PERIÓDICO TCHÊ QUÍMICA

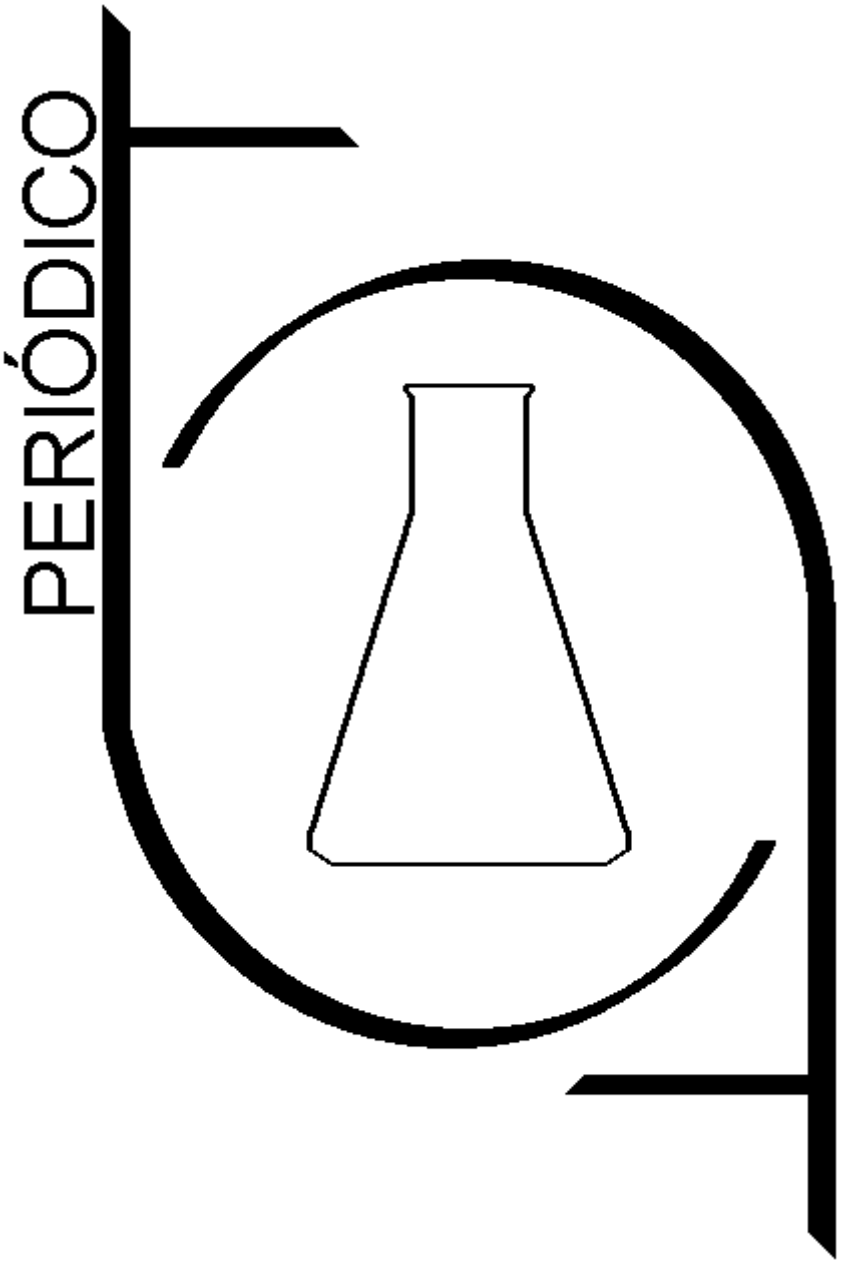

Volume 18 - Número 38 - 2021 ISSN 2179-0302

Órgão de divulgação científica e informativa

www.periodico.tchequimica.com

PERIÓDICO TCHÊ QUÍMICA

ISSN - 1806-0374 (Impresso) - ISSN - 2179-0302 (Online)

Volume 18 **Número 38 – 2021** **ISSN 2179 - 0302**

Órgão de divulgação científica e informativa.

Dados Internacionais de Catalogação na Publicação (CIP)

Periódico Tchê Química: órgão de divulgação científica e informativa [recurso eletrônico] / Grupo Tchê Química – Vol. 1, n. 1 (Jan. 2004) – Porto Alegre: Grupo Tchê Química, 2005 - Semestral.
Sistema requerido: Adobe Acrobat Reader.
Modo de acesso: World Wide Web:
<http://www.tchequimica.com>

Descrição baseada em: Vol. 14, n. 28 (ago. 2017).
ISSN 1806-0374
ISSN 2179-0302
1. Química. I. Grupo Tchê Química.

CDD 540

Bibliotecário Responsável
Ednei de Freitas Silveira
CRB 10/1262

Welcome to PERIÓDICO TCHÊ QUÍMICA

International multidisciplinary scientific journal

Periodico Tchê Quimica publishes Research Article/Original Article, Review Article, Short Report, Technical Notes, Case Studies, Interview, Book review and Forum article. Articles suitable for publication at Periodico Tchê Quimica are those that cover the traditional fields of ***Chemistry, Biology/Biochemistry, Pharmaceutical Chemistry, Medicinal Chemistry, Chemical Engineering, Chemometrics/Statistics, Phisical Chemistry, Materials Science and Science Education (Biology, Chemistry, Physiscs and Mathematics)****. We are especially interested in those submissions that are highly relevant to theoretical and* ***applied contributions in the area of chemistry and related disciplines.***

PERIÓDICO TCHÊ QUÍMICA

Volume 18 Número 38 – 2021 ISSN 2179 - 0302

Órgão de divulgação científica e informativa.

Periódico Tchê Química

ISSN - 1806-0374 (Print)
ISSN - 2179-0302 (Online)

LCCN: 2010240735

Divulgação *on-line* em
http://www.periodico.tchequimica.com
http://www.journal.tchequimica.com
http://www.tchequimica.com

Esta revista é indexada e resumida pelo CAS, EBSCO, Index Copernicus, EJL, Reaxys, Latindex, Web of Science (ESCI), OAJI.net, CAB Abstracts, ROAD, and Sumários.

Missão

O Periódico Tchê Química (PTQ) publica artigos de pesquisa originais, artigos de revisão, notas curtas (publicações científicas), revisões de livros, artigos de fórum, editoriais e entrevistas. Pesquisadores de todos os países são convidados a publicar nas páginas do PTQ.

A responsabilidade sobre os artigos é de exclusividade dos autores.

Correspondências:

Rua Anita Garibaldi, 359/603.
Bairro Mon't Serrat. CEP: 90450-001
Porto Alegre – RS. Brasil.
Skype: tchequimica
www.periodico.tchequimica.com
journal.tq@gmail.com

Índice / Index

PERIÓDICO TCHÊ QUÍMICA
ARTIGO ORIGINAL

PROCESSOS DE OXIDAÇÃO-REDUÇÃO EM SOLOS DE AGROCENOSES DE ARROZ DA REGIÃO DE KUBAN

OXIDATION-REDUCTION PROCESSES IN THE SOILS OF RICE AGROCENOSES OF THE KUBAN REGION (RUSSIA)

ОКИСЛИТЕЛЬНО-ВОССТАНОВИТЕЛЬНЫЕ ПРОЦЕССЫ В ПОЧВАХ РИСОВЫХ АГРОЦЕНОЗОВ КУБАНИ

SHEUDZHEN, Askhad Khasrethovich*; GUTOROVA, Oksana Aleksandrovna; PETRIK, Galina Fedorovna; SLYUSAREV, Valery Nikiforovich; PODKOLZIN, Oleg Anatolievich

Kuban State Agrarian University. Russian Federation.

** Correspondence author*
e-mail: sheudzhen.a.k@mail.ru

Received 20 November 2020; received in revised form 28 May 2021; accepted 14 June 2021

RESUMO

Introdução: Os estudos foram realizados na matriz de irrigação Maryano-Cheburgolsky no distrito de Krasnoarmeisky, no território de Krasnodar. **Objetivo:** Esse trabalho tem como objetivo estudar os processos de oxidação-redução e a atividade dos compostos de ferro em solos prato-chernozem e prato-pantanoso de agrocenoses de arroz da região de Kuban. **Métodos:** Foram coletadas amostras do solo das plantações de arroz e gramíneas perenes, nos quais foram determinados o valor do pH, do potencial redox (Eh, mV), da suscetibilidade magnética ($\chi \times 10^{-3}$ unidades S.I.) e a porcentagem de compostos de ferro ativos (FeO e Fe2O3, mg/100 g). **Resultados e Discussão:** Os processos redutores criados nos solos das plantações de arroz ocorridos após as inundações levaram à transformação de compostos pouco solúveis de Fe2O3 em formas mais reativas de FeO. As quantidades máximas de FeO e mínimas de Fe2O3 foram registradas durante o período em que o valor do Eh era negativo. A redução máxima do ferro em solos prato-chernozem e prato-pantanosos foi alcançada durante a fase de floração do arroz, quando foram registrados, respectivamente, os seguintes valores de Eh, pH e rH_2: Eh = -127, pH = 7.36, rH_2 = 10 e Eh = -152...-167 mV, pH = 6.89-7.10, rH_2 = 9. **Conclusões:** No solo de cultivo permanente de arroz, a dinâmica do Eh e dos compostos de ferro é similar à dos campos de rotação de culturas de arroz. Nos solos não inundados das plantações de arroz sob gramíneas perenes, prevalece o regime oxidativo e a transformação dos compostos de ferro não é manifestada. Os valores mínimos de χ coincidem com o percentual máximo de ferro ferroso nos solos com valores de Eh negativos, o que corresponde à fase de floração do arroz. Os coeficientes de correlação da variável χ com as variáveis Eh, FeO e Fe_2O_3 ficaram nos intervalos de +0,66 a +0,75, de -0,69 a -0,84 e de +0,74 a +0,77, respectivamente. O valor de χ aumenta no solo sob plantações de gramíneas perenes com predominância de processos oxidativos. O coeficiente de correlação entre as variáveis χ e Fe_2O_3 ficou no intervalo de +0,83 a +0,90.

Palavras-chave: *solo prato-chernozem, solo prato-pantanoso, plantação permanente de arroz, potencial redox, ferro ativo.*

ABSTRACT

Background: The studies were carried out on the Maryano-Cheburgolsky irrigation array in the Krasnoarmeisky district of the Krasnodar Territory. **Aim:** This work aims to study the oxidation-reduction processes and activity of iron compounds in meadow-chernozem and meadow-boggy soils of rice agrocenoses of the Kuban region. **Methods:** Soil samples were taken from paddy fields occupied by rice and perennial grasses, in which the pH value, redox potential (Eh, mV), magnetic susceptibility ($\chi \times 10^{-3}$ S.I. units), and the content of active iron compounds (FeO and Fe_2O_3, mg/100 g) were determined. **Results and Discussion**: The reductive processes created in the soils of rice fields after flooding led to the transformation of poorly soluble Fe_2O_3 compounds into more active reaction forms of FeO. The maximum content of FeO and the minimum amount of Fe_2O_3 were recorded during the period of negative Eh values. The maximum reduction of iron in meadow-boggy and meadow-chernozem soils was achieved by the phase of flowering of rice plants at Eh = -127, pH = 7.36 units,

DOI: 10.52571/PTQ.v18.n38.2021.01_ SHEUDZHEN_pgs_1_14.pdf

rH_2 = 10 and Eh = -152...-167 mV, pH = 6.89-7.10 units, rH_2 = 9, respectively. **Conclusions:** In the soil of permanent rice cultivation, the dynamics of Eh and iron compounds are similar to the fields of rice crop rotation. In non-flooded soils of rice fields under perennial grasses, the oxidative regime prevails, and the transformation of iron compounds is not expressed. The minimum values of χ coincide with the maximum content of ferrous iron in soils at negative Eh values, which corresponds to the rice flowering phase. Correlation coefficients of χ with Eh, FeO, and Fe_2O_3 equal from +0.66 to +0.75, from -0.69 to -0.84, and from +0.74 to +0.77, respectively. The χ value increases in the soil under crops of perennial grasses with a predominance of oxidative processes. The correlation coefficient between χ and Fe_2O_3 equals from +0.83 to +0.90.

Keywords: *meadow-chernozem soil, meadow-boggy soil, permanent rice cultivation, redox potential, active iron.*

АННОТАЦИЯ

Введение: Исследования проведены на Марьяно-Чебургольском массиве орошения в Красноармейском районе Краснодарского края. **Цель:** Цель работы – изучить окислительно-восстановительные процессы и подвижность соединений железа в лугово-черноземной и лугово-болотной почвах рисовых агроценозов Кубани. **Методы:** На рисовых чеках, занятых посевом риса и многолетними травами отбирались почвенные образцы, в которых определяли величину pH, окислительно-восстановительный потенциал (Eh), магнитную восприимчивость (χ) и содержание подвижных соединений железа. **Результаты и Обсуждение**: Восстановительные процессы, создающиеся в почвах рисовых полей после затопления, привели к трансформации труднорастворимых соединений Fe_2O_3 в более подвижные реакционные формы FeO. Максимум содержания FeO и минимум количества Fe_2O_3 зафиксировано в период отрицательных значений Eh. Максимальное восстановление железа в лугово-болотной и лугово-чернозёмной почвах достигалось к фазе цветения растений риса при Eh = –127, pH = 7,36 ед., rH_2 = 10 и Eh = –152...–167 mV, pH = 6,89-7,10 ед., rH_2 = 9 соответственно. **Заключение:** В почве бессменного посева риса динамика Eh и соединений железа аналогична полям рисового севооборота. В не затапливаемых почвах рисовых полей под многолетними травами преобладает окислительный режим и трансформация соединений железа не выражена. Минимальные значения магнитной восприимчивости совпадают с максимальным содержанием в почве двухвалентных соединений железа при низких величинах Eh, что соответствует фазе цветения растений риса. Коэффициенты корреляции величины χ с Eh, FeO и Fe_2O_3 составляют от + 0,66 до + 0,75; от -0,69 до -0,84 и от + 0,74 до +0,77 соответственно. Величина χ увеличивается в почве под посевами многолетних трав при преобладании окислительных процессов; коэффициент корреляции между χ и Fe_2O_3 состовляют от + 0,83 до + 0,90.

Ключевые слова: *лугово-черноземная почва, лугово-болотная почва, бессменный посев риса, окислительно-восстановительный потенциал, подвижное железо.*

1. INTRODUCTION:

The cultivation of lowland rice causes fundamental changes in soil-forming processes and the nature of the hydrological situation. During the growing season, the soils are under a water layer, which causes the creation of reductive conditions in them annually for 4-5 months. These conditions are reflected in their morphological and physical, chemical, biochemical, and biological properties (Bahmanyar, 2007; Sheudzhen and Gutorova, 2020; Sheudzhen, Gutorova, Shein, and Romanenkov, 2019; Huang, Thompson, Zhang, Chen, Han, and Gong, 2015).

Iron is a necessary and irreplaceable element of the mineral nutrition of rice plants and an active regulator of oxidation-reduction processes in the soil. The genesis of paddy soils is closely related to the transformation of iron compounds. The periodically occurring reductive processes in the soil under the rice favor the iron supply of plants. Iron enters the plant in the form of Fe^{2+} and Fe^{3+} cations and the form of chelates (Huang *et al*., 2015; Chacon, Silver, Dubinsky, and Gusack, 2006; Fageria, Baligar, and Wright, 1990; Shahid *et al*., 2017; Annisa and Nursyamsi, 2016). The reduction of $Fe^{3+}$to Fe^{2+} in the soil begins at pH = 6.0, and a decrease in the redox potential (Eh) to 220 mV and in conditions of pH = 7.0 units and Eh = 160 mV (Brümmer, 1974). This favorably affects the supply of rice plants with iron, but under certain conditions, it can also have a negative effect. In a reductive environment at low Eh values around 100-200 mV and below, ferrous iron can precipitate in an ore-like form and result in a form inaccessible to plants (Brümmer, 1974).

An excess of Fe^{2+} content in soil solution can cause toxicosis in rice plants (Li, Kronzucker, and Shi, 2016; Zaid, Ahmad, Jaleel, Wani, and Hasanuzzaman, 2020; Chérif, Audebert, Fofana,

and Zouzou, 2009). In the seedling phase, the root system of rice does not produce enough oxygen. Therefore, the reduced iron in the rhizosphere of the roots is not completely oxidized and partially penetrates the root cells, being oxidized by oxygen intended for the oxidation of intracellular processes. In this case, Fe^{2+} transforms into hydroxide forms, precipitates, and forms drusen in cells and clogs vascular vessels, leading to weakening and even thinning of seedlings (Titkov and Koltsov, 2007). Many studies determine rice yield loss due to excess iron content in the soil (Diedhiou *et al*., 2020; Sahrawat, 2005; Becker and Asch, 2005; Sahrawat, 2003).

On the other hand, with the accumulation of Fe^{2+} in the soil solution, conditions are created for binding hydrogen sulfide FeS, eliminating the products of anaerobic decomposition, which are toxic to rice. As a result of the reaction described in Equation 1.

$$FeO + H_2S \rightarrow FeS + H_2O \qquad \text{(Eq. 1)}$$

sulfurous iron, insoluble in water, is formed. This compound is harmless to rice plants, crystallizing hydrotroilite – $FeS \times nH_2O$ (Titkov and Koltsov, 2007).

Iron compounds determine the magnetic properties of the soil, which are most often characterized by the value of magnetic susceptibility (χ). This indicator for different soil types is a physical quantity that characterizes the ability of soil iron-containing minerals to magnetize. Iron minerals, which determine the magnetic susceptibility of soils, are presented as oxides and hydroxides crystallized to varying degrees and differing in the types of crystal lattices (Babanin, Trukhin, Karpachevskii, Ivanov, and Morozov, 1995). In automorphic soils with good aeration and a predominance of oxidizing conditions over reducing iron compounds, ferric oxide and hydroxides accumulate. In hydromorphic soils with a stable waterlogging regime, ferrous iron compounds predominate (Vodyanitskii and Skripnikova, 2000). The value of their magnetic susceptibility depends on the content of iron-containing minerals in soils. The soils of rice fields are dominated by iron-containing oxide and hydroxide minerals such as hematite (Fe_2O_3), goethite (α-FeOOH), lepidocrocite (γ-FeOOH), feroxyhyte ($Fe_3(OH)_8$) (Goton and Patrick, 1973; Akter *et al*., 2018). Their formation is associated with the dehydration of amorphous hydrated compounds, represented mainly by high molecular weight gels and directly with the destruction of ferruginous minerals (Zonn, 1982).

In connection with the above, the work aimed to study the oxidation-reduction regime in the soils of rice agrocenoses of the Kuban and the possibility of using the value of magnetic susceptibility as an indicator of its direction.

2. METHODS:

The studies were carried out on the Maryano-Cheburgol irrigation area of the rice irrigation system in the Krasnoarmeisky district of the Krasnodar Territory (45°23'02.77", N; 38°31'06.59", E). The research period lasted from 2016 to 2018.

A temperate continental climate characterizes the natural conditions of soil formation; a large number of positive temperatures above 10 °C, amounting to 3,600 °C; during the growing season of rice plants to 2,920-3,040 °C; low average annual precipitation (589 mm) (K.U. = 0.3-0.4); during the growing season of rice 250-350 mm; inhomogeneous relief (ridge-like near-surface rises, plain spaces and depressions); a small variety of parent rocks, represented by alluvial deposits of various granulometric composition; past growth of meadow-steppe vegetation and a high level of groundwater (1-2 m) (All-Russian Research Institute of Rice, 2005).

Per the geomorphological map of the Krasnodar Territory, the territory of the region belongs to the ancient deltaic accumulative-alluvial plain of the Kuban river. By soil geographical zoning, it belongs to the Azov-Ciscaucasian soil province of the steppe zone of ordinary and southern chernozems and the soil district of the lower reaches of the Kuban river distribution of soils of meadow-steppe and meadow types. The soil cover of the territory is represented mainly by meadow-chernozem (corresponding to Gleyic Chernozem in W.R.B. (IUSS Working Group WRB, 2015)), located on ridges and ridge-like near-river rises of the flooded plains, and meadow-boggy (corresponding to Calcic Chernic Gleysol in W.R.B. (IUSS Working Group WRB, 2015)) soils, formed in closed low regions and depressions. As a result of the construction and operation of the rice irrigation system, the natural relief was disturbed. Its anthropogenic elements are distinguished: low and high paddy fields with absolute marks from +7.2 to +10.7 m.

Within the rice irrigation system, at a short distance from each other, key areas were

selected for sowing rice and perennial grasses:

Plot 1. Meadow-chernozem soil. Sowing rice in the 1st year after a busy fallow (winter wheat).

Plot 2. Meadow-boggy soil. Sowing rice in the 1st year after a busy fallow (winter wheat).

Plot 3. Meadow-chernozem soil. Sowing perennial grasses of the 2nd year.

Plot 4. Meadow-boggy soil. Sowing perennial grasses of the 2nd year.

Plot 5. Meadow-chernozem soil. Permanent rice cultivation for 80 years without fertilization (monoculture since 1937).

Soil samples were taken simultaneously in the central part of rice paddies on counting plots in the arable (0-10 and 11-20 cm) and sub-arable (21-30 and 31-40 cm) soil layers. Samples were taken with a soil drill before the creation of a layer of water above the soil surface and after its flooding in the phases of rice plant vegetation: seedlings, tillering, flowering, and full ripeness of the grain.

In freshly collected soil samples without drying and grinding, we determined di- (FeO) and trivalent (Fe_2O3) iron in 0.1 N H_2SO_4 at a soil-to-solution ratio of 1: 5 and shaking for five minutes, followed by filtration through a dry ash-free filter with a pore diameter of 3-5 microns. The method is based on forming a soluble complex compound Fe [$C_{10}H_8N_2$] 32+ being intensely red during the interaction of α, α-dipyridyl ($C_{10}H_8N_2$ Sigma-Aldrich, USA) with bivalent iron. This compound is stable in the pH range of 3.5-8.5, and the color intensity is proportional to the concentration of iron in the solution. FeO and Fe_2O_3 are determined simultaneously in two portions of 0.1 H H_2SO_4 on a spectrophotometer Thermo Scientific GENESYS 10S UV-Vis at a wavelength of 508 nm. In the first portion, FeO was determined, in the second portion – the sum of FeO + Fe_2O_3, with FeO being previously converted into Fe_2O_3 using hydroxylamine hydrochloric acid (H_4ClNO). To do this, a buffer acetate solution was added to two portions of the filtrate, and H_4ClNO was added to the second portion, after adding α, α-dipyridyl, the volume in a volumetric flask was brought to the line with distilled water, thoroughly mixed, and after 30 min the absorption was measured on a spectrophotometer at a wavelength of 508 nm. In the first determination, the FeO content was determined. The amount of Fe_2O_3 was calculated by means of subtracting it from the results of the second determination and multiplying by a factor of 1.11 (Novitskii *et al*., 2009).

The determination of pH and redox potential (Eh, mV) was carried out simultaneously in undisturbed soil composition by a potentiometric method using a Metller Toledo pH meter (Novitskii *et al*., 2009). The value of the partial pressure of hydrogen (rH_2) was calculated using Equation 2, introduced by V. M. Clark and B. Cohen:

$$rH2 = \frac{\mathrm{Eh}}{30} + 2\mathrm{pH\ at\ 20°C} \qquad \text{(Eq. 2)}$$

This value characterizes the intensity of redox processes in the soil at different pH values of the environment. The predominance of oxidative processes corresponds to rH_2 over 27; of reductive processes – to rH_2 <27; of intensive reductive processes – to rH_2 <20 (Savich, Gukalov, and Polyakov, 2017; Savich, Kaurichev, Shishov, Nikol'skii, and Romanchik, 2004).

The magnetic susceptibility (χ) of the studied soils was measured with a Satis Geo KM-7 kappameter (Czech Republic) (Babanin *et al*., 1995; Vodyanitskii and Skripnikova, 2000). The measurements were carried out in the field at each site in 15 replicates. The method did not require chemical or physical destruction of soil samples and was applied for the first time under rice cultivation conditions. Single-mode of measurement was used to be reproduced in two stages. The first stage consisted of zeroing the device, which was removed from the studied soil samples and other magnetic or conductive objects at a distance of at least 30 cm. The direct measurement of soil samples characterized the second stage. For this, the gauge sensor was applied to the soil samples taken with a soil drill from under the water layer into a plastic bag, and then the readings were recorded with the KM-7 device. The values of the magnetic susceptibility of soils were expressed in SI units. The sensitivity of the KM 7 device was $1x10^{-6}$ SI units, and the measurement range was ± $999x10^{-3}$ SI units with automatic switching of the accuracy level, the operating frequency is 10 kHz. The data were exported to a text file by means of the KMdata software and were used for further processing in Microsoft Excel.

3. RESULTS:

The conducted analysis showed that there was a sharp change in oxidative reduction processes (Figure 1). The highest values of the redox potential were noted before their flooding at rH_2 equal to 25-28. After creating the water layer,

the soil potential gradually decreased, reaching its minimum values in the rice flowering phase. During this period, negative values of Eh = - 127 ... - 167 mV were recorded in the soil layer 0-10 cm in the range of pH = 6.89-7.36 units and rH_2 = 9-10. The difference in the interval between the redox potential indicators before soil flooding and during the period of maximum development of reductive processes (rice flowering phase) reached 502-630 mV. After the discharge of water from rice fields and drying of the soil, oxidative processes were activated, and the Eh values increased. However, due to the ability of soils to be in a state of complete moisture saturation and increased compaction of the arable layer for a certain time after rice harvesting, the process of oxidation of reduced products is difficult in them.

Different soils have unequal resistance to changes in the redox potential. Before the flooding of paddy fields, the potential difference between the soils of the meadow-boggy and meadow-chernozem types already amounted to 77-88 mV (Table 1).

Table 1. *The difference in the oxidation-reduction potential between meadow chernozem and meadow bog soils during the growing season of rice*

Rice vegetation phase	Difference Eh, mV	
	Sowing rice 1st year	Permanent sowing of rice
Before the soil is flooded	+88	+77
Seedlings	+152	+138
Tillering	+35	+131
Bloom	-40	-25
Full ripeness of grain	+111	+48

The most pronounced reductive processes were expressed in the meadow-boggy soil at the beginning of the rice-growing season (Plot 2). 30 days after its flooding, which corresponded to the germination phase, the Eh values decreased from 375 to 171 mV, and rH_2 became equal to 17. This indicated strongly reductive conditions in the upper 0-10 cm soil layer. The absence of a sufficiently developed root system in rice plants during this period can cause their suppression or death. The discharge of irrigation water from paddy fields, carried out during this period according to the agricultural technology of rice cultivation, improves soil aeration, which favorably affects the development of plants.

The best aeration conditions were observed in meadow-chernozem soil. After 30 days of the soil being in a flooded state, Eh in the 0-10 cm layer decreased from 463 to 323 mV at rH_2 = 24. This indicated the predominance of a weak, reduced environment in the soil (Plot 1). The same direction of soil processes was observed in the soil under permanent rice cultivation (Plot 5) – from 452 to 309 mV at rH_2 = 22, with the only difference was that the Eh values were lower 11-14 mV.

Later, regardless of the type of soil and the duration of rice cultivation, strong anaerobic processes developed in them. Already by the tillering phase of rice plants, rH_2 in soils dropped to 15-16. However, the reductive processes reached the greatest intensity after 90 days of soil flooding, i.e., in the flowering phase. Moreover, in the meadow-boggy soil, the Eh values were lower than in the meadow-chernozem soil. The potential difference between them equaled 25-40 mV.

After the cessation of water supply to the paddy fields and the creation of aerobic conditions in the phase of complete ripeness of the grain, the redox potential increased more intensively in the meadow-chernozem soil, which indicated rather rapid oxidation of the reduced compounds. Simultaneously, the oxidation processes in the soil under permanent rice were weaker than in rice crop rotation conditions. Lower values indicated this for Eh (236 versus 326 mV) and rH_2 (24 versus 19).

In non-flooded paddy fields under perennial grass crops, the oxidative regime was maintained throughout the irrigation period. Simultaneously, in the meadow-boggy soil, aerobic processes developed slower (Plot 4), as indicated by the low values of the redox potential, ranging from 388 to 440 mV at pH = 7.10-7.47 units and rH_2 = 27-29 (Figure 1).

The best conditions for aeration under perennial grasses were found in the meadow-chernozem soil (Plot 3). The Eh values during the entire measurement period varied in the 0-10 cm layer from 410 to 470 mV at pH = 6.59-7.57 units and rH_2 = 28-30. Compared to Plot 4, the Eh value was 20-55 mV lower.

Thus, the most intensively reductive conditions develop in the meadow-boggy soil of

rice fields than in the meadow-chernozem soil. The maximum intensity of reductive processes in flooded soils of rice agrocenoses is achieved by the flowering phase of the rice plants (Eh equals from -127 to -167 mV, pH = 6.89-7.36 units, rH_2 9-10).

Studies showed that the development of reduction processes led to the transformation of poorly soluble Fe_2O_3 compounds into more active FeO reaction forms (Figures 2, 3). After a decrease in the redox potential, the content of reduced iron in the studied soils and the quantitative ratio of FeO: Fe_2O_3 increased sharply, which indicated the creation of an anaerobic environment. The intensity of the accumulation of bivalent iron in the soil increased with the growth of reduction processes in it. During the period of anaerobiosis, the content of Fe_2O_3 in the soil decreased, and when anaerobic conditions changed with aerobic ones, their amount increased again.

Different modes of oxidation-reduction conditions in meadow-chernozem and meadow-boggy soils had a different effect on the dynamics of the content of iron compounds in them. A weak manifestation of reductive processes characterizes the meadow-boggy soil even before its flooding (rH_2 = 25). The total content of ferrous and ferric iron in the arable (0-20 cm) and sub-arable (21-40 cm) soil layers during this period was 207.24 and 191.41 mg/100 g, respectively (Plot 2). Active iron was represented by compounds of the trivalent form (FeO: Fe_2O_3<1.0). Simultaneously, in spring, before the soil was flooded, reasonably high content of under-oxidized iron was found not only in the arable layer but also in the subsoil. The share of FeO content was 8-14%, and Fe_2O_3 amounted to 86-92% of the total FeO + Fe_2O_3. Compared with meadow-chernozem soil, the FeO content was 3.0-4.5 times higher in rice crop rotation fields (Plot 1) and 1.5-2.0 times higher under permanent rice cultivation (Figures 2 and 3).

A month after the meadow-boggy soil flooding, there was a sharp increase in FeO content and a decrease in the amount of Fe_2O_3, especially in the upper 0-10 cm layer (FeO: Fe_2O_3 = 1.16). According to rice cultivation technology, this is despite the periodic discharges of water from the paddy fields in the phase of plant emergence, aimed at airing and enriching the soil with air oxygen. Although in the deeper layers of the soil, weak oxidizing conditions persisted: the ratio of FeO: Fe_2O_3 in 11-20, 21-30, and 31-40 cm soil layers equaled 0.83, 0.62, and 0.42, respectively.

In the tillering phase, the accumulation of reduced iron in the soil continued, reaching its maximum for rice flowering - FeO = 269.38 mg/100 g at Eh = –127 mV and pH = 7.36 units, rH_2 = 10. Simultaneously, as the reduction processes increased, the amount of Fe_2O_3 in the soil sharply decreased, especially in the upper layers of 0-10 and 11-20 cm. During the period of the highest intensity of the reduction regime, which corresponded to the phase of plant flowering, the Fe_2O_3 content in the 0-10 cm layer was 18.96 mg/100g, and the FeO:Fe_2O_3 ratio increased to 14.0. The anaerobic environment persisted in the lower soil layers at 11-20, 21-30, and 31-40 cm. However, the reductive processes in those layers were less pronounced (FeO: Fe_2O_3 = 3.2, 1.8, and 1.0, respectively).

Based on the statistical evaluation of the experimental data, a high negative correlation was established between Eh and the content of FeO in meadow-boggy soil, equal to r = -0.83, as well as a positive correlation with Fe_2O_3 r = 0.79, and a strong correlation between FeO and Fe_2O_3 (r = -0.97).

A completely different oxidation-reduction regime in the rice field developed in meadow-chernozem soil (Plots 1, 5). Before sowing and flooding the paddy field, the total active iron content in the arable and subsoil layers was 222.07 and 199.06 mg/100 g, respectively (Plot 1). Simultaneously, the share of FeO content accounted for 2.01-3.73% and Fe_2O_3 – 96-98% of the total FeO + Fe_2O_3. The proportion of FeO content was 1.5-2.0 times higher (4.02-5.40% of the total FeO + Fe2O3) than under rice crop rotation conditions in the soil under permanent rice cultivation. Regardless of the duration of rice cultivation, most of the undeoxidized iron was contained in the 0-10 cm layer and decreased by two times with the soil depth (Figures 2, 3).

If, before the meadow-chernozem soil flooding, the FeO content was low compared to the meadow-boggy soil, then after creating a layer of water in the paddy fields, its amount increased. However, ferric oxides still predominated in the seedling phase. This can be explained by the fact that there were discharges of water from paddy fields during this period, and the soil was well enriched with air oxygen. Nevertheless, after creating a permanent layer of water, from the tillering phase to the flowering of rice plants, an accumulation of bivalent active iron and a decrease in trivalent active iron content were noted. The maximum content of reduced iron was reached by the rice flowering phase 152.64-165.84 mg/100 g at Eh = –152 ...2

167 mV, pH = 6.89-7.10 units, and rH_2 = 9. The amount of Fe_2O_3 during this period decreased to 55.00-58.29 mg/100 g, and the ratio of FeO:Fe2O3 in layers 0-10 and 11-20 cm was 2.77-2.80 and 1.66-2.40, respectively. This indicated that recovery processes were taking place in the soil. However, at the lower soil layers, their tension noticeably weakened. The narrow range of FeO evidenced this: Fe_2O_3 ratios in the layers 21-30 and 31-40 cm, equal to 0.17-0.23 and 0.07-0.17, respectively, indicating the predominance of oxidizing conditions in the soil.

After the water was discharged from the paddy fields, the reduced iron was gradually oxidized by atmospheric oxygen. At the same time, in the meadow-boggy soil, the oxidation process in the 0-10 cm layer was slower than in the meadow-chernozem soil: FeO: Fe_2O_3 = 7.4 at Eh = 215 mV versus FeO: Fe_2O_3 = 1.3-2.3 at Eh = 236-326 mV.

Regardless of the duration of rice cultivation, the direction of the dynamics of active forms of iron compounds in the growing season of rice was the same. In the meadow-chernozem soil of the rice crop rotation, negative correlations were established between the indicators Eh and FeO (r = -0.89), FeO and Fe_2O_3(r = -0.74), positive between Eh and Fe_2O_3 (r = +0.70). In the soil of permanent rice cultivation, correlations between these indicators equaled -0.89, -0.79, and +0.73, respectively.

In non-flooded soils under perennial grass crops, the ferric iron content dominated throughout the observation period, and the oxidative regime prevailed in them (Figures 1-3). In the meadow-boggy soil (Plot 4), oxidative processes were less developed than in the meadow-chernozem soil (Plot 3). This was indicated by a lower Eh in the 0-10 cm layer, fluctuating in the range 388-440 mV at pH = 7.10-7.47 units and rH_2 = 27-29, and increased content of FeO in the soil in the range from 10.10 to 41.92 mg/100 g.

The best oxidizing conditions under crops of perennial grasses developed in meadow-chernozem soil. During the entire measurement period, the Eh values in the 0-10 cm layer varied in a small range of 410-470 mV at pH = 6.59-7.57 units and rH_2 = 28-30. Compared to the meadow-boggy soil, the FeO content was lower by 33%, in layers at 11-20 and 21-30 cm, it was lower by 41%, and in layers at 31-40 cm by 51%. Simultaneously, the content of Fe_2O_3 was higher in the 0-10 cm layer by 9.72%, in the 11-20 cm layers by 8.63%, 21-30 cm by 6.35%, and in the 31-40 cm layers by 12.67%.

In non-flooded meadow-chernozem and meadow-boggy soils under perennial grasses, a negative correlation between Eh and FeO (r = -0.84 to -0.89) was noted.

Studies showed that the dynamics of Eh and active forms of iron compounds during the flooding of soils in rice fields are associated with a change in the value of the magnetic susceptibility χ, which decreased under anaerobic conditions. Its minimum values were recorded during the period of maximum reduced iron content at low Eh values, i.e., in the flowering phase of rice plants. During this period, χ indices in the flooded soil varied in the range from 0.059-0.081 in the 0-10 cm layer to 4.7-6.6×10^{-5} S.I. units in the lower layers, i.e., 60 days after the emergence of rice seedlings, they decreased by 1.5-2.0 times (Figure 4).

The nature of magnetic susceptibility dynamics in meadow-chernozem soil under permanent rice cultivation conditions and crop rotation was approximately the same. However, during the period of maximum intensity of reductive processes, lower values of χ were achieved with permanent rice cultivation (Figure 4). This is explained by the low content of organic matter in the soil, which catalyzes biochemical reduction reactions during the period of its flooding (Sheudzhen *et al*., 2019).

The highest χ values are confined to the upper 0-10 cm soil layer; in the 11-20 cm layer, they are 1.5-2.0 times lower. Their decrease was also noted in the lower layers (at 21-30 and 31-40 cm). The χ value is always higher in the surface horizons, where the content of humic acids is increased since the latter can be catalysts for the ferromagnetisation of weakly magnetic iron compounds (Babanin *et al*., 1995).

When oxidizing conditions are created in the soil, the magnetic susceptibility increases. After the discharge of water from paddy fields relative to the rice flowering phase, the χ value increased in the 0-10 cm layer by 17-25%, in the 11-20 cm layer by 42-47, in the 21-30 cm layer by 12-26, and in the 31-40 cm layer by 10-18%.

The largest values of χ were formed in the meadow-chernozem soil. On average, during the growing season of rice, this indicator was higher than in the meadow-boggy soil by 16.0-54.0%. The lower χ values of the meadow-boggy soil reflect the low content of crystallized highly magnetic minerals (Babanin *et al*., 1995). This is due to the dissolution of iron-containing minerals

under reductive conditions (Grimley and Vepraskas, 2000; Van Bodegom, Van Reeven, and Van Der Gon, 2003).

The aerobic conditions created by the accompanying rice crop rotation favor the formation of more magnetic iron-bearing minerals (Figure 4).

In meadow-chernozem soil, the indicators of the magnetic susceptibility of soil under perennial grasses are more stable throughout the observation period and higher in the 0-10 cm layer by 3.2×10^{-5}, in the 11-20 cm layer by 5.5, in the 21-30 cm layer by 3,4, and in the 31-40 cm layer by 4.2×10^{-5} S.I. units than in flooded rice field soil. Accordingly, they are higher in the meadow-boggy area by 1.8×10^{-5}, 1.7, 1.4, and 1.1×10^{-5} S.I. units. Simultaneously, a general pattern is observed: the smallest indicators of magnetic susceptibility, both under oxidative and reducing modes, were recorded in meadow-boggy soil.

Hence, it follows that in the aerobic period of the rice field, conditions appear that determine the possibility of the formation of more magnetic iron-containing compounds in soils. When the moistening period is changed to desiccation, newly formed ferromagnets are found in them (Zonn, 1982; Vodyanitskii, Morgun, Rumyantseva, Obydenova, and Chapygina, 2009).

4. DISCUSSION:

The practice of rice cultivation, literature data, and our research indicates that the technology of rice cultivation, which provides for the maintenance of the rice field for the main part of the growing season of rice under a layer of water, is associated with a change in the oxidation-reduction conditions in the soil (Bahmanyar, 2007; Sheudzhen and Gutorova, 2020; Sheudzhen *et al*., 2019; Annisa and Nursyamsi, 2016; Goton and Patrick, 1973). The flooding factor largely determines the exclusive orientation of soil-forming processes. One of the decisive conditions for high soil fertility in rice fields is to ensure a favorable redox potential, which is regulated by measures that traditionally include a balanced use of mineral fertilizers, replenishment with fresh organic matter, scientifically substantiated introduction of crop rotation with the inclusion of perennial grasses, soil cultivation techniques for them. Oxidation during the inter-irrigation period and the accumulation of chemically bound oxygen in them, lowering the groundwater level. In this regard, diagnostic indicators are needed to characterize the oxidation-reduction regime of soils in rice agrocenoses. The previous section considered the dynamics of the redox potential and compounds of active forms of iron, which fully reflect the oxidation or reduction state of the rice field. The literature highlights the relationship between the redox potential and ferrous iron content in soils under rice. The data we obtained do not disagree with the literature (Annisa and Nursyamsi, 2016; Akter *et al*., 2018; Gardiner and James, 2012). W. Annisa and D. Nursyamsi (2016) showed a negative correlation between the Eh value and the Fe^{2+} concentration equal to $r = -0.856$.

We analyzed the possibility of using the value of the magnetic susceptibility χ as an indicator of the redox state of soils in rice fields. The literature mainly describes the profile distributions of magnetic susceptibility. It has been shown that in rice soils, there exists a more pronounced profile differentiation of iron oxides and a low magnetic susceptibility in comparison with well-drained soils (Zhang and Gong, 1993; Lu, Zhu, and Yu, 2012; Han and Zhang, 2013; Huang *et al*., 2018).

From the studies carried out, it follows that the magnitude of the magnetic susceptibility can be judged on the direction of the redox processes occurring in the flooded soils of rice fields. Its minimum values coincide with the maximum FeO content in them at negative Eh values in the flowering phase of rice plants:

χ = 5.9×10^{-5} SI units, FeO = 269.38 mg/100 g, Fe_2O_3 = 18.96 mg/100 g, Eh = -127 mV, pH = 7.36 units, rH_2 = 10 for meadow-boggy soil;

χ = 7,6-8.1×10^{-5}SI units, FeO = 152,64-165.84 mg/100 g, Fe_2O_3 = 55,00-58.29 mg/100 g, Eh = -152...-167 mV, pH = 6.89-7.10 units, rH_2 = 9 for meadow-chernozem soil.

Based on the statistical evaluation of the experimental data, the dependence of the χ values on the indicators of the redox regime of soils was noted (Table 2).

Table 2. *Correlation between the value of magnetic susceptibility and indicators of the oxidation-reduction regime of soils (p<0.05, n = 35)*

Plot/Indicator	FeO	Fe_2O_3	Eh
Plot 1. Meadow-	-0.69	0.76	0.72

chernozem soil. Sowing rice 1st year after winter wheat			
Plot 2. Meadow-boggy soil. Sowing rice in the 1st year after a busy fallow (winter wheat)	-0.84	0.77	0.66
Plot 3. Meadow-chernozem soil. Sowing perennial grasses of the 2nd year	0.41	0.90	-0.28
Plot 4. Meadow-boggy soil. Sowing perennial grasses of the 2nd year	0.27	0.83	-0.40
Plot 5. Meadow-chernozem soil. Permanent rice cultivation for 80 years without fertilization (since 1937)	-0.80	0.74	0.75

During the flooding of the meadow-boggy soil, correlations with FeO (r = -0.84) were revealed, weaker with Fe_2O_3 (r = +0.77) and Eh (r = +0.66), while during the flooding of the meadow-chernozem soil we discovered positive relations with Fe_2O_3 and Eh (r = +0.76 and +0.72, respectively) and negative relations with FeO (r = -0.69). Under conditions of permanent rice cultivation, we discovered relations with FeO, Fe_2O_3, and Eh: -0.80, +0.74, and +0.75 respectively.

The χ values increase and are more stable in dynamics with the predominance of aerobic processes in soils. In meadow-boggy and meadow-chernozem soils under perennial grasses, the highest correlation coefficients were noted between the χ value and the Fe_2O_3 content, equal to +0.83 and +0.90, respectively.

Thus, with the flooding of soils in rice fields, the value of the magnetic susceptibility decreases, which indicates a decrease in the redox potential and an increase in the content of reduced iron.

5. CONCLUSION:

The results demonstrates the possibility of using one of the characteristics of the magnetic properties of soils, the magnitude of the magnetic susceptibility, to diagnose the oxidation-reduction state of rice agrocenoses. This is the first time such research has been conducted in rice fields.

The reductive processes that occur in the soils of rice fields after flooding lead to the transformation of poorly soluble Fe_2O_3 compounds into more active reaction forms of FeO. The maximum content of FeO and the minimum amount of Fe_2O_3 were recorded during the period of negative values of the redox potential – the phase of flowering of rice plants. During this period, in the flooded meadow-boggy soil, the content of reduced iron reaches 269.38 mg/100 g, the ratio FeO:Fe_2O_3 = 14.0, Eh = –127 mV, pH = 7.36 units, rH_2 = 10; meadow chernozem – 152.64-165.84 mg/100 g, FeO:Fe_2O_3 = 2.77-2.80, Eh = –152 ...– 167 mV, pH = 6.89 ... 7.10 units, rH_2 = 9. At the same time, in the meadow-chernozem soil of permanent rice sowing, the dynamics of Eh and iron compounds are similar to the fields of rice crop rotation. In the soil of permanent rice cultivation, the dynamics of Eh and iron compounds are similar to the fields of rice crop rotation. In non-flooded soils of rice fields under perennial grasses, the oxidative regime prevails, and the transformation of iron compounds does not occur.

The minimum values of the magnetic susceptibility (χ) coincide with the maximum content of ferrous iron in the flooded soil and a low redox potential, which corresponds to the flowering phase of rice plants. The correlation (determination) coefficients between the value of χ and Eh, FeO and Fe_2O_3 are r = +0.66 ... +0.75 (r_2 = 0.44 ... 0.56); r = -0.69 ... -0.84 (r^2 = 0.48 ... 0.71) and r = +0.74 ... +0.77 (r_2 = 0.55 ... 0 , 59), respectively. Indicators of magnetic susceptibility increase in the soil under crops of perennial grasses with a predominance of oxidative processes. The correlation coefficient between χ and Fe_2O_3 is r = +0.83 ... +0.90 (r_2 = 0.69 ... 0.81).

6. REFERENCES:

1. Akter, M., Deroo, H., De Grave, E., Van Alboom, T., Kader, M. A., Pierreux, S., Sleutel, S. (2018). Link between paddy soil mineral nitrogen release and iron and manganese reduction examined in a rice pot growth experiment. *Geoderma*, 326, 9-21. https://doi.org/10.1016/j.geoderma.2018.04.002
2. Annisa, W., and Nursyamsi, D. (2016). Iron dynamics and its relation to soil redox

potential and plant growth in acid sulphate soil of south Kalimantan, Indonesia. *Journal of Agricultural Science, 17*(1), 1-8.

3. Babanin, V. F., Trukhin, V. I., Karpachevskii, L. O., Ivanov, A. V., and Morozov, V. V. (1995). *Magnetizm pochv [Soil magnetism].* Moscow, Russia: Izdatelstvo YaGTU, 222 p.
4. Bahmanyar, M. A. (2007). The Influence of Continuous Rice Cultivation and Different Waterlogging Periods on Morphology, Clay Mineralogy, Eh, pH, and K in Paddy Soils. *Pakistan Journal of Biological Sciences*, 10, 2844-2849.
5. Becker, M., and Asch, F. (2005). Iron toxicity in rice conditions and management concepts. *Journal of Plant Nutrition and Soil Science, 168*(4), 558-573. https://doi.org/10.1002/jpln.200520504
6. Brümmer, G. (1974). Redoxpotentiale und redoxprozesse von mangan-, eisenund schwefelverbindungen in hydromorphen böden und sedimenten. *Geoderma, 12*(3), 207-222.
7. Chacon, N., Silver, W. L., Dubinsky, E.A., and Gusack, D. F. (2006). Iron reduction and soil phosphorus solubilization in humid tropical forest soils: the roles of labile carbon pools and an electron shuttle compound. *Biogeochemistry*, 78, 67-84.
8. Chérif, M., Audebert, A., Fofana, M., and Zouzou, M. (2009). Evaluation of Iron Toxicity on Lowland Irrigated Rice in West Africa. *Tropicultura, 27*(2), 88-92.
9. Diedhiou, S., Goudiaby, A. O. K., Sagna, Y. P., Diatta, Y., Diallo, M. D., and Ndoye, I. (2020). Effect of Iron Toxicity on Rice Growth in Sulfato-ferruginous Lowland of South Senegal. *American Journal of Agriculture and Forestry, 8*(1), 9-14. https://doi.org/10.11648/j.ajaf.20200801.12
10. Fageria, N. K., Baligar, V. C., and Wright, R. J. (1990). Iron nutrition of plants: au overview on the chemistry and physiology of its deficiency and toxicity. *Pesq. agmpec. bras.*, *25*(4), 553-570.
11. Gardiner, D. T., and James, S. (2012). Wet Soil Redox Chemistry as Affected by Organic Matter and Nitrate. *American Journal of Climate Change*, 1, 205-209. http://dx.doi.org/10.4236/ ajcc.2012.14017
12. Goton, S., and Patrick, W. H. (1973). Transformation of Iron in a Waterlogged Soil as Influenced by Redox Potential and pH. *Soil Science Society of America, Proceedings*, 38, 66-71.
13. Grimley, D. A., and Vepraskas, M. J. (2000). Magnetic susceptibility for use in delineating hydric soils. *Soil Science Society of America Journal, 64*(6), 2174-2180.
14. Han, G. Z., and Zhang, G. L. (2013). Changes in magnetic properties and their pedogenetic implications for paddy soil chronosequences from different parent materials in south China. *European Journal of Soil Science*, 64, 435-444.
15. Huang, L., Jia, X., Shao, M., Chen, L., Han, G., and Zhan, G. (2018). Phases and rates of iron and magnetism changes during paddy soil development on calcareous marine sediment and acid Quaternary red-clay. *Scientific Reports, 8*(444), 1-11. https://doi.org/10.1038/s41598-017-18963-x
16. Huang, L. M., Thompson, A., Zhang, G. L., Chen, L. M., Han, G. Z., and Gong, Z. T. (2015). The use of chronosequences in studies of paddy soil evolution: a review. *Geoderma*, 237-238, 199-210.
17. IUSS Working Group WRB. (2015). *World Reference Base for Soil Resources 2014, update 2015. International soil classification system for naming soils and creating legends for soil maps. World Soil Resources Reports No. 106*. Rome, Italy: FAO, 192 p.
18. Li, G., Kronzucker, H. J., and Shi, W. (2016). The Response of the Root Apex in Plant Adaptation to Iron Heterogeneity in Soil. *Front Plant Sci*., 7, 344. https://doi.org/10.3389/fpls.2016.00344
19. Lu, S. G., Zhu, L., and Yu, J. Y. (2012). Mineral magnetic properties of Chinese paddy soils and its pedogenic implications. *Catena*, 93, 9-17.
20. Novitskii, M. V., Donskikh, I. N., Chernov, D. V., Nazarova, A. V., Melnikov, S. P., Baeva, N. N., and Lavrishchev, A. V. (2009). *Laboratorno-prakticheskie zanyatiya po pochvovedeniyu [Laboratory and practical classes in soil science].* St. Petersburg, Russia: Prospekt Nauki, 320 p.
21. All-Russian Research Institute of Rice (2005). Rice-growing system of the Krasnodar Territory. Krasnodar, Russia: All-Russian Research Institute of Rice, 340 p.
22. Sahrawat, K. L. (2003). Iron toxicity in wetland rice: occurrence and management through integration of genetic tolerance with plant

nutrition. *Journal of the Indian Society of Soil Science, 51*(4), 409-417.

23. Sahrawat, K. L. (2005). Iron Toxicity in Wetland Rice and the Role of Other Nutrients. *Journal of Plant Nutrition, 27*(8), 1471-1504. https://doi.org/10.1081/PLN-200025869
24. Savich, V. I., Gukalov, V. V., and Polyakov, A.M. (2017). Okislitelno-vosstanovitelnoye sostoyaniye pochv, kak kriteriy ikh plodorodiya [Oxidation-reduction state of soils as a criterion of their fertility]. *Plodorodiye*, 6, 22-24.
25. Savich, V. I., Kaurichev, I. S., Shishov, L. L., Nikol'skii, Yu. N., and Romanchik, E. A. (2004). Agronomic evaluation of the redox status of soils. *Eurasian Soil Science, 37*(6), 608-617.
26. Shahid, M., Shukla, A. K., Nayak, A. K., Rahul Tripathi, M. J., Lal, B., and Gautam, P. (2017). Root Activity and Antioxidant Enzyme Activities of Rice Cultivars under Different Iron Toxicity Mitigation Options. *Journal of the Indian Society of Soil Science, 65*(3), 341-348. https://doi.org/10.5958/0974-0228.2017.00040.8
27. Sheudzhen, A. Kh., and Gutorova, O. A. (2020). State of Humus in Soils under Rice Cultivation. *In I.O.P. Conference Series: Materials Science and Engineering*. Paper presented at the International Scientific and Practical Conference "Modern Problems of Ecology, Transport and Agricultural Technologies", held at Barnaul, June 26-27, 2020 (pp. 012022), doi:10.1088/1757-899X/941/1/012022
28. Sheudzhen, A. Kh., Gutorova, O. A., Shein, E. V., and Romanenkov, V. A. (2019). Agrogenic soil evolution of rice agrolandscapes. In *I.O.P. Conference Series: Earth and Environmental Science*. Paper presented at the International Conference "On key concepts of soil physics: development, future prospects and current applications 2019", held at Moscow, May 27-31, 2019 (pp. 012044). Institute of Physics Publishing.
29. Titkov, A. A., and Koltsov, A V. (2007). *Evolyutsiya risovykh landshaftno-meliorativnykh sistem Ukrainy [Evolution of rice landscape-ameliorative systems in Ukraine].* Simferopol, Ukraine: S.O.N.A.T., 308 p.
30. Van Bodegom, P. M., Van Reeven, J., and Van Der Gon, H. A. C. D. (2003). Prediction reducible soil iron content from iron extraction data. *Biogeochemistry, 64*(2), 231-245. https://doi.org/10.1023/A:1024935107543
31. Vodyanitskii, Yu. N., Morgun, E. G., Rumyantseva, K. A., Obydenova, L. A., and Chapygina, N. V. (2009). Geochemistry of magnetite and maghemite in soils in European Russia. *Geochemistry International, 47*(3), 297-310.
32. Vodyanitskii, Yu. N., and Skripnikova, M. I. (2000). Magnitnyi metod [Magnetic method]. In: S.A. Sycheva, *Rukovodstvo po izucheniyu paleoekologii kulturnykh sloev drevnikh poselenii [A guide to the study of paleoecology of cultural layers of ancient settlements]* (pp. 47-50). Moscow, Russia: R.A.N., M.G.U.
33. Zaid, A., Ahmad, B., Jaleel, H., Wani, S. H., and Hasanuzzaman, M. (2020). A Critical Review on Iron Toxicity and Tolerance in Plants: Role of Exogenous Phytoprotectants. In: T. Aftab and K.R. Hakeem (Eds), *Plant Micronutrients* (pp. 83-89). Cham, Switzerland: Springer.
34. Zhang, G. L., and Gong, Z. T. (1993). Geochemical features of element migration under artificial submergence. *Acta Pedol. Sin*., 30, 355-365.
35. Zonn, S. V. (1982). *Iron in Soils (genetic and geographical aspects).* Moscow, Russia: Nauka, 207 p.

7. OPEN ACCESS

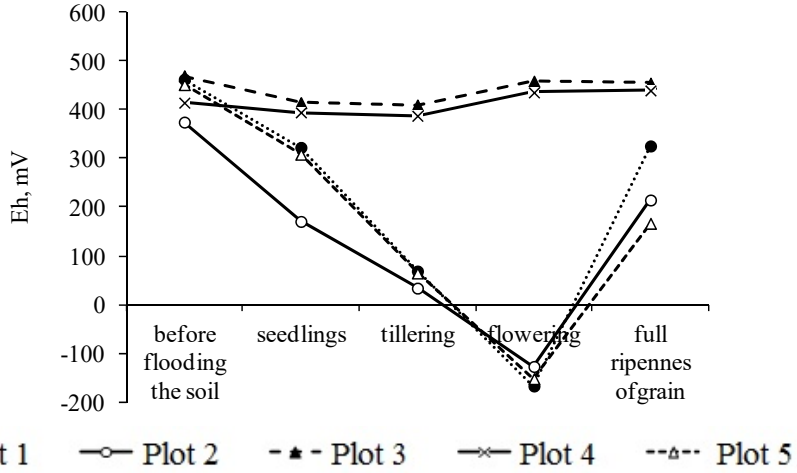

Legend: plot 1 meadow-chernozem soil (rice sowing in the 1st year after a busy fallow); plot 2 meadow-boggy soil (rice sowing in the 1st year after a busy fallow); plot 3 meadow-chernozem soil (sowing of perennial grasses of the 2nd year); plot 4 meadow-boggy soil (sowing of perennial grasses of the 2nd year); plot 5 meadow chernozem soil (rice monoculture since 1937).

Figure 1. Dynamics of the redox potential in the soils of rice fields

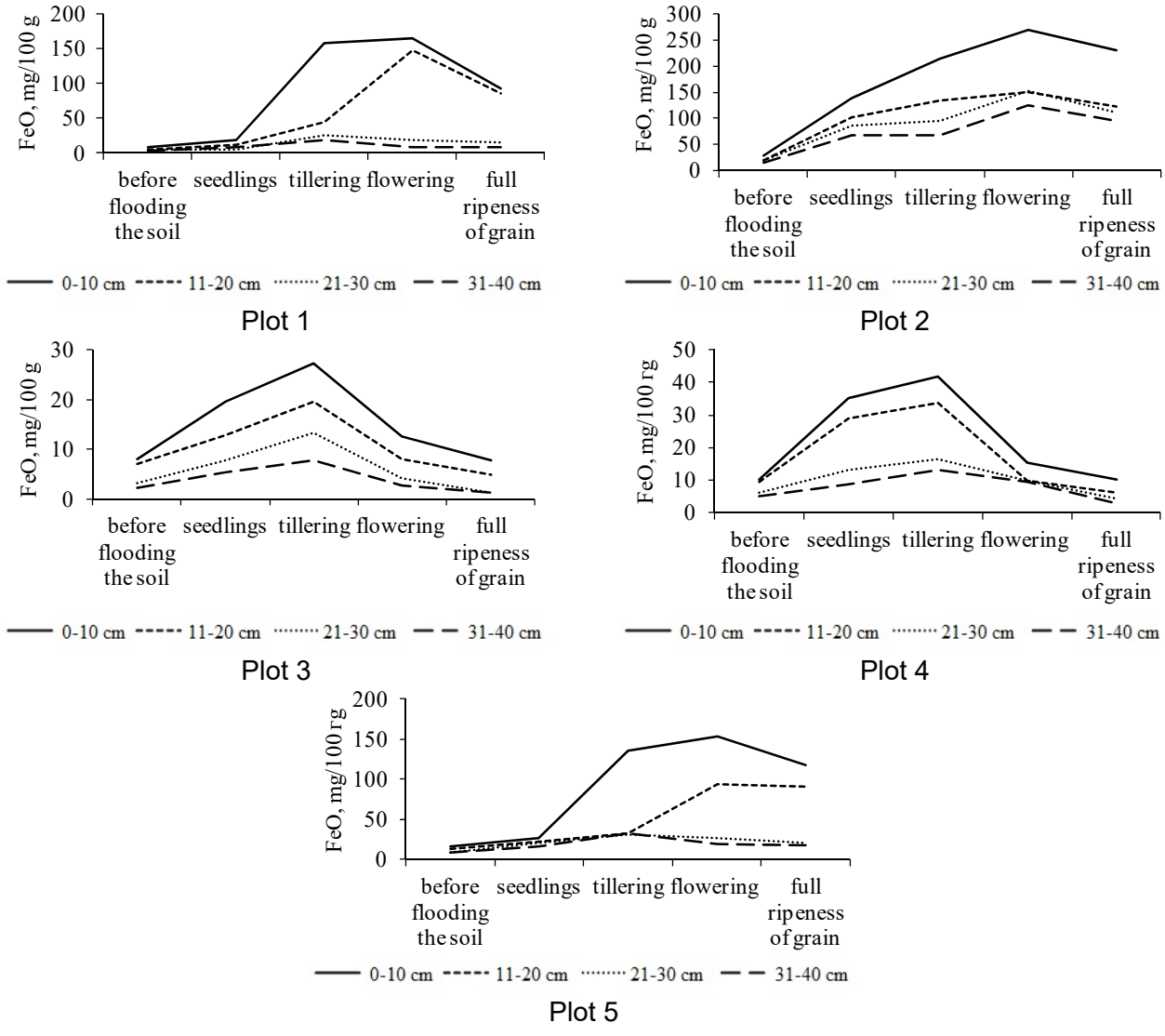

Figure 2. Dynamics of the ferrous iron content in the soils of rice fields

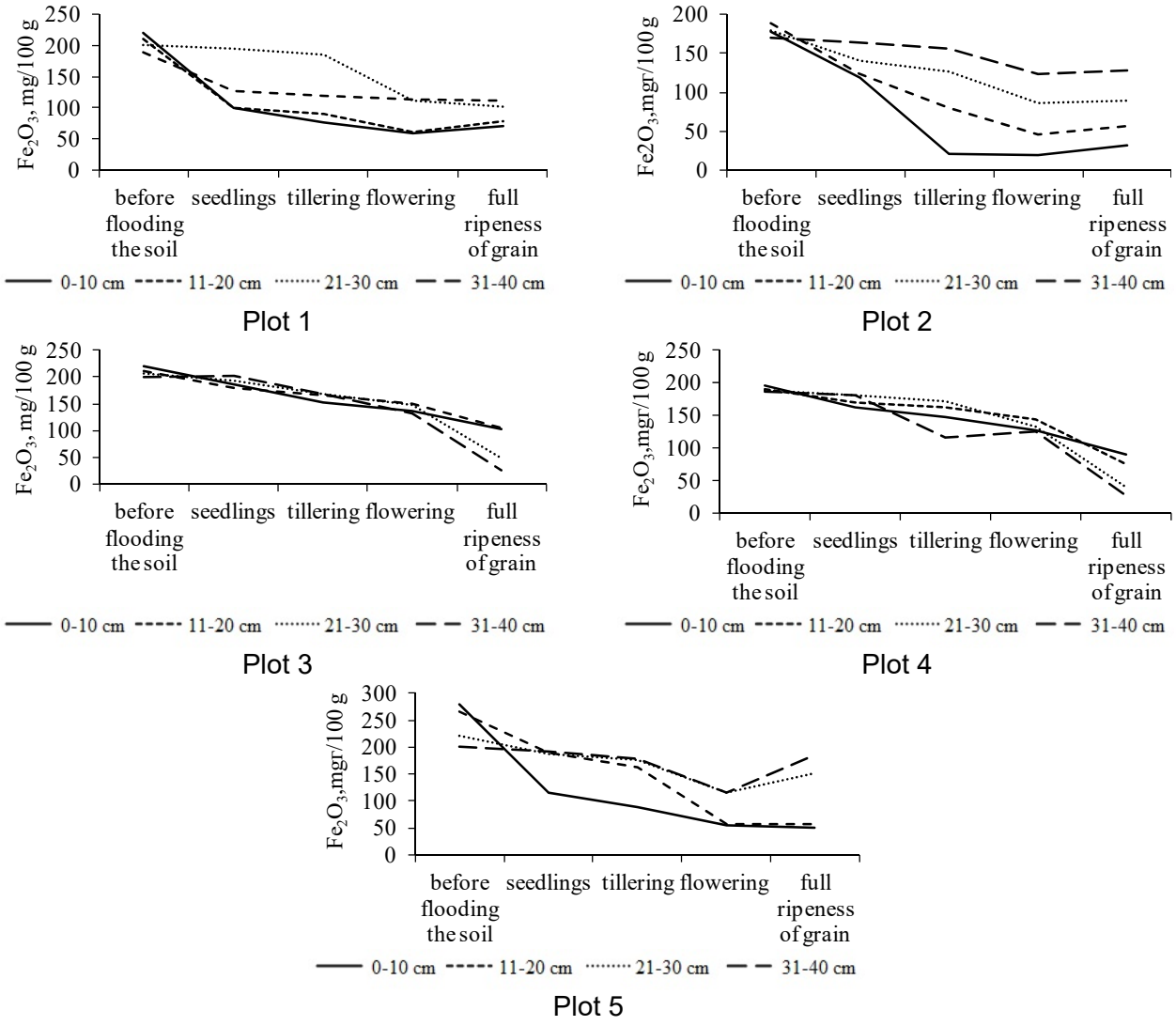

Figure 3. Dynamics of the content of ferric iron in the soils of rice fields

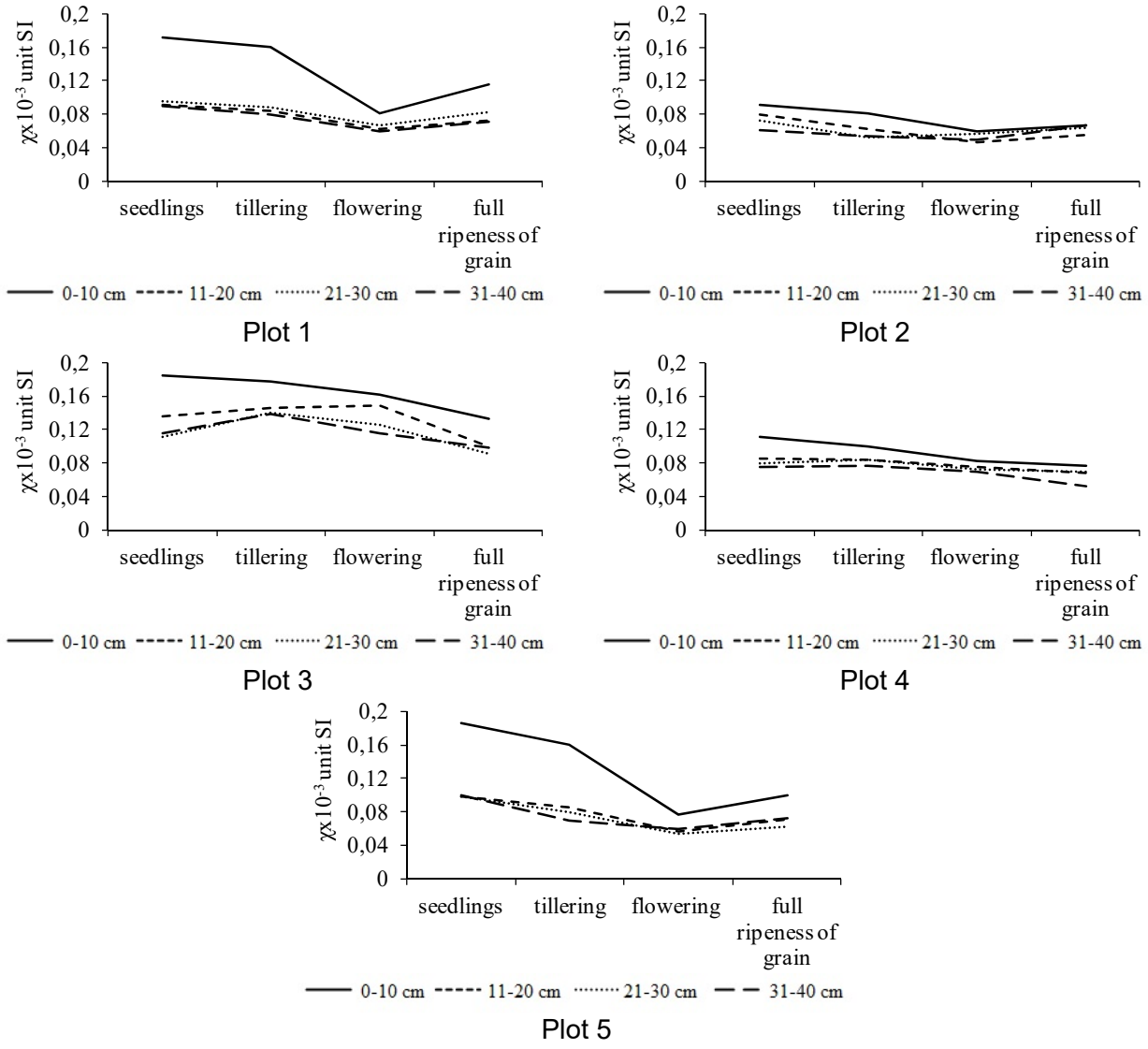

Figure 4. Change in magnetic susceptibility in the rice field soils

PERIÓDICO TCHÊ QUÍMICA
ARTIGO ORIGINAL

DESENVOLVENDO MEIOS DE APRENDIZAGEM DE GRÁFICOS DE FÍSICA NO CONCEITO DE CINEMÁTICA E SUA AVALIAÇÃO USANDO TUG-K (TEST OF UNDERSTANDING GRAPHS IN KINEMATICS)

DEVELOPING PHYSICS GRAPH LEARNING MEDIA IN THE CONCEPT OF KINEMATICS AND ITS ASSESSMENT USING TUG-K (TEST OF UNDERSTANDING GRAPHS IN KINEMATICS)

PENGEMBANGAN MEDIA PEMBELAJARAN GRAFIK FISIKA PADA KONSEP KINEMATIKA DAN PENILAIANNYA MENGGUNAKAN TUG-K (TEST OF UNDERSTANDING GRAPHS IN KINEMATICS)

MUBASIR,Yazid[1*]; SUPRIYADI, Supriyadi[2]; LIA, Roudloh M[3]

[1] Senior High School, SMA N 3 Purworejo, Purworejo, 54173, Indonesia

[2] Physic Major Universitas Negeri Semarang, Gunungpati Semarang, 50229, Indonesia

[3] Educational Research and Evaluation, Graduate School Universitas Negeri Semarang, Kelud Utara Semarang 50237, Indonesia

** Corresponding author*
e-mail: masayid09@gmail.com

Received 13 August 2020; received in revised form 10 February 2021; accepted 21 June 2021

RESUMO

Introdução: Avaliação para determinar a capacidade de dominar gráficos MRU e MRUV, nomeadamente o Teste de Compreensão de Gráficos em Cinemática (TUG-K). Por meio do TUG-K, que é ajustado às competências básicas, os professores podem formular indicadores de desempenho de competências. **Objetivos**: Este estudo teve como objetivo desenvolver meios de aprendizagem de grafos físicos (GraFIS) no conceito de cinemática, descrever a eficácia da aprendizagem após o uso de mídia GraFIS e descrever as percepções dos alunos sobre a aprendizagem usando mídia GraFIS e avaliação usando TUG-K. **Métodos**: Esta pesquisa foi uma pesquisa de PandD. Os aplicativos desenvolvidos utilizam a tecnologia HTML5 que pode ser distribuída em um aplicativo web. O software desenvolvido foi aplicado a 143 respondentes do grau X MIPA da SMA Negeri 3 Purworejo. A coleta de dados foi conduzida com o fornecimento de planilhas de validação a especialistas em materiais, especialistas em mídia e respostas a questionários de alunos, para fornecer informações sobre os produtos desenvolvidos. **Resultados e discussões**: Os resultados da pesquisa foram na forma de aplicação do graFIS como um meio adequado para uso. Os resultados da implementação das atividades de ensino e aprendizagem por meio dos planos de aula elaborados mostraram que a eficácia da aprendizagem com o aplicativo GraFIS ainda se encontrava na categoria baixa com um ganho de pontuação normalizado de 0,03, o que significava que ainda precisava de revisão e aprimoramento. Os resultados da análise das diferenças nas pontuações do pré e pós-teste usando Shapiro-Wilk obtiveram dados que não foram normalmente distribuídos, com Sig. 0,015 <0,05. Portanto, o teste continuou usando o Wilcoxon Signed Rank Test. Foram obtidos os valores de Asymp. Sig. (Bicaudal) <0,05, o que interpretou que houve diferença significativa entre os resultados do pré e pós-teste. **Conclusões**: Conclui-se que melhorias e revisões ainda são necessárias. Com base nas percepções dos alunos, o aplicativo GraFIS atendeu aos padrões de usabilidade e qualidade móvel.

Keywords: *TUG-K*, HTML5, media, *web, móvel.*

ABSTRACT

Background: Assessment to determine the ability to master GLB and GLBB charts, namely the Test of Understanding Graphs in Kinematics (TUG-K). Through TUG-K which is adjusted to basic competencies, teachers can formulate indicators of competency achievement. **Aim** : This study aimed to develop Physics Graph learning media (GraFIS) on the kinematics concept describe the effectiveness of learning after using GraFIS

DOI: 10.52571/PTQ.v18.n38.2021.02_MUBASIR_pgs_15_26.pdf

media and describe students' perceptions of learning using GraFIS media and assessing using TUG-K. **Methods:** This research is an R and D research. The developed applications used HTML5 technology that can be published on the web app. and mobile app. The application was applied to 143 respondents in grade X MIPA of SMA Negeri 3 Purworejo. Data collection was conducted by giving validation sheets to material experts, media experts, students' questionnaire responses, to provide input on the products developed. **Result and Discussion**: The results of the research were in the form of graFIS application as a suitable medium for use. The results of implementation in teaching and learning activities through lesson plans that had been prepared showed that the effectiveness of learning using the GraFIS application was still in the low category with a normalized score gain of 0.03, which meant that it still needed revision and improvement. The analysis results of differences in pretest and posttest scores using Shapiro-Wilk obtained data that were not normally distributed, with Sig. 0.015 <0.05. Therefore, testing continued using the Wilcoxon Signed Rank Test. It was obtained the values of Asymp. Sig. (2-tailed) <0.05, which interpreted that there was a significant difference between the results of the pretest and posttest. **Conclusions:** The conclusion is improvements and revisions are still needed. Based on students' perceptions, the GraFIS application met usability and mobile quality standards.

Keywords: *TUG-K*, HTML5, media, *web, mobile*

ABSTRAK

Latar Belakang : Penilaian untuk mengetahui kemampuan penguasaan grafik GLB dan GLBB yaitu Test of Understanding Graphs in Kinematics (TUG-K). Melalui TUG-K yang disesuaikan dengan kompetensi dasar, guru dapat merumuskan indikator pencapaian kompetensi. **Tujuan** : Penelitian ini bertujuan untuk mengembangkan media pembelajaran Grafik Fisika (graFIS) pada konsep kinematika, mendeskripsikan efektivitas pembelajaran setelah menggunakan media graFIS dan mendeskripsikan persepsi peserta didik terhadap pembelajaran yang menggunakan media graFIS pada konsep pemenuhan standar usability dan mobile quality serta penilaiannya menggunakan Test of Understanding Graphs in Kinematics (TUG-K). **Metode** : Penelitian ini merupakan penelitian R and D dengan desain meliputi: analisis kebutuhan, perencanaan dan pengembangan produk, pengembangan produk, evaluasi produk, produk akhir dan diseminasi presentasi. Aplikasi yang dikembangkan berteknologi HTML5 yang mampu dipublikasikan di web app. dan mobile app. Aplikasi diterapkan pada responden berjumlah 143 peserta didik kelas X MIPA SMA Negeri 3 Purworejo. Pengumpulan data dilakukan dengan pemberian lembar validasi kepada ahli materi, ahli media, angket respon peserta didik, untuk memberi masukan pada produk yang dikembangkan. **Hasil dan Pembahasan** : Hasil penelitian berupa aplikasi graFIS sebagai media yang layak digunakan. Hasil implementasi dalam kegiatan belajar mengajar melalui RPP yang telah disusun, menunjukkan bahwa efektivitas pembelajaran menggunakan aplikasi graFIS masih berada pada kategori rendah dengan gain skor ternormalisasi sebesar 0,03 sehingga masih memerlukan revisi dan perbaikan. Hasil analisis perbedaan skor pretest dan posttest menggunakan Shapiro-Wilk didapat data tidak terdistribusi normal, dengan nilai Sig. 0,015 < 0,05 oleh karena itu pengujian dilanjutkan menggunakan Wilcoxon Signed Rank Test yang diperoleh nilai Asymp. Sig. (2-tailed) < 0,05 , yang menginterpretasikan bahwa terdapat perbedaan bermakna antara hasil pretest dan posttest. **Simpulan** : Kesimpulannya, masih perlu perbaikan dan revisi. Berdasarkan hasil persepsi peserta didik, aplikasi graFIS memenuhi standar usability dan mobile quality

Keywords: *TUG-K*, HTML5, media, *web, mobile*

1. INTRODUCTION

The rational development of the 2013 curriculum emphasizes the strengthening of material through enrichment and elaboration given to students. The material needs to remain relevant to the basic competencies listed in Permendikbud (Minister of Education Regulation) number 24 of 2016. The mastery of basic competencies of students is fulfilled by the teacher through the preparation of the Indicators of Competency Achievement so that the expansion of the material requires the creativity of the teacher to be by following indicators of competency achievement. Then, the indicators are used as a basis in designing assessments that will be billed to students.

PhysPort can be used as a reference to improve the creativity of physics teachers in classroom teaching. The published content is based on research such as teaching methods, assessment, and the results of physics education research. The results of physics education research are believed to have made great progress in developing various tools to enhance students' physics learning. The purpose of PhysPort itself is to synthesize and translate the results of physics education research. Then, it can be used in a class. One menu that can be used by the teacher in Physport is an assessment guide

that contains more than 50 research-based assessment instruments that can be used to find out what learners must learn. One of which is an assessment to determine the ability to master the GLB and GLBB charts, namely TUG-K. Through TUG-K adjusted to basic competencies, teachers can formulate indicators of competency achievement.

One of the basic competencies that must be mastered by students of X grader is kinematic. Kinematics concepts in physics have been modeled graphically (Tebabal and Kahssay, 2011). The students are difficult to present data and graphs on the experimental motion results to investigate the characteristics of straight motion with constant speed (fixed) and straight motion with constant acceleration (fixed) following physical meaning. Alimisis and Boulougaris (2014) have identified serious difficulties that students encounter in drawing and interpreting graphs.

The TUG-K assessment guidance contains questions that can measure the level of graphic mastery to achieve these basic competencies. Limited time to study at school becomes an obstacle to mastering the basic competencies required. The limitedness can be found in a solution by using information technology. The use of information technology in the learning process has become a necessity and a demand in this global era (Muhson, 2010). Advances in technology and information as strength can be a solution to overcome the limited time to study at school through technological devices. Therefore, they can independently learn whenever and wherever they are.

The development of technology is currently very rapid with the presence of multimedia-based mobile technology. It is in harmony with the mindset of the 2013 curriculum, which needs to be developed from single-tool learning into multimedia-based learning. The development of multiplatform learning software is needed to adjust to the currently developed technological devices. The use of mobile applications as a learning media can help students learn independently using their smartphones. The software is also expected to run well using web-based devices through a browser on a computer, with the result that it will accommodate more technological devices owned by students and schools. Learning can be held in a computer laboratory to overcome the device gaps that students have. Collaboration and discussion in learning will be easier to do when students use computer devices.

This GraFIS application was developed to be used as a learning medium in the kinematics graph learning framework. Application development is expected to increase understanding of graphs related to kinematics material because graphs in kinematics play an important role in students' understanding of the basic concepts of physics related to motion. Graphs are abstract representations, so a student's logical thinking level might be an indicator for understanding kinematics graph (Bektasli, 2012). The Understanding Graph Test in Kinematics (TUG-K) that has been developed by Beichner will be used to measure the ability to install it.

The previous research has been carried out by Ayop and Ismail (2019), March and Singh (2016), Antwi, Savelsbergh and Eijkelhof (2018); Klein *et al*. (2019) and Zavala *et al*. (2019), which similarly adopted the TUGK from Beichner to assess students' understanding of kinematics charts. Research by Lichtenberger *et al*. (2017) related Concept Tests Kinematical, validated and addressed by FCI which the TUG-K was also indicated as resources. Eshachs (2010) researched re-examining the power of video motion analysis to promote the reading and creating of kinematic graphs. Eshachs (2014) showed intuitive rules in interpreting students' difficulties in reading and creating kinematic graphs. Then, Ayop and Ismail (2019) took on the material kinematics in the same field, but they focused on the assessment and conceptual difficulties and teaching strategies.

Based on the stated problems, one of the efforts that can be used as an alternative problem solving is through the development of PHYSICS graphics (graFIS) software based on Test of Understanding Graphs in Kinematics (TUG-K), which is designed for mastering basic competencies number 4.4 of X grade in the 2013 Curriculum. GraFIS software is not only a web-based media but can also be run on an Android smartphone.

The purpose of this research was to develop Physics Graph learning media (GraFIS) on the kinematics concept describe the effectiveness of learning after using GraFIS media and describe students' perceptions of learning using GraFIS media and assessing using TUG-K on kinematics material the concept of GLB and GLBB for high school level. In the development process, it would be carried out through the Research and Development (RnD) method of the Borg n Gall model. Therefore, in this study, the title is "Development of Physics Graph Learning Media on Kinematics Concepts Based on Tug-K."

2. MATERIALS AND METHODS:

The main objective of this research is to develop physics graphs (GraFIS) learning media on the kinematics concept by using HTML5-technology software that can be published on various platforms. Content in the software focuses on learning kinematics of graphic material, which the development refers to the assessment of TUG-K. Then, the type of research is Research and Development (RnD). Generally, the systematic of this research is to design, develop and to evaluate, process, and produce products.

The development procedure in HTML5-technology software development research published to various platforms in high school students was carried out in various stages. The development procedure showed in Figure 1 and explanation for every stage described below (Ahmed and Pearson, 2013).

2.1 Requirements Analysis

At this stage, the developer conducted a needs analysis to collect data. It was analyzing basic competency-based on *Permendikbud* No. 24, 2016. The fact shows that many students at high school, or even university level, have less ability to understand and interpret graphs in physics (Planinic, 2012). Students in schools are rarely asked to analyze graphic information and describe it, even though this skill is important at the next level of education (Chaudhury, 2015). Graphs can contain a lot of information and make it possible to predict an event to be resolved (Larkin, 1981). Analysis of material data contained in the revised 2013 curriculum of grade X on the first semester of SMA Negeri 3 Purworejo with essential material to be developed, as well as an assessment of the problems occurred.

2.2 Product Development Planning

At this stage, the developer determined by the research's team about the purpose and the character of the product, looked for sources of content from the product design to be made, arranged the stages of making products/product concepts in the form of storyboards, flowcharts, and developed initial products.

2.3 Product Development

In developing the early product, researchers had some consultations and cooperated with experts, namely material experts and media experts.

In this research and development, the trial design was that before large group trials were carried out, the product was consulted with material experts, media experts and tested on small groups. After getting advice, it was necessary to revise. This research step was expected to find weaknesses, deficiencies, errors, and suggestions for improvement. Therefore, the resulting product was valid and suitable for use.

2.4 Product Evaluation

The evaluation product stage produced a representative measurement tool in obtaining data through the validation carried out by experts. Small-scale field trials on initial products were conducted to obtain responses and product revisions by experts and students.

2.5 Final Products

The developer produced the final product based on the input and results of the initial product revision. After going through expert reviews and trials, the product was refined based on expert and student input to produce a proper and effective product (Ahmed and Pearson, 2013) The product was also implemented in X grade of MIPA to get responses from students about aspects of usability and mobile quality. This responses used instrument qualitative and quantitative)

2.6 Dissemination and Presentation

This stage aimed to disseminate products in the form of physics material applications that can be downloaded for free through the Playstore on a smartphone/gadget or accessed using a specific domain. Product dissemination was carried out through MGMP (Subject Teachers' Deliberation) and social media such as Facebook, Instagram, Twitter, WhatsApp, and others.

The subject of the trial was the target product users, namely students of SMA N 3 Purworejo. Small scale trials were tested on 32 XII grader students of MIPA-1 in SMA N 3 Purworejo, and large scale trials were tested on 143 X grader students of MIPA in SMA N 3 Purworejo.

The data obtained from this research were quantitative data that were converted into qualitative. The data were used to provide an overview of the quality of physics learning media developed, including Metaphor; Interactivity; Learning Content (Parsons and Ryu, 2006), and Learnability; Operability; Understandability (ISO, 2003).

The instrument used to collect data in this study was a questionnaire. There are three questionnaire. The first questionnaire was used as a data collection tool from material expert. The first questionnaire consists of 14 item for material expert. The second questionnaire consists of 19

item for media experts. The blue print of material experts and media experts showed on Table 1. The third questionnaire for students related to criticism, suggestions, and input that was beneficial for the quality of the product. The third questionnaire was adopted from Ahmed and Parsons (2012), which had been applied to measure the usefulness of learning applications named "Think Learn".

Table 1 The blue print of material experts and media experts

No	Statements	Evaluation aspects
S1	This mobile learning experience was enjoyable	Learning content
S2	This mobile application was easy to use	Learnability
S3	Navigation through this application was easy	Operability
S4	This application guides me to formulate a hypothesis	Understandability
S5	The given suggestions in the application were relevant	Methapor
S6	This application helps me understand the relationship between different variables	Interactivity
S7	The given suggestions help me to understand the topic	Methapor
S8	This application helps me to improve my reasoning skills	Interactivity
S9	It is an effective learning application	Learning Content

The collected data were used to analyze the quality of the product development that was produced. Qualitative data about the effectiveness, efficiency, and attractiveness of the product were used to revise the product. The data analysis technique used in this study was the percentage analysis descriptive technique (Widodo, 2014). This percentage analysis technique was used to analyze and evaluate development subjects to assess product quality and acceptability. Descriptive analysis is the accumulation of basic data in the form of descriptions only, meaning that it does not explain relationships, test hypotheses to make predictions, or draw conclusions (Muhson, 2006). It was used the one group pretest-posttest method to measure learning success, illustrated in the following Table 2.

Table 2. Research design

Pretest	Implementation	Posttest
S_{pre}	X	S_{post}

S_{pre} was the result of the pretest. X was the treatment given that was kinematics learning with graphic media, which the development was based on TUG-K. S_{post} was the result of the posttest. The pretest and posttest scores were used to analyze the effects of learning based on the normalized score gain. Analysis of questionnaire data from the application of the media used a *one-sample t-test*.

3. RESULTS AND DISCUSSION

3.1 Results of the Requirement Analysis Phase

Basic competency analysis on *Permendikbud* No. 24, 2016 for high school physics subjects in the first semester of grade X, KD (Basic Competence) 4 discusses graphics. Journal analysis found that many students had less ability to interpret graphs. Analysis at Physport.org on the assessment menu obtained Test of Understanding Graphs in Kinematics (TUG-K) can be used to test the ability to master the GLB and GLBB graphs. Analysis of material understanding of the concepts of GLB and GLBB and mathematical calculations needed to be developed through graphical analysis to obtain the quantity in question. Analysis of the problem found that many students in secondary school, or even university level, could not understand and interpret physics graphs (Planinic, 2012). Students in schools were rarely asked to analyze graphical information and

describe it, although this skill was important at the next level of education (Chaudhury, 2015).

3.2 Results of the Product Planning and Development Phase

Analysis of the design development objectives was to produce applications that had the following capabilities. Those were (1) It can be installed on any Android-based smartphone, and; (2) It can be used as a physics learning media on the subject matter of kinematics GLB and GLBB graphics. In the design stage, the developer designed a learning media product design by referring to the analysis phase and creating story-boards and flowcharts. Producing the beginning design used Jquery Mobile software of 1.4.5 version formed with the name 'graFIS' (Physics Graphs). Images of the software developed showed in Figure 4 and 5.

3.3 Product Development Stage Results

In the testing phase of media expert lecturers and material expert lecturers and trials for students, applications that had been designed at an early stage were given to material experts and media experts. They were published to student respondents to be given an assessment or validation related to aspects of the quality and feasibility of the media.

3.4 Final Product Stage Results

The average results of the pretest and posttest scores of graFIS were presented in Table 3. Results of Analysis of Normality. Test Differences in Pretest and Posttest Scores with the Kolmogorov-Smirnov were presented in Table 4, and statistical test results of pretest and posttest score were presented in Table 5.

Table 3. *Results of analysis of normality*

Z	***-2478b***
Asymp. Sig. (2-tailed)	.013

Table 4. *Test differences in pretest and posttest scores with the Kolmogorov-Smirnov*

	Kolmogorov-Smirnov	***Shapiro walk***
	sig.	sig.
diff	0.005	0.0*15*

Table 5. *Statistical test results of pretest and posttest score*

Pretest	***Posttest***	***Normalized Gain Score***
3.74	4.35	0.03

In gaining student questionnaire responses, the questionnaire was given to students after applying the GraFIS application in learning. The number of students as respondents was 4 classes with a total of 143 respondents. There were 9 statements in the questionnaire, as presented in Table 1.

The usability aspect consisting of three questionnaire statements (S2, S3, and S4) had been found in the GraFIS application, namely linearity, operability, and understandability (ISO, 2003). Student responses from statements S2, S3, and S4 revealed that the application of GraFIS was not difficult to use. The navigation was easy, and students agreed that the application guides it to make hypotheses. One sample t-test against a neutral value of 3 was used to analyze it ($t95 = 16.319$, $p < 0.05$ for P2; $t95 = 12.444$, $p < 0.05$ for P3; $t95 = 15.256$, $p < 0.05$ for P4) . According to students, GraFIS applications included interactive learning media, which were able to link various variables and help their reasoning skills. The results of interactivity aspects were confirmed ($t95 = 12{,}914$, $p < 0.05$ for P6; $t95 = 19{,}213$, $p < 0.05$ for P8). The learning content aspect through statements S1 and S9 revealed that the GraFIS application was effective in learning and provided a pleasant experience ($t95 = 17.115$, $p < 0.05$ for S1; $t95 = 21.425$, $p < 0.05$ for S9). The metaphor aspect meant that students got learning experiences through the whole learning process ($t95 = 15.047$, $p < 0.05$ for S5; $t95 = 15.150$, $p < 0.05$ for S7). Then, the qualitative responses of students were in the form of a discussion group by giving three questions in the discussion to evaluate the application after the students had got their learning experience. The questions given were related to usability and mobile quality.

This model defines usability as a combination of effectiveness, efficiency, satisfaction, learnability, and security, along with a recommended set of related measures (Nayebi *et al*., 2012). The product distribution was expanded through publications on the Google PlayStore with the keyword "grafist". Dissemination was also carried out by providing a Google PlayStore

application link on the WhatsApp of MGMP (Subject Teachers' Group) Physics Meeting at the Provincial level and the District Physics MGMP.

In this research, the development of learning media in the form of an Android-based graFIS application was used to create graphics on GLB material for high school grade X students. The product substance developed was based on the indicators in the TUG-K. The initial product development had been validated by media experts, material experts, and small groups of students. The average overall assessment of the learning media developed at the initial production stage was 80.75%, with a very good category. Thus, this media was appropriate to be used for learning media.

Implementation of learning had been carried out using RPP (Lesson Plan) learning media using the GraFIS application. The learning steps used the Jigsaw learning model so that all indicators can be studied effectively. This model provided opportunities for students to take responsibility for the mastery of the material provided. Students also seemed to cooperate in discussing issues in their respective expert groups. When students returned to their groups, they independently and politely presented the results of the discussion. Other students looked wise to pay attention to it. At the closing activity stage, students were guided by the teacher about making reports using the application. They seemed impressed that the GraFIS application was able to help make reports easily. Digital literacy indirectly grew in students' personalities. This was proofed by the existence of some of them, desiring to have the ability to create applications. Students felt proud when the teacher said that they were the first users of the GraFIS application. Applause echoed in the class as a form of appreciation for their teacher.

The results of applying GraFIS application, which had been tested through pretest and posttest based on Table 2, normalized score gain from learning that implements graFIS was 0.03. Thus, the effectiveness of learning after using GraFIS media on the kinematics concept was still in the low category. This indicated that revisions and improvements were still needed so that the learning effectiveness could increase. The results of the analysis of the differences in the pretest and posttest scores (see Table 3) used Shapiro-Wilk obtained that data were not normally distributed, with Sig. 0.015 <0.05. Therefore, testing continued using the Wilcoxon Signed Rank Test obtained by Asymp values. Sig. (2-tailed) <0.05, which interpreted that there was a significant difference between the results of the pretest and posttest.

Based on the results of the pretest and posttest scores for each TUG-K item shown in Figure 2, it was known that questions no. 2 and 13 with the same type of questions. The results of student acquisition scores tend to be stable, only slightly increased. This was supported by activity-3 and activity-4 in the application to analyze the graph by following the indicators of the problem. Big mistakes were seen in no. 1, 7, 9, 23, and 24. The numbers of students answering correctly were only under 12 of 143 students. This proved that students could not fully understand the 7th and 8th activities in the GraFIS application. A significant increase in scores was on questions no. 6, 11, 12, 19, 21, and 22. Based on these data, it can be concluded that the students quite understood the activities-1, activity-2, activity-9, and activity-10 of the GraFIS application.

4. CONCLUSIONS:

Based on the results of the pretest and posttest scores of each respondent from the TUG-K questions had been shown in Figure 1. Respondents of Class X-MIPA-1 and X-MIPA-3 obtained different pretest and posttest scores that had similar patterns, but class X-MIPA-1 had lower posttest scores than the pretest scores. The pattern looks different for class X-MIPA-2. Although the pretest and posttest results were lower than the other classes, the pattern formed showed the posttest tendency to be higher than the pretest results. For class X MIPA-4 the pattern was seen to have experienced a significant increase in the posttest results and occupied the highest score even though most respondents received a score of 0.

The implementation of GraFIS application in learning encouraged students to actively solve the problems given in their respective activity menus. Students well followed each step of the activity given until a graph showing the rendering results based on the data entered. Students enthusiastically analyzed the displayed graphs. The analysis began by answering the questions given in each activity. Then, it was developed independently by students. As a preliminary report, they carefully copied graphic images into graph paper that had been prepared in advance. The results of the analysis were also written as proof that they understood the graph.

Based on the results and analysis of the TUG-K that had been applied to 143 students, it

could provide information for the teachers to try to improve students' understanding of the topic of the graph in kinematics through better planning in making lesson plans. In this study, we present test results with a low score. Therefore, one of the classroom teaching recommendations was to focus specifically on teaching about graphs of the position toward time, the speed toward time, and the acceleration toward time from a phenomenon of moving objects. Besides, more focus was also needed for teaching about calculating the acceleration of the velocity graph toward time.

This research has produced learning media in the form of GraFIS applications. Its characteristics met usability and mobile quality standards. After using the graFIS application media on the kinematics concept, the results of learning effectiveness were still in the low category. Therefore, improvements and revisions are still needed. However, the results of the pretest and posttest based on statistical analysis showed significant differences.

5. REFERENCES:

1. Ahmed, S., and Parsons, D. (2013). Abductive science inquiry using mobile devices in the classroom. *Computers and Education*, *63*, 62-72.
2. Alimisis, D., and Boulougaris, G. (2014). Robotics in physics education: fostering graphing abilities in kinematics. *In Proceedings of 4th International Workshop Teaching Robotics, Teaching with Robotics and 5th International Conference Robotics in Education*, 2-10.
3. Antwi, V., Savelsbergh, E., and Eijkelhof, H. (2018). Understanding kinematics graphs using MBL tools, simulations, and graph samples in an interactive engagement context in a Ghanaian university. In *Journal of Physics: Conference Series*, 1076 (1),p. 012002). IOP Publishing. https://iopscience.iop.org/article/10.1088/1742-6596/1076/1/012002/meta.
4. Ayop, S. K., and Ismail, A. T. (2019). Students' Understanding in Kinematics: Assessments, Conceptual Difficulties, and Teaching Strategies. *International Journal Of Academic Research In Business And Social Sciences*, 9(2).
5. Beichner, R. J. (1994). Testing student interpretation of kinematics graphs. *American Journal of Physics*, 62(8), 750-762.
6. Bektasli, B., and White, A. L. (2012). The Relationships between Logical Thinking, Gender, and Kinematics Graph Interpretation Skills. *Eurasian Journal of Educational Research*, 48, 1-19.
7. Berryhill, E., Herrington, D., and Oliver, K. (2016). Kinematics card sort activity: Insight into students' thinking. *The Physics Teacher,* 54(9).
8. Chaudhury S., Mandeltort L., Mulnix A., Vandegrift E., Yates J.. (2015). Using Scientific Visualization to Enhance the Teaching and Learning of Core Concepts. In: Baylen D., D'Alba A. (eds*) Essentials of Teaching and Integrating Visual and Media Literac*y. Springer, Cham, pp. 185-202.
9. Collins, M.J., (2017). Pro HTML5 with CSS, JavaScript, and Multimedia: Complete Website Development and Best Practices, Springer Science+Business Media, New York.
10. Eshach, H. (2010, December). Re-examining the power of video motion analysis to promote the reading and creating of kinematic graphs. In Asia-Pacific Forum on Science Learning and Teaching, 11(2).
11. Eshach, H. (2014). The use of intuitive rules in interpreting students' difficulties in reading and creating kinematic graphs. *Canadian Journal of Physics*, 92(1), 1-8.
12. Kementrian Pendidikan dan Kebudayaan, (2017). Direktorat Pembinaan SMA Dirjen Dikdasmen, Model Pengembangan RPP.
13. Klein, P., Lichtenberger, A., Küchemann, S., Becker, S., Kekule, M., Viiri, J., and Kuhn, J. (2019). Visual attention while solving the test of understanding graphs in kinematics: An eye-tracking analysis. *European Journal of Physics*.
14. Larkin, J.H., (1981). Understanding, and Problem Solving in Physics, Research in Science Education: New Questions, *New Directions*, ,115-130.
15. Lichtenberger, A., Wagner, C., Hofer, S. I., Stern, E., and Vaterlaus, A. (2017). Validation and structural analysis of the kinematics concept test. *Physical Review Physics Education Research*, 13(1), 010115
16. Maries, A., and Singh, C. (2014). Performance of Graduate Students at Identifying Introductory Physics Students' Difficulties Related to Kinematics Graphs. *2014 PERC Proceedings.*
17. Muhson, A. (2006). Teknik analisis kuantitatif. *Universitas Negeri Yogyakarta. Yogyakarta*.
18. Muhson, A. (2010). Pengembangan media pembelajaran berbasis teknologi informasi. *Jurnal Pendidikan Akuntansi Indonesia*, 8(2).

19. Nayebi, F., Desharnais, J. M., and Abran, A. (2012, April). The state of the art of mobile application usability evaluation. In 2012 25th *IEEE Canadian Conference on Electrical and Computer Engineering (CCECE)* (pp. 1-4). IEEE.
20. Peraturan Kementerian Pendidikan dan Kebudayaan No 24 Tahun 2016. Kompetensi Inti Dan Kompetensi Dasar Pelajaran Pada Kurikulum 2013 Pada Pendidikan Dasar Dan Pendidikan Menengah, Jakarta : Kemendikbud.
21. Planinic, M., Zeljka Milin-Sipus, Helena Katic, Ana Susac, and Lana Ivanjek. (2012). Comparison Of Student Understanding Of Line Graph Slope In Physics And Mathematics, International *Journal of Science and Mathematics Education*,10, 1393 – 1414.
22. Tebabal, A., and Kahssay, G. (2011). The effects of student-centered approach in improving students' graphical interpretation skills and conceptual understanding of kinematical motion. *Latin-American Journal of Physics Education*, 5(2), 9.
23. Vaara, R. L., and Sasaki, D. G. G. (2019). Teaching kinematic graphs in an undergraduate course using an active methodology mediated by video analysis. LUMAT: *International Journal on Math, Science and Technology Education*, 7(1), 1-26.
24. Vučeljić, M and Šuškačević, M. (2016).Achievements of Montenegrian high-school students in TUG-K test (Test of Understanding Graphs – Kinematics), *AIP Conference Proceedings*, 1722 (1).
25. Zainuddin, H. M. (2015). Implementasi kurikulum 2013 dalam membentuk karakter anak bangsa. UNIVERSUM: *Jurnal KeIslaman dan Kebudayaan*, 9(1).
26. Zavala, G., Tejeda, S., Barniol, P., and Beichner, R. J. (2017). Modifying the test of understanding graphs in kinematics. *Physical Review Physics Education Research,* 13(2).
27. Widodo, D. S. (2014). Influence of leadership and work environment to job satisfaction and impact to employee performance (Study on Industrial manufacture in West Java). *Journal of Economics and Sustainable Development*, *5*(26), 2010-2015.
28. Zorrilla, M., Martin, A., Sanchez, J. R., Tamayo, I., and Olaizola, I. G. (2012, November). HTML5-based system for interoperable 3D digital home applications. In *2012 Fourth International Conference on Digital Home* (pp. 206-214). IEEE.

6. OPEN ACCESS

Figure 1 *Development flow*

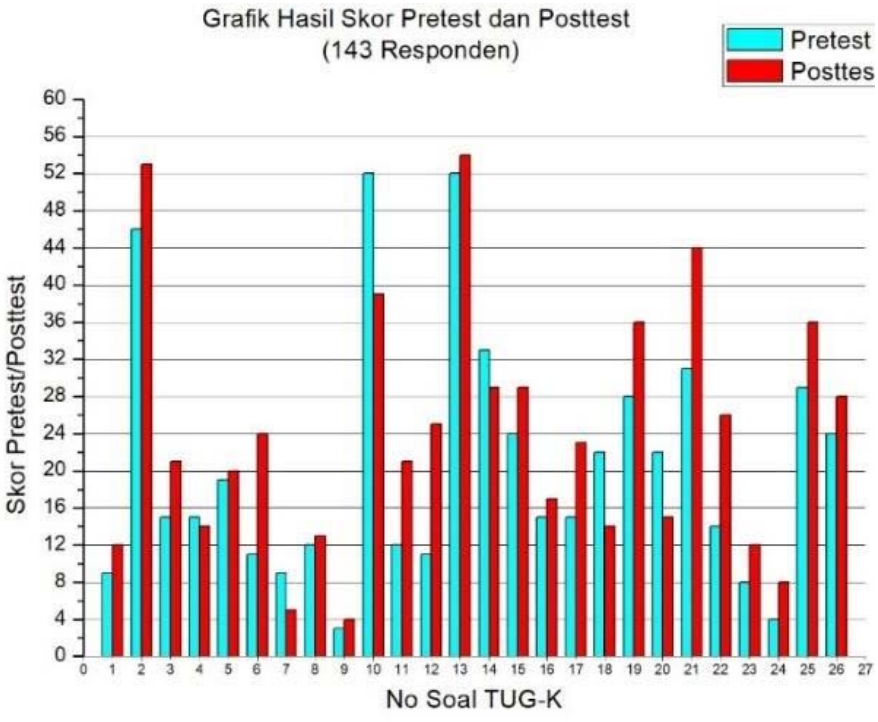

Figure 2. *Pretest score and graph results posttest for each item*

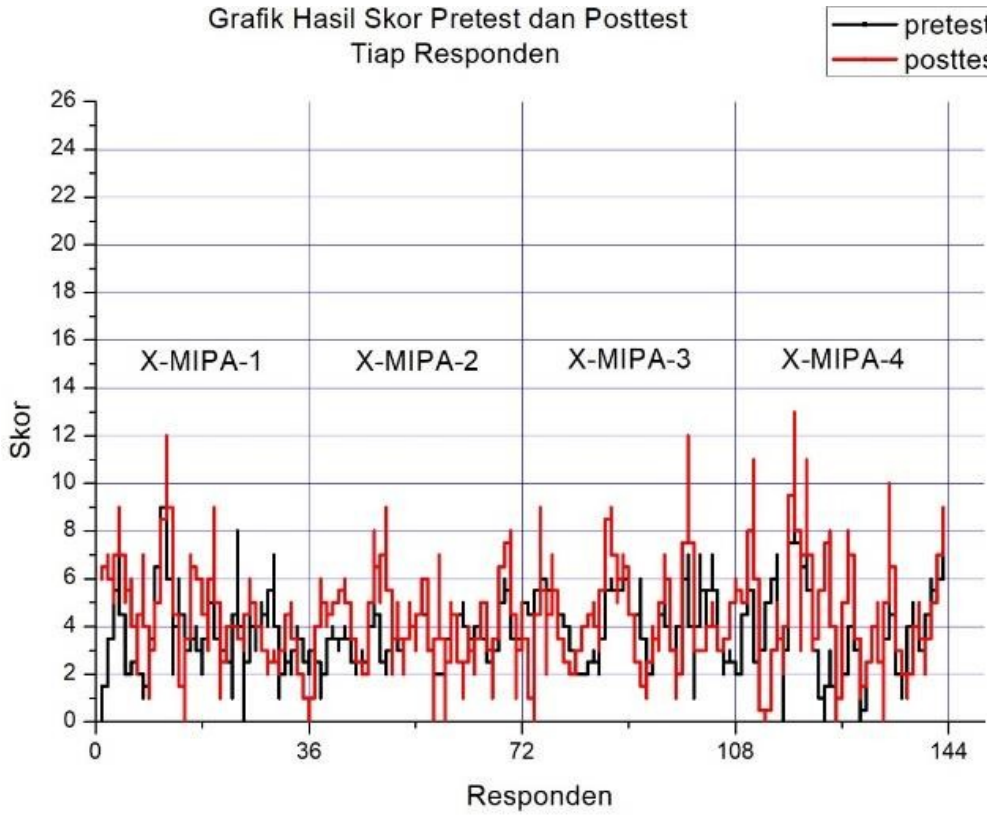

Figure 3. *Graph of pretest and posttest score for each respondent*

Figure 4. *Images the software developed (Initial view)*

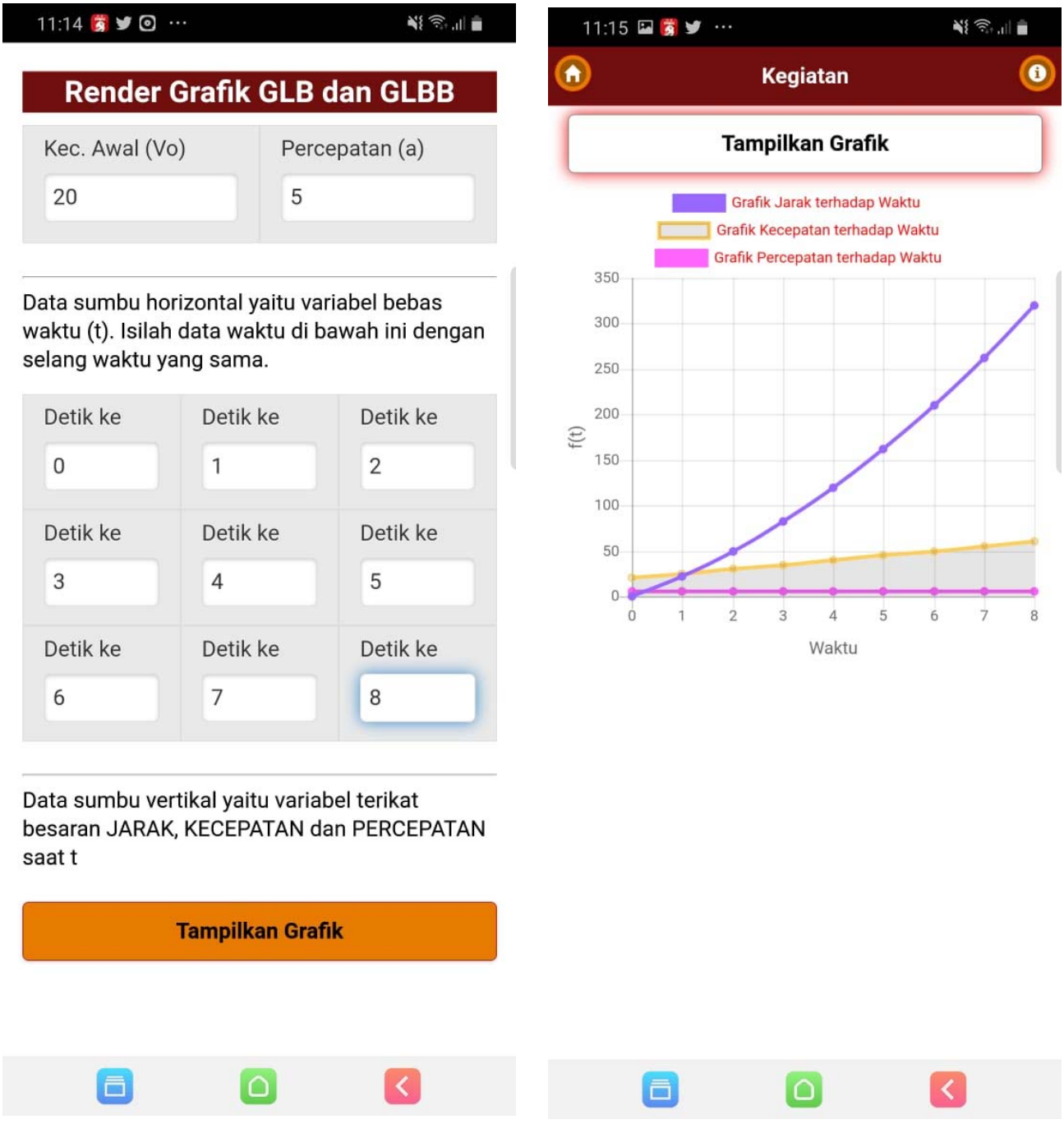

Figure 5. *Images the software developed (graphic view)*

PERIÓDICO TCHÊ QUÍMICA
ARTIGO ORIGINAL

HETEROGENEIDADE CINÉTICA DE PRODUTOS POLIMÉRICOS OBTIDOS NA PRESENÇA DE SISTEMAS CATALÍTICOS MICROHETEROGÊNEOS BASEADOS EM CROMATOGRAMAS DE GEL

KINETIC HETEROGENEITY OF POLYMER PRODUCTS OBTAINED IN THE PRESENCE OF MICROHETEROGENIC CATALYTIC SYSTEMS BASED ON GEL CHROMATOGRAMS

АНАЛИЗ КИНЕТИЧЕСКОЙ НЕОДНОРОДНОСТИ ПОЛИМЕРНЫХ ПРОДУКТОВ, ПОЛУЧАЕМЫХ В ПРИСУТСТВИИ МИКРОГЕТЕРОГЕННЫХ КАТАЛИТИЧЕСКИХ СИСТЕМ, НА ОСНОВЕ ГЕЛЬ-ХРОМАТОГРАММ

MIFTAKHOV, Eldar N.[1*]; MUSTAFINA, Svetlana A.[2]; NASYROV, Ildus Sh.[3]; DAMINOV, Azat Kh.[4];

[1,2,4] Bashkir State University, 32 Zaki Validi Str., zip code 450076, Ufa – Russian Federation.

[3] JSC "Synthesis rubber", 14 st. Technical., zip code 453110, Sterlitamak – Russian Federation

** Corresponding author*
e-mail: promif@mail.ru

Received 17 March 2021; received in revised form 25 May 2021; accepted 22 June 2021

RESUMO

Introdução: o produto polimérico obtido na presença de sistemas catalíticos microheterogêneos é caracterizado por uma distribuição de peso molecular bastante razoável (MWD), resultante de centros ativos cineticamente não equivalentes (ACs) no sistema que inicia o processo de polimerização. A natureza e a composição dos ACs são determinadas definindo e resolvendo um problema inverso na formação de MWD. Este problema é agudo porque revelar a natureza da heterogeneidade cinética explica as mudanças nos parâmetros moleculares e de consumo do produto para diferentes composições de catalisador e modos de propagação em polimerizações**. Objetivo**: o presente estudo teve como objetivo desenvolver métodos e algoritmos de interpretação de cromatogramas em gel para analisar a heterogeneidade cinética de um produto polimérico obtido industrialmente em sistemas catalíticos microheterogêneos**. Métodos:** o método de solução parte do pressuposto de que o MWD formado é uma superposição de distribuições inerentes a cada tipo de ACs. Como o problema na formulação final se refere às equações integrais de Fredholm do primeiro tipo, o método de regularização de A. N. Tikhonov é usado para sua solução numérica, com o problema original sendo preliminarmente discretizado. Esta metodologia e os algoritmos de software desenvolvidos foram usados para determinar a heterogeneidade cinética de sistemas catalíticos contendo titânio e neodímio. **Resultados e discussão**: a análise MWD revelou dois tipos de ACs com um peso molecular médio de A_{Ti} - lnM = 11.3 e B_{Ti} - lnM = 13.2 no catalisador de titânio, e três tipos de A_{Nd} - lnM = 11.1, B_{Nd} - lnM = 12.7 e C_{Nd} - lnM = 14 para o catalisador de neodímio, respectivamente. **Conclusões:** experimentos computacionais repetidos sob diferentes condições de polimerização e requisitos para a preparação de um sistema catalítico permitem revelar uma relação com a heterogeneidade resultante de ACs. Ele nos permite definir e resolver problemas de controle das características moleculares do produto polimérico resultante.

Palavras-chave: *poliisopreno, problema inverso, distribuição de peso molecular, titânio, neodímio.*

ABSTRACT

Background: the polymer product obtained in the presence of microheterogeneous catalytic systems is characterized by fairly molecular weight distribution (MWD), resulted from kinetically nonequivalent active centers (ACs) in the system that initiate the polymerization process. The nature and composition of ACs are determined by setting and solving an inverse problem on the formation of MWD. This problem is acute because revealing the nature of the kinetic heterogeneity explains changes in the molecular and consumer parameters of the product for different catalyst compositions and propagation modes in polymerizations. **Aim:** This study aimed to develop methods and algorithms for interpreting gel chromatograms to analyze the kinetic heterogeneity of a polymer product obtained industrially in microheterogeneous catalytic systems. **Methods**: the solution method is based on the

DOI: 10.52571/PTQ.v18.n38.2021.03_MIFTAKHOV_pgs_27_37.pdf

assumption that the formed MWD is a superposition of distributions inherent in each type of ACs. Since the problem in the final formulation refers to the Fredholm integral equations of the first kind, the regularization method of A. N. Tikhonov is used for its numerical solution, with the original problem being preliminary discretized. This methodology and the developed software algorithms were used to determine the kinetic heterogeneity of titanium- and neodymium-containing catalytic systems. **Results and discussion**: The MWD analysis revealed two types of ACs with an average molecular weight of A_{Ti}-lnM = 11.3 and B_{Ti}-lnM = 13.2 in the titanium catalyst and three types of ACs A_{Nd}-lnM = 11.1, B_{Nd}-lnM = 12.7 and C_{Nd}-lnM = 14 for the neodymium catalyst, respectively. **Conclusions**: repeated computational experiments under different polymerization conditions and requirements for the preparation of a catalytic system make it possible to reveal a relationship with the resulting heterogeneity of ACs. It allows us to set and solve problems of controlling the molecular characteristics of the resulting polymer product.

Keywords: *polyisoprene, inverse problem, molecular weight distribution, titanium, neodymium*.

АННОТАЦИЯ

Предпосылки: полимерный продукт, получаемый в присутствии микрогетерогенных каталитических систем, характеризуется достаточно широком молекулярно-массовым распределением, в основе формирования которого лежит наличие в системе кинетически неэквивалентных активных центров, инициирующих процесс полимеризации. Определение характера и состава активных центров проводится путем постановки и решения обратной задачи формирования молекулярно-массового распределения. Такая задача является актуальной поскольку определение характера кинетической неоднородности позволяет ответить на вопросы изменения молекулярных и потребительских параметров продукта для различного состава каталитического комплекса и режима ведения процесса. **Цель**: разработка методов и алгоритмов интерпретации гель-хроматограмм для анализа кинетической неоднородности полимерного продукта, получаемого промышленным способом в присутствии микрогетерогенных каталитических систем. **Методы**: в основе метода решения лежит предположение о том, что формируемое молекулярно-массовое распределения является суперпозицией распределений, присущих каждому типу активных центров. Поскольку задача в конечной постановке относится к интегральным уравнениям Фредгольма 1 рода, то для ее численного решения используется метод регуляризации А.Н. Тихонова, с предварительной дискретизацией исходной задачи. Данная методология и разработанные алгоритмы были использованы для определения кинетической неоднородности титан- и неодимсодержащих каталитических систем. **Результаты и обсуждение**: описанная методология и разработанные алгоритмы в программном исполнении были применены для определения кинетической неоднородности титансодержащих и неодимсодержащих каталитических систем. Проведенный анализ молекулярно-массового распределения для титанового катализатора выявил наличие двух типов активных центров с характерной средней молекулярной массой A_{Ti} – lnM = 11.3 и B_{Ti} – lnM = 13.2, для неодимового катализатора соответственно трех типов активных центров A_{Nd} – lnM = 11.1, B_{Nd} – lnM = 12.7 и C_{Nd} – lnM = 14. **Выводы**: многократное проведение вычислительных экспериментов при различных условиях полимеризации и правилах приготовления каталитического комплекса позволяет установить взаимосвязь с получаемой неоднородностью активных центров, что позволяет ставить и решать перспективные задачи управления молекулярными характеристики получаемого полимерного продукта.

Ключевые слова: *полиизопрен, обратная задача, молекулярно-массовое распределение, титан, неодим*.

---

1. INTRODUCTION:

Over the past decades, Ziegler-Natt catalysts have been actively used to produce stereoregular polydienes (Monakov *et al.,* 1988; Sabirov *et al.,* 1989; Skuratov *et al.,* 1992; Jie Liu *et al.,* 2018). Industrial production of polydienes is based on d-element (Ti, Co, V) (Uetsuki and Fujiwara, 1976; Wu and Li, 2011) and f-element catalysts (Rakhimov *et al.,* 1997; Ryo Tanaka *et al.,* 2016). The latter composites include the lanthanides. In particular, titanium-based catalytic systems can produce up to 96% of cis-1,4 polyisoprene (Marina *et al.,* 1983). Lanthanide

catalysts allow obtaining dienes with more cis units (up to 98%) (Monakov and Tolstikov, 1990). Modern industrial production is focused on getting a product with specified consumer properties, which is determined by the molecular characteristics of the resulting product. Experimental estimation of molecular parameters is based on gel chromatographic analysis of the resulting product (Belenkii and Vilenchik, 1983) and molecular weight distribution (MWD) (Rudin, 1969).

The estimation of the MWD at the initial stage of modeling allows the study of the kinetic heterogeneity of the resulting product (Usmanov *et al.,* 2004; Monakov *et al.,* 2005). Microheterogeneous Ziegler-Natt catalysts during the polymerization process entail several kinetically nonequivalent active centers (ACs) that produce macromolecules of a certain molecular weight. Subsequent polycentricity broadens the MWD of the product that cannot be described by any of the known model functions corresponding to certain kinetic mechanisms. The broad MWD leads to a deterioration in the molecular and consumer properties of the end polymer product. A successful approach for regulating the number of ACs is to change their dispersed structure by changing the chemical composition of the reaction mixture (Zakharov *et al.,* 2015) and applying hydrodynamic effects in turbulent flows (Zakharov *et al.,* 2013).

To produce a turbulent effect at the stage of the catalyst preparation, a small-sized tubular turbulent device of the diffuser-confusor design is installed that modifies the dispersion of the initial microheterogeneous catalyst components. The induced hydrodynamic effect results in lower catalyst consumption as well as a change in polydispersity nature. The mathematical interpretation of the gel chromatograms reveals the dynamics of the ACs (Bigaeva *et al.,* 2015; Garifullin *et al.,* 2004) that initiate polymerization. Information about the number and proportion of ACs gives a clear picture of polymerization kinetics. It enables to conduct an empirical study and set future-proof objectives to control polymer product formation on an industrial scale. In this regard, an urgent challenge is a methodology for analyzing the obtained MWDs to identify the number and composition of ACs and implement them in the form of programs solved with the known calculation methods and algorithms.

This study aimed to develop methods and algorithms for interpreting gel chromatograms to analyze the kinetic heterogeneity of a polymer product obtained industrially in microheterogeneous catalytic systems.

2. MATERIALS AND METHODS:

The study of the kinetic heterogeneity of polymer products is based on the solution of an inverse MWD problem (Usmanov *et al.,* 2004). The method is based on the assumption that the resulting MWD of the product can be represented as a superposition of distributions formed by each active center separately. The presence of kinetically nonequivalent ACs in the system leads to broadened MWD. The given problem is solved using model functions (Usmanov *et al.,* 2005; Usmanov *et al.,* 2003) typical for a certain kinetic mechanism. In particular, Ziegler-Natta catalysts are characterized by the monomolecular decay of ACs. In this regard, the Flory distribution represents a model function that determines the dynamics of each AC. The superposition of these distributions explains the broad nature of the resultant MWD.

Experimental studies conducted in industrial conditions determined the molecular weight distribution of the end isoprene polymerization product in titanium and neodymium catalytic systems.

In particular, to produce isoprene rubber in a $TiCl_4$TIBA (triisobutylaluminum) catalytic system, a suspension of the titanium catalytic complex was obtained at -10^{0}C by decanting toluene solutions $TiCl_4$(catalyst) with $Al(i-C_4H_9)_3$(co-catalyst), p-electron-donating diphenyloxide (DFO) and electron-donating piperylene. DFO and piperylene increase the chain propagation rate and the AC concentration, respectively. The ratio of the supplied reagents was as follows: $TiCl_4/Al(i-C_4H_9)_3$/piperylene/DFO = 1/1/0.2/0.15 mol. The process was carried out continuously at an initial temperature of -5^{0}C in a cascade of perfectly mixed reactors with a volume of 16.6 m^3 and a length of 2 or 3 reactors, depending on the requirement of the final product conversion. The reagent flowrate was 19 t/h at 15 wt % of an isoprene concentration in isopentane. The consumption of the titanium catalyst was 1 mol per 980 mol of isoprene. The polymerization was terminated, and the polymerizate was washed with demineralized water when the final product conversion reached 70-75%.

Polymer samples were taken at the delivery end of the terminal reactor. They were analysed by Waters-2000 using gel-penetrating chromatography, a method for separating a mixture of substances with different molecular weights by filtering through so-called cellular gels.

Gel filtration was necessary to determine the polymer fractions with a certain molecular weight and build a pattern of the molecular weight distribution. Figure 1 shows the MWD of the final polyisoprene based on the $TiCl_4/Al(i-C_4H_9)_3$piperylene/DFO catalytic system.

Similarly, the molecular characteristics of the isoprene polymerization product in the neodymium catalytic complex was studied. It was produced from a hydrate $NdCl_3 \cdot 0.6H_2O$(hereinafter $NdCl_3$) with isopropyl alcohol in a liquid paraffin medium at 25 ˚ C to get a 9 % suspension weight. The initial molecular ratio of reagents$NdCl_3$ /IPA=1/3. The catalytic complex of the composition$NdCl_3 \cdot nИПС/Al(i-C_4H_9)$ /piperylene = 1/13/2.6 mol was prepared in toluene. Polymerization was carried out in isopentane with isoprene concentrations of 16.6 wt%. The catalyst rate was 1 mol (according to $NdCl_3$) per 24.97 thousand mol of isoprene. The ratio of the supplied reagents was as follows: $NdCl_3/Al(i-C_4H_9)_3$/piperylene = 1/12/2. The process was carried out in a continuous manner in a cascade of perfectly mixed reactors with a volume of 16.6 m3. The reagent flowrate was 19 t/h at 15 wt % of an isoprene concentration in isopentane. The molecular weight was regulated by supplied diisobutylaluminium hydride in the volume of 0.04 kg per 1 ton of monomer. The process was terminated when the conversion rate of the final product reached 72-75%.

A gel chromatographic analysis to build the molecular weight distribution of the final polyisoprene based on the $NdCl_3/Al(i-C_4H_9)_3$/piperylene catalytic system was conducted in the same way.

Based on the fact that every AC is characterized by a certain value of the statistical parameter λ underlying the Flory distribution, the experimental curve of the MWD q_{exp} (M) can be described by Equation 1.

$$q_{exp}(M) = \int_0^{\infty} \varphi(\lambda) K(\lambda, M) d\lambda, \qquad \text{(Eq.1)}$$

where $K(\lambda, M) = \lambda^2 M \exp(-\lambda M)$ is the function that reflects the polymerization mechanism (Flory distribution), $\varphi(\lambda)$ is the distribution function of the ACs.

Since the gel chromatography determines the MWD of the product in coordinates binding q_w with lnM, it is advisable to use new variables $x = lnM$ and $s = ln\lambda$. Equation 1 will take the form of Equation 2.

$$q_{exp}(M) = \int_{-\infty}^{+\infty} \psi(s) e^{2(s+x)-\exp(s+x)} ds. \text{ (Eq.2)}$$

The equation $\exp[2(s+x) - \exp(s+x)]$ under the integral sign is a function $K(\lambda, M)$ in new coordinates (s, x).

Then the inverse MWD problem is reduced to finding a subintegral function $\psi(s)$. Its analysis identifies the patterns in distributing polymerization centres of different types in the catalytic system. The problem of finding a function $\psi(s)$ in the Equation 2 refers to the Fredholm integral equations of the first kind (Polyanin and Manzhirov, 2003), i.e., it is ill-posed. The correct solution to the inverse problem accepts the Tikhonov regularization method (Tikhonov and Arsenin, 1986; Tikhonov *et al.,* 1990), involving a composite function and minimizing the following functional (3):

$$M_\alpha[\varphi] = \int_c^d \left[\int_a^b \varphi(s) K(s,x) ds - q_{exp}(x)\right]^2 dx + \alpha \int_a^b \left[\varphi^2 + \left(\frac{d\varphi}{ds}\right)^2\right] ds \to min, \quad \text{(Eq.3)}$$

where α is the regularization parameter, finding its value is a separate task.

Since it is impossible to find an analytical solution to the problem (Equation 3), the equation will be preliminary discretized. The given function will be approximated (Tikhonov *et al.,* 1983; Verlan and Sizikov, 1986). To do this, there will be added a uniform $[a, b]$ grid $[c, d]$ with points $\{s_j\}: j = 1, \dots, n$ and n on intervals $\{x_i\}: i = 1, \dots, m$ and m points, respectively. Grid step $h_s = (b-a)/(n-1)$ and $h_x = (d-c)/(m-1)$. As a result of discrete transformations and replacement of the integral expression by the trapezoid formula, Equation 3 is reduced to a system of linear algebraic equations:

$$W_\alpha Z = WZ + \alpha CZ = V, \qquad \text{(Eq.4)}$$

where vector $V_j = \sum_{i=1}^m \beta K(s_j, x_i) q_i h_x$, $W_{jk} = \sum_{i=1}^m \beta(k) K(s_k, x_i) \beta(j) K(s_j, x_i) q_i h_x$, $\beta(x) = 0.5$, if $x = 1, n$, otherwise $\beta(x) = 1$. The square matrix C has a dependence on the size of the grid step:

$$C = \begin{bmatrix} 1 + \frac{1}{{h_s}^2} & -\frac{1}{{h_s}^2} & \dots & 0 \\ -\frac{1}{{h_s}^2} & 1 + \frac{2}{{h_s}^2} & \dots & 0 \\ \dots & \dots & \dots & \dots \\ 0 & 0 & \dots & 1 + \frac{1}{{h_s}^2} \end{bmatrix}.$$

The solution of the inverse problem of MWD given in Equation 4 is reduced to finding a vector Z whose values form a discrete function $\psi(s)$. The classical approach to such problems is reduced to the use of numerical methods for solving systems of linear equations. Since the matrix W_α is symmetric, and the dimension depends on the number of partition points of the original segment, it is optimal to use exact solution methods, for

example, the square root method. However, these methods do not always meet the nonnegativity requirement Z of the vector. In this case, it is more convenient to write the original problem (equation 4) in the form of a linear programming problem with nonnegativity requirements of the vector elements V and apply the appropriate numerical methods for solving it (the simplex method, the method of internal points).

In particular, the original problem for the simplex method can be represented as Equation 5:

$$|WZ + \alpha CZ - V| \to min, \qquad \text{(Eq.5)}$$
$$Z \geq 0, \qquad i = \overline{1,n}.$$

The regularization parameter in the numerical solution is of great interest α. Its choice determines the correctness and accuracy in solving the inverse problem of the MWD. The regularization parameter α is selected based on the minimum conditions of the residual Equation 6:

$$\beta(\alpha) = \left\|\varphi(s)K(s,x) - q_{exp}(x)\right\|^2 = \delta^2. \text{ (Eq.6)}$$

To make a correct choice of the value α, the multiple solutions of the problem (4) are carried out in the interval [0;1] with a step not exceeding the value of the permissible accuracy. Then, based on the minimum condition of the functional, the value α and $\varphi(s)$ are fixed. When the described method is solved utilizing a computer, such iteration does not cause difficulties.

3. RESULTS AND DISCUSSION:

3.1. Results

This research uses the described approach to study kinetic heterogeneity on the example of polyisoprene obtained in titanium-based catalytic systems.

Since the developed methodology requires a discrete representation of the MWD, a graph of the polymer product's MWD (Fig.1) with a step of 0.1 included a grid and values that formed a curve $q_{\text{эксп}}(x)$. These values determine the vector components $q_{exp}(x)$ necessary to solve the problem (3) in a discrete form. After fixing 30 points, the inverse MWD problem in the formulation (4) was solved. The Flory distribution was used as the core of the original $K(s,x)$ integral equation 4. To find a vector forming a discrete view Z, an algorithm, and a software $\varphi(s)$ implementation of the internal point method were used (Zorkaltsev and Mokryi, 2018). The solution of the inverse problem and the function $\varphi(s)$ of active center distribution are shown in Figure 2.

Each maximum on the curve $\varphi(s)$ (Figure 2) corresponds to a specific type of polymerization centers that form a polymer fraction with an average molecular weight of lnM. The value of the average molecular weight is determined based on the value corresponding to the next peak of the curve. The conducted MWD analysis proves that the system has at least two types of ACs: A_{Ti}-lnM = 11.3 and B_{Ti}-lnM = 13.2. Besides, the curve determines the position of the maxima, i.e., the average molecular weight formed on this type of ACs. However, detailed characteristics of the AC behavior can be obtained by evaluating the contribution of each centre to the overall polymerization process. To do this, the function $\varphi(s)$ was divided into elementary functions of the Gauss distribution according to the Equation 7

$$\varphi(s) = \sum_{k=1}^{n} p_k \frac{1}{\sigma_k\sqrt{2\pi}} \exp\left(-\frac{(s_i - s_k)^2}{2\sigma_k^2}\right), \text{ (Eq.7)}$$

where n is the number of ACs in the system, s_k is the position of the maxima, σ_k is the width of the Gauss distribution, p_k is the proportion of each AC in the catalytic system, and $p_1 + p_2 + \cdots p_k = 1$. Since the figure depicts the presence of two types of active centers, then n=2.

In the studied case, the maxima in Figure 2 overlap each other. The effect of each type of active centre can be evaluated roughly. Since the original problem was presented in a discrete form, there was another problem created to find parameters $p_1, p_2, \sigma_1, \sigma_2$ corresponding to the first and second types of the active centre:

$$\sum_{i=1}^{m}\left[\varphi(s_i) - p_1 \frac{1}{\sigma_1\sqrt{2\pi}} \exp\left(-\frac{(s_i - s_1)^2}{2\sigma_1^2}\right) - p_2 \frac{1}{\sigma_2\sqrt{2\pi}} \exp\left(-\frac{(s_i - s_2)^2}{2\sigma_2^2}\right)\right] \to min, \qquad \text{(Eq.8)}$$

where m is the number of segment division points. The algorithm for problem-solving in a statement (8) is reduced to selecting a value for system parameters $p_1, p_2, \sigma_1, \sigma_2$ when at each step of the initial discrete partition the deviation of the sum of Gaussian distributions from the complex function $\varphi(s)$ will be minimal

The optimization problem (8) for parameter identification $p_1, p_2, \sigma_1, \sigma_2$ was solved by the configuration method (Hooke-Jeeves) (Panteleev and Letova, 2015). Since $p_1 + p_2 = 1$, the value p_2 is used instead $1 - p_1$ in the expression (8). Then problem (8) is the problem of finding three parameters of the system. As the initial condition of the problem (5), the parameters $\sigma_1 = 0.5$, $\sigma_2 = 0.5$, $p_1 = 0.1$, $p_1 = 0.9$ are used. The initial conditions for p_1, p_2 were proposed based on the quadrature error estimate of the curve in Figure 2. In particular, the authors used the trapezoid

method.

The minimization problem (8) solution provided the values $\sigma_1 = 0.44,\ \sigma_2 = 0.65,\ p_1 = 0.15,\ p_2 = 0.85$. Then the proportion of A_{Ti} centres is 0.15, the proportion of B_{Ti} centres is 0.85. To find the deviation of the resulting calculated curve, which is the sum of the Gaussian distributions from the original curve $\varphi(s)$, an absolute difference was recorded at each point of the discrete partition. Figure 3 displays a graphical representation of the resulting distributions. The mean-square deviation of the Gauss distribution from the calculated curve $\varphi(s)$ reached 5.4%.

In practice, the number of AC types usually reaches four. The small number of AC types in the very study is explained by the multi-component chemical composition of the reaction mixture (Zakharov *et al.,* 2015) and the hydrodynamic effect in turbulent flows (Nasyrov *et al.,* 2016).

To get isoprene on the catalytic system $NdCl_3/Al(i-C_4H_9)_3$/piperylene, the inverse MWD problem is solved. To solve the inverse problem and determine the number and composition of ACs, the same methodology was used in the titanium catalyst. As a method of solving the problem in the form (4), internal points were used. The number of partition points to represent the original problem in discrete form was set to 30. The solution of the problem for the function $\varphi(s)$ is shown in Figure 4.

The result of the inverse MWD problem solution gives grounds for stipulating that there are three AC types in the system A_{Nd}-lnM = 11.1, B_{Nd}-lnM = 12.7, and C_{Nd}-lnM = 14. To find additional parameters of the system, the AC distribution function was expanded in Gauss distributions by minimizing the functional of the following form (Equation 9):

$$\sum_{i=1}^{m}\left[\varphi(s_i) - \sum_{j=1}^{3} p_j \frac{1}{\sigma_j\sqrt{2\pi}} e^{-\frac{(s_i - s_j)^2}{2\sigma_j^2}}\right] \rightarrow min. \quad \text{(Eq.9)}$$

Since the number of types of ACs has increased to 3, the task of identifying the system parameters is reduced to identifying 6 parameters, the initial approximation of the parameters p_1, p_2 and p_3 is of great importance. They were found by estimating the areas under each peak using the trapezoid method

The minimization problem solution provided the values $\sigma_1 = 0.15,\ \sigma_2 = 0.26,\ \sigma_3 = 0.26,\ p_1 = 0.12,\ p_2 = 0.48,\ p_2 = 0.4$. Thus, the proportion of A_{Nd} centers is 0.12, the proportion of B_{Nd} centers equals 0.48, and the share of C_{Nd} centers is 0.4.

3.2. Discussion

The research results of titanium catalyst heterogeneity depict two AC types: A_{Ti}-lnM = 11.3 and B_{Ti}-lnM = 13.2. The proportion of active centers forming fractions with the lowest molecular weight is small and does not exceed 15%. An additional impact on the catalytic complex can lead to a further reduction in the proportion of A_{Ti}-type centers and make the system monocentric (Zakharov *et al.,* 2013).

Studies of a neodymium catalyst system show that there are at least three types of active centers: A_{Nd}-lnM = 11.1, B_{Nd}-lnM = 12.7, and C_{Nd}-lnM = 14. The proportion of active centers with a typical low molecular weight does not exceed 12%, with the B_{Nd} and C_{Nd} AC types being very close in molecular weight.

4. CONCLUSIONS:

The solution of the inverse MWD problems provides a clear picture of the AC dynamics that initiate the polymerization process. The developed methods and algorithms based on the regularizing operator of A.N. Tikhonov have been successfully applied to analyze the nature of polycentricity of titanium-and neodymium-based catalytic systems. As a result, industrial polymer samples are characterized in terms of their nature and the AC composition.

Repeated computational experiments under different polymerization conditions and catalytic complex preparation reveal a relationship with the resulting heterogeneity of the active centers. In the future, it can be used to control the polymerization process with modeling tools.

The MWD width is often estimated using the polydispersity value, expressed as the ratio of the average mass and the average calculated molecular mass. However, polymer products have the same width but a completely different number and the ratio of ACs. Accurate data on the nature and composition of the ACs lays the basis for modeling the polymerization kinetics and answering the questions on developing polymer product's consumer and molecular properties during empirical studies.

In addition, the control of the kinetic polymerization product heterogeneity remains an urgent target of industrial production in the search for better catalyst system modification and preparation modes. This explains the need for continuous gel chromatographic analysis of the product at different stages of its preparation and analysis of the MWD being built up.

5. ACKNOWLEDGMENTS:

The study was carried out within the framework of the state assignment of the Ministry of Science and Higher Education of the Russian Federation (scientific topic code FZWU-2020-0027).

6. REFERENCES:

1. Belenkii, B. G. and Vilenchik, L. Z. (1983). Chapter 3 Interpretation of data on the analysis of polymers by gel chromatography. *Journal of Chromatography Library, 25*, 117-148.

   DOI: 10.1016/S0301-4770(08)61038-6.

2. Bigaeva, L. A., Latypov, I. I., Usmanov, S. M., Nabiullin, A. R., Shiyan, D. A., and Ulitin, N. V. (2015). On the problem of solving an inverse ill-posed problem in the chemical technology of polymers: interpretation gel chromatograms. *Bulletin of Kazan Technological University*, *18*(3), 86-92.

3. Garifullin, R. N., Spivak, S. I., Garifullina, R. N., Sigaeva, N. N., and Monakov, Yu. B. (2004). Algorithm for calculating the kinetic inhomogeneity of active centers of ion-coordination catalytic systems. *Bulletin of the Bashkir University, 9*(4), 7–12.

4. Jie Liu, Xiaodong, Fan, Xin Min, Xiuzhong Zhu, Na Zhao, and Zichao Wang. (2018). Synthesis of high cis-1,4 polybutadiene with narrow molecular weight distribution via a neodymiumbased binary catalyst. *RSC Adv., 8*, 21926–21932.

   doi: 10.1039/C8RA02656D.

5. Marina, N. G., Monakov, Yu. B., Rafikov, S. R. and Ponomarenko, V. I. (1983). Relationship between the nature of the components of titanium-containing Ziegler systems with their activity and stereospecificity in the polymerization of dienes. *Uspekhi khimii, 52*, 733-753.

6. Miftakhov, E. N., Nasyrov, I. Sh., Mustafina, S. A., Zakharov, V. P. (2021). Study of kinetics of isoprene polymerization in the presence of neodymium-containing catalytic systems modified in turbulent flows. *Russian Journal of Applied Chemistry*, *94*(1), 77–83.

   doi: 10.1134/S1070427221010110.

7. Monakov, Yu. B., Marina, N. G. and Tolstikov, G. A. (1988). On the formation and structure of active centers of lanthanide coordination catalysts for cis-polymerization of dienes. *Chemie Stosowana, 32*(3-4), 547-558.

8. Monakov, Yu. B., Sigaeva, N. N. and Urazbaev, V. N. (2005). *Active sites of polymerization. Multiplicity: stereospecific and kinetic heterogeneity.* Leiden: Brill Academic Publishers.

9. Monakov, Yu. B. and Tolstikov, A. G. (1990). *Catalytic polymerization of 1,3 dienes.* Moscow, Russian Federation: Nauka.

10. Morozov, Yu. V., Nasyrov, I. Sh., Zakharov, V. P., Mingaleev, V. Z., Monakov, Yu. B. (2011). Enhancement of the Activity of the Titanium Catalyst for Isoprene Polymerization by Improving the Step of Active Site Formation. *Russian Journal of Applied Chemistry, 84*(8), 1434-1437.

    doi: 10.1134/S1070427211080258.

11. Nasyrov, I. Sh. Zhavoronkov, D. A., Faizova, V. Yu., Zakharov, V. P. and Zakharova, E. M. (2016). Evaluation of the efficiency of using a tubular turbulent apparatus in the step of titanium catalyst preparation in isoprene rubber production. *Russian Journal of Applied Chemistry, 89*(6), 960-964.

12. Panteleev, A. V. and Letova, T. A. (2015). *Optimization methods in examples and problems: a tutorial*. St. Petersburg, Russian Federation: Lan.

13. Polyanin A.D. and Manzhirov A.V. (2003). *Integral Equations Handbook*. Moscow, Russian Federation: Fizmatlit.

14. Rakhimov, R. Kh., Kutuzov, P. I., Bazhenov, Yu. P. and Nasyrov, I. Sh. (1997). Properties and applications of cis-1,4-polyisoprene, obtained industrially using a lanthanide catalytic complex. *Bashkir Chemical Journal*, *4*(2), 14-17.

15. Rudin, A. Molecular weight distributions of polymers. (1969). *J. Chem. Educ.*, *46*(9), 595.

    doi: 10.1021/ed046p595.

16. Ryo Tanaka, Kaede Yuuya, Hiroki Sato, Peter Eberhardt, Yuushou Nakayamaa and Takeshi Shiono. (2016). Synthesis of

stereodiblock polyisoprene consisting of cis-1,4 and trans-1,4 sequences by using a neodymium catalyst: change of the stereospecificity triggered by an aluminum compound. *Polym. Chem., 7*, 1239-1243.

DOI: 10.1039/C5PY01872B.

17. Sabirov, Z. M., Minchenkova, N. K. and Monakov Yu. B. (1989). Diene polymerizations with lanthanide coordination catalysts. Kinetic stereocontrol of polybutadiene microstructure. *Inorganica Chimica Acta*, *160*, 99-101.

    doi: 10.1016/S0020-1693(00)85407-9.

18. Skuratov, K. D., Lobach, M. I., Shibaeva, A. N., Churlyaeva, L. A., Erokhina, T. V., Osetrova, L. V., Kormer, V. A. (1992). Structure of initial and ultimate chain units of polydienes obtained with rare-earth catalysts as revealed by 2H nuclear magnetic resonance spectroscopy. *Polymer*, *33*(24), 5202-5207.

    DOI: 10.1016/0032-3861(92)90802-4.

19. Tikhonov, A. N. and Arsenin V. Ya. (1986). *Methods for solving ill-posed problems*. Moscow, Russian Federation: Nauka.

20. Tikhonov, A. N., Goncharskiy, A. V., Stepanov, V. V., Yagola, A. G. (1983). *Regularizing algorithms and a priori information*. Moscow, Russian Federation: Nauka.

21. Tikhonov, A.N., Goncharsky, A.V., Stepanov, V.V. and Yagola, A.G. (1990). *Numerical methods for solving ill-posed problems.* Moscow, Russian Federation: Nauka.

22. Uetsuki, M. and Fujiwara, Y. (1976). Structure of Ziegler-Natta Catalysts for the Polymerization of Isoprene. *Bulletin of the Chemical Society of Japan, 49*(12), 3530-3539.

    doi: 10.1246/bcsj.49.3530.

23. Usmanov, A. S., Gaisin, F. R., Spivak, S. I. (2003). Molecular weight distribution and model functions in polymers. *Bulletin of BirSPI. 1*, 48-54.

24. Usmanov, A. S., Ismailov, R. P., Usmanov, T. S., Spivak, S. I. and Usmanov, S. M. (2005). Model functions in the ill-posed problem of the formation of molecular weight distributions. *Bashkir Chemical Journal*, *12*(2), 67-74.

25. Usmanov, T. S., Saitova, F. F., Ionova, I. A., Glukhov, E. A., Gareev, A. R., Monakov, Yu. B., Bazhenov, Yu. P., Nasyrov, I. Sh. (2004). Modification of ticl4-based catalytic systems by electron donors: effect on kinetic parameters of polymerization, molecular characteristics of polyisoprene, and kinetic nonuniformity of catalysts. *Polymer Science. Series B*, *46*(1), 1-5.

26. Usmanov, T.S., Spivak, S.I. and Usmanov, S.M. (2004). *Inverse problems of the formation of molecular weight distributions*. Moscow, Russian Federation: Chemistry.

27. Verlan, A. F., Sizikov, V. S. (1986). *Integral equations: methods, algorithms, programs*. Reference manual. Kiev, Ukraine: Naukova Dumka.

28. Wu, J. Q., and Li, Y. S. (2011). Well-defined vanadium complexes as the catalysts for olefin polymerization. *Coord. Chem*. *Rev*. *255*, 2303–2314.

    doi: 10.1016/j.ccr.2011.01.048.

29. Zakharov, V. P., Mingaleev, V. Z., Berlin, A. A., Nasyrov, I. Sh., Zhavoronkov, D. A., Zakharova, E. M. (2015). Kinetic heterogeneity of titanium and neodymium catalysts for the production of 1,4-cis-polyisoprene. *Chemical Physics, 34*(3), 69-75.

    doi: 10.7868/S0207401X15030139.

30. Zakharov, V. P., Mingaleev, V. Z., Zakharova, E. M. *et al.* (2013) Improvement of the neodymium catalyst preparation step in isoprene rubber production. *Russ. J. Appl. Chem., 86***,** 909–913.

    doi: 10.1134/S1070427213060219

31. Zakharov, V. P., Sadykov, I. V., Minsker, K. S., Berlin, A. A., Monakov, Yu. B. (2004). Molecular characteristics of cis-1,4-polyisoprene during the formation of the catalytic system TiCl4-Al(i-C4H9)3 in turbulent mode. *Vysokomolekulyarnye soedineniya*, *46*(10), 1765-1769.

32. Zakharov, V. P., Zakharova, E. M. and Mingaleev, V. Z. (2013). Influence of the dispersed composition of the titanium catalyst on the kinetic heterogeneity of the centers of isoprene polymerization. *Vysokomolekulyarnye soedineniya, 55*(9), 1201-1212.

33. Zhavoronkov, D. A., Morozov, Yu. V., Nasyrov, I. Sh., Petrunina, A. V., Faizova, V. Yu., Khairullin, I. I. Method of obtaining alcohol solvate of neodymium chloride: Patent 2468995 Russian Federation. 2011123051/05, declared 07.06.2011, published 10.12.2012, 34.

34. Zorkaltsev, V. I. and Mokryi, I. V. (2018). Interior point algorithms in linear optimization. *Siberian math. zhurn. industrial mat*., *21*(1), 11–20.

doi: 10.17377/sibjim.2018.21.102.

7. OPEN ACCESS:

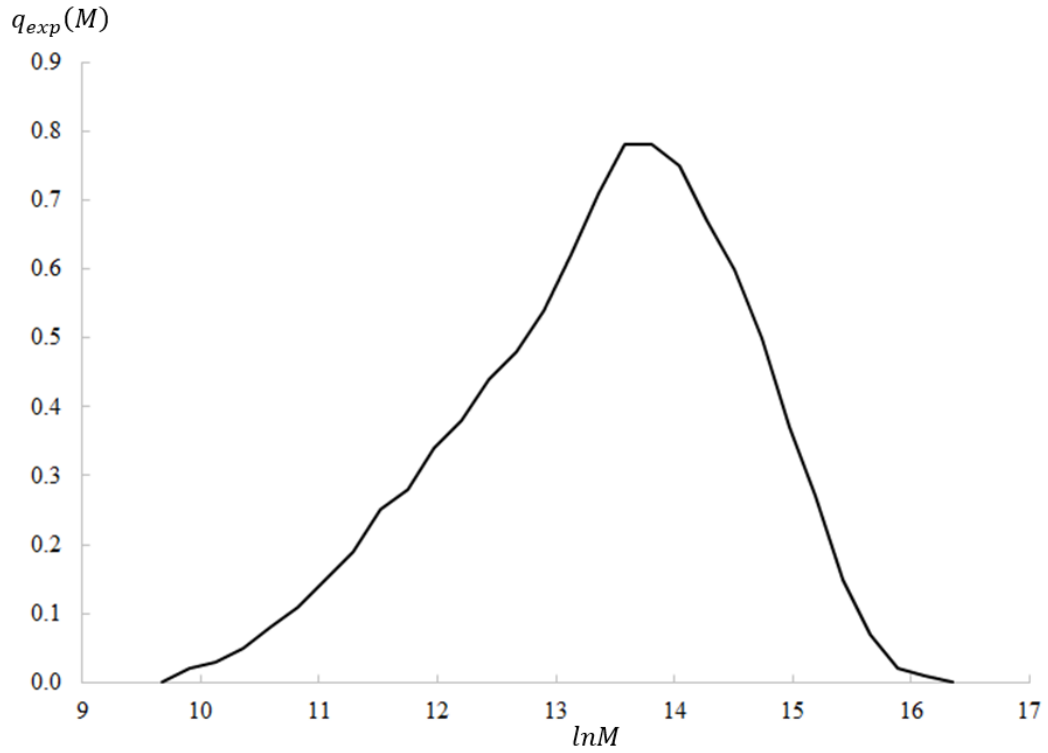

Figure 1. *The MWD of the isoprene polymerization product on the catalytic system* $TiCl_4/Al(i-C_4H_9)_3$ */piperylene/DFO. Source: the author*

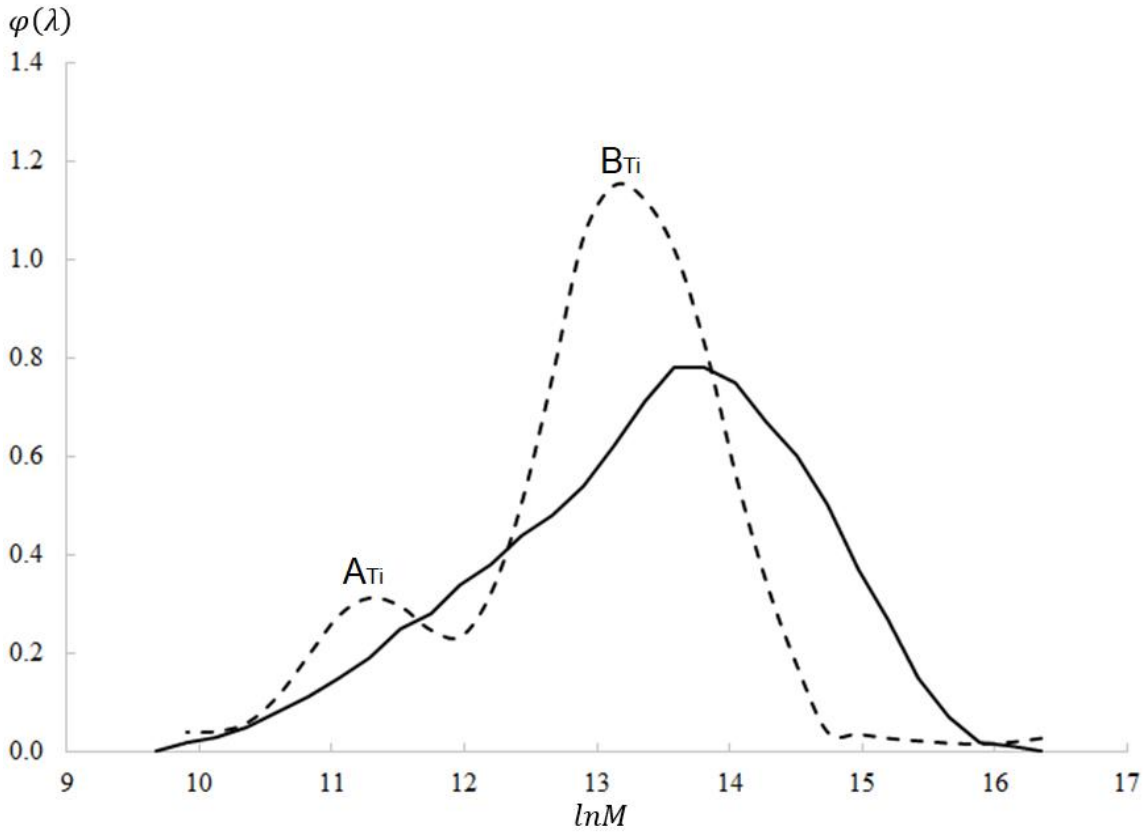

Figure 2*. The solution results of the inverse MWD problem for isoprene on a catalytic system*$TiCl_4/Al(i-C_4H_9)_3$*/piperylene/DFO (a continuous line presents the initial distribution of the product, a dotted line shows the AC distribution). Source: the author*

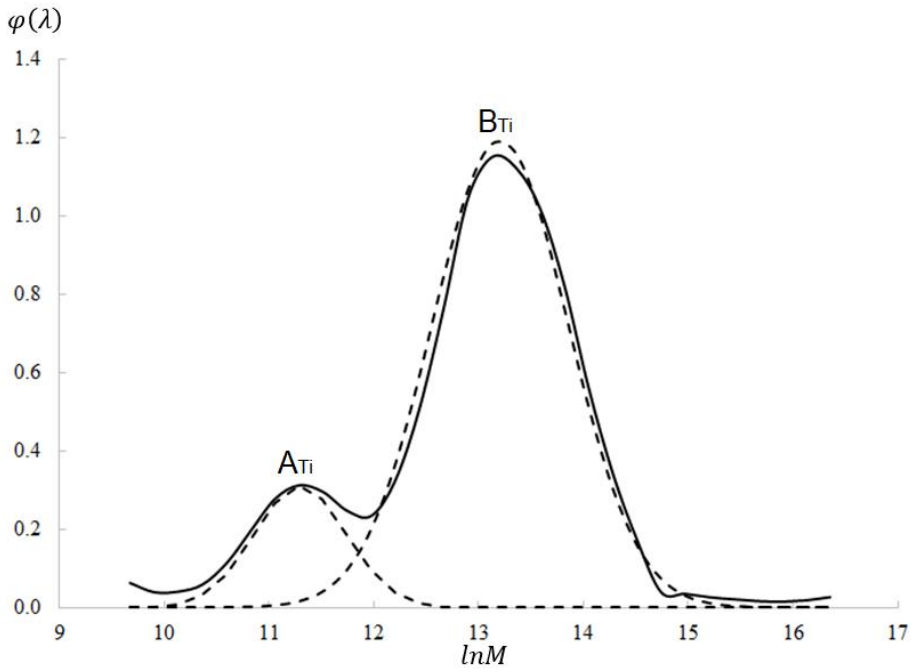

***Figure 3**. Expansion of the AC distribution function into the Gauss distribution (a continuous line is a calculated function $\varphi(s)$, a dotted line stands for the Gauss distribution for each AC). Source: the author*

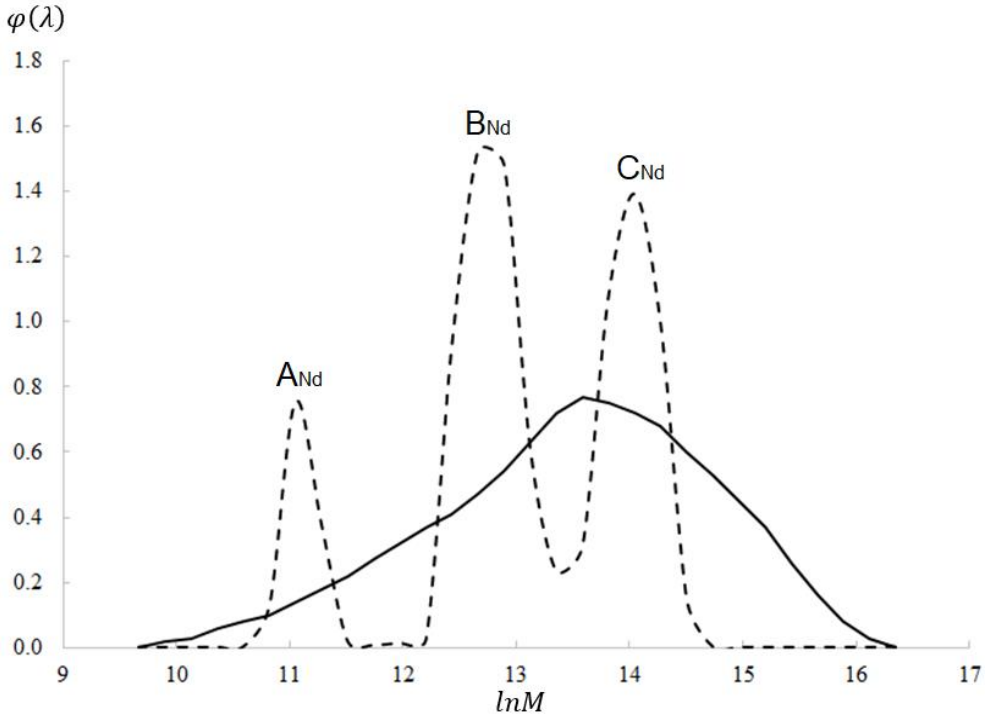

***Figure 4**. The results of the inverse isoprene MWD problem solution for a catalytic system $NdCl_3/Al(i-C_4H_9)_3$/piperylene (a continuous line presents the initial distribution of the product, a dotted line shows the AC distribution). Source: the author*

PERIÓDICO TCHÊ QUÍMICA
ARTIGO ORIGINAL

VARIAÇÃO SAZONAL DE FENÓIS E FLAVONOIDES EM FOLHAS NÃO-GALHADAS E GALHADAS DE *CARYOCAR BRASILIENSE* (CARYOCARACEAE)

SEASONAL VARIATION OF PHENOLS AND FLAVONOIDS IN NON-GALLED AND GALLED LEAVES OF *CARYOCAR BRASILIENSE* (CARYOCARACEAE)

TEIXEIRA, Edson Cardoso[1]; FERREIRA, Rafaela Oliveira[2*]

[1] Universidade Federal do Tocantins, Programa de Pós-Graduação em Química, Brasil

[2] Universidade Federal do Recôncavo da Bahia, Centro de Ciências Exatas e Tecnológicas, Brasil

** Autor correspondente*
e-mail: rafaelaoliveira@ufrb.edu.br

Received 12 April 2021; received in revised form 13 May 2021; accepted 21 June 2021

RESUMO

Introdução: Os insetos galhadores manipulam o desenvolvimento de suas plantas hospedeiras. Galhas são ricas em metabólitos secundários, como compostos fenólicos e terpenos. *Caryocar brasiliense* atua como hospedeira de insetos galhadores. Poucos estudos relatam os impactos desta interação planta-inseto na morfologia, fisiologia e metabolismo secundário da espécie. **Objetivo:** A finalidade deste estudo foi verificar se existe correlação entre os teores de fenóis totais e flavonoides de extratos de folhas de *C. brasiliense* e variáveis ambientais, como temperatura e precipitação, ao longo do ano, e avaliar como os insetos galhadores podem interferir nessa sazonalidade. **Métodos:** Os extratos em etanol de folhas foram obtidos por extração em soxhlet. As principais classes de metabólitos secundários foram detectadas por prospecção fitoquímica e os teores de fenóis totais e flavonoides foram quantificados pelos testes de Folin-Dennis e reação de complexação com cloreto de alumínio, respectivamente. Através do coeficiente de correlação de Pearson, os teores de fenóis e flavonoides foram correlacionados com a média das temperaturas máximas mensais e acúmulo de precipitação, respectivamente, registrados em Gurupi - Tocantins. **Resultados e Discussão:** A prospecção fitoquímica indicou a presença de flavonoides, saponinas, taninos, triterpenos, esteroides e alcaloides em ambos os extratos. Em *C. brasiliense*, as amostras de folhas sadias sofreram maior variação nos teores de fenóis (68,39±2,3 a 279,34±3,1 mg EAG g^{-1} extrato) e flavonoides (164,06±3,0 a 269,03±3,6 mg EQ g^{-1} extrato) em comparação às amostras de folhas com galhas. Através da correlação de Pearson, constatou-se uma forte correlação positiva entre os teores de fenóis totais e as temperaturas máximas e uma forte correlação negativa com a precipitação. **Conclusões:** As variações observadas nos teores de fenóis e flavonoides dos extratos de *C. brasiliense* parecem estar relacionadas aos fatores abióticos e a herbivoria promovida pelo inseto galhador.

Palavras-chave: *Insetos; galhas; pequi; fenólicos; sazonalidade*

ABSTRACT

Introduction: Galling insects manipulate the development of their host plants. Galls are rich in secondary metabolites, such as phenolic compounds and terpenes. *Caryocar brasiliense* acts as a host of galling insects. Few studies report the impacts of this plant-insect interaction on the species' morphology, physiology, and secondary metabolism. **Objective**: The purpose of this study was to verify if there is a correlation between the levels of total phenols and flavonoids in *C. brasiliense* leaf extracts and environmental variables, such as temperature and precipitation, throughout the year, and to evaluate how galling insects can interfere in this seasonality. **Methods**: Ethanol extracts from leaves were obtained by soxhlet extraction. The main classes of secondary metabolites were detected by phytochemical prospecting. The levels of total phenols and flavonoids were quantified by the Folin-Dennis tests and complexation reaction with aluminum chloride, respectively. Pearson 's correlation coefficient shows that the levels of phenols and flavonoids were correlated with the average monthly maximum temperatures and precipitation accumulation, respectively, recorded in Gurupi - Tocantins. **Results and Discussion**: Phytochemical prospecting indicated flavonoids, saponins, tannins, triterpenes, steroids, and alkaloids in both extracts. In *C. brasiliense*, the samples of healthy leaves suffered a greater variation in the levels of phenols (68.39±2.3 to 279.34±3.1 mg GAE g^{-1} extract) and flavonoids (164.06± 3.0 at 269.03±3.6 mg QE g^{-1} extract) compared to leaf samples with galls. A strong positive correlation was found between the contents of total phenols and maximum temperatures and a strong negative correlation with precipitation through Pearson's correlation. **Conclusions**: The variations observed in the levels of phenols and flavonoids in the extracts of *C. brasiliense* seem to be related to abiotic factors and the herbivory promoted by the galling insect.

DOI: 10.52571/PTQ.v18.n38.2021.04_TEIXEIRA_pgs_38_46.pdf

Keywords: Insects; galls; pequi; phenolic; seasonality

1. INTRODUÇÃO:

As galhas são resultado da hipertrofia e/ou hiperplasia dos tecidos vegetais causadas pela presença de um agente indutor, como vírus, bactérias, nematoides e insetos. As galhas possuem elevado conteúdo de nutrientes, além de acumularem substâncias do metabolismo secundário. O organismo indutor utiliza a galha como um sítio seguro para alimentação, proteção contra inimigos naturais e condições ambientais adversas (Formiga *et al*., 2009; Damasceno *et al*., 2010). As plantas hospedeiras podem apresentar deformação nas folhas, redução na taxa fotossintética e propriedades medicinais modificadas, esta última, provavelmente decorrentes de alterações no metabolismo secundário (Patel *et al*., 2018).

O perfil de metabólitos secundários das plantas, responsáveis pelas suas atividades biológicas, podem sofrer alterações qualitativas e quantitativas dependendo de estímulos ambientais. Além dos fatores bióticos, como as interações planta-inseto, fatores como disponibilidade hídrica, intensidade luminosa, temperatura, nutrientes do solo e fases fenológicas da planta podem provocar alterações nas rotas metabólicas e na distribuição de metabólitos secundários. Estudos relacionados a variabilidade destes compostos são considerados importantes para orientar pesquisas que visam o isolamento de produtos naturais, especialmente para espécies de interesse medicinal (Gobbo-Neto e Lopes, 2007; Ouerghemmi *et al*., 2016; Yao *et al*., 2016; Ribeiro *et al*., 2019).

O mecanismo de resistência das plantas compreende uma série de eventos bioquímicos, dentre estes, a produção de metabólitos de defesa como os compostos fenólicos e terpenos. A ação defensiva destes metabólitos inclui a toxicidade, a inibição do crescimento e redução de digestibilidade. Comumente, os tecidos das galhas apresentam maiores teores de compostos fenólicos quando em comparação ao tecido foliar sadio (Mota el al., 2005; Formiga *et al*., 2009; Ferreira *et al*., 2014).

A família Caryocaraceae é da ordem dos Malpighiales, possui 2 gêneros e 25 espécies espalhadas pelas Américas do Sul e Central (Fleming *et al*., 2009). O gênero *Caryocar* apresenta cerca de 16 espécies no Brasil, dentre estas destaca-se a *Caryocar brasiliense* (Figura 1), conhecida popularmente por pequizeiro (Nunes e Gil, 2016). O pequizeiro é considerado uma das espécies do Cerrado de maior interesse econômico, principalmente devido ao uso do seu fruto na alimentação, na extração de óleos para a fabricação de cosméticos e na medicina popular (Carvalho *et al*., 2015).

Figura 1*. Espécime de Caryocar brasiliense com presença de galhas foliares. Fonte: O Autor, 2019*

Alguns trabalhos relatam *C. brasiliense* como hospedeira de vários insetos galhadores (Leite *et al*., 2009; Leite *et al*., 2011; Castro *et al*., 2012; Santos *et al*., 2015). Apesar disso, poucos estudos foram descritos sobre essa interação planta-inseto galhador e seus possíveis efeitos na morfologia, fisiologia e metabolismo secundário da espécie.

Neste contexto, esse estudo teve como objetivo discutir o efeito de fatores abióticos sazonais, como estresse hídrico e temperatura, na biossíntese de fenóis e flavonoides em extratos de folhas sadias e galhadas de *C. brasiliense* e como os agentes galhadores podem interferir nessa sazonalidade.

2. PARTE EXPERIMENTAL:

2.1. Solventes, produtos químicos e aparelhos

Os reagentes e solventes P.A. (Merck, Sigma-Aldrich, Nox chemicals e Quimex) foram utilizados sem purificação prévia. Os extratos foram concentrados em evaporador rotatório Fisatom 802. As análises fotométricas foram registradas em espectrofotômetro UV-VIS T60, PG instruments.

2.2. Material vegetal

O material vegetal foi coletado em Gurupi – TO (11°44'21" S; 49°05'25" W). Uma exsicata foi depositada no herbário do Recôncavo da Bahia (HURB) da UFRB (número 26019). O procedimento de acesso ao patrimônio genético foi realizado e o projeto foi registrado no SisGen (Cadastro A10589B). As coletas de folhas sadias e galhadas de *C. brasiliense* foram realizadas nos dias 15/06/2018 (floração), 15/10/2018 (frutificação), 15/02/2019 (período vegetativo) e 15/06/2019 (floração). As amostras de folhas sadias foram nomeadas S1; S2; S3 e S4; de forma similar, as amostras de folhas galhadas foram nomeadas, respectivamente G1; G2; G3 e G4.

2.3. Preparo dos extratos

As folhas sadias e com galhas de *C. brasiliense* foram secas ao ar livre. Em seguida, foram trituradas em um liquidificador. As folhas (10 g) em pó foram submetidas a extração em soxhlet com etanol P.A. por 2 horas. Os extratos obtidos foram filtrados e concentrados em evaporador rotativo e secos até peso constante

2.4. Análises químicas

2.4.1 Prospecção fitoquímica

A triagem fitoquímica foi realizada por meio da análise qualitativa da composição química dos extratos foliares. Observou-se a formação de espuma, reações colorimétricas e/ou de precipitação para identificar os principais grupos químicos naturais como taninos, saponinas, flavonoides, catequinas, alcaloides, xantonas, triterpenos e esteroides (Matos, 1997). As reações gerais nesta análise, descritas a seguir, revelaram a presença ou ausência dessas classes de metabólitos secundários nos extratos analisados.

2.4.1.1 Taninos

Para realizar o ensaio utilizou-se 1,0 mL de extrato EtOH, sendo adicionada gota a gota uma solução de gelatina 2,5 %. A presença de precipitado branco indicaria reação positiva.

2.4.1.2 Triterpenos e esteroides

Neste ensaio realizou-se a reação de Lierberman-Burchard (anidrido acético + ácido sulfúrico concentrado). Coloração azul evanescente seguida de verde indicaria presença de esteroides/triterpenos.

2.4.1.3 Alcaloides

Em 1,0 mL de extrato adicionou-se quinze gotas de hidróxido de sódio a 1%, 2,0 mL de água destilada e 2,0 mL de clorofórmio. A fração aquosa foi desprezada e a fração clorofórmica acrescida de quinze gotas de ácido clorídrico a 1%, em seguida extraída com 2,0 mL de água destilada. A fração aquosa de clorofórmio foi desprezada e os testes foram realizados com a fração aquosa ácida, onde se acrescentou três gotas do reagente de Dragendorff. A formação de precipitados insolúveis e floculosos indicaria a presença de alcaloides.

2.2.1.4 Saponinas

Em 2,0 mL de extrato adicionou-se 2,0 mL de clorofórmio e 5,0 mL de água destilada logo após filtrou-se para um tubo de ensaio. Agitou-se a solução por 3 minutos e observou-se a formação de espuma. Presença de espuma persistente e abundante indicaria reação positiva.

2.4.1.5 Flavonoides, chalconas e xantonas

Em três tubos de ensaio foram adicionados 1,0 mL de extrato. O tubo 1 foi acidificado com HCl 0,5 mol.L^{-1} (pH 3). Os tubos 2 e 3 foram alcalinizados com NaOH 0,5 mol L^{-1} (pH 8 e 11). O aparecimento de coloração vermelha, lilás e azul púrpura nos tubos 1, 2 e 3, respectivamente, indicaria a presença de antocianidinas. A coloração amarela no tubo 3, indicaria a presença de flavonas, flavonóis e xantonas. A coloração vermelha nos tubos 1 e 3 indicaria a presença de chalconas e auronas. A coloração vermelho-laranja no tubo 3, indicaria a presença de flavanonois.

2.4.1.6 Leucoantocianidinas, Catequinas e Flavanonas

Em dois tubos de ensaio foram adicionados 1,0 mL de extrato. Os pH dos tubos 1 e 2 foram ajustados para 3 e 11, respectivamente. Posteriormente, os tubos foram aquecidos em bico de Bunsen. A coloração vermelha ou amarela no tubo 1 indicaria a presença de leucoantocianidinas ou catequinas, respectivamente. A coloração vermelho-laranja no tubo 2, indicaria a presença de flavanonas.

2.4.2 Teor de fenóis totais

O teor de fenóis totais foi determinado usando o método de Folin-Dennis modificado (Singleton *et al*., 1999). Misturou-se 0,5 mL do extrato (0,1 mg·mL^{-1} em metanol) com 2,5 mL do

reagente de Folin-Denis e, após 5 minutos, adicionaram-se 2,0 mL de uma solução de carbonato de sódio a 14% (Na_2CO_3). Após 2 h, mensurou-se a absorbância da mistura reacional em espectrofotômetro a 760 nm, usando metanol como branco. O teor de fenóis totais foi expresso em miligramas de equivalentes de ácido gálico por grama de extrato (mg EAG.g^{-1} de extrato).

2.4.3 Teor de flavonoides

O teor de flavonoides foi determinado utilizando um método colorimétrico descrito por MEDA *et al*., 2005, com modificações. Misturaram-se 2,0 mL de uma solução metanólica de cloreto de alumínio a 2% ($AlCl_3$) com 2,0 mL de solução do extrato (0,1 mg·mL^{-1} em metanol). Após 30 min, mensurou-se a absorbância a 415 nm, usando metanol com branco. O teor de flavonoides totais foi expresso em equivalentes de quercetina (mg EQ.g^{-1} de extrato).

2.5. Dados climatológicos

Os teores de fenóis totais e flavonoides dos extratos foram correlacionados através do coeficiente de correlação de Pearson com as médias das temperaturas máximas de Gurupi – TO registradas no mês de coleta das amostras e com a precipitação acumulada no quadrimestre anterior a coleta de cada amostra. As correlações foram avaliadas de acordo com a abordagem clássica para distribuição de Pearson com a utilização dos seguintes critérios: $|r|<0,3$ (correlação fraca), $0,3\leq|r|<0,6$ (correlação moderada) e $|r|\geq0,6$ (correlação forte).

Os dados climatológicos utilizados neste estudo foram extraídos do Instituto Nacional de Meteorologia (INMET), disponibilizados na plataforma online AGRITEMPO.

2.6. Análises estatísticas

Os testes foram realizados em três repetições, com todos os valores expressos em média±desvio padrão. As médias foram comparadas pelo teste de Tukey a 5% de probabilidade. As análises estatísticas foram realizadas usando Microsoft Excel e GraphPad 5.0 DEMO.

3. RESULTADOS E DISCUSSÃO:

A triagem fitoquímica é um procedimento importante para a bioprospecção de espécies vegetais de interesse farmacológico e/ou toxicológico. A triagem fitoquímica de extratos de folhas sadias e galhadas de *C. brasiliense* (Tabela 1), nos diferentes períodos de coleta, detectou a presença de flavonoides, taninos, esteroides e triterpenos, saponinas, catequinas e alcaloides em ambos os extratos. Esses resultados são parcialmente semelhantes aos relatados por Magalhães *et al*. (1988), que detectou a ausência de alcaloides nas folhas de *C. brasiliense*.

Tabela 1. *Triagem fitoquímica dos extratos de folhas sadias e galhadas de C. brasiliense*

Classes de metabólitos secundários	**Extratos em EtOH**	
	Folhas Galhadas	**Folhas Sadias**
Saponina	+	+
Taninos	+	+
Alcaloides	+	+
Esteroides e triterpenos	+	+
leucoantocianidinas	-	-
Catequinas	+	+
Flavanonas	-	-
Antocianinas e antocianidinas	-	-
Flavonas, flavonóis e xantonas	+	+
Chalconas e auronas	-	-
Flavanonóis	-	-

(+) Presente; (-) Ausente

Em relação aos fatores climáticos, Gurupi - TO caracteriza-se pela distinção entre uma estação seca (maio a outubro) e outra chuvosa (novembro a abril), característica do bioma Cerrado. Observou-se uma variação significativa na precipitação no decorrer do período de coleta (Figura 2), o maior acúmulo de precipitação foi observado entre novembro/2018 a fevereiro/ 2019 (889,28 mm) e o menor índice registrado entre julho/2018 a outubro/2018 (69,6 mm). A temperatura apresentou resultados relativamente constantes durante o período em estudo, mínimas na faixa de 20°C de madrugada e máximas na faixa de 30°C pela tarde. As temperaturas mais baixas foram registradas nos meses de maio/2018 a julho/2018 e as temperaturas mais elevadas nos meses de agosto/2018 a outubro/2018 (Figura 2).

Os teores de fenóis totais quantificados em extratos de folhas de *C. brasiliense* estão descritos na Figura 3. Os extratos S1, S2 e S4

apresentaram teores de fenóis totais significativamente maiores com relação a G1, G2 e G4, respectivamente ($p<0,05$). Somente nas amostras coletadas em fevereiro/2019, o teor de fenóis totais foi superior no extrato de folhas galhadas (G3) em comparação ao de folhas sadias (S3).

Com relação aos fatores climáticos, o teor de fenóis totais apresentou uma forte correlação com as temperaturas máximas ($r= 0,817$ para folhas sadias e $r= 0,666$ para folhas galhadas) registradas nos meses de coleta. Considerando-se o acúmulo de precipitação hídrica, observou-se uma forte correlação negativa com os teores de fenóis em folhas sadias ($r= -0,918$) e galhadas ($r= -0,826$), respectivamente.

O pico no teor de fenóis totais no período de estudo foi observado nas amostras coletadas em outubro/2018 (S2 com 279,34±3,1 mg EAG g^{-1}; G2 com 157,58±2,2 mg EAG g^{-1}), que coincide com a fase reprodutiva do pequi e com o período de estação seca na região. Os menores teores de fenóis totais (S3 com 68,39±2,3 mg EAG g^{-1}; G3 com 117,01±1,7 mg EAG g^{-1}) foram registrados em fevereiro/2019, que compreende o período vegetativo do pequi e a estação chuvosa no Cerrado.

De maneira geral, observou-se uma maior produção de fenóis em períodos mais secos e/ou com temperaturas elevadas. Similarmente, a restrição hídrica proporcionou maiores teores de fenóis totais em *Vitis vinífera L.* (Chavarria *et al*., 2011). Em flores de *Hypericum perforatum* observou-se o aumento na concentração de flavonoides, hipericinas e ácido clorogênico (Gray *et al*., 2003). Os fenóis contribuem para a absorção e neutralização de radicais livres gerados pelo aumento do estresse oxidativo nas plantas provocado pelo déficit hídrico (Detoni *et al*., 2010). Resultados similares foram observados por Formiga *et al*. (2009), que indicaram o impacto de fatores físicos na produção de fenóis em folhas sadias e com galhas de *Aspidosperma spruceanum*.

Em sinergia com a estação seca, os eventos reprodutivos, como a frutificação do pequi, podem estimular a produção de fenóis como um mecanismo de defesa vegetal em resposta a atração de insetos (Kaplan *et al*., 2008; Ribeiro *et al*., 2019).

Os menores teores de fenóis totais observados em folhas sadias (S3) e galhadas (G3) podem estar relacionados ao período vegetativo do pequi, onde ocorre uma translocação de carbono para o metabolismo primário em detrimento ao metabolismo secundário, o que pode explicar o déficit de fenóis neste período (Pimpão, 2009). Adicionalmente, alguns trabalhos relatam a menor atividade da enzima fenilalanina amônia-liase PAL, enzima chave na biossíntese de compostos fenólicos (Cartea *et al*., 2010), nas estações chuvosas (Castro *et al*., 2005).

A análise das curvas de precipitação e temperaturas mensais durante o período de estudo em conjunto com os teores de fenóis totais (Figuras 2 e 3), sugere que fatores abióticos estejam atuando em conjunto com a galhas na modulação da resposta química da planta hospedeira. Essa tendência é reforçada considerando-se que a diferença entre os teores de fenóis totais das galhas e dos tecidos sadios foi significativa ($p<0,05$) em todos os meses analisados.

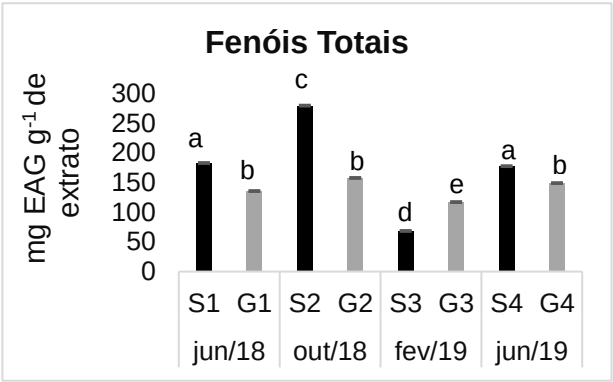

Figura 3. *Teor de fenóis totais em extratos de folhas de C. brasiliense. Médias seguidas da mesma letra não diferem entre si pelo teste de Tukey (0,05)*

Com relação ao teor de flavonoides (Figura 4), os extratos S1, S3 e S4 apresentaram teores de flavonoides similares aos de G1, G3 e G4, respectivamente. Analogamente, Rehill e Schultz (2012) não observaram diferenças no teor de fenóis de galhas e folhas sadias de *Hamamelis virginiana*. Nas amostras coletadas em outubro/2018, os teores de flavonoides foram significativamente maiores nas folhas sadias (S2) em comparação as folhas galhadas (G2) ($p< 0,05$). Ferreira *et al*. (2014) e Motta *et al*. (2005) detectaram maiores teores de flavonoides em folhas sadias de *Clusia lanceolata* e *Tibouchina pulchra*, respectivamente, em comparação as folhas galhadas.

Com relação aos fatores climáticos, o teor de flavonoides totais apresentou uma forte correlação com as temperaturas máximas para

folhas sadias (r= 0,511) e galhadas (r= 0,648), respectivamente. Considerando o acúmulo de precipitação hídrica, observou-se uma moderada correlação negativa com os teores de fenóis em folhas sadias (r= -0,448) e uma forte correlação com folhas galhadas (r= -0,687), respectivamente.

Os flavonoides atuam na modulação do transporte e nas respostas dependentes de auxinas, influenciando a arquitetura das plantas (Peer e Murphy, 2007; Buer *et al*., 2010). Bedetti *et al*. (2014), correlacionou o acúmulo de fenólicos em galhas de *Piptadenia gonoacantha* ao controle de auxinas (IAA). Bedetti *et al*. (2017), observaram que os locais de acúmulo de IAA e fenólicos coincidiram com as regiões mais hipertrofiadas, influenciando na determinação da forma final das galhas em *P. gonoacantha*.

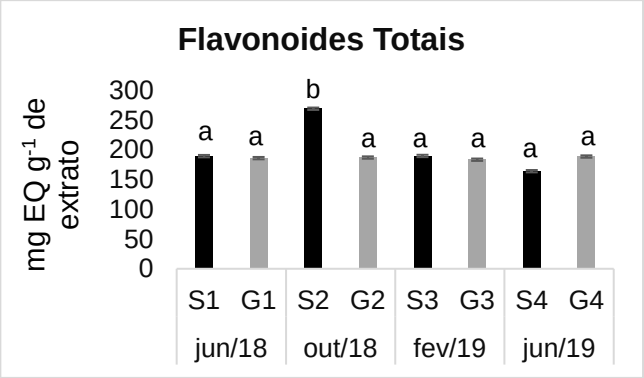

Figura 4. *Teor de flavonoides totais em extratos de folhas de C. brasiliense. Médias seguidas da mesma letra não diferem entre si pelo teste de Tukey (0,05)*

A amplitude das variações no conteúdo de fenóis totais foi maior nas folhas sadias do que nas folhas galhadas durante todo o período analisado (junho/2018 a junho/2019). Detoni *et al*. (2011) relataram maior variação no perfil fenólico em tecidos sadios de *Calliandra brevipes* e sugeriram que os insetos galhadores possuem algum mecanismo para limitar essa variação, provavelmente para sua própria defesa. Entretanto, essa menor variação sazonal dos teores de fenóis e flavonoides em tecidos galhados pode estar relacionado ao papel regulador da hipertrofia celular em galhas exercido por esses grupos de substâncias.

4. CONCLUSÕES:

Os resultados obtidos sugerem que em *C. brasiliense*, os fatores abióticos, como precipitação e temperatura, estejam atuando em conjunto com a herbivoria promovida pelo inseto galhador na modulação da defesa vegetal. O teor de fenóis totais apresentou uma forte correlação com as temperaturas máximas e uma forte correlação negativa com a precipitação, respectivamente. Os extratos de folhas sadias sofreram uma maior variação nos teores de fenóis em comparação aos extratos com galhas, sugerindo que os insetos possuem algum mecanismo de controle para evitar mudanças bruscas no conteúdo destas substâncias, provavelmente ligado à sua defesa ou ao papel de regulação da hipertrofia celular desempenhado por essas substâncias nas galhas.

5. AGRADECIMENTOS:

Ao PPGQ-UFT

6. REFERÊNCIAS:

1. Bedetti, C. S., Modolo, L. V., *and* Isaias, R. M. S. (2014). The role of phenolics in the control of auxin in galls of *Piptadenia gonoacantha* (Mart.) MacBr (Fabaceae: Mimosoideae). *Biochemical Systematics and Ecology*, 55, 53–59.
2. Bedetti, C. S., Bragança, G. P., *and* Isaias, R. M. S. (2017). Influence of auxin and phenolic accumulation on the patterns of cell differentiation in distinct gall morphotypes on *Piptadenia gonoacantha* (Fabaceae). *Australian Journal of Botany*, 65, 411–420.
3. Buer, C. S., Imin, N., *and* Djordejevic, M. A. (2010). Flavonoids: new roles for old molecules. *Journal of Integrative Plant Biology*, 52, 98–111.
4. Castro, A.H.F., Alvarenga, A.A., Soares, A.M., Young, M.C.M., *and* Purcino, A.A.C. (2005). Avaliação sazonal da atividade da fenilalanina amônia-liase e dos teores de fenóis e taninos totais em *Byrsonima verbascifolia* Rich. ex A. Juss.: uma espécie medicinal do cerrado. *Revista Brasileira de Plantas Medicinais*, 7(3), 45-55.
5. Cartea, E.M., Francisco, M., Soengas, P. *and* Velasco, P. (2010). Phenolic compounds in *Brassica* vegetables. *Molecules,* 6, 251-280.
6. Chavarria, G., Bergamaschi, H., Silva, L. C., Santos, H. P., Mandelli, F., Guerra, C. C., Flores, C. A., *and* Tonietto, J. (2011). Relações hídricas, rendimento e

compostos fenólicos de uvas Cabernet Sauvignon em três tipos de solo. *Bragantia*, *70*(3), 481-487.

7. Castro, A. C. R., Leite, G. L. D., Oliveira, D. C., *and* Isaias, R. M. S. (2012). Morphological Patterns of a Hymenopteran Gall on the Leaflets of *Caryocar brasiliense* Camb. (Caryocaraceae). American *Journal of Plant Sciences*, 3, 921-929.
8. Carvalho, L. S., Pereira, K. F., *and* Araújo, E. G. (2015). Características botânicas, efeitos terapêuticos e princípios ativos presentes no pequi (*Caryocar brasiliense*). *Arquivos de Ciências da Saúde da UNIPAR*, 19(2), 147-157.
9. Damasceno, F. C., Nicolli, K. P., Caramao, E. B., Soares, G. L. G., *and* Zini, C. A. (2010). Changes in the volatile profile of *Schinus polygamus* (Anacardiaceae) and *Baccharis spicata* (Asteraceae) induced by galling psyllids. *Journal of the Brazilian Chemical Society*, 21, 556-563.
10. Detoni, M. L., Vasconcelos, E. G., Scio, E., Aguiar, J. A., Isaias, R. M. S., *and* Soares, G.L.G. (2010). Differential biochemical responses of *Calliandra brevipes* (Fabaceae, Mimosoidae) to galling behaviour by *Tanaostigmodes ringueleti* and *T. mecanga* (Hymenoptera, Tanaostigmatidae). *Australian Journal of Botany*, 58, 280-285.
11. Detoni, M. L., Vasconcelos, E. G., Rust, N. M., Isaias, R. M. S., *and* Soares, G. L. G. (2011). Seasonal variation of phenolic content in galled and non-galled tissues of *Calliandra brevipes* Benth (Fabaceae: Mimosoidae). *Acta Botanica Brasilica*, 25(3), 601-604.
12. Ferreira, B. G., *and* Isaias, R. M. S. (2014). Floral-like destiny induced by a galling Cecidomyiidae on the axillary buds of *Marcetia taxifolia* (Melastomataceae). *Flora*, 209, 391–400.
13. Ferreira, R. O., Carvalho Junior, A. R., Silva, T. M. G., Castro, R. N., Silva, T. M. S., *and* Carvalho, M. G. (2014). Distribution of metabolites in galled and non-galled leaves of *Clusia lanceolata* and its antioxidant activity. *Revista Brasileira de Farmacognosia*, 24(6), 617-625.
14. Fleming, T. H., Geiselman, C., *and* Kress, W. J. (2009). The evolution of bat pollination: a phylogenetic perspective. *Annals of Botany*, 104, 1017–1043.
15. Formiga, A. T., Gonçalves, S. J. M. R., Soares, G. L. G., *and* Isaias, R. S. S. (2009). Relações entre o teor de fenóis totais e o ciclo das galhas de Cecidomyiidae em *Aspidosperma spruceanum* Mull. Arg. (Apocynaceae). *Acta Botânica Brasílica*, 23, 93-99.
16. Gray, D.E., Pallardy, S.G., Garrett, H.E. *and* Rottinghaus, G.E. (2003). Effect of acute drought stress and time of harvest on phytochemistry and dry weight of St. John's wort leaves and flowers. *Planta Medica*, 69(11), 1024-1030.
17. Gobbo-Neto, L., *and* Lopes, N. P. (2007). Plantas medicinais: fatores de influência no conteúdo de metabólitos secundários. *Química Nova*, 30(2), 374-381.
18. Kaplan, I., Halitschke, R., Kessler, A., Sardanelli, S., *and* Denno, R. F. (2008). Constitutive and induced defenses to herbivory in above- and belowground plant tissues. *Ecology*, 89(2), 392-406.
19. Leite, G. L. D., Veloso, R. V. S., Silva, F. W. S. S., Guanabens, R. E. M., *and* Fernandes, G. W. (2009). Distribuição espacial de galhas induzidas por *Eurytoma* (Hymenoptera, Eurytomidae) em plantas de *Caryocar brasiliense* (Caryocaraceae). *Revista Brasileira de Entomologia*, 53(4), 643-648.
20. Leite, G. L. D., D'ávila, V. A., Cerqueira, V. M., Nascimento, A. F., *and* Fernandes, G. W. (2011). Spatial distribution of a spherical gall (Hymenoptera, Eulophidae) on *Caryocar brasiliense (*Caryocaraceae). *Revista Brasileira de entomologia*, 55(3), 396-400.
21. Magalhães, H. G., Monteiro Neto, H., Lagrota, M. H., Wigg, M. D., Guimarães, L. A. S., Loja, M. A. S. O., *and* Araújo, R. R (1988). Estudo estrutural do pequizeiro *Caryocar brasiliense* Camb. Caryocaraceae, sob o aspecto farmacoquímico e botânico. Revista Brasileira de Farmácia, 69(3), 31-41.
22. Matos, F.J.A. (1997). Introdução à fitoquímica experimental. Edições UFC, Fortaleza.
23. Meda, A., Lamien, C. E., Romito, M., Millogo, J., *and* Nacoulma, O. G. (2005). Determination of the total phenolic, flavonoid, and proline contents in *Burkina Fasan* honey, as well as their radical

scavenging activity. *Food Chemistry*, 91, 571-577.

24. Motta, L. B., Kraus, J. E., Salatino, A., *and* Salatino, M. L. F. (2005). Distribution of metabolites in galled and non-galled foliar tissues of *Tibouchina pulchra*. *Biochemical Systematics and Ecology*, 33, 971-981.
25. Nunes, C. S., *and* Gil, A. S. B. (2016). Flora das cangas da Serra dos Carajás, Pará, Brasil: Caryocaraceae. *Rodriguésia*, 67(5), 1281-1283.
26. Ouerghemmi, S., Sebei, H., Siracusa, L., Ruberto, G., Saija, A., Cimino, F., *and* Cristani, M. (2016). Comparative study of phenolic composition and antioxidant activity of leaf extracts from three wild Rosa species grown in different Tunisia regions: rosa canina L., Rosa moschata Herrm. and Rosa sempervirens L. Industrial Crops and Products, 94,167–177.
27. Peer, W., *and* Murphy, A. (2007). Flavonoids and auxin transport: modulators or regulators? *Trends in Plant Science*, 12, 556–563.
28. Pimpão, R.S.S. (2009). Compostos fenólicos e suas actividades antioxidantes em espécies de *Juniperus*: Análise de produção sazonal e sob condições de stresse. Dissertação de Mestrado, Universidade de Lisboa, Portugal.
29. Patel, S., Rauf, A., *and* Khan, H. (2018). The relevance of folkloric usage of plant galls as medicines: Finding the scientific rationale. *Biomedicine and Pharmacotherapy*, 97, 240-247.
30. Rehill, B. J., *and* Schultz, J. C. (2012). *Hormaphis hamamelidis* Fundatrices Benefit by Manipulating Phenolic Metabolism of Their Host. *Journal of Chemical Ecology*, 38, 496-498.
31. Ribeiro, D.A., Macêdo, D.G., Boligon, A.A., Menezes, I.R.A., Souza, M.M.A., *and* Costa, J.G.M. (2019). Influence of seasonality on the phenolic composition of Secondatia floribunda A.DC (Apocynaceae) during its phenological cycle. Acta Physiologiae Plantarum, 41, 185.
32. Santos, C. S., Sampaio, A. C., Silva, P. C., Barbosa, D. S., *and* Dantas, S. P. (2015). Descrição morfológica das galhas foliares de *Caryocar brasiliense* Camb. (Caryocaraceae): uma espécie super hospedeira. *Journal of Bioenergy and Food Science*, 02(4), 194-200.
33. Singleton, V. L., Orthofer, R., *and* Lamuela-Raventós, R. M. (1999). Analysis of total phenols and other oxidation substrates and antioxidants by means of folin-ciocalteu reagent. *Methods in Enzymology*, 299, 152-178.
34. Yao, X.H., Zhang, Z.B., Song, P., Hao, J.Y., Zhang, D.Y., *and* Zhang, Y.F. (2016). Different harvest seasons modify bioactive compounds and antioxidant activities of *Pyrola incarnata*. *Industrial Crops and Products*, 94, 405-412.

7. OPEN ACCESS:

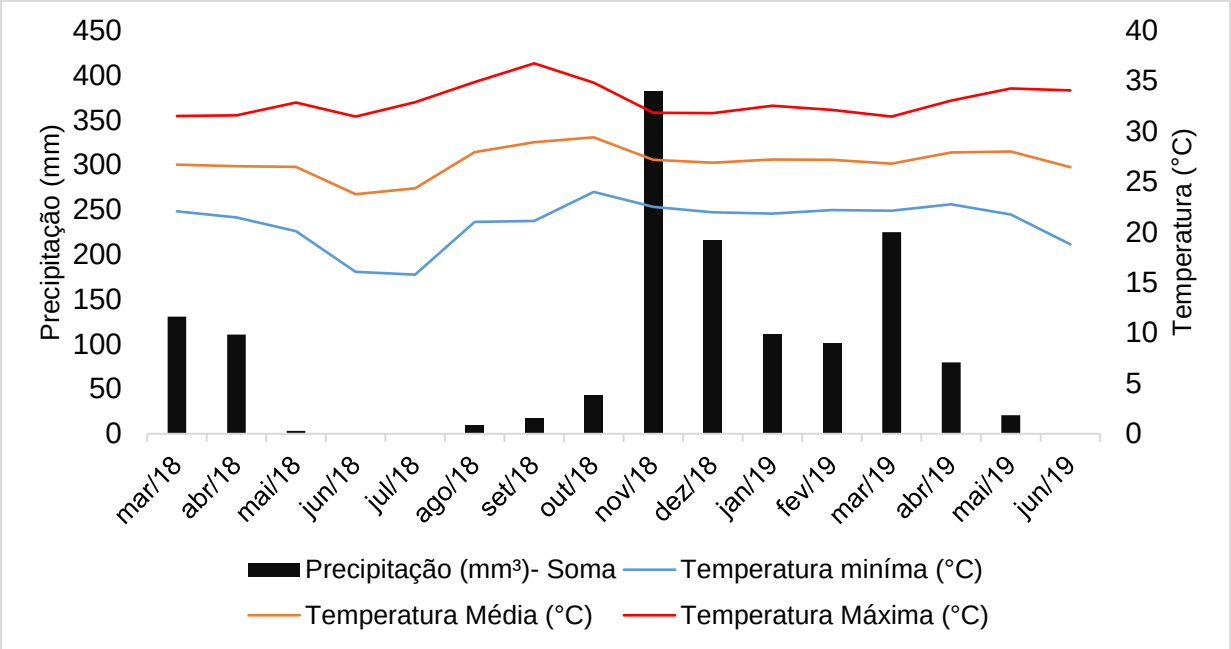

Figura 2. *Dados climatológicos (precipitação mensal, médias das temperaturas mínima, média e máxima) do município de Gurupi – TO, referentes aos meses de março/2018 a junho/2019, fornecidos pelo INMET através do sistema Agritempo*

PERIÓDICO TCHÊ QUÍMICA
ARTIGO ORIGINAL

PROJETO DE ESPECTRÔMETRO FOTOACÚSTICO DE EXTRACAVIDADE BASEADO EM DIODO LASER AZUL NA DETECÇÃO DE GÁS NO_2 (DIÓXIDO DE NITROGÊNIO)

DESIGN OF EXTRA CAVITY PHOTOACOUSTIC SPECTROMETER BASED ON BLUE DIODE LASER IN NO_2 (NITROGEN DIOXIDE) GAS DETECTION

RANCANG BANGUN SPEKTROMETER FOTOAKUSTIK EKSTRAKAVITAS BERSUMBERKAN LASER DIODA BIRU DALAM PENDETEKSIAN GAS NO_2 (NITROGEN DIOKSIDA)

HARJUM[1*]; UTOMO, Agung Bambang Setio[2.]; MITRAYANA[3.]

[1,2,3] Universitas Gadjah Mada, Mathematics and Natural Science Faculty, Physic Department, Indonesia

** Corresponding author*
e-mail: harjumfisika@gmail.com

Received 17 April 2021; received in revised form 06 June 2021; accepted 14 July 2021

RESUMO

Introdução: A detecção de NO_2 é necessária porque o NO_2 é um poluente do ar que causa poluição fotoquímica e chuva ácida. Além disso, as doenças respiratórias são causadas por altos níveis de NO_2 no ar inspirado. **Objetivo.** O objetivo deste estudo foi detectar NO_2 usando PAS utilizando Arduino Uno, uma pesquisa fácil, simples e de baixo custo. **Métodos:** Foi realizada a detecção do gás Dióxido de Nitrogênio (NO_2) com um Espectrômetro Fotoacústico (PAS) usando um microcontrolador Arduino Uno. O sistema PAS usa um laser de diodo azul com comprimento de onda de 450 nm como fonte de radiação porque esse comprimento de onda é adequado para gás NO_2. A intensidade do feixe de laser é modulada usando um sistema de modulação com um esquema liga-desliga usando o Arduino Uno. A frequência de modulação foi variada para obter a frequência máxima de detecção. A célula fotoacústica usada foi uma única célula fotoacústica ressonadora com sensores de som tipo H. Sensor de som e fotodiodo foram usados nesta medição. A amplificação do sinal foi feita utilizando o amplificador Lock-in, e o tempo de amplificação também foi determinado para otimizar o PAS. O gás nitrogênio foi usado para detectar sinais de fundo. **Resultados e Discussão:** A partir da otimização do espectrômetro fotoacústico, os resultados obtidos foram uma freqüência de diodo laser de 1.000 Hz com ciclo de trabalho de 50% e uma amplificação Lock-in de 10.000 vezes com tempo constante de 3,3 ms. A concentração máxima alcançada nesta medição foi de 6 ppm. O sinal de fundo obtido nesta medição foi 0,00002 V / W. O limite de detecção mais baixo alcançado nesta medição foi de 0,0064 ppm. **Conclusões:** Os recipientes de amostra de gás contendo NO_2 com tamanhos maiores tendem a ter uma concentração maior. Às vezes, a concentração de NO_2 do grande recipiente de amostra de gás foi ultrapassada pelo pequeno recipiente de amostra.

Palavras-chave: *Espectrômetro fotoacústico de laser azul, dióxido de nitrogênio, células fotoacústicas, modulação, Arduino Uno.*

ABSTRACT

Background: NO_2 detection is necessary because NO_2 is an air pollutant causing photochemical smog and acid rain. In addition, respiratory diseases are caused by high levels of NO_2 in the inhaled air. **Aim:** The purpose of this study was to detect NO_2 using PAS utilizing Arduino Uno, an easy, simple, and low-cost research. **Methods:** The detection of Nitrogen Dioxide (NO_2) gas with a Photoacoustic Spectrometer (PAS) using an Arduino Uno microcontroller has been carried out. The PAS system uses a blue diode laser with a wavelength of 450 nm as the radiation source because this wavelength is suitable for NO_2 gas. The intensity of the laser beam is modulated using a modulation system with an on-off scheme using the Arduino Uno. The modulation frequency has been varied to get the maximum detection frequency. The photoacoustic cell used was a single resonator photoacoustic cell with type H. Sound sensor and photodiode were used in this measurement. The amplification of the signal was done by utilizing the Lock-in amplifier, and the constant time of Lock-in amplifier was also determined to optimize the PAS. Nitrogen gas was used to detect background signal. **Results and Discussion:** From the photoacoustic spectrometer optimization, the results obtained were a laser diode frequency of 1,000 Hz with a duty cycle of 50% and a Lock-in amplifier amplification of 10,000 times with a constant time of 3.3 ms. The maximum concentration reached in this measurement was 6 ppm. The background signal achieved in this measurement was 0.00002 V/W. The lowest detection limit achieved in this measurement was 0.0064 ppm.

DOI: 10.52571/PTQ.v18.n38.2021.05_HARJUM_pgs_47_61.pdf

Conclusion: The gas sample containers containing NO_2 with larger sizes tend to have a greater concentration. Sometimes, the NO_2 concentration of the large sample gas container was overtaken by the small sample container.

Keywords*: Blue Laser Photoacoustic Spectrometer, Nitrogen dioxide, Photoacoustic Cell, Modulation, Arduino Uno.*

ABSTRAK

Latar Belakang: Deteksi NO_2 diperlukan karena NO_2 sebagai polutan udara yang menyebabkan kabut asap fotokimia dan hujan asam**.** Selain itu penyakit pernapasan disebabkan oleh tingginya kadar NO_2 dalam udara yang dihirup.**Tujuan:** Tujuan dari penelitian ini adalah untuk mendeteksi NO_2 yang menggunakan SFA yang memanfaatkan Arduino Uno yang merupakan sebuah riset yang mudah, sederhana dan biaya murah. **Metode:** Pendeteksian gas Nitrogen Dioksida (NO_2) dengan Spektrometer Fotoakustik (SFA) yang menggunakan mikrokontroller Arduino Uno telah dilakukan. Sistem SFA menggunakan laser dioda biru dengan panjang gelombang 450 nm sebagai sumber radiasinya karena panjang gelombang tersebut sesuai untuk gas NO_2. Sinar laser dimodulasi intensitasnya dengan menggunakan sistem modulasi berskema *on-off* dengan menggunakan Arduino Uno. Frekuensi modulasi telah divariasi untuk mendapatkan frekuensi dengan deteksi maksimum. Sel fotoakustik yang digunakan adalah sel fotoakustik resonator tunggal dengan tipe H. Sensor bunyi dan Fotodioda digunakan dalam pengukuran ini. Penguatan sinyal dilakukan dengan memanfaatkan Lock-in amplifair dan waktu tetapan Lock-in amplifair juga ditentukan dalam rangka mengoptimasi SFA. Gas nitrogen digunakan untuk mendeteksi sinyal latar. **Hasil dan Diskusi:** Dari optimasi spektrometer fotoakustik, hasil-hasil yang diperoleh adalah frekuensi laser dioda 1.000 Hz dengan *duty cycle* 50%, dan penguatan Lock-in amplifair 10.000 kali dengan waktu tetapan 3,3 ms. Konsentrasi maksimum yang dicapai dalam pengukuran ini adalah 6 ppm. Sinyal latar yang dicapai dalam pengukuran ini adalah 0,00002 V/W. Batas deteksi terendah yang tercapai dalam pengukuran ini adalah 0,0064 ppm. **Kesimpulan:** Wadah sampel gas yang mengandung NO_2 dengan ukuran-ukuran yang lebih besar cenderung mempunyai konsentrasi yang lebih besar. Kadang-kadang konsentrasi NO_2 wadah sampel gas yang besar dikalahkan oleh wadah sampel yang kecil.

Kata kunci: *Spektrometer Fotoakustik Laser Biru, Nitrogen dioksida, Sel fotoakustik, Modulasi, Arduino Uno.*

1. INTRODUCTION:

1.1. Background

NO_2, as the most common air pollutant, can cause health problems for humans. NO_2 causes photochemical smog and acid rain. The primary sources of ambient NO_2 are anthropogenic combustion processes, such as the emissions from cars, power plants, and factories. There has been respectable interest in building a sound and cost-effective NO_2 sensor system (Yin *et al*., 2017). NO_2 can become toxic if it has a high concentration and is inhaled (Dong *et al*., 2020). NO_2 concentrations above 100 ppmV are chronic human exposure, so NO_2 is classified as a highly hazardous substance. It can cause pulmonary edema leading to death (Ruck *et al*., 2017).

Greenhouse gases such as NO_2, CO_2, and CH_4, are also responsible for global warming (Yehya and Chaudhary, 2012). Electrochemical-based sensors are used to detect NO_2, but these sensors lack long-term stability and undergo cross-sensitivity to other gases (Breitegger *et al*., 2020). IR absorption photometers used to measure NO_2 are very large and costly (Kapp *et al*., 2018). Accurate and easy measurement of NO_2 at ppb levels is essential for monitoring environmental pollution and can be used to maintain a healthy living environment. NO_2 characterized by broadband absorption in the visible region of the spectrum has been a subject of frequent research. Gas detection using photoacoustic with blue diode laser sources is a perfect, well-established, and sensitive detection technique for NO_2 gas based on the generation of sound waves (Kalkman dan Kesteren, 2008).

The increasing use of photoacoustic techniques to control trace gases is mainly due to the constant growth of short, medium, and long-wavelength infrared semiconductor lasers (Ruck *et al*., 2017). Photoacoustic Spectroscopy has characteristics like a fast response, high selectivity and sensitivity, and compact detection module, so it is widely used for detecting trace gas (Gong *et al*., 2020).

The disadvantage of lasers derived from lead-salt equipment is that they are cryogenically cooled. DFB lasers are high-priced lasers and work in only a few windows between 0.7 and 1.9 µm. The simple Fabry-Perot diode laser is more suitable for integrated, portable, and low-cost sensors (Gianfrani *et al*., 1997). Extra cavity configuration was chosen because it made

instruments easier to combine with the lowest detection limit achieving the ppt order for ethylene gas (Mitrayana *et al*., 2011). A different design for photoacoustic cells had been suggested, namely resonant cells with one resonator and two acoustic buffers. It aims to obtain efficient noise reduction, thereby increasing the signal-to-noise ratio results (Elia *et al*., 2009).

The modulation method used in the green diode laser modulation was the amplitude-shift keying method (ASK) with the On-Off Keying modulation type (OOK). Calibration of the laser modulation system with a database technique is expected to improve accuracy with the recommended frequency of 500 Hz to 9,500 Hz with 500 Hz intervals (Rakhmadi *et al*., 2018). The molecular concentration directly relates to obtained signal in on-off modulation, so it becomes the best practical modulation way. At atmospheric pressure, finding a wavenumber where no atmospheric molecule absorbs is quite impossible, but the absorption that can be low enough enables very weak error in using this detection method. (Grossel *et al*., 2007). Laser intensity modulation for continuous wave laser can be applied at a fixed frequency or variable frequency with the laser light periodically turned on and off to form square wave fluctuations in photoacoustic imaging. The 532 nm diode laser modulation can affect photoacoustic image quality. Therefore, laser modulation must be applied in the optimum duty cycle to obtain the best quality from photoacoustic images (Widianingrum *et al*., 2017).

Slezak carried out a simple experiment to detect NO_2 using visible laser photoacoustic with various wavelengths (Slezak, 2001). Elia *et al*. used a differential photoacoustic cell with two resonators for NO_2 gas with a concentration of 0.5 ppb for a continuous wave quantum cascade laser with λ = 6.25 μm and 80 ppb for a pulsed quantum cascade laser with λ = 6.2 μm (Elia *et al*., 2009). Pushkarsky *et al*. reported detecting NO_2 levels of subparts per billion using photoacoustic spectroscopy based on a 350 nm tunable continuous-wave quantum cascade laser with minimum detection of 0.5 ppb (Pushkarsky *et al*., 2006). Mitrayana *et al*. had successfully designed and built a PAS with a blue laser light source and used it to measure NO_2 gas with a detection limit of 10 ppbV (Mitrayana *et al*., 2007). Zheng, H *et al*. used a sub ppb level QEPAS NO_2 nitrogen dioxide sensor built utilizing a cost-effective broad line diode laser emitting at 450 nm (Zheng *et al*., 2015).

The H-type longitudinal resonant PA cell has easy processing, good matching with axisymmetric laser beams, and good cooperating with axisymmetric PA fields. It has been utilized in recent years. Though researches on the structure optimization of an H-type PA cell are seldom. (Gong *et al*., 2020).

1.2. Theory

1.2.1 Blue Laser

The layering of atomic orbitals in a semiconductor makes the electrons form a continuous band structure. The band structure consists of a conduction band and a valence band separated by an energy gap of typically 0.5-2.5eV. In undoped semiconductors, the electrons in the conduction band and holes in the valence band can move almost freely because the continuous band structure is approximately represented as an electron gas. Holes are the electrons lost in the valence band that can shift so that they flow current. Semiconductors are N-doped if group V atoms dope a semiconductor with the atom in group IV. Semiconductors are P-doped if a semiconductor with the atom in group IV is doped by group III atoms (Fuchs, 2006). A one-dimensional energy diagram for electrons and holes can be seen in Figure 1.

When an electric current is passed in a forward direction through a p-n semiconductor diode, the electrons and holes can rearrange in the p-n junction. They can emit recombinant energy in the form of electromagnetic radiation. The line width of the spontaneous emission is up to several cm^{-1}. The wavelength is determined by the energy difference between the energy levels of electrons and the holes, which is mainly determined by the bandgap (Demtroder, 2002).

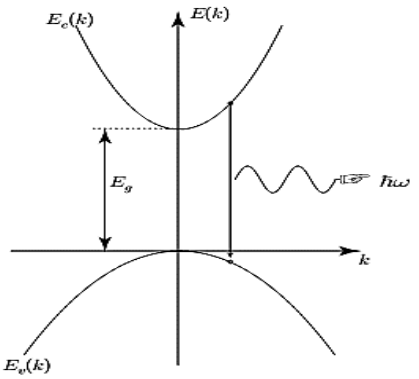

Figure 1. *One-dimensional energy diagram for electrons and holes. E_c is the energy of the conduction band, E_v is the energy of the valence band. Because of the combination of electrons with holes, photon energy can be emitted (Fuchs, 2006)*.

With the undoped layer of p-i-n heterostructure defined as a small area where the recombination

process is known to occur, the conditions for laser light amplification can also be met in this region.

The p-i-n structure acts as a waveguide using total internal reflection because the undoped layer has a higher refractive index than the surrounding cladding layer (Fuchs, 2006). Thus, in a simple bulk laser, the active region does not confine the optical radiation produced by stimulated recombination of electron-hole pairs, and absorption processes outside the active (or gain) medium surpass a significant fraction of the optical radiation (Nakamura *et al*., 2000).

1.2.2 Photoacoustic Spectroscopy

Photoacoustic spectroscopy is based on the absorption of electromagnetic radiation by analyte molecules. Non-radiative relaxation processes (such as collisions with other molecules) induce local heating of the reference sample. Pressure fluctuations generated by thermal expansion can be detected in the form of acoustic or ultrasonic waves (Bageshwar *et al*., 2010).

The acoustic signal is converted to an electric signal by equation 1.

$$S(\nu) = C_{cell} I_{po} S(T) g(\nu) N \quad (1)$$

(Jiang *et al*., 2016).

The eigenfrequency is the same for an open-open or closed-closed cavity and is given by equation 2.

$$\omega_j = 2\pi f_j = \pi c_s \sqrt{\left(\frac{k}{L}\right)^2 + \left(\frac{\alpha_{mn}}{R_c}\right)^2}. \quad (2)$$

The eigenvalues represent the longitudinal, azimuthal and radial indices, respectively (Besson and Thevenaz, 2006). For both sides of the open or closed resonator tube, the maximum resonance amplification frequency f_{res} is related to the effective tube length L_{eff} through the speed of sound following equation 3.

$$f_{res} = n \frac{c}{2L_{eff}} \quad (3)$$

(Ruck *et al*., 2017).

The acoustic pressure equation is obtained using equation 4

$$p_j(r,\omega) = \begin{matrix}\cos \\ \sin\end{matrix}(m\Phi)\left[AJ_m(k_r r) + BY_m(k_r r)\right]\left[C\sin(k_z z) + D\cos(k_z z)\right] \quad (4)$$

with $m = 0, n = 0, n_z = 1$ so that $\alpha_{mn} = 0$ and $J(0) = 1$ result in equation 5 for the buffer space

$$\tilde{p}_b(z,\omega_1) = \frac{Q_{1b}}{\omega_1}\left[\frac{\beta \tilde{I}(\gamma - 1)}{V_{ob}}\right]\frac{1}{\sqrt{2}}\cos\left(\frac{\pi}{l} z\right), \quad (5)$$

and in the resonator space (equation 6)

$$\tilde{p}_b(z,\omega_1) = \frac{Q_{1r}}{\omega_1}\left[\frac{\beta \tilde{I}(\gamma - 1)}{V_{or}}\right]\frac{1}{\sqrt{2}}\cos\left(\frac{\pi}{l} z\right) \quad (6)$$

(Mitrayana *et al*., 2014).

The electronic transition ${}^2B_1 \leftarrow X^2A_1$ and ${}^2B_1 \leftarrow X^2A_1$ are the suitable broad absorption spectrum of NO_2 (Ruck *et al*., 2017).

In a range of 460-370 nm, absorption occurs from the ground state to the ${}^2B_1$ and ${}^2B_2$levels, and above 600 nm, the transition occurs only to ${}^2B_2$ (Slezak., 2001). The wavelength that photochemical dissociation can occur is below 415 nm (Zheng *et al*., 2015). Figure 2 shows energy exchange between and from low electronic levels of NO_2 in the presence of N_2.

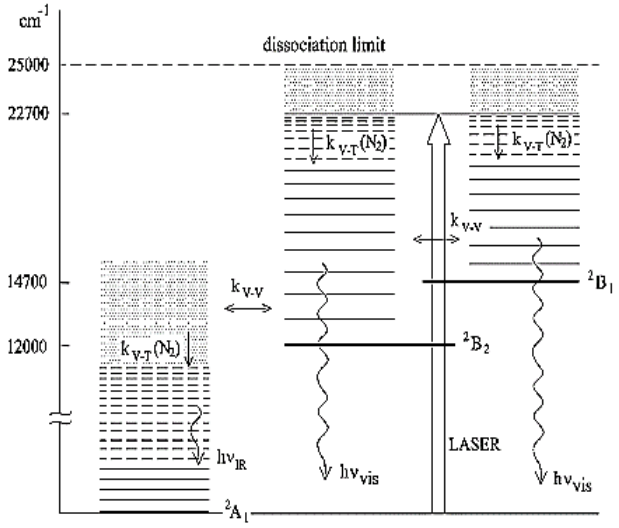

Figure 2. *Energy exchange between and from low electronic levels of NO_2 in the presence of N_2 (Slezak, 2001).*

1.2.3 Arduino UNO R3 and Amplitude Shift Keying (ASK) Methode

Arduino Uno R3 is a microcontroller development board based on the ATmega328P chip. Software used to develop microcontroller applications, starting from writing source programs, compiling, uploading compilation results, and testing them in a serial terminal, is IDE (Integrated Development Environment). Arduino Uno board can be seen in Figure 3.

Amplitude-Shift Keying (ASK) modulation modulates the amplitude of the carrier signal output to be changed by the modulation signal. Changes in the carrier signal amplitude will occur in this ASK method according to the logic of input signal bits. Bit 1 and bit 0 are used to symbolize

digital information signals.

The duty cycle can be used to adjust the number of high logic and low logic in a signal with the equation 7:

$$Duty\ cycle = \frac{T_{on}}{T_{on}+T_{off}} \times 100\%. \quad (7)$$

(Solihah, 2016).

1.2.4 Nitrogen dioxide

Nitrogen dioxide is a strong oxidant, is reddish-brown, and is soluble in water. Nitrogen dioxide is an important atmospheric trace gas. In addition to its health effects, it absorbs visible solar radiation. Thus, it contributes to the visibility of a damaged atmosphere. It is an absorber of visible radiation, potentially impacting global climate change if concentrations are high enough. Figure 4 ilustrates nitrogen dioxide structural formula.

NO_2, together with NO, becomes the primary regulator of the oxidizing power of free troposphere by controlling the addition and destruction of radical types, including hydroxyl radicals and NO_2. Moreover, it plays a critical role in determining the concentration of ozone (O_3) in the troposphere. Whether in a polluted or unpolluted atmosphere, the photolysis of nitrogen dioxide is the only key initiator of the photochemical formation of ozone (WHO, 2000).

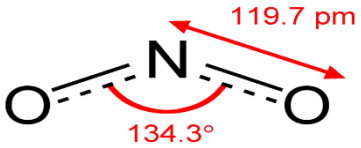

Figure 4. *Nitrogen dioxide structural formula (Mills, B., 2007).*

Therefore, this study aimed to make a simple, easy, and low-cost experiment in detecting NO_2 gas using PAS with a blue laser diode utilizing on-off modulation.

2. MATERIALS AND METHODS:

NO_2 detection was carried out using a photoacoustic spectrometer with a blue laser source with a wavelength of 450 nm. The photoacoustic cell used is a single resonator photoacoustic cell with type H. In most studies, a mechanical chopper is used to modulate the laser beam. In contrast, an Arduino Uno microcontroller can be used to modulate laser beam working on-off according to frequency input (Rakhmadi *et al*., 2019). The blue diode laser intensity is modulated using an on-off scheme. The modulation period is adjusted until the maximum photoacoustic signal value is found. Nitrogen gas is used to determine the background signal that plays a role in determining the concentration of NO_2.

The equipment and material of this study are the Blue Diode Laser with a wavelength (λ) of 450 nm, class IIIA position, 12 V DC voltage, and 2W power. Other instruments are the actuator system, which is a series consisting of a power supply, TTL laser, and Arduino Uno, whose system modulates laser current by adjusting the modulation frequency of the Arduino UNO microcontroller programming, resistors, lock-in amplifier, computer, a photodiode sensor, multi-size gas containers, Outcoupling window glass, an Arduino UNO sound sensor, BNC oscilloscope cables, male and female circuit cables. Figure 5 shows the series of tools. The material used was gases containing NO_2, such as motor vehicle exhaust gas and environmental air.

The photoacoustic cell consists of a single cylindrical channel as an acoustic resonator. The channel length is 90 mm, and the channel diameter is 8 mm. Photoacoustic cell can be seen in Figure 6.

An electric condenser microphone is placed against the wall in the middle of the channel to detect acoustic pressure. Two identic buffer volumes have 10 mm long and 30 mm diameter. The distance between the two windows is 110 mm.

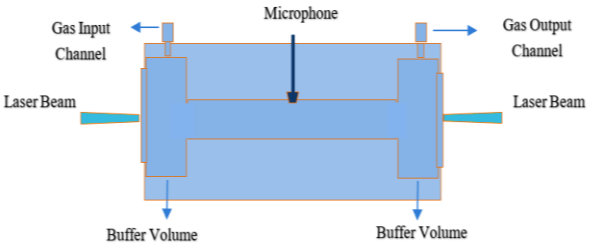

Figure 6. *Photoacoustic Cell.*

The difference between this research and others is that in optimizing and characterizing the blue diode laser spectrometer and determining the resonance curve, we used a gas containing NO_2 instead of pure NO_2 gas. For the linearity curve, it refers to another reference to get a gradient variable. A Diagram of the research phase can be seen in Figure 7.

Determining the lock-in amplifier amplification was carried out by inserting 1.5 liters of gas containing NO_2 into the photoacoustic cell and irradiating it for 2 minutes, respectively, from 1 to 10,000. On turning the buttons, care was required to be taken so it was not to overload. The lock-in amplifier constant time was determined by inserting 1.5 liters of gas containing NO_2 into the

photoacoustic cell and irradiating it for 2 minutes, respectively, from 3.3 ms to 1s. On turning the buttons, attention should be given to avoid overloading.

The duty cycle laser was determined by inserting 5 liters of gas containing NO_2 into the photoacoustic cell and irradiating it for 2 minutes, respectively, from 16.67% to 83.33%. The photoacoustic signal appearing not associated with absorption in the medium under investigation is called the background signal. These signals are caused by the absorption of radiation in the walls and windows of the photoacoustic cells, by scattered radiation entering the acoustic detector, by the presence of impurities that are extraneous to the absorption bands in the spectrum range in the study, and others (Zharov dan Lethokov, 1986). Measurement of background signal was carried out by passing nitrogen to the photoacoustic cell.

Determination of the resonance curve and quality factor was done by modulating the diode with the on-off method to see the maximum signal frequency at the 2 L gas sample and determine the quality factor. The linearity curve is determined by referring to a selected reference. It was referred from an article by author Yi Hongming *et al*. in 2011 entitled "*Application of a broadband blue laser diode to trace NO_2 detection using off-beam quartz-enhanced photoacoustic spectroscopy*". The linearity curve graph is presented in Figure 8 with a gradient of 24.51 and a mean laser power of 7 mW.

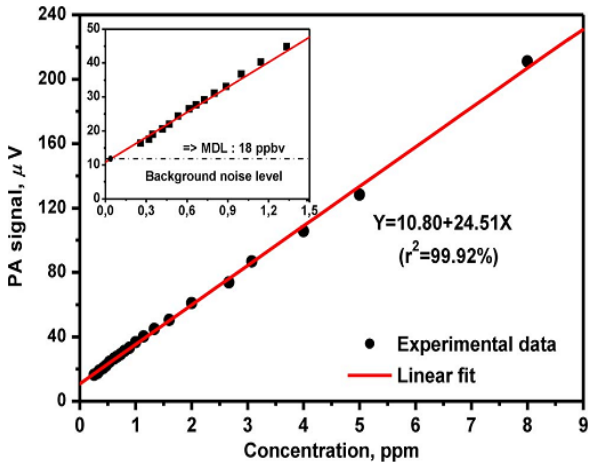

Figure 8. *NO_2 linearity curve (Yi et al., 2011).*

Measurement of noise and the lowest detection limit of PAS was done by injecting 250 ml of gas containing NO_2, turning off the blue laser, and recording the signal.

Testing NO_2 concentration from gases containing NO_2 was carried out by injecting gas containing NO_2 from various motor vehicle exhaust gases and from environmental air in multi-size containers. Calculating the concentration of the signal can be done with equation 8:

$$\text{Concentration} = \frac{S_N - S_{background}}{Gradient} \quad (8)$$

(Mitrayana, 2008).

Measurement of NO_2 gas was carried out by taking gas samples containing NO_2 in 4 types of vehicles and campus air on the same six gas containers. One type of vehicle was varied in the collection time, namely 1 minute and 2.5 minutes.

3. RESULTS AND DISCUSSION:

3.1. Results

From the experiment, the lock-in amplifier amplification achieved is 10,000 times. We can see the result of the experiment in Figure 9.

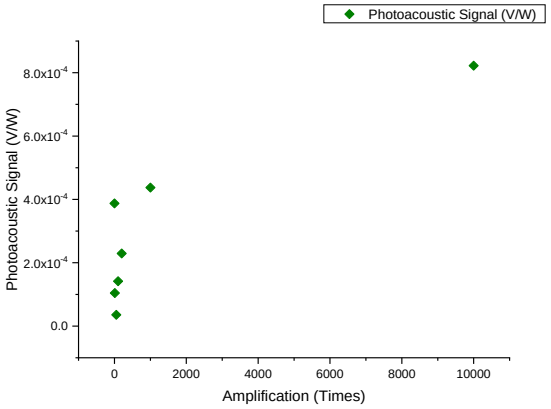

Figure 9. *Lock-in amplifier amplification graph.*

It was achieved 3.3 ms for lock-in amplifier constant time from the experiment like in Figure 10.

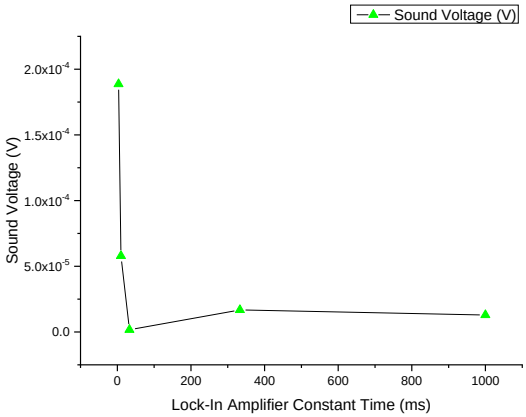

Figure 10. *Lock-In Amplifier constant time graph.*

The experiment result of lock-in amplifier

constant time can be seen in Table 1 and the experiment result of the lock-in amplifier amplification is in Table 2.

Table 1. *Lock-in Amplifier constant time.*

Lock-in Amplifier constant time (ms)	Sound sensor value (Bit)	Sound Voltage (V)
3.3	386	0.000189
10	118.5	0.000058
33	3.5	0.000002
333	34.3	0.000017
1,000	26.5	0.000013

The duty cycle achieved was 50%, as shown in Figure 11 and Table 3.

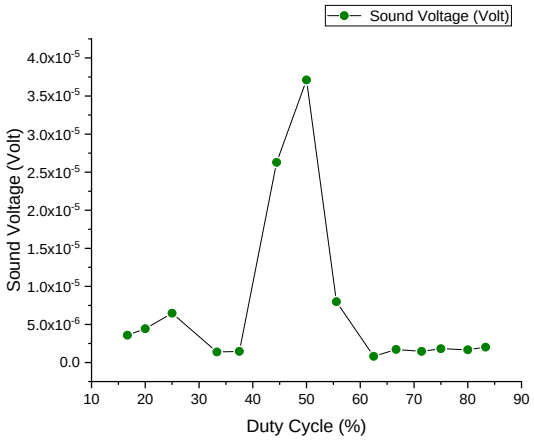

Figure 11. *Duty cycle curve of blue diode laser modulation.*

The background signal gotten was 0.00002 V/W. Figure 12 shows a graph of the background signal, and the experiment result can be seen in Table 4. The quality factor obtained is Q = 6.67.

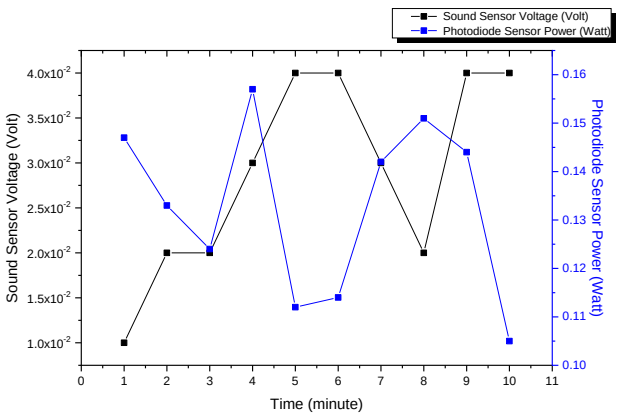

Figure 12. *Graph of the background signal.*

According to the experimental results, the resonant frequency obtained was 1,000 Hz. Figure 13 shows resonance curve, and the experiment result can be seen in Table 5. The maximum laser output power received by the photodiode is 0.193353 Watt. The airflow rate to the photoacoustic cell is 24 liters/hour.

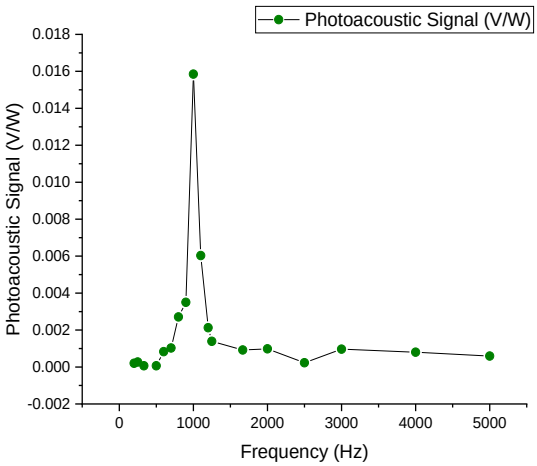

Figure 13. *Resonance curve.*

The lowest detection limit obtained at 250 mL volume was 0.00640 ppm or 6.40 ppb with a signal noise of 3.97 V/W or 0.011 V, and Table 6 shows the experiment result.

In detecting NO_2 gas from motor vehicle exhaust gases and campus air, Figures 14, 15, 16, 17, 18 and 19 show the experiment result of gas sample container from vehicle A for 1 minute take time, vehicle A for 2.5 minutes take time, vehicle B, vehicle C, vehicle D, and campus air respectively. The experiment result can be seen in Table 7.

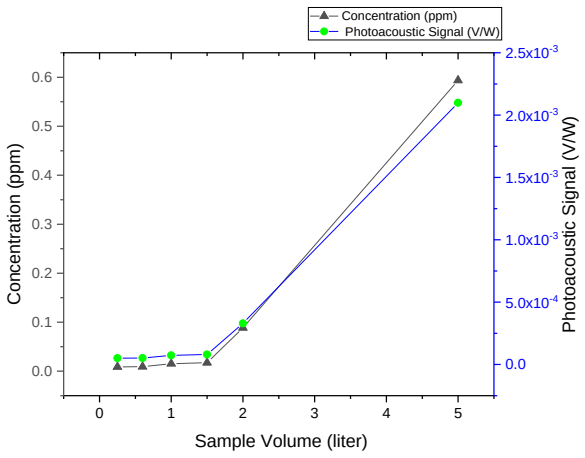

Figure 14. *NO_2 concentration curve for vehicle A (t = 1 minute).*

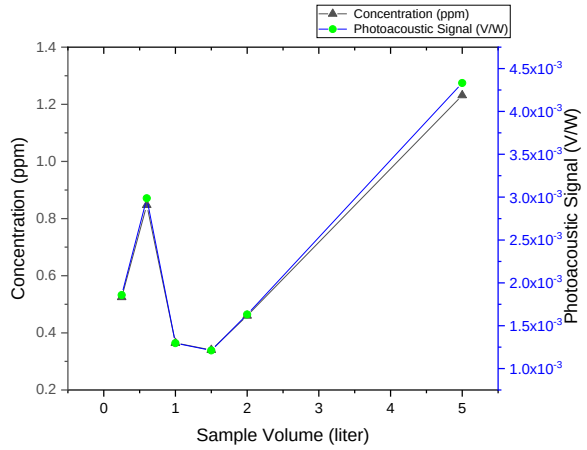

Figure 15. *NO_2 concentration curve for vehicle A (t = 2.5 minutes).*

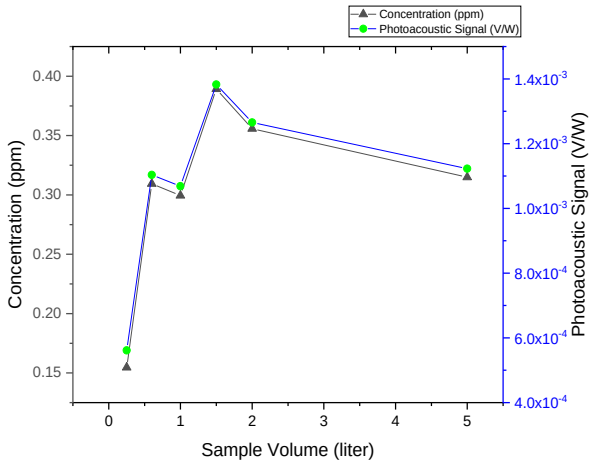

Figure 16. *The curve of the NO_2 concentration of vehicle B.*

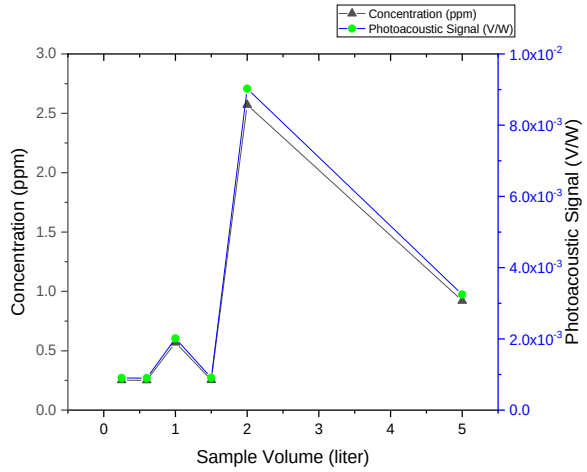

Figure 17. *The curve of NO_2 concentration for vehicle C.*

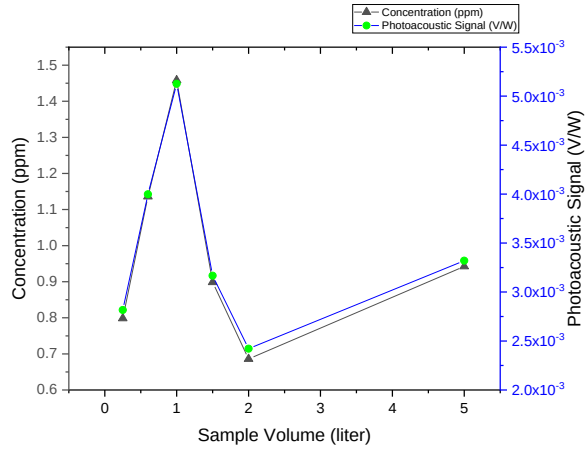

Figure 18. *The curve of NO_2 concentration for vehicle D.*

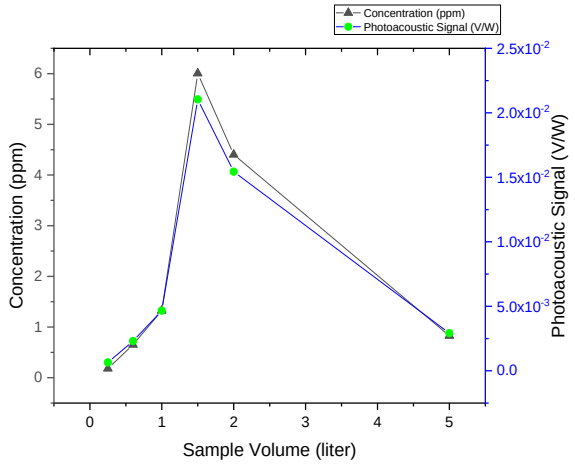

Figure 19. *The curve of air NO_2 concentration in the campus environment.*

3.2 Discussion

In using a photoacoustic spectrometer, the resonance curve is first determined to know what the maximum modulation frequency measurement is. Likewise, the amplification and the constant time of lock-in amplifier, and the blue diode laser duty cycle are determined in advance to maximize the photoacoustic signal.

The extra cavity blue diode laser photoacoustic spectrometer designed was successfully tested by detecting NO_2-containing gases from motor vehicle exhaust gases and the campus air. The extra cavity blue diode laser photoacoustic spectrometer utilizing Arduino Uno is used to measure the concentration of NO_2 gas in a gas sample whose performance can increase by increasing its sensitivity. The design and use of the right equipment can improve the accuracy of measurement. Optimization needs to be done to find the maximum measurement conditions.

The nitrogen dioxide concentration in each sample shows the number of NO_2 molecules accommodated in each sample. In taking campus environment air, the sample air was taken in the night to avoid the dissociation effect. From the calculations using achieved photoacoustic signals, larger volumes of gas show a tendency to increase in concentration even though some are decreasing.

From the analysis of the variables needed to determine the concentration, these variables have increased, and some have decreased, especially in the sound sensor voltage and photodiode power. The final concentration result is that it generally increases. The estimation is that NO_2 gas breaks out during sampling from the concentration decrease undergone in the measurement. The estimated cause is that the sampling process is still simple, so there is a possibility that NO_2 gas will come out when closing the container. Another factor is the possibility of frequent shifting of the equipment during sampling, which can change the laser and photodiode alignment position. The alignment that is less than the maximum can affect the measurement results. Another possibility is the number and the size of other exhaust gas types that dominate more than NO_2 occupying each container. The amount of NO_2 is surpassed by the number of other exhaust gases. PAS was arranged only to detect NO_2 gas.

From the six sample containers used, the 5-liter volume of the container often has the highest concentration calculation of the six types of sample sources. Likewise, the second-largest 2-liter container is always in second place even though it is in the first place with the most concentration. From these results, the greater container volume tends to have the greater concentration. In addition, the sample container that the time of the take from a vehicle is longer has NO_2 concentration higher.

The maximum measurement achieved by the blue diode laser PAS tool in this experiment is up to 6 ppm. This measurement has the lowest detection limit of 6.4 ppb. However, it is not so far from Ruck *et al*., in 2017, having a detection limit of 2.0 ppbV NO_2. The resonance frequency based on theory is 1,559 Hz, but the practical resonance frequency in this measurement was 1,000 Hz.

4. CONCLUSIONS:

It can be concluded that large gas sample storage containers tend to contain more significant NO_2. The concentration number tends to increase from small sample volumes to large sample volumes, although some have decreased. The decrease undergone is based on the estimation that some gases were wasted when the exhaust gas was entered into the container, and other exhaust gases surpassed NO_2. The maximum concentration obtained is six ppm. Paying attention to the take time of the sample is required in determining NO_2 concentration from a vehicle.

Arduino Uno can be used to modulate the beam of diode laser in replacing mechanic chopper. Optimation is needed by choosing the appropriate duty cycle and maximum frequency to achieve maximum measurement. The proper amplification and the proper constant time of lock-in amplifier must be chosen to get the maximum measurement.

This photoacoustic spectrometer with blue diode laser utilizing Arduino Uno can achieve low ppb levels for the measurement result. It is sensitive enough to detect gas. The experiment having been done can be more straightforward, more effortless, and low-cost. Modulation of the laser beam with Arduino Uno can be applied to detect other gases with different wavelengths and colors of laser using the photoacoustic spectrometer.

5. ACKNOWLEDGMENTS:

Thank you for Indonesia Endowment Fund For Education (LPDP) from the Finance Ministry of Republic Indonesia as the sponsor of this research.

6. REFERENCES:

1. Bageshwar, D. V, Pawar, A. S., Khanvilkar, V. V, and Kadam, V. J., 2010, Photoacoustic Spectroscopy and Its Applications–*A Tutorial Review, Eurasian Journal of Analytical Chemistry*,*5* (December 2009), 187–203, Retrieved from http://www.eurasianjournals.com/index.php/ejac/article/view/290.
2. Besson, J. P., and Thévenaz, L. (2006). Photoacoustic spectroscopy for multi-gas sensing using near infrared lasers. *Laboratoire de Nanophotonique et Métrologie*, *Ph.D.*(Thèse No. 3670 (2006)), 1–189. https://doi.org/10.5075/epfl-thesis-3670
3. Breitegger, P., Schweighofer, B., Wegleiter, H., Knoll, M., Lang, B., and Bergmann, A. (2020). Photoacoustics Towards low-cost QEPAS sensors for nitrogen dioxide

detection. *Photoacoustics*, *18*(March), 100169. https://doi.org/10.1016/j.pacs.2020.100169

4. Demtroder, W., 2002, *Laser Spectroscopy Volume 1 Basic Principle. Kaiserslauten* Germany: Springer.
5. Dong, Y., Gu, M., Zhu, G., Tan, T., Liu, K., and Gao, X. (2020). *Fully Integrated Photoacoustic NO 2 Sensor for Sub - ppb Level Measurement*. (2). https://doi.org/10.3390/s20051270
6. Elia, A., Lugarà, P. M., di Franco, C. and Spagnolo, V., 2009, Photoacoustic techniques for trace gas sensing based on semiconductor laser sources, *Sensors*, *9*(12), 9616–9628. https://doi.org/10.3390/s91209616.
7. Fuchs M., 2006, Development of a high power stabilized diode laser system, *Thesis.*US: University of Oregon, http://atomoptics-nas.uoregon.edu/publications/matthias-fuchs-thesis.pdf.
8. Gianfrani, L., Gagliardi, G., Pesce, G., and Sasso, A., 1997, High-sensitivity detection of NO_2 using a 740 nm semiconductor diode laser, *Applied Physics B-Lasers and Optics*, *64*(4), 487–491, https://doi.org/10.1007/s003400050204
9. Gong, Z., Gao, T., Chen, Y., Zhang, B., Peng, W., Yu, Q., and Chen, K. (2020). Journal of Quantitative Spectroscopy & Radiative Transfer Sub-ppb level detection of nitrogen dioxide based on an optimized H-type longitudinal acoustic resonator and a lock-in white-light interferometry demodulation algorithm. *Journal of Quantitative Spectroscopy and Radiative Transfer*, *253*(2), 107136. https://doi.org/10.1016/j.jqsrt.2020.107136
10. Grossel, A., Zéninari, V., Parvitte, B., Joly, L., and Courtois, D. (2007). Optimization of a compact photoacoustic quantum cascade laser spectrometer for atmospheric flux measurements: Application to the detection of methane and nitrous oxide. *Applied Physics B: Lasers and Optics*, *88*(3), 483–492. https://doi.org/10.1007/s00340-007-2719-2
11. Jiang, Y., Li, G., and Wang, J. (2016). Photoacoustic Compound Fire Alarm System for Detecting Particles and Carbon Monoxide in Smoke. *Fire Technology*, *52*(5), 1255–1269. https://doi.org/10.1007/s10694-015-0542-6.
12. Kalkman, J., and Van Kesteren, H. W., 2008, Relaxation effects and high sensitivity photoacoustic detection of NO_2 with a blue laser diode*, Applied Physics B: Lasers and Optics*, *90*(2), 197–200, https://doi.org/10.1007/s00340-007-2895-0.
13. Kapp, J., Weber, C., Schmitt, K., Pernau, H.-F., and Wöllenstein, J., 2019, Resonant Photoacoustic Spectroscopy of NO2 with a UV-LED Based Sensor, *Sensors*, https://doi.org/10.3390/s19030724
14. Mills, B., 2007, Nitrogen-dioxide-2D-dimensions, (https://commons.wikimedia.org/wiki/File:Nitrogen-dioxide-2D-dimensions.png., accessed on 05-09-2018).
15. Mitrayana, 2008, Rancang Bangun Spektrometer Fotoakustik dan Spektrometer Modulasi Panjang Gelombang Laser. Kajian Deteksi Gas Biomarker C_2H_4, C_3H_6O, NH_3, NO_2 dan NO dalam bidang Kedokteran, *Disertasi*, Yogyakarta: Universitas Gadjah Mada.
16. Mitrayana, Pierera, T., Persijn, S., Naus, H., and Rochmah, W., 2007, Diode-Laser Based Photo -Acoustic Spectroscopy in Atmospheric NO_2 Detection*, Berkala MIPA,* (2)*,* 21–26.
17. Mitrayana, Wasono, M.A.F., and Ikhsan, M.R. 2014, Spektroskopi Fotoakustik Laser dan Aplikasinya, Yogyakarta: Gadjah Mada University Press.
18. Mitrayana, Wasono, M.A.J. and Karno, 2011, Optimasi Spektrometer Fotoakustik Laser CO_2 dan Aplikasinya Dalam Pendeteksian Konsentrasi Etilen di Dalam Tanah, *Prosiding Pertemuan Ilmiah XXV HFI Jateng & DIY, ISSN 0853-0823*.
19. Pushkarsky, M., Tsekoun, A., Dunayevskiy, I. G., Go, R., and Patel, C. K. N., 2006, Sub-parts-per-billion level detection of NO_2 using room-temperature quantum cascade lasers, *Proceedings of the National Academy of Sciences*, *103*(29), 10846–10849, https://doi.org/10.1073/pnas.0604238103.
20. Nakamura, S., Pearton, S. and Fasol, G., 2000, *The Blue Laser Diode,* Berlin: Springer-Verlag.
21. Rakhmadi, F. A., Mitrayana and Shalihah, H., (2018), Design of Green Laser Modulation System Based on Arduino Uno Microcontroller, *AIP Conference Proceedings 2014, 20149* (September), https://doi.org/10.1063/1.5054553.

22. Rakhmadi, F. A., Mitrayana and Alifin, M.A.,(2019), Design of modulation frequency regulator to optimize the green laser photoacoustic spectroscopy, *AIP Conference Proceedings 2202, 020033,* (December), https://doi.org/10.1063/1.5141646.

23. Rück, T., Bierl, R., and Matysik, F.-M., 2017, Low-cost photoacoustic NO_2 trace gas monitoring at the pptV-level, *Sensors and Actuators A: Physical*, *263*(2), 501–509, https://doi.org/10.1016/j.sna.2017.06.036.

24. Rück, T., Bierl, R., and Matysik, F. M., 2017, Development and characterization of a laboratory setup for photoacoustic NO_2 determination based on the excitation of electronic $^2B_2$ and $^2B_1$ states using a low-cost semiconductor laser, *Sensors and Actuators, A: Physical*, *258*(2), 193–200, https://doi.org/10.1016/j.sna.2017.03.024.

25. Solihah, H., 2016, Rancang Bangun Sistem Modulasi Laser Hijau Berbasis Mikrokontroler Arduino Uno, *Skripsi*, Yogyakarta: Uin Sunan Kalijaga.

26. Slezak, V. (2001). High-precision pulsed photoacoustic spectroscopy in NO_2-N_2. *Applied Physics B: Lasers and Optics*, *73*(7), 751–755. https://doi.org/10.1007/s003400100686.

27. Wicaksono, 2017, Dasar Teori Arduino UNO R3, [pdf], (http://eprints.akakom.ac.id/3905/3/3_133310002_BABII., accessed on 21 Agustus 2018).

28. Widyaningrum, R., Gracea, R.S., Agustina, D., Mudjosemedi, M., and Mitrayana, 2017, Influence of Diode Laser Intensity Modulation on Photoacoustic Image Quality for Oral Soft Tissue Imaging, Yogyakarta: UGM, https://arxiv.org/ftp/arxiv/papers/1712/1712.01832.pdf.

29. World Health Organization (WHO), 2000, Chapter 7.1 Nitrogen dioxide, Air Quality Guidelines for Europe-*Second Edition, 3(2),* 175–180, Retrieved from http://www.euro.who.int/__data/assets/pdf_file/0017/123083/AQG2ndEd_7_1nitrogendioxide.pdf.

30. Yehya, F., and Chaudhary, A. K. (2012). Time-resolved time-dependent photoacoustic spectroscopy of NO_2 in a high frequency multi-resonant cavity. *Applied Physics B: Lasers and Optics*, *106*(4), 953–959. https://doi.org/10.1007/s00340-011-4815-6

31. Yi, H., Liu, K., Chen, W., Tan, T., Wang, L., and Gao, X., 2011, Application of a broadband blue laser diode to trace NO_2 detection using off-beam quartz-enhanced photoacoustic spectroscopy, *Optics Letters*, *36*(4), 481–483. https://doi.org/10.1364/OL.36.000481.

32. Yin, X., Dong, L., Wu, H., Zheng, H., Ma, W., Zhang, L., and Tittel, F. K., 2017, Sub-ppb nitrogen dioxide detection with a large linear dynamic range by use of a differential photoacoustic cell and a 3.5 W blue multimode diode laser*, Sensors and Actuators, B: Chemical*, *247*, 329–335. https://doi.org/10.1016/j.snb.2017.03.058.

33. Zharov, V.P., and Letokhov, V.S., 1986, Laser Optoacoustic Spectroscopy, Berlin: Springer-Verlag.

34. Zheng, H., Dong, L., Yin, X., Liu, X., Wu, H., Zhang, L., and Jia, S., 2015, Ppb-level QEPAS NO_2 sensor by use of electrical modulation cancellation method with a high power blue LED, *Sensors and Actuators, B: Chemical*, *208*(2), 173–179, https://doi.org/10.1016/j.snb.2014.11.015.

35. Zheng, H., Dong, L., Ma, Y., Wu, H., Liu, X., Yin, X., and Jia, S. (2016). Scattered light modulation cancellation method for sub-ppb-level NO_2 detection in a LD-excited QEPAS system. *Optics Express*, *24*(10), A752. https://doi.org/10.1364/OE.24.00A752

7. OPEN ACCESS:

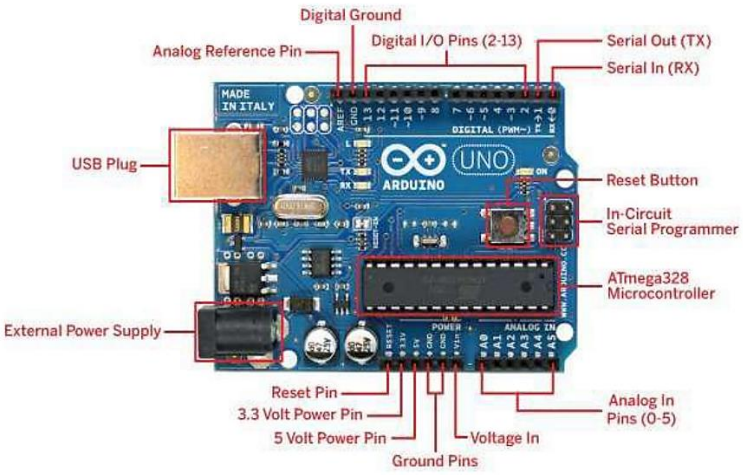

Figure 3. *Arduino Uno (Wicaksono, 2017).*

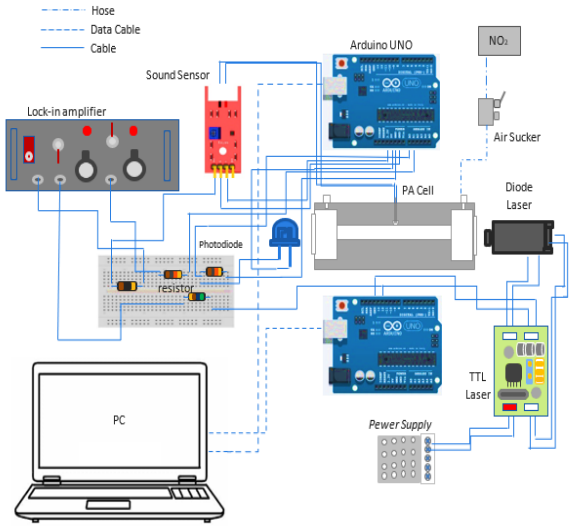

Figure 5. *Series of Tools.*

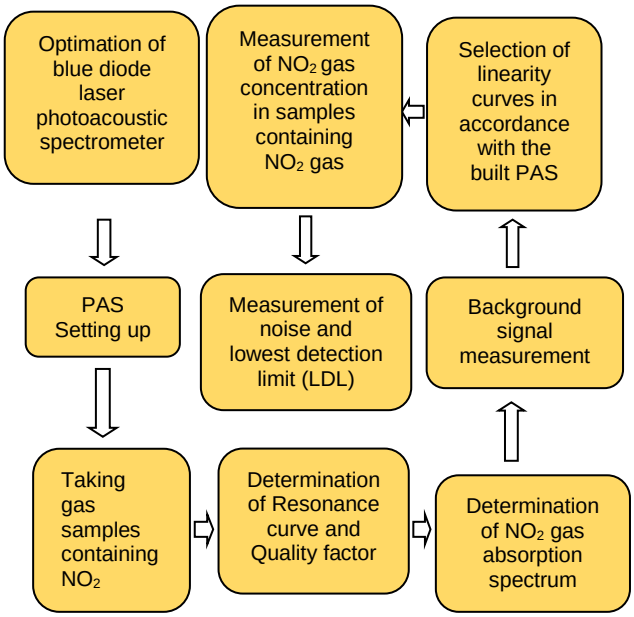

Figure 7. *Diagram of the research phase.*

Table 2. *Lock-In Amplifier Amplification.*

No	Lock-In Amplification (Time)	Sound Sensor Value (Bit)	Photodiode Sensor Value (Bit)	Photodiode Power (W)	Sound Sensor Voltage (V)	Photoacoustic Signal (V/W)
1.	1	150.3	970	0.1896	0.00007346	0.00038745
2.	10	40.5	970	0.1896	0.00001979	0.00010440
3.	50	138.25	970	0.1896	0.00000921	0.00004857
4.	100	55	971	0.1896	0.00002688	0.00014178
5.	200	89	970	0.1896	0.00004350	0.00022943
6.	1,000	169.67	970	0.1896	0.00008293	0.00043738
7.	10,000	319	970	0.1896	0.00015591	0.00082233

Table 3. *Blue Diode Laser Modulation Duty Cycle Curve.*

No	Duty Cycle	Photodide Sensor Value (Bit)	Sound Sensor Value (Bit)	Sound Sensor Voltage (Volt)
1.	16.67%	43.44444444	7.333333333	0.00000358
2.	20%	15.17647059	9.090909091	0.00000444
3.	25%	28	13.25	0.00000648
5.	33.33%	32.46666667	2.833333333	0.00000138
6.	37.50%	18.28571429	3	0.00000147
7.	44.44%	221.3658537	53.78333333	0.00002629
8.	50%	570	75.92941176	0.00003711
9.	55.56%	365.6842105	16.35416667	0.00000799
10.	62.50%	316.4285714	1.666666667	0.00000081
11.	66.67%	404.6666667	3.5	0.00000171
12.	71.42%	760.7826087	3	0.00000147
13.	75%	503.7241379	3.727272727	0.00000182
14.	80%	502.4310345	3.419354839	0.00000167
15.	83.33%	445.8	4.142857143	0.00000202

Table 4. *Background Signal*

Time (minute)	Sound Sensor Value (Bit)	Sound Voltage (Volt)	Photodiode Power (W)	Photodiode Sensor Value (Bit)
1	2	0.01	0.147	754.5
2	4	0.02	0.133	685
3	4	0.02	0.124	637
4	7	0.03	0.157	807
5	8	0.04	0.112	573
6	9	0.04	0.114	586
7	6	0.03	0.142	727
8	5	0.02	0.151	772
9	9	0.04	0.144	740
10	8	0.04	0.105	559

Background Signal = (0.029/0.1329)/10,000=0.21/10,000 V/W=0.00002 V/W

Table 5. *Resonance Curve.*

No	Frequency (Hz)	Photodiode Sensor Value (Bit)	Sound Sensor Value (Bit)	Photodiode Power (Watt)	Sound Voltage (V)	Photoacoustic Signal (V/W)
1.	200	65.822	5.359	0.01287	0.026192446	0.00020354
2.	250	64.226	6.941	0.01256	0.033925594	0.00027019
3.	333.33	364.9	9.949	0.07134	0.04862521	0.00006816
4.	500	468.45	11.932	0.09158	0.058319665	0.00006368
5.	600	21.909	7.273	0.00428	0.035546077	0.00082988
6.	700	21.333	8.75	0.00417	0.042766373	0.00102539
7.	800	20.667	22.385	0.00404	0.109406722	0.00270782
8.	900	14.476	20.2632	0.00283	0.099037917	0.00349939
9.	1000	551.455	357.667	0.10781	1.748126426	0.01585014
10.	1100	20.929	5.167	0.00410	0.025252525	0.00603303
11.	1200	14.333	12.2	0.00280	0.059628543	0.00212791
12.	1250	31.7436	17.684	0.00621	0.086433092	0.00139274
13	1666.67	68.833	25.364	0.01346	0.123966942	0.00092120
14.	2000	17.84	7	0.00349	0.034213099	0.00098094
15.	2500	229.75	21.4	0.04595	0.10459433	0.00022763
16.	3000	6.615	2.556	0.00129	0.012490496	0.00096576
17.	4000	9.385	3	0.00183	0.014662757	0.00079918
18.	5000	77.5	18.364	0.01515	0.089753843	0.00059238

Table 6. *Noise Signal and Lowest Detection limit*

No	Photodiode Sensor Value (Bit)	Sound Sensor Value (Bit)	Photodiode Volatge (V)	Photodiode Power (W)	Sound Voltage (V)	Photoacoustic Signal (V/W)
1.	88.2167	3.0976	0.4312	0.0172	0.01514	0.8778
2.	14.1765	2.25	0.0693	0.0028	0.011	3.9678

Table 7. *Concentration Calculation of measurement samples*

Type	Sample (L)	PD Sensor Value (Bit)	Sound Sensor Value (Bit)	PD Power (W)	Sound Voltage (V)	PA Signal (V/W)	Concentration (ppm)
Vega (A) t=60 s	0.25	557.100	11.333	0.1089	0.000006	0.000051	0.0088
	0.6	757.025	15.706	0.1480	0.000008	0.000052	0.0091
	1	531.630	15.630	0.1039	0.000008	0.000074	0.0153
	1.5	584.630	18.841	0.1143	0.000009	0.000081	0.0173
	2	563.060	74.300	0.1101	0.000036	0.000330	0.0885
	5	15.000	12.592	0.0029	0.000006	0.002099	0.5937

Vega (A) t=150 s	0.25	3.172	2.357	0.0006	0.000001	0.001858	0.5248
	0.6	4.261	5.091	0.0008	0.000002	0.002987	0.8474
	1	5.631	2.920	0.0011	0.000001	0.001296	0.3646
	1.5	6.828	3.308	0.0013	0.000002	0.001211	0.3402
	2	6.427	4.191	0.0013	0.000002	0.001630	0.4599
	5	5.825	10.091	0.0011	0.000005	0.004331	1.2313
Versa (B)	0.25	23.533	5.283	0.0046	0.000003	0.000561	0.1546
	0.6	21.567	9.519	0.0042	0.000005	0.001103	0.3094
	1	24.200	10.345	0.0047	0.000005	0.001069	0.2995
	1.5	14.638	8.096	0.0029	0.000004	0.001383	0.3892
	2	15.689	7.942	0.0031	0.000004	0.001266	0.3557
	5	14.673	6.590	0.0029	0.000003	0.001123	0.3149
Tiger (C)	0.25	10.672	3.847	0.0021	0.000002	0.000901	0.2517
	0.6	8.098	2.909	0.0016	0.000001	0.000898	0.2508
	1	7.551	6.077	0.0015	0.000003	0.002012	0.5689
	1.5	11.400	4.143	0.0022	0.000002	0.000909	0.2538
	2	4.828	17.429	0.0009	0.000009	0.009025	2.5717
	5	7.333	6.333	0.0014	0.000005	0.003245	0.9210
Force (D)	0.25	6.500	7.322	0.0013	0.000004	0.002816	0.7986
	0.6	4.475	7.155	0.0009	0.000003	0.003998	1.1360
	1	4.885	10.016	0.0010	0.000005	0.005126	1.4582
	1.5	4.250	5.383	0.0008	0.000003	0.003167	0.8987
	2	5.571	5.397	0.0011	0.000003	0.002422	0.6859
	5	5.587	7.419	0.0011	0.000004	0.003320	0.9424
Campus Environment Air	0.25	11.492	3.000	0.0022	0.000001	0.000653	0.1807
	0.6	4.567	4.212	0.0009	0.000002	0.002306	0.6528
	1	5.689	10.607	0.0011	0.000005	0.004661	1.3256
	1.5	13.741	115.667	0.0027	0.000057	0.021043	6.0043
	2	11.032	68.111	0.0022	0.000033	0.015435	4.4026
	5	5.016	5.862	0.0010	0.000003	0.002922	0.8287

PERIÓDICO TCHÊ QUÍMICA
ARTIGO ORIGINAL

CONHECIMENTO E ATITUDES SOBRE QUESTÕES ÉTICAS E MEDICOLEGAIS NO TRATAMENTO DA PANDEMIA DE COVID-19 ENTRE MÉDICOS RESIDENTES NO HOSPITAL ZAINOEL ABIDIN, ACEH, INDONÉSIA

KNOWLEDGE AND ATTITUDES REGARDING ETHICAL AND MEDICOLEGAL ISSUES IN HANDLING THE COVID-19 PANDEMIC AMONG RESIDENT DOCTORS AT ZAINOEL ABIDIN HOSPITAL, ACEH, INDONESIA

PENGETAHUAN DAN SIKAP MENGENAI ISU-ISU ETIKA DAN MEDIKOLEGAL DALAM PENANGANAN PANDEMI COVID-19 DI KALANGAN DOKTER RESIDEN PADA RUMAH SAKIT ZAINOEL ABIDIN, ACEH, INDONESIA

SURYADI, Taufik[1*]; SUARDI, Hijra Novia[2]; ZAIN, Hanifah[3]; HAYATI, Zinatul[4]; YANTI, Budi[5]

[1] Department of Forensic Medicine and Medicolegal, Faculty of Medicine, Universitas Syiah Kuala, Indonesia.

[2] Department of Pharmacology, Faculty of Medicine, Universitas Syiah Kuala, Indonesia.

[3] Medical Student, Faculty of Medicine, Universitas Syiah Kuala, Indonesia.

[4] Department of Microbiology, Faculty of Medicine, Universitas Syiah Kuala, Indonesia.

[5] Department of Pulmonology and Respiratory Medicine, Faculty of Medicine, Universitas Syiah Kuala, Indonesia.

** Corresponding author*
e-mail: taufiksuryadi@unsyiah.ac.id

Received 09 March 2021; received in revised form 05 June 2021; accepted 24 June 2021

RESUMO

Introdução: A doença coronavírus 2019 (COVID-19) se espalhou pelo mundo e se tornou uma pandemia, deixando todo o setor de saúde sobrecarregado. Os hospitais, como instalações de serviços de saúde, se esforçam continuamente para fornecer um serviço ideal aos pacientes com infecção confirmada por COVID-19. Os pacientes com COVID-19 no Hospital Zainoel Abidin (ZAH) são geralmente atendidos por médicos residentes. Como a linha de frente no tratamento da pandemia de COVID-19, esses médicos residentes devem ter conhecimento adequado e boas atitudes no tratamento de pacientes com COVID-19, especialmente no que diz respeito à ética e médico-legal. **Objetivo:** o objetivo deste estudo é conhecer o nível de conhecimento e as atitudes dos médicos residentes no enfrentamento da pandemia de COVID-19 no ZAH, Aceh. **Métodos:** Trata-se de um estudo transversal realizado entre médicos residentes (n = 80) do ZAH no período de novembro a dezembro de 2020 com questionário online autoaplicável. A validade foi testada por especialistas com Índice de Validade de Conteúdo / CVR de 0,738 e confiabilidade de 0,732. Os dados foram analisados por meio do teste de distribuição de frequência (univariada) e do teste de correlação do Qui quadrado (bivariada). **Resultados e Discussão:** Os resultados mostram que a maioria dos entrevistados tinha conhecimento inadequado sobre questões éticas e médico-legais no manejo da pandemia de COVID-19 (70,0%); no entanto, tiveram atitude positiva na superação de questões éticas e médico-legais, ou seja, 77,5%. O resultado do teste estatístico Qui-quadrado mostra que não houve correlação entre conhecimento e atitude com p-valor de 0,077 (p-valor> 0,05). **Conclusões:** Conclui-se, portanto, que o conhecimento teórico dos médicos não foi suficiente para identificar as questões éticas e médico-legais, mas a atitude no trato das questões éticas e médico-legais foi satisfatória. Este resultado oferece uma nova oportunidade e desafio para aumentar a consciência dos médicos na aplicação de seus conhecimentos e atitudes para lidar com a pandemia COVID-19.

Palavras-chave: *COVID-19, ética, médico-legal, conhecimento, atitude*

ABSTRACT

Background: Coronavirus Disease 2019 (COVID-19) has spread throughout the world to become a pandemic, making the entire health sector overwhelmed. Hospitals as health service facilities continuously strive to provide

DOI: 10.52571/PTQ.v18.n38.2021.06_SURYADI_pgs_62_84.pdf

optimal service to patients with the confirmed COVID-19 infection. Resident doctors usually handle COVID-19 patients at the Zainoel Abidin Hospital (ZAH). As the front liner in handling the COVID-19 pandemic, these resident doctors must have adequate knowledge and good attitudes in dealing with COVID-19 patients, especially regarding ethical and medicolegal. **Aim:** This study aims at finding out the level of knowledge and attitudes of resident doctors in dealing with the COVID-19 pandemic at the ZAH, Aceh. **Methods:** This was a cross sectional study conducted among resident doctors (n=80) in the ZAH during November-December 2020 with a self-administered online questionnaire. It had been tested for validity by experts with a Content Validity Ratio / CVR of 0.738 and reliability of 0.732. The data were analyzed using the frequency distribution test (univariate) and the Chi square correlation test (bivariate). **Results and Discussion**: The results show that the majority of respondents had inadequate knowledge of ethical and medicolegal issues in handling the COVID-19 pandemic (70.0%); however, they had a positive attitude in overcoming ethical and medicolegal issues, i.e.77.5%. The chi square statistical test result shows no correlation between knowledge and attitude with a p-value of 0.077 (p-value >0.05). **Conclusions:** Therefore, it can be concluded that the theoretical knowledge of doctors was not sufficient to identify ethical and medicolegal issues, but the attitude in dealing with ethical and medicolegal issues was satisfactory. This result offers a new opportunity and challenge to increase the awareness of doctors in applying their knowledge and attitudes towards handling the COVID-19 pandemic.

Keyword: *COVID-19, ethical, medicolegal, knowledge, attitude*

ABSTRAK

Pendahuluan: Coronavirus Disease 2019 (COVID-19) saat ini merupakan penyakit yang tersebar ke seluruh dunia sehingga menjadi pandemi. Seluruh sektor kesehatan kewalahan menghadapi pandemi ini. Rumah sakit sebagai sarana pelayanan kesehatan terus menerus berupaya memberikan pelayanan optimal pada pasien terkonfirmasi COVID-19. Penanganan pasien COVID-19 di Rumah Sakit Zainoel Abidin (RSZA) biasanya dilakukan oleh dokter residen. Sebagai garda terdepan dalam menghadapi pandemi COVID-19, dokter tersebut harus memiliki kesadaran akan pengetahuan dan sikap yang tinggi dalam menangani pasien COVID-19 terutama terkait masalah dan tantangan etika dan medicolegal. **Tujuan:** Penelitian ini bertujuan untuk mengetahui gambaran tingkat pengetahuan dan sikap dokter residen dalam menghadapi pandemi COVID-19 di RSZA. **Metode:** Ini adalah studi cross sectional yang dilakukan pada dokter residen (n = 80) di RSZA selama November-Desember 2020 dengan kuesioner online yang diberikan sendiri. Yang telah diuji validitas oleh para ahli dengan Content Validity Ratio/CVR sebesar 0.738 dan reabilitas 0.732. Analisis yang digunakan adalah uji distribusi frekuensi (univariat) dan uji korelasi Chi square (bivariat). **Hasil dan Pembahasan:** Hasil penilitian didapatkan mayoritas responden memiliki pengetahuan yang terbatas tentang isu etika dan medicolegal terkait penanganan pandemi COVID-19 (70.0%), namun mempunyai sikap yang positif dalam mengatasi isu etika dan medikolegal tersebut yaitu sebanyak 77.5%. Berdasarkan hasil uji statistic Chi square menunjukkan tidak ada korelasi antara pengetahuan dan sikap dengan nilai p sebesar 0.077 (p-value>0.05). **Kesimpulan:** Pengetahuan teoritis dokter residen belum memadai untuk mengidentifikasi isu etika dan medikolegal, namun sikap dalam menghadapi isu etika dan medikolegal cukup memuaskan. Hal ini merupakan peluang dan tantangan baru untuk meningkatkan kesadaran dokter dalam mengimplementasikan pengetahuan dan sikapnya terhadap penanganan pandemi COVID-19.

Kata kunci: *COVID-19, etika, medicolegal, pengetahuan, sikap*

1. INTRODUCTION:

Severe Acute Respiratory Syndrome Coronavirus 2 (SARS-CoV-2), which was originally named novel coronavirus or 2019-nCoV, is one of the single-stranded RNA viruses of the seven coronaviridae - 229E, OC43, NL63, HKU1, Severe Acute Respiratory Syndrome Coronavirus (SARS-CoV), and Middle East Respiratory Syndrome (MERS-CoV) - which are known to infect humans (Nicola *et al*., 2020; Wu *et al*., 2020). On 11 February, WHO announced that the epidemic disease was caused by 2019-nCoV: coronavirus disease (COVID-19). Regarding the name of the virus, the International Committee on Taxonomy of Viruses has changed the name of the virus from 2019-nCoV to Severe Acute Respiratory Syndrome Coronavirus-2 (SARS-CoV-2) and the name of the disease as Coronavirus disease 2019 (COVID-19) (Lai *et al*., 2020; Wang *et al*., 2020; World Health Organization, 2020). The COVID-19 was declared a pandemic on 11 March 2020 by the World Health Organization (WHO). Currently, the COVID-19 pandemic is the biggest challenge for the health sector worldwide (McGuire *et al*., 2020).

To date, 216 countries have contracted the SARS-CoV-2 virus according to data from the Task Force for the Acceleration of Handling COVID-19 of the Republic of Indonesia as of 21 August, 2020. COVID-19 is a contagious disease

that can spread directly or indirectly, from one person to another. This has led the Indonesian government to implement a strict policy to break the chain of its spread. The spike in COVID-19 cases has overwhelmed health systems worldwide, including Indonesia, which declared the COVID-19 as a national disaster on 14 March 2020.

The condition of the COVID-19 pandemic has created several ethical challenges in the form of a lack of public trust in the existence of this outbreak due to a lack of knowledge and public awareness of the dangers of the virus, which has claimed many human lives (Asghari and Tehrani, 2020). Several efforts to control the spread of COVID-19 have been carried out in various ways, for example, limiting large-scale social activities, social distancing, travel restrictions, quarantine, and lockdown (Xafis *et al*., 2020).

In preventing the spread of the COVID-19 pandemic in some areas, there may still be an inability to meet facilities and infrastructure needs. The obstacles that often occur in hospitals are the lack of hospital beds, limited staff, medicines, and equipment. Along with the increasing number of COVID-19 cases, the allocation criteria for using sophisticated medical devices such as ventilators are widely discussed. In making decisions about resource allocation, a priority scale is needed by assessing the balance between benefits and risks and looking at the probability of recovery from patients (Robert *et al*., 2020).

The COVID-19 pandemic has caused various problems, both medical and ethical-medicolegal. It is always emphasized that a doctor maintains ethical competence, morals, and medical professionalism. Considering the significance of doctor knowledge on ethical and medicolegal issues in dealing with the COVID-19 pandemic, research on this topic is essential. In this study, the ethical and medicolegal issues discussed are diagnostic and therapeutic, allocation of resources, facilities and infrastructure, and delivery of personal information for COVID-19 patients (Asghari and Tehrani, 2020; Huxtable, 2020; Yusof *et al.*, 2020; McGuire. *et al.*, 2020).

Doctors who are currently undergoing specialization education (often referred to as resident doctors in Indonesia) are the frontline health service providers in dealing with COVID-19 patients. Resident doctors inevitably have to study issues related to the COVID-19 pandemic; however, they should not rule out medical ethics because many issues related to medical ethics are developing in the midst of society. Therefore, resident doctors must identify issues of medical ethics as a means of fulfilling their competence in the field of noble professionalism of the medical profession (IMC, 2019).

Based on the 2019 National Standards for Indonesian Medical Professional Education compiled by the Indonesian Medical Council (IMC), there are nine expected graduate profiles, one of which is to fulfill noble professional competencies, namely being able to carry out professional medical practice following the values and principles of Godliness, noble morals, ethics, discipline, law, socio-culture, and religion in local, regional and global contexts in managing health problems of individuals, families, and communities (IMC, 2019). The medical profession emphasizes ethical competence, morals and medical professionalism. This is because this competence will support the participation of health workers in patient safety, which is central to better medical services (Kusumaningtyas and Hermasari, 2017).

Medical practice is closely related to ethics and medicolegal. In line with the times, ethics and medicolegal have become an inseparable part of medicine because it will guarantee a good doctor-patient relationship. On the other hand, some consequences must be faced if there is dissatisfaction on the side of the patient, which can cause the patient to sue the doctor. Resident doctors are guarded by a medical code of ethics and laws that always guide their practice (Taufan, 2019; Afandi *et al.*, 2010).

There are four ethical principles, namely: (1) Autonomy, which is recognizing the right of individuals to make their own decisions for what is best for themselves, (2) Beneficence, which describes the principle of doing good, showing goodness (demonstrating kindness), showing affection (showing compassion), and helping others, (3) Non-maleficence, which is an ethical principle that requires doctors (caregivers) to avoid things which can endanger patients, and (4) Justice, which is an obligation to be fair in the distribution of benefits and risks. Justice demands that people in the same condition be treated equally (Pozgar, 2020; Afandi, 2017).

These principles have a profound effect, not only in the field of medical ethics academically but also in their application in clinical situations to making ethical clinical decisions (Henky, 2018). Medical ethics will enable physicians to make a difference, recognize difficult situations and go through them properly according to ethical and medicolegal principles.

Significantly, a study is conducted to assess the knowledge and attitudes of resident doctors at the Zainoel Abidin Hospital (ZAH) regarding ethical and medicolegal issues in handling the COVID-19 pandemic. Therefore, the current research is intended to answer the following research questions: (1) what is the level of knowledge and attitudes of resident doctors at ZAH regarding ethical and medicolegal issues in handling the COVID-19 pandemic? (2) Is there a relationship between knowledge and attitudes of resident doctors regarding ethical and medicolegal issues in handling the COVID-19 pandemic?

Thus, this study aimed to obtain information about resident doctors knowledge and attitudes regarding ethics and medicolegal issues in handling the COVID-19 pandemic at ZAH, Aceh, Indonesia.

2. MATERIALS AND METHODS:

2.1. Design and research subjects

This research falls under an observational with a cross-sectional design. The population in this study was 394 resident doctors who were pursuing a specialization education from 2016-2020 at the ZAH. In this study, the sample size was determined using the Slovin equation 1 as follows:

$$n = \frac{N}{1+N(d^2)} \qquad \text{(Eq.1)}$$

where: N: Total population, n: Number of samples, d: Percentage of error rate in research (10%), with the following calculations:

$$n = \frac{N}{1 + N\,(d^2)}$$
$$n = \frac{394}{1 + 394(0{,}1^2)}$$
$$n = \frac{394}{1 + 394(0{,}01)}$$
$$n = \frac{394}{4.94} = 79{,}7 \approx 80$$

The minimum sample size used in the study based on the Slovin equation was 80 respondents. Respondents who participated in this study were resident doctors who met the inclusion criteria. The sampling technique used in this study was non-probability sampling (consecutive sampling), namely sampling by dividing a population into strata, selecting a simple random sample from each stratum, combining it into the sample to determine population parameters. The calculation of the number of samples per stratum uses the following equation 2:

$$n = \frac{\Sigma\ per\ department}{\Sigma\ total\ population}\, x\ number\ of\ sampels \qquad \text{(Eq.2)}$$

Inclusion Criteria:1) registered and active as a resident doctor of medical faculty, Universitas Syiah Kuala, 2) have been a resident doctor for at least six months, 3) have handled COVID-19 patients. Exclusion Criteria: 1) resident doctor taking academic leave, 2) resident doctor who is currently receiving an academic sanction.

2.2. Instruments

The instrument used is an online questionnaire (google form) (see appendix) which has been tested for validity using a Content Validity Ratio/CVR by experts. The CVR validity test was conducted from 17 July to 12 August 2020. The assessment of each questionnaire item involved nine panelists consisting of 5 bioethicists and four medical experts in handling COVID-19. The average result of the CVR value was 0.738. The reliability test was conducted on 8 - 10 September 2020. The reliability test involved ten respondents. The results show that the Cronbach coefficient of the validated questionnaire is 0.732. This value meets the reliability requirements because it is higher than 0.70. From this CVR value, it can be concluded that the level of the instrument content validity is high level (Suryadi and Kulsum, 2020).

2.3. Procedure of data collection

Before collecting the data, the researchers explained the purpose of the study, the benefits of the research, and how to fill out the questionnaire, and respondents who participated in the study were voluntary. All respondents agreed to participate in the study by signing the consent sheet in Google form before answering the questionnaire.

This study used primary data collected using an online questionnaire (APPENDIX 1) delivered through Google Forms, which was prepared by researchers and distributed via social media by enumerators to help gather resident doctors in filling out the questionnaire. The data collection began on 26 November and concluded on 31 December 2020. All respondents completed the questionnaire independently. The questionnaire consists of doctors knowledge (29 statements: S1-S29), and attitudes related to ethical and medicolegal issues (29 statements:

S1-S29).

Knowledge is a respondent ability to identify the ethical principles of medicine (autonomy, beneficence, non-maleficence, and justice) related to ethical and medicolegal in handling the COVID-19 pandemic. Respondents were asked to determine which basic ethical principles are included in the statements in the questionnaire. The measurement scale used was an ordinal scale, and the categories were divided into good and less using the Guttman scale. Each correct answer was assigned a value of one, and the wrong answer was assigned a score of zero (Saryono, 2011). The criteria for assessing respondent knowledge were determined using the cut-off point method, namely by determining the cut-off point of the variable with the equation 3 (Sitorus *et al*., 2018).

Attitude is a response or what a respondent does to ethical and medicolegal issues in handling the COVID-19 pandemic as measured by asking the respondent's opinion. Respondents were asked to determine the attitude they take on the statements in the questionnaire. Statement items were similar to those in the knowledge variable. Attitude was measured using a 5-point Likert scale (5 = strongly agree to 1 = strongly disagree). After the data were collected, the answers were grouped into two categories: the agree group consisting of answers strongly agree and agree and disagree group consisting of answers to doubtful, disagree, and strongly disagree. The measurement scale used was ordinal, and the categories of which were divided into right and wrong. The criteria for assessing the respondent's attitude were determined using the cut-off point method, namely by determining the cut-off point of the variable with equation 3 (Sitorus *et al*., 2018).

$$\text{Natural cut} - \text{off point} = \frac{(\max \text{score} - \min \text{score})}{2} \quad \text{(Eq.3)}$$

2.4. Data analysis

This study used a univariate and bivariate data analysis to describe each variable. Descriptive statistics were used to describe the characteristics of respondents, the knowledge, and attitudes of doctors related to ethical and medicolegal issues. The correlation between knowledge and attitudes was determined by using the Chi square's test at 90% confidence intervals, at the significance level of 0.05. The data were processed and analyzed by using SPSS version 22.

2.5. Ethical statement

This study was approved by the Health research ethics committee at the Medical Faculty of Universitas Syiah Kuala / Zainoel Abidin Hospital No. 281/EA/FK-RSUDZA/2020.

3. RESULTS AND DISCUSSION:

3.1. Results

3.1.1 General characteristics of research subjects

This study involved 80 resident doctors who met the inclusion criteria. Data collection was carried out from 26 November to 31 December 2020 using an online questionnaire distributed directly to resident doctors at ZAH Aceh. Table 1 shows the general characteristics of the respondents.

Table 1. *General characteristics of respondents*

Characteristics	Frequency (N=80)	Percentage (%)
Sex		
Male	44	55%
Female	36	45%
Age (years)		
26-27	4	5%
28-29	9	11%
30-31	17	21.3%
32-33	22	27.5%
34-35	14	17.5%
36-37	14	17.5%
Study Program		
Surgery	7	8.8%
Internal medicine	18	22.5%
Obstetrics and Gynecology	15	18.8%
Pediatrics	10	12.5%
Neurology	10	12.5%
Pulmonology	2	2.5%
Oto-rhino-laryngology	7	8.8%
Anesthesiology	6	7.5%
Cardiology	5	6.3%

Based on Table 1, there were 80 respondents who participated in this study. There were 36 female respondents and 44 male respondents, and the majority of respondents were between 32 and 33 years old (27.5%). Most respondents were majoring in Internal Medicine and Obstetrics Gynecology, namely 18 respondents and 15 respondents respectively.

3.1.2 Doctor knowledge regarding medical ethical issues in handling the COVID-19 pandemic

The distribution of respondent answers can be seen in Table 2, which shows that the correct answer was the statement S14, which was answered correctly by 47 respondents (58.8%), and the statement S4, answered correctly by 45 respondents (56.3%). Statements that had been validated consisting of 29 points were answered with one of the four basic rules of medical ethics (Suryadi and Kulsum, 2020). The answer to the statement was based on the four basic principles of medical ethics, namely beneficence, non-maleficence, autonomy, and justice, with the characteristics of each basic ethical principle.

The results show that the highest score for knowledge was 21 and the lowest was 4 (out of 29), so based on the natural cut-off point, the cut-off point was determined to be 8.5. Based on this calculation, it was considered good knowledge if the score was between 12.6 and 21, while limited knowledge is concluded when the score was between 4 and 12.5.

Table 3. *Distribution of analysis of doctors knowledge on issues of medical ethics and medicolegal in handling the COVID-19 pandemic*

Knowledge	Frequency (N=80)	Percentage (%)
Good	24	30%
Limited	56	70%

Table 3 shows that as many as 56 respondents (70%) had limited knowledge of medical ethics and medicolegal issues in handling the COVID-19.

3.1.3 Doctor attitudes regarding ethical and medicolegal issues in handling the COVID-19 pandemic

Based on the research results on respondent attitudes towards ethical and medicolegal issues related to handling the COVID-19, the distribution of respondents' answers is shown in Table 4. Answers to the attitudes that respondents should take are adjusted to the applicable laws in Indonesia, regulations of the minister of health of the Republic of Indonesia, and the Indonesian Medical Code of Ethics (IMCE) compiled by the Medical Ethics Honors Council (MEHC) in 2012.

The results show that the highest score for attitude was 25 and the lowest one was 10 (out of 29), so the cut-off point was 7.5, based on the natural cut-off point. From this calculation, the attitude is considered a positive attitude if the score is between 17.6 and 25, and it is negative if the score is between 10 and 17.5.

Table 5 shows that 62 respondents (77.5%) had a positive attitude regarding medical ethics issues in handling COVID-19.

Table 5. *Distribution of analysis of doctors attitudes regarding ethics and medicolegal in handling the COVID-19*

Attitudes	Frequency (N=80)	Percentage (%)
Positive	62	77.5%
Negative	18	22.5%

3.1.4 The relationship between doctor knowledge and attitudes regarding ethical and medicolegal issues in handling the COVID-19 pandemic

The distribution of the number and percentage of correct answers related to respondent knowledge and attitudes towards ethical and medicolegal issues in handling the COVID-19 pandemic can be seen in Table 6. Statistical analysis regarding relationship between doctor knowledge and attitudes regarding ethical and medicolegal issues in handling the COVID-19 pandemic using the Chi square test can be seen in Table 7.

Based on the data presented in Table 7, as many as 40 respondents with limited knowledge had positive attitudes, and 22 respondents (27.5%) had good knowledge and positive attitudes. In this study, the majority of respondents had limited knowledge of basic principles of ethics, namely 56 respondents (70%), but the majority of respondents had a positive attitude in dealing with ethical and medicolegal issues related to COVID-19, i.e.62 respondents (77.5%).

Based on the statistical data analysis there was no correlation between the respondent knowledge and attitudes regarding the ethical and medicolegal issues in handling COVID-19. The

Chi-square test results gave a p-value of 0.077 (p value >0.05).

3.2. Discussion

The following discusses the respondent knowledge of ethical and medicolegal issues based on basic principles of ethics and medicolegal consideration related to handling the COVID-19 pandemic as well as how a resident doctor behaves towards these ethical and medicolegal issues.

This study discusses several ethical and medicolegal issues related to handling COVID-19 such as protection when doing medical practice, keeping personal data and information, diagnostic and treatment, quarantine and isolation, discrimination and stigmatization, vaccination, resource allocation, and respecting individual rights.

3.2.1 Protection when doing medical practice

The statements S1, S2, S7, and S21 are related to protection while performing medical practice. The statement S1 reads, "Doctors who are not equipped with complete Personal protective Equipment (PPE) may refuse to examine patients who are suspected of having COVID-19". The statement P2 is "Doctors who are not equipped with PPE may refuse to treat patients suspected of having COVID-19". Finally, statement S7 is "Doctors, nurses and other health workers have the right to receive protection in the form of the use of complete PPE while working during the COVID-19 pandemic". The correct answers from the respondents for the knowledge category of each statement were S1 (26.3%), S2 (23.8%), S7 (21.3%), while for attitudes indicate S1 (92.5%), S2 (86.3%), S7 (91.3 %). The basic ethical principles for statements S1, S2, and S7 relate to beneficence.

The beneficence principle is the responsibility of doctors to take actions that benefit patients and support the moral role of protecting and defending the rights of others, preventing damage, eliminating conditions that can cause harm, helping people with disabilities, and saving people in danger (Varkey, 2020). In a medical context, general beneficence is defined as improving the patient's well-being (Papanikitas, 2013). According to Beuchamp and Childress, in general, the basics of beneficence aim to help people exceed their interests (Beuchamp and Childress, 2013).

Respondents did not realize that protection at work is included in the act of beneficence, namely preventing badness. Most respondents considered it non-maleficence, and this is expected because the principles of beneficence and non-maleficence in certain conditions are not easily differentiated. However, according to Beauchamp and Childress, the non-maleficence obligation is not to inflict evil or harm, while the consecutive beneficence obligations are to prevent evil or harm, to remove evil or harm, and to do or promote goodness (Beuchamp and Childress, 2013).

For statements of attitude related to statements S1, S2, and S7, most respondents had a positive attitude. Based on the Indonesian Medical Code of Ethics (IMCE) article 20 concerning the doctor's obligation to protect themselves, "Every doctor is always obliged to maintain his or her health so that he or she can work well" (MEHC, 2012). The objective of maintaining a doctor's health is to stay healthy while performing their duties, become a role model for patients and society, and prevent risks to patients that can be avoided (preventing transmission and preventing harm to patients) (MEHC,2012). For statements S1, S2 and S7 related to the Law of the Republic of Indonesia No. 36 of 2014 concerning health providers, article 57 letter d, the health providers in carrying out their practices receive protection for occupational safety and health (Law of Republic of Indonesia No.36, 2014).

The statement S21 reads, "The replacement of the doctor in charge of the patient, who provides care for COVID-19 patients is carried out regularly according to needs" The correct answers from the respondents for the knowledge (33.8%) and attitude (86.3%). The statement S21 is related to the justice principle. The term distributive justice refers to fair, equitable, and appropriate distribution in society determined by justified norms that structures the terms of social cooperation (Beuchamp and Childress, 2013).

Inadequate knowledge of the respondents regarding the S21 statement might be caused by confusion in distinguishing between the principles base of ethics, i.e., beneficence, non-maleficence, and justice principles. On the one hand, changing the guard duty is similar to beneficence because the goal is to prevent harm when the doctor is too tired. However, it can also be non-maleficence because working extra can harm the patient. However, in the context of the S21 statement, it is closer to the justice system for all doctors on duty, so the principle is justice.

According to the standard guidelines for doctor protection in the era of the COVID-19 pandemic, compiled by the Executive Board of the Indonesian Medical Association (IMA), doctors as one of the providers of COVID-19 services have an important meaning in handling COVID-19. With the determination of COVID-19 as a disease that can cause an epidemic, it is necessary to provide doctors as health workers with legal and social protection. Resident doctors as the front liners are at risk for various hazards, including exposure to pathogens, long working hours, psychosocial distress, fatigue, occupational burnout, and stigma (IMA, 2021).

According to IMCE, if the doctor in charge is absent, a replacement doctor who has a valid registration certificate and licenses to practice with the same competence as the doctor in charge of the patient can be appointed. In handling COVID-19 patients, doctors must be completely fit both physically and mentally. If they are not in mental and physical fitness, they should not take part in treating patients. One of the other professional attitudes of doctors is that doctors must take care of their health to avoid endangering themselves and their patients (MEHC,2012).

3.2.2 Keeping personal data and information

In this study, the statements of points S3, S4, and S26 are related to keeping personal data and information. The statement S3 is "Doctors may notify patient data to the general public to prevent the spread of COVID-19" In the statement S26 "Personal data of COVID-19 patients may be published". The correct answers from the respondents for the knowledge were 26.3%, and attitude was 56.3%. These statements are related to autonomy principle.

Autonomy means self-control. In essence, autonomy is the ability to 1) provide reasons and think about choices for themselves; 2) decide how to behave; and 3) to behave by decisions, without obstruction from others (Varkey, 2013). Autonomy is defined as the right to determine fate, and it is related to privacy, authority, freedom, and self-power. Respect for autonomy is an important ethical basis because this point emphasizes self-worth and trust and emphasizes that a person can determine what is best for himself or herself, even though his or her choice is detrimental to his health (Beuchamp and Childress, 2013; Manoppo, 2020).

In principle, doctors should not disseminate any information on COVID-19 patients because this is a medical confidentiality. The ethical aspect of confidentiality for COVID-19 patients is that there is a moral obligation in terms of preventing stigmatization, discrimination, and errors in disseminating information related to and related to COVID-19 (Yusof *et al.*, 2020). Ethical issues can arise from the process of health surveillance activities as a basic action in handling conditions The Covid-19 outbreak requires extensive patient data information. Patient identification information must be protected, and disclosure of medical information is limited to those relevant to tracing transmission. It is feared that this could lead to stigmatization in the community and increase the government difficulty in controlling the outbreak (Agustin *et al.*, 2020; Page, 2012). In pandemic conditions, the principle is to protect those who are most vulnerable (Coghlan *at al.*, 2020).

According to Agustin *et al.* transparency in providing health-related information needs to be done because handling the COVID-19 outbreak is currently an urgent matter, but in the process, patient identification information must be protected and the disclosure or publication of medical information is only limited to information relevant to tracing transmission (Agustin *et al*., 2020).

Legal aspects of patient confidentiality for COVID-19 states that every patient has the right to privacy and confidentiality of the illness, including medical data. This is regulated in Article 32 of Law Number 44 of 2009 concerning Hospitals, concerning patient rights and hospital obligations. Thus each hospital must keep medical secrets, which can only be disclosed for the benefit of patient health and to fulfill requests from law enforcement official with the patient's own consent (Law of Republic of Indonesia No.44, 2009).

The statement S4 states that "The doctor can ask the patient's travel history for tracing," Statement S4 was mostly answered correctly, i.e.45 respondents (56.3%). Based on the principle of beneficence, doctors are obliged to take actions that benefit patients and support a moral role to protect and defend the rights of others, prevent damage, and eliminate conditions that cause harm (Varkey, 2020). By asking about the patient's travel history, doctors can make early anticipations to anticipate losses that may occur, such as the transmission of the coronavirus to the people around them. In the Law of the Republic of Indonesia No. 29 of 2004 concerning medical practice, article 50c states that "In carrying out medical practice, doctors have the right to obtain complete and honest information from patients or their families (Law of Republic of Indonesia No.29, 2004).

3.2.3 Diagnostic and treatment

In statement S12, "A person with symptoms similar to COVID-19 without a swab result needs to undergo treatment for COVID-19" The correct answers from the respondents for the knowledge was 36.3% and 48.9% for the attitude. This statement is related to non-maleficence. In accordance with the principle of non-maleficence, the obligation to prevent injury to people is much stronger (Papanikitas, 2013).

To diagnose a corona virus infection, it is necessary, to begin with a history or medical interview. For this purpose, a doctor asks about the symptoms or complaints experienced by the patient. In addition, the doctor also performs a physical examination and blood tests to help make a diagnosis. The diagnosis of COVID-19 must be confirmed by reverse transcription-polymerase chain reaction (RT-PCR) or gene sequencing for respiratory or blood specimens as a critical indicator for hospitalization. Furthermore, the patient can do a Computerized Tomography (CT) scan or thorax photo (Susilo *et al*., 2020; Burhan *et al*., 2020).

When this article was prepared, there were no specific management recommendations for COVID-19 patients, including antivirals or vaccines. Management that could be done was symptomatic therapy and oxygen. In patients with respiratory failure, mechanical ventilation could be performed. China's National Health Commission (NHC) had studied several drugs that had the potential to overcome SARS-CoV-2 infection, including interferon-alpha (IFN-α), Lopinavir/Ritonavir, Ribavirin, Chloroquine phosphate, Remdesvir, and Umifenovir (Arbidol). In addition, several other antiviral drugs were being tested elsewhere (WHO, 2020; Burhan *et al*., 2020). Thus, patients who had symptoms similar to COVID-19 but had no PCR swab results did not need to be treated as COVID-19 patients.

The statement S19 is related to justice, i.e. "Patients with COVID-19 and not COVID-19 have the right to receive appropriate treatment according to their illness". The correct answer from the respondents for the knowledge was 42.5%and 47.5% for the attitude. Every individual has the right to get health services according to their medical needs (Wasisto *et al*., 2020). The principle of justice in a medical context demands equal rights to fair treatment in the health system. Every individual has the right to get health services according to their medical needs (Beuchamp and Childress, 2013; Manoppo, 2020).

The statement S23 states that "COVID-19 patients who have a history of comorbid diseases are prioritized to be hospitalized,", and the statement S24 reads "Patients with elderly COVID-19 are prioritized to get treatment at the hospital". Statement S23 and S24 are also related to justice. The principle of justice basically treats all patients the same, unless there are reasons for different treatment, for example choosing priority vulnerabilities based on age, gender, economic status or disease severity.

Justice is generally defined as treating someone fair, equal, and appropriate (Beuchamp and Childress, 2013). According to Aristotle, justice is more than just equality because someone can feel that they are not treated properly even though they have been treated the same. Beauchamp and Childress stated that the philosophical theory of justice related to the wholeness of one life applies throughout life. This theory is closely associated with being fair to others, such as who needs health assistance is first considered based on the severity of the disease (Afandi, 2017).

In statement S5, "Doctors give drugs circulating in the market to treat COVID-19 patients, and it is permissible even without going through the stage III clinical trial stage for the treatment of COVID-19 during the pandemic period". The statement S6 states that "Consumption of drugs circulating in the market to treat COVID-19 patients who are self-isolating in their living quarters is allowed even without a doctor's recommendation and has not passed stage III clinical trials to treat COVID-19 during the pandemic period". Statement P5 and P6 are related to goodwill.

The beneficence principle is the principle that prioritizes good deeds. In a medical context, beneficence means improving the patient's well-being. The principle of beneficence is the golden rule principle: to treat patients as they should commonly, where every medical practice must be compassionate, altruistic, full of kindness, and respect for human dignity (Mappaware *et al*., 2020).

In principle, COVID-19 treatment is usually given based on symptomatic, so it is allowed for the doctor to provide drugs on the market or for the patient to take over-the-counter medications without a doctor's recommendation as long as the patient feels the symptoms. In principle, all medicines sold in the market have gone through phase III clinical trials before being distributed to the public.

The statements S5 and S6 are related to the regulation of the Ministry of Health (MOH) Republic of Indonesia. According to the Ministry of Health (MOH) the Republic of Indonesia, drugs circulating in the market are divided into four groups: free drugs, limited free drugs, strong/psychotropic drugs, and narcotic drugs. Therefore, the administration of drugs must still be under the supervision of a doctor (MOH, 2007).

3.2.4 Quarantine and isolation

Statements S8, S9, S10, and S11 are related to quarantine and isolation. In statement S8, "Doctors can force someone who is in close contact with probable or confirmed to do self-isolation". Statement S8 is related to the principle of non-maleficence.

Non-maleficence is related to the Latin phrase *primum non nocere* which means “for the most part, do not cause harm/damage” (Varkey, 2020). This principle aims to protect individuals who are unable or individuals who do not have the ability to autonomy themselves. The beneficence principle also protects this individual. On the principle of non-maleficence, the obligation not to hurt others is much stronger than the obligation to do goodness (Beuchamp and Childress, 2013).

According to the Law of the Republic of Indonesia No. 6 of 2018, article 1 paragraph 6, quarantine is a limitation of activities and/or separation of a person who is exposed to an infectious disease even though he has not shown any symptoms or is in the temporary incubation phase. According to article 1 paragraph 7, isolation is the separation of sick people from healthy people, carried out in health facilities to get treatment and care. Self-isolation is carried out at home or a designated place. Based on article 3, the objective of quarantine is to protect, prevent, and ward off diseases and public health risk factors that can cause public health emergencies. Based on article 9, everyone is obliged to comply with and participate in implementing health quarantine (Law of Republic of Indonesia No. 6, 2018).

In statement 9, "Patients with suspicion or close contact with probable/ confirmed patients have the right to refuse to self-isolate". Statement P9 is related to the principle of autonomy. The principle of autonomy is related to equality and freedom of choice as the basis of the human rights paradigm. The principle of autonomy is defined as the right to make choices, which relates to the concepts of privacy, authority, freedom, and self-management. However, the rights and freedoms outlined in law can be limited by other laws for public order and the interests of the state (Ranasinghe *et al.*, 2020).

In the statement S10, "Suspected patients or patients who had a close contact with probable/confirmed patients who do not want to self-isolate may be forcibly picked up so as not to infect the people around them”, and statement S11 reads "A person who has been confirmed with COVID-19 and refuses to be treated can be forced to be isolated". Statements S10 and S11 are related to the principle of justice.

The principle of justice in the medical context refers to allocating or distributing resources to the population. This principle demands the same treatment in the health system. However, there is no single definite answer as to what is meant by fair and equal distribution. The possible answers are (Papanikitas, 2013): a) Equality - each person receives the available resources in equal proportion, b) Need - each person receives the appropriate resources according to how much someone needs them, c) Deserve - each person receives a resource based on how much they deserve it (in terms of contribution, effort, or worth it or not), and d) Desire - everyone got what they wanted.

3.2.5 Discrimination and stigmatization

In the statement S13, “People who reject COVID-19 patients in their environment commit ethical violations”. In statement S14, "People who reject the dead bodies of COVID-19 patients are violating ethics." Under the principle of justice, every individual must be treated fairly, equally, and properly (Papanikitas, 2013).

Based on the principle of justice, a person must be treated equally and cannot be discriminated (Afandi, 2017). This study is contrary to the principle of justice if there is unfair treatment due to discrimination and stigmatization from the surrounding community. Everyone must be given an understanding that everyone can be infected with COVID-19. An explanation must be conveyed to the public that COVID-19 can affect anyone, and this disease is not a disgrace that the public must stigmatize. Therefore, what must be done in the community is to work hand in hand to reduce the risk of transmission by limiting activities outside the home, maintaining physical distance, wearing masks, and always washing hands (Xafis *et al.*, 2020). Thus, after the public understands that discriminatory actions against patients or bodies confirmed to have COVID-19 can harm themselves because they may become the next

patient. Thus, the most important thing for society is to treat other people the way they want to be treated.

3.2.6 Vaccination

In statement S15, "Phase III COVID-19 vaccine trials may be carried out directly on humans". Statement point S15 states that most respondents answered correctly, namely 33 respondents (41.3%). In this study, statement S15 is related to the principle of non-maleficence.

Statement number S15 reads "Clinical trials of the COVID-19 vaccine phase III may be carried out directly on humans". Like clinical trials of drugs, clinical trials of vaccines are conducted to test safety, immunogenicity, and tolerability. Preclinical trials use experimental animals, while phase III clinical trials include human subjects. The implementation of clinical trials of drugs or vaccines is based on the Declaration of Helsinki (CIOMS, 2016).

Before clinical trials in humans are carried out, preclinical trials are carried out on experimental animals to gather information on toxicity and activity testing. The toxicity test results provide information related to the safety level of a substance/material in experimental animals or other biological substances before the substance/ material is used in clinical trials. Meanwhile, the activity test (efficacy) provides information regarding the correctness of the effectiveness of a test material that is scientifically proven using the methodology and parameters determined based on the intended use of the test material to be used in clinical trials. In phase III, the clinical trial evaluates the drug/vaccine compared to existing treatments. This phase is carried out to ensure that new drugs/vaccines are truly efficacious by comparing them with standard drugs/vaccines proven useful (Manoppo, 2020).

Clinical trials are carried out based on the International Conference on Harmonization (ICH) principles, namely following the ethical principles of the Declaration of Helsinki. Research subjects are given informed consent to explain the basic elements and additional elements that include an explanation of research activities, research objectives, potential risks and unpleasant feelings that the prospective subject will experience, direct benefits to the subject, alternative procedures, and data confidentiality. A statement that the subject can be excluded from the research, intensive for the subject (if any), the possibility that unknown risks may arise, the potential danger that will occur if the subject resigns, and so on (CIOMS, 2016).

3.2.7 Resource allocation

In the statement S16, "New patients who are not COVID-19 patients should not be treated in the hospital because the hospital prioritizes a place to treat COVID-19 patients". In the statement S17, "Patients who are not COVID-19 patients who have been hospitalized but have not fully recovered are discharged because the hospital needs a place to treat COVID-19 patients". Statement S16 and S17 are related to justice principle. Everyone has the right to obtain health services under their medical needs (Wasisto *et al*., 2020).

The statement S18 reads "All rapid tests or COVID-19 swab tests should be free so that all people can be examined". Statement S18 is related to justice principle. Based on the principle of justice, everyone must be treated fairly. If we comply to the principle of justice equality, everyone receives the available resources in the same proportion (Papanikitas, 2013).

In statement S20, "Allocation of funding to health services should be prioritized for COVID-19 patients". Based on the principle of justice need, everyone receives appropriate resources based on how much someone needs these resources (Papanikitas, 2013).

3.2.8 Respecting individual right

The statement S22 states that "Citizens with a high risk of contracting COVID-19 have the right to refuse the COVID-19 rapid test". Although individuals have their respective autonomous rights, mutual safety is much more important (Papanikitas, 2013; Law of Republic of Indonesia No. 6, 2018).

In the statement S25, "Every person has the right to use or not use a mask because this is an individual autonomous right. Autonomy (self-determination) can decide how individuals behave without hindrance to others, even though the choice will be detrimental to their health (Papanikitas, 2013; Manoppo, 2020).

In statement S27, "The lockdown of the territory during the pandemic violates individual rights." Considering Law No. 6 of 2018 concerning health quarantine letter c "... Indonesia must fully respect the dignity, human rights, the basics of freedom of a person, and its universal application" and article 2 states that its implementation is carried out based on humanity, benefits, protection, justice, non-discrimination, public interest, cohesiveness, legal awareness, and state sovereignty. The public interest in question is to

prioritize the public interest over individuals or certain groups (Law of Republic of Indonesia No. 6, 2018).Quarantine is carried out to limit the movement of the community; however, this is done to ensure the health of all citizens so as not to become infected.

Thus, quarantine cannot be categorized as a violation of human rights. In Law No. 39 of 1999 concerning human rights, article 73 regarding restrictions and prohibitions, "the rights and freedoms outlined in this law can only be limited by and based on law, solely to guarantee recognition and respect for human rights and basic freedoms of people, morality, public order, and the interests of the nation "(Law of Republic of Indonesia No. 39, 1999).

In the statement S28, "Families have the right to bring COVID-19 patients home." In the statement S29, "Families have the right take the dead bodies of COVID-19 patients". In handling a pandemic, people must follow government regulations. In Law No. 4 of 1984 concerning Communicable Disease Outbreaks article 5 paragraph 1 of the handling of bodies due to outbreaks is regulated by government regulations (Law of Republic of Indonesia No. 4,1984). In addition, if a body is taken, it will endanger the health of the person who takes the body because he or she could be infected with the SARS-CoV-2 virus from liquid or aerosol from the body.

3.2.9 Basic principles of ethics

Not many previous studies have discussed resident doctors' knowledge of medical ethics issues (especially those related to the basic principles of ethics) in handling the COVID-19. A similar study conducted by Adhikari *et al*. found that two-third of physicians were aware of the contents of the Hippocratic oath. The Hippocratic oath is the initial foundation for the formation of basic principles of ethics. In this study, there were also differences of opinion between doctors and nurses regarding the importance of including medical ethics in the undergraduate curriculum and the paternalistic attitudes of doctors. Differences influenced differences in opinion among health providers in the intensity of professional training. This research is limited to assessing the code of ethics and has not analyzed knowledge of the basic principles of ethics (Adhikari *et al*., 2020).

It is challenging to determine which basic ethical principles are the most dominant. Sensitivity and continuous training are required to identify ethical issues in health services (Kemparaj and Kadalur, 2018). Likewise, it was evident in this study. Many resident doctors had different opinions in determining ethical issues that arose in handling the COVID-19 pandemic. In this study, it was most difficult to distinguish between beneficence and non-maleficence and justice from autonomy and beneficence from justice. In practice, no one principle is higher than another. The principles are applied depending on the situation at hand. Four basic ethical principles need to be fulfilled, unless there is a conflict in certain conditions with the same or stronger principles (Kirchhoffer, 2020).

In a study conducted by Singh *et al.* it was stated that 75% of doctors had good knowledge and attitudes towards medical ethics (Singh *et al*., 2016). However, resident doctors were advised to gain more understanding by attending symposiums, conferences, and training. In contrast to this study, it was found that only 27.5% (about one-third) had adequate knowledge and attitudes about ethical issues. This result is expected because the knowledge tested in research was very specific regarding the basic principles of ethics, which are certainly not easy to identify because they depend on the situation and conditions in the medical practice.

The results of the research by Al-Shehri *et al*, with the characteristics of resident doctor respondents in Aseer Province, Saudi Arabia, most of the respondents had sufficient knowledge (44.1% of respondents), followed by 35.6% of respondents having limited knowledge, and 20.3% of respondents having good knowledge (Al Shehri*et al.,* 2020).

A research study was conducted by Ranasinghe *et al.* regarding doctors' knowledge of medical ethics in three teaching hospitals in Sri Lanka. It was found that 81.2% of participating doctors had limited knowledge with postgraduate trainees having a higher level of knowledge (60.7%) than other doctors (44.4 %) (Ranasinghe *et al*., 2020).

However, there is a research study on medical ethics knowledge of pre-clinical and clinical students. The research results by Manurung *et al.* (2019) show that the pre-clinic and clinical student respondents at the University of Lampung having a mean value of 3 with a maximum score of 8 indicate that the students' knowledge is still not adequate (Manurung *et al*., 2019).

As with knowledge, we have not found an adequate number of studies examining the attitudes of resident doctors regarding the issue of

medical ethics in handling COVID-19 pandemic. However, there were several studies related to attitudes such as research conducted by Jatana *et al*. who examined the attitudes of preclinical students towards medical ethics. In this study, it was found that the majority of the pre-clinical students' attitudes towards the core values of the guidelines, doctors duties towards patients, and learning medical ethics in the curriculum were positive (Jatana *et al*., 2018). Research conducted by Ranasinghe *et al*. on doctors' attitudes towards medical ethics in three teaching hospitals in Sri Lanka found that most respondents (95%) showed good attitudes towards gaining knowledge and the need for training (Ranasinghe *et al*., 2020).

Until this research report was written, we had not found other studies examining the relationship of knowledge to resident doctors' attitudes regarding medical ethics in handling the COVID-19 pandemic. However, based on the research results conducted by Manurung et al., there is a relationship between knowledge of basic principles of ethics on the moral assessment of pre-clinical and clinical students at the Faculty of Medicine, University of Medicine Lampung (Manurung*et al*., 2019).

The theory of Beauchamp and Childress states that the basic principles of ethics include specific rules that can influence concrete actions and one judgment on the analysis of problems in the biomedical field (Beuchamp and Childress, 2013). Knowledge of bioethical principles is related to the cognitive abilities possessed by respondents to increase the ability to think critically and logically (Manurung *et al*., 2019). In this study, respondents were exposed to medical ethics events, but respondents did not understand or forgot the basic principles of medical ethics. This is caused by many factors, such as lack of opportunity to read books or journals related to medical ethics.

Resident doctors lack of ability to identify ethical issues that arise when dealing with the COVID-19 pandemic is influenced by the lack of exposure to ethical issues in their education. In this study, respondents were less able to identify the basic principles of ethics on the ethical issue of the COVID-19 pandemic. This can be explained by the fact that when undergoing education for resident doctors, the emphasis is more on the technical side of medicine (medical skills) and clinical facts that must be studied continuously. However, it turns out that every medical action and decision-making was strongly influenced by ethical decisions (Hébert, 2009; Muhaimin *et al*., 2019).

3.2.10 Advantage and limitation of the study

The strength of this study is that it used a questionnaire that the researchers constructed and the content validity has been tested by experts who assessed the relevance of the contents of the questionnaire. Therefore, much information was generated from this study so that it can be re-explored into several quantitative and qualitative studies.

As for the limitations of this study, the researcher did not investigate the practice directly in the field for the attitude item, but instead asked what attitude the respondent would take due to the impossible situation in the field. In addition, the results of the study could not be generalized without caution to the context outside the resident doctors at ZAH because the sample was drawn from the resident doctors at ZAH as the population of this study.

4. CONCLUSIONS:

Resident doctor knowledge about ethical and medicolegal issues is needed in dealing with the COVID-19 pandemic. In this study, it was found that resident doctor knowledge regarding ethical and medicolegal issues in handling the COVID-19 pandemic by using the basic principles of bioethics was not satisfactory, so it is necessary to increase their competence through continuous professional development such as seminars, workshops or case studies.

Adequate ethical and medicolegal decision making is very helpful in making medical decisions. This study found that ethical and medicolegal decision making through resident doctor attitudes regarding ethical and medicolegal issues in handling the COVID-19 pandemic was adequate. Still, it is necessary to raise their awareness of specific ethical and medicolegal issues through a joint conference to discuss difficult cases.

The relationship between knowledge and attitude was not significantly based on our analysis. Education of health care professionals is needed, especially to discuss ethical issues following basic ethical principles. There is also a need for intensive programs such as bioethics courses. A consultative committee will also be helpful to discuss cases of ethical dilemmas and to continuously discuss the ethical perspectives of patients in various clinical situations.

5. ACKNOWLEDGMENTS

The authors express their most profound appreciation to the participants who participated in this study.

6. COMPETING INTEREST

The authors declare that there are no competing interests related to the study

7. FUNDING

This study did not require funding.

8. REFERENCES:

1. Nicola, M., O'Neill, N., Sohrabi, C., Khan, M., Agha, M., and Agha, R. (2020). Evidence-based management guideline for the COVID-19 pandemic - Review article. *Int J Surg*, 77, 206–216. Available from: https://doi.org/10.1016/j.ijsu.2020.04.001

2. Wu, Y. C., Chen, C. S., and Chan, Y.J. (2020). The outbreak of COVID-19 -An overview. *J Chin Med Assoc*, 217–20.

3. Lai, C. C., Shih, T. P., Ko, W. C., Tang, H. J., and Hsueh, P. R. (2020). Severe acute respiratory syndrome coronavirus 2 (SARS-CoV-2) and coronavirus disease-2019 (COVID-19): The epidemic and the challenges. *Int J Antimicrob Agents* [Internet], 55(3):105924. Available from: https://doi.org/10.1016/j.ijantimicag.2020.105924

4. Wang, L., Wang, Y., Ye, D., and Liu, Q. (2020). Review of the 2019 novel coronavirus (SARS-CoV-2) based on current evidence. *International Journal of Antimicrobial Agents* [Internet]. 2020;(XXXX):105948. Available-from: https://doi.org/10.1016/j.ijantimicag.2020.105948

5. WHO Coronavirus Disease (COVID-19) [Internet]. [cited 2020 Sep 3]. Available from: https://covid19.who.int/

6. McGuire, A. L., Aulisio, M. P., Davis, F. D., Erwin, C., Harter, T. D., Jagsi, R., Klitzman, R., Maccauley, R., Racine, E., Wolf, S. M., Wynia, M., Wolpe, P.R., and The COVID-19 Tarsk Force of the Association of Bioethics Program Directors (APBD). (2020). Ethical challenges arising in the COVID-19 pandemic: an overview from the Association of Bioethics Program Directors (ABPD) task force. *The American Journal of Bioethics,* 1-13. Available from: https://doi.org/10.1080/15265161.2020.1764138

7. Asghari, F., and Tehrani, S. S. (2020). Ethical issues responding to the COVID-19 pandemic; a narrative review. *Adv J Emerg Med,* 4(2s): e60.

8. Xafis, V., Schaefer, G. O., Labude, M. A., Zhu, Y., and Hsu, L.Y. (2020). The perfect moral strom; Diverse ethical consideration in the COVID-19. *Asian Bioethics Review*, 12, 65-83.

9. Robert, R., Barnes, N, K., Boyer, A., Laurent, A., Azoulay, E., and Reignier, J. (2020). Ethical dilemmas due to the COVID-19 pandemic. *Ann Intensive Care*, 10:84, 1-9. Available from: https://doi.org/10.1186/s13613-020-00702-7

10. Huxtable, R. (2020). COVID -19: where is the national ethical guidance?. *BMC Medical Ethics*, 21(32), 1-3.

11. Yusof, A. N. M., Muuti, M. Z., Ariffin, L. A., and Tan, M. K. M. (2020). Sharing information on COVID-19 : the ethical challenges in the Malaysian setting, *Asian Bioethics Review* 1-13.

12. Indonesian Medical Council (IMC). (2019). *National Standards for Indonesian Medical Professional Education.*

13. Kusumaningtyas, H.H., and Hermasari, B.K. (2017). The correlation between sensitivity of medical ethics and patient satisfaction. *Nexus Pendidik Kedokt Kesehat*, 6(1),1–8.

14. Taufan, A. (2019). The relationship between young doctors' knowledge level about types of malpractice and health law curriculum at the medicolegal forensic stage. *J Soshum Insentif,* 164–72.

15. Afandi, D., Mursa, L. B., Novitasari, D., and Faulina, M. R. (2010). The relationship between the knowledge level of basic bioethics and the level of moral assessment ability of students of the Faculty of Medicine,

University of Riau, *Maj Ked Indones,* 60(1): 27–31.

16. Pozgar, G.D. (2020). Legal and ethical issues for health professions. 5th Ed. *Jones & Bartlett Learning*; 443.

17. Afandi, D. (2017) The basic principles of bioethics in ethical clinical decision making. *Andalas Med J*, 40:2, 111-121.

18. Henky, H. (2018). Clinical Ethics Services. *Indones J Medical Ethics*; 2(2), 59.

19. Suryadi, T., and Kulsum, K. (2020). Content validity for the research instrument regarding ethical issues in handling the COVID-19 pandemic. *Periódico Tchê Química,* 17(36), 100-118.

20. Saryono, S. (2011). Health *research methodology - a practical guide for beginners.* Yogyakarta: Mitra Cendikia.

21. Sitorus, Z., Suherman, S., and Wahyuni, M. S. (2018). Mapping model of the cut point method to find out the location of the hospital's ICU room. *Int J Res Dev,* 2(2), 90–96.

22. Varkey, B. (2020). Principles of clinical ethics and their application to practice. *Med Princ Pract.*

23. Papanikitas, A. (2013). Crash course - medical ethics and sociology. 2nd Ed. Horton-Szar D, editor. Elsevier Ltd.

24. Beauchamp, T. L., and Childress J. F. (2013). Principles of biomedical ethics (7th ed). New York: *Oxford University Press*, 190-317.

25. Medical Ethics Honors Council (MEHC).(2012). Indonesian Medical Code of Ethics and Guidelines for Implementing Indonesian Medical Code of Ethics.

26. Law of Republic of Indonesia No. 36, 2014, concerning the health worker.

27. Indonesian Medical Association (IMA). (2021). Standard guidelines for doctor protection in the era of the COVID-19 pandemic. Jakarta.

28. Manoppo, P. J. (2020). From the paradigm of "Listen to the Doctor" to "Listen to the Patient." *J Etika Kedokt Indones,* 4(2), 53–56.

29. Agustin, R., Anna, R., Hatta, G. F., and Prawiroharjo, P. (2020). Ethical review of disclosure of medical secrets and patient identities in the situation of the COVID-19 pandemic and its relation to efforts to fight positive patient stigma. *J Etika Kedokt Indones*, 4(2), 41–45.

30. Page, K. (2012). The four principles: Can they be measured and do they predict ethical decision making? [Internet]. Available from: http://www.biomedcentral.com/1472-6939/13/1/10

31. Coghlan, N., Archard, D., Sipanoun, P., Hayes, T., and Baharlo, B.. (2020). COVID-19: legal implications for critical care. *Anaesthesia*, 75(11):1517–1528.

32. Law of Republic of Indonesia No.44, 2009 concerning hospital.

33. Law of Republic of Indonesia No. 29, 2004, concerning the medical practice.

34. Susilo, A., Rumende, C. M., Pitoyo, C. W., Santoso, W. D., Yulianti, M., and Sinto, R. (2020). Coronavirus Disease 2019: Updated Literature Review Coronavirus Disease 2019: Review of Current Literatures. *Indonesian Internal Medicine,* 7 (1): 45–67.

35. Burhan, E., Isbaniyah, F., and Susanto A. D., (2020). Pneumonia COVID-19 (Diagnosis and Management in Indonesia). *Indonesian Association of Pulmonologist*. Jakarta, 1–58.

36. World Health Organization (WHO). (2020). Naming the coronavirus disease (COVID-19) and the virus that causes it [Internet]. Geneva.

37. Wasisto, B., Librianty, N., and Harinda, F. (2020). Ethical review of health promotive efforts to postpone to the doctor except potential emergency cases or services that cannot be delayed. *J Etika Kedokt Indones,* 4(2), 63–66.

38. Mappaware, N. A, Sima, S., Syahril, E., Mokhtar, S., Royani, I., and Mursyid, M. (2020). Stage III-B cervical-cancer of young age in medical, bioethics, and clinical ethics perspectives. *Indian J Forens Med Toxicol,* 14(2): 2565-70.

39. Ministry of Health (MOH) Republic of Indonesia. (2007). Guidelines for the Use of

Free Medicines and Limited Over-the-Counter Drugs. Directorate of Community and Clinical Pharmacy Development, Directorate General of Pharmaceutical and Medical Devices Development.

40. Law of Republic of Indonesia No. 6, 2018, concerning the health quarantine.

41. Ranasinghe, A. W. I. P., Fernando, B., Sumathipala, A., and Gunathunga, W. (2020). Medical ethics: knowledge, attitude and practice among doctors in three teaching hospitals in Sri Lanka. *BMC Med Ethics*, 21(1),1–10.

42. The Council for International Organization of Medical Sciences (CIOMS). (2016). *International ethical guideline for health related research involving humans.*

43. Law of Republic of Indonesia No. 39, 1999, concerning the human right.

44. Law of Republic of Indonesia No. 4, 1984, concerning the infectious disease outbreak.

45. Adhikari, S., Paudel, K., Aro, A. R., Adhikari, T. B., Adhikari, B., and Mishra, S. R. (2016). Knowledge, attitude and practice of healthcare ethics among resident doctors and ward nurses from a resource poor setting, Nepal. *BMC Med* Ethics [Internet], 17(1):1–8. Available from: http://dx.doi.org/10.1186/s12910-016-0154-9

46. Kemparaj, V. M., and Kadalur, U. G. (2018). Understanding the principles of ethics in health care: a systematic analysis of qualitative information. *Int J Community Med Public Heal,* 5(3):822.

47. Kirchhoffer, D. G. (2020). Dignity, Autonomy, and Allocation of Scarce Medical Resources During COVID-19. *J Bioeth Inq*. 2020.

48. Singh, S., Sharma, P., Bhandari, B., and Kaur, R. (2016). Knowledge, awareness and practice of ethics among doctors in tertiary care hospital. *Indian J Pharmacol,* 48(7):S89–93.

49. Al-Shehri, E., Siddiqui, A. F., and Khalil, S. U. N. (2020). Knowledge, attitude and practice of medical ethics among resident physicians of specialty certificate in Aseer Province, Saudi Arabia. *J Liaquat Univ Med Heal Sci,* 19(1), 48–54.

50. Manurung, W. P., Sari, M. I., Aries, R., and Oktaria, D. (2019). The Relationship between knowledge of principles base of bioethics and moral attitudes Assessment on pre-clinical and clinical students, Faculty of Medicine, University of Lampung. *Majority*, 8, 25–9. Available from: http://repository.lppm.unila.ac.id/11752/1/Widya.pdf

51. Jatana, S. K.., Soe, H. T. K., Soe, K, Phyu, K. L., Lwin, H., and Than, N. N. (2018). A survey on knowledge and attitudes towards medical ethics among undergraduate medical students. Education [Internet]. 2018;8(3):48–53. Available from: https://www.researchgate.net/publication/326734894

52. Hébert, P. C. (2009). *Doing Right: A Practical Guide to Ethics for Medical Trainees and Physicians*. 3rd Ed. Oxford University Press, 354.

53. Muhaimin, A., Willems, D. L., Utarini, A., and Hoogsteyns, M. (2019). What do students perceive as ethical problems ? a comparative study of Dutch and Indonesian medical students in clinical training, *Asian Bioethics Review*, 391–408.

9. OPEN ACCESS:

Table 2. *Distribution of respondent answers regarding knowledge related to issues of ethics and medicolegal in handling the COVID-19 pandemic*

Statement	Key answers	Autonomy N(%)	Beneficence N(%)	Nonmalaficence N(%)	Justice N(%)
S1	Beneficence	24 (30%)	21 (26,3%)	25 (31,3%)	10 (12,5%)
S2	Beneficence	24 (30%)	19 (23,8%)	22 (27,5%)	15 (18,8%)
S3	Autonomy	21 (26,3%)	25 (31,3%)	24 (30%)	10 (12,5%)
S4	Beneficence	14 (17,5%)	45 (56,3%)	32 (40%)	9 (11,3%)
S5	Beneficence	5 (6,3%)	32 (40%)	38 (47,5%)	5 (6,3%)
S6	Beneficence	14 (17,5%)	18 (22,5%)	40 (50%)	8 (10%)
S7	Beneficence	14 (17,5%)	17 (21,3%)	10 (12,5%)	39 (48,8%)
S8	Non maleficence	13 (16,3%)	31 (38,8%)	18 (22,5%)	18 (22,5%)
S9	Autonomy	39 (48,8%)	8 (10%)	22 (27,5%)	11 (13,8%)
S10	Justice	11 (13,8%)	29 (36,3%)	22 (27,5%)	18 (22,5%)
S11	Justice	13 (16,3%)	24 (30%)	23(28,8%)	20 (25%)
S12	Non maleficence	9 (11,3%)	35 (43,8%)	29 (36,3%)	7 (8,8%)
S13	Justice	17 (21,3%)	12 (15%)	12 (15%)	39 (48,8%)
S14	Justice	16 (20%)	9 (11,3%)	8 (10%)	47 (58,8%)
S15	Non maleficence	19 (23,8%)	18 (22,5%)	33 (41,3%)	10 (12,5%)
S16	Justice	10 (12,5%)	20 (25%)	23 (28,8%)	27 (33,8%)
S17	Justice	9 (11,3%)	20 (25%)	20 (25%)	31 (38,8%)
S18	Justice	11 (13,8%)	24 (30%)	6 (7,5%)	39 (48,8%)
S19	Justice	9 (11,3%)	25 (31,3%)	6 (7,5%)	40 (50%)
S20	Justice	7 (8,8%)	25 (31,3%)	14 (17,5%)	34 (42,5%)
S21	Justice	4 (5%)	17 (21,3%)	32 (40%)	27 (33,8%)
S22	Autonomy	37 (46,3%)	7 (8,8%)	24 (30%)	12 (15%)
S23	Justice	8 (10%)	39 (48,8%)	17 (21,3%)	16 (20%)
S24	Justice	3 (3,75%)	45 (56,3%)	11 (13,8%)	21 (26,3%)
S25	Autonomy	40 (50%)	8 (10%)	16 (20%)	16 (20%)
S26	Autonomy	27 (33,8%)	10 (12,5%)	21 (26,3%)	22 (27,5%)
S27	Justice	15 (18,8%)	21 (26,3%)	25 (31,3%)	19 (23,8%)
S28	Autonomy	41 (51,3%)	5 (6,3%)	22 (27,5%)	12 (15%)
S29	Autonomy	38 (47,5%)	6 (7,5%)	23 (28,8%)	13 (16,3%)

Table 4. *Distribution of respondent answers regarding doctors attitudes towards ethical and medicolegal issues in handling the COVID-19 pandemic*

No	Statements	Key answers	Strongly Disagree	Disagree	Doubtful	Agree	Strongly Agree

			N (%)	N (%)	N (%)	N (%)	N (%)
1	S1	Agree	2 (2,5%)	3 (3,8%)	1 (1,3%)	21 (26,3%)	53 (66,3%)
2	S2	Agree	3 (3,8%)	3 (3,8%)	5 (6,3%)	20 (25%)	49 (61,3%)
3	S3	Disagree	14 (17,5%)	9 (11,3%)	22 (27,5%)	9 (11,3%)	26 (32,5%)
4	S4	Agree	1 (1,3%)	0(0%)	5 (6,3%)	12 (15%)	62 (77,5%)
5	S5	Agree	15 (18,8%)	16 (20%)	25 (31,3%)	15 (18,8%)	9 (11,3%)
6	S6	Disagree	17 (21,3%)	17 (21,3%)	25 (31,3%)	12 (15%)	9 (11,3%)
7	S7	Agree	1 (1,3%)	1 (1,3%)	5 (6,3%)	10 (12,5%)	63 (78,8%)
8	S8	Agree	2 (2,5%)	2 (2,5%)	13(16,3%)	30 (37,5%)	33 (41,3%)
9	S9	Disagree	25 (31,3%)	19 (23,8%)	7 (8,8%)	15 (18,8%)	14 (17,5%)
10	S10	Agree	2 (2,5%)	6 (7,5%)	19 (23,8%)	22 (27,5%)	31 (38,8%)
11	S11	Agree	0(0%)	4 (5%)	17 (21,3%)	25 (31,3%)	34 (42,5%)
12	S12	Disagree	3 (3,8%)	7 (8,8%)	29 (36,3%)	29 (36,3%)	12 (15%)
13	S13	Agree	4 (5%)	1 (1,3%)	12 (15%)	24 (30%)	39 (48%)
14	S14	Agree	5 (6,3%)	2 (2,5%)	11 (13,8%)	23 (28,8%)	39 (48,8%)
15	S15	Disagree	12 (15%)	13 (16,3%)	20 (37,5%)	14 (17,5%)	11 (13,8%)
16	S16	Disagree	11 (13,8%)	25 (31,3%)	15 (18,8%)	19 (23,8%)	10 (12,5%)
17	S17	Disagree	9 (11,3%)	15 (18,8%)	23 (28,8%)	16 (20%)	17 (21,3%)
18	S18	Agree	2 (2,5%)	0(0%)	13 (16,3%)	19 (23,8%)	46 (57,5%)
19	S19	Agree	1 (1,3%)	0(0%)	7 (8,8%)	20 (25%)	52 (65%)
20	S20	Agree	0(0%)	9 (11,3%)	34 (42,5%)	18 (22,5%)	19 (23,8%)
21	S21	Agree	1 (1,3%)	0(0%)	10 (12,5%)	27 (33,8%)	42 (52,5%)
22	S22	Disagree	22 (27,5%)	23 (28,8%)	13 (16,3%)	10 (12,5%)	12 (15%)
23	S23	Disagree	1 (1,3%)	2 (2,5%)	9 (11,3%)	29 (36,3%)	39 (48,8%)
24	S24	Disagree	1 (1,3%)	1 (1,3%)	13 (16,3%)	30 (37,5%)	35 (43,8%)
25	S25	Agree	36 (45%)	18 (22,5%)	10 (12,5%)	8 (10%)	8 (10%)
26	S26	Disagree	16 (20%)	24 (30%)	20 (25%)	8 (10%)	12 (15%)
27	S27	Disagree	20 (25%)	20 (25%)	22 (27,5%)	11 (13,8%)	7 (8,8%)
28	S28	Disagree	20 (25%)	16 (20%)	27 (33,8%)	11 (13,8)	6 (7,5%)
29	S29	Disagree	25 (31,3%)	14 (17,5%)	20 (25%)	11 (13,8)	10 (12,5%)

Table 6. *Recapitulation of correct answers about respondent knowledge and attitudes*

No	**Statements**	**Knowledge**		**Attitude**	
		Key answer	**Correct answers n (%)**	**Key answer**	**Correct answers n (%)**

1	S1	Beneficence	21 (26,3%)	Agree	74 (92.5%)
2	S2	Beneficence	19 (23,8%)	Agree	69 (86.3%)
3	S3	Autonomy	21 (26,3%)	Disagree	45 (56.3%)
4	S4	Beneficence	45(56,3%)	Agree	74 (92.5%)
5	S5	Beneficence	32 (40.0%)	Agree	24 (30.0%)
6	S6	Beneficence	18 (22,5%)	Disagree	59 (73.8%)
7	S7	Beneficence	17 (21,3%)	Agree	73 (91.3%)
8	S8	Non maleficence	18 (22,5%)	Agree	63 (78.8%)
9	S9	Autonomy	39 (48,8%)	Disagree	49 (61.3%)
10	S10	Justice	18 (22,5%)	Agree	53 (66.3%)
11	S11	Justice	20 (25.0%)	Agree	59 (73.8%)
12	S12	Non maleficence	29 (36,3%)	Disagree	39 (48.7%)
13	S13	Justice	39 (48,8%)	Agree	63 (78.8%)
14	S14	Justice	47 (58,8%)	Agree	62 (77.5%)
15	S15	Non maleficence	33 (41,3%)	Disagree	45 (56.3%)
16	S16	Justice	27 (33,8%)	Disagree	51 (63.8%)
17	S17	Justice	31 (38,8%)	Disagree	47 (58.8%)
18	S18	Justice	39 (48,8%)	Agree	65 (81.3%)
19	S19	Justice	40 (50.0%)	Agree	72 (90.0%)
20	S20	Justice	34 (42,5%)	Agree	37 (46.3%)
21	S21	Justice	27 (33,8%)	Agree	69 (86.3%)
22	S22	Autonomy	37 (46,3%)	Disagree	58 (72.5%)
23	S23	Justice	16 (20.0%)	Disagree	12 (15.0%)
24	S24	Justice	21 (26,3%)	Disagree	15 (18.8%)
25	S25	Autonomy	40 (50.0%)	Agree	16 (20.0%)
26	S26	Autonomy	27 (33,8%)	Disagree	60 (75.0%)
27	S27	Justice	19 (23,8%)	Disagree	62 (77.5%)
28	S28	Autonomy	41 (51,3%)	Disagree	63 (78.8%)
29	S29	Autonomy	38 (47,5%)	Disagree	59 (73.8%)

Table 7. *Statistical analysis*

Knowledge	**Attitude**			**p-value**
	Positive	**Negative**	**Total**	
Good	22	2	24	
Limited	40	16	56	0,077
Total	62	18	80	

APPENDIX. 1. *Original online questionnaire in Indonesian*

QUESTIONNAIRE SHEET

Knowledge and attitudes regarding ethical and medicolegal issues in handling the COVID-19 pandemic among resident doctors at Zainoel Abidin Hospital, Aceh, Indonesia

1. Respondent data

a. Serial number :
b. Place of duty :
c. Gender :
d. Age :

2. Questionnaires

Choose the answer that suits your opinion by clicking on the available answer choices.

Item No.	Statement Items	Knowledge	Attitudes
		What ethical principles are contained in the statement?	What is your attitude towards that statement?
S1	Doctors who are not equipped with complete personal protective equipment (PPE) have the right to refuse to examine patients suspected of having COVID-19.	☐ Beneficence ☐ Nonmaleficence ☐ Justice ☐ Autonomy	☐ Strongly disagree ☐ Disagree ☐ Doubtful ☐ Agree ☐ Strongly agree
S2	Doctors who are not equipped with personal protective equipment (PPE) have the right to refuse to treat patients suspected of having COVID-19.	☐ Beneficence ☐ Nonmaleficence ☐ Justice ☐ Autonomy	☐ Strongly disagree ☐ Disagree ☐ Doubtful ☐ Agree ☐ Strongly agree
S3	Doctors may notify patient data to the general public to prevent the spread of COVID-19.	☐ Beneficence ☐ Nonmaleficence ☐ Justice ☐ Autonomy	☐ Strongly disagree ☐ Disagree ☐ Doubtful ☐ Agree ☐ Strongly agree
S4	The doctor has the right to ask about the patient's travel history for tracking purposes	☐ Beneficence ☐ Nonmaleficence ☐ Justice ☐ Autonomy	☐ Strongly disagree ☐ Disagree ☐ Doubtful ☐ Agree ☐ Strongly agree
S5	During a pandemic, using drugs on the market to treat COVID -19 patients is allowed even without going through the clinical trial stage.	☐ Beneficence ☐ Nonmaleficence ☐ Justice ☐ Autonomy	☐ Strongly disagree ☐ Disagree ☐ Doubtful ☐ Agree ☐ Strongly agree

S6	During a pandemic, taking drugs on the market to treat COVID -19 patients isolated independently in their homes is allowed even without a doctor's prescription.	☐ Beneficence ☐ Nonmaleficence ☐ Justice ☐ Autonomy	☐ Strongly disagree ☐ Disagree ☐ Doubtful ☐ Agree ☐ Strongly agree
S7	Doctors have the right to receive protection while working during the COVID-19 pandemic	☐ Beneficence ☐ Nonmaleficence ☐ Justice ☐ Autonomy	☐ Strongly disagree ☐ Disagree ☐ Doubtful ☐ Agree ☐ Strongly agree
S8	The doctor has the right to ask someone who is categorized as a suspect or close contact with a probable/confirmed COVID-19 person to self-isolate.	☐ Beneficence ☐ Nonmaleficence ☐ Justice ☐ Autonomy	☐ Strongly disagree ☐ Disagree ☐ Doubtful ☐ Agree ☐ Strongly agree
S9	A person categorized as a suspect or in close contact with a probable/confirmed COVID -19 person has the right to refuse self-isolation.	☐ Beneficence ☐ Nonmaleficence ☐ Justice ☐ Autonomy	☐ Strongly disagree ☐ Disagree ☐ Doubtful ☐ Agree ☐ Strongly agree
S10	A person categorized as a suspect or in close contact with a probable/confirmed COVID -19 person who does not want to perform self-isolation may be forcibly picked up.	☐ Beneficence ☐ Nonmaleficence ☐ Justice ☐ Autonomy	☐ Strongly disagree ☐ Disagree ☐ Doubtful ☐ Agree ☐ Strongly agree
S11	A person who has been confirmed as COVID-19 and refuses to be treated can be forced into isolation.	☐ Beneficence ☐ Nonmaleficence ☐ Justice ☐ Autonomy	☐ Strongly disagree ☐ Disagree ☐ Doubtful ☐ Agree ☐ Strongly agree
S12	Someone who has symptoms similar to COVID-19 but there is no result of the swab being treated for COVID-19	☐ Beneficence ☐ Nonmaleficence ☐ Justice ☐ Autonomy	☐ Strongly disagree ☐ Disagree ☐ Doubtful ☐ Agree ☐ Strongly agree
S13	People who reject COVID-19 patients in their environment are violating social ethics	☐ Beneficence ☐ Nonmaleficence ☐ Justice ☐ Autonomy	☐ Strongly disagree ☐ Disagree ☐ Doubtful ☐ Agree ☐ Strongly agree
S14	People who reject the dead bodies of COVID-19 patients are violating social ethics	☐ Beneficence ☐ Nonmaleficence ☐ Justice ☐ Autonomy	☐ Strongly disagree ☐ Disagree ☐ Doubtful ☐ Agree ☐ Strongly agree

S15	COVID-19 vaccine trials can be carried out directly on humans.	☐ Beneficence ☐ Nonmaleficence ☐ Justice ☐ Autonomy	☐ Strongly disagree ☐ Disagree ☐ Doubtful ☐ Agree ☐ Strongly agree
S16	New non- COVID-19 patients should not be hospitalized because hospitals need a place to treat COVID-19 patients	☐ Beneficence ☐ Nonmaleficence ☐ Justice ☐ Autonomy	☐ Strongly disagree ☐ Disagree ☐ Doubtful ☐ Agree ☐ Strongly agree
S17	Non- COVID-19 patients who have been hospitalized should be discharged because hospitals need a place to treat COVID-19 patients	☐ Beneficence ☐ Nonmaleficence ☐ Justice ☐ Autonomy	☐ Strongly disagree ☐ Disagree ☐ Doubtful ☐ Agree ☐ Strongly agree
S18	All rapid tests / RT-PCR should be made free so that all people can be examined for COVID-19 detection	☐ Beneficence ☐ Nonmaleficence ☐ Justice ☐ Autonomy	☐ Strongly disagree ☐ Disagree ☐ Doubtful ☐ Agree ☐ Strongly agree
S19	COVID-19 and non- COVID-19 patients deserve the same treatment	☐ Beneficence ☐ Nonmaleficence ☐ Justice ☐ Autonomy	☐ Strongly disagree ☐ Disagree ☐ Doubtful ☐ Agree ☐ Strongly agree
S20	Allocation of funding for health services is prioritized for COVID-19 patients	☐ Beneficence ☐ Nonmaleficence ☐ Justice ☐ Autonomy	☐ Strongly disagree ☐ Disagree ☐ Doubtful ☐ Agree ☐ Strongly agree
S21	Changes in professional care providers such as doctors, nurses and other health workers for COVID-19 patients are carried out regularly according to needs	☐ Beneficence ☐ Nonmaleficence ☐ Justice ☐ Autonomy	☐ Strongly disagree ☐ Disagree ☐ Doubtful ☐ Agree ☐ Strongly agree
S22	Residents with a high risk of contracting COVID-19 have the right to refuse the rapid test / RT-PCR.	☐ Beneficence ☐ Nonmaleficence ☐ Justice ☐ Autonomy	☐ Strongly disagree ☐ Disagree ☐ Doubtful ☐ Agree ☐ Strongly agree
S23	COVID-19 patients who have a history of comorbid diseases are prioritized for hospitalization.	☐ Beneficence ☐ Nonmaleficence ☐ Justice ☐ Autonomy	☐ Strongly disagree ☐ Disagree ☐ Doubtful ☐ Agree ☐ Strongly agree

S24	COVID-19 patients who are elderly are prioritized for getting treatment at the hospital.	☐ Beneficence ☐ Nonmaleficence ☐ Justice ☐ Autonomy	☐ Strongly disagree ☐ Disagree ☐ Doubtful ☐ Agree ☐ Strongly agree
S25	Each person has the right to use or not use masks during a COVID-19 pandemic because this is an individual's autonomous right.	☐ Beneficence ☐ Nonmaleficence ☐ Justice ☐ Autonomy	☐ Strongly disagree ☐ Disagree ☐ Doubtful ☐ Agree ☐ Strongly agree
S26	Personal data of COVID-19 patients may be published.	☐ Beneficence ☐ Nonmaleficence ☐ Justice ☐ Autonomy	☐ Strongly disagree ☐ Disagree ☐ Doubtful ☐ Agree ☐ Strongly agree
S27	Lockdowns during a COVID-19 pandemic violate the rights of individual freedoms.	☐ Beneficence ☐ Nonmaleficence ☐ Justice ☐ Autonomy	☐ Strongly disagree ☐ Disagree ☐ Doubtful ☐ Agree ☐ Strongly agree
S28	Families of COVID-19 patients can forcibly bring COVID-19 patients home.	☐ Beneficence ☐ Nonmaleficence ☐ Justice ☐ Autonomy	☐ Strongly disagree ☐ Disagree ☐ Doubtful ☐ Agree ☐ Strongly agree
S29	Families of COVID-19 patients can forcibly take the dead bodies of COVID-19 patients.	☐ Beneficence ☐ Nonmaleficence ☐ Justice ☐ Autonomy	☐ Strongly disagree ☐ Disagree ☐ Doubtful ☐ Agree ☐ Strongly agree

PERIÓDICO TCHÊ QUÍMICA
ARTIGO ORIGINAL

O COMPOSTO QUATERNÁRIO DE CALCOGENIDA $Ag_2FeGeSe_4$: UMA REVISÃO DE SUA ESTRUTURA CRISTAL E PROPRIEDADES MAGNÉTICAS

THE QUATERNARY CHALCOGENIDE COMPOUND $Ag_2FeGeSe_4$: A REVISION OF THEIR CRYSTAL STRUCTURE AND MAGNETIC PROPERTIES

EL COMPUESTO CALCOGENURO CUATERNARIO $Ag_2FeGeSe_4$: UNA REVISIÓN DE SU ESTRUCTURA CRISTALINA Y PROPIEDADES MAGNÉTICAS

DELGADO, Gerzon E.[1*]; DELGADO-NIÑO, Pilar[2], QUINTERO, Eugenio[3]

[1] Laboratorio de Cristalografía, Departamento de Química, Facultad de Ciencias, Universidad de Los Andes, Mérida, Venezuela

[2] Departamento de Ingeniería Ambiental, Facultad de Ingeniería, Universidad Libre, Bogotá, Colombia

[3] Centro de Estudios de Semiconductores, Departamento de Física, Facultad de Ciencias, Universidad de Los Andes, Mérida, Venezuela

** Correspondence author*
e-mail: gerzon@ula.ve

Received 8 April 2021; received in revised form 18 May 2021; accepted 22 June 2021

RESUMO

Introdução: Quaternary compounds bellowing to the I_2-II-IV-VI_4 system are of considerable technological interest due to their possible use in the preparation of solar cell and thermoelectric materials devices. In recent years considerable attention has been focused on the detailed study of quaternary chalcogenide compounds related to the chalcopyrite compounds, particularly $AgInSe_2$ which has emerged as a leading material for the preparation of photovoltaic devices due to their potential applications in solar cell technology. **Objetivos**: This work focuses on the synthesis, chemical analysis, thermal study, magnetism measurement and crystal structural characterization of the quaternary semiconductor $Ag_2FeGeSe_4$, an important member of the family I_2-II-IV-VI_4. **Métodos**: This material was synthesized by the melt and anneal technique, the chemical analysis was carried out by scanning electron microscopy (SEM), thermal study was performed by differential thermal analysis (DTA) measurements, magnetic susceptibility (χ) as a function of temperature and magnetization as a function of the magnetic field were performed, and crystal structure analysis was made employing the Rietveld method with powder X-ray diffraction data. **Resultados e Discussão**: The preparation confirms the formation of the quaternary compound with stoichiometric 2:1:1:4 according to the chemical analysis. This quaternary compound melt at 1015 K, and show an antiferromagnetic behavior with Neel temperature T_N of 240 K. The Debye temperature (θ_D) estimated for this compound was 194 K. The quaternary chalcogenide compound $Ag_2FeGeSe_4$ crystallizes in the orthorhombic space group $Pmn2_1$, Z = 4, with unit cell parameters: a = 7.6478(1) Å, b = 6.5071(1) Å, c = 6.4260(1) Å, and V = 319.79(1) Å^3, in a wurtzite-stannite arrangement with a Cu_2CdGeS_4-type structure, which is characterized by a three-dimensional arrangement of slightly distorted $AgSe_4$, $FeSe_4$, and $GeSe_4$ tetrahedra connected by corners. In this structure, each Se atom is coordinated by four cations located at the corners of a slightly distorted tetrahedron, and each cation is tetrahedrally bonded to four anions. **Conclusão**: The melt and anneal method remains effective for preparing compounds chalcogenides as the quaternary $Ag_2FeGeSe_4$, a new member of I_2-II-IV-VI_4 family of semiconductors which crystallizes in the non-centrosymmetric space group $Pmn2_1$ with diamond-like structure. The crystal structure information of this compound allows explaining their magnetic properties which in combination with its semiconductor properties make this material a potential aspirant for different applications, mainly in solar cells.

Palavras-chave: *Semicondutores, difração de raios-X em pó, estrutura cristalina, método de Rietveld, magnetismo.*

ABSTRACT

Background: Quaternary compounds bellowing to the I_2-II-IV-VI_4 system are of considerable technological interest due to their possible use in the preparation of solar cell and thermoelectric materials devices. In recent years, considerable attention has been focused on the detailed study of quaternary chalcogenide compounds related to the chalcopyrite compounds, particularly $AgInSe_2$, which has emerged as a leading material for the

DOI: 10.52571/PTQ.v18.n38.2021.07_DELGADO_pgs_85_99.pdf

preparation of photovoltaic devices due to their potential applications in solar cell technology. **Aims**: This work focuses on synthesis, chemical analysis, thermal study, magnetism measurement, and crystal structural characterization of the quaternary semiconductor $Ag_2FeGeSe_4$, an essential member of the family I_2-II-IV-VI_4. **Methods**: This material was synthesized by the melt and anneal technique. The chemical analysis was carried out by scanning electron microscopy (SEM) and differential thermal analysis (DTA). Magnetic susceptibility (χ) as a function of temperature and magnetization as a function of the magnetic field were also performed, and crystal structure analysis was made employing the Rietveld method with powder X-ray diffraction data. **Results and Discussion**: The preparation confirms the formation of the quaternary compound with stoichiometric 2:1:1:4 according to the chemical analysis. This quaternary compound melt at 1015 K, and show an antiferromagnetic behavior with Neel temperature T_N of 240 K. The Debye temperature (θ_D) estimated for this compound was 194 K. The quaternary chalcogenide compound $Ag_2FeGeSe_4$ crystallizes in the orthorhombic space group *Pmn2₁*, Z = 4, with unit cell parameters: *a* = 7.6478(1) Å, *b* = 6.5071(1) Å, *c* = 6.4260(1) Å, and V = 319.79(1) Å^3, in a wurtzite-stannite arrangement with a Cu_2CdGeS_4-type structure, which is characterized by a three-dimensional arrangement of slightly distorted $AgSe_4$, $FeSe_4$, and $GeSe_4$ tetrahedra connected by corners. In this structure, each Se atom is coordinated by four cations located at the corners of a slightly distorted tetrahedron, and each cation is tetrahedrally bonded to four anions. **Conclusions**: The melt and anneal method remains effective for preparing compounds chalcogenides as the quaternary $Ag_2FeGeSe_4$, a new member of I_2-II-IV-VI_4 family of semiconductors, which crystallizes in the non-centrosymmetric space group *Pmn2₁* with diamond-like structure. The crystal structure information of this compound allows explaining their magnetic properties, which in combination with its semiconductor properties make this material a potential aspirant for different applications, mainly in solar cells.

Keywords: *Semiconductors, powder X-ray diffraction, crystal structure, Rietveld method, Magnetism.*

RESUMEN

Antecedentes: Los compuestos cuaternarios pertenecientes al sistema I_2-II-IV-VI_4 son considerados de interés tecnológico debido a sus posibles usos en la preparación de celdas solares y dispositivos como materiales termoeléctricos. En años recientes, una considerable atención se ha enfocado en el estudio detallado de compuestos calcogenuros cuaternarios, particularmente AgInSe2, el cual ha emergido como un material líder en la preparación de dispositivos fotovoltaicos debido a sus potenciales usos en tecnología de celdas solares. **Objetivos**: Este trabajo se enfoca en la síntesis, análisis químico, estudio térmico, medidas de magnetismo y la caracterización estructural del semiconductor cuaternario $Ag_2FeGeSe_4$, un importante miembro de la familia I_2-II-IV-VI_4. **Métodos**: Este material se sintetizó utilizando la técnica de fusión y recocido. El análisis químico se llevó a cabo por microscopia electrónica de barrido (SEM) y por análisis térmico diferencial (DTA). Se realizaron medidas de susceptibilidad magnética (χ) como función de la temperatura y de la magnetización (M) como función del campo aplicado, y el análisis de la estructura cristalina se realizó empleando el método de Rietveld con datos de difracción de rayos-X en muestras policristalinas. **Resultados y discusiones**: La preparación confirmó la formación del compuesto cuaternario con estequiometria 2:1:1:4 de acuerdo con el análisis químico. Este compuesto cuaternario funde a1015 K, y muestra un comportamiento anti ferromagnético con una temperatura de Neel T_N de 240 K. La temperatura de Debye (θ_D) estimada para este compuesto es de 194 K.El compuesto calcogenuro cuaternario $Ag_2FeGeSe_4$ cristaliza en el grupo especial ortorrómbico *Pmn2₁*, Z = 4, con parámetros de celda unidad : *a* = 7.6478(1) Å, *b* = 6.5071(1) Å, *c* = 6.4260(1) Å, y V = 319.79(1) Å^3, en un arreglo wurtzita-estanita con estructura tipo Cu_2CdGeS_4, la cual se caracteriza por un arreglo tridimensional de tetraedros $AgSe_4$, $FeSe_4$, y $GeSe_4$ ligeramente distorsionados conectados por las esquinas. En esta estructura, cada átomo de selenio esta coordinado a cuatro cationes localizados en las esquinas de un tetraedro ligeramente distorsionado, y cada catión, a su vez, esta enlazado tetraédricamente a cuatro aniones. **Conclusions**: El método de fusión y recocido sigue siendo efectivo en la preparación en compuestos calcogenuros como el cuaternario $Ag_2FeGeSe_4$, un nuevo miembro dela familia de semiconductores I_2-II-IV-VI_4, los cuales cristalizan in el grupo espacial no-centrosimétrico con una estructura tipo diamante. La información sobre la estructura cristalina de este compuesto permite explicar sus propiedades magnéticas las cuales en combinación con sus propiedades semiconductoras hacen de este material un potencial aspirante para diferentes aplicaciones, principalmente in celdas solares.

Palabras clave: *Semiconductores, difracción de rayos-X en muestras policristalinas, estructura cristalina, método de Rietveld, magnetismo.*

1. INTRODUCTION:

The family of quaternary diamond-like semiconductors: I_2-II-IV-VI_4 with (I = Cu, Ag; II = Zn, Cd, Mn, Fe; IV = Ge, Sn; VI = S, Se) are formed from the tetrahedrally coordinated derivatives of the II-VI binaries (Parthé, 1995; Nikiforov, 1999) and can be defined as tetrahedral chalcogenides because their closest neighbors fourfold surround anions and cations. These materials have received increasing consideration for their promising physical properties and wide applications, mainly the Cu-based compounds which have been used as thermoelectric materials (Shi *et al*., 2009; Sevik and Cagin, 2010; Ibañez *et al*., 2012), solar-cell (Guo *et al*., 2009; Ahn *et al*., 2010; Todorov *et al*., 2010) and photocatalysts (Tsuji *et al*., 2010). Cu_2ZnSnS_4, for example, can be employed as photovoltaic devices because of its environmentally friendly thin-film solar-cell absorber, large absorption coefficient (~10^5 cm^{-1}), and optimum direct bandgap energy (~1.5 eV) (Wei *et al*., 2012; Liu *et al*., 2013).

When this family of semiconductor compounds is introduced, a paramagnetic cation as cation II, such as Mn^{+2}, Fe^{+2}, Co^{+2}, or Ni^{+2}, higher capacity as magneto-optical materials are produced (Shapira *et al*., 1988). These types of materials are known as semimagnetic compounds.

This family of quaternary compounds complies with the rules of adamantane formation (Parthé, 1995). According to this rule, when substituting cations, the average number of valence electrons per atom (4) and the ratio of valence electrons to the number of anions (8) are maintained. The general composition diagram for these quaternary compounds and their related binary and ternary compounds can be represented as shown in Figure 1.

From the structural point of view, these materials crystallize in sphalerite derivatives with tetragonal symmetry in a Cu_2FeSnS_4-type structure (stannite, space group $I\bar{4}2m$) or a Cu_2ZnSnS_4-type structure (kesterite, space group $I\bar{4}$) (Hall *et al*., 1978), or wurtzite derivatives with orthorhombic symmetry in a Cu_2CdGeS_4-type structure (wurtzite-stannite, space group $Pmn2_1$) (Parthé *et al*., 1969) or with monoclinic symmetry (wurtzite-kesterite, space group *Pn*) (Joubert-Bettan *et al*., 1969). Figure 2 shows the unit cells of each of the structures mentioned above. The slight differences lie in the distribution of the cations in the tetrahedral sites. It has been shown that there is a close relationship between the properties of the wurtzite-kesterite and kesterite structures as between wurtzite-stanite and stannite structures (Chen *et al*., 2010).

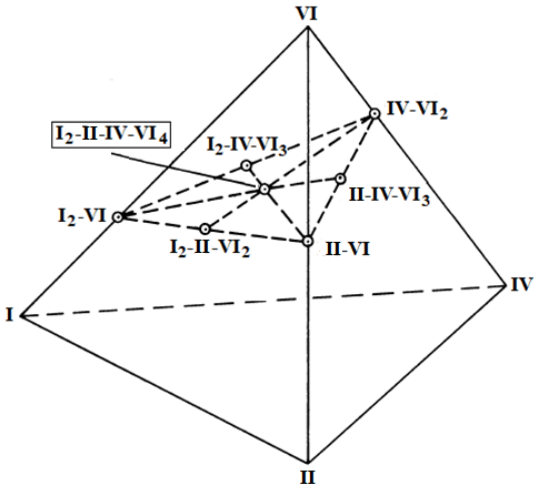

Figure 1. *General composition diagram showing the I_2-II-IV-VI_4 compounds.*

Several studies carried out in recent years on the structural characterization and physical properties of these I_2-II-IV-VI_4 quaternary semiconductor chalcogenides have been reported (Delgado *et al*., 2004; Quintero *et al*., 2007; Caldera *et al*., 2008; Moreno *et al*., 2009; Rincón *et al*., 2011; Dong *et al*., 2015; Wei and Nolas, 2015; Delgado *et al*., 2018). Nevertheless, the semimagnetic compounds of the Ag_2-II-IV-VI_4 family have received minor attention, although these Ag-based quaternary compounds also exhibit remarkable magnetic properties (Parasuk *et al*., 2002; Parasyuk *et al*., 2005; Davydyuk *et al*., 2011; Brunetta *et al*., 2012a; Brunetta *et al*., 2012b; Quintero *et al*., 2001; Wooley *et al*., 2003; Marquina *et al*., 2017), with photocatalyst and photo-electrochemical applications as in the case of Ag_2ZnSnS_4 (Li *et al*., 2013; Yeh and Cheng, 2014).

Table 1 shows the structural information found in the literature about the Ag_2-II-IV-VI_4 quaternary compounds with II= Mn, Fe, Zn, Cd, IV= Si, Ge, Sn, and VI= S, Se, Te, where the more relevant crystallographic parameters as unit cell, volume and bond distances together with the crystalline system and the space group are shown. Is possible observe that most compounds with detailed structural studies are those containing sulfur as anion.

In particular, as regards the quaternary $Ag_2FeGeSe_4$, which could be of interest because it was reported that it shows antiferromagnetic behavior down to 60K and an appreciably larger ferromagnetic effect below this temperature

(Wooley *et al*., 2003), and a low-temperature phase was identified in the equilibrium phase space of the system Ag-Fe-Ge-Se using thermodynamic calculations (Moroz *et al*., 2021). However, its crystal structure has not been established.

In the literature and crystallographic databases, Powder Diffraction File (PDF-ICDD, 2019), Inorganic Crystal Structure Database (ICSD, 2018), and Springer Materials (SpringerMaterials, 2021) only appear to report the same information corresponding only with the cell parameters obtained from a Güinier X-ray photographic data study (Quintero *et al*., 1999), without structural details such as the space group and atomic positions of cations and anions in the crystal packing.

The structural characterization of this quaternary compound could be used to explain and understand its interesting magnetic properties reported, and for this reason, this work is focused on the synthesis and complete crystal structure analysis of the semimagnetic compound $Ag_2FeGeSe_4$ using powder X-ray diffraction data.

2. MATERIALS AND METHODS:

2.1. Synthesis

The sample was synthesized by the melt and annealed technique. Highly pure components (silver 99.98 %, iron 99.97 %, germanium 99.99 %, and selenium 99.99 from Goodfellow) of 1 g sample were sealed under vacuum (≈ 10^{-5} Torr) in a small quartz ampoule which had previously been carbonized to prevent interaction of the components with the quartz. The components were heated up to 470 K and kept for about 1-2 h, and then the temperature was raised to 770 K using a rate of 40 K/h and held at this temperature for 14 hours. After, the sample was heated from 770 °C to 1070 K at a rate of 30 K/h and kept at this temperature for another 14 hours. Then it was raised to 1420 K at 60 K/h, and the components were melted together at this temperature. The furnace temperature was brought slowly (4 K/h) down to 870 K, and the sample was annealed at this temperature for 1 month. Then, the sample was slowly cooled to room temperature using a rate of about 2 K/h.

2.2. Chemical analysis (EDS)

The stoichiometric relations of the sample were investigated by scanning electron microscopy (SEM) technique, using Hitachi S2500 equipment. The microchemical composition was found by an energy-dispersive X-ray spectrometer (EDS) coupled with a computer-based multichannel analyzer (MCA, Delta III analysis, and Quantex software, Kevex). For the EDS analysis, K_α lines were used. The accelerating voltage was 15 kV. The samples were tilted 35 degrees. A standardless EDS analysis was made with a relative error of ± 5-10% and detection limits of the order of 0.3 wt %, where the k-ratios are based on theoretical standards. Table 2 shows the experimental results on the stoichiometry of the quaternary $Ag_2FeGeSe_4$, for which three different regions of the ingot were evaluated. These results indicate that the composition corresponds to the ratio 2: 1: 1:4.

2.3. Thermal analysis (DTA)

Differential thermal analysis (DTA) measurements were obtained, in the temperature range between 295 and 1150 K, using a Perkin-Elmer DTA-7 with aluminum and gold used as reference materials. The charge was of a powdered sample of approximately 100 mg weight. The error in determining these temperatures is about ±10K. The value of the melting point for the compound was obtained from the peaks on the DTA cooling curve. Melting temperature was determined from the baseline intercept of the tangent to the leading edge of the peak in the difference signal. The cooling DTA melting peak is shown in Figure 3. $Ag_2FeGeSe_4$ melt at 1015 K.

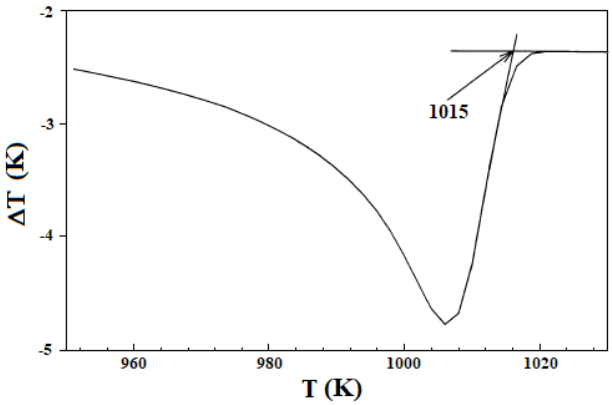

***Figure 3**. DTA curve for the quaternary $Ag_2FeGeSe_4$.*

2.4. Magnetization measurement

Measurements of magnetic susceptibility (χ) as a function of temperature (T) were made using a Quantum Design SQUID magnetometer with an external magnetic field of $1x10^{-2}$ T. Measurements were made in the range of 2 to 300

K. The magnitude of χ vs T variations serves to determine the temperatures at which magnetic transitions occurred and to estimate the type of transition.

Figure 4 shows the magnetic susceptibility curves (χ vs T) in the temperature range 2K to 300 K., where are shown the heating curve (zero-field cooled) and cooling curve (field cooled). The form of the curves indicates that the transition is an antiferromagnetic type, with Neel temperature T_N of 240 K, and a weak ferromagnetic contribution, which has been observed previously in similar compounds (Quintero *et al*., 2001).

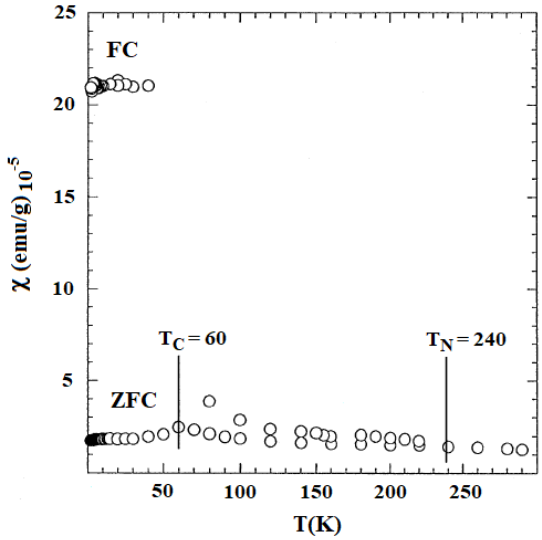

Figure 4*. Variation of magnetic susceptibility (χ) with temperature (T) for zero-field cooled (ZFC) and field cooled (FC) conditions. Vertical lines show transitions T_N and T_C.*

Measurements of magnetization (M) as a function of applied field (B) were made at helium temperatures using the high field pulsed technique for fields up to 35 T, and using the SQUID steady-field system with fields up to 6 T. Figure 5 show the variations of M with B for the quaternary $Ag_2FeGeSe_4$. In this figure is possible observe the spin-flop behavior for measurements using pulsed field system, where an appreciable hysteresis is present with a B_f with a value of approximately 16 T.

These results indicate that $Ag_2FeGeSe_4$ has a Neel temperature of 240 K and shows mainly antiferromagnetic behavior with a very weak superimposed ferromagnetic component down to 60K. At 4.2 K, a transition occurs resulting in an appreciably larger ferromagnetic effect below the transition.

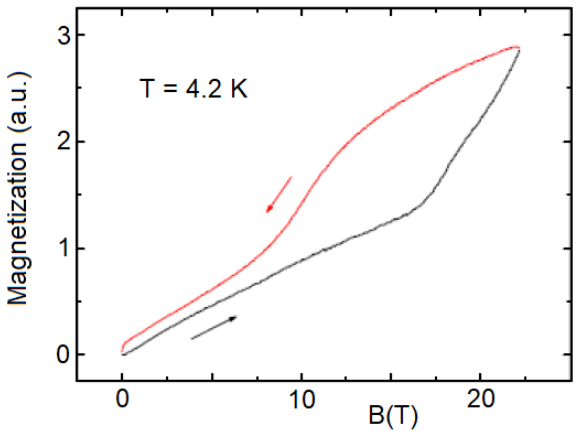

Figure 5. *Magnetization measurement (M) vs applied magnetic field (B) of the chalcogenide $Ag_2FeGeSe_4$ at 4.2 K.*

Additionally, the Debye temperature θ_D, was calculated by using the Lindemann's expression $\theta_D \approx C\,(T_M/W)^{1/2}(1/a_e)$ (Deus *et al*., 1981). Where, *C* is a constant (*C* ≈ 300 for I_2-II-IV-VI_4 tetrahedral bonded quaternary compounds) (Dong *et al*., 2015), T_M is the melting temperature of the compound (1015 K), *W* is the molecular weight, and a_e is the effective lattice parameter $a_e = (V/Z)^{1/3}$ (a_e = 5.7354 Å) where *V* is the volume of the unit cell (in Å^3) and *Z* the number of molecules per cell (Z = 2). For $Ag_2FeGeSe_4$ the θ_D value obtained was ≈ 194 K, which agree well with those reported, from 185 to 310 K (Quintero *et al*., 2014),.for related semimagnetic semiconductor compounds.

2.5. Powder X-ray diffraction (PXRD)

A small quantity of the sample was ground in an agate mortar and pestle. The resulting fine powder, sieved to a grain size of fewer than 46 μm, was mounted on a flat zero-background holder. The X-ray diffraction data were measured, in θ/θ reflection mode, using a Siemens D5005 diffractometer equipped with an X-ray tube (CuKα radiation: λ = 1.5418 Å; 40kV, 30 mA) and a diffracted beam graphite monochromator. Data were collected at room temperature. The specimen was scanned in the 2θ range of 10 to 80°, the scan step was 0.02°, and the time of counting in every step was 10 s. Quartz was used as an external standard. The precise determination of peak positions was carried out employing the Winplotr analytical software (Roisnel and Rodríguez-Carvajal, 2001).

3. RESULTS AND DISCUSSION:

Figure 6 shows the resulting powder X-ray diffraction pattern for the $Ag_2FeGeSe_4$ compound. A single-phase is observed. The powder pattern was indexed using the Dicvol program (Boultif and Löuer, 2004). An orthorhombic cell of dimensions *a* = 7.650(1) Å, *b* = 6.508(1) Å, and *c* = 6.425(1) Å was obtained. These cell values are close to those previously reported in PDF: 052-0986 (PDF-ICDD, 2019). The systematic absence indicated a *P*-type cell. The crystallographic characteristics of $Ag_2FeGeSe_4$, such as the sample composition, cell parameters, and lattice-type indicate that this material crystallizes with a Cu_2CdGeS_4-type structure (Parthé et al., 1969) similarly with other related I_2-II-IV-VI_4 compounds. So, to refine the structural parameters of $Ag_2FeGeSe_4$, the space group *Pmn2₁* (Nº 31) and the atomic position parameters of Cu_2CdGeS_4 were taken as the starting values.

The Rietveld refinement (Rietveld, 1969) was performed using the Fullprof program (Rodríguez-Carvajal, 1993; Rodríguez-Carvajal, 2021). The refinement parameters were scale factor, background, unit cell parameters, peak profile, atomic coordinates, and overall isotropic temperature factor. The unit cell parameters obtained in the indexing were used as starting data. The angular dependence was described using the Cagliotti formula (Cagliotti *et al*., 1958) and the peak shapes were described by the Thompson-Cox-Hastings pseudo-Voigt profile function (Thompson *et al*., 1987). The background was refined with a polynomial of six coefficients. An overall isotropic temperature factor was refined for described the thermal motion of the atoms. The final Rietveld refinement led to agreement factors of: R_p = 7.7%, R_{wp} = 8.4%, R_{exp} = 6.6%, and S = 1.3, for 4001 step intensities and 145 independent reflections. Table 3 summarizes the Rietveld refinement results. Figure 6 shows the observed calculated and different profile for the final cycle of the refinement. Atomic coordinates, occupancy factors, and isotropic temperature factors are given in Table 4. Figure 7 shows the unit cell diagram for $Ag_2FeGeSe_4$. Bond distances and angles are given in Table 5.

$Ag_2FeGeSe_4$ crystallize with orthorhombic symmetry, space group *Pmn2₁*, and unit cell parameters: *a* = 7.6478(1) Å, *b* = 6.5071(1) Å, *c* = 6.4260(1) Å, and V = 319.79(1) $Å^3$, in a wurtzite-stannite structure. This structure can be defined as closest-packed array, in hexagonal fashion, of selenide anions with Ag^+, Fe^{2+}, and Ge^{4+} occupying tetrahedral holes, and is characterized by a three-dimensional arrangement of slightly distorted $AgSe_4$, $FeSe_4$, and $GeSe_4$ tetrahedra connected by corners. Every Ag, Fe, or Ge atom is surrounded by four Se atoms, forming $AgSe_4$, $FeSe_4$, or $GeSe_4$ units; every selenium atom has four nearest-neighbor atoms: two Ag atoms, one Fe atom, and one Ge atom. This array is expected for adamantane compounds (Parthé, 1995).

The tetrahedrons containing the Ge atoms [mean Se…Se distance 3.470(9) Å] are slightly smaller than those containing the Fe atoms [means Se…Se distance 3.946(9) Å] and Ag atoms [mean Se…Se distance 3.996(9) Å] respectively. The bond distances are slightly shorter than the sum of the ionic radii of the atoms involved (rAg^+ = 1.14 Å, rFe^{2+} = 0.77 Å, rGe^{4+} = 0.53 Å, rSe^{2-} = 1.84 Å) for structures tetrahedrally bonded (Shannon, 1976). Bond distances in Table 5 show an average Ag-Se bond length of 2.450(8) Å. This distance compare well to those found for the related ternary $AgInSe_2$ with 2.612(2) Å (Delgado *et al*., 2015) and for the quaternary $Ag_2CdSnSe_4$ with 2.572(2) Å (Parasyuk *et al*., 2002). The Fe-Se bond has an average length of 2.417(8) Å which compare well with those observed in compounds as CuFe(Al,Ga,In)Se_3 (Mora *et al*., 2007) and $CuFe_2$(Al,Ga,In)Se_4 (Delgado *et al*., 2008). The Ge-Se [mean value 2.126(8) Å] is also in good agreement with similar distances in Cu_2GeSe_3 (Rincón *et al*., 2008), Cu_2GeSe_4 (Chi *et al*., 2013; Delgado *et al*., 2015) $Cu_2ZnGeSe_4$ (Parayuk *et al*., 2001) and $Cu_2CdGeSe_4$ (Gulay *et al*., 2002). All these structures were found in the Inorganic Crystal Structure Database (ICSD, 2018).

4. CONCLUSIONS:

The quaternary chalcogenide compound $Ag_2FeGeSe_4$ was synthesized by the melt and anneals technique from the pure elements and its crystal structure was characterized by X-ray diffraction analysis. Rietveld refinement from the powder X-ray data allowed us to determine the crystal structure of this compound.

This compound crystallizes in the wurtzite-stannite structure, space group *Pmn2₁*, characterized by a three-dimensional arrangement of slightly distorted $AgSe_4$, $FeSe_4$, and $GeSe_4$ tetrahedra connected by corners, and correspond to one new member of the quaternary chalcogenide material belonging to the I_2-II-IV-VI_4 family of semiconductors.

This quaternary compound melt at 1015 K, and show an antiferromagnetic behavior with Neel temperature T_N of 240 K. The Debye temperature

(θ_D) estimated for this compound was 194 K.

The crystal structure information of this compound allows explaining their magnetic properties which in combination with its semiconductor properties make this material a potential aspirant for different applications, mainly in solar cells.

5. ACKNOWLEDGMENTS:

The authors want to thank CDCHT-ULA and FONACIT, Venezuela.

6. REFERENCES:

1. Ahn, S., Jung, S., Gwak, J., Cho, A., Shin, K., Yoon, K., Park, D., Cheong, H., Yun, J.H. (2010). Determination of band gap energy of thin films: On the discrepancies of reported band gap values. *Applied Physics Letters, 97*(2): 0219051-3. https://doi.org/10.1063/1.3457172.
2. Boultif, A., Löuer, D. (2004). Powder pattern indexing with the dichotomy method. *Journal of Applied Crystallography, 37*(5)**:** 724-731. http://dx.doi.org/10.1107/S0021889804014876.
3. Brunetta, C.D., Balamurugan, K., Rosmus, K.A., Aitken, J.A. (2012a). The crystal and electronic band structure of the diamond-like semiconductor Ag_2ZnSiS_4. *Journal of Alloys and Compounds, 516*(1-2): 65-72. https://doi.org/10.1016/j.jallcom.2011.11.133.
4. Brunetta, C.D., Brant, J.A., Rosmus, K.A., Henline, K.M., Karey, E., MacNeil, J.H., Aitken, J.A. (2013). The impact of three new quaternary sulfides on the current predictive tools for structure and composition of diamond-like materials. *Journal of Alloys and Compounds, 574*(8): 495-503. http://dx.doi.org/10.1016/j.jallcom.2013.05.141.
5. Brunetta, C.D., Minsterman III, W.C., Lake, C.H., Aitken, J.A. (2012b). Cation ordering and physicochemical characterization of the quaternary diamond-like semiconductor Ag_2CdGeS_4. *Journal of Solid State Chemistry, 187*(3): 177-185. http://dx.doi.org/10.1016/j.jssc.2011.12.032.
6. Cagliotti, G., Paoletti, A., Ricci, F.P. (1958). Choice of collimators for a crystal spectrometer for neutron diffraction. *Nuclear Instruments, 3*(4): 223-228. http://dx.doi.org/10.1016/0369-643X(58)90029-X.
7. Caldera, D., Quintero, M., Morocoima, M., Quintero, E., Grima, P., Marchan, M., Moreno, E., Bocaranda, P., Delgado, G.E., Mora, A.E., Briceño, J.M., Fernandez, J.L. (2008). Lattice parameters values and phase diagram for the $Cu_2Zn_{1-z}FezGeSe_4$ alloy system. *Journal of Alloys and Compounds, 457*(1-2): 221-224. https://doi.org/10.1016/j.jallcom.2007.03.033.
8. Caye, R., Laurent, Y., Picot, P., Pierrot, R., Levy, C. (1968). La hocartite, Ag_2SnFeS_4, une nouvelle espece minerale. *Bulletin de la Societe Francaise de Mineralogie et de Cristallographie, 91*(4): 383-387. https://www.persee.fr/doc/bulmi_0037-9328_1968_num_91_4_6244.
9. Chen, W., Waslsh, A., Luoe, Y., Yang, J.H., Gong, X.G., Wei, S.H. (2010). Wurtzite-derived polytypes of kesterite and stannite quaternary chalcogenide semiconductors. *Physical Review B: covering condensed matter and materials physics, 82*(19): 195203. https://doi.org/10.1103/PhysRevB.82.195203.
10. Choi, S.G., Donohue, A.L., Marcano, G., Rincón, C., Gedvilas, L.M., Li, J., Delgado, G.E. (2013). Optical properties of cubic-phase Cu_2GeSe_4 single crystal. *Journal of Applied Physcis, 114*(3): 033531. https://doi.org/10.1063/1.4816051.
11. Davydyuk, G.E., Myronchuka, G.L., Kittyk, I.V., Danyl'chuk, S.P., Bozhko, V.V., Parasyuk, O.V. (2011). Ag_2CdSnS_4 single crystals as promising materials for optoelectronic. *Optical Materials, 33*(8): 1302-1306. https://doi.org/10.1016/j.optmat.2011.03.003.
12. Delgado, G.E., Contreras, J.E., Marcano, G., Rincón, C., Nieves, L. (2015). Caracterización estructural del semiconductor ternario Cu_2GeSe_4. *Revista LatinoAmericana de Metalurgia y Materiales, 35*(1): 34-38. http://www.rlmmjournal.com/index.php/path/article/download/120/118.

13. Delgado, G.E., Mora, A.J., Grima-Gallardo, P., Quintero, M. (2008). Crystal structure of $CuFe_2InSe_4$ from X-ray powder diffraction. *Journal of Alloys and Compounds, 454*(1-2): 306-309. https://doi.org/10.1016/j.jallcom.2006.12.057.

14. Delgado, G.E., Mora, A.J., Pineda, C., Ávila, R., Paredes, S. (2015). X-ray powder diffraction data and Rietveld refinement of the ternary semiconductor chalcogenides $AgInSe_2$ and $AgInTe_2$. *LatinAmerican Journal of Metallurgy and Materials, 35*(1): 110-117. http://www.rlmm.org/ojs/index.php/rlmm/article/view/546.

15. Delgado, G.E., Quintero, E., Tovar, R., Quintero, M. (2004). X-ray powder diffraction study of the semiconducting alloy $Cu_2Cd_{0.5}Mn_{0.5}GeSe_4$. *Crystal Research and Technology, 39*(9): 807-810. https://doi.org/10.1002/crat.200310257.

16. Delgado, G.E., Sierralta, N., Quintero, E., Quintero, M., Quintero, E., Moreno, E., Flores, J.A., Rincón, C. (2018). Synthesis, structural characterization and differential thermal analysis of the quaternary compound Ag_2MnSnS_4. *Revista Mexicana de Física, 64*(3): 216-221. https://doi.org/10.31349/RevMexFis.64.216.

17. Deus, P., Schneider, H.A., Voland, U. (1981). Estimation of the Debye temperature of diamond-like semiconducting compounds by means of the Lindemann rule. *Crystal Research and Technology, 16*(8): 941-948. https://doi.org/10.1002/crat.19810160814.

18. Dong, Y., Wojtas, L., Martin, J., Nolas, G.S. (2015). Synthesis, crystal structure, and transport properties of quaternary tetrahedral chalcogenides. *Journal of Materials Chemistry C, 3*(40): 10436-10441. https://doi.org/10.1039/C5TC01606A.

19. Friedrich, D., Greil, S., Block, T., Heletta, L., Pöttgen, R., Pfitzner, A. (2018). Synthesis and characterization of Ag_2MnSnS_4, a new diamond-like semiconductor. *Zeitschrift für anorganische und allgemeine Chemie, 644*(24): 1707-1714. http://dx.doi.org/10.1002/zaac.201800142.

20. Gulay, Y.E., Romanyuk, L.V., Parasyuk, L.D. (2002). Crystal structures of low- and high-temperature modifications of $Cu_2CdGeSe_4$. *Journal of Alloys and Compounds, 347*(1-2): 193-197. https://doi.org/10.1016/S0925-8388(02)00790-9.

21. Guo, Q., Hillhouse, W.W., Agrawal R. (2009). Synthesis of Cu_2ZnSnS_4 nanocrystal ink and its use for solar cells. *Journal of American Chemical Society, 131*(33): 11672-11673. https://doi.org/10.1021/ja904981r.

22. Hall, S.R., Szymanski, J.T., Stewart, J.M. (1978). Kesterite, $Cu_2)(Zn,Fe)SnS_4)$, and stannite, $Cu_2)(Fe,Zn)SnS_4)$, structurally similar but distinct minerals. *Canadican Mineralogist, 16*(2): 131-137. http://canmin.geoscienceworld.org/content/16/2/131.extract.

23. Ibañez, M., Cacavid, M., Zamani, R., García-Castelló, N., Izquierdo-Roca, V., Li, W., Fairbrother, A., Prades, J.D., Shavel, A., Arbiol, J., Pérez-Rodríguez, A., Morante, J.R., Cabot, A. (2012). Composition control and thermoelectric properties of quaternary chalcogenide nanocrystals: The case of stannite $Cu_2CdSnSe_4$. *Chemistry of Materials, 24*(3): 562-570. https://doi.org/10.1021/cm2031812.

24. ICSD-*Inorganic Crystal Structure Database*. Gemlin Institute, Kalrsruhe, Germany, 2018.

25. International Centre for Diffraction Data. *PDF-ICDD-Powder Diffraction File (Set 1-71)*. Newtown Square, PA, USA, 2019.

26. Johan, Z., Picot, P. (1982). La pirquitasite, Ag_2ZnSnS_4, un nouveau membre du groupe de la stannite. *Bulletin de la Societe Francaise de Mineralogie et de Cristallographie, 105*(3): 229-235. https://www.persee.fr/doc/bulmi_0180-9210_1982_num_105_3_7610.

27. Joubert-Bettan, C.A., Lachenal, R., Bertaut, E.F., Parthé, E. (1969). The crystal structures of Na_2ZnSiO_4, Na_2ZnGeO_4, and Na_2MgGeO_4. *Journal of Solid State Chemistry, 1*(1): 1-5. https://doi.org/10.1016/0022-4596(69)90001-2.

28. Li, K., Chai, B., Peng, T., Mao, J., Zan, L. (2013). Synthesis of multicomponent sulfide Ag_2ZnSnS_4 as an efficient

photocatalyst for H_2 production under visible light irradiation. *RSC Advances, 3*(1): 253-258. https://doi.org/10.1039/C2RA21481D.

29. Liu, W., Guo, B., Mak, C., Li., A., Wu, X., Zhang, F. (2013). Facile synthesis of ultrafine Cu_2ZnSnS_4 nanocrystals by hydrothermal method for use in solar cells. *Thin Solid Films, 535*(5): 39-43. https://doi.org/10.1016/j.tsf.2012.11.073

30. Marquina, J., Sierralta, N., Quintero, M., Rincón, C., Morocoima, M., Quintero, E. (2017). Study of the critical-fields and the thermal broadening in polycrystalline $Ag_2FeGeSe_4$ semiconducting compound. *Revista Mexicana de Física, 63*(5): 456-460. https://rmf.smf.mx/ojs/rmf/article/view/366/211.

31. Mora, A.J., Delgado, G.E., Grima-Gallardo, P. (2007). Crystal structure of $CuFeInSe_3$ from X-ray powder diffraction data. *physica status solidi (a): applications and materials science, 204* (2): 547-554. https://doi.org/10.1002/pssa.200622395.

32. Moreno, E., Quintero, M., Morocoima, M., Quintero, E., Grima-Gallardo, P., Tovar, R., Bocaranda, P., Delgado, G.E,, Contreras, J.E., Mora, A.E., Briceño, J.M., Avila, R., Fernandez, J.L., Henao, J.A., Macías, M.A. (2009). Lattice parameter values and phase transitions for the $Cu_2Cd_{1-z}Mn_zSnSe_4$ and $Cu_2Cd_{1-z}Fe_zSnSe_4$ alloys". *Journal of Alloys and Compounds, 486*(1-2): 212-218. https://doi.org/10.1016/j.jallcom.2009.07.066.

33. Moroz, M., Tesfaye, F., Demchenko, P., Prokhorenko, M., Rudyk, B., Soliak, L., Lindberg, D., Reshetnak, O., Hupa, L. (2021). Thermodynamic examination of quaternary compounds Ag-Fe-(Ge,Sn)-Se systems by solid-state EMF method. *In Materials Processing Fundamentals, The Minerals, metals & Materials Series*; JohnWiley & Sons, Ltd. Hoboken, NJ, USA, pp. 271-290. https://doi.org/10.1007/978-3-030-65253_1_24.

34. Nikiforov, K.G. Magnetically ordered multinary semiconductors. (1999). *Progress in Crystal Growth and Characterization of Materials, 39*(1-4): 1-104. https://doi.org/10.1016/S0960-8974(99)00016-9.

35. Parasyuk, L.D., Gulay, Y.E., Romanyuk, L.V., Piskach, L.V. (2001). Phase diagram of the Cu_2GeSe_3-ZnSe system and crystal structure of the $Cu_2ZnGeSe_4$ c compound. *Journal of Alloys and Compounds, 329*(1): 202-207. https://doi.org/10.1016/S0925-8388(01)01606-1.

36. Parasyuk, O.V., Fedorchuk, A.O., Kogut, Y.M., Piskach, L.V., Olekseyuk, I.D. (2010). The Ag_2S-ZnS-GeS_2 system: Phase diagram, glass-formation region and crystal structure of Ag_2ZnGeS_4. *Journal of Alloys and Compounds,* 500(1), 26-29. https://doi.org/10.1016/j.jallcom.2010.03.198.

37. Parasyuk, O.V., Gulay, L.D., Piskach, L.V., Olekseyuk, I.D. (2002). The Ag_2Se-CdSe-$SnSe_2$ system at 670 K and the crystal structure of the $Ag_2CdSnSe_4$ compound. *Journal of Alloys and Compounds, 335*(1-2): 176-180. https://doi.org/10.1016/S0925-8388(01)01845-X.

38. Parasyuk, O.V., Olekseyuk, I.D., Piskach, L.V., Volkov, S.V., Pekhnyo, V.I. (2015b). Phase relations in the Ag_2S-CdS-SnS_2 system and the crystal structure of the compounds. *Journal of Alloys and Compounds, 399*(1-2): 173-177. http://dx.doi.org/10.1016/j.jallcom.2005.03.023.

39. Parasyuk, O.V., Piskach, L.V., Olekseyuk, I.D., Pekhnyo, V.I. (2005a). The quasi-ternary system Ag_2S-CdS-GeS_2 and the crystal structure of Ag_2CdGeS_4. *Journal of Alloys and Compounds, 397*(1-2): 95-98. https://doi.org/10.1016/j.jallcom.2004.12.043.

40. Parthé, E., in: Westbrook JH, Fleischer RL (Eds.), *Intermetallic compounds, principles and applications*. Jhon Wiley & Sons; Chichester, UK, 1995. Vol 1, Chap. 14.

41. Parthé, E., Yvon, K., Deitch, R.H. (1969). The crystal structure of Cu_2CdGeS_4 and other quaternary normal tetrahedral structure compounds. *Acta Crystallographica Section B: Structural Science, Crystal Engineering and Materials, 25*(6): 1164-1174. http://dx.doi.org/10.1107/S0567740869003670.

42. Quintero, E., Tovar, R., Quintero, M., Delgado, G.E., Morocoima, M., Caldera, D., Ruiz. J., Mora, A.E., Briceño, J.M., Fernandez, J.L. (2007). Lattice parameter values and phase transitions for the $Cu_2Cd_{1-z}Mn_zGeSe_4$ and $Cu_2Cd_{1-z}Fe_zGeSe_4$ alloys. *Journal of Alloys and Compounds, 432*(1-2): 142-148. https://doi.org/10.1016/j.jallcom.2006.05.126.
43. Quintero, M., Barreto, A., Grima-Gallardo, P., Quintero, E., Sánchez Porras, G., Ruiz, J., Woolley, J.C., Lamarche, G., Lamarche, A.M. (1999). Crystallographic properties of I_2-Fe-IV-VI_4 magnetic semiconductor compounds. *Materials Research Bulletin, 34*(14-15): 2263-2270. https://doi.org/10.1016/S0025-5408(00)00166-5.
44. Quintero, M., Cadenas, R., Tovar, R., Quintero, E., Gonzalez, J., Ruiz, J., Woolley, J.C., Lamarche, J.C., Lamarche, A.M., Broto, J.M., Rakoto, H., Barbaste, R. (2001). Magnetic spin-flop and magnetic saturation in $Ag_2FeGeSe_4$, $Ag_2FeSiSe_4$ and $Cu_2MnGeSe_4$ semiconductor compounds. *Physica B: Consended Matter, 294-295*(1): 471-474. https://doi.org/10.1016/S0921-4526(00)00702-X.
45. Rietveld, H.M. (1969). A profile refinement method for nuclear and magnetic structures. *Journal of Applied Crystallography, 2*(2)**:** 65-71. https://doi.org/10.1107/S0021889869006558
46. Rincón, C., Marcano, G., Marín, G., Mora, A.J., Delgado, G.E., Herrera-Pérez, J.L., Mendoza-Alvarez, J.G., Rodríguez, P. (2008). Raman scattering and X-ray diffraction study in Cu_2GeSe_3. *Solid State Communications, 146*(1-2): 65-68. https://doi.org/10.1016/j.ssc.2008.01.018.
47. Rincón, C., Quintero, M., Moreno, E., Power, Ch., Quintero, E., Henao, J.A., Macías, M.A., Delgado, G.E., Tovar, R., Morocoima, M. (2011). X-ray diffraction, Raman spectrum and magnetic susceptibility of the magnetic semiconductor Cu_2FeSnS_4. *Solid State Communication, 151*(1-2): 947-951. https://doi.org/10.1016/j.ssc.2011.04.002.
48. Rodriguez-Carvajal J. (1993). Recent advances in magnetic structure determination by neutron powder diffraction. *Physica B: Condensed Matter, 192*(1-2)**:** 55-69. http://dx.doi.org/10.1016/0921-4526(93)90108-I.
49. Rodriguez-Carvajal, J. Fullprof program: Rietveld pattern matching analysis of powder patterns (version 7.4), Laboratoire Léon Brillouin (CEA-CNRS), France, 2021.
50. Roisnel, T., Rodríquez-Carvajal, J. (2001). WinPLOTR: A windows tool for powder diffraction pattern analysis. *Materials Science Forum, 378-381*(1): 118-123. https://www.scientific.net/MSF.378-381.118
51. Sevik, C., Cagin, T. (2010). *Ab initio* study of thermoelectric transport properties of pure and doped quaternary compounds. *Physical Review B: covering condensed matter and materials physics, 82*(4): 045202. http://dx.doi.org/10.1103/PhysRevB.82.045202.
52. Shannon, R.S. (1976). Revised effective ionic radii and systematic studies of interatomic distances in halides and chalcogenides. *Acta Crystallographica Section A: Foundations and Advances, 32*(5): 751-767. http://dx.doi.org/10.1107/S0567739476001551.
53. Shapira, Y., McNiff, E.J., Oliveira, N.F., Honig, E.D., Dwight, K., Wold, A. (1988). Magnetic properties of antiferromagnetic interactions in the wurtz-stannite structure. *Physical Review B: covering condensed matter and materials physics, 37*(1): 411-418. https://doi.org/10.1103/PhysRevB.37.411.
54. Shi, X.Y., Huang, F.Q., Liu, M.L., Chen, L.D. (2009). Thermoelectric properties of tetrahedrally bonded wide-gap stannite compounds $Cu_2ZnSn_{1-x}In_xSe_4$. *Applied Physics Letters, 94*(12): 122103. https://doi.org/10.1063/1.3103604.
55. SpringerMaterials, https://materials.springer.com. Access in 30/03/2021.
56. Thompson, P., Cox, D.E., Hastings, J.B. (1987). Rietveld refinement of Debye-Scherrer synchrotron X-ray data from Al_2O_3. *Journal of Applied Crystallography, 20*(): (1987) 79-83. http://dx.doi.org/10.1107/S0021889887087090.

57. Todorov, T.K., Reuter, K.B., Mitzi, D.B. (2010). High-efficiency solar cell with earth-abundant liquid-processed absorber. *Advanced Materials, 2*(22): E156-E159. https://doi.org/10.1002/adma.200904155.

58. Tsuji, I., Shimodaira, Y., Kato, H., Kobayashi, H., Kudo, A. (210). Novel stannite-type complex sulfide photocatalysts A^{I}_2-Zn-A^{IV}-S_4 (A^{I} = Cu and Ag; A^{IV} = Sn and Ge) for sydrogen evolution under visible-light irradiation. *Chemistry of Materials, 22*(4): 1402-1409. https://doi.org/10.1021/cm9022024.

59. Wei, K., Nolas, J.S. (2015). Synthesis, characterization and alloying of Cu_2ZnSnQ_4 (Q= S, Se and Te) nanocrystals. *Journal of Solid State Chemistry, 226*(3): 215-218. https://doi.org/10.1016/j.jssc.2015.02.027.

60. Wei, M., Du., Q., Wang, D., Liu, W., Jiang, G., Zhu, C. Synthesis of spindle-like kesterite $Cu_2Zn_SnS_4$ nanoparticles using thiorea as sulfur source. *Materials Letters, 79*(7): 177-179. https://doi.org/10.1016/j.matlet.2012.03.080

61. Wooley, J.C., Lamarche, G., Lamarche, A.M., Rakoto, H., Broto, J.M., Quintero, M., Morocoima, M., Quintero, E., Gonzalez, J., Tovar, R., Cadenas, R., Bocoranda, P., Ruiz, J. (2003). High field magnetic properties of $Ag_2FeGeSe_4$ in the temperature range 2-300 K. *Journal of Magnetism and Magnetic Materials, 257*(1): 87-94. https://doi.org/10.1016/S0304-8853(02)01051-X.

62. Yeh, L.-Y., Cheng, K.-W. (2014). Preparation of the Ag-Zn-Sn-S quaternary photoelectrodes using chemical bath deposition for photoelectrochemical applications. *Thin Solid Films, 558*(5): 289-293. https://doi.org/10.1016/j.tsf.2014.02.046.

7. OPEN ACCESS:

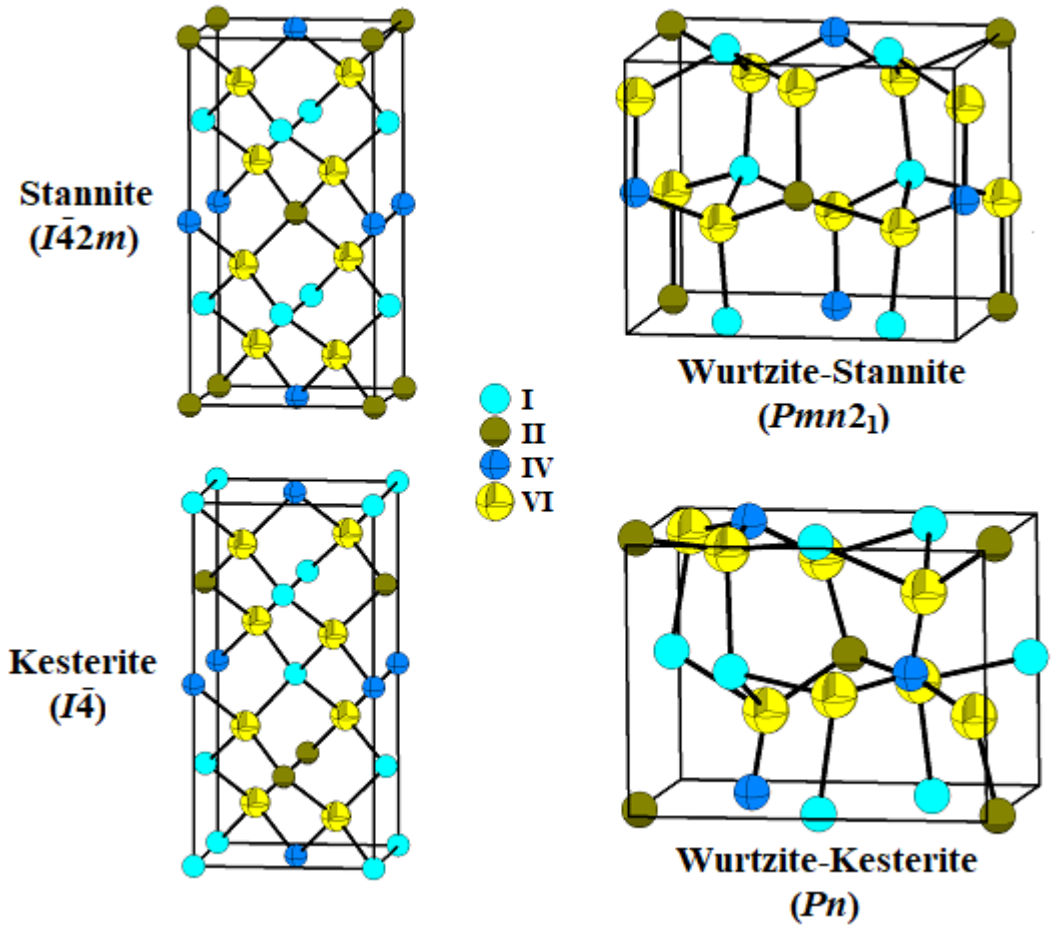

Figure 2. *Unit cell diagrams of the different structures that describe the I_2-II-IV-VI_4 family of compounds.*

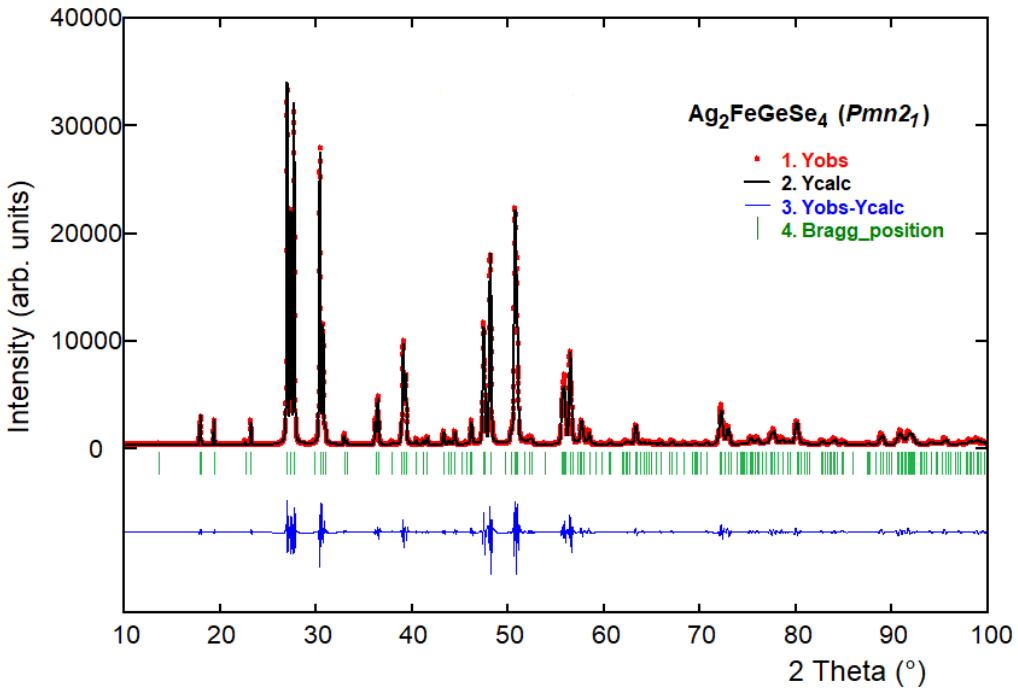

Figure 6. *Observed (·), calculated (-), and difference plot of the final Rietveld refinement of $Ag_2FeGeSe_4$. The Bragg reflections for the studied phase are indicated by vertical bars.*

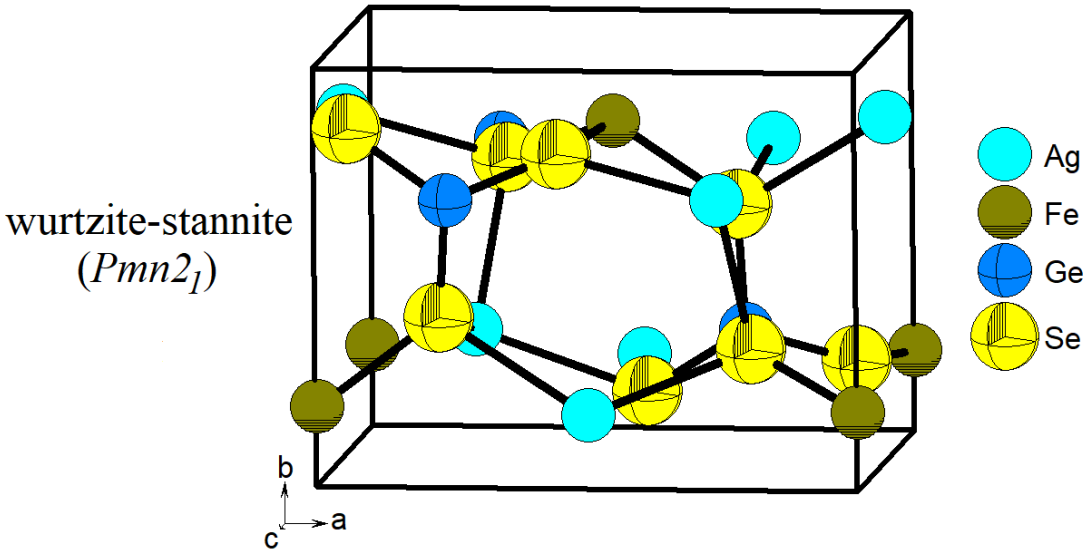

Figure 7. *Unit cell diagram of $Ag_2FeGeSe_4$ viewed in the* ***ba*** *plane of the space group $Pmn2_1$.*

***Table 1**. Crystallographic information about the quaternaries I_2-II-IV-VI_4 with I =Ag, II = Fe, Mn, Zn, Cd, IV = Si, Ge, Sn, VI = S, Se, Te.*

Molecular Formula	**System**	**Space group**	***a*, *b*, *c*, *β*** **(Å,°)**	**V (Å³)**	**Ag-VI (Å)**	**II-VI (Å)**	**IV-VI (Å)**	**Ref.**
Ag_2FeSiS_4	Mon.	*Pn* Z= 2	6.4220(1) 6.6185(1) 7.8650(1) 90.614(1)	334.28(1)	2.546(1)	2.354(1)	2.129(2)	Brunetta *et al*., 2013
Ag2FeSnS4	Tetr.	$I\bar{4}2m$ Z= 2	5.74(3) 10.96(5)	361.11	-	-	-	Caye *et al*., 1968
Ag_2MnSnS_4	Ortho.	$Pmn2_1$ Z= 2	8:1705(5) 6:9413(5) 6:6532(5)	377:33(5)	2.5982)	2.56(2)	2.25(2)	Delgado *et al.*, 2018
	Mon.	*Pc* Z= 2	6.651(1) 6.943(1) 10.536(2) 129.15(1)	377.3(1)	2.933(5)	2.401(4)	2.428(6)	Friedrich *et al*., 2018
Ag_2ZnSiS_4	Mon.	*Pn* Z= 2	6.4052(1) 6.5484(1) 7.9340(1) 90.455(1)	332.77(1)	2.2557(2)	2.344(2)	2.128(4)	Brunetta *et al*., 2012a
Ag_2ZnGeS_4	Tetr.	$I\bar{4}2m$ Z= 2	5.74996(9) 103434(3)	341.98(2)	2.578(5)	2.372(5)	2.332(5)	Parasyuk *et al*., 2010
Ag_2ZnSnS_4	Tetr.	$I\bar{4}$ Z= 2	5.786 10.829	362.53	-	-	-	Johan *et al*., 1982
Ag_2CdGeS_4	Ortho.	$Pmn2_1$ Z= 2	8.0338(3) 6.8680(2) 6.5866(3)	363.43(4)	2.55(1)	2.52(1)	2.22(1)	Parasyuk *et al*., 2005a
	Ortho.	$Pna2_1$ Z= 4	13.7415(8) 8.0367(5) 6.5907(4)	727.85(8	2.558(2)	2.526(2)	2.214(3)	Brunetta *et al*., 2012b
Ag_2CdSnS_4	Ortho.	$Cmc2_1$ Z= 8	4.1015(3) 7.0224(4) 6.6946(4)	192.82(4)	2.478(4)	2.496(5)	2.557(7)	Parasyuk *et al*., 2005b
$Ag_2FeSiSe_4$	Ortho.	$Pmn2_1$	7.653 6.529 6.638	318.79	-	-	-	Quintero *et al*., 1999
$Ag_2FeGeSe_4$	Ortho.	$Pmn2_1$	7.658 6.515 6.434	321.04	-	-	-	Quintero *et al*., 1999
	Ortho.	$Pmn2_1$ Z= 2	7.6478(1) 6.5071(1) 6.4260(1)	319.79(1)	2.450(8)	2.417(8)	2.126(8)	this work
$Ag_2FeSnSe_4$	Ortho.	$Pmn2_1$	7.398 6.993 6.401	331.12	-	-	-	Quintero *et al*., 1999
$Ag_2CdSnSe_4$	Ortho.	$Cmc2_1$ Z= 8	4.2640(2) 7.3170(3) 6.9842(4)	217.6(1)	2.572(2)	2.627(4)	2.649(3)	Parasyuk *et al*., 2002
$Ag_2FeSiTe_4$	Ortho.	$Pmn2_1$	7.721 6.657 6.588	338.65	-	-	-	Quintero *et al*., 1999
$Ag_2FeGeTe_4$	Ortho.	$Pmn2_1$	8.048 6.668 6.450	346.15	-	-	-	Quintero *et al*., 1999
$Ag_2FeSnTe_4$	Ortho.	$Pmn2_1$	8.098 6.785 6.335	348.05	-	-	-	Quintero *et al*., 1999

Mon.= monoclinic, Ortho.= orthorhombic, Tetr.= tetragonal

***Table 2**. SEM experimental results for the sample $Ag_2FeGeSe_4$.*

Composition	MW (g/mol)	Nominal Stoichiometry (%)	Experimental Stoichiometry (%)
$Ag_2FeGeSe_4$	660.03	Ag = 25.0 Fe = 12.5 Ge = 12.5 Se = 50.0	Ag = 25.1 ± 0.2 Fe = 11.2 ± 0.2 Ge = 11.5 ± 0.2 Se = 52.2 ± 0.4

***Table 3.** Results of the Rietveld refinement for $Ag_2FeGeSe_4$.*

Molecular formula	$Ag_2FeGeSe_4$	D_{calc} (g.cm^{-3})	6.85
Molecular weight (g/mol)	660.03 (g/mol)	N° step intensities	4001
a (Å)	7.6478(1)	independent refl.	145
b (Å)	6.5071(1)	Peak-shape profile	Pseudo-Voigt
c (Å)	6.4260(1)		
V (Å^3)	319.79(1)	R_{exp}	6.6 %
System	Orthorhombic	R_p	7.7 %
Space group	*Pmn2$_1$* (N° 31)	R_{wp}	8.4 %
Z	2	S	1.3

$R_p = 100\ \sum|y_{obs} - y_{calc}| / \sum|y_{obs}|$ $\quad R_B = 100\ \sum_k|I_k - Ic_k| / \sum_k |I_k|$ $\quad S = [R_{wp} / R_{exp}]$

$R_{wp} = 100\ [\sum_w|y_{obs} - y_{calc}|^2 / \sum_w|y_{obs}|^2]^{1/2}$ $\quad R_{exp} = 100[(N+C)/\sum_w(y_{obs}^2)]^{1/2}$ $\quad$ N-P+C= degrees of freedom

***Table 4.** Atomic coordinates, occupancy factors and isotropic temperature factor for $Ag_2FeGeSe_4$.*

Atom	Ox.	Wyck.	*x*	*y*	*z*	foc	B (Å^2)
Ag	+1	4*b*	0.255(1)	0.317(1)	0	1	0.51(5)
Fe	+2	2*a*	0	0.849(1)	0.987(1)	1	0.51(5)
Ge	+4	2*a*	0	0.186(1)	0.490(1)	1	0.51(5)
Se1	-2	4*b*	0.237(1)	0.324(1)	0.387(1)	1	0.51(5)
Se2	-2	2*a*	0	0.186(1)	0.822(1)	1	0.51(5)
Se3	-2	2*a*	0	0.885(1)	0.366(1)	1	0.51(5)

***Table 5.** Distance lengths (Å) and bond angles (º) for $Ag_2FeGeSe_4$.*

Ag-Se1	2.491(6)	Fe-Se1^{iv}	2.393(8)	Ge-Se1	2.128(8)
Ag-Se1^{i}	2.447(9)	Fe-Se1^{vi}	2.393(8)	Ge-Se1^{vii}	2.128(8)
Ag-Se2^{ii}	2.416(8)	Fe-Se2^{v}	2.436(9)	Ge-Se2	2.133(9)
Ag-Se3^{i}	2.445(8)	Fe-Se3^{iii}	2.447(9)	Ge-Se3^{viii}	2.115(9)
Se1-Ag-Se2^{ii}	115.8(2)	Se3^{iii}-Fe-Se1^{iv}	108.2(2)	Se1^{vii}-Ge-Se2	108.1(2)
Se1-Ag-Se3^{i}	113.8(2)	Se3^{iii}-Fe-Se1^{vi}	108.2(2)	Se1^{vii}-Ge-Se3^{viii}	105.9(2)
Se1-Ag-Se1^{i}	106.3(2)	Se3^{iii}-Fe-Se2^{v}	110.3(3)	Se1^{vii}-Ge-Se1	116.8(3)
Se1^{i}-Ag-Se3^{i}	112.9(2)	Se2^{v}-Fe-Se1^{iv}	107.9(2)	Se2-Ge-Se3^{viii}	112.1(4)
Se1^{i}-Ag-Se2^{ii}	102.5(2)	Se2^{v}-Fe-Se1^{vi}	107.9(2)	Se2-Ge-Se1	108.1(2)
Se2^{ii}-Ag-Se3^{i}	105.2(2)	Se1^{iv}-Fe-Se1^{vi}	114.4(3)	Se3^{viii}-Ge-Se1	105.9(2)

Symmetry codes: (i) 0.5-x, 1-y, -0.5+z; (ii) x, y, -1+z; (iii) x, y, 1+z; (iv) -0.5+x, 1-y, 0.5+z; (v) x, 1+y, z; (vi) 0.5-x, 1-y, 0.5+z; (vii) -x, y, z; (viii) x, -1+y, z.

PERIÓDICO TCHÊ QUÍMICA
ARTIGO ORIGINAL

O IMPACTO DA PECUÁRIA INTENSIVA DE NOVILHAS HOLSTEIN AUSTRALIANAS NAS PROPRIEDADES FÍSICO-QUÍMICAS DO LEITE DE VACA

THE IMPACT OF INTENSIVE RAISING OF AUSTRALIAN HOLSTEIN HEIFERS ON THE PHYSICOCHEMICAL PROPERTIES OF COW MILK

ВЛИЯНИЕ ИНТЕНСИВНОГО ВЫРАЩИВАНИЯ ГОЛШТИНСКИХ ТЕЛОК АВСТРАЛИЙСКОЙ СЕЛЕКЦИИ НА ФИЗИКО-ХИМИЧЕСКИЕ СВОЙСТВА МОЛОКА КОРОВ

ZABASHTA, Sergey Nikolaevich[1]; KARATUNOV, Vyacheslav Anatolievich[1]; TUZOV, Ivan Nikiforovich[1]; KOSHCHAEV, Andrey Georgievich[1*]; SHANTYZ, Aliy Yusufovich[1]

[1]Kuban State Agrarian University. Russia.

** Correspondence author*
e-mail: kagbio@mail.ru

Received 20 March 2021; received in revised form 29 April 2021; accepted 25 June 2021

RESUMO

Antecedentes: O estudo das características de crescimento, desenvolvimento e produtividade do gado importado da Austrália para o Território Krasnodar é de grande interesse científico e prático, que é tópico. Uma vez que as características produtivas dos genótipos importados não foram estudados suficientemente, não apenas nas fazendas do Território Krasnodar, mas também em outras regiões da Rússia, eles requerem um estudo mais aprofundado e melhoramento sob as novas condições de alimentação e alojamento. **Objetivo:** a pesquisa teve como objetivo estudar a influência da criação intensiva de novilhas de reposição da raça Holandesa de seleção australiana sobre os indicadores de qualidade do leite de vaca. **Métodos:** Os estudos foram conduzidos na Artex-Agro LLC, distrito de Kushchevsky do Território de Krasnodar, sobre os descendentes do gado holandês importado da Austrália. Sessenta e quatro novilhas foram selecionadas para o estudo. As novilhas de substituição experimentais foram criadas usando as taxas de alimentação de leite aumentadas e o produto probiótico Cellobacterin. Eles foram criados intensivamente e inseminados aos 14 meses de idade. A produtividade do leite das vacas e as propriedades físico-químicas do leite foram estudadas durante três lactações após o parto. **Resultados e Discussão:** A produtividade de leite das vacas dos grupos experimentais excedeu um de seus companheiros de rebanho do grupo controle em 450 - 1.360 kg. Os melhores indicadores das propriedades físico-químicas do leite foram determinados no leite das vacas criadas a partir de novilhas alimentadas com 450 kg de leite integral durante os primeiros 50 dias até os seis meses de idade. **Conclusões:** Os autores acreditam que a criação intensiva de novilhas de reposição afetou positivamente o grau de desenvolvimento do trato gastrointestinal e melhorou o nível de produção de leite e seus parâmetros físico-químicos.
Palavras-chave: *novilhas de reposição, pecuária, produção de leite, acidez, densidade, composição de aminoácidos.*

ABSTRACT

Background: The study of growth, development and productivity features of imported cattle from Australia to the Krasnodar Territory is of great scientific and practical interest, which is topical. Since the productive features of the imported genotypes have not been studied sufficiently, not only in the farms of the Krasnodar Territory but also in other regions of Russia, they require further, more in-depth study and improvement under the new conditions of feeding and housing. **Aim:** The research aimed to study the influence of intensive rearing of replacement heifers of the Holstein breed of Australian selection on cow milk quality indicators. **Methods:** The studies were conducted at Artex-Agro LLC, Kushchevsky District of the Krasnodar Territory, concerning the descendants of the imported Australian Holstein cattle. Sixty-four heifers were selected for the study. The experimental replacement heifers were raised using the enhanced milk feeding rates and the Cellobacterin probiotic product. They were raised intensively and inseminated when they were 14 months old. The milk productivity of cows and the physicochemical properties of milk were studied during three lactations after calving. **Results and Discussion**: The milk productivity of the cows from the experimental groups has exceeded one of their herd mates from the control group by 450 – 1,360 kg. The best indicators of the

DOI: 10.52571/PTQ.v18.n38.2021.8_ZABASHTA_pgs_100_122.pdf

physicochemical properties of milk have been determined in the milk of the cows raised from the heifers fed with 450 kg of the whole milk during the first 50 days until they were six months old. **Conclusions:** The authors believe that intensive rearing of replacement heifers positively affected the degree of development of their gastrointestinal tract and improved the level of milk yield and its physicochemical parameters.

Keywords: *replacement heifers, raising, milk production, acidity, density, amino acid composition*.

АННОТАЦИЯ

Предпосылки: Изучение особенностей роста, развития и продуктивности импортированного скота из Австралии в Краснодарский край представляет большой научный и практический интерес, что является актуальным. Поскольку продуктивные особенности завезенных генотипов недостаточно изучены, не только в хозяйствах Краснодарского края, но и в условиях других регионов РФ, они требуют дальнейшего более углубленного изучения и совершенствования в новых условиях кормления и содержания. **Цель:** Целью наших исследований являлось изучение влияния интенсивного выращивания ремонтных телок голштинской породы австралийской селекции на качественные показатели молока коров. **Методы:**Исследования проводились в ООО “Артекс-Агро” Кущевского района Краснодарского края, на потомках импортного скота голштинской породы австралийской селекции. Для исследований было отобрано 64 телочки. Подопытные ремонтные телки были выращены с использованием повышенных норм выпойки молока при добавлении пробиотического препарата целлобактерина. Они выращивались интенсивно, и были осеменены в 14 месячном возрасте. После отела на протяжении трех лактаций изучена молочная продуктивность коров и физико-химические свойства молока. **Результаты и Обсуждение:** По уровню молочной продуктивности коровы опытных групп превышали сверстниц контрольной на 450-1360 кг, лучшие показатели по физико-химическим свойствам молока были у коров, выращенных из телок, которым скормили до 6-месячного возраста за первые 50 дней – 450 кг цельного молока. В результате исследований установлено, что коровы III группы превосходили сверстниц контрольной и опытных групп по физико-химическим показателям молока. **Заключение:** Интенсивное выращивание ремонтных телок (которым за первые 50 дней выращивания было скормлено – 450 кг цельного молока, а с 50-ти и до 110-ти дневного возраста они потребили – 600 кг обезжиренного молока) положительно повлияло на степень развития их желудочно-кишечного тракта и позволило улучшить уровень молочной продуктивности коров и физико-химические показатели молока.

Ключевые слова:*ремонтные телки, молочная продуктивность, кислотность, плотность, аминокислотный состав.*

1. INTRODUCTION:

Holstein cattle of the USA, Canada, and Israel are the most highly-productive breed in the world. Its milk production is the highest compared to other breeds (Kargar, Habibi, and Karimi-Dehkordi, 2019; Ma *et al*., 2019; Rodrigues *et al*., 2019; Stepurina *et al*., 2019).In the Russian Federation, dairy cattle breeding remains one of the most important branches of agriculture (Gorlov *et al*., 2018; Ratoshny *et al*., 2018). Improving milk production and quality is one of the top priority problems of the agricultural sector of the country (Gorlov *et al*., 2019; Tuzov *et al*., 2018).

To considerably improve the milk production and dairy cattle and promote the Holstein breed, purebred Holstein cattle were imported (Haselmann *et al*., 2019). Holstein cows are characterized by the high genetic potential for dairy productivity (Anisimova, Koshchaev, and Eremenko, 2019; Gurtsieva *et al*., 2018; McKay *et al*., 2019). Cattle of this breed are well adapted to modern milk production (Gorlov *et al*., 2019; Karatunov, Tuzov, and Zelenkov, 2014). Cows of the Holstein breed are distinguished by high milk yield with a high milk constituents content; cows recompense well the fodder with milk yield (Ferreira *et al*., 2019; Krasnova, Batanov and Lebengarts, 2018; Weiss, 2019).

Under the conditions of loose housing and balanced feeding, the milk yield of Holstein cows in breeding herds reaches more than 8,000 kg when produced industrially, with the mass fraction of fat in milk being 3.5-4.1% on average.(Ferreira *et al*., 2019; Krasnova, Batanov, and Lebengarts, 2018; Reynolds *et al*., 2019). To obtain optimal milk yield, the diet of lactating cows should contain raw fiber constituted 18-28% of dry matter (A. S. Gorelik, O. V. Gorelik, and Kharlap, 2016; Gorelik *et al*., 2016; Olagarav *et al*., 2019). It is known that an insufficient amount of raw fiber in the diet leads to serious disorders of cicatricial digestion and negatively affects the level of milk yield (Deen *et al*., 2019; Haskell, Simm, and Turner, 2014).

The development of replacement heifers during the rearing period is the basis on which the organism is formed with all its physiological and adaptive characteristics. In the first months of the life of young animals, the cardiovascular, respiratory, and digestive systems develop intensively. Therefore, the rearing of replacement heifers should be carried out with complete and balanced feeding during all animal growth (Knoblock *et al*., 2019; Raza and Kim, 2018; Sun, Plastow, and Guan, 2019).

The feeding of animals should be organized properly to ensure the conditions for effective fodder and regulation of microbiological digestion processes. The normal microflora of the gastrointestinal tract of an animal is of great importance, along with a balanced diet. The deficiency of normal microflora negatively affects various body functions. Various factors of modern livestock industry technologies, such as limited contact of young animals with their mothers, excessive density of livestock per unit area, unsanitary conditions of farms, antibiotic treatment, inadequate and unbalanced feeding rations, further lead to disruption of intestinal microflora. Against the foregoing background, the normal intestinal microflora in animals is violated, which leads to dysbiosis, a decrease in natural resistance, and productivity. One solution to this problem is the inclusion of probiotics in the animal feed (Kok *et al*., 2019; Sehested *et al*., 2019; Wang and Kadarmideen, 2019).

In cattle diets, Cellobacterin combines functions of two feed additives: a feed enzyme and a probiotic. Cellobacterin is a cellulolytic probiotic, a collection of living microorganisms *Enterococcus faecium* isolated from the rumen of cattle. It is used for feeding animals as a separate supplement or as part of a compound feed. When calves consume this product, the maturation of the cicatricial microflora is accelerated, and the digestive system is normalized. In addition, the Cellobacterin destroys the fiber and increases the digestibility of grain feed (30).

The research aimed to study the impact of intensive raising of replacement heifers of the Australian Holstein breed on the qualitative indices of cow milk.

The following tasks were set:

1. To develop methods of intensive breeding of Holstein young stock, using increased doses of milking, contributing to the early introduction of the herd of replacement heifers into use;

2. To determine the features of lactation activity of cows in three lactations.

2. MATERIALS AND METHODS:

2.1. General information

The studies were carried out at Artex-Agro LLC in the Kushchevsky District of the Krasnodar Territory concerning imported Australian Holstein cattle descendants.

2.2. Samples

For the experiment, calves were obtained from the Reflection Showering line cows, and four groups of experimental animals were formed (n = 64). Sixteen heifers were selected for each group: I – the control group, and II, III, and IV – the experimental groups. Table 1.

All groups were formed according to the principle of analogs. The groups differed by the raising technology: the animals of the control group I – up to six months old – were raised using traditional technology. They received 200 kg of whole milk (for 50 days) and 400 kg of skimmed milk (from 50 to 110 days). The heifers received concentrated fodder, including pre-feed fodder – 50 %, and corn grains – 50 %. The heifers from the experimental groups received the same percentage of fodder. The heifers of the II experimental group were fed with 200 kg of whole milk for 25 days, and at the age between 25 and 60 days, they consumed 400 kg of skimmed milk. During the first 50 days, the animals from the III experimental group ate 450 kg of whole milk, and at the age of 50 and 110 days, they consumed 600 kg of skimmed milk. The herd mates of the IV experimental group consumed 450 kg for 60 days, and at the age between 60 and 120 days, they were fed with 600 kg of skimmed milk.

Simultaneously, the heifers of all experimental groups were fed with 3 g of the Cellobacterin probiotic product (purchased from BIOTROF LLC) (Biotrof, n.d.) per day for each animal.

After the dairy period, the heifers of all groups were raised intensively. After the fruitful insemination of the heifers and their transfer to bred heifers, they had the ordinary farm diet. The daily diet consisted of the following feeds: corn silage (11 kg), alfalfa hay (2 kg), gramineous hay (0.7 kg), grass haylage (2.5 kg), brewing grains (3.8 kg), forage molasses (0.25 kg), a mixture of concentrates (1.5 kg), monocalcium phosphate 0.038 kg). The daily nutritional structure of the diet was as follows: roughage - 30%, succulent fodder - 45%, concentrated - 25%. The

experimental animals were kept under identical conditions.

2.3. Materials and reagents

The calcium content in milk was determined according to the titrimetric method (ISO 12081-2013).

Consumables and reagents specified in the method were used.

1. Application area: a titrimetric method for determining the calcium content in milk.

2. Terms and definitions: the following term was used in this method, and an appropriate definition was given:

2.1. Calcium content in milk: mass fraction of substances determined by the method. The calcium content was expressed as a percentage by weight.

3. Principle: protein substances were precipitated in the analyzed sample with trichloroacetic acid and then filtered. Calcium was precipitated in the filtrate in the form of calcium oxalate and separated by centrifugation. The washed and dissolved precipitate was titrated with potassium permanganate.

4. Reagents and Materials: unless otherwise specified, only reagents of recognized analytical grade were used, as well as distilled or demineralized water or water of equivalent purity.

4.1. Trichloroacetic acid solution I ($C_2HCl_3O_2$), concentration 200 g/dm^3.

4.2. Trichloroacetic acid solution II, concentration 120 g/dm^3.

4.3. Ammonium oxalate ($C_2H_8N_2O_4$), saturated cooled solution.

4.4. Methyl red solution

Methyl red ($C_{15}H_{15}N_3O_2$) in the amount of 0.05 g was dissolved in100 ml^{3}of ethanol (96% by volume).

4.5. Acetic acid solution ($C_2H_4O_2$), 20% by volume.

4.6. Ammonia solution I

Equal volumes of ammonia (NH_3) solution (25% by a mass fraction) and water were mixed.

4.7. Ammonia II solution

Ammonia solution in the amount of 2 cm^3 (25% by a mass fraction) was diluted with water to 100 cm^3.

4.8. Sulfuric acid (H_2SO_4)

20 cm^3 of sulfuric acid (98% by a mass fraction) was added to 80 ml of water.

4.9. Titrated solution of potassium permanganate, $c(KMnO_4)$=0.004, mol/dm^3 ± 0.0001 mol/dm^3

The titer was checked according to the normal laboratory practice with oxalic acid or sodium oxalate.

Reagents and equipment: potassium permanganate solution ("0.05 n); 2 n sulfuric acid solution; standard 0.05 n oxalic acid solution (M_e=1/2M($H_2C_2O_4$)); burette; glass funnel; 100 ml conical flasks; Mohr pipettes; 50 ml glass cylinder; electric hotplate. Potassium permanganate solution is poured into a clean burette and prepared for titration. In a conical flask for the titration 10.00 ml of oxalic acid solution is selected with a Mohr pipette, 10 ml of 2 n sulfuric acid is added, the solution in the flask is heated to 70-80 °C (without boiling, in which the oxalic acid decomposes) and the hot solution is titrated with a solution of potassium permanganate. Potassium permanganate solution should be added slowly, drop by drop, while continuously shaking the solution. Each next drop is added only after the previous one has been discolored. At first, the decolorization of potassium permanganate will be slow, but as manganese (II) is formed, it will accelerate.

The titration is stopped when an excessive drop of potassium permanganate gives the solution a pale crimson color that does not disappear within 1-2 minutes. It is convenient to count by the upper edge of the burette because the lower one is hardly visible. The titration is repeated 2-3 times. From the converging counts, take the average titration result and calculate the normality (C_E) of potassium permanganate solution by the Equation 1:

$$N = C_E(KMnO4) = \frac{V(H_2C_2O_4)\times C_E(H_2C_2O_4)}{V(KM_nO_4)};\text{mol/l} \quad \text{(Eq.1)}$$

V – volumes of the corresponding solutions, ml.

5. Equipment and materials: common laboratory equipment was used, including the following.

5.1. Analytical balance capable of weighing with an accuracy of 0.01 g, with the possibility of reading to 0.001 g.

5.2. Volumetric flask with one mark with a capacity of 50 cm^3, according to A.S. Gorelik, O.V. Gorelik, and S.Y. Kharlap (2016), class A.

5.3. Pipette, 20 cm^3, according to Deen and co-authors (2019), class A.

5.4. Centrifuge providing radial acceleration of 1,400 g.

5.5. Centrifuge tubes, cylindrical, with a round bottom, the capacity of approximately 30 ml^3, graduated to 20 cm^3.

5.6. Pipettes, with a capacity of 2 cm^3 and 5 cm^3, according to Deen and co-authors (2019), class A.

5.7. Suction device with a capillary tube.

5.8. Water bath capable of maintaining water at boiling point

5.9.Graduated burette with the graduation of 0.02 cm^3, according to Anisimova, Koshchaev, and Eremenko (2019), class A.

5.10. Ashless filter paper for slow filtration.

6. Sampling: sampling was not included in the method specified in this standard. The recommended sampling method was given in Ferreira *et al*. (2019). It was important to deliver a truly representative sample to the laboratory that had not been damaged or altered during transport or storage.

7. Preparation of the test sample: the test sample for milk or reconstituted milk was brought to a temperature of (20 ± 2)°C and mixed thoroughly. If homogeneous dispersion of fat was not formed, the sample was slowly heated to 40°C, then gently mixed by repeated overturn and cooled to a temperature of (20 ± 2)°C.

8. Procedure of analysis:

8.1.Test sample for analysis:

Approximately 20 g of the prepared test sample (see 7) was transferred into the volumetric flask (5.2) using the pipette (5.3). The sample was weighed to the nearest 0.01 g.

8.2. Definition:

8.2.1. Precipitation of protein substances: the trichloroacetic acid solution I (4.1) was gradually added, with shaking, to the test sample (8.1) until the volume of 50 $cm^3$was obtained. The test sample was shaken vigorously for a few seconds and left at rest for 30 min. The filter paper (5.10)was used for filtering; the filtrate had to be clear.

8.2.2. Precipitation of calcium as oxalate and separation of oxalate: 5 cm^3 of clear filtrate (8.2.1), 5 cm^3 of trichloroacetic acid solution II (4.2), 2 cm^3 of ammonium oxalate solution (4.3), two drops of methyl red solution (4.4) and 2 cm^3 of acetic acid solution (4.5)were added with a pipette (5.6) into a centrifuge tube (5.5) and stirred with shaking.

Ammonia solution I (4.6) was added dropwise to the solution obtained in the test tube until the color turned pale yellow. Then a few drops of acetic acid solution (4.5) were added until the color turned pink. The solution was left for 4 hours at room temperature. The contents of the centrifuge tube were diluted with water to 20 cm^3. The tube was centrifuged at 1,400 g for 10 min. The clear supernatant was removed from the centrifuge tube using the suction device (5.7). Next, the centrifuge tube walls were flushed with 5 cm^3 of ammonia II solution (4.7) to not affect the calcium oxalate precipitate. The tube was centrifuged at 1,400 g for 5 min. The supernatant was removed from the centrifuge tube using a suction device (5.7). The washing procedure was repeated twice.

8.2.3. Titration: 2 cm^3 of sulfuric acid (4.8) and 5 cm^3 of water were added to the calcium oxalate precipitate (8.2.2). The test tube was placed in a boiling water bath (5.8) to dissolve the calcium oxalate precipitate completely. Then, the dissolved calcium oxalate was titrated with the potassium permanganate solution (4.9) until the pink color remained. During the titration, the temperature of the solution should remain above 60°C. The volume (in cm^3) of potassium permanganate solution consumed was recorded to the nearest 0.01 cm^3.

8.2.4. Control experiment: in parallel with the sample testing, a control experiment was carried out using 20 cm^3 of water instead of a sample for analysis. The volume of potassium permanganate solution consumed was recorded, in cm^3, to the nearest 0.01 cm^3.

Milk productivity of cows was monitored using Afimilk milking equipment with a subsequent calculation for 305 days of lactation.

Average milk samples were taken from five cows from each experimental group using Afimilk software (https://www.afimilk.com/) devaluation milking equipment.

Physicochemical indicators (acidity, density, NFMS, fat, protein, ash, calcium, phosphorus) of milk were studied once a month.

In the average milk sample, the content of NFMS, fat, protein, and density were determined by the milk quality analyzer Laktan 1-4 model 220. The analyzer allowed determining the six most important parameters – protein, fat, NFMS,

density, temperature, and mass fraction of added water – in a sample of fresh, canned, pasteurized, normalized, skimmed, reconstituted, and long-term storage milk without the use of chemical reagents for 130 seconds.

Acidity was determined by the titrimetric method. The method was based on titration of milk with an alkali solution (sodium or potassium hydroxide) in the presence of phenolphthalein indicator. It was necessary to measure 10 ml of milk and add 20 ml of distilled water and 3 drops of 1% phenolphthalein solution. Water was needed in order to more clearly see the pink tint during titration. The resulting mixture was stirred and titrated with a solution of 0.1 N sodium hydroxide until a faint pink color appeared, which did not disappear within 1 min. The analysis results were obtained by calculating the amount of alkali left for titration multiplied by 10. If milk had just been milked, it had an acidity index of 16-18 ºT. The acidity rose after two hours if milk had not been refrigerated. As microorganisms developed, the fermentation process took place, respectively, the acidity also increased. An increase in acidity leads to the fact that proteins became less resistant to heating. Therefore milk with the acidity of 21 ºT was off-grade, and with the acidity of 22 ºT, it was already on the verge of fresh and sour and could not be sold to processing plants.

Phosphorus in milk was determined by the spectrometric method (ISO 9874:2006).

1 The field of application.

This standard specifies a spectrometric method for the determination of the mass fraction of total phosphorus in milk.

2 Mass fraction of total phosphorus: Mass fraction of total phosphorus in milk as measured by the method specified in this standard and expressed as a percentage.

3 Essence of the method. The method was based on the destruction of organic substances in a milk sample under the action of sulfuric acid and hydrogen peroxide (wet mineralization) or under the action of high temperature (dry mineralization), the addition of a solution of sodium molybdate in ascorbic acid, the spectrometric determination of the optical density of the formed molybdenum blue at the wavelength of 820 nm and determination of the mass fraction of total phosphorus in milk according to the calibration graph.

4 Measurement instrumentation: Molecular absorption spectrometer, allowing measurements at a wavelength of 820 nm, permissible measurement error of transmission coefficient ± 1%, equipped with a cuvette with an optical path length of 10 mm; laboratory liquid non-mercury thermometer with a measurement range from 0°C to 150 °C and scale interval 0.5 °C; an electric circulating muffle kiln, capable of holding tests at temperatures between 500°C and 550°C; a thermostatically controlled water bath, capable of holding temperatures of (100±2)°C; a desiccator, capable of holding temperatures of (100±2)°C. An electric hotplate.

5 Utensils

Flasks, pipettes, cylinders, beakers, glass beads, 5 mm diameter; Kjeldahl flask for mineralization or test tubes of 50 cm^3 capacity.

6 Reagents: Monopotassium phosphate (KH_2PO_4), ascorbic acid, a solution of mass concentration 50 g/dm^3, sulphuric acid, a solution of mass fraction 50%; hydrochloric acid, a solution of mass concentration 36 g/dm, hydrogen peroxide in a solution of mass concentration 300 g/dm^3, free from phosphorus compounds; sodium molybdate dihydrate, mass fraction of basic substance - not less than 99,5%, insoluble substances - not more than 0,005%, phosphate - not more than 5 mln^{-1}; distilled water

7 Measurement conditions.

The following conditions are to be observed during measurements in the laboratory

ambient air temperature (20±5) °C

relative humidity (55±25)%;

(95±10)kPa atmospheric pressure.

8 Preparation for measurements

8.1 Before taking a sample for analysis, the milk shall be heated slowly to (40±2) °C, stirred gently, and cooled to (20±2) °C.

8.2 All glassware shall be washed thoroughly with phosphorus-free detergent and then with distilled water before use.

8.3 Preparation of reagents

8.3.1 A solution of sulphuric acid with a mass fraction of 50%: 278 cm^3 of concentrated sulphuric acid is carefully added, stirring the solution constantly, to 722 cm^3 of distilled water. The solution should be kept for no longer than 1 month at (20±5) °C in a dark glass container.

8.3.2 A solution of hydrochloric acid with a mass concentration of 36 g/dm^3 (intended for dry mineralization): 83 cm^3 of concentrated

hydrochloric acid (1.19 g/cm^3) is placed in a 1000 cm^3 volumetric flask and carefully add distilled water.

The volume of the solution is topped up with distilled water to the mark. The solution is stored for no more than 1 month at (20±5) °C in a dark glass vial.

8.3.3 Sodium molybdate solution with mass concentration of 25 g/dm^3 - in a volumetric flask of 100 cm^3 contain (2.5000±0.0001) g of sodium molybdate dihydrate ($Na_2M_oO_4 \times 2H_2O$), add a solution of sulfuric acid (8.3.1) in an amount sufficient to dissolve the sodium molybdate crystals, stir it and then the volume of the solution is topped up to the mark with the same acid solution. The solution is stored in the refrigerator for not more than 7 days.

8.3.4 Ascorbic acid solution with mass concentration of 50 g/dm^3 - in a 100 cm3 volumetric flask, place (5.0000±0.0001) g of ascorbic acid and dissolve in a small amount of distilled water. The volume of the solution is brought to the mark with distilled water.

The solution shall be used freshly prepared.

8.3.5 Solution of sodium molybdate in ascorbic acid: The solution is prepared immediately before use. Pour 10 cm^3 of ascorbic acid solution (see 8.3.4) into a 100 cm^3 volumetric flask and add 25 cm3 of sodium molybdate solution (see 8.3.3) small amount of distilled water, and mix. Add distilled water to the mark.

8.3.6 Standard solution of phosphorus A, containing 100 mg of phosphorus in 1 dm^3: In a 50 cm^3 beaker, weigh (1.0±0.1) g of monosodium phosphate, place in a desiccator, and dry for at least 48 hours. In a 1000 cm^3 volumetric flask, add (0.4394±0.0001) g of dried potassium phosphate, and add a small amount of distilled water and mix.

The volume of the solution is topped up to the mark with distilled water. The mass concentration of phosphorus in solution A is 100 μg/cm^3.

The solution shall be used freshly prepared.

8.3.7 A standard solution of phosphorus B containing 10 mg of phosphorus in 1 dm^3:

Into a 100 cm^3 volumetric flask, add 10 cm^3 of phosphorus A standard solution (see 8.3.6) by pipetting, add a small amount of distilled water, and mix. The volume of the solution is topped up to the mark with distilled water. The mass concentration of phosphorus in solution B is 10 μg/cm^3. The solution is to be used freshly prepared.

9 Conducting the measurements

9.1 Wet saline method

9.1.1 Place (1,500±0,001) g of the milk prepared according to 8.1 into a flask for mineralization. Add three glass beads and 4 cm^3 of concentrated sulfuric acid.

9.1.2 Place the flask in an inclined position in a well-ventilated fume cupboard and heat it over an electric hotplate. Keep the foaming in the flask to a minimum during heating.

Keep the flask at a gentle boil. Local overheating and heating of the flask above the liquid level is not allowed.

9.1.3 Once the flask has stopped foaming, and it shall be cooled in the air to a temperature of (20 ± 2)°C. Carefully add 2 cm^3 of hydrogen peroxide solution and heat again. Repeat this procedure until the contents of the flask become clear and colorless. During heating, periodically stir the flask contents by gently turning the flask to avoid local overheating.

9.1.4 Cool the mixture in the air to (20±2) °C and wash the neck of the flask with about 2 cm^3 distilled water. Heat the contents of the flask again until the water has evaporated. Boil the liquid for (30±1) min to eliminate all traces of hydrogen peroxide. Local overheating is not allowed.

9.1.5 Cool the mixture in the air to a temperature of (20±2) °C. Next, quantify the mixture in a 100 cm^3 volumetric flask and add distilled water to the volume of solution in the flask.

9.1.6 With a pipette, take 2 cm^3 of the mixture into a 50 cm^3 volumetric flask and add about 25 cm^3 of distilled water. Then add 2.0 cm^3 of sodium molybdate solution in ascorbic acid (see 8.3.5) to the flask, stir and bring the volume of the solution in the flask to the mark with distilled water.

9.1.7 Boil the contents of the flask for 15 min in a water bath.

9.1.8 Cool the flask with the mixture to a temperature of (20±2) °C in cold water. Then carry out the tests according to 9.5. The mixture shall be testable for 1 hour.

9.2 Dry mineralization method

9.2.1 Place (10,000±0.001) g of the milk prepared according to 8.1 in a platinum or quartz crucible.

9.2.2 Evaporate the sample to dryness in a desiccator at (100±2)°C or in a water bath.

9.2.3 The test sample is calcined in a muffle furnace at 500 °C to 550 °C until white (or almost white) ash is formed.

Preferably, before placing the crucible in the muffle furnace, heat it on an electric cooker to burn off the flammable components.

9.2.4 The crucible with its contents is cooled together with the muffle furnace and then covered with a watch glass. Dissolve the ashes in a 2 to 3 cm^3 solution of hydrochloric acid (see 8.3.2) and add about 3 cm^3 of distilled water.

9.2.5 Transfer the ash solution to a 100 cm^3 volumetric flask by rinsing the watch glass and crucible with distilled water and discarding the washing water in the flask. Add the volume of the solution in the flask to the mark with distilled water. Filter the solution through filter paper.

9.2.6 Using a pipette, pour 10 cm^3 of the filtrate into a 100 cm^3 volumetric flask. Add the volume of the solution in the flask to the mark with distilled water.

9.2.7 Pour 2 cm^3 of the filtrate solution into a 50 cm^3 volumetric flask and add 25 cm^3 distilled water. Then add 2.0 cm^3 sodium molybdate in ascorbic acid (see 8.3.5). Add the volume of the solution in the flask to the mark with distilled water.

9.2.8 Boil the contents of the flask in a water bath for 15 min.

9.2.9 Cool the flask with the mixture by placing it in a bath of running water to a temperature of (20±2)°C. Then carry out the tests according to 9.5. The mixture is suitable for measurements for 1 hour.

9.3 Control measurement

Simultaneously with the measurement of the sample, a control measurement is carried out using the same procedure as for the test sample (see 9.1 or 9.2) but with 1.5 cm^3 or 10 cm^3 respectively of phosphorus-free distilled water instead of the test sample.

9.4 Drawing a graduation chart

9.4.1 Pour 0, 1, 2, 3, and 5 cm^3 respectively of phosphorus B standard solution into five 50 cm^3 volumetric flasks.

9.4.2 Add 2.0 cm^3 of sodium molybdate solution in ascorbic acid to the contents of each volumetric flask (see 8.3.5). Next, add the volume of each solution in the flask to the mark with distilled water. The prepared solutions contain 0, 10, 20, 30, and 50 μg of phosphorus, respectively.

9.4.3 The contents of the flasks are boiled in a water bath for (15±1) min.

9.4.4 Cool the solutions to a temperature of (20±2)°C in cold water. For 1 h, measure with a spectrometer equipped with a cuvette at 820 nm the optical density of each calibration solution compared to the phosphorus-free solution (see 9.4.2). If the optical density of the phosphorus-free solution in 50 cm^3 of the solution is high, check the reagents.

9.4.5 Plot the chart of the corresponding value of the optical density on the mass in micrograms of phosphorus contained in the calibration solutions (see 9.4.2).

9.5 Spectrometric measurement

Measure the optical density of the cooled mixtures according to 9.1.8 and 9.2.9 on a spectrometer at a nominal value of 820 nm relative to the control sample (see 9.3).

10 Processing of measurements

10.1 The mass of phosphorus corresponding to the measured optical density of the test solution shall be determined from the calibration chart.

The mass fraction of total phosphorus (W) in the sample, %, is calculated using equations 2 and 3:

a) wet mineralization method

$$W = \frac{m_1 100}{200 m_0}, \qquad \text{(Eq. 2)}$$

b) dry mineralization method

$$W = \frac{m_1 100}{20 m_0}, \qquad \text{(Eq. 3)}$$

where W - mass of phosphorus determined from the calibration curve, μg;

200 and 20 - sample dilution factor;

m_0 - sample weight, g.

The final result is the arithmetic mean of the results of two parallel measurements, rounded to the third decimal place.

The water content in milk was determined by Equation 5:

$$B = 100 - C, \qquad \text{(Eq. 5)}$$

where C was the dry matter (%), and B was the water content in milk (%). Determination of the presence of the studied indicators. Fluctuations of the dry matter in milk in cows were in the range of 11.3-14.5%. A glass weighing bottle with 20-30 g of well-washed and calcined sand and a glass rod that did not protrude beyond the edges of the bottle was placed in the drying cabinet and kept at (102 ± 2)^{0}C for 30-40 minutes. After that, the weighing bottle was removed from the drying cabinet, covered with a lid, cooled in a desiccator for 40 minutes, and weighed with an error of not more than 0.001 g. 10 cm^3 of milk was added to the same weighing bottle with a pipette, covered with a lid and immediately weighed. The contents were thoroughly mixed with a glass rod, and the open weighing bottle was heated in a water bath, with repeated stirring of the contents until a crumbling mass was obtained. Then the open weighing bottle and the lid were placed in the drying cabinet with a temperature of (102 ± 2) ºC. After 2 hours, the weighing bottle was removed from the drying cabinet, covered with the lid, cooled in the desiccator for 40 minutes, and weighed. Subsequent weighings were carried out after drying for 1 hour until the difference between two successive weighings was equal to or less than 0.001 g. If an increase in mass was found during one of the weighings after drying, the previous weighing results were taken for calculations. The mass fraction of dry matter (c) in percent was calculated by Equation 4:

$$C = \frac{m_1 - m_0}{m - m_0} \times 100 \qquad \text{(Eq. 4)}$$

where $m_0$was the mass of a weighing bottle with sand and a glass rod, g;

m was the mass of a weighing bottle with sand and a glass rod and a weighed portion of the test sample before drying, g;

$m_1$was the mass of a weighing bottle with sand and a glass rod and a test sample after drying, g;

The discrepancy between parallel determinations had to be no more than 0.1%. The arithmetic mean of two parallel determinations was taken as the final result.

11. Determination of ash in milk.

Determination technique.

1. Temper the porcelain crucible in a muffle furnace, cool it in a desiccator, and weigh it on an analytical scale. Then weigh about 25 g of milk into the crucible or measure this quantity with a pipette. In the latter case, correct the density of the milk.
2. Evaporate the milk to dryness in a water bath or desiccator and char the dry residue over a low flame. At the end of the emission of smoke, intensify the heating and continue until a dark grey residue is obtained.
3. Cool the crucible, add 15 mL distilled water, and heat gently. Then filter through an ash-free filter. Treat the residue in the crucible 2-3 times with small portions (5-6 mL each) of hot water and transfer to a filter.
4. After filtration, the filter is transferred into a crucible with the undissolved residue, dried in the desiccator and further, calcined in a muffle furnace or on high heat until greyish white ash is obtained in the crucible.
5. Pour the filtrate obtained by washing the precipitate into a crucible with the ash, evaporate to dryness, and incinerate over low heat.
6. Cool the crucible in a desiccator; weigh it on an analytical scale, and calculate the amount of ash in the milk according to the formula 6:

$$A = \frac{c - a}{b - a} \times 100 \qquad \text{(Eq. 6)}$$

where A is the amount of ash in the milk (%); a is the mass of the empty crucible (g); b is the mass of the crucible with the milk (g); c is the mass of the crucible with the ash (g).

Preparation of samples for analysis:

1. Using a microdoser, take 5 ml of milk into a vial and add 5 ml of HCl hydrochloric acid (36%).
2. Close the vial tightly with an iron lid and place it in a desiccator at t=+110ºC for 16-20 hours for hydrolysis.
3. The resulting hydrolysate should be filtered through a paper filter.
4. Evaporate 0.5 ml of filtered hydrolysate with a hairdryer to a dry residue.
5. Add 1 ml of buffer-2,2 pH to the dry residue to dilute the sample.
6. The dilution occurs twice. Transfer the tube (Eppendorf) filled sample to the amino acid analyzer for analysis.

Collection and processing of the chromatographic data were done using the software Multichrome (https://multichrom.ru/).

2.4. Experimental Procedures

The NFMS, fat, protein, and density were

determined in an average milk sample using a Lactan 1-4 model 220 milk quality analyzer (https://sibagropribor.ru/en/).

Acidity was determined by titration of milk with alkaline solution (sodium or potassium hydroxide) in the presence of phenolphthalein indicator.

The essence of the ash determination method is to burn a sample of milk and weigh the resulting ash.

The spectrometric method of determining the mass fraction of total phosphorus is based on the destruction of organic substances of milk sample under the influence of sulfuric acid and hydrogen peroxide (wet mineralization) or under the influence of high temperature (dry mineralization), adding sodium molybdate solution in ascorbic acid, spectrometric determination of the optical density of the formed molybdenum blue at wavelength 820 nm, and determination of the mass fraction of total phosphorus in milk using the graduation chart (ISO 9874|IDF 42:2006).

The titrimetric method of calcium determination is based on the precipitation of calcium by ammonium oxalate in the filtrate obtained after precipitation of milk proteins by trichloroacetic acid, followed by titrimetric determination of the mass fraction of calcium (ISO 12081|IDF 36:2010).

The amino acid composition of milk was determined by high-performance liquid chromatography (HPLC) using an LC-10 chromatograph (Shimadzu) with a fluorometric detector and precolumn derivatization (DataApex, Clarity, 2020).

2.5. Ethics

The research was approved under the regulations of Kuban State Agrarian University, and the data collected was published for scientific and research purposes only.

2.6. Statistics

The data were statistically processed: (M) - arithmetic mean;σ - sigma, standard deviation; Cv - coefficient of variation; m - error of arithmetic mean; td - criterion of reliability.

Experimental data were biometrically processed using Microsoft Excel, to which the presented formulas were added:

$$M = \frac{\sum V}{n}; \quad \text{(Eq. 7)}$$

$\sum V$ – is the sum of the indicators for the studied animals;

n - number of studied animals.

$$\sigma = \frac{Vmax - Vmin}{K}; \quad \text{(Eq. 8)}$$

K – coefficient of sigma calculation according to the number of studied animals in the group;

$Vmax$ – the highest index;

$Vmin$ – the lowest index.

$$Cv = \frac{\sigma * 100}{M}; \quad \text{(Eq. 9)}$$

$$m = \frac{\sigma}{\sqrt{n}}; \quad \text{(Eq. 10)}$$

$$td = \frac{M1 - M2}{\sqrt{m1^2 + m2^2}}; \quad \text{(Eq. 11)}$$

$M1 - M2$ and $m1$ and $m2$ – the compared values by the group.

Suppose td criterion is equal to or greater than 2 (td ≥ 2), corresponding to infallible probability P (probability significance level) equal or greater than 95% (P ≥ 95%). In that case, the difference should be considered credible (significant), i.e., conditioned by some factor that would be valid in general. If td < 2, the probability of error-free prediction P < 95% means that the difference is unreliable, random, i.e., not due to any regularity (not due to the influence of any factor).

3. RESULTS AND DISCUSSION:

3.1 RESULTS

The study aimed at researching the effect of various doses of dairy feed on the growth and development of replacement heifers, subject to adding 3 g of the probiotic product Cellobacterin per heifer from the experimental groups since the age of ten days on an everyday basis. The positive effect of the enhanced doses of whole milk and the probiotic product Cellobacterin was determined.

The cows from the experimental groups gave more milk than those from the control group during lactation III: II and Ist groups – by 700 kg, III and I – by 1860 kg, and IV and I – by 1560 kg (Table 2).

According to three lactations, the dynamics of changes in the milk production of the cows and the physicochemical composition of

milk were studied. Table 1 shows the change in the milk yield and the physicochemical properties of milk.

The milk yield of the experimental cows for the I lactation in the control group was 6,590 kg. Milk yield per lactation was determined using Afimilk milking equipment. In the experimental groups, the milk yield was as follows: II – 7,120 kg, III – 7,860 kg, and IV – 7,720 kg, respectively. Moreover, the milk yield was higher by 7.4 % in the II experimental group than in the control group, by 16.2 % in the III one, and by 14.6 % in the IV one; accordingly, for the II lactation – by 8.4 %, by 18.5 % in the III group, by 16.9 % in the IV group, and similarly for the III lactation – by 8.8 %, by 20.4 % in the III group, and by 17.7 % in the IV group.

The milk productivity of the cows from the control group increased during the II lactation when compared with the I lactation – by 260 kg (3.8 %), II – by 360 kg (4.8 %), III – by 540 kg (6.4 %), and IV – by 520 kg (6.3 %); respectively, during the III lactation – by 680 kg (9.4 %), II – by 850 kg (10.7 %), III – by 1,270 kg (13.9 %) and IV – by 1,110 kg (12.6 %).

When studying the physicochemical composition of milk by lactation, it was determined that the acidity of the milk of the animals from the experimental groups was within the standard. The acidity norm of whole milk was 16-21ºT. The statistical differences by the acidity of milk from lactation I to III in groups were not significant – $P < 0.95$.

The water content in the milk of the cows from the experimental groups was slightly less than the control one. The water content in the milk of the cows from lactation I to III decreased. The fluctuations were within 0.1 %. These differences from lactation I to III with the animals from the experimental groups were not significant – $P < 0.95$.

During the lactation, the dry matter amount changed and depended on feeding, age, and other factors. The nutritional content of milk depends on the content of dry matter and dry skimmed milk rest. The content of fat in milk slightly increased in the experimental groups as compared to the control one.

The content of fat in milk slightly increased in the experimental groups as compared to the control one. The fat content in the milk of the cows from group III was higher than the herd mates. The differences in fat content in the milk from lactation I to III were not significant in the groups – $P < 0.95$.

The protein content was slightly higher with the cows from group IIIthan the herd mates from groups I, II, and IV. The differences in protein content in the milk from lactation I to III were not significant – $P < 0.95$.

The indicators for the cows from group III were a bit higher as compared to their herd mates. The calcium and phosphorus content differences in the milk from lactation I to III were not significant – $P < 0.95$.

The cows from the experimental groups had slightly better indicators of the chemical composition of milk as compared to the control group.

Table 3 shows the change in fat content in the milk of the experimental cows by months of lactation.The qualitative composition of the milk of the experimental cows made it possible to determine the changes in fat content in the milk of the experimental cows during the lactation.

The cows from groups II, III, and IV surpassed their herd mates from control group I by the fat content in the milk during three lactations. There was an increase in the content of fat in the milk from lactation I to III in the experimental groups. As compared to the control group, the difference between the groups during lactation I was as follows: II and I – by 0.03 %; III – I – by 0.08 %;IV – I – by 0.06 %. In the III lactation, the difference was, respectively: II and I – by 0.04 %, III – I – by 0.11 %, and IV – I – by 0.09 %

The cows from group III had a slightly higher fat content than their experimental herd mates. This was because the intensive heifer breeding methods positively affected both the milk production of cows and its properties.

Table 4 contains the data on the protein content in the milk by months of lactation. The provided data indicate that the protein content in the milk differs both between the groups and between the lactations. The protein content in the milk for lactation I between the groups of the cows from the experimental groups (II, III, and IV) was higher compared to control group I, but the differences were insignificant – $P < 0.95$.

The decrease in the average value of protein for lactation I with the experimental cows between groups is different as compared to the fat content of milk: III – I – by 2.5 %, III-II – by 1.5 %, IV – III and IV – I – by 1.2 %, IV-II – by 0.3 %, and II – I – 0.9 %. Analyzing the protein content in the milk during lactation II and III, it was

determined that the cows from group III surpassed their herd mates from the control group. There was an enhanced protein content in the milk from lactation I to III in the experimental groups compared to the control group. The difference for lactation III was as follows: I and II – by 0.05 %, I – III – by 0.11 %, and I – IV – by 0.09 %.

The cows from group III raised using intensive technology slightly surpassed their herd mates from the experimental groups in protein content for III lactations. However, the differences were not significant – P < 0.95.

The fat in the milk of cows was a thin emulsion with a considerable amount of tiny fat globules. The fat globules were surrounded by a protein-lecithin shell distributed evenly among the aqueous portion of the milk. After the milk gravity separation, the fat part was located on the top because the specific density of fat was less than water. Table 5 shows the data on the content of milk fat.

It was determined that the fat content in the milk of the cow differed between groups and in lactation. In terms of the fat content in milk, in lactation, I the cows from experimental groups II, III, and IV surpassed their herd mates from the control group.

The milk fat content in lactation II increased in groups I and II for up to three months and in groups III and IV for up to four months. Then the milk fat decreased by the 10th month of lactation. However, the differences were not significant – P < 0.95. Thus, in terms of milk fat content, the cows from the experimental groups surpassed the control one.

It was determined for lactation I to III by groups that the milk fat content in the milk of the cows from group I had increased by 26.2 kg (9.5 %) and 26.0 kg (8.9 %) for the herd mates from group II. The highest difference was with the cows from group III. It was 39.2 kg (11.9 %). The analogs of group IV, according to the indicator, understudy took the intermediate position between groups I, II, III – by 34.1 kg (10.6 %).

The obtained data indicate that in terms of fat content in the milk, the cows from the experimental groups in III lactations surpassed their herd mates from the control group, which indicates the efficiency of the methods used when raising heifers.

The determined differences in the milk protein content in the cow's milk for the analyzed lactations differ both between groups and by lactations (Table 6).

The cows from the experimental groups exceeded their herd mates from the control group by milk protein content. It was determined that the milk protein content in the milk had increased from lactation I to III. The difference betweengroups was as follows: I – by 30.4 kg (12.4 %), II – by 32.3 kg (12.3 %), III – by 47 kg (15.2 %), and IV – by 42.9 kg (14.4 %). The milk protein content in the milk from lactation I to II increased in the experimental groups compared to the control group of lactation I: I and II – by 18.3 %, I – III – by 30.4 %, and I – IV – by 27.6 %.

The cows from the experimental groups that received the enhanced daily milk and the probiotic product when raised surpassed their herd mates from the control group by the milk protein content in III lactations. It was determined that the control group cows were inferior to the analogs from the experimental groups by the content of milk fat and milk protein.

The data presented in Table 5 indicate the superiority of the animals from the experimental groups over the control one by the indicator under study. This was a consequence of the efficient breeding of heifers using intensive technology involving the Cellobacterin probiotic product.

Tables 7 and 8 show the composition of amino acids in the milk by groups of cows. The essential amino acids cannot be synthesized in mammals and must come from food. When raising young mammals, there are metabolic disorders if at least one essential amino acid is missing.

Calculation and expression of results: Calculation: the calcium content, W_{Ca}, wt%, was calculated according to Equation12:

$$W_{Ca} = 0.0004(V - V_0) \times \frac{1000f}{m} = 0.4(V - V_0) \times \frac{f}{m}$$ (Eq. 12)

where V was the volume of potassium permanganate solution consumed during the titration of a sample for analysis (see 8.2.3); V_0 was the volume of potassium permanganate solution consumed in the control experiment (see 8.2.4); m was the mass of the sample for analysis, g; ʃ was the correction factor given in Table 9 for the volume of sediment obtained by precipitation with trichloroacetic acid.

Table 9. *Correction factor ʃ as a function of fat content in a sample*

Content of fat in a sample,wt%	Correction factor
3.5-4.5	0.972
3	0.976
2	0.980
1	0.985
<0.1	0.989

Expression of results: the result was expressed to the third decimal place.

3.2 DISCUSSION

Considering the total content of nonessential amino acids in the milk of the cows from lactation I to III, it was determined that by the content of replaceable amino acids in their milk, the cows in group III surpassed their herd mates in the I control group, as well as from the II and IV experimental groups.

Regarding the content of essential amino acids in the milk, the control group cows were inferior to the herd mates from the experimental groups for all lactations under analysis.

The provided data indicate a consistent increase in the total number of essential and nonessential amino acids in all experimental groups of cows from lactation I to III.

Considering the data from Tables 6 and 7, there is an increase in essential amino acids in lactations. Compared to their experimental herd mates, the enhanced content of essential amino acids in the milk of cows from group III was determined. This is because they had been raised intensively from their birth till 18 months and had been given the probiotic product.

The determined superiority of the cows from group III by the total content of essential and nonessential amino acids as compared to their herd mates confirms that the intensive growth of young animals had a positive effect on the amino acid composition of the milk of the cows from the experimental groups as compared to the control one.

The amino acid index determines the ratio of essential amino acids to nonessential ones. The higher it is, the higher the nutritional value of milk is. It characterizes the nutritional and biological usefulness of milk. The highest amino acid index was determined for groups III and IV. Statistically, these differences are of low quality – $P < 0.95$.

4. CONCLUSION:

The cows from group III have exceeded their herd mates from the experimental groups and the control one regarding the indicators under study.

During the I lactation, higher milk yield was obtained from the III group cows compared to the cows from the other experimental groups.

The replacement heifers from the experimental groups surpassed their herd mates from the control group by growth and development. They reached economic maturity earlier.

It has been established that intensive rearing of replacement heifers using Cellobacterin has positively impacted the development of their gastrointestinal tract, which is confirmed by the results of conducted research. It has been found that cows of the III experimental group surpassed the cows of the other experimental groups in terms of milk productivity and the physicochemical properties of milk.

The study of the physicochemical properties of milk makes it possible to conclude that intensive raising of replacement heifers using enhanced milk feed rates and the Cellobacterinprobiotic product allowed obtaining milk with better physicochemical properties from the cows in the experimental groups as compared to the ones in the control group.

5. REFERENCES:

1. Anisimova, E.I., Koshchaev, A.G., and Eremenko, O.N. (2019). Economic efficiency of productive features of various dairy cattle genotypes. *International Journal of Innovative Technology and Exploring Engineering*, *8*(8), 3207-3211.
2. Deen, A.U., Tyagi, N., Yadav, R. D., Kumar, S., Tyagi, A. K., and Singh, S. K. (2019). Feeding balanced ration can improve the productivity and economics of milk production in dairy cattle: A comprehensive field study. *Tropical Animal Health and Production,* 51(4), 737-744. DOI:10.1007/s11250-018-1747-8
3. Ferreira, G., Richardson, E. S., Teets, C. L., andAkay, V. (2019). Production performance and nutrient digestibility of

lactating dairy cows fed low forage diets with and without the addition of a live yeast supplement. *Journal of Dairy Science,* 102(7), 6174-6179. DOI:10.3168/jds.2019-16396
4. Gorelik, A.S., Gorelik, O.V.,Kharlap, S.Y. (2016). Lactation performance of cows, quality of colostral milk, and calves' livability when applying "Albit-bio". *Advances in Agricultural and Biological Sciences*, 2 (122 1), 5-12.
5. Gorelik, O.V., Dolmatova, I.A.,Gorelik, A.S.,Gorelik V.S. (2016).The effectiveness of dietary supplements Ferrourtikavit usage for the dairy cows. *Advances in Agricultural and Biological Sciences,* 2 (2), 27-33.
6. Gorlov, I. F.,Fedotova, G. V., Mosolova, N. I.,Sergeev, V. N.,Glushchenko, A.V., Vorontsova E. S. (2019). Assessment of the current state of dairy production in Russia. *Izvestiya NV AUK*, 2 (54). 189-197. DOI: 10.32786 / 2071-9485-2019-02-23.
7. Gorlov, I. F., Slozhenkina, M. I., Mosolova, N. I., Mishina, O. Y., andVorontsova, E. S. (2019). Productivity and biological value of milk of cows of various eco-genetic types. *IOP Conference Series: Earth and Environmental Science,* 341(1) DOI:10.1088/1755-1315/341/1/012043.
8. Gorlov, I.F., Mokhov, A.S.,Vorontsova, E.S.,Karetnikova, A.R.,Mosolova, N.I.,Slozhenkina, M.I.,Ovchinnikov, A.S.,Fomin S.D. (2018). Economic and biological peculiarities of golshchinsky breed cows of different ecological-genetic types. *ARPN Journal of Engineering and Applied Sciences,* 13 (7), 2562-2570.
9. Gurtsieva, D. O.,Kokaeva, M. G., Baeva, Z. TTsalieva, L. V. (2018). Influence of antioxidants on the physical, chemical, and technological properties of milk of lactating cows. *Izvestiya gorskogo gosudarstvennogo agrarnogo universiteta,*54(3), 76-81.
10. Haskell, M. J., Simm, G., and Turner, S. P. (2014). Genetic selection for temperament traits in dairy and beef cattle. *Frontiers in Genetics*, 5(OCT) DOI:10.3389/fgene.2014.00368
11. Karatunov, V.A., Tuzov, I.N., Zelenkov, P.I. (2014). Peculiarities of growth of the live weight of Australian Holstein young cattle when reared intensively. *Veterinary Pathology,* 2(48): 81–88.
12. Kargar, S., Habibi, Z., and Karimi-Dehkordi, S. (2019). Grain source and chromium supplementation: Effects on feed intake, meal and rumination patterns, and growth performance in Holstein dairy calves. *Animal,* 13(6), 1173-1179. DOI:10.1017/S1751731118002793
13. Knoblock, C. E., Shi, W., Yoon, I., and Oba, M. (2019). Effects of supplementing a saccharomyces cerevisiae fermentation product during the periparturient period on the immune response of dairy cows fed fresh diets differing in starch content. *Journal of Dairy Science*, 102(7), 6199-6209. DOI:10.3168/jds.2018-16224
14. Kok, A., Chen, J., Kemp, B., and Van Knegsel, A. T. M. (2019). Review: Dry period length in dairy cows and consequences for metabolism and welfare and customized management strategies. *Animal,* 13(S1), S42-S51. DOI:10.1017/S1751731119001174
15. Krasnova, O.A.,Batanov, S.D., Lebengarts, Y.Z. (2018). Increase of dairy and meat productivity of cattle when using biologically active substances. *Feeding of farm animals and feed production,* 5, 20-36.
16. Ma, Z. Y., Zhang, X. M., Wang, M., Wang, R., Jiang, Z. Y., Tan, Z. L., and Muhammed, A. (2019). Molecular hydrogen produced by elemental magnesium inhibits rumen fermentation and enhances methanogenesis in dairy cows. *Journal of Dairy Science,* 102(6), 5566-5576. DOI:10.3168/jds.2018-15647
17. McKay, Z. C., Lynch, M. B., Mulligan, F. J., Rajauria, G., Miller, C., and Pierce, K. M. (2019). The effect of concentrate supplementation type on milk production, dry matter intake, rumen fermentation, and nitrogen excretion in late lactation, spring-calving grazing dairy cows. *Journal of Dairy Science,* 102(6), 5042- 5053. DOI:10.3168/jds.2018-15796
18. Olagaray, K. E., Sivinski, S. E., Saylor, B. A., Mamedova, L. K., SaulsHiesterman, J. A., Yoon, I., and Bradford, B. J. (2019). Effect of saccharomyces 116 cerevisiae fermentation product on feed intake parameters, lactation performance, and metabolism of transition dairy cattle. *Journal of Dairy Science,* 102(9), 8092-8107. DOI:10.3168/jds.2019-16315
19. Ratoshny, A.N., Soldatov, A.A., Kononenko, S. I., Tuzov, I. N., Koshchaev, A.G. (2018). Organization of

feeding dairy cows for preventing metabolic disorders. *Journal of Pharmaceutical Sciences and Research,* 10(12): 3273-3276.
20. Raza, N., and Kim, K. -. (2018). Quantification techniques for important environmental contaminants in milk and dairy products. *Trends in Analytical Chemistry,* 98, 79-94. DOI:10.1016/j.trac.2017.11.002
21. Reynolds, M. A., Borchers, M. R., Davidson, J. A., Bradley, C. M., and Bewley, J. M. (2019). Technical note: An evaluation of technology-recorded rumination and feeding behaviors in dairy heifers. *Journal of Dairy Science,* 102(7), 6555-6558. DOI:10.3168/jds.2018-15635
22. Rodrigues, R. O., Rodrigues, R. O., Ledoux, D. R., McFadden, T. B., Rottinghaus, G. E., Borutova, R., and Averkieva, O. (2019). Feed additives containing sequestrant clay minerals and inactivated yeast reduce aflatoxin excretion in milk of dairy cows. *Journal of Dairy Science,* 102(7), 6614-6623. DOI:10.3168/jds.2018- 16151
23. Sehested, J., Gaillard, C., Lehmann, J. O., Maciel, G. M., Vestergaard, M., Weisbjerg, M. R., Kristensen, T. (2019). Review: Extended lactation in dairy cattle. *Animal,* 13(S1), A65-A74. DOI:10.1017/S1751731119000806
24. Stepurina, M. A.,Struk, V. N, Varakin, A. T.,Khakimov, I. N.,Vorontsova, E. S. (2019). Feed additives to increase the nutritional value of rations and productivity of lactating cows. *Izvestiya NV AUK,*4(56),170-179. DOI: 10.32786 / 2071-9485-2019-04-21.
25. Sun, H. Z., Plastow, G., and Guan, L. L. (2019). Invited review: Advances and challenges in the application of feedomics to improve dairy cow production and health. *Journal of Dairy Science,* 102(7), 5853-5870. DOI:10.3168/jds.2018-16126
26. Tuzov, I.N., Ryadchikov, V.G., Ratoshniy, A.N., Kulikova, N.I., Koshchaev, A.G. (2018). Using Holstein Cattle in Conditions of the Krasnodar Territory. *Journal of Pharmaceutical Sciences and Research*, 10(12): 3160-3163.
27. Wang, X., andKadarmideen, H. N. (2019). Metabolomics analyses in high-low feed efficient dairy cows reveal novel biochemical mechanisms and predictive biomarkers. *Metabolites,* 9(7) DOI:10.3390/metabo9070151
28. Weiss, W. P. (2019). Effects of feeding diets composed of corn silage and a corn milling product with and without supplemental lysine and methionine to dairy cows. *Journal of Dairy Science,* 102(3), 2075-2084. DOI:10.3168/jds.2018- 15535
29. Biotrof, (n.d.). Cellobacterin + Enzymatic Probiotic for Cattle. Retrieved from http://biotrof.ru/produkciya/cellobakterin/
30. ISO 12081-2013. Milk. Determination of calcium content. Titrimetric method.
31. DataApex, Clarity (2020), Shimadzu LC-10/20 System. Retrieved from https://downloads.dataapex.com/documentation/clarity/manuals/controls/controls-shimadzu-lc10_20systems.pdf

7. OPEN ACCESS

Table 1. *Scheme of the experiment*

Group	n	Scheme of technology for raising Holstein cattle
I control	16	Up to 6 months of age - traditional (T): 200 kg of milk (in 50 days) and 400 kg of swill (from 50 to 110 days); pre-starter (50%) with maize (50%). From 7 to 16 months of age - rearing, insemination.
II experimental	16	Up to 6 months of age - increased milking rate (in 25 days) of 200 kg and 400 kg of swill (from 25 to 60 days); pre-starter (50%) with maize (50%); probiotic "Cellobacterin" - 3 g/goal daily (before insemination). From 7- to 15-months of age - intensive rearing (IR), insemination.
III experimental	16	p to 6 months of age, increased rate of milking (in 50 days) - 450 kg and milk (from 50 to 110 days) - 600 kg of swill; pre-starter (50%) with maize (50%); probiotic "Cellobacterin" - 3 g/goal daily (before insemination). From 7 to 14 months of age - (IR), insemination/
IV experimental	16	Up to 6-months of age increased milking rate (in 60 days): 450 kg of milk (60 to 120 days); heifers: 600 kg, steers: 800 kg; pre-starter (50%) with maize (50%); "Cellobacterin" probiotic: 3 g/head daily (before insemination). From 7 to 14 months of age - (IR), insemination.

Table 2. *Cow Productivity and Physicochemical Composition of Milk for 305 Lactation Days (n = 5)*

Indicator	Group			
	I	II	III	IV
Lactation I				
Milk yield, kg	6590 ± 200.0	7120 ± 144.8	7860 ± 334.2	7720 ± 281.7
Acidity, °T	16.82 ± 0.2	16.79 ± 0.3	16.49 ± 0.2	16.53 ± 0.2
Density, °A	30.08 ± 0.4	29.87 ± 0.5	29.83 ± 0.5	29.85 ± 0.5
Water, %	88.21 ± 0.3	87.93 ± 0.4	87.25 ± 0.4	87.44 ± 0.5
Dry matter, %	11.79 ± 0.2	12.07 ± 0.2	12.75 ± 0.3	12.56 ± 0.2
Nonfat milk solids, %	9.05 ± 0.3	8.95 ± 0.3	8.87 ± 0.4	8.89 ± 0.3
Fat, %	3.75 ± 0.1	3.74 ± 0.1	3.65 ± 0.09	3.70 ± 0.1
Protein %	3.22 ± 0.2	3.25 ± 0.1	3.29 ± 0.1	3.27 ± 0.1
Ash, %	0.68 ± 0.09	0.73 ± 0.07	0.79 ± 0.06	0.76 ± 0.05
Calcium, %	0.145 ± 0.004	0.146 ± 0.005	0.149 ± 0.005	0.148 ± 0.004
Phosphorus, %	0.1045 ± 0.001	0.1047 ± 0.001	0.1048 ± 0.001	0.1048 ± 0.0008
Lactation II				
Milk yield, kg	6850 ± 129.5	7480 ± 151.4	8400 ± 348.2	8240 ± 329.1
Acidity, °T	16.78 ± 0.2	16.72 ± 0.3	16.47 ± 0.3	16.50 ± 0.2
Density, °A	30.01 ± 0.4	29.83 ± 0.2	29.80 ± 0.3	29.82 ± 0.4
Water, %	88.15 ± 0.5	87.86 ± 0.4	87.19 ± 0.4	87.35 ± 0.4
Dry matter, %	11.85 ± 0.3	12.14 ± 0.3	12.81 ± 0.3	12.65 ± 0.2
Nonfat milk solids, %	9.01 ± 0.2	8.90 ± 0.2	8.81 ± 0.2	8.83 ± 0.3
Fat, %	3.72 ± 0.1	3.70 ± 0.2	3.64 ± 0.1	3.69 ± 0.1
Protein %	3.25 ± 0.2	3.28 ± 0.2	3.31 ± 0.2	3.30 ± 0.1
Ash, %	0.69 ± 0.07	0.73 ± 0.08	0.80 ± 0.07	0.79 ± 0.05
Calcium, %	0.146 ± 0.005	0.147 ± 0.003	0.151 ± 0.003	0.150 ± 0.006
Phosphorus, %	0.1047 ± 0.002	0.1049 ± 0.002	0.1052 ± 0.003	0.1051 ± 0.002
Lactation III				
Milk yield, kg	7270 ± 184.6	7970 ± 208.3	9130 ± 407.9	8830 ± 330.5
Acidity, °T	16.72 ± 0.2	16.68 ± 0.2	16.43 ± 0.2	16.47 ± 0.3
Density, °A	29.95 ± 0.5	29.76 ± 0.5	29.72 ± 0.4	29.75 ± 0.4
Water, %	88.11 ± 0.4	87.81 ± 0.5	87.15 ± 0.4	87.31 ± 0.5
Dry matter, %	11.89 ± 0.3	12.19 ± 0.3	12.85 ± 0.2	12.69 ± 0.3
Nonfat milk solids, %	8.98 ± 0.2	8.88 ± 0.3	8.78 ± 0.2	8.80 ± 0.2
Fat, %	3.71 ± 0.2	3.69 ± 0.1	3.62 ± 0.1	3.65 ± 0.1
Protein %	3.29 ± 0.1	3.33 ± 0.08	3.39 ± 0.05	3.37 ± 0.07
Ash, %	0.70 ± 0.03	0.74 ± 0.03	0.84 ± 0.02	0.83 ± 0.03
Calcium, %	0.147 ± 0.006	0.149 ± 0.003	0.153 ± 0.006	0.152 ± 0.007
Phosphorus, %	0.1048 ± 0.001	0.1051 ± 0.002	0.1054 ± 0.001	0.1053 ± 0.002

Table 3. *Content of Fat in Milk of the Experimental Cows, % (n = 5)*

Group	Lactation month										Average fat content per lactation
	1	2	3	4	5	6	7	8	9	10	
Lactation I											
I	3.64 ± 0.02	3.65 ± 0.05	3.70 ± 0.04	3.74 ± 0.03	3.77 ± 0.03	3.59 ± 0.02	3.54 0.02	3.53 ± 0.02	3.50 ± 0.02	3.35 ± 0.02	3.60
II	3.69 ± 0.02	3.70 ± 0.03	3.71 ± 0.04	3.76 ± 0.02	3.80 ± 0.02	3.64 ± 0.02	3.60 ± 0.02	3.54 ± 0.02	3.51 ± 0.02	3.32 ± 0.02	3.63
III	3.74 ± 0.02	3.89 ± 0.02	3.88 ± 0.01	3.83 ± 0.02	3.78 ± 0.02	3.70 ± 0.02	3.62 ± 0.02	3.59 ± 0.02	3.50 ± 0.02	3.31 ± 0.01	3.68
IV	3.72 ± 0.02	3.81 ± 0.03	3.84 ± 0.02	3.86 ± 0.02	3.75 ± 0.02	3.67 ± 0.02	3.59 ± 0.02	3.58 ± 0.01	3.51 ± 0.02	3.31 ± 0.02	3.66
Lactation II											
I	3.67 ± 0.02	3.71 ± 0.03	3.76 ± 0.03	3.78 ± 0.02	3.67 ± 0.03	3.62 ± 0.02	3.59 ± 0.02	3.55 ± 0.02	3.52 ± 0.02	3.31 ± 0.02	3.62
II	3.73 ± 0.02	3.80 ± 0.02	3.86 ± 0.02	3.86 ± 0.02	3.75 ± 0.02	3.67 ± 0.03	3.60 ± 0.02	3.58 ± 0.02	3.51 ± 0.02	3.26 ± 0.02	3.66
III	3.76 ± 0.02	3.84 ± 0.02	3.90 ± 0.01	3.89 ± 0.02	3.79 ± 0.02	3.71 ± 0.02	3.62 ± 0.02	3.61 ± 0.02	3.56 ± 0.02	3.27 ± 0.02	3.70
IV	3.74 ± 0.02	3.81 ± 0.02	3.88 ± 0.02	3.85 ± 0.02	3.76 ± 0.02	3.67 ± 0.02	3.62 ± 0.02	3.59 ± 0.02	3.52 ± 0.02	3.35 ± 0.02	3.68
Lactation III											
I	3.69 ± 0.02	3.73 ± 0.04	3.78 ± 0.03	3.80 ± 0.02	3.69 ± 0.03	3.63 ± 0.02	3.61 ± 0.02	3.56 ± 0.02	3.52 ± 0.02	3.28 ± 0.02	3.63
II	3.75 ± 0.02	3.79 ± 0.03	3.84 ± 0.02	3.85 ± 0.02	3.76 ± 0.02	3.69 ± 0.03	3.67 ± 0.03	3.59 ± 0.02	3.54 ± 0.02	3.24 ± 0.03	3.67
III	3.80 ± 0.02	3.90 ± 0.01	3.86 ± 0.01	3.88 ± 0.02	3.83 ± 0.02	3.75 ± 0.02	3.69 ± 0.02	3.64 ± 0.02	3.60 ± 0.02	3.40 ± 0.02	3.74
IV	3.81 ± 0.02	3.85 ± 0.03	3.88 ± 0.02	3.87 ± 0.02	3.85 ± 0.02	3.72 ± 0.02	3.70 ± 0.02	3.61 ± 0.02	3.60 ± 0.02	3.27 ± 0.02	3.72

Table 4. *Content of Protein in Milk of the Experimental Cows, % (n = 5)*

Group	Lactation month										Average content of protein in milk per lactation
	1	2	3	4	5	6	7	8	9	10	
Lactation I											
I	3.25 ± 0.02	3.48 ± 0.04	3.39 ± 0.03	3.39 ± 0.03	3.33 ± 0.02	3.20 ± 0.04	3.22 ± 0.03	3.21 ± 0.03	2.79 ± 0.03	2.67 ± 0.03	3.19
II	3.21 ± 0.02	3.29 ± 0.03	3.50 ± 0.04	3.40 ± 0.03	3.41 ± 0.02	3.35 ± 0.02	3.26 ± 0.03	3.25 ± 0.03	2.83 ± 0.02	2.69 ± 0.03	3.22
III	3.30 ± 0.02	3.31 ± 0.03	3.33 ± 0.02	3.39 ± 0.03	3.44 ± 0.02	3.42 ± 0.04	3.31 ± 0.03	3.28 ± 0.02	2.99 ± 0.03	2.88 ± 0.03	3.27
IV	3.30 ± 0.02	3.29 ± 0.03	3.29 ± 0.02	3.33 ± 0.02	3.40 ± 0.02	3.41 ± 0.04	3.30 ± 0.03	3.24 ± 0.03	2.91 ± 0.03	2.82 ± 0.02	3.23
Lactation II											
I	3.33 ± 0.02	3.35 ± 0.03	3.44 ± 0.02	3.43 ± 0.02	3.35 ± 0.02	3.26 ± 0.02	3.14 ± 0.02	3.13 ± 0.02	3.10 ± 0.02	2.72 ± 0.02	3.23
II	3.34 ± 0.02	3.37 ± 0.03	3.46 ± 0.02	3.45 ± 0.02	3.36 ± 0.03	3.28 ± 0.02	3.19 ± 0.02	3.15 ± 0.03	3.14 ± 0.02	2.77 ± 0.04	3.25
III	3.36 ± 0.03	3.39 ± 0.03	3.46 ± 0.03	3.48 ± 0.03	3.38 ± 0.03	3.32 ± 0.02	3.24 ± 0.02	3.23 ± 0.02	3.17 ± 0.02	2.91 ± 0.03	3.29
IV	3.36 ± 0.02	3.38 ± 0.02	3.45 ± 0.02	3.47 ± 0.02	3.37 ± 0.03	3.28 ± 0.02	3.20 ± 0.02	3.21 ± 0.02	3.15 ± 0.02	2.87 ± 0.03	3.27
Lactation III											
I	3.37 ± 0.02	3.38 ± 0.02	3.39 ± 0.02	3.39 ± 0.03	3.38 ± 0.02	3.37 ± 0.02	3.21 ± 0.02	3.19 ± 0.03	3.16 ± 0.02	2.80 ± 0.04	3.26
II	3.41 ± 0.02	3.42 ± 0.02	3.44 ± 0.03	3.47 ± 0.02	3.40 ± 0.02	3.39 ± 0.02	3.23 ± 0.03	3.22 ± 0.02	3.18 ± 0.02	2.89 ± 0.02	3.31
III	3.42 ± 0.03	3.43 ± 0.02	3.43 ± 0.03	3.51 ± 0.03	3.52 ± 0.03	3.41 ± 0.03	3.38 ± 0.03	3.33 ± 0.02	3.19 ± 0.02	3.10 ± 0.04	3.37
IV	3.40 ± 0.02	3.42 ± 0.03	3.42 ± 0.03	3.50 ± 0.03	3.52 ± 0.03	3.40 ± 0.02	3.36 ± 0.02	3.27 ± 0.02	3.18 ± 0.02	3.00 ± 0.07	3.35

Table 5. *Milk Fat in the Cow's Milk, kg (n = 5)*

Group	Lactation month										Milk fat obtained per 305 days of lactation
	1	2	3	4	5	6	7	8	9	10	
Lactation I											
I	26.4 ± 0.7	29.6 ± 0.6	28.5 ± 0.9	27.9 ± 0.9	27.8 ± 0.9	26.3 ± 0.6	24.9 ± 0.6	22.6 ± 0.6	20.4 ± 0.5	16.5 ± 0.4	250.9
II	29.0 ± 0.7	30.6 ± 0.6	31.5 ± 0.7	31.2 ± 0.9	30.8 ± 0.7	26.2 ± 0.8	25.8 ± 0.5	24.4 ± 0.6	20.8 ± 0.4	16.0 ± 0.3	266.3
III	31.9 ± 1.0	33.3 ± 0.7	34.7 ± 0.9	35.1 ± 0.7	32.9 ± 0.8	30.3 ± 0.8	27.8 ± 0.8	25.2 ± 0.6	22.8 ± 0.6	17.3 ± 0.5	291.3
IV	32.2 ± 0.9	32.9 ± 0.7	34.2 ± 0.8	34.4 ± 0.7	32.6 ± 0.8	30.8 ± 0.9	28.7 ± 0.8	25.6 ± 0.5	20.7 ± 0.5	16.1 ± 0.4	288.2
Lactation II											
I	27.4 ± 0.8	29.5 ± 0.9	31.0 ± 0.8	30.2 ± 1.0	28.8 ± 0.7	26.9 ± 1.0	25.7 ± 0.8	23.2 ± 0.7	19.7 ± 0.8	16.1 ± 0.8	258.5
II	29.6 ± 1.0	31.2 ± 0.9	33.5 ± 0.8	32.8 ± 0.8	30.9 ± 0.7	29.3 ± 0.6	26.9 ± 0.9	25.3 ± 0.7	20.6 ± 0.7	16.7 ± 0.7	276.8
III	33.5 ± 0.9	36.1 ± 1.0	36.3 ± 0.9	37.2 ± 0.9	34.7 ± 0.9	31.8 ± 0.9	29.5 ± 0.9	26.3 ± 0.7	23.0 ± 0.6	17.4 ± 0.8	305.8
IV	33.0 ± 0.9	35.8 ± 1.0	36.7 ± 0.9	37.5 ± 0.9	34.2 ± 0.8	32.0 ± 0.9	29.3 ± 1.0	26.2 ± 0.7	22.6 ± 0.6	16.8 ± 0.7	304.1
Lactation III											
I	29.5 ± 0.9	33.7 ± 0.8	32.9 ± 0.7	31.4 ± 0.8	31.4 ± 0.6	29.3 ± 0.8	26.7 ± 0.6	25.4 ± 0.7	20.5 ± 0.7	16.3 ± 0.7	277.1
II	31.6 ± 0.8	33.7 ± 0.8	34.8 ± 0.7	36.4 ± 0.8	33.2 ± 0.8	30.2 ± 0.7	27.6 ± 0.7	25.0 ± 0.8	22.5 ± 0.7	17.3 ± 0.9	292.3
III	36.4 ± 0.7	37.3 ± 0.8	37.4 ± 0.9	39.0 ± 0.8	40.6 ± 1.0	34.7 ± 0.8	32.3 ± 0.9	28.1 ± 0.8	24.8 ± 0.8	19.9 ± 1.0	330.5
IV	35.7 ± 0.8	36.1 ± 0.7	37.0 ± 0.7	37.6 ± 0.7	39.3 ± 0.9	35.3 ± 0.8	31.6 ± 0.7	27.8 ± 0.7	23.5 ± 0.8	18.4 ± 0.8	322.3

Table 6. *Milk Protein in the Cow's Milk, kg (n = 5)*

Group	Lactation month										Milk protein obtained per 305 days of lactation
	1	2	3	4	5	6	7	8	9	10	
Lactation I											
I	22.6 ± 0.7	26.4 ± 0.8	24.5 ± 0.9	23.1 ± 0.8	24.6 ± 0.9	23.8 ± 1.0	21.7 ± 0.8	19.9 ± 0.7	15.8 ± 0.9	13.0 ± 0.4	215.4
II	25.1 ± 0.8	25.5 ± 1.0	28.5 ± 0.8	27.2 ± 0.9	26.9 ± 0.8	24.0 ± 0.9	22.8 ± 0.8	21.9 ± 0.8	16.3 ± 0.9	13.2 ± 0.3	231.4
III	28.5 ± 0.9	29.6 ± 0.9	30.6 ± 1.0	31.3 ± 1.0	30.7 ± 0.9	28.5 ± 0.8	25.5 ± 0.9	23.2 ± 0.8	19.4 ± 0.9	15.2 ± 0.5	262.5
IV	28.3 ± 0.8	28.5 ± 0.7	29.7 ± 0.8	30.4 ± 0.9	28.5 ± 0.8	28.4 ± 0.8	25.8 ± 0.9	23.1 ± 0.8	17.0 ± 0.9	15.0 ± 0.4	254.7
Lactation II											
I	24.2 ± 0.8	25.7 ± 0.9	27.3 ± 0.9	26.7 ± 0.9	25.4 ± 1.0	23.7 ± 0.9	22.2 ± 0.7	20.1 ± 0.9	17.2 ± 0.9	13.4 ± 0.9	225.9
II	26.5 ± 0.8	27.6 ± 0.8	29.8 ± 0.8	29.8 ± 0.9	27.6 ± 0.8	26.2 ± 0.9	23.7 ± 0.9	22.2 ± 1.0	18.4 ± 0.9	13.8 ± 0.7	245.3
III	30.7 ± 0.9	32.2 ± 0.8	33.6 ± 0.9	33.6 ± 0.7	31.9 ± 0.8	29.2 ± 0.8	26.6 ± 0.9	23.9 ± 0.8	20.7 ± 0.8	15.3 ± 0.9	278.0
IV	29.7 ± 0.9	31.8 ± 0.8	33.0 ± 0.9	33.0 ± 0.9	30.7 ± 1.0	28.6 ± 0.7	26.0 ± 0.9	23.5 ± 0.7	20.3 ± 0.7	14.8 ± 0.8	271.9
Lactation III											
I	26.6 ± 0.9	27.7 ± 0.9	28.7 ± 0.8	29.4 ± 0.8	28.2 ± 0.9	26.7 ± 0.8	23.7 ± 0.9	22.6 ± 0.8	18.4 ± 0.8	13.8 ± 0.8	245.8
II	29.0 ± 0.9	30.4 ± 0.8	31.4 ± 0.8	32.1 ± 0.9	30.1 ± 1.0	27.9 ± 0.8	24.8 ± 0.8	22.5 ± 0.8	20.4 ± 0.8	15.1 ± 0.8	263.7
III	34.3 ± 0.8	35.5 ± 0.7	35.5 ± 0.9	36.8 ± 0.8	36.9 ± 0.8	32.9 ± 0.7	30.8 ± 0.8	26.5 ± 0.8	22.6 ± 0.8	18.2 ± 1.0	309.5
IV	33.0 ± 0.8	34.0 ± 0.9	34.1 ± 0.8	35.2 ± 0.7	35.4 ± 0.7	32.9 ± 0.9	29.5 ± 0.9	25.7 ± 0.6	21.3 ± 0.9	16.5 ± 0.9	297.6

Table 7. *Amino Acid Composition of Milk in Groups I and II, g/100g (n = 5)*

Amino acid	Group I lactation I	I lactation II	I lactation III	II lactation I	II lactation II	II lactation III
Essential amino acids:						
Lysine	0.205 ± 0.007	0.242 ± 0.005	0.254 ± 0.006	0.268 ± 0.004	0.274 ± 0.003	0.279 ± 0.005
Leucine	0.211 ± 0.008	0.263 ± 0.007	0.278 ± 0.006	0.273 ± 0.007	0.285 ± 0.006	0.290 ± 0.006
Isoleucine	0.170 ± 0.006	0.183 ± 0.007	0.294 ± 0.005	0.197 ± 0.008	0.205 ± 0.006	0.208 ± 0.005
Phenylalanine	0.130 ± 0.004	0.153 ± 0.005	0.161 ± 0.004	0.162 ± 0.003	0.177 ± 0.007	0.185 ± 0.005
Threonine	0.095 ± 0.004	0.129 ± 0.008	0.136 ± 0.007	0.122 ± 0.003	0.128 ± 0.005	0.131 ± 0.004
Methionine	0.152 ± 0.005	0.174 ± 0.005	0.181 ± 0.008	0.174 ± 0.004	0.184 ± 0.008	0.192 ± 0.008
Valine	0.157 ± 0.007	0.161 ± 0.008	0.170 ± 0.006	0.169 ± 0.005	0.173 ± 0.007	0.178 ± 0.006
Essential amino acids, in total	1.140	1.305	1.374	1.365	1.426	1.463
Nonessential amino acids:						
Glycine	0.048 ± 0.003	0.052 ± 0.004	0.053 ± 0.005	0.050 ± 0.004	0.053 ± 0.006	0.055 ± 0.005
Cystine	0.054 ± 0.005	0.055 ± 0.007	0.057 ± 0.008	0.055 ± 0.005	0.057 ± 0.007	0.058 ± 0.008
Serine	0.102 ± 0.007	0.103 ± 0.009	0.104 ± 0.007	0.103 ± 0.006	0.104 ± 0.007	0.106 ± 0.009
Proline	0.101 ± 0.006	0.105 ± 0.008	0.107 ± 0.008	0.102 ± 0.008	0.106 ± 0.006	0.108 ± 0.008
Tyrosine	0.172 ± 0.008	0.176 ± 0.008	0.178 ± 0.007	0.174 ± 0.007	0.178 ± 0.007	0.179 ± 0.008
Alanine	0.103 ± 0.007	0.105 ± 0.008	0.106 ± 0.009	0.104 ± 0.007	0.106 ± 0.005	0.107 ± 0.009
Glutamine acid	0.578 ± 0.04	0.580 ± 0.02	0.589 ± 0.02	0.581 ± 0.02	0.584 ± 0.02	0.593 ± 0.013
Aspartic acid	0.193 ± 0.007	0.196 ± 0.03	0.198 ± 0.012	0.194 ± 0.007	0.198 ± 0.03	0.199 ± 0.012
Arginine	0.128 ± 0.02	0.129 ± 0.007	0.128 ± 0.005	0.129 ± 0.004	0.130 ± 0.006	0.131 ± 0.007
Histidine	0.101 ± 0.005	0.104 ± 0.008	0.103 ± 0.008	0.102 ± 0.007	0.104 ± 0.005	0.104 ± 0.007
Nonessential amino acids, in total	1.580	1.605	1.623	1.594	1.620	1.640
Amino acids, in total	2.720	2.910	2.997	2.959	3.046	3.103
Amino acid index*	0.72	0.81	0.84	0.86	0.88	0.89

Note: *The amino acid index was determined by the ratio of essential to nonessential amino acids.

Table 8. *Amino Acid Composition of Milk in Groups III and IV, g/100g (n = 5)*

Amino acid	Group					
	I			II		
	lactation			lactation		
	I	II	III	I	II	III
Essential amino acids:						
Lysine	0.280 ± 0.004	0.288 ± 0.005	0.302 ±0.006	0.273 ± 0.005	0.283 ± 0.006	0.295 ± 0.007
Leucine	0.289 ± 0.007	0.298 ± 0.006	0.310 ± 0.005	0.282 ± 0.006	0.291 ± 0.008	0.302 ± 0.006
Isoleucine	0.216 ± 0.005	0.223 ± 0.006	0.236 ± 0.004	0.213 ± 0.006	0.215 ± 0.005	0.230 ± 0.006
Phenylalanine	0.186 ± 0.004	0.191 ± 0.004	0.196 ± 0.006	0.181 ± 0.005	0.187 ± 0.006	0.190 ± 0.006
Threonine	0.135 ± 0.005	0.138 ± 0.007	0.148 ± 0.008	0.134 ± 0.005	0.132 ± 0.006	0.145 ± 0.007
Methionine	0.198 ± 0.006	0.226 ± 0.005	0.249 ± 0.006	0.190 ± 0.006	0.214 ± 0.009	0.238 ± 0.008
Valine	0.184 ± 0.008	0.198 ± 0.007	0.215 ± 0.005	0.182 ± 0.008	0.191 ± 0.006	0.208 ± 0.005
Essential amino acids, in total	1.488	1.562	1.656	1.455	1.513	1.608
Nonessential amino acids:						
Glycine	0.057 ± 0.006	0.061 ± 0.005	0.064 ± 0.006	0.056 ± 0.006	0.059 ± 0.007	0.062 ± 0.005
Cystine	0.061 ± 0.007	0.067 ± 0.007	0.069 ± 0.006	0.059 ± 0.006	0.065 ± 0.008	0.067 ± 0.005
Serine	0.109 ± 0.006	0.114 ± 0.008	0.119 ± 0.007	0.106 ± 0.006	0.111 ± 0.005	0.117 ± 0.006
Proline	0.121 ± 0.003	0.125 ± 0.006	0.129 ± 0.005	0.119 ± 0.003	0.122 ± 0.007	0.125 ± 0.006
Tyrosine	0.183 ± 0.006	0.186 ± 0.005	0.189 ± 0.006	0.181 ± 0.007	0.184 ± 0.008	0.185 ± 0.008
Alanine	0.112 ± 0.004	0.116 ± 0.004	0.118 ± 0.006	0.111 ± 0.005	0.114 ± 0.004	0.116 ± 0.006
Glutamine acid	0.592 ± 0.03	0.608 ± 0.02	0.617 ± 0.005	0.590 ± 0.03	0.604 ± 0.02	0.614 ± 0.009
Aspartic acid	0.212 ± 0.007	0.216 ± 0.013	0.219 ± 0.009	0.210 ± 0.004	0.214 ± 0.03	0.217 ± 0.005
Arginine	0.133 ± 0.007	0.137 ± 0.006	0.139 ± 0.007	0.132 ± 0.007	0.135 ± 0.006	0.136 ± 0.006
Histidine	0.103 ± 0.008	0.106 ± 0.007	0.108 ± 0.006	0.102 ± 0.006	0.104 ± 0.005	0.106 ± 0.006
Nonessential amino acids, in total	1.683	1.737	1.771	1.666	1.712	1.745
Amino acids, in total	3.171	3.299	3.427	3.121	3.225	3.353
Amino acid index*	0.88	0.90	0.94	0.87	0.88	0.92

Note: *The amino acid index was determined by the ratio of essential to nonessential amino acids.

PERIÓDICO TCHÊ QUÍMICA
ARTIGO ORIGINAL

USO DE NOVOS COMPOSTOS DA SÉRIE QUINOLINA COMO ESTIMULANTES DE CRESCIMENTO E RENDIMENTO DE CULTURAS AGRÍCOLAS

USE OF NEW COMPOUNDS OF THE QUINOLINE SERIES AS GROWTH AND YIELD STIMULANTS OF AGRICULTURAL CROP

ИСПОЛЬЗОВАНИЕ НОВЫХ СОЕДИНЕНИЙ ХИНОЛИНОВОГО РЯДА КАК СТИМУЛЯТОРОВ РОСТА И УРОЖАЙНОСТИ СЕЛЬСКОХОЗЯЙСТВЕННЫХ КУЛЬТУР

VOSTRIKOVA, Tatiana V.[1]*; KALAEV, Vladislav N.[2]; POTAPOV, Andrey Yu.[3]; MANAKHELOKHE, Gizacheu M.[4]; SHIKHALIEV, Khidmet S.[5]

[1]Federal State Budgetary Scientific Institution "A.L. Mazlumov All-Russian Research Institute of Sugar Beet and Sugar", Russian Federation.

[2]Voronezh State University, Department of Genetics, Cytology, and Bioengineering, Russian Federation.

[3,5]Voronezh State University, Department of Organic Chemistry, Russian Federation.

[4]University of Gondar, Department of Chemistry, College of Natural and Computational Sciences, Ethiopia.

** Correspondence author*
e-mail: tanyavostric@rambler.ru

Received 28 November 2020; received in revised form 02 February 2020; accepted 27 June 2021

RESUMO

Introdução: Diversos métodos foram desenvolvidos para sintetizar compostos orgânicos que possuem atividades biológicas específicas. **Objetivo:** O objetivo desta pesquisa foi estudar o efeito de compostos orgânicos sintetizados de fórmula geral: 1-alquil-2,2,4-trimetil-6-aminocarbotioil-1,2-dihidroquinolina e 1-alquil-2,2,4-trimetil-6-aminocarbotioil-1,2,3,4-tetra-hidroquinolina em indicadores de crescimento (como a germinação da semente, a altura, comprimento, largura e número de folhas da planta) e o rendimento da colheita agrícola. **Métodos**: Para identificar os efeitos biológicos dos compostos orgânicos sintetizados, foram selecionados parâmetros morfométricos de uma cultura anual de hortaliças (*Solanum melongena* L.). Foi analizasa a germinação de sementes, processos de crescimento e produtividade. Os processos de crescimento foram estudados por indicadores biométricos. Os indicadores biométricos incluíram a altura da planta, comprimento, largura e número de folhas. **Resultados e discussão:** Os estimuladores de crescimento mais eficazes de compostos da série 1-alquil-2,2,4-trimetil-6-aminocarbotioil-1,2-di-hidroquinolina e 1-alquil-2,2,4-trimetil-6-aminocarbotioil-1,2,3,4-tetraidroquinolina para berinjela comum foram revelados. As substâncias mais eficazes para *Solanum melongena* são 1,2,2,4-tetrametil-6- (1-piperidinilcarbotioil)-1,2,3,4-tetrahidroquinolina cloridrato e 4-[(1,2,2,4-tetrametil)Cloridrato de -1,2-dihidro-6-quinolinil)carbotioil]-1-piperazinilcarbaldeído nas concentrações testadas (0,01%; 0,05% e 0,1%), bem como os compostos da fórmula geral: 1- alquil-2,2,4-trimetil-6-aminocarbotioil-1,2,3,4-tetra-hidroquinolina em concentrações de 0,05% e 0,1%. Foi estabelecido que as substâncias químicas sintetizadas estimulam o crescimento da berinjela em comparação com a preparação comercial existente. Compostos da série 1-alquil-2,2,4-trimetil-6-aminocarbotioil-1,2-di-hidroquinolina e 1-alquil-2,2,4-trimetil-6-aminocarbotioil-1,2,3,4- a tetraidroquinolina aumenta a germinação das sementes de *Solanum melongena* de 30 a 80%, a massa vegetativa - de 10 a 40%, rendimento - de 28 a 46%. **Conclusões**: As tetraidroquinolinas são mais eficazes como estimulantes dos processos de crescimento (e produtividade) da berinjela comum. Os compostos contendo um substituinte di-hidro-6-quinolinil estimulam o crescimento e também aumentam o rendimento de *Solanum melongena*. A conveniência dos compostos da série quinolina para a produção de cultivo de vegetais é mostrada. Os estimuladores de crescimento usados aumentam o potencial adaptativo de *Solanum melongena*.

Palavras-chave*: reguladores de crescimento, processos de crescimento, compostos orgânicos sintetizados, germinação de sementes, rendimento*.

DOI: 10.52571/PTQ.v18.n38.2021.9_VOSTRIKOVA_pgs_123_136.pdf

ABSTRACT

Background: Productivity is increased with breeding techniques and modes for obtaining highly productive cultivars, various agricultural activities, and the use of new technologies for growing planting material. Some of modes to increase productivity are simple. They use different growth stimulants. Many methods were developed to synthesize organic compounds that have stimulating biological activity and can be used as growth stimulants for agricultural crop. **Aim:** The purpose of this research was to study the effect of synthesized organic compounds of the general formula: 1-alkyl-2,2,4-trimethyl-6-aminocarbothioyl-1,2-dihydroquinoline and 1-alkyl-2,2,4-trimethyl-6-aminocarbothioyl-1,2,3,4-tetrahydroquinoline on growth indicators (by which we meant seed germination and plant height, length, width, and the number of leaves) and the yield of the agricultural crop. **Methods:** To identify the biological effects of the synthesized organic compounds, morphometric parameters of an annual vegetable crop (*Solanum melongena* L.) were selected. It is investigated seed germination, growth processes, and yield. Growth processes were studied by biometric indicators. Biometric indicators included the plant height, length, width, and the number of leaves. **Results and Discussion:** The most effective growth stimulators from compounds of the series 1-alkyl-2,2,4-trimethyl-6-aminocarbothioyl-1,2-dihydroquinoline and 1-alkyl-2,2,4-trimethyl-6-aminocarbothioyl-1,2,3,4-tetrahydroquinoline for common eggplant were revealed. The most effective substances for *Solanum melongena* are 1,2,2,4-tetramethyl-6-(1-piperidinylcarbothioyl)-1,2,3,4-tetrahydroquinoline hydrochloride and 4-[(1,2,2,4-tetramethyl-1,2-dihydro-6-quinolinyl)carbothioyl]-1-piperazinylcarbaldehyde hydrochloride in tested concentrations (0,01 %; 0,05 % and 0,1 %), as well as the compounds of the general formula: 1-alkyl-2,2,4-trimethyl-6-aminocarbothioyl-1,2,3,4-tetrahydroquinoline in concentrations of 0,05 % and 0,1 %. It was established that the synthesized chemical substances cause stimulation of the eggplant growth compared with existing commercial preparation. Compounds of the series 1-alkyl-2,2,4-trimethyl-6-aminocarbothioyl-1,2-dihydroquinoline and 1-alkyl-2,2,4-trimethyl-6-aminocarbothioil-1,2,3,4-tetrahydroquinoline increase the seed germination of *Solanum melongena* from 30 to 80 %, the vegetative mass - from 10 to 40 %, yield - from 28 to 46 %. **Conclusions:** Tetrahydroquinolines are most effective as stimulants of growth processes (and productivity) for common eggplant. Compounds containing a dihydro-6-quinolinyl substituent stimulate the growth and also increase the yield of *Solanum melongena.* The expediency of quinoline series compounds for the production of vegetable growing is shown. Used growth stimulators increase the adaptive potential of *Solanum melongena.*

Keywords: *growth regulators, growth processes, synthesized organic compounds, seed germination, yield*.

АННОТАЦИЯ

Предпосылки: Урожайность повышается за счет селекционных технологий и способов получения высокопродуктивных сортов, различных сельскохозяйственных работ и использования новых технологий выращивания посадочного материала. Некоторые из способов повышения продуктивности просты. Они используют разные стимуляторы роста. Разрабатываеся множество методов синтеза органических соединений, которые обладают стимулирующей биологической активностью и могут использоваться как стимуляторы роста сельскохозяйственных культур. **Цель:** Цель исследования состояла в изучении эффектов соединений общей формулы: 1-алкил-2,2,4-триметил-6-аминокарботиоил-1,2-дигидрохинолин и 1-алкил-2,2,4-триметил-6-аминокарботиоил-1,2,3,4-тетрагидрохинолин на ростовые показатели (под которыми мы понимали всхожесть семян и высоту растения, длину, ширину и количество листьев) и урожайность сельскохозяйственной культуры. **Методы:** Для выявления биологического действия синтезированных органических соединений были выбраны морфометрические параметры однолетней овощной культуры (*Solanum melongena* L.). Исследуется всхожесть семян, процессы роста и урожайность. Процессы роста изучали по биометрическим показателям. Биометрические показатели включали высоту растения, длину, ширину и количество листьев. **Результаты и Обсуждение:** Выявлены наиболее эффективные стимуляторы роста из соединений ряда 1-алкил-2,2,4-триметил-6-аминокарботиоил-1,2-дигидрохинолина и 1-алкил-2,2,4-триметил-6-аминокарботиоил-1,2,3,4-тетрагидрохинолина для баклажана обыкновенного. Наиболее эффективными веществами для *Solanum melongena* являются 1,2,2,4-тетраметил-6-(1-пиперидинилкарботиоил)-1,2,3,4-тетрагидрохинолин гидрохлорид и 4-[(1,2,2,4-тетраметил)-1,2-дигидро-6-хинолинил)карботиоил]-1-пиперазинилкарбальдегида гидрохлорид в тестируемых концентрациях (0,01 %; 0,05 % и 0,1 %), а также соединения общей формулы: 1- алкил-2,2,4-триметил-6-аминокарботиоил-1,2,3,4-тетрагидрохинолин в концентрациях 0,05 % и 0,1 %. Установлено, что синтезированные химические вещества вызывают стимуляцию роста баклажанов по сравнению с существующим коммерческим препаратом. Соединения ряда 1-алкил-2,2,4-триметил-6-аминокарботиоил-1,2-дигидрохинолин и 1-алкил-2,2,4-триметил-6-аминокарботиоил-1,2,3,4-тетрагидрохинолин увеличивают всхожесть семян *Solanum melongena* с 30 до 80 %, вегетативную массу - с 10 до 40 %, урожайность - с 28 до 46 %. **Выводы:** Тетрагидрохинолины наиболее эффективны в качестве стимуляторов ростовых процессов (и продуктивности) для баклажана

обыкновенного. Соединения, содержащие дигидро-6-хинолинильный заместитель, стимулируют рост, а также увеличивают урожайность *Solanum melongena*. Показана целесообразность применения соединений хинолинового ряда для овощеводства. Используемые стимуляторы роста повышают адаптационный потенциал *Solanum melongena*.

Ключевые слова: *регуляторы роста, ростовые процессы, синтезированные органические соединения, всхожесть семян, урожайность*

1. INTRODUCTION

In recent years vegetable growing has been faced with many problems associated with an extreme increase in air temperature, lack of soil moisture, and the search for the most stable and unpretentious crops that can grow in such conditions. Breeding and testing are carried out and aimed at increasing the yield, resistance of agricultural plants to adverse environmental conditions (Dyakov *et al.*, 2009). Productivity is increased with breeding techniques and modes for obtaining highly productive cultivars, various agricultural activities, and the use of new technologies for growing planting material. It is known that different genetic systems control the productivity potentials of cultivated plants and their environmental sustainability and relatively independent (Zhuchenko, 1994, 1995, 2009; Kilchevsky, Khotyleva, 1997). It was noted that the productivity of the fruiting plant and its resistance to adverse factors are antipodal in nature since the same metabolites are involved in their creation but in different quantities (Doroshenko, 2000). Thus, productivity and stability are formed from the same photosynthesis products but redistributed in different directions following genetic regulation (Doroshenko *et al*., 2010). Studies show the presence of negative genetic correlation or even significant incompatibility between the high yield potential and tolerance to adverse conditions in many species of cultivated plants (Azzi, 1959; Rosielle, Hamblin, 1981; Kadyrov *et al*., 1984), which indicates the need for a search other (non-breeding) methods for solving this problem, which may be the treatment of planting material with chemical stimulators.

Last years a lot of new compounds are recommended for use as plant growth and seed germination stimulants, fertilizers for vegetables, field (including sugar beet), and fruit crops used for food by humans. In this connection, ecologically safe substances play an important role. For example, when reproducing sugar beet hybrids, an increase in yield and sugar content of mother roots after the treatment of seeds with humic compounds has been revealed (Tsareva, 2013). Further, planting of these roots for the reproduction of hybrids improves the yield and sowing properties (germinating capacity) of seeds (Tsareva, 2013).

Maintenance of seed quality is mandatory for the sale of seed and assuring required plant population and final yields to end-user. Seed lots are evaluated based on their germination capabilities and vigor (Sudhakar *et al*., 2016). However, many tests used to evaluate seed physiological characteristics require time and skilled labor, making it a costly process (Baranova, 2013; Sudhakar *et al*., 2016). However, there are simple characteristics, for example, biometric indicators included plant height, length, width, and several leaves. They are suitable for the study of the agricultural crop.

One of the agricultural plants cultivated in recent years in Russia, in the Central Black Earth region, and even in the Non-Chernozem zone due to the more cold-resistant varieties obtained in breeding tests is an ordinary eggplant (Mamedov, 2002; Guber and Shentseva, 2011). Its fruits are tasty and healthy; they contain antioxidants in the seeds – steroid glycosides. These natural compounds delay the aging of living organisms and thereby contribute to their resistance to stress and disease (Mamedov, 2002). Due to the long vegetation period of eggplant common (*Solanum melongena* L.) in this zone, accelerated production of planting material is necessary, which is achieved using growth stimulators and seed germination, including synthesized chemical compounds.

Several researches have been carried out related to the development of methods for the synthesis of organic compounds that have certain types of biological activity and are promising drugs (Kashaev *et al.*, 2010 a, b, 2011). At the same time, one of the key problems of the functionally-oriented molecular design of new pharmacologically active compounds was and remained the problem of choosing an accessible substrate with great preparative capabilities (Kashaev *et al.*, 2010 a, b, 2011).

Heterocyclic series, including quinoline derivatives, being polyfunctional substrates, fully meet these requirements. A significant amount of data on the biological activity of compounds

containing a quinoline fragment, including the activity and toxicity, has been published in the literature (Abadi, Brun, 2003; Saudi *et al.*, 2003; Abdel-Gawad *et al.*, 2005; Kashaev *et al.*, 2010 a, b, 2011). Some compounds have found application as chemotherapeutic drugs with antimicrobial, antiprotozoal, antifungal, and bronchodilatory activity (montelukast, quinifuril, chlorquinaldol, hydroxychlorin, chlorin) (Abadi, Brun, 2003; Saudi *et al.*, 2003; Abdel-Gawad *et al.*, 2005; Kashaev *et al.*, 2010 a, b, 2011; Ghoneim and Assy, 2015). Effective antimalarial drugs have been found among aminoquinolines. Iso-propylamide 2- (4-chloroanilino) cinchoninic acid exhibits anti-inflammatory and analgesic activity (Kashaev *et al.*, 2010 a, b, 2011).

Despite the fairly widespread use of derivatives quinolines, the potential for their research is far from being exhausted. A promising area of work, in connection with the growing need for the development of effective and safe preparation, is the synthesis of new heterocyclic systems containing other groups along with a quinoline fragment. It was shown that the most stable is the quinoline nucleus by the mass spectrometric method (Kashaev *et al.*, 2010 a, b, 2011).

Last years there are a lot of organic and inorganic compounds (Pentelkina and Pentelkina, 2002; Vasin *et al*., 2008, 2009; Ostroshenko and Ostroshenko, 2011; Kadyrov and Schuchka, 2005; Baranova, 2013; Khodaei-Joghan *et al*., 2018; Nesterkina *et al*., 2019) and other original modes for growth-regulating (Shibaeva *et al*., 2018). In the greenhouse production of several vegetables and ornamental plant species, a short diurnal temperature drop is used to reduce stem elongation as an alternative to chemical growth retardants (Shibaeva *et al*., 2018). It was determined the effects of applying organic and chemical fertilizers under different irrigation regimes on sunflower (*Helianthus annuus* L.) morphological traits, yield components, grain yield, and grain quality (Khodaei-Joghan *et al*., 2018). There are new effective synthesized quinoline compounds (Abadi and Brun, 2003; Saudi *et al.*, 2003; Abdel-Gawad *et al.*, 2005; Shujiang *et al.*, 2005; Denmark, Venkatraman, 2006; Kashaev *et al.*, 2010 a, b, 2011; Mosalam *et al.*, 2011 a, b; Azizian *et al.*, 2014; Shikhaliev *et al.*, 2014; Ghoneim and Assy, 2015).

A wide range of derivatives of 4-quinolinecarboxylic acid hydrazides has been obtained, containing 1,3,4-oxadiazole, 1,2,4-triazine, and 1,2,4-triazole rings, along with the quinoline fragment (Kashaev *et al.*, 2010 a, b, 2011). The synthesis of 2-R-6-R′-(5-X-2-oxo-1,2-dihydro-3H-indol-3-ylidene) quinoline-4-carbohydrazides was carried out by condensation of hydrazides of 4-quinolinecarboxylic acids with isatins (Kashaev *et al.*, 2010 b). Based on 2-methyl-4- (1,3,4-oxadiazol-2-yl) quinolines, the corresponding 2- [2- (2-nitrophenyl) -1-ethenyl] -6-R-4- (1,3 , 4-oxadiazol-2-yl) quinolines of the E-configuration. The cyclization of 2-[2-(2-am_ inophenyl)-1-ethenyl]-4-(1,3,4-oxadiazol-2-yl)qui_ noline, which is a reduction product of 2-[2- (2-nitrophenyl) -1- ethenyl] -4- (1,3,4-oxadiazol-2-yl) quinoline, 4-(1,3,4-oxadiazol-2-yl)-2,3-biquinoline was synthesized under the conditions of the Vilsmeier reaction (Kashaev *et al.*, 2010 a). Based on the results of biological tests of the synthesized substances, the expediency of searching for new physiologically active compounds in the series of 4-hetarylquinolines was confirmed (Kashaev *et al.*, 2011). Thus a lot of newly synthesized compounds containing the quinoline fragment show physiological activity.

The main objectives of this research were to study the effect of synthesized organic compounds of the general formula: 1-alkyl-2,2,4-trimethyl-6-aminocarbothioyl-1,2-dihydroquinoline and 1-alkyl-2,2,4-trimethyl-6-aminocarbothioyl-1,2,3,4-tetrahydroquinoline on growth indicators (by which we meant seed germination and plant height, length, width, and the number of leaves) and the yield of *Solanum melongena.*

2. MATERIALS AND METHODS

2.1. The synthesis of organic compounds

Acrylonitrile was copolymerized with 8-methacryloxy-quinoline in Dimethylformamide using azobisisobutyronitrile as the initiator. Both homopolymer and copolymers were characterized by different spectral and thermal methods (Mosalam *et al.*, 2011 b).

The monomer 8-methacryloxy-quinoline (MAQ) was prepared by the reaction of 8-hydroxyquinoline with either methacryloyl chloride or methacrylic acid in the presence of triethylamine and N,N′-dicyclohexylcarbodiimide, respectively (Mosalam *et al.*, 2011 a). Binary copolymerization of this new monomer with methyl acrylate (MA), acrylonitrile (AN) methyl methacrylate (MMA), styrene (ST), were performed in Dimethylformamide, using 1 mol% azobisisobutyronitrile as initiator at 65 °C (Mosalam *et al.*, 2011 a). The monomer reactivity ratios for the systems MAQ-MA, MAQ-AN, MAQ-MMA and MAQ-ST were found to be r1 = 0.695 ±

0.036, r2 = 0.62 ± 0.235; r1 = 0.273 ± 0.087, r2 = 0.259 ± 0.67; r1 = 0.356 ± 0.015, r2 = 1.615 ± 0.052 and r1 = 0.097 ± 0.003, r2 = 0.339 ± 0.027 respectively (Mosalam *et al.*, 2011 a).

Novel pyrimido[4,5-b]quinoline-tetraones (4 a-m) were prepared by the three-component reaction of 2-hydroxynaphthalene-1,4-dione (1), 6-amino-uracils (2), and aromatic aldehydes (3) in aqueous media and catalyzed by *p*-toluenesulfonic acid (Figure 1). This reaction provides a simple one-step procedure with the advantages of easy workup, good yield of products, and environmental friendliness (Azizian *et al.*, 2014). Sulfur as the element present in the synthesis of new hydroquinoline derivatives.

2–Amino–4-phenyl–5,6,7,8–tetrahydroqui_ noline–3–carbonitrile (3) was synthesized by treating cyclohexanone (1) with 2–benzylidenemalononitrile (2) in the presence of ammonium acetate (Elkholy and Morsy, 2006). The treatment of cyclohexanone (1) with the α,β-unsaturated nitrile derivative 2 in the presence of ammonium acetate afforded the tetrahydroquinoline derivative 3 (Elkholy and Morsy, 2006). A solution of cyclohexanone (1, 0.01 mol) in absolute ethanol (30 mL) containing an excess of ammonium acetate and the arylidene derivative 2 (0.01 mol) was heated under reflux from 3 to 5 h (Elkholy and Morsy, 2006). The separated solid material during the heating was collected by filtration and recrystallized from ethanol to yield the tetrahydroquinoline derivative 3 (Elkholy and Morsy, 2006). The reactivity of compound 3 towards dimethylformamide dimethyl acetal, carbon disulfide, urea, thiourea, formamide, formic acid, acetyl chloride, and isothiocyanate was studied (Elkholy and Morsy, 2006).

It was developed a three-component method for the synthesis of new thiocarboxamides containing in their composition the gidroquinoline cycle. The elemental sulfur was used in Wilgerodt-Kindler reaction for the thioamides synthesis. The thioamides series synthesis of hydroquinoline derivatives is based on Wilgerodt-Kindler reaction for 1-alkylhydroquinoline-6-carbaldehydes, amines, and sulfur. The structures of compounds were characterized by NMR-1H spectroscopy and elemental analysis. The data of NMR-1H (nuclear magnetic resonance) thioamides spectra are presented below.

Figure 2 is a general scheme for the synthesis of organic compounds of the series 1-alkyl-2,2,4-trimethyl-6-aminocarbothioyl-1,2-dihydroquinoline and 1-alkyl-2,2,4-trimethyl-6-aminocarbothioyl-1,2,3,4-tetrahydroquinoline.

A mixture of the corresponding hydroquinoline carboxaldehyde (1 mmol), amine (1.33 mmol), and elemental sulfur (1.33 mmol) in dimethylformamide (2 ml) was heated under reflux until the completion of the reaction (the control by the thin layer chromatography). After cooling, the reaction mass was poured into 5 ml of ice water with vigorous stirring. The solidified after grinding, and the precipitate was filtered, washed with water, and recrystallized from 75% ethanol. Non-hardening thiocarboxamides were treated with a double excess of hot 2M hydrochloric acid, filtered, and recrystallized from ethanol.

The structures of synthesized organic compounds are presented in Figures 3-7.

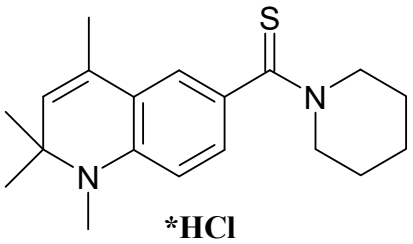

Figure 3. *1,2,2,4-tetramethyl-6-(1-piperidinylcarbothioyl)-1,2-dihydroquinoline hydrochloride (compound 1).*

The data of NMR-1H thioamides spectra: 1.29 (6H, s, (CH3) 2 -C2); 1.45-1.60 (6H, br.s, 3CH2 - piperidine); 1.89 (3H, s, CH3 -C4); 2.76 (3H, s, N-CH3); 3.60-4.30 (4H, br.s, 2CH2 - piperidine); 5.39 (1H, s, CH-DHC); 6.44 (1H, d, J = 8.54, arom); 6.95 (1H, d, J = 2.18, arom); 7.05 (1H, dd, J = 8.46, J = 2.18, arom.).

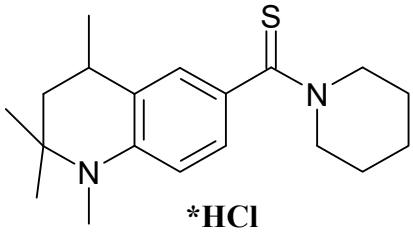

Figure 4. *1,2,2,4-tetramethyl-6-(1-piperidinylcarbothioyl)-1,2,3,4-tetrahydroquinoline hydrochloride (compound 2).*

The data of NMR-1H thioamides spectra: 1.17 (3H, s, (CH3) 2A-C2); 1.26 (3H, s, (CH3) 2B-C2); 1.27 (3H, d, J = 6.59, CH3 -C4); 1.40 (1H, t, J = 12.85, CH2A); 1.44-1.65 (6H, br.m., 3CH2 -piperidine); 1.83 (1H, dd, J = 13.04, J =

4.44, CH2B); 2.76 (1H, m, CH); 2.78 (3H, s, N-CH3); 3.50-4.30 (4H, br.m., 2CH2 -piperidine); 6.47 (1H, d, J = 9.18, arom); 7.03 (1H, dd, J = 6.79, J = 2.16, arom.); 7.04 (1H, s, arom.).

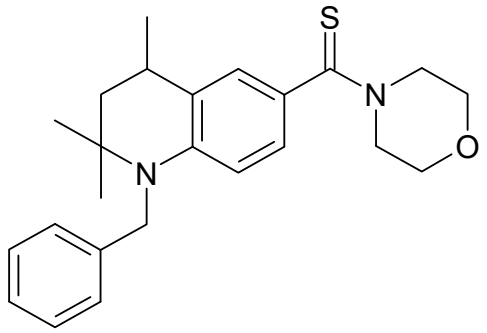

Figure 5. *1-benzyl-2,2,4-trimethyl-6-(4-morpholinylcarbothioyl)-1,2,3,4-tetrahydroquinoline (compound 3).*

The data of NMR-1H thioamides spectra: 1.24 (3H, s, (CH3) 2A-C2); 1.26 (3H, s, (CH3) 2B-C2); 1.32 (3H, d, J = 6.59, CH3 -C4); 1.64 (1H, t, J = 12.98, CH2A); 1.90 (1H, dd, J = 13.03, J = 4.72, CH2B); 2.96 (1H, m, CH); 3.50-4.20 (8H, m br, 4CH2 - morpholine); 4.26 (1H, d, J = 18, CH2A-benzyl); 4.78 (1H, d, J = 18.07, CH2B-benzyl); 6.13 (1H, d, J = 8.65, aroma.); 6.90 (1H, dd, J = 8.63, J = 2.13, arom); 7.15- 7.35 (6H, m, arom).

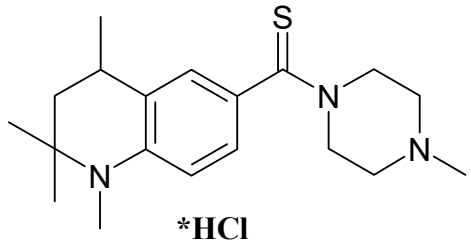

Figure 6. *1,2,2,4-tetramethyl-6-[(4-methyl-1-piperazinyl)carbothioyl]-1,2,3,4-tetrahydroquinoline hydrochloride (compound 4.)*

The data of NMR-1H thioamides spectra: 1.19 (3H, s, (CH3) 2A-C2); 1.28 (3H, s, (CH3) 2B-C2); 1.30 (3H, d, J = 7.31, CH3 -C4); 1.42 (1H, t, J = 12.45, CH2A); 1.85 (1H, dd, J = 13.08, J = 4.52, CH2B); 2.75 (3H, d, J = 4.55, N-CH3 -piperazine); 2.81 (3H, s, N-CH3 -TGQ); 3.08 (1H, m, CH); 4.10-4.70 (8H, br.m., 4CH2 -piperazine); 6.50-7.35 (3H, m, aroma.); 11.25 (1H, s, HCl).

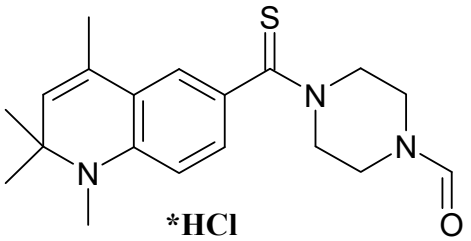

Figure 7. *4-[(1,2,2,4-tetramethyl-1,2-dihydro-6-quinolinyl)carbothioyl]-1-piperazinylcarbaldehyde hydrochloride (compound 5).*

2.2. The treatment of planting material

As an object of research, common eggplant (*Solanum melongena* L.) cv. Black Beauty was chosen. The material was purchased seeds of "Aelita" (Moscow) with a guaranteed shelf life, the quality of which corresponds to Russian Standards of high quality (varietal purity - 92-98 %, germination - not less 60%, humidity - no more 11 %). Seeds were soaked in water solutions of the synthesized compounds. The seeds of *Solanum melongena* were kept in water solutions of the above chemical compounds at concentrations of 0.01%, 0.05%, and 0.1% for 18 hours. As a traditional stimulator, the commercial preparation Epin-Extra (Russian produced by NNPP NEST M) in a working concentration according to the instructions for use - 0.05%. The control seeds were soaked in tap water. The experiment was carried out in triplicate (100 seeds in each). Seeds were germinated under laboratory conditions at a constant temperature of 22 °C.

The eggplant seedlings were counted to study laboratory germination and planted in boxes in a covered ground (greenhouse) on the 14th day after the germination. The laboratory germination of seeds was determined as the ratio of the number of germinated seeds to the total number of seeds and was expressed in %. Biometric indicators (the plant height, length, and width of leaves) were measured on the 50th day of the start of the experiment using a ruler. The plants were transferred from the greenhouse to the open ground on the 50th day of the beginning of the experiment, after preliminary hardening the seedlings (from 30 days). A field experiment was laid according to B. A. Dospehov (1985) by the method of split plots in triplicate. Eggplant seedlings were planted in open ground at the rate of 5 plants per 1 m^2 (50 thousand plants per 1 ha). Biometric indicators included the plant height, length, width, and the number of leaves. The number of leaves, which is considered the most objective sign of the degree of plant

development (Korovkin, 2007, Zhidkih *et al*., 2012), was calculated on the 50th day of the start of the experiment. The number of leaves was counted from 50 plants of each variant and was found the average value. The yield was determined after fruit harvesting on 70th day after planting in open ground (120th day of the start of the experiment). The mass of fruits was measured using a balance from 4 m^2 and calculated for 1 m^2 (was devided at 4). The yield was expressed in kg/m^2.

Computer statistical processing was performed using the Stadia software package. Data on 50 plants of each variant were analyzed. The seed germination in control and experimental variants was compared according to the frequency agreement criterion using Z-statistics. The comparison of the mean values was carried out using Student's t-test according to A. P. Kulaichev (2006) work. The influence of the chemical treatment factor at different concentrations on growth rates was determined using a two-way analysis of variance.

3. RESULTS AND DISCUSSION:

The virtual screening of the obtained compounds is carried out with the help of PASS programe developed at the Institute of Bioorganic Chemistry of the Russian Academy of Medical Sciences (Moscow). Therefore opportunities for the practical use of substances were predicted. As it turned out, hydroquinoline thioamides with a high degree of probability (more than 70%) are biologically active compounds. Pharmacological side effects such as mutagenicity, carcinogenicity, teratogenicity ness, and embryotoxicity for synthesized substances are not predicted. It should also be marked that it is predicted the high growth-stimulating activity regarding plants for all thioamides.

The results of the influence of tested chemical compounds on the germination capacity of common eggplant (*Solanum melongena* L.) seeds of cv. Black Beauty is presented in Table 1. The greatest effect of increasing the germination capacity of ordinary eggplant was produced by compounds of the series 1-alkyl-2,2,4-trimethyl-6-aminocarbothioyl-1,2,3,4-tetrahydroquinoline, which are tetrahydroquinolines. There is a distinct tendency to increase seed germination with decreasing concentration in all considered compounds belonging to this series. Stimulators 1 (dihydroquinoline) and 5 (containing the dihydro-6-quinolinyl substituent) did not stimulate germination. The germination of eggplant seeds under the influence of synthesized organic substances in the tested concentrations increases from 32.4 to 89.3 %.

The height of the common eggplant plant grown from seeds treated with synthesized chemical compounds is shown in Table 2. It can be found from the table that stimulators 2 and 5 express the greatest stimulating effect in all tested concentrations. Stimulators 3 and 4 are effective in concentrations of 0.05 % and 0.1 %. All tested compounds exhibit a stimulating effect at a concentration of 0.1 %. Plant height under the influence of synthesized organic substances in the tested concentrations increases from 13.9 to 43.1%.

The leaf length of *Solanum melongena* after treating the seeds with synthesized chemical compounds is presented in Table 3. The table shows that their effect is similar to that on the plant height: stimulators 2 and 5 exhibits the greatest stimulating effect in all tested concentrations. Stimulators 3 and 4 are effective in concentrations of 0.05 % and 0.1 %. All tested compounds exhibit a stimulating effect at a concentration of 0.1%. The leaf length increases from 15.9 to 20.6 %.

All tested compounds at a concentration of 0.05 % and 0.1 % had a stimulating effect on the leaf width of common eggplant (Table 4), except for stimulator 1, which was effective only in a 0.1 % solution. The greatest effect was stimulators 2 and 5. The leaf width increases from 21.7 to 45.7 %.

The stimulating effect of chemical compounds on the number of leaves of *Solanum melongena* (Table 5) differed from that of the height of the plant and the leaf length. The most effective stimulator was 2. The number of leaves under the influence of synthesized organic substances in the tested concentrations increases from 3.9 to 28.9 %.

All the tested compounds at all concentrations, except for a 0.01 % solution of the stimulator 1, had a stimulating effect on eggplant yield (Table 6). The yield under the influence of synthesized organic substances in the tested concentrations increased from 28.1 to 46.9 %. The results of two-way analysis of variance confirm the influence of the factor of seed treatment with chemical compounds and concentration on biometric indicators: plant height ($P<0.01$), leaf length ($P<0.01$), leaf width ($P<0.01$), number of leaves ($P<0.05$) and yield

(P<0.05). Therefore, the obtained data shows that used growth stimulators increase the adaptive potential of *Solanum melongena.* Though productivity potentials of cultivated plants and their environmental sustainability are controlled by different genetic systems (Zhuchenko, 2009), it was noted that productivity and environmental sustainability is risen by several chemical substances (Titov *et al*., 2011; Bashmakov *et al*., 2012). Our data is confirmed by the results of other authors. The investigations about the influence of organic and inorganic compounds for woody plants seedlings that leads to the growth activity increase (Pentelkina and Pentelkina, 2002; Ostroshenko and Ostroshenko, 2011), to the better development of oilseed radish seedlings (*Raphanus sativus* L. var. *oleiferus* Metzg.) (Nesterkina *et al*., 2019). The effect of seed treatment with growth stimulants were positive for corn and barley growing (Vasin *et al*., 2008, 2009), for soybean yield (Kadyrov and Schuchka, 2005) for sunflower (*Helianthus annuus* L.) morphological traits, yield components, grain yield and grain quality (Khodaei-Joghan *et al*., 2018).

Obtained results are consistent with earlier studies by R. G. Gafurov and co-workers on carbon N- and O-benzyl-containing compounds that have bright auxin activity, which is ensured by the presence of a benzyl group at the nitrogen or oxygen atom (Gafurov and Makhmutova, 2003, 2005). These compounds contain effector fragments that together determine the stress-protective activity, namely, the quaternary ammonium and benzyl groups and the hydroxyethyl group - an analog of the benzoxyethyl group (Budykina *et al*., 2005; Timeyko *et al*., 2005). Tested substances contain similar fragments, so they also show bright auxin activity. Based on the literature data (Budykina *et al*., 2005; Timeyko *et al*., 2005; Titov *et al*., 2011; Bashmakov *et al*., 2012) and the results of our research, it can be assumed that used compounds have the stress-protective activity for important vegetable culture – *Solanum melongena*. They can be accepted as growth stimulators.

4. CONCLUSIONS:

Compounds 2 and 5 were the most effective from the tested chemical substances. The compounds carry out the greatest stimulation of the growth processes and productivity of the common eggplant (*Solanum melongena* L.): 1,2,2,4-tetramethyl-6-(1-piperidinylcarbothioil)-1,2,3,4-tetrahydroquinoline hydrochloride and 4-[(1,2,2,4-tetramethyl-1,2-dihydro-6-quinolinyl)carbothioyl] -1-piperazinylcarbaldehyde hydrochloride in all tested concentrations. Compounds of the series 1-alkyl-2,2,4-trimethyl-6-aminocarbothioyl-1,2,3,4-tetrahydroquinoline at concentrations of 0.05 % and 0.1 % are effective. All tested compounds increase the plant height, length, width, the number of leaves, and the yield of common eggplant at a concentration of 0.1%. The synthesized chemical compounds cause stimulation of these characteristics compared with existing commercial preparations, for example, Epin-Extra. Compounds of the series 1-alkyl-2,2,4-trimethyl-6-aminocarbothioyl-1,2-dihydroquinoline and 1-alkyl-2,2,4-trimethyl-6-aminocarbothioyl-1,2,3,4-tetrahydroquinoline can be used as growth stimulants. They can increase the germination capacity of *Solanum melongena* seeds from 30 to 80 %, increase the vegetative mass from 10 to 40 %, and yield from 28 to 46 %. Thus, tetrahydroquinolines are most effective as stimulators of growth processes (and productivity) for common eggplant. Compounds containing a dihydro-6-quinolinyl substituent stimulate growth and also increase the yield of *Solanum melongena*.

5. ACKNOWLEDGMENTS:

The study received financial support from the Ministry of Science and Higher Education of the Russian Federation within the framework of State Contract with universities regarding scientific research in 2020–2022, project No. FZGU-2020-0044.

6. REFERENCES:

1. Abdel-Gawad, S. M., El-Gagy, M. S. A., Heiba, H. I., Aly, H. M., Ghorab, M. M. (2005). Synthesis and radiation stability of some new biologically active hydroquinoline and pyrimido[4,5-b]quinoline derivatives. *J. Chin. Chem. Soc*., *52*, 1227-1236.
2. Abadi, A. H., Brun, R. (2003). Synthesis and evaluation of novel 7-trifluoromethyl-4-(4-substituted anilino) quinolines as antiparasitic and antineoplastic agents *Arzneimforsch. Drug. Res*., *53*, 655–663.
3. Azizian, J., Delbari A. S., One-Pot, K. Y. (2014). Three-Component Synthesis of Pyrimido[4,5-b]quinoline-tetraone Derivatives in Water. *Synthetic Commun*, *44 (22)*, 3277-3286. DOI: 10.1080/00397911.2011.626139

4. Azzi, J. (1959). Agricultural Ecology. Moscow: IL.

5. Baranova, T. V. (2013). Accelerated production of plants resistant to urban conditions. *Ecology and Industry of Russia*, *4*, 65–67.

6. Bashmakov, D. I., Pynenkova, N. A., Sazanova, K. A., Lukatkin, A. S. (2012). Effect of the synthetic growth regulator Cytodef and heavy metals on oxidative status in cucumber plants. *Russian Journal of Plant Physiology*, 59(1), 59-64.

7. Budykina, N. P., Drozdov, S. N., Kurets, V. K., Timeyko, L. V., Gafurov, R. G. (2005). The effect of etiol and benzihole on tomato plants due to changes in temperature conditions. *Agricultural chemistry*, *4*, 32-36.

8. Davidchuk, N. V. Borodina, N. N., Demidova, V. P. (2007). The use of wastewater for the correction of seed germination and morphogenesis of plant seedlings of the species *Cerasus vulgaris*. *Problems of regional ecology*, *3*, 99-103.

9. Davidchuk, N. V., Eremeeva, N. V. (2011). Comparison of the response of Brassica napus L. plants to the use of wastewater. *Bulletin of Tambov University. Series: Natural and Technical Sciences*, *16(6)*, 1583–1585.

10. Denmark, S., Venkatraman, S. (2006). On the mechanism of the Skraup-Doebner-Von Miller quinoline synthesis. *J. Org. Chem*., *71*, 1668–1676.

11. Doroshenko, T. N. (2000). Physiological and environmental aspects of southern fruit growing. Krasnodar: KubSAU.

12. Doroshenko, T. N., Zakharchuk, N. V., Ryazanova, L. G. (2010). Adaptive potential of fruit plants in the south of Russia: Monograph. Krasnodar: Publishing House LLC "Enlightenment-South".

13. Dospekhov, B. A. (1985). The methodology of field experience (with the basics of statistical processing of research results). Textbook: benefits for high school. Moscow: Agropromizdat**.**

14. Dyakov, A. B. Trunova, M. V., Vasiliev, T. A. (2009). Evaluation of the potentials of productivity and drought tolerance of soybean varieties. *Oilseeds. Scientific and Technical Bulletin of the All-Russian Research Institute of Oilseeds*, *2 (141)*, 78-86.

15. Elkholy, Y. M., Morsy, M. A. (2006). Facile Synthesis of 5, 6, 7, 8-Tetrahydropyrimido [4, 5-b]- quinoline Derivatives. *Molecules*, *11*, 890-903.

16. Gafurov, R. G., Makhmutova, A. A. (2003). A new group of synthetic auxin biomimetics: N- and O-benzyl-containing compounds. *Reports of the Russian Academy of Sciences*, *391*, 562-565.

17. Gafurov, R. G., Makhmutova, A. A. (2005). Growth-regulating activity of N- and O-benzyl-containing compounds - a new group of synthetic analogues of natural auxins. *Applied Biochemistry and Microbiology*, *41(2)*, 245-249.

18. Ghoneim, A. A., Assy, M. G. (2015). Synthesis of Some New Hydroquinoline and Pyrimido[4,5-b] Quinoline Derivatives. *Current Research in Chemistry*, *7(1),* 14-20. DOI: 10.3923/crc.2015.14.20)

19. Guber, K. V., Shentseva, E. V. (2011). Growing early eggplants using tunnel shelters. Melioration and water management, 1, 36-38.

20. Kadyrov, M. A., Grib, S. I., Baturo, F. N. (1984). Some aspects of selection of varieties with wide agroecological adaptation. *Selection and seed production*, *7*, 8-11.

21. Kadyrov, S. V., Shchuchka, R. V. (2005). The effect of seed treatment with growth stimulants on soybean yield. *Aspects of modern technologies: Sat. scientific tr. VSAU*, Voronezh, 38-40.

22. Kashaev, A. G., Zimichev, A. V., Rybakov, V. B., Klimochkin, Y. N., Zemtsova, M. N. (2010 a). 2,6–Dimethyl–4–(1,3,4-oxadiazol–2–yl)quinoline. *Acta Crystallogr*, *66*, 3333.

23. Kashaev, A.G., Zimichev, A.V., Rybakov, V.B., Klimochkin, Y.N., Zemtsova, M.N. (2010 b). 4-Allyl-3-(2-methyl-4-quinolyl)-4,5-dihydro-1H-1,2,4-triazole-5-thione. *Acta Crystallogr*, *66*, 3090.

24. Kashaev, A. G., Zimichev, A. V., Zemtsova, M. N., Klimochkin, Yu. N. (2011). Synthesis and anti-tuberculosis activity of quinoline isosteres of isoniazid. *Chem-farm. Magazine*, 45(4), 21-23.

25. Khodaei-Joghan, A., Gholamhoseini, M.,

Agha-Alikhani, M., Habibzadeh, F., Sorooshzadeh, A., Ghalavand, A. (2018). Response of sunflower to organic and chemical fertilizers in different drought stress conditions. *Acta agriculturae Slovenica*, *111(2)*, 271–284. doi:10.14720/aas.2018.111.2.03.

26. Kilchevsky, A. V., Khotyleva, L. V. (1977). Ecological plant breeding. Minsk: Tekhnologiya.

27. Korovkin, O. A. (2007). Anatomy and morphology of higher plants: a dictionary of terms. Moscow: Drofa**.**

28. Kulaichev, A. P. (2006). Methods and tools for integrated data analysis. Moscow: FORUM: INFA-M.

29. Lopatina, E. A. (2011). Change in the properties of sod-podzolic soil, productivity, and environmental quality of plant products in the aftermath of sewage sludge (WWS). Ph.D. in Biological thesis. Moscow.

30. Mamedov, M. I. (2002). Scientific substantiation and development of methods for breeding varieties and heterosis hybrids F1 of nightshade crops for adaptability: Tomato, pepper, eggplant: Ph.D. in Agriculture thesis. Moscow**.**

31. Mosalam, M. A., El Hamouly, S. H., Mahmoud, A. A., Khalil, A. (2011 a). Binary copolymerizations of 8-methacryloxy-quinoline with methyl methacrylate, methyl acrylate, styrene, and acrylonitrile. *Journal of Polymer Research*, *18(6)*, 2141–2150. doi:10.1007/s10965-011-9624-4

32. Mosalam, M. A., El Hamouly, S. H., Mahmoud, A. A., Khalil, A. (2011 b). Thermal Behavior of 8-methacryloxy-quinoline-Acrylonitrile Copolymers. *International Journal of Chemistry*, *3(2)*, 14-22. DOI: 10.5539 / ijc.v3n2p14

33. Nesterkina, I. S., Musalov, M. V., Gurina, V. V., Ozolina, N. V., Spiridonova, E. V., Tretyakova, A. V., Potapov V. A., Amosova, S. V., Yakimov, V. A. (2019). The effect of a new non-toxic, water-soluble selenorganic substance on antioxidant protection and development of seedlings of oilseed radish (*Raphanus sativus* L. var. *oleiferus* Metzg.). *Acta agriculturae Slovenica*,*114(1)*, 61–67.

34. Ostroshenko, V. V., Ostroshenko, L. Yu. (2011). Influence of the seed pretreatment with growth stimulators on their sowing qualities. *Bulletin of Krasnoyarsk State Agrarian University*, *5*, 12–15.

35. Pentelkina, N. V. Pentelkina, Yu. S. (2002). Stimulating effect of zircon on the growth of coniferous seedlings anditroducents. *Forestry Bulletin*, 2 (22), 24-29.

36. Rosielle, A. A., Hamblin, J. (1981). Theoretical aspects of selection for yield in stress and non-stress environments. *Crop Science*, *21(6)*, 943-946.

37. Saudi, M. N. S., Rostom, S. A., Fahmy, H. T. Y., El-Ashmawy I. (2003). Synthesis of 2-(4Biphenylyl)quinoline-4-carboxylate and Carboxamide Analogues. *Article in Chem Inform*, *34(39)*.doi:10.1002 / chin.200339123

38. Shibaeva, T. G., Sherudilo, E. G., Ikonen, E. N., Titov, A. F. (2018). Responses of young cucumber plants to a diurnal temperature drop at different times of day and night. *Acta agriculturae Slovenica*, *111-3*, 567-573.

39. Shikhaliev, H. S., Selemenev, V. F., Medvedeva, S. M., Ponomareva, L. F., Kopteva, N. I. (2014). Mass-spectrometric analysis of 1-acyl-2,2,5-trimethyl-4,4-dichlorocyclopropane [c] quinolines. *Sorption and chromatographic processes*, *14 (2)*, 332–337.

40. Shujiang, T. U., Fang, F., Tuanjie, L., Songlei, Z., Xiaojing, Z. (2005). An efficient one-pot synthesis of novel pyrimidoquinoline derivative under microwave irradiation without catalyst. *J. Heterocycl. Chem*., *42*, 707-710.

41. Sudhakar P., Latha P., Reddy P. V. (2016). Seed physiological and biochemical traits In: *Phenotyping Crop Plants for Physiological and Biochemical Traits*, 17-24.

42. Timeyko, L. V., Drozdov, S. N., Budykina, N. P., Gafurov, R. G. (2005). The effect of etiol on the thermal resistance and productivity of cucumber in spring film greenhouses in Karelia. *Agricultural chemistry*, *7*, 36-42.

43. Titov, V. N., Smyslov, D. G., Dmitrieva, G. A., Bolotova, O. I. (2011). Plant growth regulators as a biological factor in

reducing the level of heavy metals in a plant. *Vestnik OrelGAU*, *31(4),* 4–6.

44. Tsareva, L. E. (2013). Technique of improving yielding features of seeds in reproduction of sugar beet hybrids. *Bulletin of Altai State Agrarian University*, 1 (99), 17–19.
45. Valitova, A.R. (2006). Agroecological assessment of phytomelioration of sandy loamy sod-podzolic soil contaminated with heavy metals as a result of fertilizer by sewage sludge. PhD in Biolgical thesis. Moscow**.**
46. Vasin, A. V., Darmin, A. V., Brezhnev, V. V. (2009). Using growth stimulators for corn and barley growing. *Fodder Production*, *2*, 17–18.
47. Vasin, V. G., Darmin, A. V., Vasin, A. V. (2008). Effective use of growth stimulators for corn growing. *Proceedings of Samara State Agrarian University*, *4*, 22–24.
48. Zhidkih, O. Yu. Sorokopudov, V. N., Sorokopudova, O. A., Brindza, I. (2012). Some features of the ontogenesis of Mahonia aquifolium (Pursh) Nutt. *Scientific reports of Belgorod State University. Ser. Natural Sciences*, *21–1(140)*, 62-67.
49. Zhuchenko, A. A. Strategy for adaptive intensification of agriculture (concept). Pushchino: ONTI PNC RAS, 1994.
50. Zhuchenko, A. A. (1995). Ecological genetics of cultivated plants: theory and practice. *Agricultural biology, ser. biol. rast*, *3*, 4-31.
51. Zhuchenko, A. A. Trukhanov, A. I. (2009). Environment-Improving Phytotechnologies in Northern Megacities. Moscow: KRASAND.

7. OPEN ACCESS

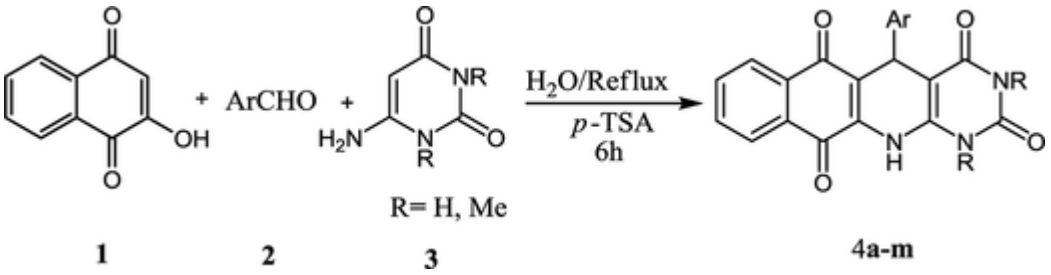

Figure 1. *The general scheme for the synthesis of pyrimido[4,5-b]quinoline-tetraones.*

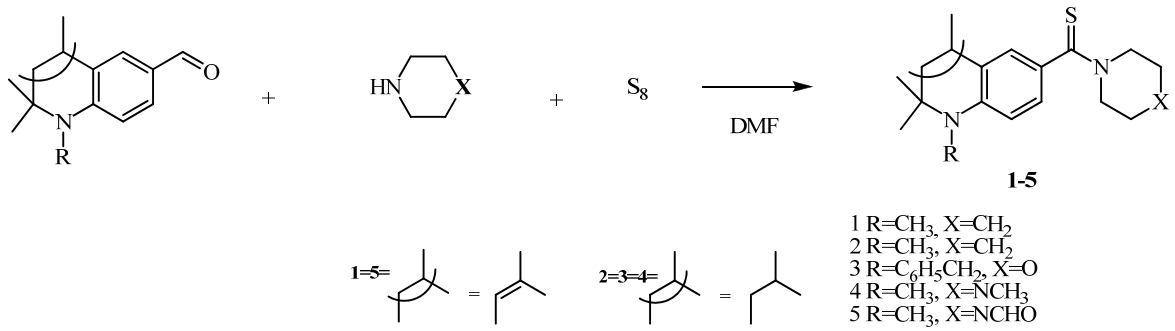

Figure 2. *The general scheme for the synthesis of 2,2,4-tetramethylhydroquinolin-6-ylcarbothioamides 1-5.*

Table 1. *The seed germination (in %) of Solanum melongena (cv. Black Beauty) treated with synthesized organic compounds*

Concentration	Control group	Epin group	compound 1	compound 2	compound 3	compound 4	compound 5
0,01%	41.1	42.2	33.3	61.1**[2]	77.8***[3]	62.2**[2]	47.8
0,05%			32.2	55.6*[1]	75.6***[3]	48.9	43.3
0,1%			31.1	54.4*[1]	73.3***[3]	46.7	42.2

Note for Table 1-6:

** – differences with the control group are reliable (p<0.05)*

*** – differences with the control group are reliable (p<0.01)*

**** – differences with the control group are reliable (p<0.001)*

[1] - differences with the Epin group are reliable (p<0.05);

[2] - differences with the Epin group are reliable (p<0.01);

[3] - differences with the Epin group are reliable (p<0.01);

1,2,2,4-tetramethyl-6-(1-piperidinylcarbothioyl)-1,2-dihydroquinoline hydrochloride (compound 1);
1,2,2,4-tetramethyl-6-(1-piperidinylcarbothioyl) -1,2,3,4-tetrahydroquinoline hydrochloride (compound 2);
1-benzyl-2,2,4-trimethyl-6-(4-morpholinylcarbothioyl)-1,2,3,4-tetrahydroquinoline (compound 3);
1,2,2,4-tetramethyl-6-[(4-methyl-1-piperazinyl)carbothioyl]-1,2,3,4-tetrahydroquinoline hydrochloride (compound 4);
4-[(1,2,2,4-tetramethyl-1,2-dihydro-6-quinolinyl)carbothioyl]-1-piperazinylcarbaldehyde hydrochloride (compound 5).

Table 2. *The height (in cm) of Solanum melongena plant grown from seeds treated with synthesized chemical compounds*

Concentration	Control group	Epin group	compound 1	compound 2	compound 3	compound 4	compound 5
0.01%	6.5±0,1	6.6±0,1	6.4±0,1[1]	8.1±0,2***[3]	6.6±0,1	6.7±0.2	7.8±0.2***[3]
80.05%			6.6±0,1	8.8±0,2***[3]	7.6±0,1***[3]	7.6±0.1***[3]	8.8±0.2***[3]
0.1%			7.4±0,1***[2]	9.3±0,2***[3]	8.6±0.1***[3]	7.7±0.2***[3]	9.0±0.1***[3]

Table 3. *The leaf length (in cm) of Solanum melongena after treating the seeds with synthesized chemical compounds*

Concentration	Control group	Epin group	compound 1	compound 2	compound 3	compound 4	compound 5
0.01%	6.3±0,1	6.4±0,1	6.0±0,2	7.6±0,2***[3]	6.4±0,1	6.4±0.1	7.6±0.2***[3]
0.05%			6.5±0,1	8.7±0,2***[3]	7.6±0,2***[3]	7.5±0.1***[3]	8.6±0.2***[3]
0.1%			7.3±0,1***[2]	9.0±0,2***[3]	8.3±0.2***[3]	7.6±0.1***[3]	8.8±0.1***[3]

Table 4. *The leaf width (in cm) of Solanum melongena after treating the seeds with synthesized chemical compounds*

Concentration	Control group	Epin group	compound 1	compound 2	compound 3	compound 4	compound 5
0.01%	4.5±0,1	4.6±0,1	4.8±0,2[1]	5.7±0,1***[3]	5.4±0,2	4.5±0.1	5.7±0.1***[3]
0.05%			5.1±0,1	6.4±0,1***[3]	6.0±0,2***[3]	5.0±0.1***[3]	6.3±0.2***[3]
0.1%			5.6±0,1***[2]	6.7±0,1***[3]	6.3±0.1***[3]	5.2±0.1***[3]	6.8±0.2***[3]

Table 5. *The number of leaves of Solanum melongena after treating the seeds with synthesized chemical compounds*

Concentration	Control group	Epin group	compound 1	compound 2	compound 3	compound 4	compound 5
0.01%	5.2±0,1	5.6±0,2**	5.4±0,2*[1]	5.6±0,2**	5.4±0,1*[1]	5.4±0.2*[1]	5.3±0.1[1]
0.05%			5.6±0,2**	6.5±0,2***[3]	5.6±0,2**	5.6±0.2**	5.8±0.1**[1]
0.1%			5.7±0,2**	6.7±0,2***[3]	5.7±0.2**	5.8±0.2**[1]	5.8±0.1**[1]

Table 6. *The yield (in kg/m^2) of Solanum melongena plant grown from seeds treated with synthesized chemical compounds*

Concentration	Control group	Epin group	compound 1	compound 2	compound 3	compound 4	compound 5
0.01%	3.2±0,1	3.3±0,1	3.5±0,1	5.1±0,1**[2]	4.2±0,2*[1]	4.5±0.1**[2]	5.3±0.1**[2]
0.05%			4.1±0,1*[1]	5.4±0,1***[3]	4.4±0,2**[2]	4.8±0.1**[2]	5.5±0.2***[3]
0.1%			4.6±0,1**[2]	5.6±0,1***[3]	4.6±0.1**[2]	4.8±0.1**[2]	5.7±0.2***[3]

PERIÓDICO TCHÊ QUÍMICA
ARTIGO ORIGINAL

PROPRIEDADES TÉRMICAS E ELETROQUÍMICAS DE ELETRÓLITOS SÓLIDOS DE BIOPOLÍMEROS DE AMIDO DE DIFERENTES ORIGENS BOTÂNICAS

THERMAL AND ELECTROCHEMICAL PROPERTIES OF SOLID BIOPOLYMER ELECTROLYTES FROM STARCH OF DIFFERENT BOTANICAL ORIGIN

PROPIEDADES TÉRMICAS Y ELECTROQUÍMICAS DE ELECTROLITOS SÓLIDOS DE BIOPOLÍMEROS DE ALMIDÓN DE DIFERENTE ORIGEN BOTÁNICO

ARRIETA, Alvaro[1*]; MENDOZA, Jorge[2]; BARRERA, Isora[3];

[1] University of Sucre, Faculty of Education and Science, Department of Biology and Chemistry. Sincelejo, Colombia.

[2] University of Córdoba, Faculty of Engineering, Department of Mechanical Engineering. Monteria, Colombia.

[3] Mercedes Abrego Educational Institution, Diag. 6-119, Tv. 1 #6-1, Montería, Colombia.

** Corresponding author*
e-mail: alvaro.arrieta@unisucre.edu.co

Received 28 May 2021; received in revised form 29 June 2021; accepted 11 July 2021

RESUMO

Introdução: Eletrólitos de biopolímero sólido são um tipo de material com alto potencial tecnológico utilizado no desenvolvimento de células solares, baterias, células a combustível, entre outros, devido à sua natureza biodegradável e baixo impacto ambiental. **Objetivo:** Este estudo teve como objetivo avaliar o efeito da origem botânica do amido utilizado na preparação de filmes eletrolíticos sólidos biopoliméricos sobre suas propriedades eletroquímicas e térmicas e estabelecer as variações nas temperaturas de decomposição térmica e potenciais redox em função da origem botânica do amido utilizado. **Métodos:** Filmes de eletrólito de biopolímero sólido foram feitos por processos de síntese termoquímica utilizando amido de milho, amido de mandioca, amido de batata, glicerol, polietilenoglicol e glutaraldeído como plastificantes e sal perclorato de lítio. As soluções de síntese foram levadas à estufa a 70 °C por 48 horas. Os filmes foram caracterizados eletroquimicamente por voltametria cíclica em célula eletroquímica seca e termicamente por calorimetria exploratória diferencial e análise termogravimétrica. **Resultados e Discussão:** Os resultados mostraram que o comportamento eletroquímico dos filmes foi semelhante em termos de processos redox registrados. Entretanto, os valores potenciais de oxidação e redução foram diferentes, assim como a estabilidade e intensidade dos processos. Por outro lado, a análise térmica permitiu estabelecer dois processos de decomposição em cada um dos filmes estudados; o primeiro processo foi devido aos fenômenos de desidratação e despolimerização nos filmes. As temperaturas registradas foram 59,0 °C, 58,9 °C e 89,9 °C para os filmes de amido de batata, amido de mandioca e amido de milho, respectivamente. O segundo processo evidenciou a decomposição térmica que ocorreu em diferentes temperaturas, 267,7 °C nos filmes de amido de batata, 280,6 °C nos filmes de amido de milho e 287,1 °C nos filmes de amido de mandioca. **Conclusões:** Pode-se concluir que a origem botânica do amido utilizado na síntese de filmes eletrolíticos de biopolímero sólido afeta seu comportamento e estabilidade eletroquímica e térmica.

Palavras-chave: *Estabilidade, Voltametria cíclica, Milho, Mandioca, Batata*.

ABSTRACT

Background: Solid biopolymer electrolytes are a type of material with high technological potential used in the development of solar cells, batteries, fuel cells, among others, due to their biodegradable nature and low environmental impact. **Aim:** This study aimed to evaluate the effect of the botanical origin of the starch used to prepare solid biopolymeric electrolyte films on its electrochemical and thermal properties and to establish the variations in thermal decomposition temperatures and redox potentials depending on the botanical origin of the starch used. **Methods:** Films of solid biopolymer electrolyte were made by thermochemical synthesis processes using corn starch, cassava starch, potato starch, glycerol, polyethylene glycol, and glutaraldehyde as plasticizers and lithium perchlorate salt. The synthesis solutions were taken to an oven at 70 °C for 48 hours. The films were characterized electrochemically by cyclic voltammetry using a dry electrochemical cell and thermally by differential scanning calorimetry and thermogravimetric analysis. **Results and Discussion**: The results showed that the

DOI: 10.52571/PTQ.v18.n38.2021.10_ARRIETA_pgs_137_148.pdf

electrochemical behavior of the films was similar in terms of registered redox processes. However, the potential values of the oxidation and reduction were different, as are the stability and intensity of the processes. On the other hand, the thermal analysis allowed establishing two decomposition processes in each of the films studied; the first process was due to dehydration and depolymerization phenomena in the films. The temperatures recorded were 59.0 °C, 58.9 °C, and 89.9 °C for potato starch, cassava starch, and corn starch films. The second process evidenced the thermal decomposition at different temperatures, 267.7 °C in potato starch films, 280.6 °C in corn starch films, and 287.1 °C in cassava starch films. **Conclusions:** It could be concluded that the botanical origin of the starch used in the synthesis of solid biopolymer electrolyte films affects its behavior and electrochemical and thermal stability.

Keywords: *Stability, Cyclic voltammetry, Corn, Cassava, Potato*.

RESUMEN

Antecedentes: Los electrolitos de biopolímer sólido son un tipo de material con alto potencial tecnológico utilizado en el desarrollo de celdas solares, baterías, celdas de combustible, entre otros, debido a su naturaleza biodegradable y bajo impacto ambiental. **Objetivo:** Este estudio tuvo como objetivo evaluar el efecto del origen botánico del almidón utilizado para preparar películas sólidas de electrolitos biopoliméricos sobre sus propiedades electroquímicas y térmicas y establecer las variaciones en las temperaturas de descomposición térmica y los potenciales redox en función del origen botánico del almidón utilizado. **Métodos:** Se elaboraron películas de electrolito de biopolímero sólido mediante procesos de síntesis termoquímica utilizando almidón de maíz, almidón de yuca, almidón de papa, glicerol, polietilenglicol y glutaraldehído como plastificantes y sal de perclorato de litio. Las soluciones de síntesis se llevaron a un horno a 70 °C durante 48 horas. Las películas se caracterizaron electroquímicamente mediante voltamperometría cíclica utilizando una celda electroquímica seca y térmicamente mediante calorimetría de barrido diferencial y análisis termogravimétrico. **Resultados y Discusión:** Los resultados mostraron que el comportamiento electroquímico de las películas es similar en términos de procesos redox registrados. Sin embargo, los valores potenciales de oxidación y reducción son diferentes, al igual que la estabilidad e intensidad de los procesos. Por otro lado, el análisis térmico permitió establecer dos procesos de descomposición en cada una de las películas estudiadas; el primer proceso se debió a fenómenos de deshidratación y despolimerización en las películas. Las temperaturas registradas fueron 59.0 °C, 58.9 °C y 89.9 °C para las películas de almidón de papa, almidón de yuca y almidón de maíz, respectivamente. El segundo proceso evidenció la descomposición térmica que tuvo lugar a diferentes temperaturas, 267.7 °C en películas de almidón de papa, 280.6 °C en películas de almidón de maíz y 287.1 °C en películas de almidón de yuca. **Conclusiones:** Se pudo concluir que el origen botánico del almidón utilizado en la síntesis de películas de electrolítos de biopolímero sólido afecta su comportamiento y estabilidad electroquímica y térmica.

Palabras clave: *Estabilidad, Voltamperometría cíclica, Maíz, Yuca, Papa*.

1. INTRODUCTION:

In recent decades, conducting polymers have attracted the attention of many research groups due to their great technological potential (Le *et al.*, 2017; Isikli and Ryan, 2020; Shirakawa, 2001; Ngai *et al*., 2016). These polymeric materials, because they are organic conductors, combine properties of traditional polymers such as resistance to corrosion, organic and inorganic solvents, flexibility, and metals such as high electrical conductivity and magnetic properties, which makes them attractive for applications in organic electronics. This is why they have been tested for use in chemical and physical sensors, electromagnetic shielding, intelligent windows, artificial nerves, actuators, corrosion protection, among others (Shi *et al*., 2021; Salgado *et al*., 2021; Nuñez *et al*., 2016)

The conducting polymers can be divided into two large groups; intrinsic conducting polymers (ICPs), which are capable of conducting electric current through their structure of conjugated bonds (alternating double and single bonds), which can transmit a charge generated in the polymer chain through oxidation or reduction processes (Le *et al.*, 2017; Shirakawa, 2001; Bredas and etreet, 1985). On the other hand, solid polymeric electrolytes (SPEs) are capable of conducting the electric current and making artificial muscles, flexible batteries, fuel cells, among others. Due to the displacement of ions (i.e., electrolytes) through the polymer matrix, in this case, the polymer chains have fixed electrical charges that allow them to interact with species ionic mobiles to maintain their electroneutrality (Isikli and Ryan, 2020; Ngai *et al*., 2016; Owens, 2000). These polymers are mostly of petrochemical origin and therefore generate contamination from the production of the raw material they produce to their final disposal. Therefore, work has been done to generate conducting polymers from natural sources that can

be used as solid electrolytes to store charge for batteries, fuel cells, transistors, organic actuators and diodes (Nuñez *et al*., 2016; Acosta *et al*., 2015).

Polymeric materials obtained from renewable sources have attracted the attention and interest of the scientific community and the industrial sectors in recent years. "Biopolymers or bioplastics" unlike other traditional materials synthesized from petrochemical sources, have an interesting set of advantages among which are, generate a lower environmental impact, need low energy consumption for their production, their resource status renewable, the potential to add value to products and waste from industries and its particular biodegradability. Its applications are numerous and varied; they can be found as constituents of packaging, medical materials, reinforced plastics, edible films, among others (Reddy *et al*., 2015; Zhang *et al*., 2021; Vijavendra and Shamala, 2013; Jorgensen *et al*., 2020; Salikova *et al*., 2020).

The explosion of technological developments based on electronic systems has generated great concern due to that electronic devices are a source of contamination due to its relatively short shelf life. Electronic devices contain polymers, heavy metals, and other polluting materials. For this reason, work has been done to develop biomaterials capable of conducting electric current. In this way, the elaboration of biopolymers capable of conducting electric current has been reported. These biopolymers have been called Solid Biopolymer Electrolytes (SBPEs) and have been used in the development of light-emitting diodes (LEDs), artificial muscles, sensors, batteries, fuel cells, among others (Ma and Sahai, 2013; Singh *et al*., 2016; Rosnah *et al*., 2020; Nuñez *et al*., 2016; Monisha *et al*., 2016).

Recent research has established that polysaccharides such as starch found in plants can be used to produce biopolymers. This polysaccharide can be modified through a plasticization and doping process to obtain films with high ionic conductivity (Arrieta *et al.,* 2011; Singh *et al.,* 2014). Electrolytes based on plasticized cassava starch and lithium salt contents have been proposed as solid biopolymer electrolytes and tested in applications such as artificial muscles and electrochemical accumulators (Nuñez *et al*., 2016; Arrieta *et al.,* 2011; Acosta *et al*., 2015). The starch synthesized in plants is made up of two types of polymers: amylopectin and amylose. The ratio of amylose to amylopectin varies, depending on the source of the starch (botanical origin). This generates differences in the morphology, size, crystallinity and molecular macrostructure of the polymer chains in the grains, affecting the properties of the solid biopolymer electrolytes generated from starches.

The aim of this study was to determine the effect generated by the botanical origin of the starch used to produce films of solid biopolymer electrolyte on its thermal and electrochemical properties studied through cyclic voltammetry, thermogravimetry and differential scanning calorimetry.

2. MATERIALS AND METHODS:

In this work, the synthesis of solid biopolymer electrolytes of starch from different botanical sources, specifically corn, cassava, and potato are presented and an evaluation of the effect of the origin of starch on the electrochemical and thermal properties in the biopolymeric materials was made.

2.1. Materials and Reagents

The following reagents were used in this work: glycerol ($HOCH_2CH(OH)CH_2OH$), polyethylene glycol ($H(OCH_2CH_2)nOH$), glutaraldehyde ($OHC(CH_2)_3CHO$) and lithium perchlorate ($LiClO_4$). These reagents were purchased from Sigma-Aldrich. Potato starch and corn starch ($(C_6H_{10}O_5)n$) were purchased from Merck. Cassava starch was extracted in the laboratory by the traditional method that includes, washed of the material, peeled with a manual peeler, disintegrated by blending with an industrial blender at 24,000 r.p.m., sieved with a 200 µm sieve and dried in an oven at 50 °C for 24 H. The purity of the extracted cassava starch was verified by FTIR-ATR spectroscopy analysis. The spectra were recorded from 650 - 4000 cm^{-1} at a resolution of 4 cm^{-1} by 100 scans. The IR spectra of the starches were recorded, normalized and corrected with the air background. Additionally, the official method of AOAC (Association of Official Analytical Chemists) was used. All solutions were prepared using milli Q grade ultrapure water.

2.2. Synthesis of Solid Biopolymer Electrolyte Films of Starch

The synthesis of the films was carried out by means of a thermochemical process that consisted of using 3g of starch which was dispersed in 100 mL of water with a pH of 9.0 for 15 min, with constant agitation (1500 r.p.m.). The

starch dispersion was heated to 75°C and once the starch was completely dissolved, it was allowed to cool to room temperature to add the plasticizers glycerol (1g), polyethylene glycol (1g) and glutaraldehyde (2g), and 1.5 g of lithium perchlorate were also added. The mixture was heated to 75°C with constant stirring of 1500 r.p.m. The mixtures were deposited in Teflon petri dishes and taken to an oven at 70°C for 48 hours. This procedure was applied without variations for each one of the starches studied. Each of the films were made in triplicate. Once processed, the samples could be detached from the petri dishes without breaks or cracks and allowed to cool to room temperature.

2.3. Electrochemical characterization of Solid Biopolymeric Electrolyte Films

Characterizations were carried out on each of the samples. In the electrochemical characterization, sample sections of 1 x 1 cm were taken. The samples were placed in a dry electrochemical cell, which consisted of two stainless steel sheets supported on acrylic sheets. Figure 1 shows an image of the dry cell used. The samples were sandwiched in the cell and the characterization was performed by cyclic voltammetry using a sweep speed of 100 mV s^{-1} and a sweep range of -2.0 V to 2.0 V. The voltage measurements were carried out with the open circuit potential (OCP) as reference which had a value of 0.10 V. The voltammograms were analyzed using PowerSuite Software V 2.60.

2.4. Thermal characterization of Solid Biopolymeric Electrolyte Films

Thermal characterization was carried out using differential thermogravimetric analysis (DTG), thermogravimetric analysis (TGA) and differential scanning calorimetry (DSC), which were performed with a simultaneous thermal analyzer (STA-625/DSC/TGA) of Rheometric Scientific. All measurements were carried out in triplicate and the averages were used to calculate the thermal parameters. The thermograms were analyzed using the Advantage / Universal Analysis (UA) Software V 5.5.24.

The TG analyzes and DTG were carried out in an argon atmosphere with a constant gas flow of 100 L min^{-1}. The experiments were carried out using 5 mg samples, which were deposited in aluminum crucibles and empty crucibles were used as a reference. The samples were heated from 30 to 800 °C at heating rate of 10 °C min^{-1}.

For DSC analysis, 5 mg of starch samples were placed in hermetically sealed aluminum capsules and hydrated with 3 parts of distilled water (75%). The samples were kept at 30 °C for 30 min and subsequently heated to 800 °C at a heating rate of 10 °C min^{-1}. An Argon purge was performed at a flow rate of 100 L min^{-1}. The calibration of the equipment was performed prior to the measurements using an empty aluminum capsule. The enthalpy expressed as J g^{-1} of starch, were determined by integrating the area under the peaks of the thermal processes. The parameters onset temperature (*To*), peak temperature (*Tp*), conclusion temperature (*Tc*) and enthalpy of the process (*H*), of the observed thermal processes were determined from the DSC curves.

3. RESULTS AND DISCUSSION:

Figure 2 presents images of solid biopolymeric electrolyte films from corn starch (Figure 2a), potato starch (Figure 2b) and cassava starch (Figure 2c). In all cases, the films showed a transparent white color and had a stable consistency to handling. It can be seen that it does not present cracks or breaks since it could be removed from the mold without difficulty.

It has been reported that the use of plasticizing agents allows obtaining starch films with good mechanical properties to be obtained because these compounds form hydrogen bonds between the polymeric starch chains, giving the films flexibility, wetting and mechanical resistance (Arrieta *et al*., 2011).

The voltammetric response obtained from the electrochemical characterization applied to the films, was recorded during 50 consecutive cycles so that, in addition to evaluating their redox activity, their stability could also be evaluated. Figure 3 shows the voltammograms recorded in the solid biopolymeric electrolyte films elaborated with the starch from corn (Figure 3a), starch from potato (Figure 3b) and starch from cassava (Figure 3c). It can be observed that although there is a similar trend regarding the number of redox processes, the current intensities and the position of the oxidation/reduction peaks are different from each other.

In general terms, the voltammetric signals are formed by three well-defined redox processes, which are indicated in Figure 3 such as PI, PII and PIII. The processes registered with the solid biopolymer electrolytes of starch from corn, present more intense and better-defined peaks, in

that same order the cassava starch films have well defined but less intense peaks than those observed in the corn starch films.

On the other hand, the signal obtained with potato starch films shows less defined and less intense peaks. Although if the stability of the signals is compared, the recordings carried out with the potato starch films after 50 consecutive cycles showed less loss of intensity, so they are more stable. Otherwise, the signals recorded with the cassava starch film showed a moderate and less marked stability than that registered with the films made from corn starch.

Regarding the potentials registered in the oxidation/reduction processes in the three types of starch films, it was observed that the position (i.e. potentials) varies between them. The oxidation potentials (EO) of potato starch films are more positive than those observed in the voltammetric curves of cassava starch films. These, in turn, are more positive than the potentials observed in corn starch films. The reduction potentials (ER) also present different values for each one of the films studied. However, a trend as marked as in the case of oxidation potentials is not observed. Table 1 shows the oxidation and reduction potentials of the films and the medium peak potentials (Ep/2) for each case.

The Ep/2 presented in Table 1 show that the redox processes of starch potato films are more positive than the Ep/2 values of cassava starch and corn starch films, which have values close to each other. These differences in electrochemical behavior may be caused by the different amylose/amylopeptin ratio of starches and the amount of charges formed during the thermochemical synthesis process. Due to that during the process of solid biopolymeric electrolyte synthesis of starch, the glucose chains, in their hydroxyl groups (OH) experiment the alkilinization reaction and are converted to alkoxide groups (RO-), which generates charges on the polymeric chains of the starch and allows the ionic interactions in the matrix that confer the ability to conduct electric current through ion movement (Arrieta *et al*., 2019; Chin *et al*., 2014).

This characterization allowed determining the thermal stability of the conductive films synthesized from starch from different plant sources. The curves recorded in the thermogravimetric analysis are presented in figure 4 and correspond to the characterization curves by differential thermogravimetric analysis (Figure 4a) and thermogravimetric analysis (Figure 4b). In all of them, two thermal decomposition processes occurred, which in the case of the DTG is evidenced in the peaks of the graphs and in the TGA they are evidenced in the abrupt falls of the weights (%).

The first process occurs at 59.0 °C, 58.9 °C, and 89.9 °C for potato starch, cassava starch, and corn starch films, respectively. This first process may be due to dehydration of the films, so the dehydration of the potato and cassava starch films are similar. In contrast, the dehydration of the corn starch films occurs at much higher temperatures and with weight loss higher. This difference may be due to the different amylase/amylopeptin ratios of each of the starch molecules in these plant species, affecting the amount of plasticizer and water molecules that the polymers can contain. The solid biopolymer electrolyte films of potato starch and cassava starch showed a weight loss of about 16.1% during the first thermal process. In comparison, the films made of corn starch presented a weight loss of approximately 22.8%.

On the other hand, the second process evidenced in the graphs is observed at temperature values of 267.7 °C in potato starch films, 280.6 °C in corn starch films, and 287.1 °C in cassava starch films. The percentage of weight lost was lower in the corn starch films (about 78.7%), while the potato and cassava starch films showed loss percentages of 79.9% and 80.1%, respectively. This second thermal decomposition process, it corresponds to the depolymerization of the polymeric starch chains and the elimination of the polyhydroxyl groups. When comparing the temperatures of the second process, it is observed that the potato starch films have lower thermal stability than those of corn at almost 13 °C. The thermal stability of the cassava starch films is greater than those of corn and potato at approximately 7 °C and 20 °C, respectively. These temperatures are lower than those reported for pure starch films around 315 °C (Wang *et al*., 2009; Noivoil and Yoksan, 2020). This may be due to plasticizing agents that act as cross-linkers, separating the polymeric chains in the starch matrix. The difference between the depolymerization temperatures of the starch films from different plant sources may be due, not only to the differences between the amylose/amylopeptin ratios of each, but also to the number of charges that form in the polymers during the process of thermochemical synthesis and that in addition to affecting the thermal properties, they also affect the electrochemical properties as evidenced in the electrochemical characterization.

The thermograms obtained from the DSC analysis are shown in Figure 5. All the samples presented curves with two thermal processes, which correspond to those obtained in the TG analyzes. The first process associated with the dehydration of the films was observed in a broad endothermic peak between approximately 35 and 100 ºC. The water contained in the films interacts with the polymer chains and plasticizers, being evaporated at this temperature range, this process is typical in this type of biopolymer. Table 2 shows a summary of the transition temperatures (*To*, onset; *Tp*, peak; and *Tc*, conclusion) and enthalpy of the process (*H*) of the DSC thermosgrams obtained for the solid biopolymer electrolytes of corn, potato and cassava starch.

The behavior of the solid biopolymer electrolyte samples from cassava starch, corn starch and potato starch was very similar in this first thermal process. The *To* and *Tc* values were close to each other. However, the *Tp* and *H* present a small difference, with the lowest values (*Tp* = 59.7 °C and *H* = 1.6 J g^{-1}) being observed in the films made with cassava starch, followed by the films made with potato starch (*Tp* = 60.1 °C and *H* = 1.8 J g^{-1}) and finally those of corn starch (*Tp* = 75.2 °C and *H* = 2.4 J g^{-1}) These differences associated with the interaction of water with the polymer matrix and plasticizers may be due to the crystallinity levels of the starch molecules in each case.

The second endothermic peak could be seen between approximately 247 at 345 ºC. Although the *To* were close to each other (next to 248 °C), the *Tp*, *Tc* and *H* present some variation in their values. The solid biopolymer electrolyte films from corn starch presented Tp, Tc and H values of 287.6 °C, 345.9 °C and 10.8 J g-1 respectively, the films made with potato starch presented Tp = 275.6 °C, Tc = 331.1 °C and H = 9.3 J g-1 and the cassava starch films registered a Tp = 286.8 °C, Tc = 322.2 °C and H = 7.2 J g-1. This second process showed differences in the behavior of solid biopolymer electrolytes made with cassava, corn, and potato starches. These differences may be mainly due to the particularities of the polymeric matrix of the starches used, generated by their botanical origin.

4. CONCLUSIONS:

Stable and consistent solid biopolymer electrolyte films could be made from the use of starch from different plant sources. The electrochemical characterization by cyclic voltammetry showed that, although the response is similar in trend and number of processes, the botanical origin of the starch used affected the values registered for the oxidation and reduction potentials of the processes and also in the signal strengths and stability.

Besides, the characterization of the thermal stability allowed establishing that regardless of the botanical origin of the starch used to make the solid biopolymeric electrolyte films, there are two thermal processes, one consisting of dehydration and the other of depolymerization and decomposition of the starch polymer chains. The temperatures of the thermal processes and the enthalpies showed significant differences in the decomposition process of the polymeric chains of cassava, potato and corn starches. While the dehydration processes were more uniform in the films of the three types of starches studied

5. ACKNOWLEDGMENTS:

The authors Acknowledgment the Sucre University for financial support.

6. REFERENCES:

1. Acosta, M.F., Arrieta, A., Ávila, A., Martínez, A., Palacio, M., Nova, V. (2015). Development of Charge Electrochemical Accumulator of Conductive Polypyrrole/ Cassava Starch Biopolymers. *ASME-Energy*. 6A, 1-5.
2. Arrieta, A., Gañán, P.F., Márquez, S.E., Zuluaga, R. (2011). Electrically conductive bioplastics from cassava starch. *Journal of the Brazilian Chemical Society*, 22(6), 1170–1176.
3. Arrieta, A. Garcia, C., Combatt, E. (2019). Effect of elaboration ph on the electroactivity of cassava starch solid biopolymer electrolyte films. *Rasayan Journal of Chemistry*, 12(4), 1766 –1773.
4. Bredas J.L., Street, G.B. (1985). Polarons, bipolarons, and solitons in conducting polymers. *Accounts of Chemical Research*, 18(10), 309-315.
5. Chin, S.F., Azman, A., Pang, S.C. (2014). Size Controlled Synthesis of Starch Nanoparticles by a Microemulsion Method. *Journal of Nanomaterials*, 2014, 1-7.
6. Isikli, S., Ryan, K.M. (2020). Recent advances in solid-state polymer electrolytes and innovative ionic liquids based polymer electrolyte systems.

Current Opinion in Electrochemistry, 21, 188-191.

7. Jorgensen, M.R., Räägel, H., Rollins, T. S. (2020). Advances in Biocompatibility: A Prerequisite for Biomedical Application of Biopolymers. Bernd Rehm, M. Fata Moradali Editors. *Biopolymers for Biomedical and Biotechnological Applications*, 1–17.
8. Le, T.H., Kim, Y., Yoon, H. (2017). Electrical and Electrochemical Properties of Conducting Polymers. *Polymers*, 9(12), 1-32.
9. Ma, J., Sahai, Y. (2013). Chitosan biopolymer for fuel cell applications. *Carbohydrate Polymers*, 92(2), 955–975.
10. Monisha, S., Selvasekarapandian, S., Mathavan, T., Milton Franklin Benial, A., Manoharan, S., Karthikeyan, S. (2016). Preparation and characterization of biopolymer electrolyte based on cellulose acetate for potential applications in energy storage devices. *Journal of Materials Science: Materials in Electronics*, 27(9), 9314–9324.
11. Ngai, K.S., Ramesh, S., Ramesh, K., Juan, J. (2016). A review of polymer electrolytes: fundamental, approaches and applications. *Ionics*, 22(8), 1259–1279.
12. Noivoil, N., Yoksan, R. (2020). Compatibility improvement of poly(lactic acid)/thermoplastic starch blown films using acetylated starch. *Journal of Applied Polymer Science*. 49675, 1-16.
13. Nuñez, Y.E., Arrieta, A.A., Segura, J.A., Bertel, S.D. (2016). Synthesis of an air-working trilayer artificial muscle using a conductive cassava starch biofilm (manihot esculenta, cranz) and polypyrrole (PPy). *Journal of Physics: Conference Series*, 687, 1-7.
14. Owens, B.B. (2000). Solid state electrolytes: overview of materials and applications during the last third of the Twentieth Century. *Journal of Power Sources*, 90(1), 2–8.
15. Reddy, N., Reddy, R., Jiang, Q. (2015). Crosslinking biopolymers for biomedical applications. *Trends in Biotechnology*, 33(6), 362–369.
16. Rosnah Mustapa, S., Min Aung, M., Rayung, M. (2020). Physico-Chemical, Thermal, and Electrochemical Analysis of Solid Polymer Electrolyte from Vegetable Oil-Based Polyurethane. *Polymers (Basel)*, 13(1), 132-152.
17. Salado, M., Lanceros-Mendez, S., Lizundia, E. (2021). Free-standing intrinsically conducting polymer membranes based on cellulose and poly(vinylidene fluoride) for energy storage applications. *European polymer journal*, 144, 110240.
18. Salikova, N.S., Bektemissova, A.U., Nazarova, V.D., Begenova, B.E., Ostafeichuk, N.V. (2020). Preparation of mixed hydrogels based on biopolymers and the study of their rheological properties. *Periódico Tchê Química*, 17(35), 23-40.
19. Saviour, A.U., Moses, M.S. (2019). Protective polymeric films for industrial substrates: A critical review on past and recent applications with conducting polymers and polymer composites/nanocomposites. Progress in materials science, 104, 380-450.
20. Shi, H., Dai, Z., Sheng, X., Xia, D., Sha, P., Yang, L., Luo, X. (2021). Conducting polymer hydrogels as a sustainable platform for advanced energy, biomedical and environmental applications. *Science of the total environment*, 786, 147430.
21. Shirakawa, H. (2001). The Discovery of Polyacetylene Film: The Dawning of an Era of Conducting Polymers (Nobel Lecture). *Angewandte Chemie International Edition*, 40(14), 2574-2580.
22. Singh, R., Baghel, J., Shukla, S., Bhattacharya, B., Rhee, H.W., Singh, P.K. (2014). Detailed electrical measurements on sago starch biopolymer solid electrolyte. *Phase Transitions*, 87(12), 1237–1245.
23. Singh, R., Polu, A.R., Bhattacharya, B., Rhee, H.W., Varlikli, C., Singh, P. K. (2016). Perspectives for solid biopolymer electrolytes in dye sensitized solar cell and battery application. *Renewable and Sustainable Energy Reviews*, 65, 1098–1117.
24. Vijayendra, S.V.N., Shamala, T.R. (2013). Film forming microbial biopolymers for commercial applications—A review. *Critical Reviews in Biotechnology*, 34(4), 338–357.

25. Wang, N., Zhang, X., Liu, H., Wang, J., (2009). N, N dimethylacetamide/lithium chloride plasticized starch as solid biopolymer electrolytes. *Carbohydrate Polymers*, 77, 607–611.

26. Zhang, S., Bilal, M., Zdarta, J., Cui, J., Kumar, A., Franco, M., Romanholo Ferreira, LF., Iqbal, HMN. (2021). Biopolymers and nanostructured materials to develop pectinases-based immobilized nano-biocatalytic systems for biotechnological applications. *Food Research International*, 140, 109979.

7. OPEN ACCESS:

Figure 1. *The dry electrochemical cell used for the electrochemical characterization of solid biopolymeric electrolyte films*

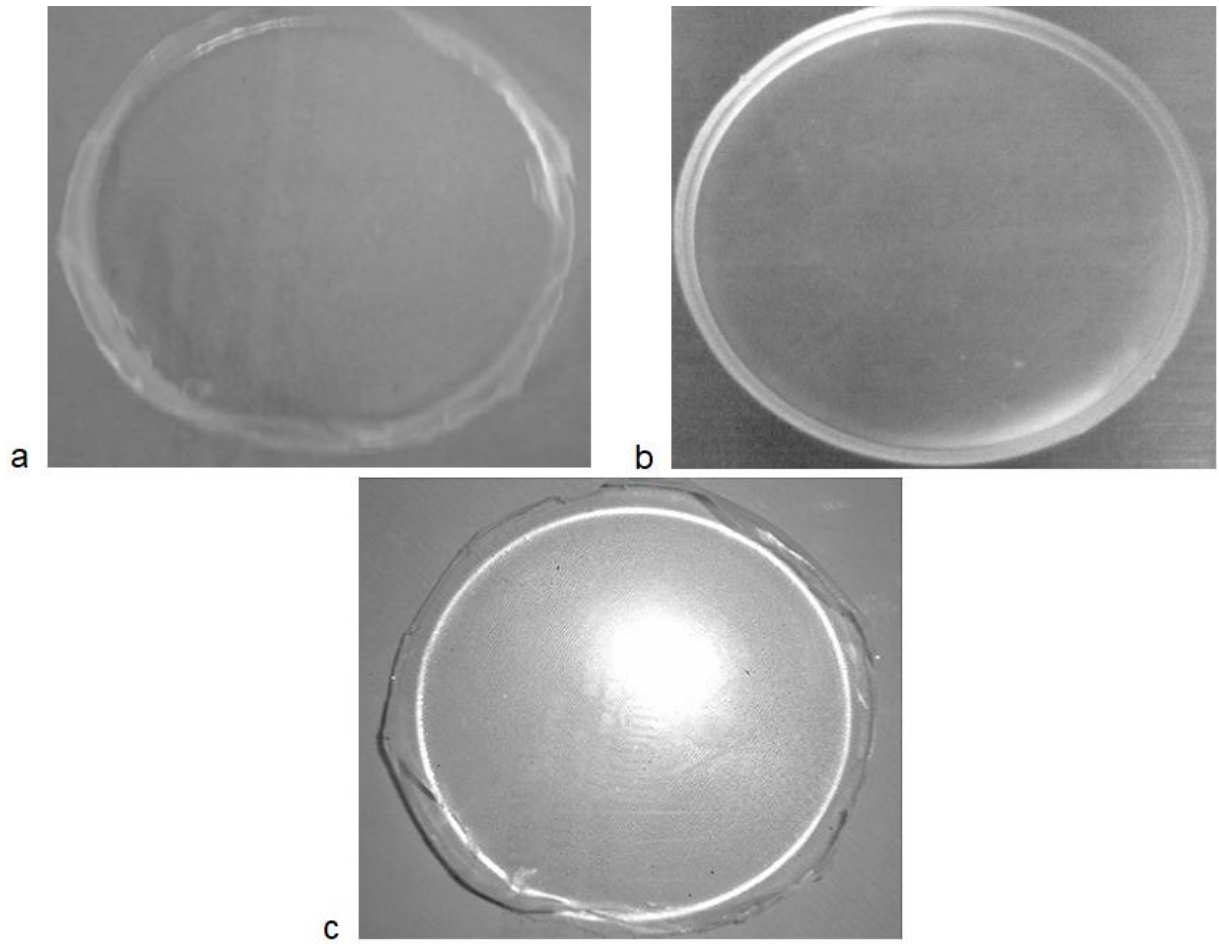

Figure 2. *Image of a solid biopolymer electrolyte films of a) starch from corn b) starch from potato, and c) starch from cassava*

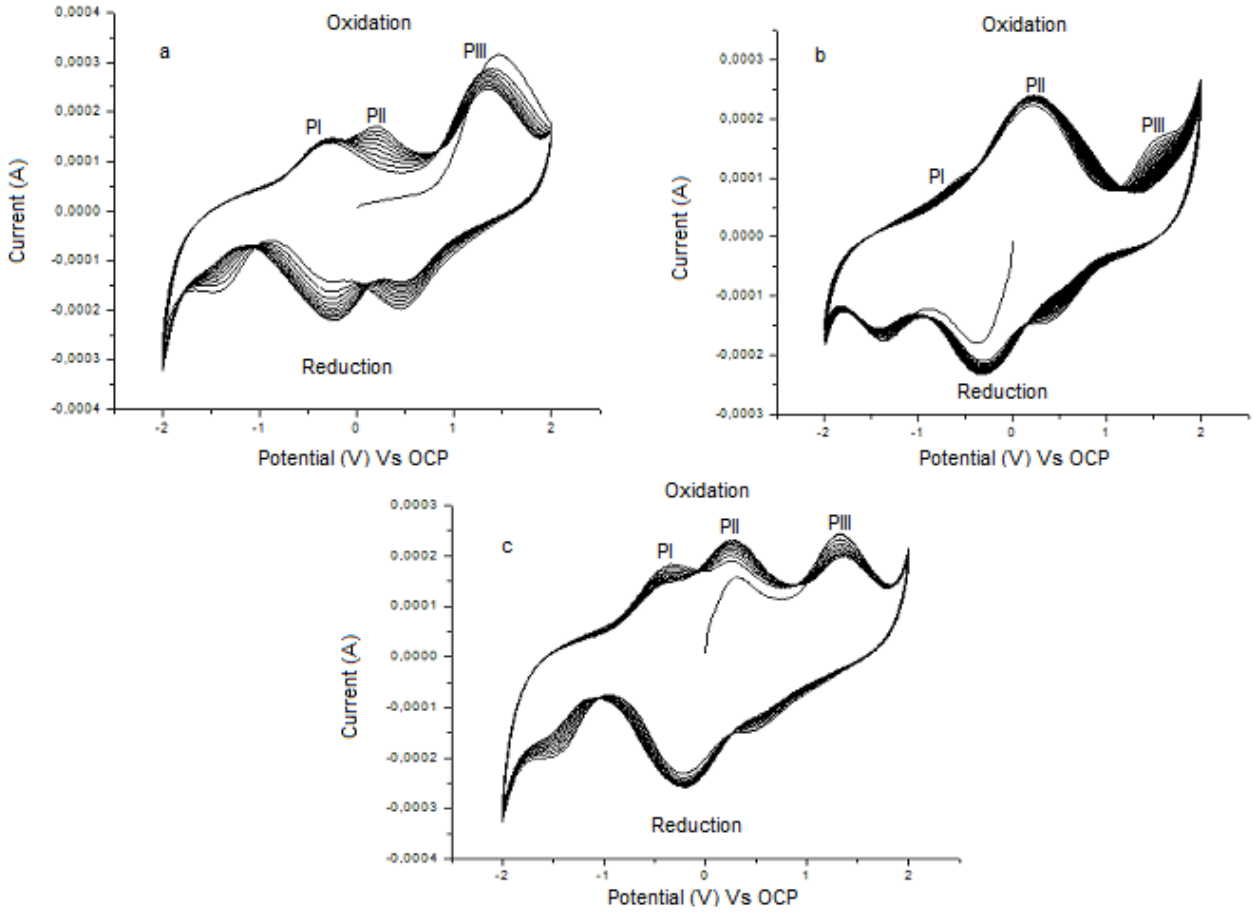

Figure 3. *Cyclic voltammetry recorded with solid biopolymer electrolyte films of starch from a) corn, b) potato, and c) cassava*

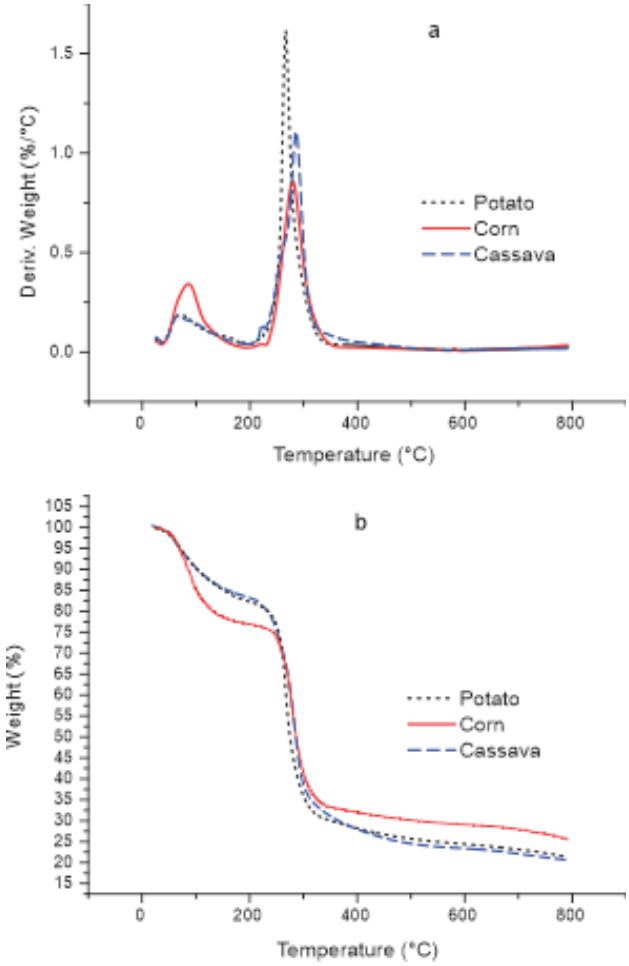

Figure 4. *Graphs of differential thermogravimetric (a) and thermogravimetric analysis (b) of solid biopolymer electrolyte films from potato starch, corn starch, and cassava starch*

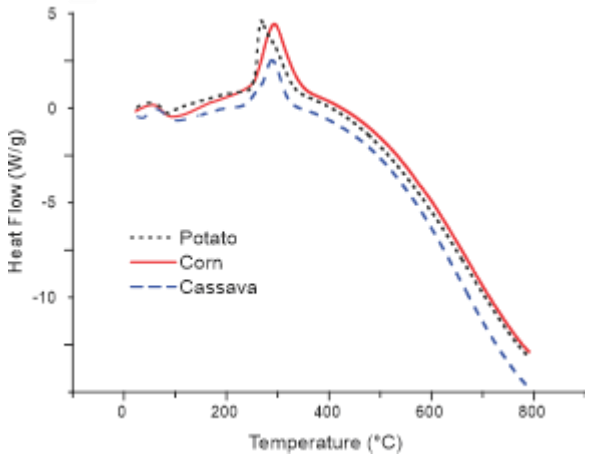

Figure 5. *Differential scanning calorimetry thermograms of solid biopolymer electrolyte films from potato starch, corn starch, and cassava starch*

Table 1. *Values of oxidation/reduction potentials and medium peak potentials recorded in the solid biopolymeric electrolyte films from corn starch, potato starch, and cassava starch*

Process		SBPE Films		
		Corn	**Potato**	**Cassava**
PI	**EO**	-0.50 V	-0.63 V	-0.45 V
	ER	-1.48 V	-1.39 V	-1.42 V
	$E_{p/2}$	-0.99 V	-1.01 V	-0.93 V
PII	**EO**	0.25 V	0.38 V	0.29 V
	ER	-0.36 V	-0.40 V	-0.19 V
	$E_{p/2}$	-0.05 V	-0.01 V	-0.05 V
PIII	**EO**	1.15 V	1.49 V	1.21 V
	ER	0.49 V	0.46 V	0.51 V
	$E_{p/2}$	0.82 V	0.97 V	0.86 V

Table 2. *Values of onset temperature, peak temperature, conclusion temperature, and enthalpy of the process of solid biopolymer electrolytes from corn starch, potato starch, and cassava starch*

SBPE Films	Peak 1				Peak 2			
	To **(°C)**	***Tp*** **(°C)**	***Tc*** **(°C)**	***H*** **(J g^{-1})**	***To*** **(°C)**	***Tp*** **(°C)**	***Tc*** **(°C)**	***H*** **(J g^{-1})**
Corn	35.0	75.2	98.7	2.4	247.8	287.6	345.9	10.8
Potato	34.7	60.1	97.9	1.8	247.6	275.6	331.1	9.3
Cassava	35.0	59.7	97.6	1.6	247.8	286.8	322.2	7.2

PERIÓDICO TCHÊ QUÍMICA
ARTIGO ORIGINAL

ESTIMATIVA DO VALOR DO NÚMERO REPRODUTIVO BÁSICO DA COVID-19 E DO EFEITO DAS MEDIDAS ANTI-EPIDÊMICAS E DO "FATOR SAZONAL" NESTE VALOR

ESTIMATION OF THE VALUE OF THE COVID-19 BASIC REPRODUCTIVE NUMBER AND THE EFFECT OF ANTI-EPIDEMIC MEASURES AND "SEASONAL FACTOR" ON THIS VALUE

ОЦЕНКА ВЕЛИЧИНЫ РЕПРОДУКТИВНОГО ЧИСЛА Ro ПРИ COVID-19 И ВЛИЯНИЯ НА НЕГО ПРОТИВОЭПИДЕМИЧЕСКИХ МЕРОПРИЯТИЙ И СЕЗОННОГО ФАКТОРА

GERASIMOV, Andrey[1]*; SEMENYCHEVA, Irina[2]; BELAIA, Olga[3]; VOLCHKOVA, Elena[4]; GOROBCHENKO, Andrey[5]

[1-5] I.M. Sechenov First Moscow State Medical University (Sechenov University), Moscow, Russia

** Corresponding author*
e-mail: andr-gerasim@yandex.ru

Received April 29 2021; received in revised form 01 July 2021; accepted July 12 2021

RESUMO

Introdução: O surgimento do COVID-19 tem levado a uma maior atenção aos modelos matemáticos da epidemiologia sendo um dos principais parâmetros o número reprodutivo básico R_0. O seu valor determina a dinâmica da incidência e o nível das medidas antiepidêmicas. É desejável ter um método bastante preciso para avaliar R_0 para cada dia. **Objetivo:** desenvolver uma metodologia para avaliar o valor de R_0 para COVID-19, levando em consideração uma mudança bastante rápida e significativa em seu valor ao longo do tempo. **Métodos:** foi proposto um método de cálculo do número de reprodução R_0 para avaliação do COVID-19 R_0 levando-se em consideração a mudança na contagiosidade das pessoas infectadas durante o processo infeccioso. **Resultados e Discussão:** Na Rússia, em junho-agosto de 2020, a taxa de reprodução era ligeiramente inferior a 1, mas, em setembro, o R_0 começou a crescer, ultrapassou 1, o que causou um aumento notável na incidência. Durante junho, no Brasil, R_0 estabilizou em um valor 1. A atividade de transmissão do patógeno é influenciada por mudanças sazonais na taxa de reprodução R_0, bem como no nível de estado imunológico da comunidade. Com base na avaliação da dinâmica da incidência de outras pneumonias, verificou-se que a variação do R_0 durante o ano é de cerca de 10%, com um mínimo no verão. **Conclusões:** embora mantendo a atividade atual de medidas antiepidêmicas devido a fatores sazonais da atividade do mecanismo de transmissão e acúmulo de indivíduos imunes nos próximos meses, a situação na Federação Russa se agravará com um aumento na incidência que dobrará em seis meses e, no Brasil, em seis meses - melhora com diminuição da incidência em 10 vezes. No entanto, a dinâmica da incidência será determinada principalmente pelo trabalho da administração e das autoridades sanitárias e pela conscienciosidade dos cidadãos.

Palavras-chave: *COVID-19, avaliação do R_0, modelos matemáticos do processo epidêmico*

ABSTRACT

Background: The emergence of COVID-19 has led to increased attention to mathematical models of epidemiology, one of the main parameters of which is the basic reproductive number R_0. Its value determines both the dynamics of the incidence and the level of anti-epidemic measures. Therefore, it is desirable to have a fairly accurate method for assessing R_0 for each day. **Aim:** Develop a methodology for determining the R_0 value for COVID-19, taking into account a reasonably rapid and significant change in its value over time**.** **Methods:** a method for calculating reproduction number R_0 was proposed for assessing COVID-19 R_0, taking into account the change in the contagiousness of the infected people during the infectious process. **Results and Discussion:** In Russia in June-August 2020, the reproduction rate was slightly less 1, but in September R_0 began to grow, exceeded 1, which was caused a noticeable increase in the incidence. During June in Brazil, R_0 stabilized at a value of 1. The activity of transmission of the pathogen is influenced by seasonal changes in the reproduction rate R_0 and the level of community immune status. Based on the assessment of the dynamics of the incidence of other pneumonia, it was found that the change of R_0 during the year is about 10%, with a

DOI: 10.52571/PTQ.v18.n38.2021.11_GERASIMOV_pgs_149_163.pdf

minimum in summer. **Conclusions:** while maintaining the current activity of anti-epidemic measures due to seasonal factors of the activity of the transmission mechanism and accumulation of the immune individuals in the coming months, the situation in the Russian Federation will worsen with an increase in the incidence doubled within six months, and in Brazil in six months — improve with a decrease in the incidence ten times. However, the dynamics of the incidence will be determined primarily by the work of the administration and health authorities and the conscientiousness of citizens.

Keywords: *COVID-19, R_0 estimation, mathematical models of the epidemic process*

АННОТАЦИЯ

Введение. Появление COVID-19 привело к повышенному вниманию к математическим моделям эпидемиологии, одним из основных параметров которых является число репродукции R_0. Его величина определяет как динамику заболеваемости, так и уровень противоэпидемических мероприятий. Желательно иметь достаточно точную методику оценки R_0 на каждый день. **Цель:** разработать методологию оценки значения R_0 для COVID-19 с учетом довольно быстрого и значительного изменения его значения с течением времени. **Методы.** Метод расчета репродуктивного числа R_0 был предложен для оценки COVID-19 R_0 с учетом изменения заразности инфицированных людей в ходе инфекционного процесса. **Результаты.** В России в июне-августе 2020 года коэффициент воспроизводства был немного меньше 1, но в сентябре R_0 начал расти, превысив 1, что вызвало заметный рост заболеваемости. В течение июня в Бразилии R_0 стабилизировался на уровне 1. На активность передачи патогена влияют сезонные изменения скорости воспроизводства R_0, а также уровень иммунного статуса сообщества. На основании оценки динамики заболеваемости другими пневмониями установлено, что изменение R_0 в течение года составляет около 10% с минимумом летом. **Заключение:** при сохранении текущей активности противоэпидемических мероприятий за счет сезонных факторов активности механизма передачи и накопления иммунных особей в ближайшие месяцы ситуация в Российской Федерации будет ухудшаться с увеличением заболеваемости вдвое в течение шести месяцев, а в Бразилии через полгода - улучшение со снижением заболеваемости в 10 раз. Однако, динамика заболеваемости будет определяться, прежде всего, работой администрации и органов здравоохранения и сознанием граждан.

Ключевые слова: COVID-19, оценка R_0, математические модели эпидемического процесса

---

1. INTRODUCTION:

1.1. Background

The onset of the pandemic disease caused by the new coronavirus COVID-19 has drawn attention to mathematical models of the epidemic process, as only with their help the dynamics of incidence of a new disease under different scenarios of anti-epidemic measures can be predicted. In particular, a “contact number” or “basic reproductive number” terms, traditionally referred to as R_0, has come into use (WHO, 2020; WHO, March 5, 2020; Euro WHO, 2020; Madabhavi, 2020; CDC, 2020; Anderson and May 1992; Li *et al*.,1999).

The basic reproductive number is defined as the average number of infected from one infected at universal susceptible. Similar terms exist in population biology and are defined as the ratio of populations of offspring and parents under the most favorable conditions: food excess, absence of predators, and parasites (Svirezhev and Logofet,1978).

Since the activity of the transmission mechanism depends on both the properties of the pathogen and the characteristics of the host population, including both biological and social aspects, the attention to mathematical models of the epidemiology, one of the main parameters of which is the basic reproductive number even for the same pathogen varies in different cities and countries and changes over time has increased. Typhoid fever is an example. Even 100 years ago, there was mass infection for typhoid fever. However, after introducing the practice of disinfecting food and water, the incidence of typhoid fever began to decline. Currently, in most countries, there are isolated cases of typhoid fever (WHO, 2018).

1.2. Basic models of the epidemic process and their development in the models of the COVID-19 epidemic process.

The first models of the epidemic process date back to the first half of the 20th century (Kermack and McKendrick,1927). Their use was limited, as the successful use of mathematical

models requires a fairly good understanding of the phenomenon under study (Longini,1978; Olsen,1988; Qiu,2020; Zhao,2020). Progress in epidemiology is accompanied by increasingly active use of mathematical models of the epidemic process. (Cabore *et al*., 2020; Carvalho *et al*. 2019).

The reason for this is that mathematical models use incidence data and knowledge about the epidemiology of the disease under study. As knowledge accumulates, the models and prognoses created on their basis are refined. So, in early 2020, it was believed that most of the infected patients with COVID-19 fall ill in severe form, with a mortality rate of more than 5% (Zhou *et al*., 2020; Guo *et al*., 2020). As a result, the obtained prognosis of damage from a pandemic in the absence of active anti-epidemic measures gave a situation of a global catastrophe (Diop *et al*.,2020) with the number of deaths in several hundred million people. Now, from the reports of the Moscow Government on the results of mass screening of city residents the presence of antibodies to COVID-19 is about 20% (Mos.ru,2020). It was also found that the likelihood of disease and its severity dramatically increases with age (Giordano *et al*., 2020; Zheng *et al*., 2020; Han *et al*., 2020; Ge *et al*., 2020; Silva *et al*., 2020; Sharma *et al*., 2020; CDC,2020).

As a result, the estimate of the maximum damage decreased by about ten times. On the other hand, the mathematical models of the COVID-19 epidemic correctly predicted that if no effective measures are taken to limit the spread of the pathogen, the incidence will grow exponentially with an increase in the number of cases in a month several tens of times until a significant proportion of the population will be infected (Ngonghala *et al*., 2020). At the same time, the maximum incidence will be such that the number of patients who need hospitalization will be many times higher than the capacity of health care. Furthermore, estimates of the activity of the transmission mechanism unambiguously showed that the spread of the pathogen will not be limited to one country but will be global.

Therefore, projections based on mathematical models served as one of the factors that prompted the health care system and government to take immediate practical measures to limit the rate of increase in the incidence (Euro WHO, 2020; WHO, March 5, 2020; Billah *et al*., 2020; Zhang *et al*., 2020). However, at the same time, it is still unknown how long the immunity will be after the disease (Zhang and Guo, 2020; Chams, 2020). Therefore, there is no data required to create mathematical models of long-term dynamics of incidence or mathematical models of the epidemic process of COVID-19. We have to limit ourselves to models of the COVID-19 epidemic for no more than several years.

Formally, the mathematical model of the epidemic is obtained from the model of the epidemic process, if we do not take into account the process of the population turnover due to the birth of new members of the population or the loss of specific immunity in some of those who have been ill. Therefore, the epidemic model can be used for short-term or medium-term prognosis, for not more than several years, even for infectious diseases with an expressed lifelong immunity.

1.3. Compartmental models in epidemiology

Traditionally, models of the epidemic process are divided according to a set of possible states. The most commonly used model is SIR (Matveev, 2020), in which members of a population can be in one of three states (S – Susceptible; I – Infectious; R – Recovered). Transition $S \rightarrow I$ — infection of a susceptible person, $I \rightarrow R$ — recovery, $R \rightarrow S$ — population turnover.

Population turnover occurs due to the loss of specific immunity or a pair of events "death of the insusceptible person" + "birth of a new member of the population". The SI model corresponds to infectious diseases from which one cannot recover, ending in death or life-long carriage; SIS model — diseases that do not have post-infectious immunity. In the SEIR model, another state is "sterile infected", "Exposed"— in the stage of the disease before the onset of the shedding of the pathogen. One more condition has been added in the MSIR and MSEIR models, corresponding to children with passive immunity due to breastfeeding (Matveev, 2020).

The specificity of the disease course may necessitate further complications of the model by introducing additional states and transition stages. So, for tuberculosis, an infected person is in a “healthy carrier” state. From this state, a transition to the state of an active infectious process is possible. The state of active tuberculosis can be divided into several variants: with and without bacterial excretion, with or

without active drug treatment, and so on (Avilov, 2007).

The epidemic model differs from the epidemic process model in that it does not account for the RS update process R → S. It should be noted that the selection of conditions in the models under consideration is done from the point of view of an epidemiologist, not a clinician. Being in the “Infectious” state ends with the end of the pathogen shedding and not with clinical recovery, that is, the disappearance of the clinical signs of the disease. Accordingly, the transition E → I is the beginning of the release of the pathogen, and not the appearance of clinical signs of the disease, that is, the duration of stay in the “Infectious” state does not coincide with the duration incubation period.

However, the classification of the infected persons into the "Exposed"/"Infectious" states is rather rough since the increase and decrease in the contagiousness of the infected occur gradually. Therefore, within the framework of this work, for a more accurate assessment of the activity of the transmission mechanism, we will consider the average contagiousness of an infected person as a function of the time elapsed after infection.

The dynamics of incidence, that is, the S → I transition activity, is determined not only by the current proportion of the infected persons, their contagiousness, and the activity of the pathogen transmission mechanism but also by the level of the community immune status. When comparing the results obtained using mathematical modeling with actual data, the following should be considered: (1) In the mathematical model, I is the proportion of those infected persons (not sick). For most infectious diseases, the number of cases, those diagnosed and officially reported, is only a small proportion of the total number of infected persons, since most infections are asymptomatic or without medical resource utilization. The ratio between sick and infected patients can be obtained using screening studies to assess the proportion of the immune proportion of the population and compare its value with the incidence; and (2) The value of community immune status is determined not so much by the total proportion of the immune persons as by the proportion of the immune persons in high-risk groups.

The following criteria can determine risk groups: A high risk of infection, by high infectivity, and by severe disease. The first two criteria relate to the spread of the disease, the third to the severity of the complications.

The risk groups for infection and contagiousness traditionally include healthcare providers (Wang W., 2020). The risk group for disease severity for COVID-19 consists of older adults, high body mass index, and chronic diseases (Zhou, 2020; Du, 2020). Unfortunately, it is challenging not only for COVID-19 but even for well-studied diseases to obtain an estimate of the distribution of members of the population in terms of individual infectiousness and risk of infection (Wang X.*et al*., 2020). The main part of this article is devoted to assessing the rate of increase in the incidence and the activity of the spread of the pathogen. For this part of the article, these difficulties in interpreting the simulation results do not affect the obtained conclusions. Also, these difficulties do not affect the analysis of the initial phase of the epidemic, when the proportion of the immune is still small in all groups, including the risk group. However? These difficulties should be considered when highlighting the influence of the community immune status on the dynamics of morbidity at a sufficiently high incidence rate. This paper concerns the analysis of the current incidence of COVID-19 in Moscow, where the proportion of seropositive persons is already about 25% (Mos.ru, 2020).

The convenience of using a reproductive number lies in the comprehensibility of interpretation. If R_0<1, then the number of sick people will decrease, and the pathogen will naturally be eliminated. If R_0>1, in the absence of additional anti-epidemic interventions, the incidence will increase until a high enough level of collective immune status is reached. To reach it, a large enough part of the population must be immune. (Billah *et al*., 2020; Van Damme *et al*.,2020; Ngonghala *et al*.,2020).

1.4. Simplest homogeneous model and collective immune status.

Under the simplest homogeneous model, the level of collective immunity is given by the fraction of the susceptible portion of the population *S*, so that from one infected, an average of $S \times R_0$ susceptible are infected, and if $S \times R_0$>1, the incidence increases, and if $S \times R_0$<1, it decreases. With constant incidence *S*=1/*Ro*. To protect the population from mass incidence by vaccination, it is necessary to vaccinate in a way that more than (1-1/*Ro*) proportion of the population obtains post-vaccinal immunity,

infecting against infestation. For example, if *Ro*=5, it is necessary to vaccinate the population so that at least 80% of the population has strenuous immunity. At the same time, vaccination coverage should be higher, as not all vaccinated produce the necessary level of immune response (Zimmermann and Curtis, 2019).

It is advisable to vaccinate with some reserve, as one case of brought disease will trigger on average $(S \times R_0)/(1-S \times R_0)$ contacted. For example, with R_0=5 and a proportion of immunes equal to 85%, one brought case will account for an average of 3 contacted (Horn *et al*.,2016). Similarly, the necessary intensity of other anti-epidemic measures, including those aimed at social disintegration and the active detection and isolation of those affected, can also be estimated. Since for COVID-19, the basic reproductive number is slightly less than 3, it is necessary to reduce the number of contacts by more than 3 times to control morbidity (Liu *et al*.,2020). However, to produce a high enough level of collective immune status, not most of the population needs to be immune — enough is that only high-risk groups in the probability of infection and contagion have immunity (Gerasimov,2008; Munday,2018).

In estimating the expected level of morbidity, it is also necessary to consider that the formation of collective immunity means the immunity of all those infected, not just those infected in a manifested form (Yu and Yang,2020). During the study of the COVID-19 pandemic, estimates of the proportion of cases with pronounced symptoms have changed significantly. In January-February, researchers believed that prominent symptoms accompanied virtually all cases. This was due both to the complexity of laboratory diagnosis of the disease and to the fact that the causative agent COVID-19 was considered an analog of other coronaviruses, SARS and MERS, in which virtually all cases of infections led to disease in a severe form (Wang Y.*et al*., 2020).

Then asymptomatic forms were identified, and estimates of the proportion of expressed cases began to decrease to 80%, then to 50%, and then to 20% (Yu and Yang,2020). According to mass research of residents of Moscow, the proportion of expressed cases is about 10% - at the beginning of July about 220.000 cases were recorded at about 20% of seropositivity among residents of Moscow. Accordingly, if at first it was expected that about half of the inhabitants of the Earth would suffer new coronavirus infection (with pronounced clinical symptoms), now the prognosis is ten times lower.

Individual protection and social separation measures have a positive impact on the incidence of COVID-19. Still, their long and intensive appliance by most countries' leadership is considered unacceptable because of the grievances of citizens and the negative impact on the economy. At the moment, methods for assessing the average value of the reproductive number R_0 for pathogens of infectious diseases are actively used, provided that the conditions of the course of the epidemic process of process remain unchanged (Wells *et al*., 2020). For COVID-19, these methods are not very successful, since in this case active anti-epidemic measures are used, the set of which and the intensity of their use are constantly changing over time.

At the same time, it cannot be said that the infectivity of COVID-19 is very high. Estimating the reproduction rate R_0 for COVID-19 gives a value of no more than 3 (see text below). At the same time, for measles, mumps, diphtheria, and many other infectious human diseases R_0 is higher (Anderson and May 1922). This, in particular, offers good prospects for controlling the spread of COVID-19 through vaccination. However, since the causative agent COVID-19 is new to the human population and it has not yet passed the stage of evolutionary adaptation to the host organism, the emergence of new, more infectious variants of the pathogen is also quite likely (Belyakov *et al*., 1987).

The need for constant monitoring of the situation and quick action follows from the experience of the initial stage of the COVID-19 epidemic. The incidence increased tenfold in a month. This technique will make it possible to assess the effectiveness of the anti-epidemic measures used and predict morbidity dynamics under different scenarios. The development of a more perfect mathematical model of the epidemic process by calculating the rapidly and significantly changing reproductive (contact) number of R_0 is an urgent task of modern epidemiology.

This study aimed to develop a methodology for assessing the value of the reproductive (contact) number R_0 for COVID-19, taking into

account a fairly rapid and significant change in its value over time.

2. MATERIALS AND METHODS

2.1. Mathematical modeling

The study used epidemiological and mathematical modeling methods for studying the proposed mathematical model using the example of the incidence of COVID-19 in Russia and Brazil in the period of March-September 2020. The study used open data from official sources on the incidence of COVID-19 in Russia (https://covid.observer/ and https://yandex.ru/covid19/stat) and Brazil (Painel coronavirus - https://covid.saude.gov.br/).

At the initial stage of development of the epidemic of a new disease, when no noticeable immune layer has formed, and no anti-epidemic measures were taken, the incidence grew exponentially, as $c \times e^{\lambda t}$, where *c* is the constant, λ is the exponential growth rate, t is the time in days. At the same time, the ratio of the number of people who fell ill for this and the previous day is equal $e^{\lambda t} - 1$.

Within the simplest homogeneous model (MacIntyre and Heslop, 2020), the number of infected J(t) dynamics at the first stage is described by equation 1.

$$\frac{dJ}{dt} = \frac{(R_0 - 1)}{T} J \qquad \text{(Eq.1)}$$

Substituting the (1) $J(t) = c \times e^{\lambda t}$, it turns out equation 2.

$$R_0 = 1 + \lambda T \qquad \text{(Eq.2)}$$

Therefore, for a new infectious disease, the reproduction rate R_0 can be estimated from the rate of increase in the incidence and duration of the disease. So, for SARS with a characteristic duration of the disease of about ten days at the initial period of the epidemic, the incidence doubled in about three weeks, which corresponds to a reproduction rate of about 1.5 (Liu *et al*.,2020). This is an estimate obtained using a highly simplified “standard” model. We further propose a more accurate assessment method and compare our values with these.

2.2. Statistical Analysis

Statistical analysis of the data was carried out using the statistical software package IBM SPSS Statistics 22.0.

3. RESULTS AND DISCUSSION:

At the initial stage of exponential growth, under conditions maintained, both the number of ill patients per day and the total number of patients (incident and prevalence), the number of hospitalized, and the number of deceased shall increase at the same rates. For example, figure 1 shows that from late March to mid-April, the incidence of COVID-19 in Russia and Brazil grew exponentially, so that on the logarithmic scale, the incidence graph was close to linear, after which the rate of morbidity began to decrease.

No new cases were reported for May 20 in Brazil, and there were more than usual on May 19 and 21. Since the logarithm of zero is infinite, the data for May 19-21 were averaged for further calculations. Also, Figure 1 clearly shows the difference in the used disease registration system. In Brazil, the number of reported cases of COVID-19 on weekends is several times lower than on weekdays. There are no such differences in Russian Federation and Moscow.

The dynamics of the incidence of COVID-19 has changed. From March 31 to May 15 — a period of exponential growth; From May 16 to June 30 — the incidence continues to change, but at a slower rate; From July 1 to August 31 — the incidence is relatively stable; From September 1 to September 18 — an increase in the incidence began in the Russian Federation.

For the period from March 31 to May 15, the average exponential growth rate for Moscow was $\lambda \approx 0.0735$, for Russia excluding Moscow $\lambda \approx 0.0958$ and for Brazil $\lambda \approx 0.0389$, which corresponds to a 7.63%, 10.05% and 3.97% increase in the number of patients per day, respectively (Gerasimov, 2020). If the average duration of the disease is ten days, for Moscow, it is $R_0 \approx 1.735$, for Russia except for Moscow - $R_0 \approx 1.958$ and for Brazil - $R_0 \approx 1.398$. However, an estimate of the average R_0 value over a relatively long period is only of relative value, since the situation with the spread of COVID-19 changes in a matter of days. Therefore, the obtained estimates R_0 1.735 for Moscow, 1.958 for Russia except for Moscow, and 1.398 for Brazil need to be clarified.

In determining the duration of the disease, clinicians focus on clinical symptoms the appearance and disappearance of which may not coincide with the beginning and end of the release of the pathogen. Epidemiologists give the maximum duration of the contagious period, as needed to determine the quarantine period. In this case, the dependence of the average contagiousness of the infected on time after infection is required.

Then if $K(n)$, $n = 1,2,\ldots$ is the relative average in *n* days after infection case, $K(1) + K(2)+\ldots = 1$, then the dynamics of the number of infected per day *N* is given by equation 3

$$A(N) = R_0(A(N-1)K(1) + A(N-2)K(2)+\ldots)$$

(Eq.3)

Now there are at least two approaches to determining the dynamics of contagiousness $K(n)$, $n = 1,2,\ldots$: by the disease picture and by the deviation of the incidence dynamics from the exponential. It is believed that for manifested cases, the release of the pathogen begins on the second to third day after infection and is increasing as the severity of the clinical picture increases, which corresponds to increase in the content of virions in the body of the patient. The diagnosis is made on 5th-7th day, after that the number of contacts of a sick person drastically decreases (both when hospitalized and treated at home). Further, the average contagion continues to decrease, including through recovery or death, and by mid of the third week, it becomes small (Lauer *et al*.,2020; Liu *et al*.,2020; Madabhavi *et al*.,2020; Zhai *et al*.,2020).

For asymptomatic cases, discharge begins a few days later, and ends in 2-3 weeks after infection, and is less intense. In general, the average number of infected from one asymptomatic carrier is lower than from one person with a pronounced form of the disease, but since the proportion of cases expressed is less than half, the proportion of infected patients with pronounced symptoms and asymptomatic are comparable (Giordano *et al*.,2020).

Table 1 shows the dependence of the average infectivity of the infected K(n) (contagiousness of patients with COVID-19) on the number of days n, which have passed since the moment of infection. These are used below to analyze the actual data. Another approach of $K(n)$ estimation is based on the deviation of dynamics from the predicted model based on Eq.3. Since in the case of development of mass COVID-19 morbidity active anti-epidemic activities were introduced, the value R_0 in equation 3 should not be considered as a constant value but as a function of time.

In this case, the expected number of cases *a*(*N)* per day N is shown in equation 4.

$$a(N) = R_0E(N)(A(N-1)K(1) + A(N-2)K(2)+\ldots)$$

(Eq.4)

Further, based on actual data on disease patterns, different countries address the following challenge: at what function the $K(n)$ the expected values of *a*(n) will be as close as possible to the actual values of *A*(n) with the simplest form of the functions *E*(n).

Both approaches give the same results — starts to differ from zero after two days, grows to the 7th day, then begins to decrease, with the rate of reduction about one and a half or two times less than the build-up speed contagion. Unfortunately, at the moment, it is no possible to provide links to publications on the second approach. Such calculations became possible only after the transition of the morbidity dynamics to the second (the slowdown in the incidence compared to the exponential) and the third (the stabilization and reduction of the incidence) stage and require quite long calculations using supercomputers, so here it has to rely on the results of the articles reviewed, including not yet published, reports and private messages.

According to equation (Eq.3) the expected value of the contact number for day *N* can be calculated as shown in equation 5

$$R_0(N) = \frac{A(N)}{A(N-1)K(1)+A(N-2)K(2)+\ldots} \qquad \text{(Eq.5)}$$

where *A*(*k*) is the number of cases per day number k.

Figure 2 shows that before May 15, there was a decrease in pathogen transmission activity, after which it remained at the same level. From May 16 to June 30, the average R_0 for Moscow was 0.783, which resulted in an about ten times decrease of the incidence. In contrast, for Russia, excluding Moscow, the average R_0

was 1.033, and the incidence remained at the same level, while for Brazil, the average R_0 was 1.213, resulting in continuing rapid growth of morbidity.

For Moscow, for the period July 1 — August 31, the average R_0 value was 0.969 and the incidence rate remained approximately at the same level. For Russian Federation (excluding Moscow), the average R_0 was 0.953, which led to a decrease in the incidence by about 20%. In the period from 1 to September 18 in Moscow the average value of R_0 was 1.034, in Russia (excluding Moscow) 1.058. By itself, an increase in the reproduction rate to a value of 1.05 corresponds to an incidence rate of about 15% per month, however, the alarming moment is that the value of R_0 in September is constantly growing.

For Brazil, the average R_0 value for the period from July 1 to September 18 is 1.025, which corresponds to a slow increase in the incidence. The average value of the change per day R_0 -0.00205, the correlation between the R_0 value and the date is statistically insignificant, p = 0.298. In addition to anti-epidemic measures, the dependence of the activity of the transmission mechanism on the time of year and the accumulation of immune ones affect the dynamics of morbidity given by equation (3), as shown in equation 6

$$R_0(t) = \bar{R}_0 S(t) E(t) V(t) \qquad \text{(Eq.6)}$$

where $\bar{R}_0$ is the "base" value of the basic reproductive number estimated above $S(t)$ is the proportion of the susceptible part of the population $E(t)$ is the current effectiveness of the anti-epidemic activities. The function V (t) corresponds to the dependence of the activity of the transmission mechanism on the season. For an unambiguous definition, it is assumed that its average value is equal to one.

The dynamics of morbidity in the absence of anti-epidemic measures can be described by equations 7 and 8 (Yu,1927)

$$I(N) = \bar{R}_0 S(N-1) V(N) \sum_{n=1} K(n) I(N-n) \qquad \text{(Eq.7)}$$

$$S(N) = S(N-1) - I(N) + \gamma(1 - S(N-1)) \qquad \text{(Eq. 8)}$$

where $I(N)$ is the proportion of infected per day number N, $S(N)$ is the proportion of infected per day number N, $1/\gamma$ is the average life expectancy in days for infections with strenuous lifetime immunity or the average duration of immunity retention for infections of temporal immunity.

Numerical calculations show that the logarithm of the ratio of maximum and minimum intra-annual morbidity depends almost linearly on the amplitude of fluctuations in the activity of the transmission mechanism, that is, if $V(N) = 1 + \alpha \times f(N)$, the ratio of maximum and minimum morbidity is almost equal to $e^{\alpha\beta}$ where β is determined by values R_0, γ, $K(n)$, and the form of function f. For life expectancy of 75 years of the contagiousness given above the $K(n)$ and the sinusoidal dependence of transmission mechanism activity on the time of year at R_0=2 we get that $\beta \approx 16.17$, and at R_0=3 $\beta \approx 16.43$.

During the year, the incidence of out-of-hospital pneumonia in Russia changes by about four times (Bondarenko *et al*., 2016). Since the duration of the disease and the activity of the transmission mechanism for COVID-19 and other out-of-hospital pneumonias are quite similar from the ratio obtained above as shown in equation 9

$$\alpha = \frac{ln\,4}{\beta} \qquad \text{(Eq.9)}$$

This gives $a \approx 0.0857$ for R_0=2 and $a \approx 0.0843$ for R_0=3. Consequently, the expected value of seasonal variation in transmission mechanism activity for COVID-19 is about 8.5%.

By mid-spring, the contact number for Moscow, Russia, and Brazil was roughly 2.5. For Moscow, reduction of activity of the transmission mechanism due to accumulation of the immune layer can be estimated at 0.8, and due to reduction of activity of the transmission mechanism from mid-spring to mid-summer — 0.915 times, which in total according to (Eq.6) gives a reduction in the activity of the transmission mechanism by 1.366 times. In fact, the activity of the transmission mechanism decreased from about 2.75 to 0.759, that is 3.62 times. Consequently, due to anti-epidemic measures and the decrease in the social activity of the population, the activity of transmission of the virus decreased by 2.65 times.

If 228.678 cases were registered in Moscow at present, then in Russia as a whole — 720.547, which at a manifestation of 10% gives the share of immune in Russia except Moscow at a level of 4.2%. As shown above, now Moscow has R_0 of about 0.82 and Russia except Moscow — of about 1. From the difference of 0.23 due to differences in the severity of the immune layer, 0.2-0.042=0.158 can be explained. About 2/3 of the difference in the activity of propagation of the pathogen is explained by differences in the immune layer.

Suppose the incidence present at the beginning of July lasts for the whole summer until the beginning of autumn, about 30.000 cases of COVID-19 will be recorded in Moscow. In that case, taking into account not manifested cases will increase the proportion of the immune layer by another about 2.5%. For Russia except for Moscow, the increase in the immune layer will also be approximately 2.5% if the incidence remains at the same level as it is now. Since due to seasonal change of R_0, in autumn the activity of propagation of the pathogen will be about 9%, the overall situation with the incidence of COVID-19 will deteriorate even with the preservation of existing anti-epidemic activities.

For Brazil, the situation is also quite unfavorable. On July 29, 2.552.265 cases were recorded, which at 10% manifesto yields to about 12.3% seropositive (Amorim Filho *et al*., 2020; Aguas *et al*., 2020; Vieira *et al*., 2020; Hallal *et al*., 2020). Therefore, the current R_0 value of 1.192, taking 10% amplitude of the transmission mechanism activity fluctuations, will increase to about 1.3 by mid-autumn. Consequently, doubling the proportion of seropositive will make R_0 less than 1. Therefore, if the current anti-epidemic activities in Brazil are maintained, it is possible to expect that by early autumn, the number of residents affected by COVID-19 will double, after which the incidence will begin to decline noticeably. So, at the initial period of the COVID-19 epidemic in Russia and Brazil, the contact number R was in the region of 2.5 - 3. However, due to the introduction of anti-epidemic measures, R_0 was reduced to about 1. Thus, the dynamics of the incidence of COVID-19 is determined, according to (Eq.6), by three components — the activity of the transmission mechanism, taking into account the anti-epidemic measures, the activity of seasonal factors of transmission, and the level of community immune status.

As of September 19, 2020, 275.354 cases of the disease were registered in Moscow, which is 2.17% of the total population. According to the statements of the Moscow Government, as a result of the screening, it was obtained that about 20% of Moscow residents have antibodies to the new coronavirus (Mos.ru,2020). Consequently, the proportion of manifest registered cases for Moscow is about 8.7%.

Currently, about 800 cases of COVID-19 are registered in Moscow per day. Considering the obtained share of documented cases of the disease in 8.7%, this increases the share of immune Muscovites per day by 0.073%. On the other hand, due to the activation of seasonal factors, the activity of the transmission mechanism will increase at a rate of about 0.093% per day. Consequently, at the current level of morbidity, the increase in the collective immune status and the activation of seasonal factors of transmission almost completely compensate each other

For Russia, with the exclusion of Moscow from it, 821.164 cases of COVID-19 were registered, which corresponds to 0.61% of the population and gives the proportion of the immune persons at 7.05%. With the current incidence of about 5000 new cases per day, this gives an increase in the proportion of immune people by 0.043% per day, which compensates for half of the seasonal increase in the activity of the transmission mechanism and corresponds to a twofold increase in the incidence by the end of winter.

In Brazil, there are 4.495.181 registered COVID-19 cases, accounting for 2.13% of the population. Since the ratio of registered cases, as well as the magnitude of seasonal changes in the activity of the transmission mechanism in Brazil, may differ from Russia, it can be said only as a very rough estimate that due to an increase in community immunity and a seasonal decrease in the activity of the transmission mechanism, which in this case will be summed up, while maintaining the current activity of anti-epidemic measures, an approximately 10-fold decrease in the incidence of COVID-19 in Brazil is expected.

4. CONCLUSIONS:

In total, while maintaining the current activity of anti-epidemic measures, the incidence in Moscow will remain at the same level. In the Russian Federation, except for Moscow, it will

increase and in six months should increase by about two times. In Brazil, it will decrease and in six months should decrease by about 10 time. Therefore, the main factor that will determine the dynamics of incidence in the Russian Federation and Brazil is anti-epidemic measures, which must be increased compared to the current level, although this causes popular discontent.

These estimates were obtained within the framework of the simplest homogeneous model, in which community immunity is determined by the proportion of the susceptible part of the population. However, as mentioned earlier, in reality, community immunity is higher since the proportion of susceptible people in high-risk groups in terms of the probability of infection is lower than the average for the population.

5. CONFLICT OF INTEREST:

The authors declare there is no conflict of interest

6. REFERENCES:

1. Amorim Filho L., Szwarcwald C.L., Mateos S., Ponce de Léon A.C.M.., Medronho RA., Veloso V.G. *et al*. (2020). Seroprevalence of IgG and IgM anti-SARS-CoV-2 among blood donors in Rio de Janeiro, Brazil. Published online 2020 July 1 Rev Saude Publica. 54-69.

2. Aguas R., Corder R.M, King J.G., Gonçalve G., Ferreira M.U., Gomes M.G.M. Herd immunity thresholds for SARS-CoV-2 estimated from unfolding epidemics. Preprints. https://www.medrxiv.org/content/10.1101/2020.07.23.20160762v3

3. Anderson R.M. and May R.M. Infectious Diseases of Humans: Dynamics and Control 766 pages. Oxford: Oxford University Press; 1991. ISBN: 9780198540403

4. Avilov K. K., Romaniukha A. A. (2007). Mathematical models of tuberculosis extension and control of it (Review). (Matematicheskie modeli rasprostraneniia i kontrolia tuberkuleza (obzor), Mathematical Biology and Bioinformatics), 2(2), 188-318 [In Russian].

5. Belyakov V.D.; Golubev D.B.; Kaminskiy G.D.; Tets V.V. Self-regulation of parasitic systems: (molecular genetic mechanisms). Medicine, 1987. 240 p. [In Russian].

6. Billah M.A, Miah M.M, Khan M.N. (2020). Reproductive number of coronavirus: A systematic review and meta-analysis based on global level evidence. PLoS ONE 2020; 15(11): e0242128.

7. Bondarenko A.P.; Shmylenko V.A.; Trotsenko O.E.; Zaitseva T.A.; Karavyanskaya T.N.; Butakova L.V.; Korita T.V. (2016). Intra-annual dynamics of pneumococcus carriage levels and the incidence of community-acquired pneumonia in Khabarovsk in 2015. Bulletin of physiology and pathology, 62,16-21. [In Russian].

8. Brasil. Painel coronavírus / COVID-19 Brasil [Internet]. Brasília: Ministério daSaúde; 2020 [updated 2020 May 30; cited 2020 May 31]. Available from: https://covid.saude.gov.br/.

9. Cabore JW, Karamagi HC, Kipruto H, *et al*. (2020). The potential effects of widespread community transmission of SARSCoV-2 infection in the World Health Organization African Region: a predictive model. BMJ Global Health 5: e002647.

10. Carvalho S.A.; da Silva S.O.; Charret I.D.C. (2019). Mathematical modeling of dengue epidemic: control methods and vaccination strategies. Theory Biosci, 138(2),223-239.

11. CDC: https://www.cdc.gov/coronavirus/2019-ncov/need-extra-precautions/older-adults.html

12. Chams N, Chams S, Badran R, Shams A, Araji A, Raad M, Mukhopadhyay S, Stroberg E,Duval EJ, Barton LM and Hajj Hussein I . COVID-19: A Multidisciplinary Review. Front. Public Health 2020; 8:383

13. Diop B.Z., Ngom M, Biyong C.P., Biyong J.N.P. (2020). The relatively young and rural population may limit the spread and severity of COVID-19 in Africa: a modelling study. BMJ Glob Health, 5:e002699.

14. COVID-19 World Statistics: https://covid.observer/

15. Du RH.; Liang LR.; Yang CQ.; Wang W.; Cao TZ.; Li M.; Guo GY.; Du J.; Zheng CL.; Zhu Q.; Hu M.; Li XY.; Peng P.; Shi HZ. (2020) Predictors of mortality for patients with COVID-19 pneumonia caused by SARS-CoV-2: a prospective cohort study. Eur Respir J., 55(5), 2000524.

16. EURO WHO: https://www.euro.who.int/ru/health-topics/health-emergencies/ coronavirus-covid-19/news/news/2020/3/who-announces-covid-19-outbreak-a-pandemic.

17. Ge H., Wang X.,Yuan X., Xiao G., Wang C. Deng T., Tuan Q., Xiao X. (2020). The epidemiology and clinical information about COVID-19. European Journal of Clinical Microbiology & Infectious Diseases Jun;39(6):1011-1019

18. Gerasimov A. (2020). Assessment of Vaccination Coverage Required for Covid-19 Incidence Control. Cohesive J Microbiol Infect Dis. 4(3). CJMI. 000590. 2020.

19. Gerasimov A.N., Razzhevajkin V.N. (2008). Dynamics of the epidemic process in a heterogeneous not completely isolated population taking into account seasonal options in the activity of the transmission mechanism. Journal of computational mathematics and mathematical physics, 48(8),1488-1499 [In Russian].

20. Giordano G.; Blanchini F.; Bruno R.; Colaneri P.; Di Filippo A.; Di Matteo A..; Colaneri M. (2020). Modelling the COVID-19 epidemic and implementation of population-wide interventions in Italy. Nature Medicine, 26, 855-860.

21. Guo G, Ye L, Pan K, Chen Y, Xing D, Yan K, Chen Z, Ding N, Li W, Huang H, Zhang L, Li X and Xue X. (2020). New Insights of Emerging SARS-CoV-2: Epidemiology, Etiology, Clinical Features, Clinical Treatment, and Prevention. Front. Cell Dev. Biol. 8:410.

22. Hallal P.C., Horta B.L., Barros A.J.D., Dellagostini O.A., Hartwig F.P., Pellanda L.C. *et al*. (2020). Trends in the prevalence of COVID-19 infection in Rio Grande do Sul, Brazil: repeated serological surveys. Ciência & Saúde Coletiva, 25(Supl.1):2395-2401.

23. Han Y, Luo Z, Zhai W, Zheng Y, Liu H, Wang Y, *et al*. (2020) Comparison of the clinical manifestations between different age groups of patients with overseas imported COVID-19. PLoS ONE 15(12): e0243347

24. Horn J.; Karch A.; Damm O.; Kretzschmar M.E.; Siedler A.; Ultsch B.; Weidemann F.; Wichmann O.; Hengel H.; Greiner W.; Rafael T Mikolajczyk R.T. (2016). Current and future effects of varicella and herpes zoster vaccination in Germany - Insights from a mathematical model in a country with universal varicella vaccination. Hum Vaccin Immunother, 12(7), 1766-1776.

25. Kermack W.O.; McKendrick A.G. (1927). Contribution to the Mathematical Theory of Epidemics. Proceedings of the Royal Society of London. Series A. 115 (772), 700-772

26. Lauer SA, Grantz KH, Bi Q, Jones FK, Zheng Q, Meredith HR, Azman AS, Reich NG, Lessler J. (2020). The Incubation Period of Coronavirus Disease 2019 (COVID-19) From Publicly Reported Confirmed Cases: Estimation and Application. Ann Intern Med. 172(9):577-582.

27. Li M.Y.; Graef J.R.; Wang L.; Karsai J. (1999). Global dynamics of a SEIR model with varying total population size. Math Biosci. 160(2), 191-213.

28. Liu Y, Gayle AA, Wilder-Smith A, Rocklöv J. The reproductive number of COVID-19 is higher compared to SARS coronavirus. J Travel Med. 13;27(2):taaa021.

29. Longini I.M.; Ackerman E.; Elveback L.R. (1978). An optimization model for influenza A epidemics. Mathematical Biosciences, 38,141-157.

30. MacIntyre C.R.; Heslop D.J. (2020). Public health, health systems and palliation planning for COVID-19 on an exponential timeline. Med J Aust., 212(10), 440-442.

31. Madabhavi I.; Sarkar M.; Kadakol N.M. (2020). COVID-19: a review. Monaldi Archives for Chest Disease, 2020; 90:1298:248-258

32. Matveev Alexandr. (2020) The mathematical modeling of the effective measures against the COVID-19 spread. National security and strategic planning, 1, 23-39

33. Mos.ru: https://www.mos.ru/news/item/76180073/?utm_source=search&utm_term=serp

34. Munday J.D.; van Hoek A.J.; Edmunds W.J.; Atkins K.E. (2018). Quantifying the impact of social groups and vaccination on inequalities in infectious diseases using a mathematical model BMC Med. 2018; 16: 162.

35. News.mail.ru: https://news.mail.ru/coronavirus/stat/world/

36. Ngonghala C.N., Iboi E., Eikenberry S, Scotch M, Chandini Raina MacIntyre C.R., Bonds M.H., Gumel A.B. (2020) Mathematical assessment of the impact of non-pharmaceutical interventions on curtailing the 2019 novel Coronavirus. Mathematical Biosciences 325, 108364

37. Olsen L.F.; Truty G.L.; Schaffer W.M. (1988). Oscillations and chaos in epidemics: a nonlinear dynamic study of six childhood diseases in Copenhagen, Denmark. Theor Popul Biol, 33(3), 344-370.

38. Qiu Y.; Chen X.; Shi W. (2020). Impacts of social and economic factors on the transmission of coronavirus disease 2019 (COVID-19) in China, J Popul Econ. 9,1-46.

39. Sharma A., Tiwari S., Deb M.K., Marty J.L. Severe acute respiratory syndrome coronavirus-2 (SARS-CoV-2): a global pandemic and treatment strategies. International Journal of Antimicrobial Agents 56 (2020) 106054.

40. Silva AAM, Lima Neto LG, Azevedo CMPS, Costa LMM, Bragança MLBM, BarrosFilho AKD, *et al*. Population-based seroprevalence of SARS-CoV-2 and the herd immunity threshold in Maranhão. Rev Saude Publica. 2020; 54:131-144.

41. Svirezhev Yu.M.; Logofet D.O. Sustainability of biological communities. Publisher: M.: Nauka, 1978, 352 p. [In Russian]

42. Van Damme W, Dahake R, Delamou A, *et al*.The COVID-19 pandemic: diverse contexts; different epidemics—how and why?BMJ Global Health2020;5:e003098.

43. Vieira M.A.C.S., Vieira C.P.B., Borba A.S., Melo M.C.C.M., Oliveira M.S., Melo R.M., Nunes V.V., Santana W.S. and Aguiar Y.A. (2020). Sequential serological surveys in the early stages of the coronavirus disease epidemic: limitations and perspectives. Revista da Sociedade Brasileira de Medicina Tropical Journal of the Brazilian Society of Tropical Medicine Vol.:53:(e20200351)

44. Wang X.; Liu W.; Zhao J.; Lu Y.; Wang X.; Yu C.; Hu S.; Shen N.; Liu W.; Sun Z.; Li W. (2020). Clinical characteristics of 80 hospitalized frontline medical workers infected with COVID-19 in Wuhan, China. J Hosp Infect, 105(3), 399-403.

45. Wang Y.; Wang Y.; Chen Y.; Qin Q.J. (2020). Unique epidemiological and clinical features of the emerging 2019 novel coronavirus pneumonia (COVID-19) implicate special control measures. Med Virol. 92(6), 568-576. Epub 2020 March 29

46. Wang W, Xu Y, Gao R, Lu R, Han K, Wu G, *et al*. (2020) Detection of SARS-CoV-2 in different types of clinical specimens. JAMA, 2020;323:1843–1844.

47. Wells CR.; Fitzpatrick MC.; Sah P.; Shoukat A.; Pandey A.; El-Sayed AM.; Singer BH.; Moghadas SM.; Galvani AP. (2020). Projecting the demand for ventilators at the peak of the COVID-19 outbreak in the USA. Lancet Infect Dis. 3099 (20), 30315.

48. WHO,2018: https://www.who.int/ru/news-room/fact-sheets/detail/typhoid

49. WHO March 5 2020. Emergencies, preparedness, response. Pneumonia of unknown origin – China, Dis. Outbreak News: https://www.

who.int/csr/don/05-january-2020-pneumonia-of-unkown-cause-china/en/.

50. WHO, 2020. Report of the WHO-China Joint Mission on Coronavirus Disease 2019 (COVID-19)–https://www.who.int/

docs/default-source/coronaviruse/who-china-jointmission-on-covid-19-final-report.pdf

51. Yu X.; Yang R. (2020). COVID-19 transmission through asymptomatic carriers is a challenge to containment. Version 2. Influenza Other Respir Viruses. 14(4), 474-475.

52. Zhai P.; Ding Y.; Wu X.; Long J.; Zhong Y.; Li Y. (2020). The epidemiology, diagnosis and treatment of COVID-19. Int J Antimicrob Agents. 55(5),105955.

53. Zhang B, Zhou H, Zhou F (2020) Study on SARS-CoV-2 transmission and the effects of control measures in China. PLoS ONE 15(11): e0242649.

54. Zhang L, Guo H. (2020). Biomarkers of COVID-19 and technologies to combat SARSCoV. Advances in Biomarker Sciences and Technology 2 1e23.

55. Zhao S.; Stone L.; Gao D.; Musa S.S.; Chong M.K.C.; He D.; Wang M.H. (2020). Imitation dynamics in the mitigation of the novel coronavirus disease (COVID-19) outbreak in Wuhan, China from 2019 to 2020. Ann Transl Med, 8(7), 448-462.

56. Zheng Y.; Xu H.; Yang M.; Zeng Y.; Chen H.; Liu R.; Li Q.; Zhang N'; Wang D. Epidemiological characteristics and clinical features of 32 critical and 67 noncritical cases of COVID-19 in Chengdu. (2020) Journal of Clinical Virology. 10(127), 104366.

57. Zhou F; Yu T; Du R; Fan G; Liu Y; Liu Z; Xiang J; Wang Y; Song B; Gu X; Guan L; Wei Y; Li H; Wu X; Xu J; Tu S; Zhang Y; Chen H; Cao B. (2020). Clinical course and risk factors for

mortality of adult inpatients with COVID-19 in Wuhan, China: a retrospective cohort study. Lancet, 395 (10229), 1054-1062

58. Zimmermann P.; Curtis N. (2019). Factors That Influence the Immune Response to Vaccination. Clin Microbiol Rev, 32(2), e00084-18.

7. OPEN ACCESS:

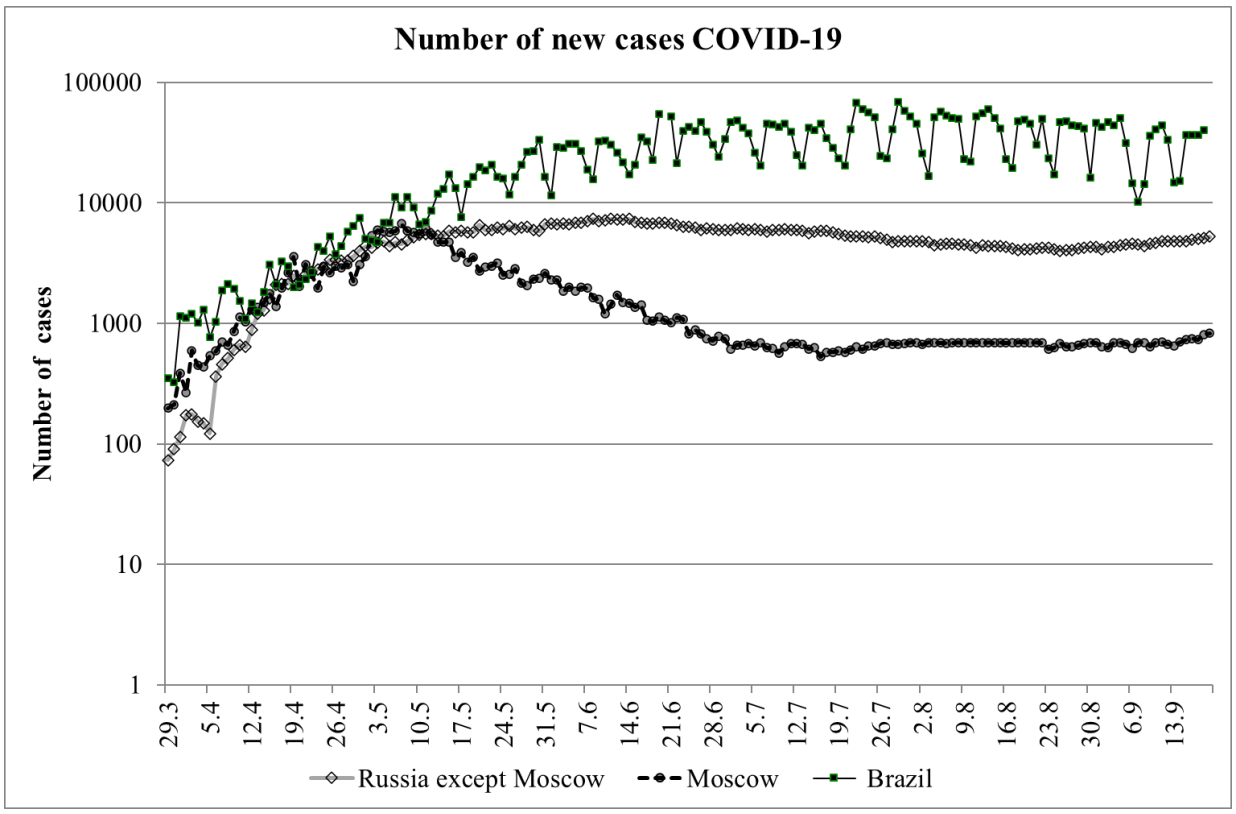

Figure 1. *Dynamics of new COVID-19 cases detected per day in Moscow, Russia excluding Moscow, and Brazil.*

Notes: The x-axis is the date (day. month) of registration of new cases in 2020.

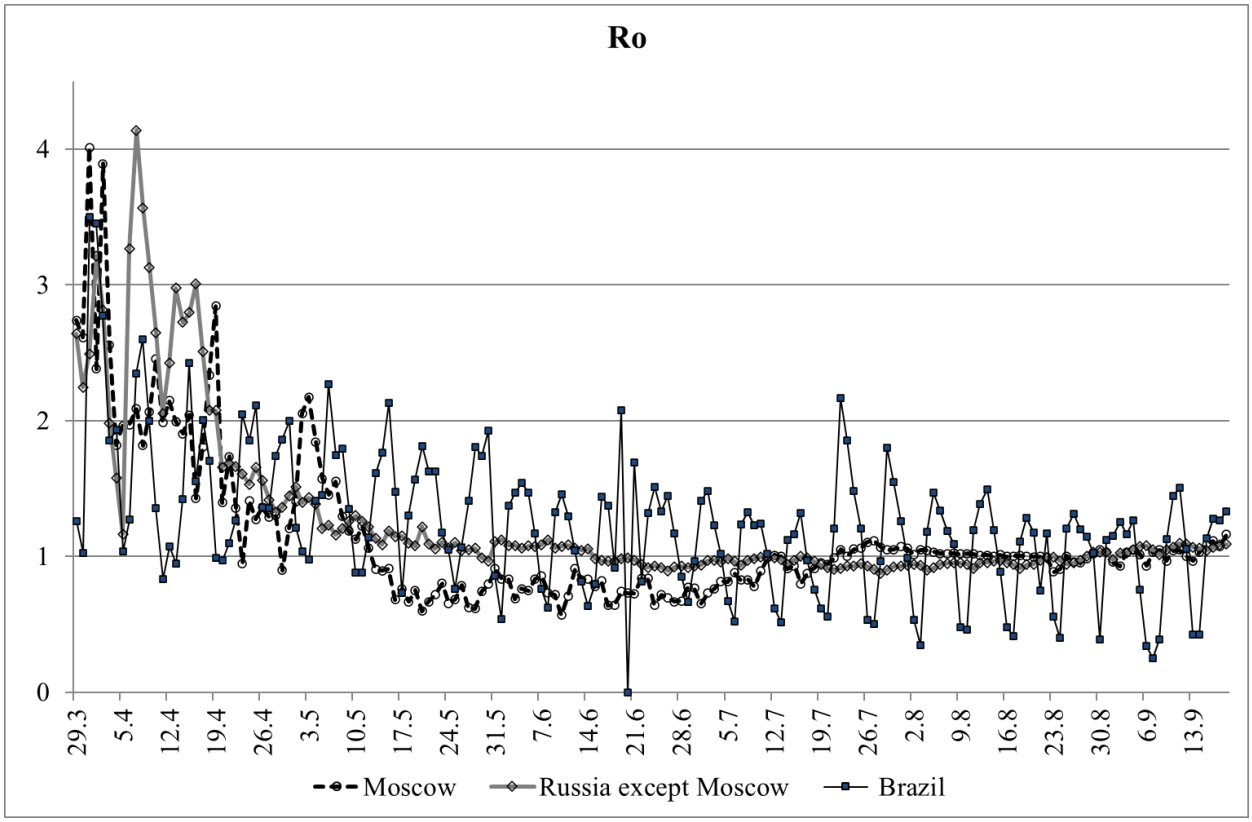

Figure 2. *Dynamics of reproductive number R_0 (average number of infected from one infected person) estimation for a given day.*

Notes: The x-axis is the date of R_0 calculation (day.month) in 2020. The y-axis is the calculated coefficient R_0 for a given day in 2020.

Table 1. *Change in contagiousness of patients (K(n) with COVID-19, depending on the time (day) elapsed since the moment of infection.*

n (day)	***K(n)***	***n*** (day)	***K(n)***
1	0	15	0.0242
2	0.142	16	0.0211
3	0.142	17	0.0179
4	0.142	18	0.0147
5	0.101	19	0.0115
6	0.0477	20	0.0083
7	0.0477	21	0.0052
8	0.0452	22	0.0045
9	0.0427	23	0.0039
10	0.0401	24	0.0032
11	0.037	25	0.0026
12	0.0338	26	0.0019
13	0.0306	27	0.0013
14	0.0274	28	0.0006

PERIÓDICO TCHÊ QUÍMICA
ARTIGO ORIGINAL

EFEITO DA TEMPERATURA E DO TEMPO NA MIGRAÇÃO DE ÍONS DE CHUMBO (PB) EM BEBIDAS DE SUCO DE LARANJA EM LATA USANDO ANÁLISE DE ESPECTROFOTOMETRIA DE ABSORÇÃO ATÔMICA

THE EFFECT OF TEMPERATURE AND TIME ON THE MIGRATION OF LEAD METAL (PB) IONS IN CANNED ORANGE JUICE DRINK USING ATOMIC ABSORPTION SPECTROPHOTOMETRY ANALYSIS

PENGARUH SUHU DAN WAKTU TERHADAP MIGRASI ION LOGAM TIMBAL (PB) PADA MINUMAN JUS JERUK KALENG MENGGUNAKAN ANALISIS SPECTROPHOTOMETRY ABSORPSI ATOM

RONI, Kiagus Ahmad[1]; ELFIDIAH, Elfidiah[1]*; PASONGKO, Ryan[2]; KHARISMA, Dian[2]; MARTINI, Sri[1]

[1] Muhammadiyah Palembang University, Faculty of Engineering, Department of Chemical Engineering, South Sumatera 30251, Palembang-Indonesia.

[2] Muhammadiyah Palembang University, Postgraduate Program Chemical Engineering Study, South Sumatera 30251, Palembang- Indonesia.

** Corresponding author*
e-mail: gemaelfidiah@yahoo.com

Received 15 December 2020; received in revised form 29 June 2021; accepted 20 July 2021

RESUMO

Introdução: A Indonésia é um país que tem um clima tropical ao longo do ano, juntamente com uma diferença de temperatura relativamente menor durante as estações seca e chuvosa. A comunidade móvel influencia o interesse das pessoas por bebidas embaladas, incluindo sucos de frutas em lata. No entanto, o primeiro obstáculo é a condição do local e a migração do metal pesado chumbo (Pb) relacionado à temperatura nas bebidas em lata de suco de laranja. **Métodos**: Este estudo enfocou a relação entre o teor de metal Pb, o tratamento de armazenamento, a temperatura de armazenamento e o tempo de armazenamento. Este estudo utilizou uma bebida de suco de laranja em lata do armazém do distribuidor da cidade de Palembang, Pb padrão $(NO_3)_2$ (Merck) em pó, soluções concentradas de HNO_3 0,5 mol / l (Merck), solução concentrada de HCl (Merck), água desmineralizada, pH do tampão 4.7 e 10. A amostra foi conduzida de 5 °C a 40 °C com o período de teste dentro de 1-30 dias. A amostra em determinados intervalos de dias seria então testada para alterar o pH e a concentração de íons Pb usando o teste de Espectrofotometria de Absorção Atômica (AAS). **Resultados e Discussão**: Neste estudo, a amostra de suco de laranja recebeu diferentes tratamentos, sendo que cada tratamento possui um código de análise diferenciado composto por S-SBJ-1-1 (Armazém do distribuidor) para um dia de armazenamento, e os códigos para 10 de tempo de armazenamento são S-SBJ-10-1 (Freezer, temperatura 5 ° C), S-SJB-10-2 (Geladeira, temperatura 20 °C), S-SJB-10-3 (Homeroom, temperatura 28 °C), S-SJB-10-4 (Forno, temperatura 40 ° C), S-SJB-10-5 (Espaço aberto, temperatura 22 °C - 38 °C). Além disso, os códigos para 30 dias de armazenamento de amostra são S-SBJ-30-1 (freezer, temperatura 5 °C), S-SJB-30-2 (refrigerador, temperatura 20 °C), S-SJB-30-3 (Casa da sala, temperatura 28 ° C, S-SJB-30-4 (Forno, temperatura 40 ° C) e S-SJB-30-5 (Espaço aberto, temperatura 22 °C - 38 °C). **Conclusões**: Temperatura e O tempo tem uma influência significativa na migração do metal pesado chumbo (Pb) da lata para as bebidas de suco de laranja e, para o valor mínimo de pH, há uma alteração menos significativa. Em geral, o suco de fruta em lata deve ser armazenado em temperatura abaixo de 28 °C, e a bebida é protegida da luz solar direta e de alta umidade..

Palavras-chave: *adsorção, latas de bebidas, tempo de armazenamento, temperatura*

DOI: 10.52571/PTQ.v18.n38.2021.12_RONI_pgs_164_175.pdf

ABSTRACT

Background: Indonesia is a country that has a tropical climate throughout the year along with relatively less difference of temperature during both dry and rainy seasons. The mobile community influences people's interest in packaged drinks, including canned fruit juice. However, the first obstacle is the condition of the place and the temperature-related heavy metal lead (Pb) migration in canned orange juice drinks. **Methods:** This study focused on the relationship between Pb metal content, storage treatment, storage temperature, and storage time. This study used a canned orange juice drink from the distributor warehouse of Palembang city, standard $Pb(NO_3)_2$ (Merck) powder, 0.5 mol/l concentrated HNO_3 solutions (Merck), concentrated HCl solution (Merck), demineralized water, Buffer pH 4.7, and 10. The sample was conducted from 5 °C to 40 °C with the testing period within 1-30 days. The sample at certain day intervals would then be tested to change pH and Pb ion concentration using the Atomic Absorption Spectrophotometry (AAS) test. **Results and Discussion:** In this study, the sample of orange juice was given different treatments, and each treatment has a differentiated analysis code consisting of S-SBJ-1-1 (Distributor warehouse) for one day of storage time, and the codes for 10 of storage time are S-SBJ-10-1 (Freezer, temperature 5 °C), S-SJB-10-2 (Refrigerator, temperature 20 °C), S-SJB-10-3 (Homeroom, temperature 28 °C), S-SJB-10-4 (Oven, temperature 40 °C), S-SJB-10-5 (Open space, temperature 22°C - 38 °C). Furthermore, codes for 30 days of sample storage are S-SBJ-30-1 (Freezer, temperature 5 °C), S-SJB-30-2 (Refrigerator, temperature 20 °C), S-SJB-30-3 (Room house, temperature 28 °C, S-SJB-30-4 (Oven, temperature 40°C), and S-SJB-30-5 (Open space, temperature 22 °C-38 °C). **Conclusions:** Temperature and time have a significant influence on the migration of the heavy metal lead (Pb) from the can to orange juice drinks, and, for the minimum pH value, there is a less significant change. Overall, canned fruit juice should be stored at a temperature below 28 °C, and the drink is protected from direct sunlight and high humidity.

Keywords: *adsorption, beverage cans, storage time, temperature*

ABSTRAK

Latar Belakang: Indonesia merupakan negara yang beriklim tropis sepanjang tahun dengan perbedaan suhu yang relatif lebih kecil baik pada musim kemarau maupun musim hujan. Komunitas mobile mempengaruhi minat masyarakat pada minuman kemasan, termasuk jus buah kalengan. Namun kendala pertama adalah kondisi tempat dan migrasi logam berat (Pb) terkait suhu pada minuman jus jeruk kaleng. **Metode**: Penelitian ini difokuskan pada hubungan antara kandungan logam Pb, perlakuan penyimpanan, suhu penyimpanan, dan waktu penyimpanan. Penelitian ini menggunakan minuman sari buah jeruk kalengan dari gudang distributor kota Palembang, serbuk standar $Pb(NO_3)_2$ (Merck), larutan HNO_3 pekat 0,5 mol/l (Merck), larutan HCl pekat (Merck), air demineral, Buffer pH 4.7, dan 10. Pengambilan sampel dilakukan dari suhu 5 °C hingga 40 °C dengan periode pengujian dalam waktu 1-30 hari. Sampel pada interval hari tertentu kemudian akan diuji perubahan pH dan konsentrasi ion Pb menggunakan uji Atomic Absorption Spectrophotometry (AAS). **Hasil dan Pembahasan**: Pada penelitian ini sampel sari buah jeruk diberi perlakuan yang berbeda, dan setiap perlakuan memiliki kode analisis yang berbeda yang terdiri dari S-SBJ-1-1 (gudang Distributor) untuk lama penyimpanan satu hari, dan kode untuk 10 lama penyimpanan adalah S-SBJ-10-1 (Freezer, suhu 5 °C), S-SJB-10-2 (Kulkas, suhu 20 °C), S-SJB-10-3 (Homeroom, suhu 28 °C), S-SJB-10-4 (Oven, suhu 40 °C), S-SJB-10-5 (Ruang terbuka, suhu 22 °C - 38 °C). Selanjutnya kode penyimpanan sampel selama 30 hari adalah S-SBJ-30-1 (Freezer, suhu 5 °C), S-SJB-30-2 (Kulkas, suhu 20 °C), S-SJB-30-3 (Ruang rumah, suhu 28 °C, S-SJB-30-4 (Oven, suhu 40 °C), dan S-SJB-30-5 (Ruang terbuka, suhu 22 °C-38 °C). **Kesimpulan**: Suhu dan Waktu memiliki pengaruh yang signifikan terhadap perpindahan logam berat timbal (Pb) dari kaleng ke minuman jus jeruk, dan untuk nilai pH minimum terjadi perubahan yang kurang signifikan. Secara keseluruhan, jus buah kalengan harus disimpan pada suhu di bawah 28 °C, dan minuman terlindung dari sinar matahari langsung dan kelembaban tinggi.

Kata kunci: *adsorpsi, kaleng minuman, lama penyimpanan, suhu*

1. INTRODUCTION:

Canned drinks and beverages are large market sectors following the market of bottled mineral water (Arif, 2020) as their price range can be considered affordable. Specifically, Indonesian consumers spend an average of 2% (percent) of their monthly income on purchasing packaged drinks (Triyono, 2013).

However, using a can as a container for a packaged drink, especially for long-term storage and longer consumption, would cause heavy metals contamination in canned orange juice drinks (St, 2011) (Paula *et al*., 2015).

Poisoning is one of the harmful effects if the can damage leading to a possible chemical reaction. This reaction would decrease the drink acidity resulting in reduction and oxidation reactions. This happens to the packaging cans that do not meet the standard requirements. The

occurrence of corrosion, a color change, and the formation of hydrogen gas can damage the can and other harmful microbiological activity. The formation of hydrogen gas (H_2) and carbon dioxide (CO2), for example, is caused by the growth of anaerobic spore-forming bacteria classified as Clostridium, including poisonous C. Botulinum. The growth of spore-forming bacteria can break down protein and produce hydrogen sulfide (H2S), so the cans would rot and turn black due to the reaction between sulfides and iron (Amin, 2015)

A can made of metal or metal alloy is definitely not an inert material. Cans that are not properly coated with an inert material (protective layer) may have some defects on their inside part, causing corrosion that can release metal elements from the can to the drink. The metal elements such as Lead (Pb), Iron (Fe), Tin (Sn), Cadmium (Cd), and Zinc (Zn) will negatively affect human health. The presence of these metals, even in small amounts, will still endanger the health of people who get long metal exposure (Sugiastuti *et al*., 2006, Martini *et al*., 2020, Roslinda *et al*., 2013).

Lead (Pb) is included in the metal group IV-A on the periodic table of chemical elements, with atomic number (NA) 82 and atomic weight (BA) 207.2. Lead (Pb) can cause chronic and acute poisoning effects (Ian Tanu, 2016). The exposure threshold for lead and lead arsenate in the air is 0.15 mg per cubic meter. Meanwhile, the exposure limit for tetramethyl lead and tetraethyl lead is 0.07 mg per cubic meter, and the threshold for lead content in food is 2.56 mg/kg (Sartono, 2012) (Nasution, 2011).

Therefore, metal corrosion should be included as an essential factor for selecting the type of can for food and drink packaging. Several aspects affecting corrosion in the inner cans are the level of remaining oxygen in the food, the presence of corrosion accelerating agents such as nitrates and other sulfur compounds, drinks pH, temperature and storage time, and material components of cans presence of corrosion-resistant coating substances.

In addition, other factors can cause detrimental effects of consuming damaged packaging cans, such as incomplete beverage processing and storage time, which significantly affect the migration of lead metal from the can to the drink. In terms of storage time, it is known that the longer the storage time, the longer the contact time between the metal and the drinks (Irawan, 2013). Following this matter, orange juice with a relatively higher acidity level and contains oxidizing agents can cause corrosion in the cans. Thus, the migration of lead (Pb) will occur (Yusrizal, 2015)

Heavy metals in the sample can be detected and measured using the wet digestion method by applying a mixture of HNO_3 and H_2O_2. It is then further identified by atomic absorption spectrophotometric instrument (AAS), Kharisma, 2006). AAS instrument has high sensitivity and selectivity levels, therefore, it is reliable to analyse metal with the ability to detect around 62 different metal elements (Suryati, 2011).

AAS can analyze quantitatively based on the absorbance measurement of sample solution. The amount of elemental content analyzed in the sample solution is calculated based on the standard graph or calibration curve. Based on Beer's law, there is a linear relationship between absorbance and the concentration of elements present in the solution (Skoog, 2004).

In this work, the main objective is to measure the influence of temperature (place of storage) and time (shelf life) of drink cans on the corrosion phenomenon, along with the possible migration of heavy metals (Pb) from the can to the drink.

2. MATERIALS AND METHODS:

This research was conducted in the laboratory of PT. Sucofindo Palembang Branch, Indonesia. This study used canned orange juice drink from the distributor warehouse of Palembang city, standard $Pb(NO_3)_2$ (Merck) powder, 0.5 mol/l concentrated HNO_3 solutions (Merck), concentrated HCl solution (Merck), demineralized water, buffer solution pH 4.7, and 10.

The sample was carried out at a temperature range of 5 °C to 40 °C with a length of time for testing 1-30 days. The sample at certain day intervals would be tested for the changes of pH and Pb ions levels using the AAS test.

Quantitative analysis of lead was carried out using an AAS analyzer with a graphite furnace. Around 20 µL of the concentrated sample, obtained from the acid process by reflux, is injected into the graphite cells. Previously, the optimal pyrolysis temperature (500 to 800 ºC) and atomization (1000 to 1700 ºC) were determined and programmed into the graphite furnace. Drying (100 ºC) and cleaning (2500 ºC) temperatures are programmed according to the instructions in the previous report. The technique used is a normal electrographic cell (Thermo Elemental Solaar) with argon flowing at a speed of 0.2 L / min and a

gap of 0.5 nm. Lead concentration was determined by constructing a calibration curve with lead concentrations ranging from 2.0 to 7.0 µg/L and reading the maximum absorbance at a wavelength of 216.9 nm. This dilution was prepared from a stock solution in 0.2% HNO_3 in a 5 mL volumetric flask. All samples were measured in triplicate, and the mean values were expressed as µgPb/Kg. (Rada-Mendoza *et al*., 2018)

The wavelength used in the analysis was 283.3 nm. Lead has the energy of 7.0134.10-8 Joule. This can cause the Pb atom to be in the ground state (Pb o) and excited to a higher energy level (Pb *). The acetylene-air flow rates used as burner and oxide for Pb metal were 2.0 L / min and 10.0 L / min. Pb standard solution is made from Pb E-Merck 1000 ppm stock solution. This standard solution was diluted to 10 ppm. It was then separately diluted again into a series of standard solutions having a concentration of 0.5; 1; 2; 3, and 4 ppm. Dilution was carried out with 0.5M HNO3 because the matrix in the standard solution must be the same as the matrix in the sample. The measurement of the absorbance of the standard solution was conducted using the AAS tool. The absorbance showed the sample's ability to absorb electromagnetic radiation at its maximum wavelength. The calibration curve of the Pb metal standard solution can be seen in the absorbance measurement of the standard solution using the AAS instrument. (Dewi, 2013).

Furthermore, the analytical validation for the lead standard curve can be stated as follows:

- The linearity of the lead standard curve (Pb) is 0.9999, meaning that ± 99% change in absorbance is influenced by changes in lead concentration (Pb), while other factors are ± 1%.

- The standard Pb curve can determine the smallest limit of an analyte based on the calculations in the appendix is LOD = 0.028 ppm and LOQ = 0.0933 ppm

- The sensitivity of the standard Pb curve is 0.00757. This value indicates that every unit change in concentration will result in a change in absorbance of 0.00757

- The accuracy values of the standard lead (Pb) curve expressed in % recovery are 91.4% for 0.5 ppm; 99.9% for 1 ppm; 98% for 2 ppm; 101.3% for 3 ppm and 99.75% for 4 ppm. Priyambodo (2011) stated that the requirement for accuracy is the percent recovery within the range of 98-102%.

- This work obtained 2.74% of precision. As the coefficient of variation for the standard lead curve (Pb) is below 5%, it can be stated that the standard curve precision has been reached as it is sensitive for analyzing lead metal (Pb). (Dewi, 2013)

The column method used in analyzing lead (Pb) was generally carried out by utilizing a 500 mL lead solution with a concentration range of 0.5-100 mg of lead used as an aliquot. Adjusting the pH of the aliquot to 9.6 was done by adding a buffer solution and then diluting it to 20 mL with distillate water. The column used was filled with PAN-naphthalene as the adsorbent, which then adjusted the acidity level to pH 9.5 by adding a 2 to 3 mL buffer solution. Aliquots were then streamed through the column at a rate of 1 mL/min. The solid metal adsorbed into the naphthalene was then dissolved with 5 mL of dimethylformamide (DMF). The analyzed sample was flown into the fire with acetylene-air fuel with a wavelength of 217.0 nm. The same treatment was carried out for reagent blanks in order to obtain a calibration chart (Taher, 2003)

Measurement of Pb level was started by measuring the standard solution. Measurements were initiated by the standard solution with the smallest concentration, then continued until the highest concentration, followed by measuring sample absorption. The sample absorption obtained was entered into the calibration curve equation in order to obtain the sample content. Measurements were made using the AAS method with the provisions of the wavelength of 283.3 nm, gas speed (acetylene) 2 L / minute, oxidant speed (air) of 15 L / minute, and burner height of 7mm. This wavelength is the most powerful wavelength absorbing the line for the electronic transition from the ground level to the excitation level. When atoms in the ground state are given the appropriate energy, it then would be absorbed, and the atoms would be excited to a higher energy level (excited state).

In contrast, unstable atoms would return to the basic energy level by releasing a certain amount of energy. The optimum wavelength of energy in the form of light for Lead (Pb) is 283.3 nm (Shimadzu, 2007; Perdana, 2019). The research flowchart of this work is displayed in figure 6.

3. RESULTS AND DISCUSSION:

3.1. Results

This study used a sample of orange juice with different treatments, and each treatment has a differentiated analysis code consisting of S-SBJ-1-1 (Distributor warehouse) for one day storage

time, for a storage time of 10 days with the code S-SBJ-10-1 (Freezer, temperature 5 °C), S-SJB-10-2 (Refrigerator, temperature 20°C), S-SJB-10-3 (Homeroom, temperature 28 °C), S-SJB-10-4 (Oven, temperature 40 °C), S-SJB-10-5 (Open space, temperature 22°C to 38 °C). For sample storage for 30 days, the codes are S-SBJ-30-1 (Freezer, temperature 5 °C), S-SJB-30-2 (Refrigerator, temperature 20 °C), S-SJB-30-3 (Room house, temperature 28 °C, S-SJB-30-4 (Oven, temperature 40 °C), S-SJB-30-5 (Open space, temperature 22°C to 38 °C). The analysis results of orange juice samples cans can be seen as follows:

For sample 1, 2, 3, and 4, the ABS values were 0.00074; 0.000725 , 0,000763 ,0,000801 , respectively. Then 0,001528 for sample 5; 0,000897 for sample 6; 0,000782 for sample 7; 0,000801 for sample 8; 0,000897 for sample 9; 0,002751 for sample 10; and for ABS sample 11 of 0,002751. Based on Indonesia government regulation, the maximum limit of Pb metal in 1 kg of fruit drink is 0.1 mg.

3.2. Discussion

Based on the measurement, it is known that the temperature can cause the migration of lead metal from the can to the drink. The release of lead metal can also be affected by the duration of storage. The longer the food is stored, the longer the contact time between the food and the tin packaging leading to higher possibility of metal migration from the can to the drink (Perdana, 2019)

In Figure 8, it is known that the treatment of the sample influences the pH value in the sample. The initial sample with code S-SBJ-1-1 has a pH value of 2.930; the sample with code S-SBJ-10-1 is 2.934. In this case, the increase in pH is 0.004. Furthermore, the pH of the orange juice sample S-SBJ-10- 2 is 2,932 and represents a 0.002 increase from the baseline sample. Sample S-SBJ-10-3 is a 2,935. Comparing the pH value of the sample S-SBJ-10-3 with the initial sample, there is an increase of 0.005. Sample S-SBJ-10-5 is 2,932; comparing its pH value with the initial sample, there is an increase of 0.002. Sample S-SBJ-30-1 is 2,946. Compared to the initial sample, the increase is 0.016. The sample S-SBJ-30-2 is 2.953, the increase from the initial sample is 0.023. Moreover, sample pH with code S-SBJ-30-3 is 2.965. sample S-SBJ-30-4 is 2.974.

In comparison with the initial sample, there is an increase of 0.044. Finally, the sample S-SBJ-30-5 is 2,982. Comparing the pH value of the initial sample, there is an increase of 0.052. Therefore, the difference in the pH value per sample depends on the treatment of the sample, which is influenced by temperature and time.

4. CONCLUSIONS:

Based on the experimental data, parameters such as temperature and storage time influence the heavy metal lead (Pb) migration from the can container to contained orange juice drinks. In addition, the proper storage area for canned drinks is below 28 ^{o}C. It also should avoid direct sunlight and high humidity. In the storage, canned drinks should not be stored at temperatures above 38°C with continuous exposure due to the high migration of lead metal (Pb) as it is harmful to the drink quality. Overall, there is an insignificant change in the pH value among the measured samples.

6. REFERENCES:

1. A Andrieti, R. (2018). Migration of Food Packaging. Posted by admin news article Center for Chemistry and Packaging, Jakarta.
2. Amin, M. (2015). Penentuan Kadar Logam Timbal (Pb) dalam Minuman Ringan Berkarbonasi Menggunakan Destruksi Basah Secara Spektroskopi Serapan Atom. Skripsi Fakultas Sains Dan Teknologi Universitas Islam Negri Malang, 1–100.
3. Azmi, Y. (2015). Atomic Absorption Spectrophotometer Analysis with Instrumentation in Engineering. www.slideshare.net. Discover, Share, and Present presentations and infographics with the world's largest professional content sharing community.
4. BPOM (Regulation of the Food and Drug Supervisory Agency) No. 05 of. (2018). Concerning the Maximum Limit of Heavy Metal Contamination in Processed Food. National Agency of Drug and Food Control Republic of Indonesia.
5. Dewi, D. C. (2013). DETERMINASI KADAR LOGAM TIMBAL (Pb) DALAM MAKANAN KALENG MENGGUNAKAN DESTRUKSI BASAH DAN DESTRUKSI KERING. Alchemy, 2(1).

https://doi.org/10.18860/al.v0i0.2299
6. Djalil, S. H., Saifuddin, Zakaria. (2011). Analysis of lead metal content in street food at SDN Aprilia, B, A Semarang. Skripsi Diponegoro University, Semarang, Central Java.
7. Dong, Z., Lu, L., Liu, Z., Tang, Y., & Wang, J. (2014). migration of toxic metals from ceramic food packaging materials into acid food Simulants. Mathematical Problems in Engineering, 2014(May). https://doi.org/10.1155/2014/759018
8. Irawan, S., Guntarti, S. (2013). Characterization of the Migration of Packaging and Polymer-Based Household Appliances. Center for Chemical and Packaging, Ministry of Industry, Republic of Indonesia, Jakarta.
9. Kharisma, W. L. (2006). Analysis of Pb, Cu, and Cd metal contamination in canned pineapple at different expiration limits by atomic absorption spectophotometry. Faculty of Pharmacy Pancasila University, Jakarta.
10. Kiki., Agus., Yulianti, K., Hanggita, S. (2012). Analysis of Heavy Metal Content. Sriwijaya University Palembang, Indonesia.
11. Nasution, S. B. (2011). Penentuan kadar timbal pada manisan buah yang berkemasan kaleng.
12. Paula, F. J. A., Guiné, R. P. F., Lopes, L. C., Duarte, A. C., Fragata, A. O. S., & Reis, M. A. L. (2015). Effects of pre-and-post-parvest factors on the selected elements contents in fruit juices. Czech Journal of Food Sciences, 33(4), 384–391. https://doi.org/10.17221/531/2014-CJFS
13. Perdana, W. W. (2019). Analisis Logam Berat Di Kemasan Kaleng. Agroscience (Agsci), 9(2), 215. https://doi.org/10.35194/agsci.v9i2.785
14. Pratiwi, R., Tristi, J., Saputri, F.A. (2018). [Review] Lead Contamination in Various Types of Food and Beverages, (7). Department of Pharmaceutical Analysis and Medicinal Chemistry, Faculty of Pharmacy, Padjadjaran, West Java, Indonesia.
15. Putra, A., Reviewed by dr. Utari, R. (2020). Variety of Orange Contents that Are Always Faithful to Make Your Body Healthy. http://www.sehatq.com.
16. Pridjosoesilo, T. (2017). Soft Drink Industry, Still Prospective, Despite Slowing Growth. Marcomm - news trend Posted by Marina Silalahi. BPS data source (2013). Central Bureau of Statistics Government Body in Jakarta, Indonesia.
17. Rada-Mendoza, M. D. P., Villamiel-Guerra, M. del M., Hoyos-Saavedra, O. L., & Alvira, L. F. (2018). Quantification of lead using atomic absorption spectrometry in thermoformed and biodegradable flexible films made from cassava (Manihot esculenta crantz). DYNA (Colombia), 85(207), 236–242. https://doi.org/10.15446/dyna.v85n207.72347
18. Roslinda, R., Humairah, & Zulharmitta. (2013). Analisis Kadmium (Cd), Seng (Zn) dan Timbal (Pb) pada Susu Kental Manis Kemasan Kaleng secara Spektrofotometri Serapan Atom (SSA). Jurnal Farmasi Higea, 5(1), 62–71.
19. Roni, K. A., Mufrodi, Z., Mustakim, I. (2020). The Production of Liquid Fuel from Plastic wastes by Using Waste Garbage Power Plant: Study on the Effect of Electric Load and Fuel / Gasoline to Solar Ratio. Jurnal Bahan Alam Terbarukan, UNNES, Semarang, Indonesia.
20. Suryati. (2011). Analysis of heavy metal content of Pb and Cu using the Atomic Absorption Spectophotometry (SSA) method on baung fish. Sultan Syarif Islamic State University, Pekanbaru Riau. Indonesia.
21. Martini, S., Afroze, S., Roni, K.A. (2020). Modified eucalyptus bark as a sorbent for simultaneous removal of COD, oil, and Cr(III) from industrial wastewater. Alexandria Engineering Journal. 59: 1637-1648.
22. Skoog, Douglas, A. (2004). Fundamentals of analytical chemistry. South Melbourne: Brooks / Cole.
23. Taher, M. A. (2003). Flame atomic absorption spectrometric determination of trace lead after solid-liquid extraction and preconcentration using 1-(2-pyridylazo)-2-naphthol. Croatica Chemica Acta, 76(3), 273–277.

7. OPEN ACCESS

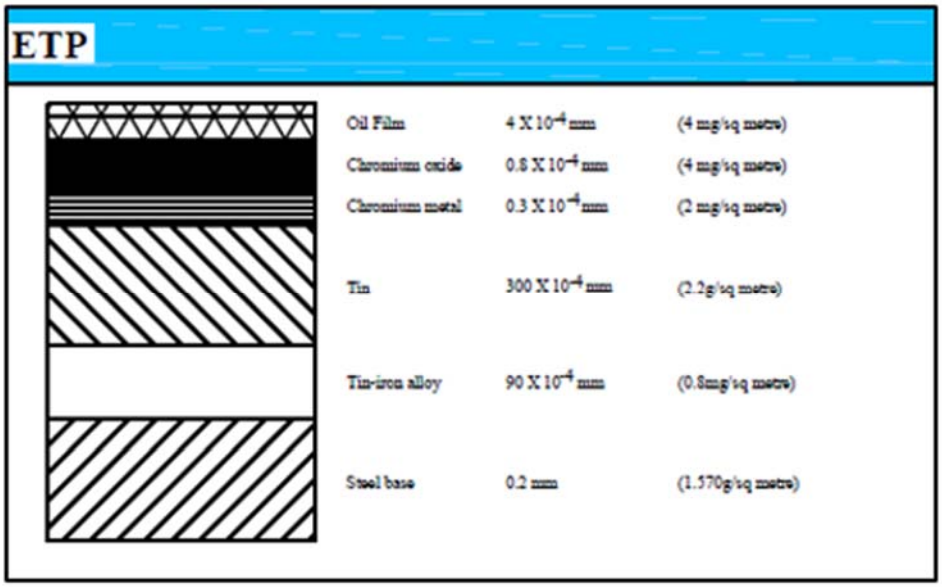

Figure 1. the layer arrangement of the electrolytic tin plate type packaging

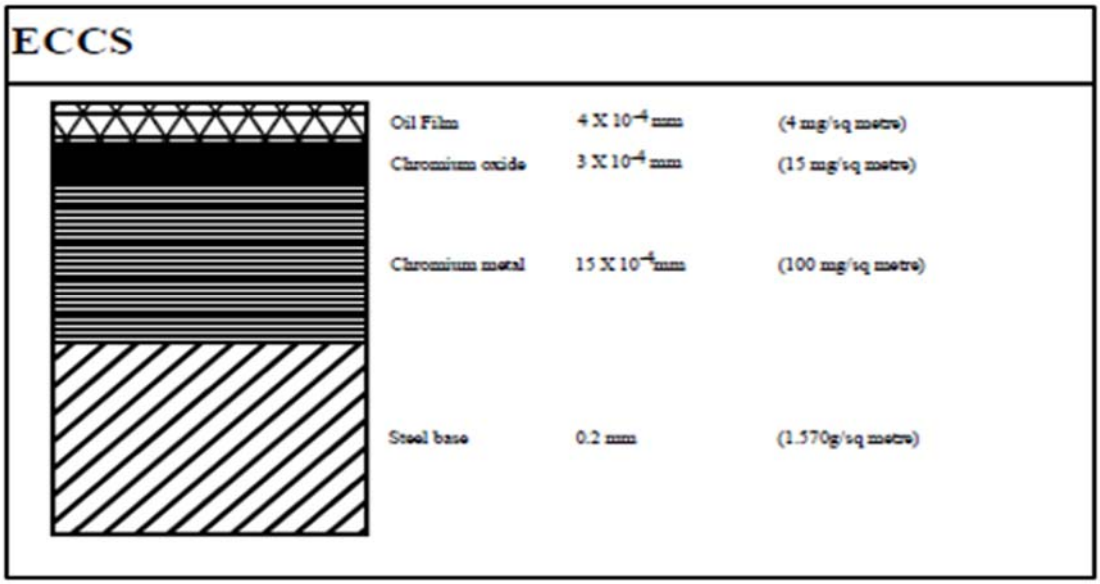

Figure 2. The layer arrangement of the electrolytic chromium-coated steel cans

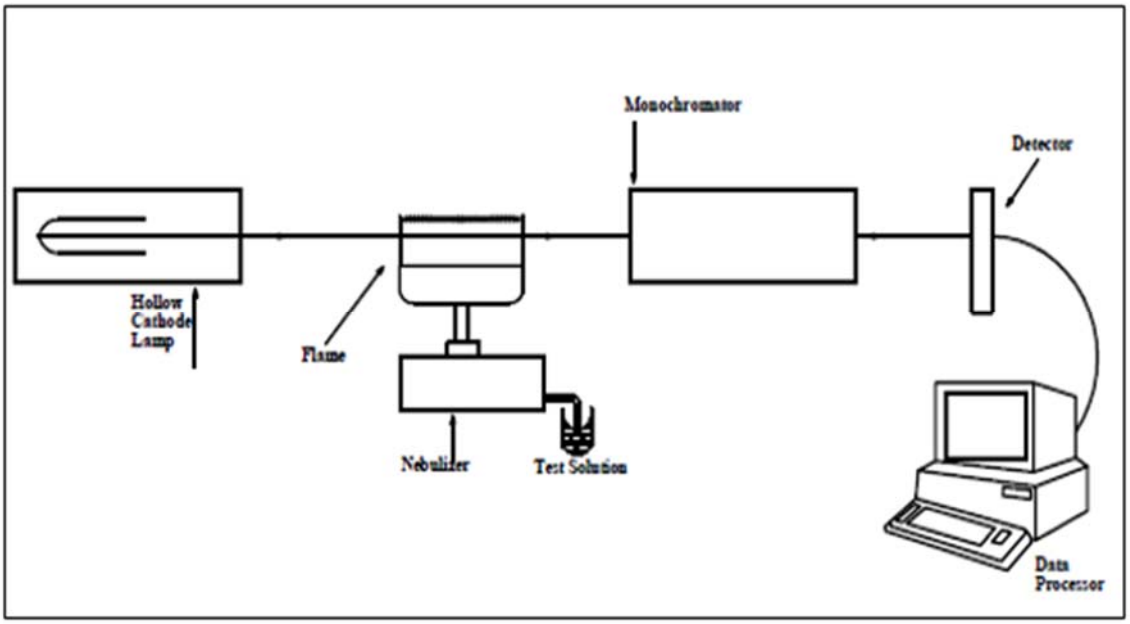

Figure 3. *Schematic Diagram Atomic Absorption Spectrophotometry*

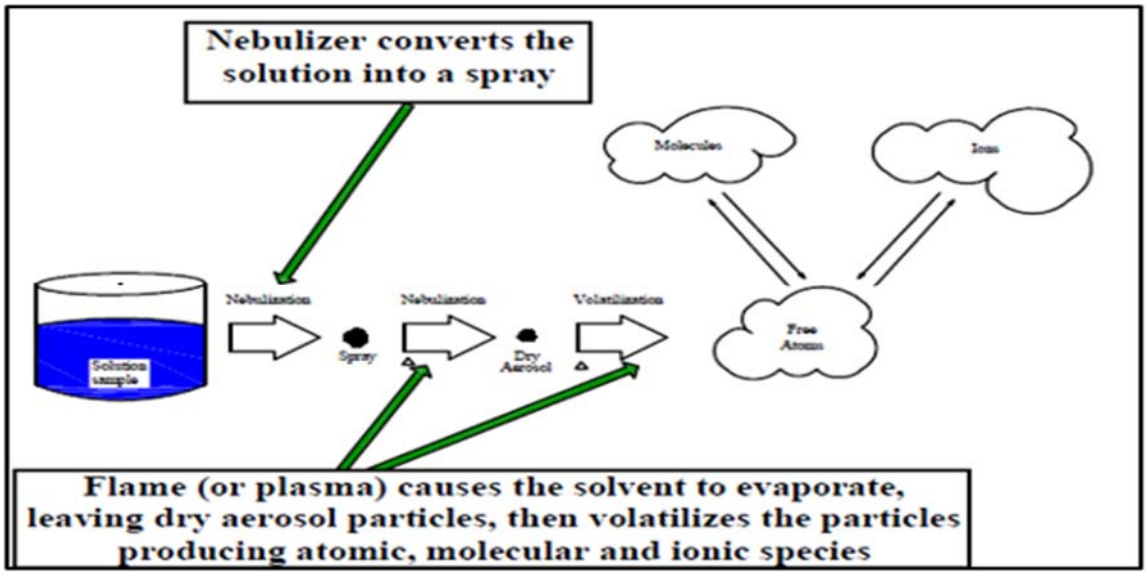

Figure 4. *Atomic Spectroscopy*

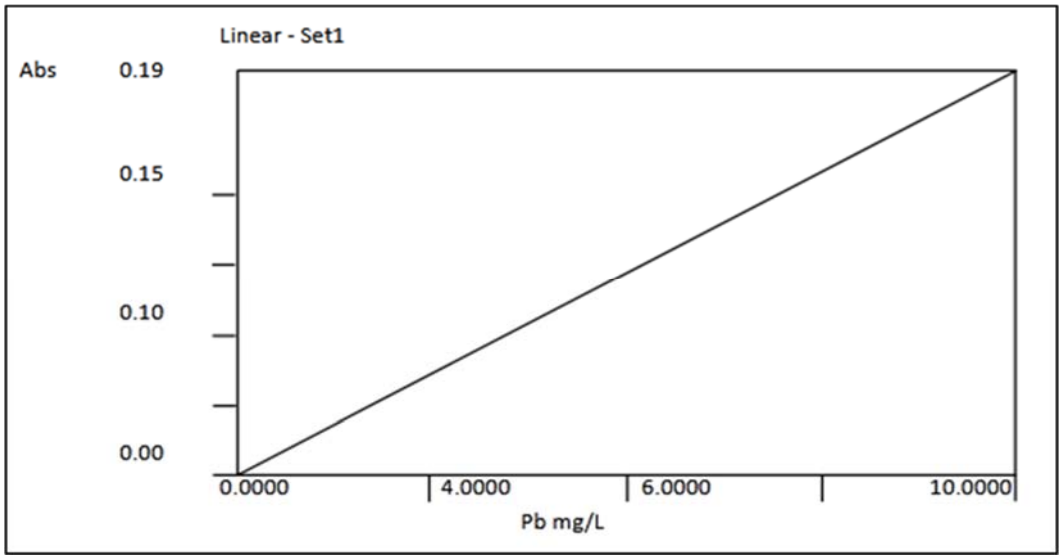

Figure 5. *Lead (Pb) Validation standard curve graph*

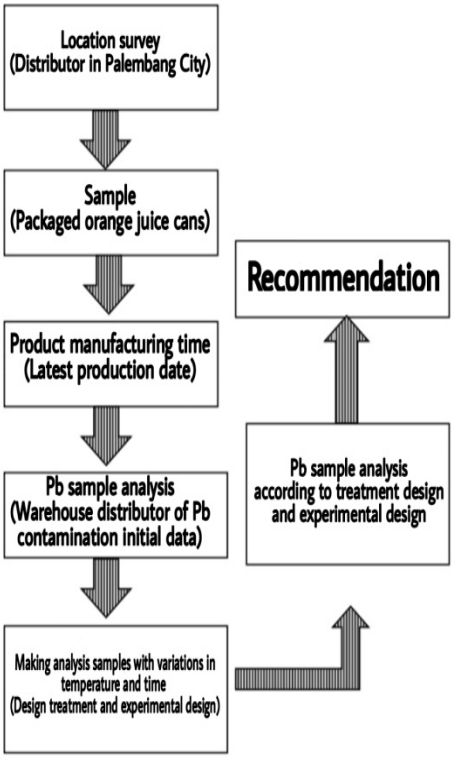

Figure 6. *Research Flowchart*

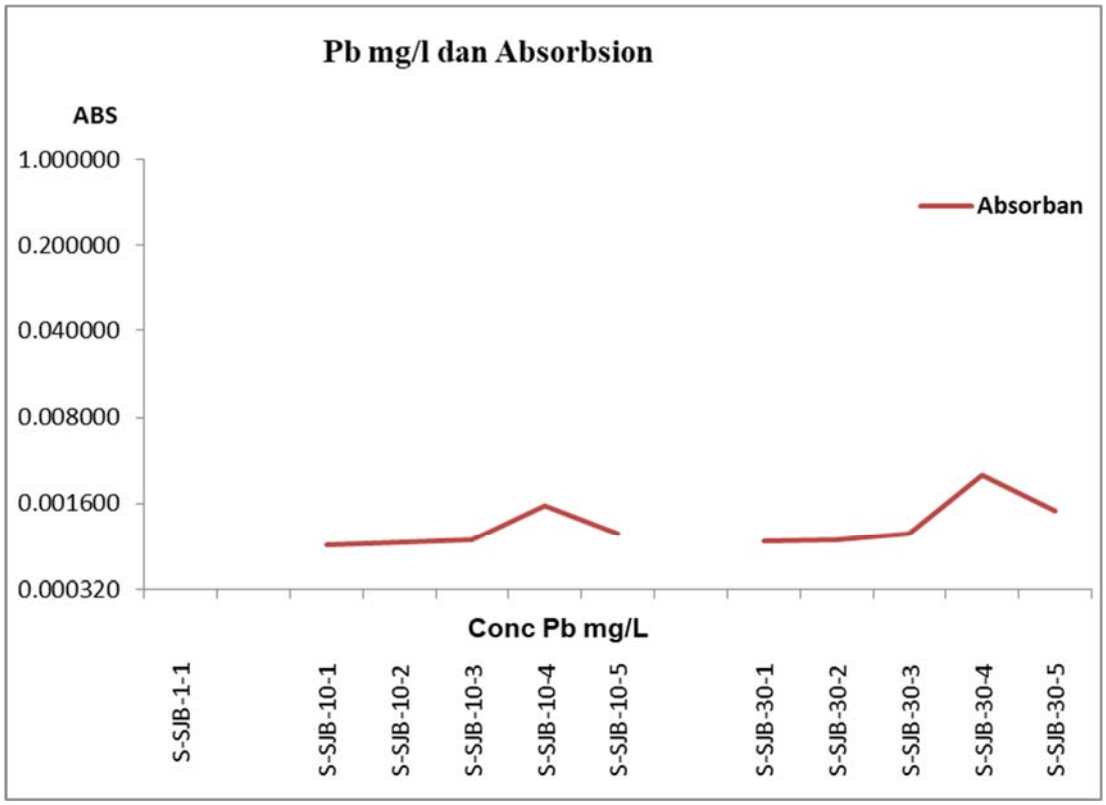

***Figure 7**. The concentration of Pb to Absorption*

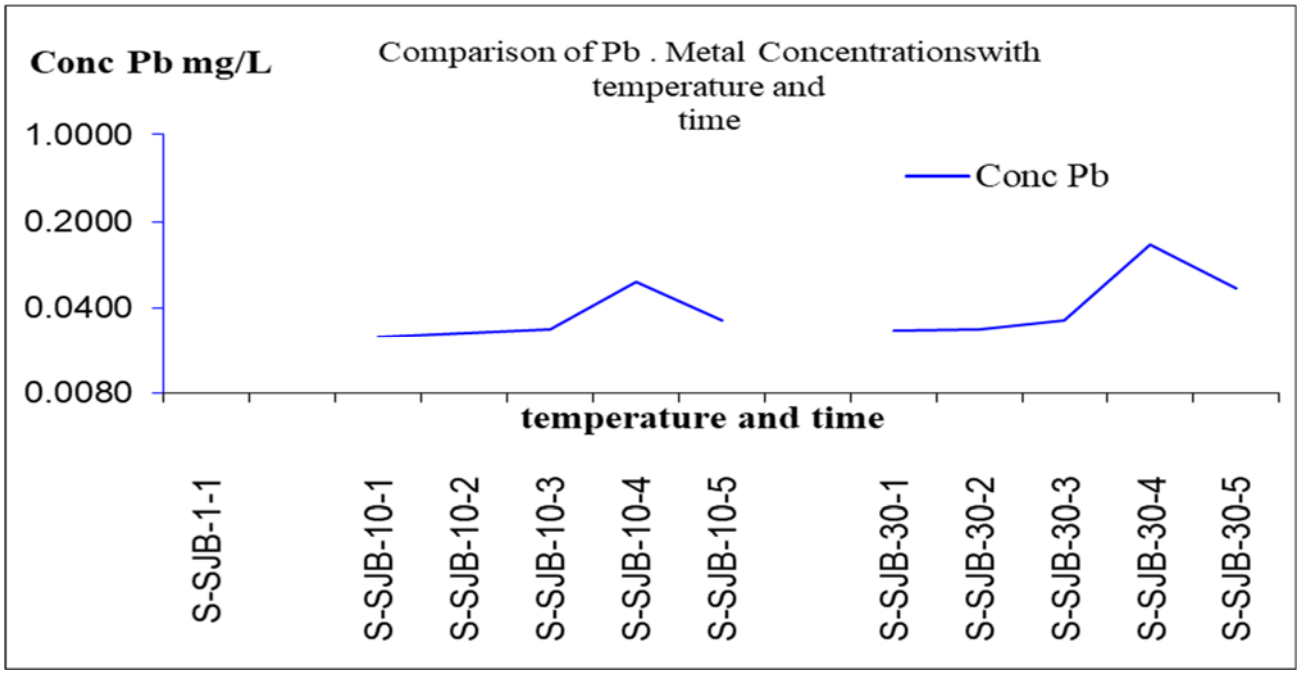

***Figure 8.** Effect of temperature and time on Pb concentration in the sample*

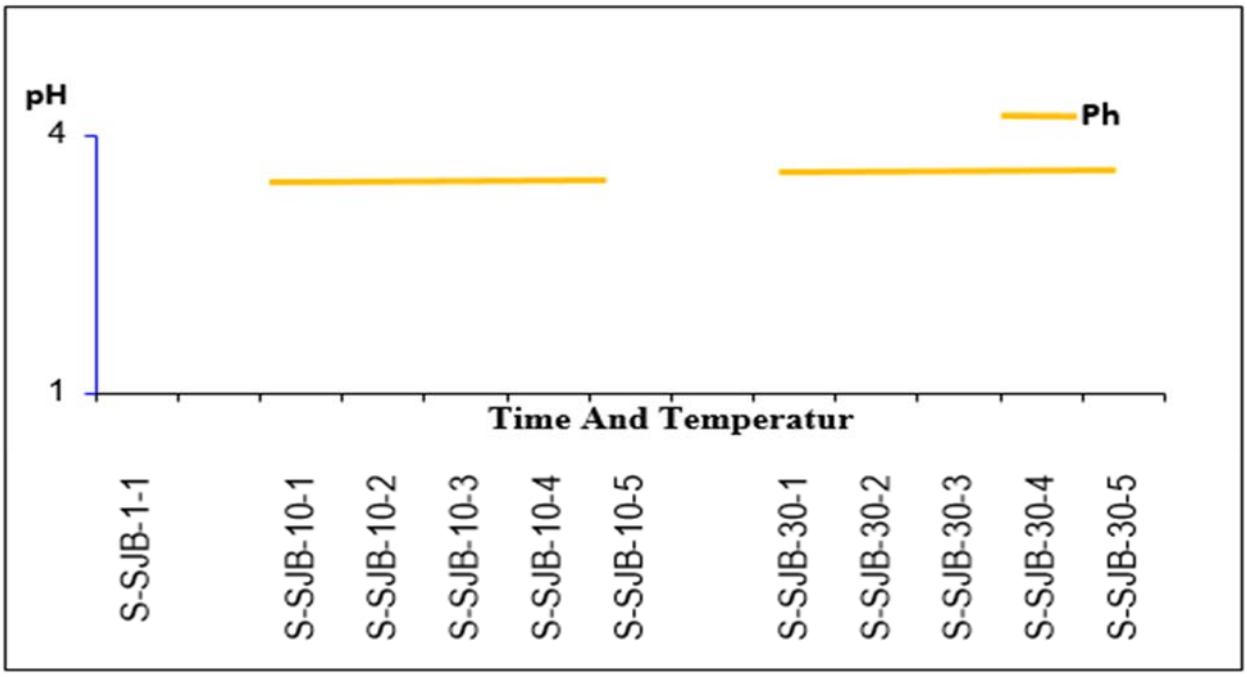

Figure 9. *Sample pH Analysis Results*

PERIÓDICO TCHÊ QUÍMICA
ARTIGO ORIGINAL

AVALIAÇÃO DOS CONHECIMENTOS, ATITUDES E PRÁTICAS DE GESTANTES EM SAÚDE PERIODONTAL E SAÚDE BUCAL E SEUS EFEITOS NO FETO DURANTE A GRAVIDEZ

INVESTIGATING THE KNOWLEDGE, ATTITUDE, AND PRACTICE OF PREGNANT WOMEN ABOUT PERIODONTAL HEALTH AND ORAL HEALTH, AND THEIR EFFECT ON THE FETUS DURING PREGNANCY

بررسی آگاهی، نگرش و عملکرد خانم‌های باردار در مورد سلامت پریودنتال و بهداشت دهان و دندان و تاثیر آن‌ها بر روی جنین در دوران بارداری

MOHAMADIMOGHADAM, Marzieh[1]; SHAKIB Seyed Hojat[2*]; SALMANI Fatemeh[3]

[1] Birjand university of medical sciences, School of Dentistry, Department of Periodontics, Iran

[2] Birjand university of medical sciences, Faculty of Dentistry, Department of Orthodontics, Iran

[3] Birjand University of Medical Sciences, Faculty of Health, Department of Epidemiology and Biostatistics, Iran

** Corresponding author*
e-mail: drmohamadi@gmail.com

Received 09 February 2021; received in revised form 24 June 2021; accepted 20 July 2021

RESUMO

Introdução: A periodontite ou piorréia leva a resultados adversos da gravidez, como parto pré-termo, baixo peso ao nascer, pré-eclâmpsia, aborto espontâneo ou perda precoce da gravidez. **Objetivo:** O objetivo deste estudo foi avaliar o conhecimento, atitude e prática de gestantes no campo da saúde periodontal e saúde bucal e seu impacto no feto. **Métodos:** O presente estudo é um estudo descritivo-analítico com 210 gestantes no primeiro e segundo trimestre de encaminhamento para os centros de saúde Birjand em 2019. O instrumento utilizado neste estudo foi um questionário de pesquisa composto por quatro seções: informações demográficas das mulheres, consciência das mulheres , atitude e prática, sua validade e confiabilidade foram confirmadas. Após a coleta de dados, os dados foram digitados no software SPSS versão 22 e, em seguida, analisados por meio de estatística descritiva, teste t de student independente e análise de variância unilateral. O Significância estatística foi considerado 0.05 em todos os testes. **Resultados e Discussão:** Neste estudo, os escores médios de conhecimento, atitude e prática das gestantes foram 5,6 ± 1,92, 55,9 ± 5,1 e 25,9 ± 3,7, respectivamente. Houve uma diferença significativa entre o escore médio de atitude e a idade das mães. Também houve diferença significativa entre os escores médios de conhecimento, atitude e prática das mulheres e conhecimento, atitude e prática de gestantes empregadas e donas de casa; Em termos de prática, houve uma diferença significativa entre donas de casa grávidas e mulheres trabalhadoras. Houve uma relação significativa entre a média desses escores e o emprego das mães, de modo que os escores médios foram maiores nas mulheres ocupadas do que nas demais. **Conclusões:** Os resultados do nosso estudo mostraram que o escore médio de conhecimento, atitude e prática das gestantes em Birjand na área de saúde bucal durante a gravidez não é desejável e adequado.

***Palavras-chave**: Conhecimento; Atitude; Prática; Mulheres grávidas*

ABSTRACT

Background: Periodontal infection leads to adverse pregnancy outcomes such as preterm delivery, low birth weight, preeclampsia, miscarriage, or early pregnancy loss. **Aim:** The aim of this study was to investigate the knowledge, attitude, and practice of pregnant women about periodontal health and oral health and their effect on the fetus. **Methods:** The present study is a descriptive-analytical study on 210 pregnant women in the first and second trimesters referring to health centers in Birjand in 2019. The tool used in this study was a researcher-made questionnaire with four parts: women's demographic information, and women's knowledge, attitude, and practice, the validity, and reliability of which were confirmed. After data collection, it was entered into SPSS software version 22 and then analyzed using descriptive statistics, independent t-test, and one-way analysis of

DOI: 10.52571/PTQ.v18.n38.2021.13_MOHAMADIMOGHADAM _pgs_176_187.pdf

variance. The significance level was considered 0.05 in all tests. **Results and Discussion**: In this study, the mean scores of knowledge, attitude, and practice of pregnant women were 5.6 ±1.92, 55.9 ± 5.1, and 25.9± 3.7, respectively. There was a significant difference between the mean attitude score and mothers' age. There was also a significant difference between the mean scores of knowledge, attitude, and practice of women and significant difference in knowledge, attitude, and practice of employee and housewife pregnant women; In terms practice, there were significant differences between pregnant housewives and self-employed women. There was a significant relationship between the mean of these scores and mothers' jobs so that the mean scores were higher in employed women than others. **Conclusions:** The results of our study showed that the average score of knowledge, attitude, and practice of pregnant women in Birjand regarding oral hygiene during pregnancy is not satisfactory and appropriate.

***Keywords**: Knowledge; Attitude; Practice, Pregnant Women*

چکیده

مقدمه: عفونت پریودنتال منجر به پیامدهای نامطلوب بارداری مانند زایمان زودرس ،نوزادادن کم وزن ، پره اکلامپسی ، سقط جنین و یا ازدست دادن بارداری در اوایل بارداری می شود. **هدف:** هدف از این بررسی آگاهی، نگرش و عملکرد خانم‌های باردار در مورد سلامت پریودنتال و بهداشت دهان و دندان و تاثیر آن‌ها بر روی جنین می باشد. **روش کار:** در یک مطالعه توصیفی تحلیلی 210 زن باردار مراجعه کننده به مراکز بهداشت در سه ماهه اول و دوم در شهرستان بیرجند در سال 1398 مورد بررسی قرار گرفتند. ابزار جمع آوری داده پرسش‌نامه محقق ساخته بود که دارای چهار قسمت: اطلاعات دموگرافیک زنان، آگاهی، نگرش و عملکرد مادران بود. داده‌ها پس از جمع‌آوری وارد نرم‌افزار SPSS نسخه 22 گردید و سپس داده‌های توصیفی بوسیله آمارهای توصیفی، و داده های تحلیلی با آزمون آنالیز واریانس و تی مستقل تجزیه و تحلیل شد. **نتایج و بحث:** در این مطالعه میانگین نمره آگاهی، نگرش و عملکرد زنان باردار بترتیب 1/92 ± 5/6، 5/1 ± 55/9 و 3/7 ± 25/9 بود. بین میانگین نمره نگرش با سن مادران اختلاف معناداری مشاهده شد (P<0.05). همچنین بین میانگین نمره آگاهی، نگرش، عملکرد زنان اختلاف معناداری وجود داشت (P<0.05).همچنین تفاوت معنی داری در آگاهی (p=0.05) و نگرش (p<0.001) و عملکرد (p=0.04) خانم های باردار کارمند و خانه دار وجود داشت؛ از نظر عملکرد نیزخانم های باردار خانه دار و خانم های دارای کار آزاد تفاوت معنی داری با هم داشتند (p<0.001). بین میانگین این نمرات و شغل مادران ارتباط معناداری مشاهده شد بطوریکه میانگین نمرات در زنان شاغل بیشتر از سایر زنان بود (p<0.05). **نتیجه گیری:** نتایج مطالعه ما نشان داد که میانگین نمره آگاهی، نگرش و عملکرد زنان باردار شهرستان بیرجند در خصوص رعایت بهداشت دهان و دندان در دوران بارداری رضایت بخش و مناسب نیست.

***واژه های کلیدی:** آگاهی؛ نگرش؛ عملکرد، زنان باردار*

1. INTRODUCTION:

Pregnancy is an important period in the life of women with various physiological changes that may occur in the body, and these changes may have a negative impact on oral health (Ambereen, Babu, Vivekananda, and Shivaprasad). Emphasis on oral health care during pregnancy has been used as an important public health issue worldwide (Gambhir, Nirola, Gupta, Sekhon, and Anand, 2015).

During pregnancy, changes in hormone levels, such as increased levels of progesterone in the bloodstream, along with poor oral hygiene, increase the incidence of oral diseases such as periodontitis, which is accompanied by redness, inflammation, and a tendency to bleed (Haririan, Mohammadpour, and Aghajanloo, 2010). Approximately 30% of women develop periodontitis during pregnancy (Lee, McWilliams, and Janchar, 1999).

Periodontal disease is an inflammatory reaction in periodontal tissues, which leads to tissue destruction, bone loss, and eventual tooth loss (Atarbashi Moghadam, Haerian Ardakani, Rashidi Meybodi, and Khabazian, 2014). Many studies have reported that the oral health needs of pregnant women are quite different from the general population (Giglio, Lanni, Laskin, and Giglio, 2009; Lee *et al*., 1999; Mills and Moses, 2002). Pregnant women pay less attention to their health due to certain conditions, strong appetite, mood swings, and mental health conditions (Mehdipoor *et al*., 2019). The American Academy of Periodontology recommends that periodontal examinations and appropriate treatment be performed for pregnant women and women planning to become pregnant (Tarannum, Prasad, Vivekananda, Jayanthi, and Faizuddin, 2013). The periodontal infection leads to adverse pregnancy outcomes such as preterm delivery, low birth weight infants, preeclampsia, miscarriage, or early pregnancy loss (Govindasamy *et al*., 2018).

Some researchers have suggested that the cause of this problem is a severe generalized inflammatory condition inside the arteries. Likewise, during childbirth, women with severe periodontal disease were at higher risk for developing preeclampsia (Brockington, 2003; Haririan *et al*., 2010). General nonspecific inflammatory mediators of periodontal disease are those that play an important role in initiating labor. In a normal delivery, labor occurs when the levels of inflammatory cytokines such as IL-1, TNF-α, and PGE2 in the placenta increase.

In the case of periodontitis, due to increased bacteremia, the level of premature inflammatory mediators that are involved in normal

delivery increases and leads to premature rupture of the placental membrane, which causes preterm delivery (Contreras *et al*., 2006; Mokeem, Molla, and Al-Jewair, 2004; Scannapieco, Bush, and Paju, 2003).

Prevention of oral diseases and its complications during pregnancy is possible with the knowledge of health issues and the attitude and proper practice of pregnant women in this case (Bamanikar and Kee, 2013). Controlling and reducing dental plaque by adopting related behaviors including brushing, flossing, and using mouthwash, as well as increasing oral care by health care providers during pregnancy, can make a significant contribution to reducing oral problems and their consequences in pregnant women (Behdani, Mosavifar, Hebrani, Soltanifar, and Mohamadnejad, 2008).

Due to hormonal changes that cause sensitivities and gingivitis, pregnant women use less toothbrush or floss, which eventually leads to the formation of microbial plaque on the teeth. Morning sickness also causes the teeth to be exposed to stomach acid, and the risk of caries increases (Christensen, Jeppe-Jensen, and Petersen, 2003). Therefore, paying attention to oral health in pregnant women is extremely important to maintain the health of themselves and the fetus (Martins, Barreto, and Pordeus, 2008). Despite the known evidence and complications of periodontal infections for mothers and their infants, this important issue has received less attention (Khalaf, Osman, Abbas, and Ismail, 2018).

This study aimed to evaluate the knowledge, attitude, and practice of pregnant women about periodontal health and oral health and their effect on the fetus during pregnancy.

2. MATERIALS AND METHODS:

In this descriptive-analytical study, 210 pregnant women in the first and second trimesters participated. Samples of pregnant women referring to health centers in Birjand were selected using the clustering method from 5 urban clusters. Health centers were selected from 5 urban clusters randomly, and pregnant women were selected through available sampling. Women were in less than 24 weeks of pregnancy, had at least basic education, and had no mental or physical illness.

2.1. Data Collection Tools

The instruments used were a researcher-made questionnaire that had four parts: women's demographic information, mothers' knowledge, attitude, and practice. The validity and reliability of this questionnaire were confirmed. The validity of the questionnaire was initially confirmed using face validity. Then, in order to check the validity of the content, the questionnaire was given to 10 professors (dental specialists, 2 health educators, 1 biostatistician) and content validity ratio (CVR) indices, the average score of the questions, and content validity index (CVI) were calculated.

The questions that were able to receive the acceptable limit remained in the questionnaire. The reliability of the questionnaire was assessed using a test and retest to assess the reliability over time, and Cronbach's alpha coefficient was used for the reliability of the questions. Reliability values for each subsector were (knowledge = 0.60 and attitude = 0.60, and practice= 0.67). After obtaining informed consent from the participants, the questions were answered by the participants. After collecting the data, they were entered into SPSS software version 22, and then the descriptive data were reported by descriptive statistics, dispersion index, frequency, and agreement tables. Kolmogorov-Smirnov test was used for normal data distribution.

The relationship between quantitative variables was analyzed by analysis of variance and independent t-test, and the relationship between qualitative variables was examined using the chi-square test. As well, in case of abnormality, Kruskal-Wallis and Mann-Whitney tests were used. The significance level was considered 0.05 in all tests.

3. RESULTS AND DISCUSSION:

3.1. Results

The results show that the mean age of women participating in the study was 27.60±6.15 years. Most of them were under 25 years old (41.9%). 35.6% (72 people) had been married for less than 2 years.85.7% were in the second trimester of pregnancy, and 45.7% were pregnant with their first child. 81% were housewives, and the spouses of 6 of them were unemployed.41% of women had a university education, and 48.6% of their husbands had a high school degree. 84.5%

had health insurance services, and the majority of the population (36.7%) had incomes of less than one million. Most of them had a moderate evaluation of their income (46.2%), and none of them rated their income as excellent (Table 1).

The mean scores of the participants in answering the questions in the section of knowledge, attitude, and practice were 5.60, 55.92, and 25.96, respectively, and their standard deviations were1.92, 5.16, and 3.79, respectively. There was a significant difference in attitude level between people who were less than 25 years old and participants who were 25-30 years old and 30-35 years old. There was also a significant difference in knowledge ($p = 0.05$) and attitude ($p < 0.001$), and practice ($p = 0.04$) of pregnant employee women and housewives. There were also significant differences in practice between pregnant housewives and self-employed women. There were also significant differences in performance between pregnant housewives and self-employed women ($p < 0.001$).

Regarding the monthly income of the family, the results in the level of knowledge, attitude, and practice showed that people who had less than 40 USD incomes were significantly different from participants who had an income of 40-80 USD, 80-120 USD and more than 120 USD. Regarding the place of residence of pregnant women living in the north, south, west, east and center of Birjand, there was a significant difference in the level of knowledge ($P = 0.037$), attitude ($P = 0.002$), and practice ($P = 0.001$) (Table 2).

Table 3 shows the frequency distribution and response rate of participants in the field of knowledge. For example, 81.4% of pregnant women did not know what dental plaque was; 91.0% did not know the cause of gingival hyperemia.93.3% knew that sweet and sticky substances increase the risk of tooth decay, and 91.1% knew that toothbrush is the best tool for hygiene and 80.5% knew that dental floss is the best tool for cleaning between teeth. 50% of the participants knew that the best time for dental treatment was the second trimester, and 50% did not know.

Table 4 shows the frequency distribution and percentage of participants' responses in the attitude area. According to it, 50% of the participants agreed and completely agreed with the fact that the calcium required by the fetus is taken from the mother's teeth, and 87.6% agreed and completely agreed that hygiene during pregnancy is more important than before pregnancy.

Table 5 shows the distribution of frequency and percentage of participants' responses in terms of practice, according to which it is found that 46.7% of women brushed their teeth every night before bed and 51.9% only occasionally used floss. 52.4% did not see a dentist before becoming pregnant, 89.5% rinsed their mouths after morning sickness and vomiting, and most participants did not use chlorhexidine and fluoride mouthwash.

3.2. Discussion

Pregnancy is a physiological process in a woman's life that causes various changes in the oral cavity. Even among healthy women, physiological changes associated with pregnancy can lead to gingivitis, periodontitis, and benign lesions (pregnancy tumors). Hormonal changes and changes in diet and frequency of eating can increase the risk of tooth decay (Patil, Thakur, Madhu, Paul, and Gadicherla, 2013). In the present, most pregnant mothers were under 25 years old. In Nogueira *et al*. (2016), mothers were between 12 and 22 years of age (Nogueira *et al*., 2016) and were in the second trimester of pregnancy. To Bedre *et al*., most pregnant mothers were referred in the second trimester (Bedre and Sharma, 2020).

In the current study, most mothers had an income of less than 40 USD and were housewives, and their assessment of income was average. However, studies have shown that income is a risk factor for the high severity of tooth decay (Campos, Bottan, Birolo, da Silveira, and Schmitt, 2010; Eigbobo and Onyeaso, 2013). In addition, the type of household occupation, income, and education are related to the severity of tooth decay (de Oliveira and Nadanovsky, 2006; Eigbobo and Onyeaso, 2013).

In the present study, most people had a university degree. Therefore, the mean score of knowledge, attitude, and practice of pregnant women about oral health in women with university education was higher than women with primary education. The study conducted by Haji Kazemi *et al*. (2005), it was stated that there is a significant relationship between the average score of knowledge and different levels of education; while in another study, it was stated that the frequency of high school education and diploma among mothers was higher than other levels of education, which did not agree with the results from the present study (Ebrahimipour, Mohamadzadeh, Niknami, Ismaili, and Vafaii Najjar, 2015). In the current study, 4.8% of pregnant women had a good level of knowledge, and 70.5% of women

had a moderate level of knowledge about oral hygiene.

According to Haji Kazemi *et al*. (2005), 5.6% of women had a good level of knowledge, and 65.9% of women had a moderate level of knowledge about oral health, which is consistent with the present study.

The present study showed that 46.7% of women brushed their teeth every night before going to bed, and 51.9% occasionally used floss. Bayat *et al*. (2016) showed that 95% of participants cited excessive tiredness and boredom as barriers to brushing. In the study by Avula *et al*. (2013), none of the women had ever flossed. In a study, Shamsi *et al*. (2013), stated that the majority of mothers knew that increasing the consumption of sweets in the diet increases the risk of tooth decay, and also 95% of mothers knew that if oral hygiene is not observed, it will lead to tooth decay. In the study of Gupta *et al*. (2013), 33.5% of non-pregnant women and 19% of pregnant women did not know which foods cause tooth decay. In the present study, most pregnant women did not know what dental plaque was and did not know the cause of gingival hyperemia. Christensen *et al*. (2003), they found that pregnant women considered symptoms such as bleeding gums while brushing to be normal and did not change the situation of their. 50% of participants knew that the best time for dental treatment was the second trimester, and 50% did not know.

Tantradi and Madanshetty(2013) believed that seeing a dentist during pregnancy was not safe. The second trimester is the safest period for dental care services due to the formation of embryonic organs (Tantradi and Madanshetty, 2013). However, more than half of the mothers in this study did not see a dentist before becoming pregnant. The study by Saddki *et al*. Showed that mothers' lack of awareness about the relationship between oral health and pregnancy outcomes was reported as the most important barrier to seeing a dentist (Saddki, Yusoff, and Hwang, 2010). In the present study, 89.5% rinsed their mouths after morning sickness and vomiting, and most participants did not use chlorhexidine and fluoride mouthwashes. Christensen *et al*. (2003) showed that nausea and vomiting expose teeth to stomach acid, which leads to tooth decay.

4. CONCLUSIONS:

The results showed that the average score of knowledge, attitude, and practice of pregnant women in Birjand regarding oral hygiene during pregnancy is unsatisfactory and inappropriate. Considering that oral care is very important during pregnancy, and pregnancy should not be considered a reason for delaying the required dental care; therefore, pregnant mothers should be educated about maintaining good oral hygiene and the expected changes in the oral cavity during regular dental visits. Moreover, women of childbearing age or expecting pregnancy should be screened for caries and oral diseases for timely control.

5. REFERENCES:

1. Ambereen, S., Babu, H. M., Vivekananda, M., and Shivaprasad, D. Practice and knowledge of periodontal health among pregnant women in Hassan, Karnataka: a cross-sectional survey. Age, 21(25), 74.
2. Atarbashi Moghadam, F., Haerian Ardakani, A., Rashidi Meybodi, F., and Khabazian, A. (2014). Evaluation of periodontal health knowledge, attitude and oral hygiene practice of pregnant women in Yazd in 2011. J Adv Periodontol Implant Dent, 5(2), 71-74.
3. Avula, H., Mishra, A., Arora, N., and Avula, J. (2013). KAP assessment of oral health and adverse pregnancy outcomes among pregnant women in Hyderabad, India. Oral Health Prev Dent, 11(3), 261-270.
4. Bamanikar, S., and Kee, L. K. (2013). Knowledge, attitude, and practice of oral and dental healthcare in pregnant women. Oman Medical Journal, 28(4), 288.
5. Bayat, F., Karimi-Shahanjarini, A., Bashirian, S., and Faradmal, J. (2016). Assessment of dental care and its related barriers in pregnant women of Hamadan city. J Educ Community Health, 3(1), 20-27.
6. Bedre, A. S., and Sharma, S. (2020). Knowledge, Attitude and Practice of Dentists Towards Provision of Dental Care to Pregnant Women. Indian J Public Health Res Dev, 11(6).
7. Behdani, F., Mosavifar, N., Hebrani, P., Soltanifar, A., and Mohamadnejad, M. (2008). Anxiety and mood disorders in infertile women referred to Montaserie infertility clinic in Mashhad, North-East Iran. Iran J Obstet Gynecol Infertil, 11(3), 15-23.
8. Brockington, I. (2003). Obstetric and gynecological conditions associated with psychiatric disorder. New Oxford textbook

of psychiatry, 1195-1217.
9. Campos, L., Bottan, E. R., Birolo, J. B., da Silveira, E. G., and Schmitt, B. H. E. (2010). Conhecimento de mães de diferentes classes sociais sobre saúde bucal no município de Cocal do Sul (SC). RSBO Revista Sul-Brasileira de Odontologia, 7(3), 287-295.
10. Christensen, L. B., Jeppe-Jensen, D., and Petersen, P. E. (2003). Self-reported gingival conditions and self-care in the oral health of Danish women during pregnancy. Journal of Clinical Periodontology, 30(11), 949-953.
11. Contreras, A., Herrera, J., Soto, J., Arce, R., Jaramillo, A., and Botero, J. (2006). Periodontitis is associated with preeclampsia in pregnant women. Journal of Periodontology, 77(2), 182-188.
12. de Oliveira, B. H., and Nadanovsky, P. (2006). The impact of oral pain on quality of life during pregnancy in low-income Brazilian women. Journal of Orofacial Pain, 20(4).
13. Ebrahimipour, H., Mohamadzadeh, M., Niknami, S., Ismaili, H., and Vafaii Najjar, A. (2015). Predictors of oral health care in pregnant women based on theory of planned behavior. J Health Syst Res, 11(3), 496-504.
14. Eigbobo, J., and Onyeaso, C. (2013). Maternal knowledge and awareness of factors affecting oral health in the pediatric population. Odonto-Stomatologie Tropicale, 36(142), 15-24.
15. Gambhir, R. S., Nirola, A., Gupta, T., Sekhon, T. S., and Anand, S. (2015). Oral health knowledge and awareness among pregnant women in India: A systematic review. Journal of Indian Society of Periodontology, 19(6), 612.
16. Giglio, J. A., Lanni, S. M., Laskin, D. M., and Giglio, N. W. (2009). Oral health care for the pregnant patient. Journal of the Canadian Dental Association. Journal de L'Association Dentaire Canadienne, 75(1).
17. Govindasamy, R., Narayanan, M., Balaji, V. R., Dhanasekaran, M., Balakrishnan, K., and Christopher, A. (2018). Knowledge, awareness, and practice among gynecologists, medical practitioners and dentists in Madurai regarding association between periodontitis and pregnancy outcomes. Journal of Indian Society of Periodontology, 22(5), 447.
18. Gupta, S., Jain, A., Mohan, S., Bhaskar, N., and Walia, P. K. (2015). Comparative evaluation of oral health knowledge, practices, and attitude of pregnant and non-pregnant women, and their awareness regarding adverse pregnancy outcomes. J Clin Diagn Res, 9(11), ZC26.
19. Haji Kazemi, E., Mohseni, S. H., Oskouie, F., and Haghani, H. (2005). The association between knowledge, attitude, and performance in pregnant women toward dental hygiene during pregnancy. Iran J Nurs, 18(43), 31-38.
20. Haririan, H. R., Mohammadpour, Y., and Aghajanloo, A. (2010). Prevalence of depression and contributing factors of depression in the infertile women referred to Kosar infertility center, 2009. Iran J Obstet Gynecol Infertil, 13(2), 45-49.
21. Khalaf, S. A., Osman, S. R., Abbas, A. M., and Ismail, A. (2018). Knowledge, attitude, and practice of oral healthcare among pregnant women in Assiut, Egypt. Int J Community Med Public Health, 5, 890-900.
22. Lee, A., McWilliams, M., and Janchar, T. (1999). Care of the pregnant patient in the dental office. Dental Clinics of North America, 43(3), 485-494.
23. Martins, A. M. E. d. B. L., Barreto, S. M., and Pordeus, I. A. (2008). Factors associated to self-perceived need of dental care among Brazilian elderly. Revista de Saúde Publica, 42, 487-496.
24. Mehdipoor, A., Danesh, M., Pouretemadi, A., Jafary Nodoushan, Z., Shabani Ghazikelayeh, M., and Saleh, A. (2019). Evaluation of Dentists' and Gynecologists' Knowledge, Attitude, and Practice Regarding Oral and Dental Care during Pregnancy in Qom, Iran, in 2017. Arch Hyg Sci, 8(3), 163-171.
25. Mills, L. W., and Moses, D. T. (2002). Oral health during pregnancy. MCN: American Journal of Maternal Child Nursing, 27(5), 275-280.
26. Mokeem, S. A., Molla, G. N., and Al-Jewair, T. S. (2004). The prevalence and relationship between periodontal disease and preterm low birth weight infants at King Khalid University Hospital in Riyadh, Saudi Arabia. Journal of Contemporary Dental Practice, 5(2), 40-56.
27. Nogueira, B. M. L., Nogueira, B. C. L., Fonseca, R. R. d. S., Brandão, G. A. M., Menezes, T. O. d. A., and Tembra, D. P. d. S. (2016). Knowledge and attitudes of pregnant women about oral health. Int J Odontostomat, 10(2), 297-302.
28. Patil, S., Thakur, R., Madhu, K., Paul, S.

T., and Gadicherla, P. (2013). Oral health coalition: knowledge, attitude, practice behaviours among gynecologists and dental practitioners. J Int Oral Health, 5(1), 8.
29. Saddki, N., Yusoff, A., and Hwang, Y. L. (2010). Factors associated with dental visit and barriers to utilisation of oral health care services in a sample of antenatal mothers in Hospital Universiti Sains Malaysia. BMC Public Health, 10(1), 1-11.
30. Scannapieco, F. A., Bush, R. B., and Paju, S. (2003). Periodontal disease as a risk factor for adverse pregnancy outcomes. A systematic review. Annals of Periodontology, 8(1), 70-78.
31. Shamsi, M., Hidarnia, A., Niknami, S., Atarha, M., and Jadidi, R. (2013). Oral health of pregnant women in Arak, Iran. Payesh Health Monit, 12(4), 355-365.
32. Tantradi, P., and Madanshetty, P. (2013). Knowledge of dental interns about management of dental needs of pregnant patients. Journal of Education and Ethics in Dentistry, 3(2), 76.
33. Tarannum, F., Prasad, S., Vivekananda, L., Jayanthi, D., and Faizuddin, M. (2013). Awareness of the association between periodontal disease and preterm births among general dentists, general medical practitioners, and gynecologists. Indian Journal of Public Health, 57(2), 92.

7. OPEN ACCESS

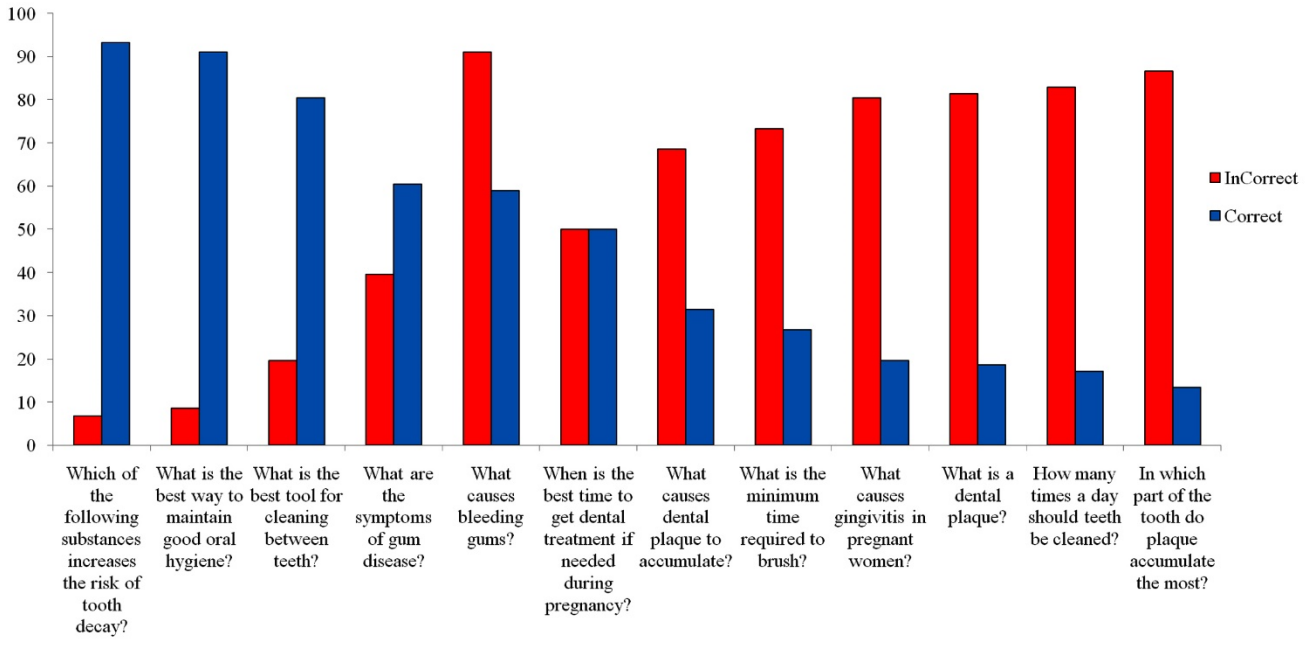

Figure 1: *Distribution of frequency and percentage of correct and incorrect answers of the participants in the field of knowledge*

Table 1: *Frequency distribution of demographic characteristics of studied pregnant women*

Variable	Specifications	Frequency (Person)	Percent
Age (Year)	<25	88	41.9
	30-25	55	26.2
	35-30	38	18.1
	40-35	26	12.4
	>40	3	1.4
Spouse Age	<25	33	15.7
	30-25	76	36.2
	35-30	59	28.1
	40-35	27	12.9
	>40	15	7.1
Duration Of Marriage (Year)	<2	72	35.6
	5-2	44	21.8
	10-5	51	25.2
	15-10	29	14.4
	>15	6	3.0
Pregnancy Weeks	<=12	27	13.0
	>12	180	87.0
Number of Children	0	96	45.7
	1	62	29.5
	2	36	17.1
	3	16	7.6
Previous Pregnancy History	Yes	91	43.3
	No	119	56.7
Job	Housewife	170	81.0
	Employee	26	12.4
	Free	10	4.7
	Manual Worker	4	1.9
Spouse Job	Unemployed	6	2.9
	Employee	69	32.9
	Free	95	45.2
	Manual Worker	40	19.0
Mother's Education	Primary	47	22.4
	High School	77	36.6
	University	86	41.0
Father's Education	Primary	21	10.0
	High School	102	48.6
	University	87	41.4
Insurance Services	Yes	177	84.7
	No	32	15.3
Monthly Income (USD)	<40	77	36.7
	40-80	73	34.8
	80-120	42	20.0
	>120	18	8.5
Income Evaluation	Low	56	26.7
	Medium	97	46.2
	Good	57	27.1

Table 2: *Comparison of knowledge, attitude and practice scores by age, occupation, income, place of residence in pregnant women participating in the study*

Variable (Age) Score	**Mean And Standard Deviation**					**Test Statistics**	**P-Value**
	<25	30-25	35-30	>35			
Knowledge	1.69±5.31	2.18±5.67	.2.01±6.00	1.90±5.86		F=1.38	0.24
Attitude	5.22±54.78	4.46±56.60	5.21±57.34	5.70±56.27		F=2.80	0.04
Practice	3.41±25.64	4.25±26.58	3.36±26.05	4.50±25.62		F=0.77	0.51
Variable (Job) Score	**Mean And Standard Deviation**					**Test Statistics**	P-Value
	Housewife	Employee	Free	Manual Worker			
Knowledge	1.95±5.42	1.58±6.76	1.15±6.00	1.82±5.00		F=4.12	0.007
Attitude	5.00±55.18	5.34±59.80	2.27±58.50	3.74±56.00		F=7.53	<0.001
Practice	3.73±25.54	3.76±27.61	2.54±29.40	2.08±24.50		F=5.61	0.001
Variable (Income) Score	**Mean And Standard Deviation**					**Test Statistics**	P-Value
	<40	40-80	80-120	>120			
Knowledge	1.83±4.96	1.94±5.80	1.68±6.11	2.03±6.38		F=5.46	0.003
Attitude	4.52±54.46	5.15±97	5.78±57.57	4.65±58.16		F=4.84	0.001
Practice	3.54±25.16	3.90±25.79	3.77±26.57	3.44±28.61		F=4.68	0.003
Variable (Place Of Residence) Score	**Mean And Standard Deviation**					**Test Statistics**	P-Value
	North	South	East	West	Center		
Knowledge	1.83±5.23	1.84±6.35	2.01±5.82	2.05±5.82	1.88±5.73	F=2.60	0.037
Attitude	4.32±54.87	6.86±58.74	4.70±56.86	4.91±55.40	4.17±55.31	F=4.53	0.002
Practice	3.50±24.89	3.33±27.89	3.23±26.69	4.71±26.36	3.63±26.00	F=5.15	0.001

Table 3: *Distribution of frequency and percentage of correct and incorrect answers of the participants in the field of knowledge*

Question	**Incorrect** answers		**correct** answers	
	Frequency (person)	**percentage**	**Frequency (person)**	**percentage**
What is a dental plaque?	171	81.4	36	18.6
What causes dental plaque to accumulate?	144	68.6	66	31.4
In which part of the tooth do plaque accumulate the most?	182	86.7	28	13.3
What causes bleeding gums?	86	91.0	124	59.0
What causes gingivitis in pregnant women?	169	80.5	41	19.5
What are the symptoms of gum disease?	83	39.5	127	60.5
Which of the following substances increases the risk of tooth decay?	14	6.7	196	93.3
What is the best way to maintain good oral hygiene?	18	8.6	191	91.0
What is the best tool for cleaning between teeth?	41	19.5	169	80.5
How many times a day should teeth be cleaned?	174	82.9	36	17.1
What is the minimum time required to brush?	154	73.3	56	26.7
When is the best time to get dental treatment if needed during pregnancy?	105	50.0	105	50.0

Table 4: *Distribution of frequency and percentage of correct and incorrect answers of participants in the field of attitude*

Question	Score 1		Score 2		Score 3		Score 4		Score 5	
	Frequency (person)	percentage	Frequency (person)	percentage	Frequency (person)	percentage	Frequency (person)	percentage	Frequency (person)	percentage
I love sweets, chocolates and snacks.	16	7.6	71	33.8	42	20.0	65	31.0	15	7.1
I believe that if we do not brush our teeth, tooth decay will happen sooner.	3	1.4	7	3.3	11	5.2	93	44.3	96	45.7
Bad breath can be due to not brushing and flossing regularly.	1	0.5	15	7.1	20	9.5	97	46.2	77	36.7
Brushing should be avoided with nausea and vomiting due to brushing.	6	2.9	36	17.1	73	34.8	79	37.6	16	7.6
I believe that I should floss at least once a day.	0	0	15	7.1	29	13.8	123	58.6	43	20.5
Tooth decay is more likely during pregnancy.	0	0	5	2.4	33	15.7	93	44.3	79	37.6
I believe that we should only go to the dentist when our teeth hurt.	6	2.9	31	14.8	26	12.4	107	51.0	40	19.0
I believe that bleeding gums and gum disease are related.	0	0	10	4.8	75	35.7	91	43.3	34	16.2
I believe gum disease can be one of the causes of bad breath.	0	0	4	1.9	45	21.4	120	57.1	41	19.5
I believe dental services can harm my fetus.	14	6.7	61	29.0	77	36.7	50	23.8	80	3.8
I believe that scaling teeth during pregnancy is harmful to the fetus.	10	4.8	44	21.0	114	54.3	33	15.7	9	4.3
I believe that pregnancy can worsen the condition and disease of the gums and increase bleeding, swelling and redness.	2	1.0	29	13.8	97	46.2	64	30.5	18	8.6
I believe that oral diseases during pregnancy can cause premature birth.	13	6.2	37	17.6	111	52.9	37	17.6	12	5.7
I believe that the calcium needed by the fetus is taken from the mother's teeth.	30	14.3	75	35.7	77	36.7	26	12.4	2	1.0
I believe that oral diseases do not affect the birth weight of my child.	14	6.7	39	18.6	110	52.4	42	20.0	5	2.4
I believe that maintaining good oral hygiene during pregnancy is more important than before pregnancy.	1	0.5	2	1.5	23	11.0	97	46.2	87	41.4

Table 5: *Frequency distribution and response percentage of participants in the field of practice*

Question	Score 1		Score 2		Score 3	
	Frequency (person)	percentage	Frequency (person)	percentage	Frequency (person)	percentage
Do you brush every night before bed?	13	6.2	99	47.1	98	46.7
Do you brush your teeth after every meal?	55	26.2	129	61.4	26	12.4
Do you brush all surfaces of your teeth carefully?	8	3.8	49	23.3	153	72.9
How often do you change your toothbrush?	39	15.6	110	52.4	61	29.0
Do you floss or toothpickyour teeth regularly?	63	30.0	109	51.9	38	18.1
Do you use fluoride toothpaste?	25	11.9	73	34.8	112	53.3
Did you see a dentist before you got pregnant?	110	52.4	13	6.2	87	41.4
Did you have an oral examination by a dentist during pregnancy?	134	63.8	12	5.7	64	30.5
Do you rinse your mouth immediately after eating sweet and sticky foods?	22	10.5	81	38.6	107	51.0
Do you rinse your mouth after morning sickness and vomiting?	7	3.3	15	7.1	188	89.5
Do you use chlorhexidine mouthwash?	183	87.1	19	9.0	8	3.8
Do you use fluoride mouthwash?	170	81.0	28	13.3	12	5.7
How often do you see a dentist?	143	68.1	57	27.1	10	4.8

PERIÓDICO TCHÊ QUÍMICA
ARTIGO ORIGINAL

ESTUDO COMPARATIVO DE CORRELAÇÕES E EQUAÇÕES EMPÍRICAS DE EFICÁCIA DE ESTADO PARA O FATOR DE COMPRESSIBILIDADE DE DETERMINAÇÃO DE GÁS NATURAL

COMPARATIVE STUDY OF EMPIRICAL CORRELATIONS AND EQUATIONS OF STATE EFFECTIVENESS FOR COMPRESSIBILITY FACTOR OF NATURAL GAS DETERMINATION

СРАВНИТЕЛЬНЫЙ АНАЛИЗ ЭФФЕКТИВНОСТИ ПРИМЕНЕНИЯ КОРРЕЛЯЦИОННЫХ ЗАВИСИМОСТЕЙ И УРАВНЕНИЙ СОСТОЯНИЯ ДЛЯ ОПРЕДЕЛЕНИЯ КОЭФФИЦИЕНТА СВЕРХСЖИМАЕМОСТИ ПРИРОДНОГО ГАЗА

MALYSHEV, Victor L.[1]; NURGALIEVA, Yana F.[2]; MOISEEVA, Elena F.[3*]

[1,3] Ufa State Petroleum Technological University, Faculty of Mining and Petroleum Engineering. Russia.

[2] Gazpromneft – Digital Solutions. Russia.

** Corresponding author*
e-mail: elena.f.moiseeva@gmail.com

Received 08 May 2021; received in revised form 23 May 2021; accepted 14 December 2021

RESUMO

Introdução: Hoje, existem quatro grupos principais de métodos de cálculo do fator de compressibilidade do gás natural: medidas experimentais, equações de estado, correlações empíricas, métodos modernos baseados em algoritmos genéticos, redes neurais, modelagem atomística (método de Monte Carlo e dinâmica molecular). Um método escolhido corretamente pode melhorar a precisão do cálculo das reservas de gás e prever sua produção e processamento. **Objetivo**: Encontrar os métodos ideais para calcular o fator z seguindo as condições termobáricas características. **Métodos**: Para determinar o melhor método para calcular o fator de compressibilidade, a eficácia do uso de várias correlações empíricas e equações de estado para prever o fator de compressibilidade de sistemas de hidrocarbonetos (gases de reservatório e gases de separação) de várias composições foi avaliada pela comparação de resultados numéricos com experimentais dados. **Resultados e discussão**: Com base em 824 valores experimentais do fator de compressibilidade para 235 várias misturas de gases na faixa de pressão de 0,1 a 94 MPa e temperaturas de 273 a 437 K, a equação de estado ideal e dependência de correlação empírica para previsão precisa do fator z foi encontrado. É mostrado que para todas as misturas de gases a equação de estado de Peng-Robinson com o parâmetro de deslocamento e a equação de estado de Brusilovsky permitem obter melhores resultados. Para esses métodos, o erro relativo absoluto médio não excede 2%. Dentre as dependências de correlação, os melhores resultados são apresentados por Sanjari e Nemati Lay; Correlações de Heidaryan, Moghadasi e Rahimi com um erro não superior a 3%. **Conclusões**: Constatou-se que, para os métodos propostos, a redução da pressão tem um efeito mais significativo na precisão dos valores calculados do que a redução da temperatura. Foi demonstrado que ao estudar misturas de gases ácidos com um teor de dióxido de carbono superior a 10%, as equações de estado descrevem melhor o comportamento de fase do sistema em comparação com as correlações empíricas.

Palavras-chave: *fator de compressibilidade, equação de estado, correlação empírica, gás natural, CO_2.*

ABSTRACT

Introduction: Today, there are four main groups of methods for calculating the compressibility factor of natural gas: experimental measurements, equations of state, empirical correlations, modern methods based on genetic algorithms, neural networks, atomistic modeling (Monte Carlo method and molecular dynamics). A correctly chosen method can improve the accuracy of calculating gas reserves and predicting its production and processing. **Aim:** To find the optimal methods for calculating the z-factor following the characteristic thermobaric conditions. **Methods:** To determine the best method for calculating the compressibility factor, the effectiveness of using various empirical correlations and equations of state to predict the compressibility factor of hydrocarbon

DOI: 10.52571/PTQ.v18.n38.2021.14_MALYSHEV_pgs_188_213.pdf

systems (reservoir gases and separation gases) of various compositions were evaluated by comparing numerical results with experimental data. **Results and Discussion:** Based on 824 experimental values of the compressibility factor for 235 various gas mixtures in the pressure range from 0.1 to 94 MPa and temperatures from 273 to 437 K, the optimal equation of state and empirical correlation dependence for accurate z-factor prediction was found. It is shown that for all gas mixtures the Peng-Robinson equation of state with the shift parameter and Brusilovsky equation of state allow achieving best results. For these methods, the average absolute relative error does not exceed 2%. Among the correlation dependences, the best results are shown by the Sanjari and Nemati Lay; Heidaryan, Moghadasi and Rahimi correlations with an error not exceeding 3%. **Conclusions:** It was found that for the proposed methods, the reduced pressure has a more significant effect on the accuracy of the calculated values than the reduced temperature. It is shown that when studying acid gas mixtures with a carbon dioxide content of more than 10%, the equations of state better describe the phase behavior of the system in comparison with empirical correlations.

Keywords: *compressibility factor, equation of state, empirical correlation, natural gas, CO_2.*

ABSTRACT

Введение: На сегодняшний день существует четыре основных группы методов для расчета коэффициента сжимаемости природного газа: экспериментальные измерения, уравнения состояния, эмпирические корреляции, а также современные методы, использующие генетические алгоритмы, нейронные сети, атомистическое моделирование (метод Монте-Карло и молекулярной динамики). Правильно выбранный метод может повысить точность подсчета запасов газа и прогнозирования его добычи и переработки. **Цель:** Найти оптимальные методики расчета z-фактора в соответствии с характерными термобарическими условиями. **Методы:** Для выбора оптимального метода расчета коэффициента сверхсжимаемости произведена оценка эффективности применения различных эмпирических корреляций и уравнений состояния для прогнозирования коэффициента сверхсжимаемости углеводородных систем (пластовые газы и газы сепарации) различного состава путем сравнения численных результатов с экспериментальными данными. **Результаты и обсуждение**: На основе 824 экспериментально полученных значений коэффициента сжимаемости для 235 составов различных газовых смесей в диапазоне давлений от 0,1 до 94 МПа и температур от 273 до 437 К произведена оценка поиска оптимального уравнения состояния и корреляционной зависимости для точного предсказания z-фактора. Показано, что для всех составов газов наилучшие результаты показывает уравнения состояния Пенга-Робинсона с шифт параметром и Брусиловского. Для этих моделей средний процент отклонения расчетных значений от экспериментальных данных не превосходит 2%. Среди корреляционных зависимостей лучшие результаты показывают зависимости Sanjari and Nemati Lay; Heidaryan, Moghadasi and Rahimi с ошибкой, не превосходящей 3%. **Заключение:** Установлено, что для большинства предложенных методов существенное влияние на точность расчетных значений в большей степени оказывает приведенное давление, чем приведенная температура. Показано, что при изучении кислых газовых составов с содержанием CO_2 свыше 10% уравнения состояния лучше описывают фазовое поведение системы в сравнении с эмпирическими корреляциями.

Keywords: *коэффициент сверхсжимаемости, уравнение состояния, эмпирическая корреляция, природный газ, диоксид углерода.*

1. INTRODUCTION:

Physical properties of natural gases, as well as their functional dependence on pressure, temperature, and molecular weight, are required for planning gas, oil, and gas condensate deposit development. The compressibility factor and viscosity of natural gas are two of the most important parameters in gas production and processing. Their importance cannot be overestimated in the context of maintaining fluid balance in the reservoir, estimating gas reserves, reservoir modeling, gas wells testing, analyzing the productivity, and predicting future gas production and processing (Heidaryan, Moghadasi, and Rahimi, 2010a; Heidaryan, Salarabadi, Moghadasi, 2010b).

All methods for the compressibility factor determination can be divided into following groups: experimental measurements, equations of state, empirical correlations, as well as modern methods using genetic algorithms, neural networks, atomistic modeling (Monte Carlo method and molecular dynamics simulations).

The most accurate approach allowing determining the z-factor is experimental measurements, based on compression-expansion process. There are a lot of experimental data in scientific journals, books and articles. Thus, one of the first experimental data on the z-factor measurements was presented in (Buxton,

Campbell, 1967). The authors determined the compressibility factors for five mixtures of methane, carbon dioxide and ethane of propane at different temperatures and mixtures. In (Ababio, McElroy, Williamson, 2001) authors published the experimental results on methane-nitrogen mixtures of various compositions, in (McElroy, Fang, Williamson, 2001) one can find data for methane+ethane+carbon dioxide mixtures. More experimental values of the compressibility factor for different mixtures can be found in (Hall, 1973; Roe, 1972; Lapshin, Volkov, Shafiev, 2011; Obuba, Ikiesnkimama, Ubani, Ekeke, 2013; Fayazi, Arabloo, Mohammadi, 2014; Bian, Du, Tang, and Du, 2012). However, this method cannot be applied to every gas mixture because of its complexity, time consuming and cost. It also needs special equipment and human resources. The authors of (Drohm, 1988) discussed also the problem of quality of experimental PVT data obtained from the experiments performed on gas condensates.

Most of the modern methods used to determine the z-factor are based on the computational capabilities of modern computers. In (Chamkalani, Maesoumi, and Sameni, 2013) authors described the theoretical basis of Particle Swarm optimization and Genetic algorithm for optimal prediction of gas deviation factor. Authors of (Baniasadi, Mohebbi, and Baniasadi, 2012) developed a new correlation of natural gas compressibility factor using an artificial neural networks while authors of (Shateri, Ghorbani, Hemmati-Sarapardeh, and Mohammadi, 2015) predicted the compressibility factor of natural gas using the most powerful modeling approach, namely Wilcoxon generalized radial basis function network for analysis of a large data bank, covering a wide range of natural gases.

One of the “young” method for the z-factor determination is the atomistic modeling, including Monte Carlo (MC) method and molecular dynamics simulations. The authors of (Ungerer, Nieto-Draghi, Rousseau, Ahunbay, Lachet, 2007) determined the compressibility factor of pure methane using MC simulations, authors of (Lagache, Ungerer, Boutin, Fuchs, 2001, 2004) did also the same thing for other hydrocarbons. In (Neubauer, Tavitian, Boutin, Ungerer, 1999; Malyshev, Moiseeva, Kalinovsky, 2018; Moiseeva, Malyshev, 2019) the applicability of the Molecular Dynamics Simulations to the z-factor determination is discussed and the computations for some natural gas components are presented.

The most reliable and time-tested methods for the compressibility factor determination are still empirical correlations and equations of state. They allow one to accurately compute the z-factor of natural gas in a wide range of thermobaric parameters. These methods are used in the majority of the software, where physical properties of gas are need to be calculated. Therefore, the problem of choosing the best empirical correlation or the equation of state is always of high importance.

This study is aimed to compare the compressibility factor for natural gas mixtures calculated using empirical correlations and equations of state and to find the optimal methods for calculating the z-factor according to the reservoir and gas separator thermobaric conditions.

2. MATERIALS AND METHODS:

The basic formula for determining the compressibility factor of natural gas is described by Equation 1:

$$Z = \frac{PV}{nRT}, \quad \text{(Eq.1)}$$

where P is the pressure, V is the volume, n is the number of moles of gas, R is the universal gas constant, T is the temperature.

Based on the theory of corresponding states, Z is also can be defined as a function of pseudo reduced pressure (P_{pr}) and pseudo reduced temperature (T_{pr}) as follows (Chamkalani et al, 2013):

$$P_{pr} = \frac{P}{P_{pc}}, \quad \text{(Eq.2)}$$

$$T_{pr} = \frac{T}{T_{pc}}, \quad \text{(Eq.3)}$$

where P_{pc} and T_{pc} stand for the pseudo critical pressure and temperature,respectively.

The physical meaning of this parameter is a correction factor, which describes the deviation of a real gas from ideal gas behavior. In this work, 13 empirical correlations and 6 equations of state used to calculate the compressibility factor were considered.

2.1. Empirical correlations

Experimental data for the compressibility factor of hydrocarbon mixtures obtained by different authors became the basis for creating convenient and easy-to-calculate correlation

dependences of the z-factor for the given pressure and temperature. To date, there are more than 20 empirical correlations (Heidaryan et al., 2010a). However, the existing applicability range imposes certain restrictions on their use in engineering calculations.

2.1.1 Azizi

In 2009, the study of Navid Azizi, Dr. R. Behbahani, Dr. M. A. Isazadeh, devoted to the z-factor of natural gas determination was published (Azizi, Behbahani, Isazadeh, 2010). The authors developed the correlation based on 3038 values of the Standing and Katz compressibility factor chart.

Equations 4-9 are suitable for calculating the compressibility factor of a dry gas for the pseudo reduced pressures and temperatures within the range of $0.2 \leq P_{pr} \leq 1$ and $1.1 \leq T_{pr} \leq 2$:

$$Z = A + \frac{B+C}{D+E}, \quad \text{(Eq.4)}$$

$$A = a_0 T_{pr}^{2,16} + a_1 P_{pr}^{1.028} + a_2 P_{pr}^{1.58} T_{pr}^{-2.1} + a_3 \ln(T_{pr})^{-0.5}, \quad \text{(Eq.5)}$$

$$B = a_4 + a_5 T_{pr}^{2.4} + a_6 P_{pr}^{1.56} + a_7 P_{pr}^{0.124} T_{pr}^{3.033}, \quad \text{(Eq.6)}$$

$$C = a_8 \ln(T_{pr})^{-1.28} + a_9 \ln(T_{pr})^{1.37} + a_{10} \ln(P_{pr}) + a_{11} \ln(P_{pr})^2 + a_{12} \ln(P_{pr}) \ln(T_{pr}), \quad \text{(Eq.7)}$$

$$D = 1 + a_{13} T_{pr}^{5.55} + a_{14} P_{pr}^{0.68} T_{pr}^{0.33}, \quad \text{(Eq.8)}$$

$$E = a_{15} \ln(T_{pr})^{1.18} + a_{16} \ln(T_{pr})^{2.1} + a_{17} \ln(P_{pr}) + a_{18} \ln(P_{pr})^2 + a_{19} \ln(P_{pr}) \ln(T_{pr}). \quad \text{(Eq.9)}$$

Coeffitients a_i are presented in table 1.

The advantage of this correlation is that it is explicit and does not require an iterative solution.

2.1.2 Bahadori

In 2007, Alireza Bahadori, Saeid Mokhatab, Brian F. Towler presented an empirical equation for calculating the gas compressibility factor (Bahadori, Mokhatab, Towler, 2007). The equation is suitable for calculating the compressibility factor of gas when $0.2 \leq P_{pr} \leq 16$ and $1.05 \leq T_{pr} \leq 2.4$.

Correlation, developed based on the Standing-Katz chart, is an explicit function that does not require an iterative solution (Equations 10-14):

$$Z = a + bP_{pr} + cP_{pr}^2 + dP_{pr}^3, \quad \text{(Eq.10)}$$

$$a = A_a + B_a T_{pr} + C_a T_{pr}^2 + D_a T_{pr}^3, \quad \text{(Eq.11)}$$

$$b = A_b + B_b T_{pr} + C_b T_{pr}^2 + D_b T_{pr}^3, \quad \text{(Eq.12)}$$

$$c = A_c + B_c T_{pr} + C_c T_{pr}^2 + D_c T_{pr}^3, \quad \text{(Eq.13)}$$

$$d = A_d + B_d T_{pr} + C_d T_{pr}^2 + D_d T_{pr}^3. \quad \text{(Eq.14)}$$

Constants A_i, B_i, C_i, D_i for the empirical dependence of Bahadory are presented in table 2.

The authors modified the correlation by introducing a correction ε for the given parameters to calculate the compressibility factor of gas mixtures with a high content of acid gas, in particular, carbon dioxide and hydrogen sulfide (Equation 15):

$$\varepsilon = \frac{a+by_{H_2S}+cy_{H_2S}^2+dy_{H_2S}^3}{1{,}8}, \quad \text{(Eq.15)}$$

where y_{H_2S}, y_{CO_2} are mole fractions of H_2S and CO_2 respectively, and the coefficients are calculated from Equations 16-19:

$$a = A_a + B_a y_{CO_2} + C_a y_{CO_2}^2 + D_a y_{CO_2}^3, \quad \text{(Eq.16)}$$

$$b = A_b + B_b y_{CO_2} + C_b y_{CO_2}^2 + D_b y_{CO_2}^3, \quad \text{(Eq.17)}$$

$$c = A_c + B_c y_{CO_2} + C_c y_{CO_2}^2 + D_c y_{CO_2}^3, \quad \text{(Eq.18)}$$

$$d = A_d + B_d y_{CO_2} + C_d y_{CO_2}^2 + D_d y_{CO_2}^3. \quad \text{(Eq.19)}$$

A_i, B_i, C_i, D_i are constants (table 3).

Then ε is used to determine the modified pseudo critical temperature (equation 20) and pressure (equation 21):

$$T_{pc}^{correct} = T_{pc} - \varepsilon, \quad \text{(Eq.20)}$$

$$P_{pc}^{correct} = \frac{P_{pc}(T_{pc}-\varepsilon)}{T_{pc}+\varepsilon y_{H_2S}(1-y_{H_2S})} \quad \text{(Eq.21)}$$

The corrected pseudocritical parameters are substituted into Equations 9-12 to calculate the compressibility factor using Equation 8.

2.1.3 Dranchuk and Abou-Kassem

In 1975, P. M. Dranchuk and J. H. Abou-Kassem proposed an empirical expression with eleven constants to calculate the gas compressibility factor (Dranchuk, Abou-Kassem, 1975):

$$Z = 1 - Z + \left(A_1 + \frac{A_2}{T_{pr}} + \frac{A_3}{T_{pr}^3} + \frac{A_4}{T_{pr}^4} + \frac{A_5}{T_{pr}^5}\right)\rho_r + \left(A_6 + \frac{A_7}{T_{pr}} + \frac{A_8}{T_{pr}^2}\right)\rho_r^2 - A_9\left(\frac{A_7}{T_{pr}} + \frac{A_8}{T_{pr}^2}\right)\rho_r^5 + \frac{A_{10}(1+A_{11}\rho_r^2)\rho_r^2}{T_{pr}^3} e^{-A_{11}\rho_r^2}, \quad \text{(Eq.22)}$$

where $\rho_r = \frac{0.27P_{pr}}{ZT_{pr}}$.

The constants for the Equation 22 presented in Table 4 were found by analyzing 1500 points of the Standing-Katz chart for pressures and temperatures within the range of $0.2 \leq P_{pr} < 30;\ 1 < T_{pr} < 3$ and $P_{pr} < 1; 0.7 < T_{pr} < 1$.

Since the compressibility factor appears on both sides of the equation, it is necessary to use an iterative solution. It is recommended to use Equation 23 representing the Newton-Raphson method:

$$Z_{n+1} = Z_n - (f_z/f_z^{'}), \quad \text{(Eq.23)}$$

where n is the index number of iteration.

Table 4. *Constants A_i for empirical dependence of Dranchuk and Abou-Kassem*

i	A_i	*i*	A_i
1	0.326	7	0.736
2	-1	8	0.184
3	-0.533	9	0.105
4	0.0156	10	0.613
5	-0.0516	11	0.721
6	0.547		

2.1.4 Dranchuk-Purvis-Robinson

Equation 24 was developed by P. M. Dranchuk, R. A. Purvis, and D. B. Robinson in 1973 (Dranchuk, Purvis, Robinson, 1974). It is based on the Benedict-Webb-Rubbin equation of state.

$$Z = \frac{0,27P_{pr}}{yT_{pr}}, \quad \text{(Eq.24)}$$

where pseudo-reduced density y is a solution of the Equation 25:

$$f(y) = 1 + R_1 y - \frac{R_2}{y} + R_3 y^2 - R_4 y^5 + \left[R_5 y^2 (1 + A_{11} y^2) e^{-A_{11} y^2}\right], \quad \text{(Eq.25)}$$

where A_i are constants from Table 4, R_i are calculated using Equations 26-30:

$$R_1 = A_1 + \frac{A_2}{T_{pr}} + \frac{A_3}{T_{pr}^3} + \frac{A_4}{T_{pr}^4} + \frac{A_5}{T_{pr}^5}, \quad \text{(Eq.26)}$$

$$R_2 = \frac{0.27P_{pr}}{T_{pr}}, \quad \text{(Eq.27)}$$

$$R_3 = A_6 + \frac{A_7}{T_{pr}} + \frac{A_8}{T_{pr}^2}, \quad \text{(Eq.28)}$$

$$R_4 = A_9 \left(\frac{A_7}{T_{pr}} + \frac{A_8}{T_{pr}^2}\right), \quad \text{(Eq.29)}$$

$$R_5 = \frac{A_{10}}{T_{pr}^3}. \quad \text{(Eq.30)}$$

2.1.5 Hall and Yarborough

In 1973, Kenneth R. Hall and Lyman Yarborough published an empirical correlation:

$$Z = 0.06125 \frac{P_{pr} t e^{-1.2(1-t)^2}}{y}, \quad \text{(Eq.31)}$$

where y is pseudo-reduced density, which can be calculated using Equation 23.

Equation 31 is developed using virial expansion and Carnahan-Starling equation of state (hard-sphere equation):

$$Z = \frac{pV}{Nk_BT} = \frac{1+\eta+\eta^2-\eta^3}{(1-\eta)^3}, \quad \text{(Eq.32)}$$

where Z denotes the compressibility factor; p is the pressure; V is volume; k_B is Boltzmann constant; T is temperature; η is packaging indicator.

An iterative solution is required to determine the compressibility factor using Equation 30. The reduced density can be found as a solution of Equation 33:

$$f(y) = -0.06125 P_{pr} t e^{-1.2(1-t)^2} + \frac{y+y^2+y^3-y^4}{(1-y)^3} - (14.76t - 9.76t^2 + +4.58t^3)y^2 + (90.7t - 242.2t^2 + 42.4t^3)y^{1.18+2.82t}, \quad \text{(Eq.33)}$$

where $t = 1/T_{pr}$.

The authors mentioned that the method is not suitable for calculating when a reduced temperature is less than unity.

2.1.6 Heidaryan et al. (2010a)

The empirical expression 34 developed by Ehsan Heidaryan, Amir Salarabadi, Jamshid Moghadas is based on 1220 values of the Standing-Katz chart for the pressure and temperature in the range of $0.2 \leq P_{pr} \leq 15$ and $1.2 \leq T_{pr} \leq 3$ (Heidaryan, Salarabadi, Moghadas, 2010). It can be written as:

$Z =$

$$\frac{A_1+A_2\ln(P_{pr})+A_3(\ln P_{pr})^2+A_4(\ln P_{pr})^3+\left(\frac{A_5}{T_{pr}}\right)+\left(\frac{A_6}{T_{pr}^2}\right)}{1+A_7\ln(P_{pr})+A_8(\ln P_{pr})^2+\left(\frac{A_9}{T_{pr}}\right)+\left(\frac{A_{10}}{T_{pr}^2}\right)},\text{(Eq.34)}$$

where A_i are the constants presented in Table 5.

Table 5. *Constants A_i for empirical expression of Heydaryan et al. (2010a)*

i	A_i	i	A_i
1	1.115323727	6	1.157531187
2	-0.079039521	7	-0.053677807
3	0.01588138	8	0.0146557
4	0.008861345	9	-1.809973749
5	-2.161907926	10	0.954860388

2.1.7 Heidaryan et al. (2010b)

Later, in (Heidaryan, Moghadasi, Rahimi, 2010), the same authors proposed a modification of the empirical expression taking into account the presence of C7+ hydrocarbons and non-hydrocarbon components of natural gas (Equation 35):

$$Z = \ln\left(\frac{A_1+A_3\,ln(P_{pr})+\frac{A_5}{T_{pr}}+A_7(ln(P_{pr}))^2+\frac{A_9}{T_{pr}^2}+\frac{A_{11}}{T_{pr}}ln(P_{pr})}{1+A_2\,ln(P_{pr})+\frac{A_4}{T_{pr}}+A_6(ln(P_{pr}))^2+\frac{A_8}{T_{pr}^2}+\frac{A_{10}}{T_{pr}}ln(P_{pr})}\right) \quad \text{(Eq.35)}$$

Constants A_i are presented in table 6.

Table 6. *Constants A_i for empirical expression of Heidaryan et al. (2010b)*

A_i	$0.2 \le P_{pr} \le 3$	$3 < P_{pr} \le 15$
A_1	2.827793	3.252838
A_2	-4.688191·10^{-1}	-1.306424·10^{-1}
A_3	-1.262288	-6.449194·10^{-1}
A_4	-1.536524	-1.518028
A_5	-4.535045	-5.391019
A_6	6.895104·10^{-2}	-1.379588·10^{-2}
A_7	1.903869·10^{-1}	6.600633·10^{-2}
A_8	6.200089·10^{-1}	6.120783·10^{-1}
A_9	1.838479	2.317431
A_{10}	4.052367·10^{-1}	1.632223·10^{-1}
A_{11}	1.073574	5.660595·10-1

2.1.8 Papay

In 1968 J. Papay proposed Equation 36 for calculating the compressibility factor (Papay, 1968):

$$Z = 1 - \frac{3.52P_{pr}}{10^{0,9813T_{pr}}} + \frac{0.274P_{pr}^2}{10^{0.8157T_{pr}}}. \quad \text{(Eq.36)}$$

2.1.9 Sanjari and Nemati Lay

In 2012 Ehsan Sanjari, Ebrahim Nemati Lay published an empirical expression (Equation 37) for the z-factor based on a virial equation (Sanjari, Nemati Lay, 2012). It was obtained by multiple regression analysis of 5844 experimental values of the compressibility factor for natural gas mixtures from 24 data sources in the range of $1.01 \le T_{pr} \le 3$ and $0.01 \le P_{pr} \le 15$:

$$Z = 1 + A_1P_{pr} + A_2P_{pr}^2 + \frac{A_3P_{pr}^{A_4}}{T_{pr}^{A_5}} + \frac{A_6P_{pr}^{(A_4+1)}}{T_{pr}^{A_7}} + \frac{A_8P_{pr}^{(A_4+2)}}{T_{pr}^{(A_7+1)}}. \quad \text{(Eq.37)}$$

Constant values can be found in table 7.

Table 7. *Constants A_i for empirical expression of Sanjari and Nemati Lay*

A_i	$0.01 < P_{pr} < 3$	$3 < P_{pr} < 15$
A_1	0.007698	0.015642
A_2	0.003839	0.000701
A_3	-0.467212	2.341511
A_4	1.018801	-0.657903
A_5	3.805723	8.902112
A_6	-0.087361	-1.136
A_7	7.138305	3.543614
A_8	0.08344	0.134041

2.1.10 Sohrab Towfighi

In 2019, Sohrab Towfighi published an empirical equation developed by regression analysis of the Standing-Katz chart using machine learning and parameter optimization based on the Levenberg-Marquardt algorithm (Towfighi, 2019). They obtained Equation 38 with 6 constants allowing the calculation of the compressibility factor. Constants are presented in Table 8:

$$Z = A_1^{\left(\left(\frac{T_{pr}}{P_{pr}}\right)+A_2\right)} + A_3^{\left(\left(\frac{A_4}{\frac{T_{pr}}{P_{pr}}}\right)\right)^{\left(\frac{T_{pr}-A_5}{\left(\frac{T_{pr}}{P_{pr}}\right)+A_6}\right)}}. \quad \text{(Eq.38)}$$

Table 8. *Constants A_i for the empirical dependence of Sohrab Towfighi*

i	A_i
1	0.2962187
2	1.285777
3	0.9946115
4	0.04115234
5	3.364051
6	0.5728996

2.1.11. Latonov-Gurevitch

In 1969 an approximation of the Standing and Katz compressibility factor chart was presented in (Latonov, Gurevich, 1969) by Russian researchers V.V. Latonov, G.R. Gurevich (Equation 39):

$$Z = \left(0.4 \lg T_{pr} + 0.73\right)^{P_{pr}} + 0.1P_{pr}. \quad \text{(Eq.39)}$$

In the literature, one can also find Equation 40 written in the following form:

$$Z = \left(0.173761 \ln T_{pr} + 0.73\right)^{P_{pr}} + 0.1P_{pr}. \quad \text{(Eq.40)}$$

These methods are recommended for dry gas over a wide range of pressure and temperature values. However, in the presence of condensate in the gas mixture, the calculation error turns out to be very high.

2.2. Equations of state

Cubic equations of state (EOS) are widely used in the oil and gas industry due to their simplicity and ability to describe the thermodynamic properties of liquids and gases with a high degree of accuracy. There are two-, three-, four- and five-parameter cubic equations of state.

2.2.1 Redlich-Kwong EOS

In 1949, O. Redlich and J. Kwong proposed a two-parameter EOS for gases (Equation 41) (Redlich, Kwong, 1949):

$$p = \frac{RT}{V-b} - \frac{a}{T^{0.5}V(V+b)}, \quad \text{(Eq.41)}$$

where a and b are constants corresponding to the considered fluid and are calculated using Equations 42-43:

$$a = \frac{0.42748R^2T_{pc}^{2.5}}{P_{pc}}, \quad \text{(Eq.42)}$$

$$b = \frac{0.08664RT_{pc}}{P_{pc}}, \quad \text{(Eq.43)}$$

where T_c, P_c are the critical temperature and pressure.

Cubic Redlich-Kwong EOS for z-factor computation is described by:

$$Z^3 - Z^2 + (A - B - B^2)Z - AB = 0. \quad \text{(Eq.44)}$$

The range of its applicability is derived from the expression $\frac{P}{P_c} < 0.5\frac{T}{T_c}$.

To calculate the properties of multicomponent systems, the coefficients a_m and b_m are used, which are calculated using equations 45-46.

$$a_m = \left(\sum_{i=1}^{N} y_i a_i^{0.5}\right)^2, \quad \text{(Eq.45)}$$

$$b_m = \sum_{i=1}^{N} y_i b_i, \quad \text{(Eq.46)}$$

where a_i, b_i are coefficients of i-th component; y_i is the mole fraction of i-th component; N is several components in the mixture.

The Redlich-Kwong equation is a successful empirical modification of the Van der Waals equation of state; the introduction of the temperature dependence $T^{0.5}$ in the denominator has no theoretical justification.

2.2.2 Soave-Redlich-Kwong EOS

The Italian scientist J. Soave proposed a modification of the Redlich-Kwong equation in 1972 (Soave, 1972). The coefficient b remained unchanged since the Equation 43, the coefficient a was presented as a function of temperature and acentric factor.

$$P = \frac{RT}{V-b} - \frac{a\alpha}{V(V+b)}, \quad \text{(Eq.47)}$$

where $a = \alpha \cdot 0.42747R^2\frac{T_{pc}^2}{P_{pc}}$; $b = 0.08664R\frac{T_{pc}}{P_{pc}}$; $\alpha = [1 + (0.48508 + 1.55171\omega - 0.15613\omega^2)(1 - T_r^{0,5})]^2$.

Cubic Soave-Redlich-Kwong equation for the z-factor determination has the same form as Equation 44 with $A = a\alpha\frac{p}{R^2T^2}$, $B = b\frac{p}{RT}$.

For multicomponent systems coefficients a_m and b_m are calculated using the additivity rule (Equations 48-49):

$$a_m = \sum_{i=1}^{N}\sum_{j=1}^{N}(1 - C_{ij})y_i y_j (a_i a_j)^{0.5}, \quad \text{(Eq.48)}$$

$$b_m = \sum_{j=1}^{N} y_i b_i, \quad \text{(Eq.49)}$$

where N is several components in the mixture; C_{ij} is pair interaction correction factor; y_i – mole fraction of the i-th component; a_i – coefficient a for pure i-th component; b_i - coefficient b for a pure i-th component.

2.2.3 Peng-Robinson EOS

Peng-Robinson equation of state has become the most used equation of state in the oil and gas industry. In 1974 D.Robinson and his graduate student Peng proposed the equation 50 (Peng, Robinson, 1976):

$$P = \frac{RT}{V-b} - \frac{a\alpha}{V(V+b)+b(V-b)}. \quad \text{(Eq.50)}$$

Cubic Peng-Robinson equation of state for z-factor computation is

$$Z^3 - (1-B)Z^2 + (A - 3B^2 - 2B)Z - (AB - B^2 - B^3) = 0. \quad \text{(Eq.51)}$$

The compressibility factor for the gas phase is determined as the smallest positive root of equation 51. Coefficients are calculated from the following expressions (Equations 52-57):

$$A = a\alpha\frac{P}{R^2T^2}, \quad \text{(Eq.52)}$$

$$B = b\frac{p}{RT}, \quad \text{(Eq.53)}$$

$$a_c = 0.457235R^2\frac{T_{pc}^2}{P_{pc}}, \quad \text{(Eq.54)}$$

$$b = 0.077796R\frac{T_{pc}}{P_{pc}}, \quad \text{(Eq.55)}$$

$$\alpha(T_{pr}, \omega) = [1 + m(1 - T_{pr}^{0.5})]^2, \quad \text{(Eq.56)}$$

$$m = \begin{cases} 0.37464 + 1.542261\omega - 0.26992\omega^2, \omega \le 0.49, \\ 0.37464 + 1.48503\omega - 0.16442\omega^2 + \\ 0.01666\omega^3, \omega > 0.49 \end{cases} \quad \text{(Eq.57)}$$

For multicomponent systems coefficients a_m and b_m are determined using Equations 48-49.

2.2.4 Peng-Robinson EOS with the shift parameter

Comparing the experimental data with the calculated values of molar volumes revealed an error that remained practically unchanged in a wide pressure range.

In 1988, Yavery and Yungren proposed introducing a linear correction c for the molar volume V of the phase calculated from the equation of state (Jhavery, Youngren, 1988). Thus, the "correct" volume of the phase $\tilde{v}$ was calculated by the formula: $\tilde{V} = V - c$. The introduction of the correction increased the accuracy of liquid density calculating and had a minimal effect on the vapor density at low and medium pressures, since its molar volume was an order of magnitude larger than the correction.

For multicomponent systems, the parameter c is determined by the mixing rule (Equation 58):

$$c = \sum_{i=1}^{N} c_i x_i, \quad \text{(Eq.58)}$$

where N is several components in the mixture; x_i is the mole fraction of the i-th component; c_i is the correction constant for the pure i-th component, which is determined by the formula $c_i = s_i b_i$. Multiplier s for some natural gas components is presented in work (Jhavery, Youngren, 1988).

Thus, the cubic Peng-Robinson equation of state with a shifting parameter is written as Equation 59:

$$P = \frac{RT}{V+c-b} - \frac{a}{(V+c)(V+c+b)+b(V+c-b)}. \quad \text{(Eq.59)}$$

The compressibility factor can be found from Equation 60:

$$Z^3 + (B + 3C - 1)Z^2 + (A - 3B^2 - 2B + 2BC + 3C^2 - 2C)Z + (AC - 2BC - C^2 + C^2B + C^3 - 3CB^2 - AB + B^2 + B^3) = 0, \quad \text{(Eq.60)}$$

Where A, B, C are derived from Equations 61-63.

$$A = \frac{aP}{R^2T^2}, \quad \text{(Eq.61)}$$

$$B = \frac{bP}{RT}, \quad \text{(Eq.62)}$$

$$C = \frac{cP}{RT}. \quad \text{(Eq.63)}$$

2.2.5 Harmens-Knapp EOS

The three-parameter equation of state, proposed by the authors A. Harmens and H. Knapp in 1980, was aimed to improve the expression of the temperature function describing

phase behavior of the superheated steam (Harmens, 1980).

$$p = \frac{RT}{V-b} - \frac{a}{V^2+bcV-b^2(c-1)}. \quad \text{(Eq.64)}$$

The cubic Harmens-Knapp Equation 64 for z-factor determination is written as Equations 65-76:

$$Z^3 + (Bc - B - 1)Z^2 + [A + B^2(1-2c) - Bc]Z + [B^3(c-1) + B^2(c-1) - AB] = 0, \quad \text{(Eq.65)}$$

$$A = a\frac{P}{R^2T^2}, \quad \text{(Eq.66)}$$

$$B = b\frac{P}{RT}, \quad \text{(Eq.67)}$$

where $a = \alpha(T_{pr})\Omega_a R^2 \frac{T_{pc}^2}{P_{pc}}$; (Eq.68)

$$b = \Omega_b R \frac{T_{pc}}{P_{cp}}; \quad \text{(Eq.69)}$$

$$c = 1 + \frac{1-3\zeta}{\beta\zeta}; \quad \text{(Eq.70)}$$

$$\Omega_a = 1 - 3\zeta + 3\zeta^2 + \beta\zeta(3 - 6\zeta + \beta\zeta), \quad \text{(Eq.71)}$$

$$\Omega_b = \zeta\beta, \quad \text{(Eq.72)}$$

$$\begin{cases} \alpha(T_r) = \left[1 + E\left(1 - T_{pr}^{0.5}\right) - F\left(1 - T_{pr}^{-1}\right)\right]^2, \ T_{pr} \le 1; \\ \alpha\left(T_{pr}\right) = 1 - (0.6258 + 1.5227\omega)lnT_{pr} + \\ (0.1533 + 0.41\omega)\left(lnT_{pr}\right)^2, \ T_{pr} > 1; \end{cases} \quad \text{(Eq.73)}$$

$$\begin{cases} E = 0.50 + 0.27767\omega + 2.17225\omega^2, \\ F = -0.022 + 0.338\omega - 0.845\omega^2, \text{when } \omega \le 0.2; \\ E = 0.41311 + 1.14657\omega, \\ F = 0.0118, \text{when } \omega > 0{,}2 \end{cases} \quad \text{(Eq.74)}$$

$$\beta = 0.10770 + 0.76405\zeta - 1.24282\zeta^2 + 0.96210\zeta^3, \quad \text{(Eq.75)}$$

$$\zeta = 0.3211 - 0.080\omega + 0.0384\omega^2. \quad \text{(Eq.76)}$$

2.2.6 Patel-Teja EOS

In 1982 Patel and Teja developed the modified equation of state (Equation 77). The key modification became the introduction of the third parameter c and Ω_c (Patel, Teja, 1982).

$$p = \frac{RT}{V-b} - \frac{a[T]}{V(V+b)+c(V-b)}. \quad \text{(Eq.77)}$$

Patel and Teja found that using the adjusted critical compressibility factor would improve the accuracy of the calculations. The cubic equation of Patel-Teja is Equation 78 with Equations 79-94.

$$Z^3 - (C-1)Z^2 + (A - 2BC - B^2 - B - C)Z + (B^2C + BC - AB) = 0. \quad \text{(Eq.78)}$$

where $A = a\frac{P}{R^2T^2}$, (Eq.79)

$$B = b\frac{P}{RT}, \quad \text{(Eq.80)}$$

$$C = c\frac{P}{RT}, \quad \text{(Eq.81)}$$

$$a[T] = \Omega_a R^2 \frac{T_{pc}^2}{P_{pc}}\alpha[T_{pr}], \quad \text{(Eq.82)}$$

$$b = \Omega_b R \frac{T_{pc}}{P_{pc}}, \quad \text{(Eq.83)}$$

$$\mathrm{c} = \Omega_c R \frac{T_{pc}}{P_{pc}}, \quad \text{(Eq.84)}$$

$$\alpha = \left[1 + F\left(1 - T_{pr}^{\frac{1}{2}}\right)\right]^2, \quad \text{(Eq.85)}$$

$$\Omega_a = 3\,\zeta_{\mathrm{c}}^2 + 3(1-2\zeta_{\mathrm{c}})\Omega_b + \Omega_b^2 + 1 - 3\zeta_c, \quad \text{(Eq.86)}$$

$$\Omega_b^3 + (2 - 3\zeta_{\mathrm{c}})\Omega_b^2 + 3\zeta_{\mathrm{c}}^2\Omega_b - \zeta_{\mathrm{c}}^3 = 0, \quad \text{(Eq.87)}$$

$$\Omega_c = 1 - 3\zeta_{\mathrm{c}}, \quad \text{(Eq.88)}$$

ζ_{c} is corrected critical compressibility factor given by the following formula

$$\zeta_{\mathrm{c}} = 0.329032 - 0.076799\omega + 0.0211947\omega^2, \quad \text{(Eq.89)}$$

$$F = 0.452413 + 1.30982\omega - 0.295937\omega^2, \quad \text{(Eq.90)}$$

$$a_{ij} = \xi_{ij}\left(a_{ii}a_{jj}\right)^{1/2}, \quad \text{(Eq.91)}$$

$$a_m = \sum_i \sum_j x_i x_j a_{ij}, \quad \text{(Eq.92)}$$

$$b_m = \sum_i x_i b_i, \quad \text{(Eq.93)}$$

$$c_m = \sum_i x_i c_i. \quad \text{(Eq.94)}$$

In particular cases, it is possible to take ζ_{c} equal to the critical compressibility factor, but this negatively affects the accuracy of calculations.

2.2.7 Brusilovsky EOS

Brusilovsky, A. I. in 1990 presented the four-parameter equation 95 (Brusilovsky, 1992):

$$P = \frac{RT}{V-b} - \frac{a(T,V)}{(V+c)(V+d)}, \quad \text{(Eq.95)}$$

where b, c, d are the constants for the considered fluid; φ is the temperature function equal to unity at a critical temperature.

In cubic form it is written as Equation 96:

$$Z^3 + (C + D - B - 1)Z^2 + (A - BC + CD - BD - D - C)Z - (BCD + CD + AB) = 0. \quad \text{(Eq.96)}$$

Coefficients A, B, C, D are derived from Equations 97-100:

$$A = a\frac{P}{R^2T^2}, \quad \text{(Eq.97)}$$

$$B = b\frac{P}{RT}, \quad \text{(Eq.98)}$$

$$C = c\frac{P}{RT}, \quad \text{(Eq.99)}$$

$$D = d\frac{P}{RT}, \quad \text{(Eq.100)}$$

The structure of the coefficients can be understood from Equations 101-110:

$$a = a_c \cdot \varphi(T_{pr}, \omega), \quad \text{(Eq.101)}$$

$$\varphi(T_{pr}, \omega) = [1 + \psi(1 - T_{pr}^{0.5})]^2, \quad \text{(Eq.102)}$$

$$a_c = \frac{\alpha R^2 T_{pc}^2}{P_{pc}}, \quad \text{(Eq.103)}$$

$$b = \frac{\beta R T_{pc}}{P_{pc}}, \quad \text{(Eq.104)}$$

$$c = \frac{\sigma R T_c}{P_{pc}}, \quad \text{(Eq.105)}$$

$$d = \frac{\delta R T_{pc}}{P_{pc}}, \quad \text{(Eq.106)}$$

$$\alpha = \Omega_c^3, \quad \text{(Eq.107)}$$

$$\beta = Z_c^* + \Omega_c - 1, \quad \text{(Eq.108)}$$

$$\sigma = -Z_c^* + \Omega_c[0.5 + (\Omega_c - 0.75)^{1/2}], \quad \text{(Eq.109)}$$

$$\delta = -Z_c^* + \Omega_c[0.5 - (\Omega_c - 0.75)^{1/2}]. \quad \text{(Eq.110)}$$

Here Z_c^*, Ω_c are independent parameters of the equation of state. Their values, along with the function $\varphi = \varphi(T)$, completely determine the equation of state of a pure substance.

It is noted that Z_c^* is not the value of the coefficient at the critical point, but for two-coefficient equations of state Z_c^* is determined by the given form of the equation, and for three- and four-coefficient equations it is to be found.

The values of the parameters ψ, Ω_c, Z_c^* for pure components are given in (Brusilovsky, 1992).

Coefficients of the Brusilovsky equation of state for a multicomponent gas mixture are calculated using Equations 111-114.

$$a = \sum_{i=1}^{N}\sum_{j=1}^{N}(1 - C_{ij})y_i y_j (a_i a_j)^{0.5}, \quad \text{(Eq.111)}$$

$$b = \sum_{j=1}^{N} y_i b_i, \quad \text{(Eq.112)}$$

$$c = \sum_{j=1}^{N} y_i c_i, \quad \text{(Eq.113)}$$

$$d = \sum_{j=1}^{N} y_i d_i, \quad \text{(Eq.114)}$$

Pair interaction coefficients depend on the temperature, as shown by Equation 115:

$$C_{ij} = e_{ij} + q_{ij}(T - 273.15) \cdot 10^{-3} + h_{ij}(T - 273.15)^2 \cdot 10^{-5}, \quad \text{(Eq.115)}$$

where e_{ij}, q_{ij}, h_{ij} are constant values represented in (Drohm, 1988).

2.3. Pseudocritical parameters

It has been experimentally proven that the method of calculating the reduced parameters for the mixture using experimentally found or calculated critical parameters gives insufficient accuracy for the compressibility factor determination using the EOS (Bretschneider, 1966) (Equations 116-117).

$$P_{pr} = \frac{P}{P_c} \quad \text{(Eq.116)}$$

$$T_{pr} = \frac{T}{T_c} \quad \text{(Eq.117)}$$

For multicomponent mixtures, there is no single rule to calculate P_c, T_c

The calculated reduced values for the mixture (Equations 118-119) should satisfy the dependencies obtained from the EOS and be suitable for a pure substance.

$$T_{pr} = T/T_{pc} \quad \text{(Eq.118)}$$

$$P_{pr} = P/P_{pc.} \quad \text{(Eq.119)}$$

Assuming that the critical parameters for mixtures can be calculated as a sum of mole fraction of each component multiplied by the corresponding critical parameter, Kay proposed a method for calculating the pseudocritical parameters T_{pcr} and P_{pcr} (Equations 120-121) (Kay, 1936).

$$T_{pc} = \sum x_i T_{ci}, \quad \text{(Eq.120)}$$

$$P_{pc} = \sum x_i P_{ci}. \quad \text{(Eq.121)}$$

Joffe, analyzing the van der Waals equation, proposed formulae for calculating pseudocritical parameters (Equations 122-123) (Joffe, Zudkevitch, 1966):

$$T_{pc} = \frac{\left[\sum_{i=1}^{N} x_i \frac{T_{ci}^{1,25}}{P_{ci}^{\frac{1}{2}}}\right]^{\frac{4}{3}}}{\left[\sum_{i=1}^{N} x_i \frac{T_{ci}}{P_{ci}}\right]^{\frac{2}{3}}}, \quad \text{(Eq. 122)}$$

$$P_{pc} = \frac{\left[\sum_{i=1}^{N} x_i \frac{T_{ci}^{1,25}}{P_{ci}^{\frac{1}{2}}}\right]^{\frac{4}{3}}}{\left[\sum_{i=1}^{N} x_i \frac{T_{ci}}{P_{ci}}\right]^{\frac{5}{3}}}. \quad \text{(Eq.123)}$$

Prausnitz and Gunn modified pseudocritical pressure calculation (Prausnitz, 1958):

$$P_{pc} = \frac{RT_{pc}}{\sum_{i=1}^{N} x_i V_{M_{ci}}} \sum_{i=1}^{N} x_i z_{ci}, \quad \text{(Eq.124)}$$

where $V_{M_{ci}}$ – critical mole volume of the component in the mixture.

Pseudocritical parameters calculated using Kay's rule differ from other rules by less than 2% if $0{,}5 < \frac{T_{c_i}}{T_{c_{i+1}}} < 2$ and $0{,}5 < \frac{P_{c_i}}{P_{c_{i+1}}} < 2$.

For P_{c_m} Kay's rule shows the same results as other rules when $P_{c_i} \approx P_{c_{i+1}}$ or $V_{c_i} \approx V_{c_{i+1}}$. The calculation results can differ up to 10% when $0{,}5 < P_{c_i}/P_{c_{i+1}} < 2$ and $T_{c_i}/T_{c_{i+1}} \approx 1$. For other conditions the difference would be greater.

To determine pseudocritical parameters, Kay's rule is most often used. If high accuracy is required, the Joffe or Praunitz and Gunn formulae are used.

For a more accurate determination of the pseudocritical parameters P_{pc}, T_{pc} of gas mixtures of gas condensate fields, it is recommended to use the equations 125-128 (Stewart, Burkhard, and Voo, 1959):

$$P_{pc} = \frac{K}{J^2}, \quad \text{(Eq.125)}$$

$$T_{pc} = \frac{K}{J}, \quad \text{(Eq.126)}$$

$$\mathrm{K} = \left[\frac{\sum x_i T_{ci}}{P_{ci}^{0,5}}\right]^2, \quad \text{(Eq.127)}$$

$$J = \frac{1}{3}\sum \frac{x_i T_{ci}}{P_{ci}} + \frac{2}{3}\left[\sum x_i \left(\frac{T_{ci}}{P_{ci}}\right)^{0,5}\right]^2, \quad \text{(Eq.128)}$$

For acid gases, if the concentration of CO_2 and H_2S is less than 25% for each and is less than 50% for both, it is recommended to use the following formulae:

$$\mathrm{P}_{pc}^{*} = \frac{\mathrm{P}_{pc}\mathrm{T}_{pc}^{*}}{\left[\mathrm{T}_{pc} + x_{\mathrm{H_2S}}(1 - x_{H_2S})\varepsilon\right]}, \quad \text{(Eq.129)}$$

$$\mathrm{T}_{pc}^{*} = \mathrm{T}_{pc} - \varepsilon, \quad \text{(Eq.130)}$$

$$\varepsilon = 14 x_{H_2S}^{-0,36} x_{CO_2}^{0,8} + 0{,}8 x_{H_2S}^{0,7}, \quad \text{(Eq.131)}$$

where x_{H_2S}, x_{CO_2}– mole fractions of H_2S and CO_2 respectively; P_{pc}, T_{pc} – pseudocritical pressure and temperature.

3. RESULTS AND DISCUSSION:

3.1. Comparison of the compressibility factors calculated by different methods

In this work, the collection and aggregation of experimental studies of various gas mixtures from the integrated field research laboratory of the Integrated Well and Reservoir Survey Department of the Branch office of Gazprom VNIIGAS LLC in Ukhta, as well as sources (Buxton, Campbell, 1967; Ababio *et al*., 2001; Drohm, 1988; McElroy *et al.*, 2001; Hall, 1973; Roe, 1972; Brusilovsky, 2002; Lapshin *et al*., 2011; Obuba *et al*., 2013; Fayazi *et al*., 2014; Bian *et al*., 2012) were carried out. There were considered 824 experimentally obtained values of the compressibility factor for 235 gas mixtures (natural gas and gas of separation) in the pressure range from 0.1 to 94 MPa and temperatures from 273 to 437 K. All the considered studies are presented in Table 9.

Samples of natural and associated petroleum gas, consisting of methane and heavier hydrocarbons (including C5 + fractions) were considered. Hydrocarbon gas mixtures with non-combustible components such as carbon dioxide, hydrogen sulfide, nitrogen, helium were also considered.

Table 9. *Experimental studies of various gas mixtures*

Number of measurements	Temperature, °C	Pressure, MPa	Compound of CH_4, %	Citation
315	11-111	0.1-34	71-92	Branch office of Gazprom VNIIGAS LLC in Ukhta
165	37-71	7-48	58-89	(Buxton and Campbell, 1967)
83	35-60	0.6-12	20-50	(Ababio, McElroy, Williamson, 2001)
61	104-164	1.4-47	55-86	(Drohm, 1988)
61	10-60	0.7-8.6	30-40	(McElroy, Fang, Williamson, 2001)
58	78-153	14-94	30-91	(Hall, 1973)
27	0-21	0.2-10.2	92-93	(Roe, 1972)
19	40	8-64	59	(Brusilovsky, 2002)
17	20	29-31	80	(Lapshin *et al.*, 2011)
12	75	2.9-31.4	89-91	(Obuba, 2013)
6	32	3.7-18.8	91	(Fayazi, 2014)

For all experimental data, the compressibility factor was calculated by the 19 methods described above. Pseudocritical parameters were calculated according to Kay's rule. The accuracy of the calculated values was assessed using mathematical statistics (Tables 10,11; Figure 1).

Types of errors are represented in Equations 132-136.

Average Absolute Relative Error (AARE),

$$AARE\% = \frac{100}{N}\sum_{i=1}^{N}\left|\frac{z_i^{pred}-z_i^{exp}}{z_i^{exp}}\right|, \qquad \text{(Eq. 132)}$$

where z_i^{pred} – the calculated value of compressibility factor, z_i^{exp}– experimental value of compressibility factor.

Mean Squared Error (MSE)

$$MSE = \frac{\sum_{i=1}^{N}(z_i^{pred}-z_i^{exp})^2}{N}. \qquad \text{(Eq.133)}$$

Root Mean Squared Error (RMSE)

$$RMSE = \sqrt{\frac{\sum_{i=1}^{N}(z_i^{pred}-z_i^{exp})^2}{N}}. \qquad \text{(Eq.134)}$$

Standard deviation (SD)

$$SD = \sqrt{\frac{1}{N-1}\sum_{i=1}^{N}\left(z_i^{pred} - average\left(z_i^{exp}\right)\right)^2}, \qquad \text{(Eq.135)}$$

where $average\left(z_i^{exp}\right)$ is the mean value of the observation.

Coefficient of determination (R^2)

$$R^2 = 1 - \frac{\sum_{i=1}^{N}(z_i^{pred}-z_i^{exp})^2}{\sum_{i=1}^{N}\left(z_i^{pred}-average\left(z_i^{exp}\right)\right)^2}. \qquad \text{(Eq.136)}$$

Calculations of the compressibility factor using empirical dependencies were carried out, taking into account the boundary conditions for reduced pressure and reduced temperature (Table 12). Calculations using the equations of state were performed for all experimental values without introducing boundary conditions.

Results presented in Tables 10-11 show that the empirical dependencies of Sanjari and Nemati Lay; Heidaryan, Moghadasi, and Rahimi; Dranchuk and Abou-Kassem, as well as the Peng-Robinson equation of state with the shift parameter and Brusilovsky equation allow achieving the most accurate results for most gas compositions. The graphs of the average absolute relative error in the coordinates $T_{pr} - P_{pr}$ – AARE (Figures 2-3) clearly shows that the accuracy of the calculated values is more influenced by the reduced pressure than the reduced temperature. For Bahadori, Papay, Heidaryan, Sohrab Towfighi, Latonov-Gurevich, Peng-Robinson, Harmens-Knapp methods, the error increases with reduced pressure (Figures 2, 3). Modification of the Peng-Robinson equation of state allows to solve this problem and significantly increases the accuracy

of compressibility factor predicting (Figure 3(a,d)).

Table 12. *The range of thermobaric conditions in which the empirical dependencies are valid*

Method	P_{pr}	T_{pr}
Azizi	$0.2 \le P_{pr} \le 11$	$1.1 \le T_{pr} \le 2$
Bahadori	$0.2 < P_{pr} < 16$	$1.05 < T_{pr} < 2.4$
Bahadori for gases with CO_2 and H_2S	$0.2 < P_{pr} < 16$	$1.05 < T_{pr} < 2.4$
Dranchuk and Abou-Kassem	$0.2 \le P_{pr} \le 30$ $P_{pr} \le 1$	$1 < T_{pr} \le 3$ $0.7 < T_{pr} \le 1$
Dranchuk Purvis Robinson	$0.2 \le P_{pr} \le 30$	$1 \le T_{pr} \le 3$
Hall and Yarborough	$0.8 \le P_{pr}$	$1.2 \le T_{pr}$
Heidaryan	$0.2 < P_{pr} < 17$	$1.2 < T_{pr}$
Heidaryan, Moghadasi and Rahimi	$0.2 < P_{pr} < 17$	$1.2 < T_{pr}$
Papay	$P_{pr} \le 8$	$T_{pr} \le 2$
Sanjari and Nemati Lay	$0.01 \le P_{pr} \le 15$	$1.01 \le T_{pr} \le 3$
Sohrab Towfighi	$0.2 \le P_{pr} \le 16$	$1.05 \le T_{pr} \le 3$
Latonov-Gurevitch	$0.2 \le P_{pr} \le 16$	$1 \le T_{pr} \le 3$

The point-by-point analysis of the results does not identify the best method in the entire range of the studied pressures and temperatures (Figure 4). However, in considering the temperature and pressure ranges corresponding to separation processes and reservoir conditions in the oil and gas industry, several conclusions can be made. In the range of temperatures and pressures not exceeding 20 ºC and 2 MPa, respectively, the Sanjari and Nemati Lay correlation among the empirical dependences turns out to be the best method, and the best equation of state is Soave-Redlich-Kwong. For temperatures and pressures characteristic for field conditions (temperature 20-100 ºC, pressure 2-40 MPa), it is recommended to choose the optimal model for predicting the compressibility factor according to Table 12.

3.2 Mixtures with high fraction of CO_2

The development of most oil and gas condensate fields with a high methane content is now entering its final stage. In recent years, more and more natural gas deposits with high CO_2 content have been found worldwide (Gachuz-Muro, Sanchez-Bujanos, Castro-Herrera, Rodriguez-Pimentel, 2011; Jokhio, Tiab Escobar, 2001). Modeling the development and operation of such facilities requires special knowledge due to the aggressiveness of carbon dioxide under conditions characteristic for processes occurring under high pressure and temperature (Koriakin, 2018; Nešić, 2011), as well as in plumes and equipment of surface facilities (Ponomarev Yusupov, 2020). The presence of CO_2 in such objects can significantly affect the value of the compressibility factor. Therefore, 212 points were analyzed for mixtures with CO2 content above 10% among the above experimental results. The accuracy of both correlation dependences and equations of state is presented in Figures 5, 6. According to Figure 5, it is possible to distinguish the pressure range in which there are certain preferences for choosing the correlation dependence.

However, the results show that for acid gases, the equations of state are more preferable. In this case, in the range of pressures not exceeding 8 MPa, the Soave-Redlich-Kwong equation of state shows good results, and for higher pressures, it's better to use the Brusilovsky and Peng-Robinson equation of state with the shift parameter.

3.3 Influence of pseudocritical parameters on the value of the z-factor

The analysis of the influence of the method for calculating pseudocritical parameters on the accuracy of the compressibility factor determination is carried out in this subsection.

The Bahadori method for calculating the compressibility factor of gas mixtures with a high content of acid components is not considered in this subsection due to the fact that it already provides the correction of the pseudocritical parameters.

The compressibility factor determined for the pseudocritical conditions calculated according to different rules are shown in Figures 7-9.

For the methods of Latonov-Gurevich with natural logarithm; Latonov-Gurevich; Sanjari and Nemati Lay; Dranchuk and Abou-Kassem; Dranchuk-Purvis-Robinson; Papay; Sohrab Towfighi, an increase in the calculation accuracy

by 0.02-0.1% is observed when using Equations 122-123. For Hall and Yarborough; Heidaryan, Moghadasi and Rahimi; Heidaryan; Bahadori methods, equations 122-123 are not recommended. When determining the z-factor of gas mixtures using the Latonov-Gurevich correlation, in order to increase the accuracy (by 0.1%), it is recommended to use equations (122-123) (Figures 7).

Figure 8 represents the pseudocritical parameters for mixtures with acid content in the range of 10-47% for pseudocritical parameters calculated using Equations 129-130 and Kay's rule (Equations 120-121). The accuracy of the z-factor determination using the empirical correlations significantly increase when the equations 129-130 are used to calculate the pseudocritical parameters. The increase in the accuracy is in the range of 0.5-1.6%.

The z-factor for P_{pc} and T_{pc} calculated using Prausnitz-Gunn rule is presented in Figure 9. It is shown that an increase in the calculation accuracy for all the empirical correlations is in the range of 0.03-0.23% when using the Prausnitz-Gunn rule. For the Sohrab Towfighi method, the calculation accuracy is increased by 0.23%. For Bahadori and Heidaryan methods, it is not recommended to apply the Prausnitz-Gunn rule.

3.3 Discussion

The results of the study shows that there is no universal method for compressibility factor calculation as natural gas is a complex mixture containing hydrocarbon and non-hydrocarbon components and its physical properties strongly depend on thermobaric conditions. That's why the development of the methods for the z-factor computation still going on and new methods and approaches appear.

It is shown that the accuracy of each method strongly depends on the gas composition. Thus, the equations of state which show good results for hydrocarbons and other simple substances are poor for substances with high content of CO_2. In this case the current study helps to establish the criteria of applicability of each method.

4. CONCLUSIONS:

In the presented work, based on 824 experimentally obtained values of the compressibility factor for 235, various gas mixtures in the pressure range from 0.1 to 94 MPa and temperatures from 273 to 437 K, the search for the optimal equation of state and correlation dependence for accurate prediction of the z-factor was evaluated. Analysis of the results allows us to make the following conclusions:

1. In the entire range of investigated pressures and temperatures for all gas mixtures, the best results are shown by the Peng-Robinson equations of state with the shift parameter and the Brusilovsky equation of state. The Average Absolute Relative Error of the calculated values compared to experimental data does not exceed 2% for these models. Among the correlation dependences, the best results are shown by Sanjari and Nemati Lay; Heidaryan, Moghadasi and Rahimi correlations with an error not exceeding 3%.
2. A point-by-point analysis of the compressibility factor shows that for most of the proposed methods, the reduced pressure has more significant effect on the accuracy of the calculated values than the reduced temperature. For the Bahadori, Papay, Heidaryan, Sohrab Towfighi, Latonov-Gurevich, Peng-Robinson, Harmens-Knapp methods, the error increases significantly with increasing reduced pressure.
3. When studying acid gas mixtures with a CO_2 content of more than 10%, preference should be given to equations of state. In the entire range of temperatures and pressures up to 8 MPa, the Soave-Redlich-Kwong equation of state has a clear advantage for such compositions. At higher pressures, preference should be given to the Peng-Robinson equation of state with the shift parameter and Brusilovsky equation.

5. ACKNOWLEDGMENTS:

The work was supported by the Grant of the President of Russian Federation (grant МК-1102.2020.8)

The authors thank Volkov A. N. and Kiian P.V. from Branch office of Gazprom VNIIGAS LLC in Ukhta for providing experimental measurements for comparison.

6. REFERENCES:

1. Heidaryan, E., Moghadasi, J., Rahimi, M. (2010). New correlations to predict natural gas viscosity and compressibility factor. *J. Petrol. Sci. Eng.,* 73, 67-72.
2. Heidaryan, E., Salarabadi, A., Moghadasi,

J. (2010). A novel correlation approach for prediction of natural gas compressibility factor. *J. Nat. Gas Chem.,* 19, 189-192.
3. Buxton, T. S., Campbell, J. M. (1967) Compressibility factors for lean natural gascarbon dioxide mixtures at high pressure. *SPE J.,* 7, 80–86.
4. Ababio, B. D., McElroy P. J., Williamson, C. J. (2001). Second and third virial coefficients for (methane + nitrogen). *The Journal of Chemical Thermodynamics,* 33(4), 413–421.
5. Drohm, J. K. (1988, June 13-15) *On the Quality of Data From Standard Gas-Condensate PVT Experiments (pp. 525–537)*. SPE Gas Technology Symposium. Dallas, Texas, USA.
6. McElroy, P. J., Fang, J., Williamson, C. J. (2001). Second and third virial coefficients for (methane + ethane + carbon dioxide). *The Journal of Chemical Thermodynamics*m, 33(2), 155–163.
7. Hall, K. R., Yarborough, L. (1973). A new equation of state for Z-factor calculations. *Oil Gas J.*, 71 (25), 82-92.
8. Roe, D. (1972) Thermodynamic Properties of Gases and Gas Mixtures at Low Temperatures and High Pressures [Doctoral Dissertation, University of London]. Imperial College London's repository.
9. Brusilovsky, A. I. (2002). Phase transitions in the development of oil and gas fields. Moscow: Graal.
10. Lapshin, V. I., Volkov, A. N., Shafiev, I. M. (2011). Koefficient szhimaemosti gazov i gazokondensatnyh smesej: eksperimental'noe opredelenie i raschety, *Nauchno-tekhnicheskij sbornik Vesti gazovoy nauki.*, 1(6), 120-131. (In russian)
11. Obuba, J, Ikiesnkimama, S. S, Ubani, C., Ekeke, I. (2013) Natural Gas Compressibility Factor Correlation Evaluation for Niger Delta Gas Fields. *Journal of Electrical and Electronics Engineering,* 6(4), 1–10.
12. Fayazi, A., Arabloo, M., Mohammadi, A. (2014). Efficient estimation of natural gas compressibility factor using a rigorous method. *Journal of Natural Gas Science and Engineering*, 16, 8–17.
13. Bian, X., Du, Zh, Tang, Yo., Du, J. (2012) Measurement and correlation of compressibility factor of high CO2-content natural gas. *Journal of Petroleum Science and Engineering,* 82-83, 38–43.
14. Redlich, O., Kwong, J. N. S (1949). On the Thermodynamics of Solutions. V. An Equation of State. Fugacities of Gaseous Solutions. *Chemical Reviews,* 44(1), 233–244.
15. Soave, G. (1972). Equilibrium constants from a modified Redliche-Kwong equation of state. *Chem. Eng. Sci.*, 27(6), 1197-1203.
16. Peng, D. Y., Robinson, D. B. (1976). A new two-constant equation of state. *Ind. Eng. Chem. Fundam.,* 15(1), 59-64.
17. Jhavery, B. S., Youngren, G. K. (1988). Three-parameter modification of the Peng-Robinson equation of state to improve volumetric predictions. *SPE Reservoir Engineering*, 3(3), 1033-1040.
18. Patel, N. C., Teja, A. S. (1982). A new cubic equation of state for fluids and fluid mixtures. *Chem. Eng. Sci.,* 37(3), 463-473.
19. Harmens, A. (1980). Three-parameter cubic equation of state for normal substances. *Ind. eng. fundamen.,* 19, 291–294.
20. Brusilovsky, A. I. (1992). Mathematical Simulation of Phase Behavior of Natural Multicomponent Systems at High Pressures With an Equation of State. *SPE Res. Eng.,* 7(01), 117–122.
21. Azizi, N., Behbahani, R., Isazadeh, M. A. (2010). An efficient correlation for calculating compressibility factor of natural gases. *J. Nat. Gas Chem.,* 19(6), 642-645.
22. Bahadori, A., Mokhatab, S., Towler, B. F. (2007). Rapidly estimating natural gas compressibility factor. *J. Nat. Gas Chem.* 16(4), 349-353.
23. Dranchuk, P. M., Abou-Kassem, J. H. (1975). Calculation of Z factors for natural gases using equations of state. *J. Can. Petrol. Technol.*, 14(3), 34-36.
24. Dranchuk, P. M., Purvis, R. A., Robinson, D. B. (1974). Computer calculation of natural gas compressibility factors using the Standing and Katz correlation. *In: Inst. Of Petroleum Technical Institute Series,* IP74-008, 1-13.
25. Papay, J. (1968). A termelestechnologiai parameterek valtozasa a gastelepek muvelese soran. *OGIL Musz, Tud, Kuzl, Budapest*, 267-273.
26. Sanjari, E., Nemati Lay, E. (2012). An accurate empirical correlation for predicting natural gas compressibility factors. *J. Nat. Gas Chem.*, 21(2), 184-188.
27. Towfighi, S. (2019). An empirical equation for the gas compressibility factor, Z, *Petroleum Science and Technology.,*

38(1), 1-4.
28. Latonov, V. V., Gurevich, G. R. (1969). Raschet koeffitsiyenta szhimayemosti prirodnogo gaza. *Gazovaya promyshlennost,* 2, 7-9 (In rus).
29. Chamkalani, A., Maesoumi, A., Sameni, A. (2013). An intelligent approach for optimal prediction of gas deviation factor using particle swarm optimization and genetic algorithm. *J. Nat. Gas Sci. Eng*., 14, 132-143.
30. Baniasadi, M., Mohebbi, A., Baniasadi, M. (2012). A new correlation based on artificial neural networks for predicting the natural gas compressibility factor. J. Eng. Thermophys., 21(4), 248-258.
31. Shateri, M., Ghorbani, Sh., Hemmati-Sarapardeh, A., Mohammadi, A. H. (2015). Application of Wilcoxon generalized radial basis function network for prediction of natural gas compressibility factor. *J. Taiwan Inst. Chem.*, 50, 131-141.
32. Ungerer, P., Nieto-Draghi, C., Rousseau, B., Ahunbay, G., Lachet, V. (2007). Molecular simulation of the thermophysical properties of fluids: From understanding toward quantitative predictions. *J. Mol. Liq.*, 134, 71-89.
33. Lagache, M., Ungerer, P., Boutin, A., Fuchs, A. H. (2001). Prediction of thermodynamic derivative properties of fuids by Monte Carlo simulation. *Phys. Chem. Chem. Phys*., 3, 4333-4339.
34. Lagache, M. H., Ungerer, P., Boutin, A. (2004). Prediction of thermodynamic derivative properties of natural condensate gases at high pressure by Monte Carlo simulation. *Fluid Ph. Equilibria*., 220, 211-223.
35. Neubauer, B., Tavitian, B., Boutin, A., Ungerer, P. (1999). Molecular simulations on volumetric properties of natural gas. *Fluid Ph. Equilibria*., 161, 45-62.
36. Malyshev, V. L., Moiseeva, E. F., Kalinovsky, Yu. V. (2018). Comparative study of the determination of thermodynamic properties of methane based on the peng-robinson equation of state and the molecular dynamics simulations. *SOCAR Proceedings*, 2, 33-40.
37. Moiseeva, E. F., Malyshev V. L. (2019). Compressibility factor of natural gas determination by means of molecular dynamics simulation. *AIP Advance*, 9(5), 055108.
38. Gachuz-Muro, H, Sanchez-Bujanos, J. L., Castro-Herrera, I, Rodriguez-Pimentel, J.A. (2011). Quebrache Field: Evaluations to Date of this Natural CO2 Reservoir. *SPE EUROPEC/EAGE Annual Conference and Exhibition*. doi:10.2118/142851-ms
39. Jokhio, S., Tiab D., Escobar, F. (2001). Quantitative Analysis of Deliverability, Decline Curve, and Pressure Tests in CO2 Rich Reservoirs. *Proceedings of SPE Permian Basin Oil and Gas Recovery Conference.* doi:10.2523/70017-ms
40. Koriakin, A. (2018) Carbon dioxide corrosion at the objects of the second district of Achimovsk deposits of Urengoy oil and gas bearing complex. *International Journal of Mechanical Engineering and Technology*, 9(8),1073-1080.
41. Nešić, S. (2011) Carbon dioxide corrosion of mild steel. *Uhlig's Corrosion Handbook.* New Jersey: John Wiley and Sons, Hoboken, 229-245. DOI:10.1002/9780470872864.ch19
42. Ponomarev, A. I., Yusupov A. D. (2020) Effect of shear stress on the wall of technological pipelines at a gas condensate field on the intensity of carbon dioxide corrosion. *Journal of Mining Institute,* 244, 439-447.
43. Bretschneider, S. (1966). Svojstva gazov i zhidkostej : inzhenernye metody rascheta : per. s pol. Moskva Leningrad: Himiya
44. Stewart, W.F., Burkhard, S.F., and Voo, D. (1959) Prediction of Pseudo Critical Parameters for Mixtures. AIChE Meeting, Kansas City, MO.
45. Prausnitz, J. M., Gunn, R. D. (1958) Volumetric properties of nonpolar gaseous mixtures. *AIChE J.*, 4(4), 430-435.
46. Joffe, J., Zudkevitch, D. (1966). Fugacity Coefficients in Gas Mixtures Containing Light Hydrocarbons and Carbon Dioxide. *Industrial & Engineering Chemistry Fundamentals*, 5(4), 455–462. doi:10.1021/i160020a003
47. Kay, W.B. (1936). Density of Hydrocarbon Gases and Vapor at High Temperature and Pressure. Ind. Eng. Chem. (Sept.), 1014–1019.

7. OPEN ACCESS

Table 1. *Constants a_i for Azizi empirical dependence*

i	a_i	i	a_i
1	0,037314	11	-24449114791,153100
2	-0,014081	12	19357955749,327400
3	0,016326	13	-126354717916,607000
4	-0,030778	14	623705678,385784
5	13843575480,943800	15	17997651104,333000
6	-16799138540,763700	16	151211393445,064000
7	1624178942,649760	17	139474437997,172000
8	13702270281,086900	18	-24233012984,095000
9	-41645509,896475	19	18938047327,520500
10	237249967625,013000	20	-141401620722,689000

Table 2. *Constants A_i, B_i, C_i, D_i for the empirical dependence of Bahadory*

i	A_i	B_i	C_i	D_i
a	0,969469	-1,349238	1,443959	-0,368600
b	-0,107783	-0,127013	0,100828	-0,012319
c	0,018481	0,052341	-0,050688	0,010870
d	-0,000584	-0,002146	0,002096	-0,000459

Table 3. *Constants A_i, B_i, C_i, D_i for the empirical dependence of Bahadory for gases with acidic components*

i	A_i	B_i	C_i	D_i
a	4,094086	$1{,}15680575 \cdot 10^2$	$-1{,}6991417 \cdot 10^2$	$5{,}62209803 \cdot 10$
b	$1{,}45517461 \cdot 10^2$	$-3{,}9672762 \cdot 10^2$	$3{,}93741592 \cdot 10^2$	$-2{,}17915813 \cdot 10^2$
c	$-1{,}95766763 \cdot 10^2$	$3{,}835331543 \cdot 10^2$	$-6{,}08818159 \cdot 10^2$	$3{,}704173461 \cdot 10^2$
d	$5{,}24425341 \cdot 10$	$-2{,}0133960 \cdot 10^2$	$3{,}51359351 \cdot 10^2$	$-2{,}20884255 \cdot 10^2$

Table 10. *Statistical data for the case of not taking into account the methods applicability range*

Method	AARE	MSE	RMSE	SD	R2
* Peng-Robinson EOS	1,870609	0,000645	0,02539	0,143565	0,970192
* Brusilovsky EOS	1,945247	0,000695	0,026358	0,146829	0,968043
* Patel-Teja EOS	1,98631	0,000814	0,028524	0,14263	0,962882
* Harmens-Knapp EOS	2,146308	0,001013	0,031831	0,134876	0,957147
Sanjari and Nemati Lay	2,887442	0,007913	0,088954	0,112872	0,646208
* Soave-Redlich-Kwong EOS	2,535057	0,00111	0,033315	0,148475	0,964145
Heidaryan, Moghadasi and Rahimi	2,916752	0,001157	0,034017	0,149505	0,961519
Dranchuk and Abou-Kassem	2,89765	0,001159	0,034049	0,148782	0,960681
Dranchuk-Purvis-Robinson	2,897658	0,001159	0,034049	0,148782	0,960681
Hall and Yarborough	2,916752	0,001157	0,034017	0,149505	0,961519
Papay	6,044089	0,050963	0,225749	0,35271	0,85031
Azizi	3,037741	0,001245	0,035284	0,154106	0,96068
* Peng-Robinson EOS with shift-parameter	3,219377	0,001616	0,040197	0,136433	0,957737
Sohrab Towfighi	3,783834	0,006905	0,083099	0,105103	0,736031
Latonov-Gurevitch (formula with with ln)	3,553486	0,00261	0,051085	0,15244	0,888272
Latonov-Gurevitch	3,554237	0,00261	0,051089	0,152443	0,888263
Heidaryan	5,373959	0,008287	0,091031	0,166027	0,741604
Bahadori for gases containing CO_2 and H_2S	4,570042	0,003594	0,05995	0,152738	0,855099
Bahadori	5,86146	0,004977	0,070546	0,159061	0,839022

Table 11. *Statistical data for the case of taking into account the methods applicability range*

Method	AARE	MSE	RMSE	SD	R2	C
* Peng-Robinson EOS	1,906302	0,000652	0,025528	0,1159	0,952893	28
* Brusilovsky EOS	1,985446	0,000706	0,026569	0,119445	0,950558	28
* Patel-Teja EOS	2,010508	0,000805	0,028372	0,116145	0,942481	28
* Harmens-Knapp EOS	2,14359	0,000942	0,030685	0,109613	0,933218	28
Sanjari and Nemati Lay	2,272306	0,001024	0,032005	0,11211	0,922934	14
* Soave-Redlich-Kwong EOS	2,59733	0,001136	0,033702	0,120254	0,944163	28
Heidaryan, Moghadasi and Rahimi	2,853375	0,001075	0,032781	0,121569	0,944274	91
Dranchuk and Abou-Kassem	2,998977	0,001205	0,034706	0,150798	0,960601	32
Dranchuk-Purvis-Robinson	2,998978	0,001205	0,034706	0,150798	0,960601	32
Hall and Yarborough	3,183188	0,001246	0,035292	0,157492	0,963785	187
Papay	2,924742	0,00156	0,039493	0,088955	0,812701	114
Azizi	3,157948	0,001294	0,035977	0,106037	0,912075	106
* Peng-Robinson EOS with shift-parameter	3,214932	0,001433	0,037856	0,112618	0,937865	28
Sohrab Towfighi	3,502897	0,003257	0,05707	0,099716	0,796591	44
Latonov-Gurevitch (formula with ln)	3,539731	0,001948	0,044138	0,100205	0,870776	44
Latonov-Gurevitch	3,540538	0,001949	0,044144	0,100209	0,870753	44
Heidaryan	4,177206	0,001965	0,044324	0,132446	0,925592	91
Bahadori for gases containing CO_2 and H_2S	4,302181	0,002872	0,053596	0,134157	0,846081	44
Bahadori	5,605219	0,004128	0,064252	0,139824	0,824332	44

Reference: Column ‘C’ is the number of values not taken into statistics because thermobaric conditions did not satisfy the applicability range of the method.

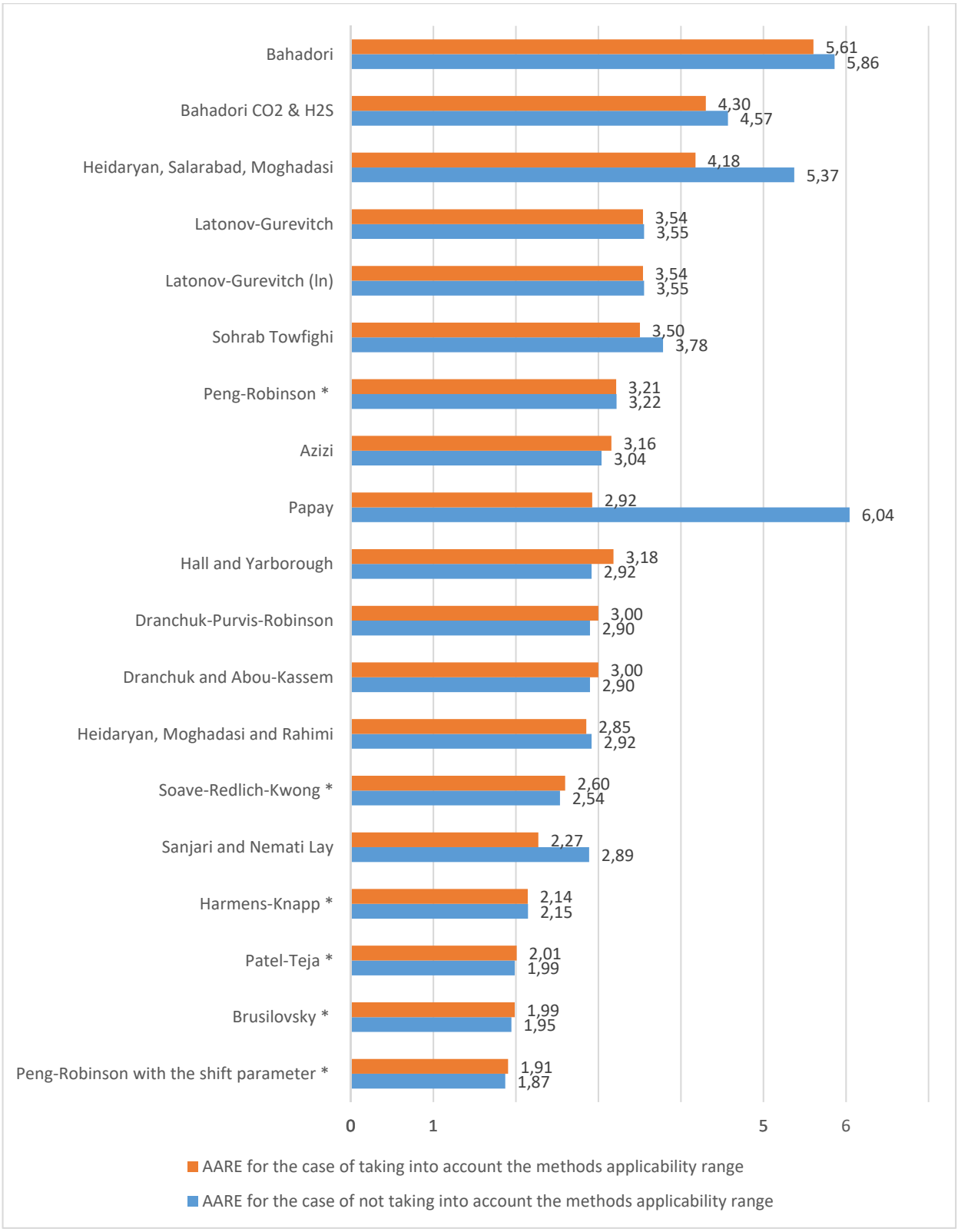

Figure 1. *AARE for different methods of compressibility factor calculation*

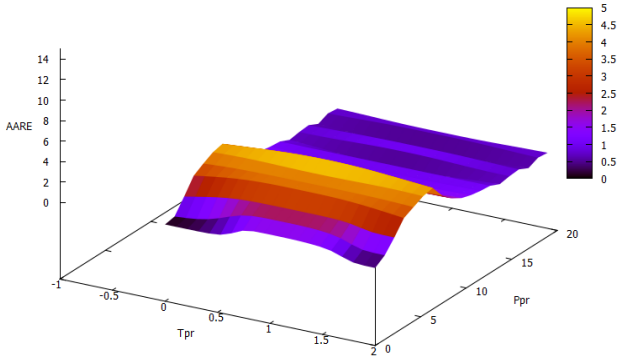

a) Azizi

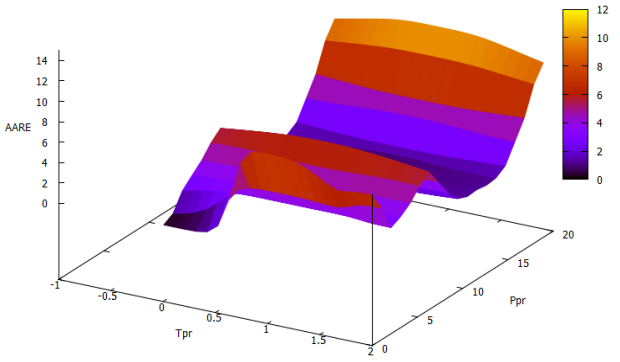

b) Bahadori

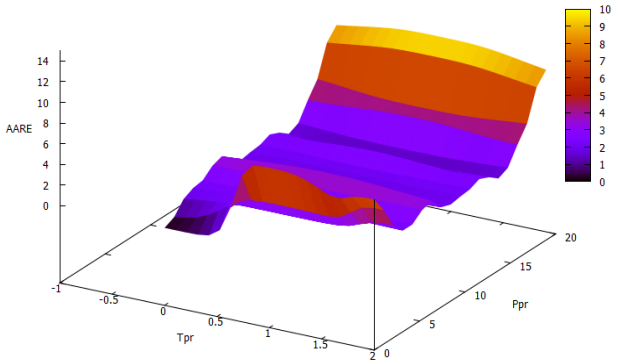

c) Bahadori with hig content of $_2$ and H_2S

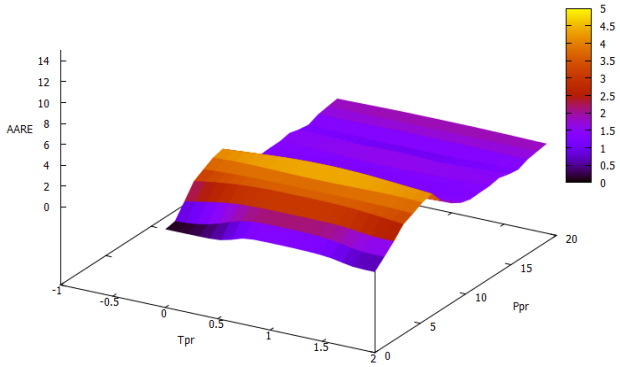

d) Dranc k Purvis Robinson

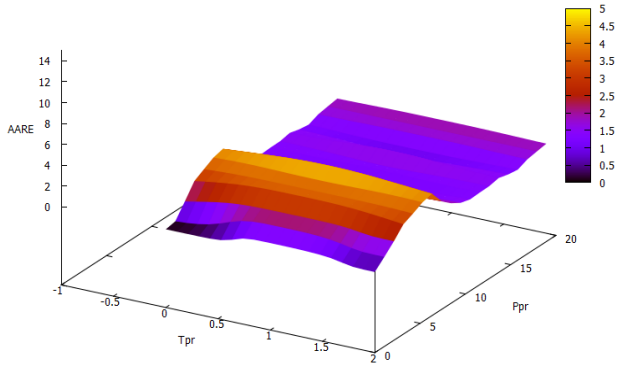

e) Dranc k and Abou-Kassem

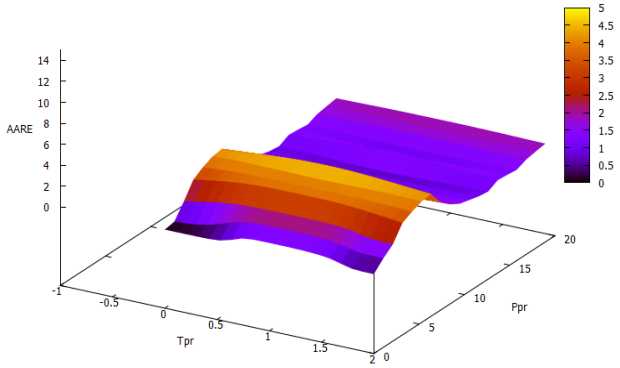

f) Hall and Yarboro h

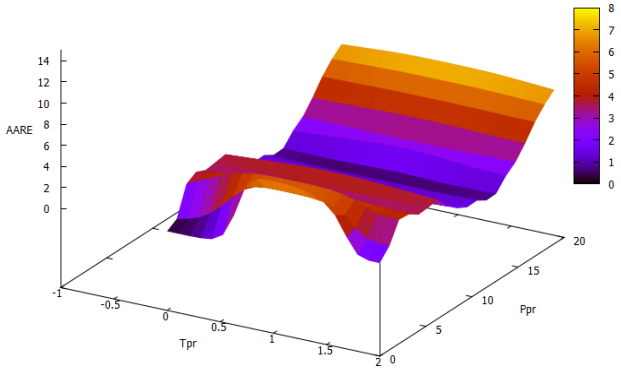

g) Heidary

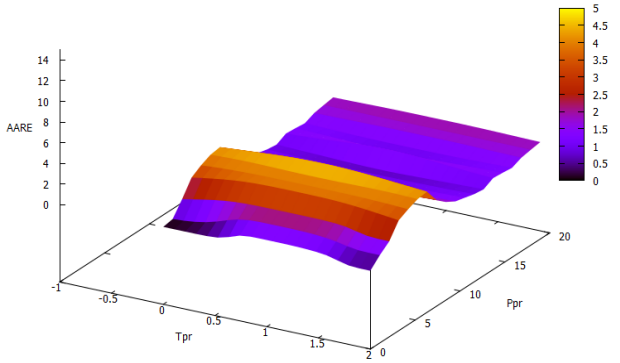

h) Heidaryan Moghadasi and Rahimi

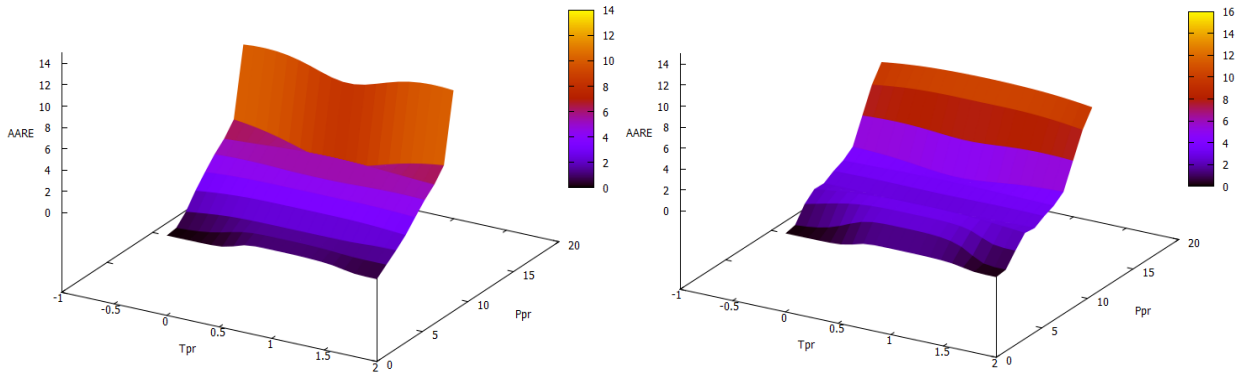

i) Papay ***j) Sohrab Towfighi***

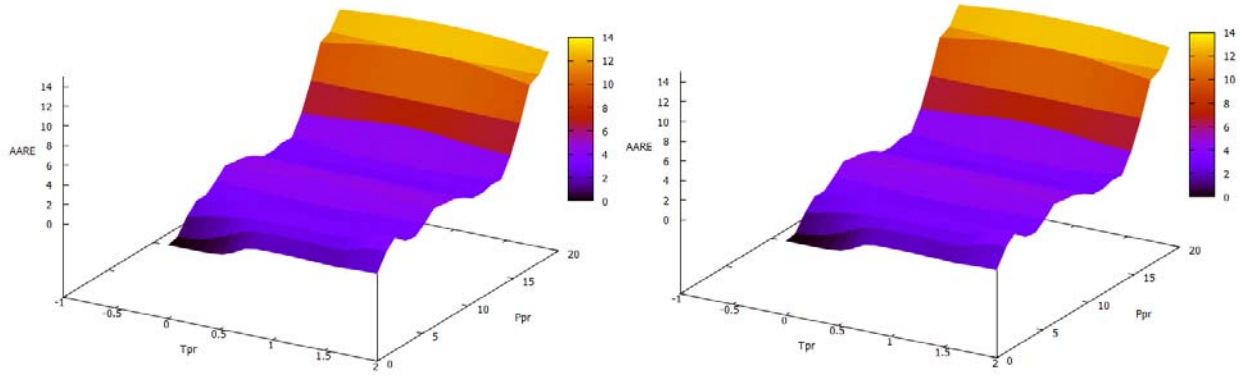

k) Latonov-Gurevitch with In ***l) Latonov-Gurevitch***

Figure 2. *AARE for the empirical correlations*

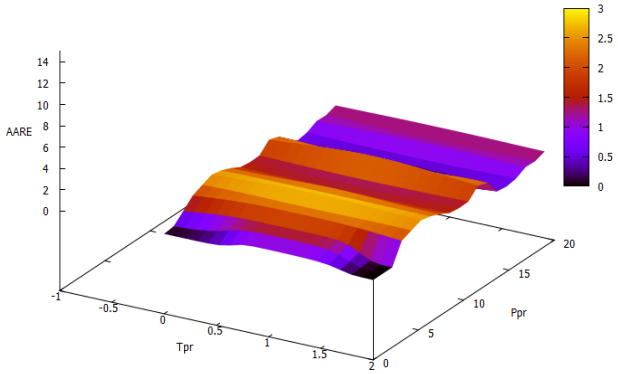

a) Brusilovsky EOS

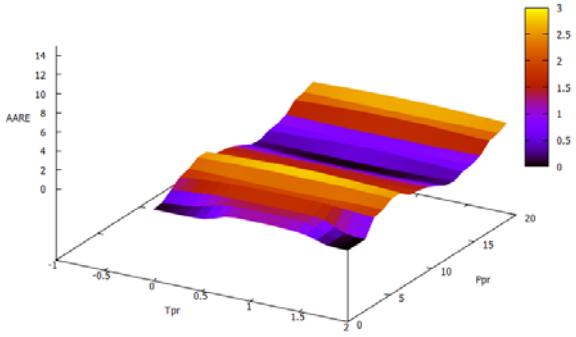

b) Patel-Teja EOS

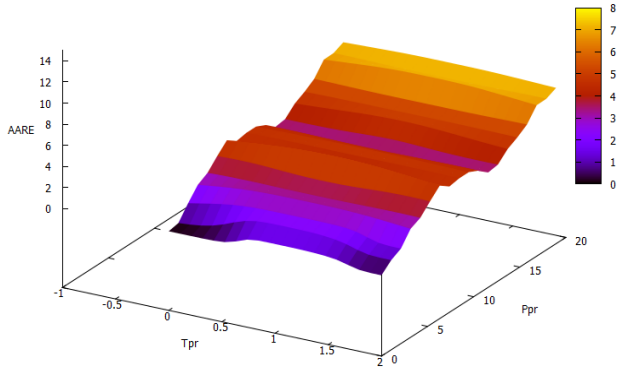

c) Peng-Robinson EOS

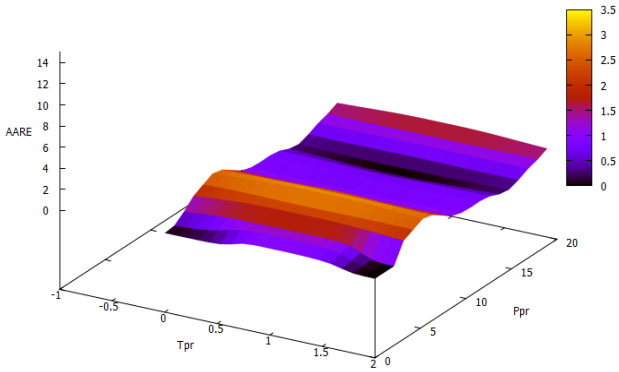

d) Peng-Robinson EOS with shift-parameter

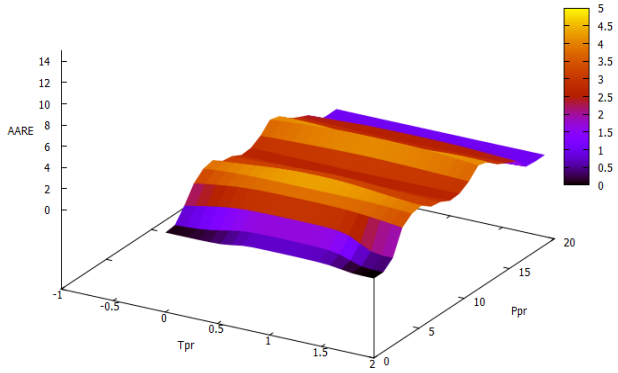

e) Soave-Redlich-Kwong EOS

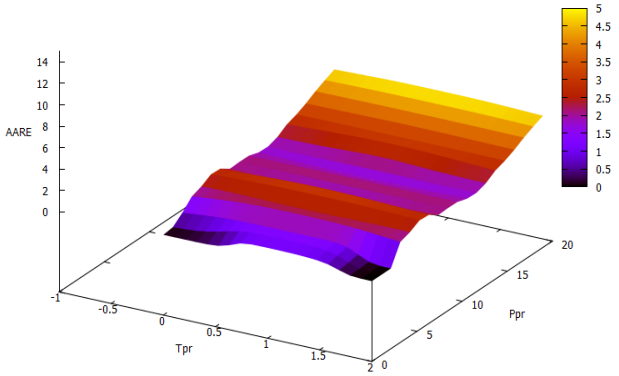

f) Harmens-Knapp EOS

Figure 3. *AARE for the equations of state*

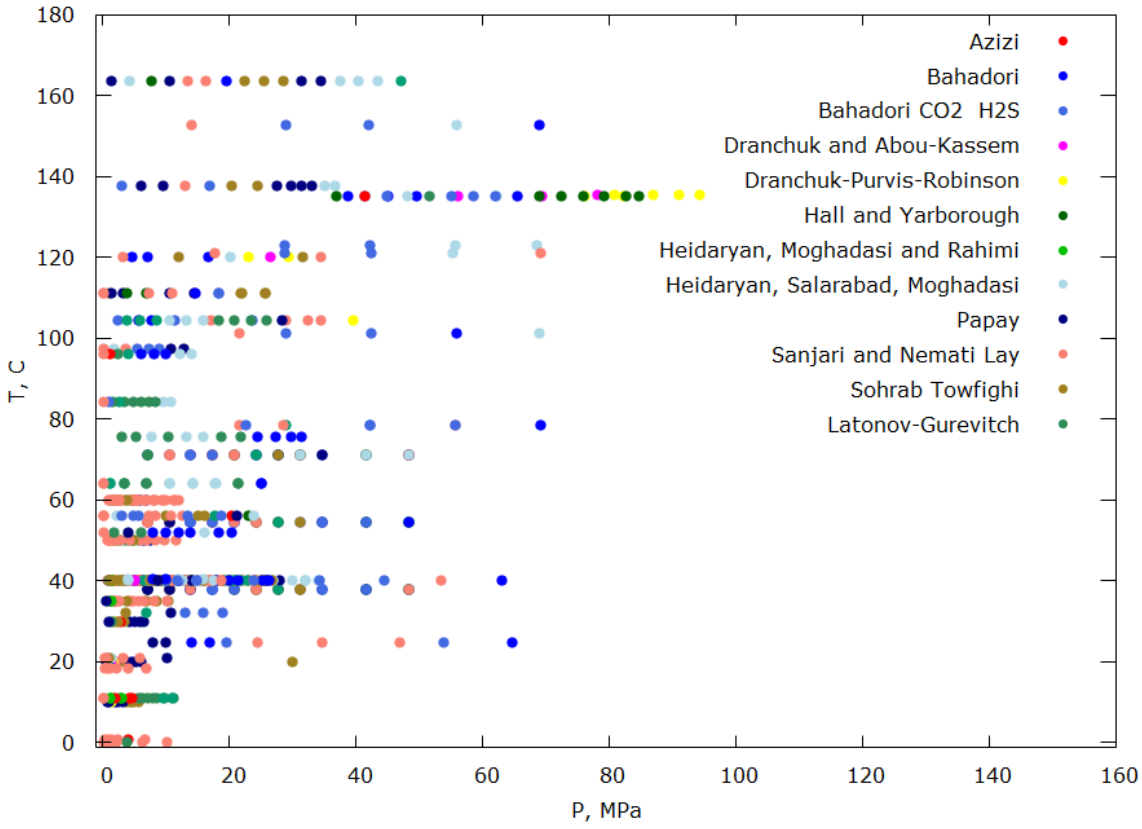

Figure 4. *Best methods (by AARE) among the empirical dependencies*

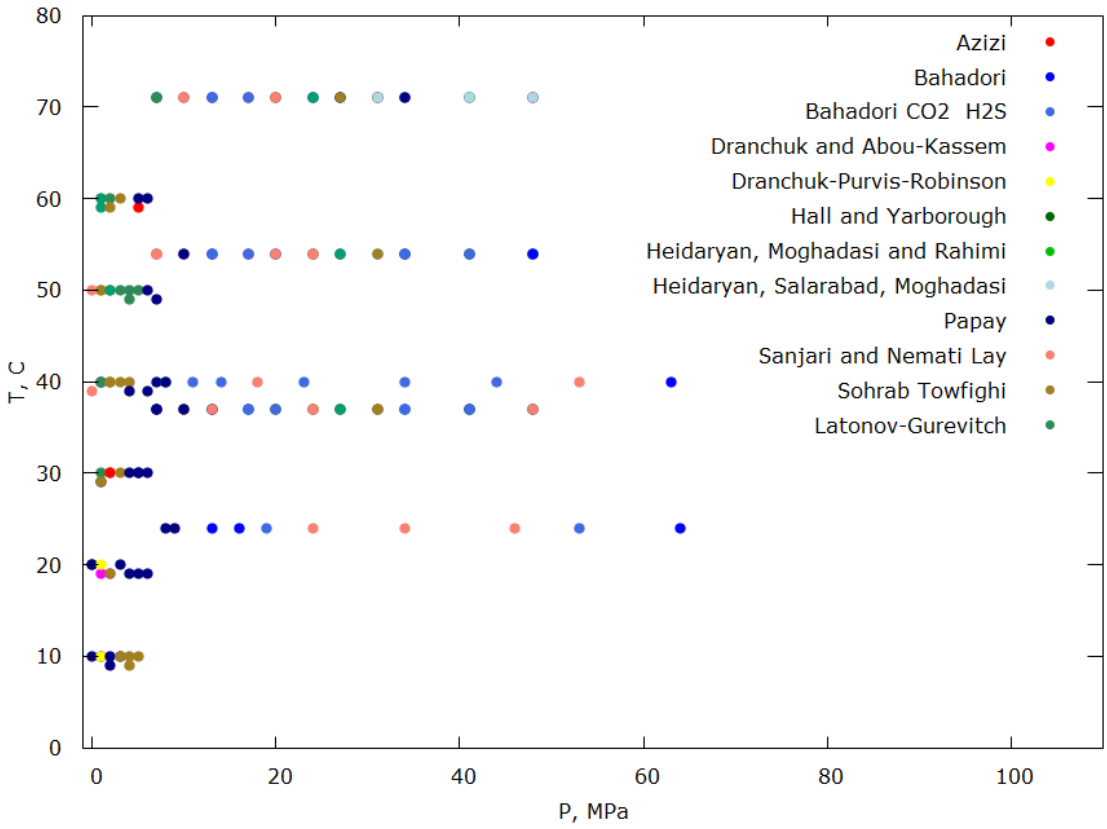

Figure 5. *Best methods (by AARE) among the empirical dependencies for mixtures with high fraction of CO_2*

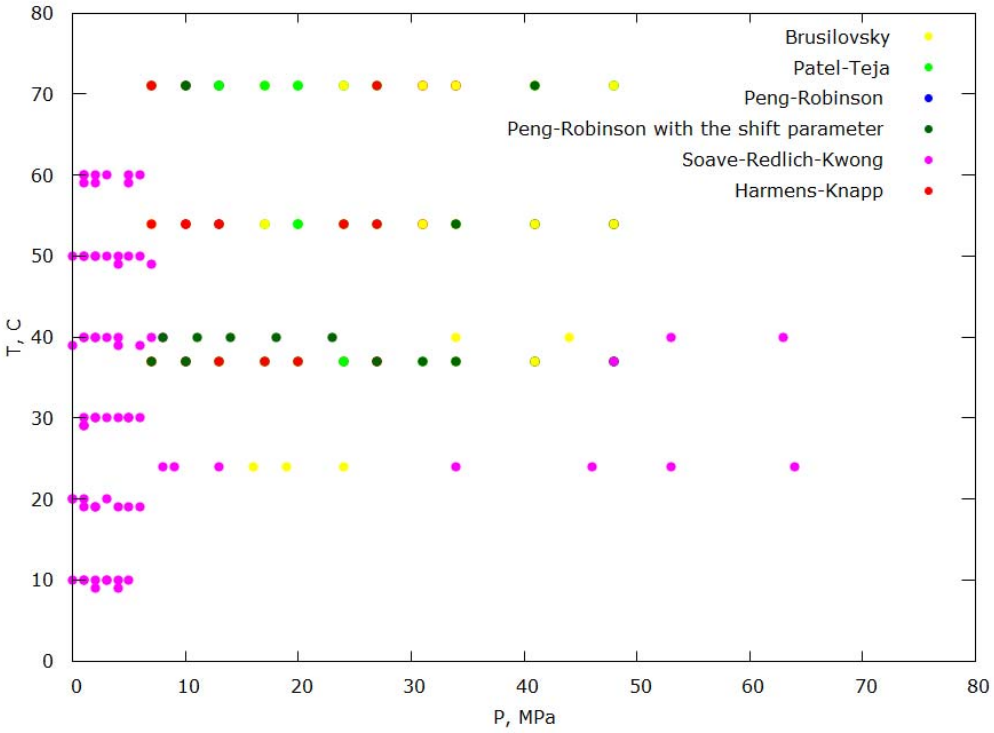

Figure 6. *Best methods (by AARE) among the equations of state for mixtures with high fraction of CO_2*

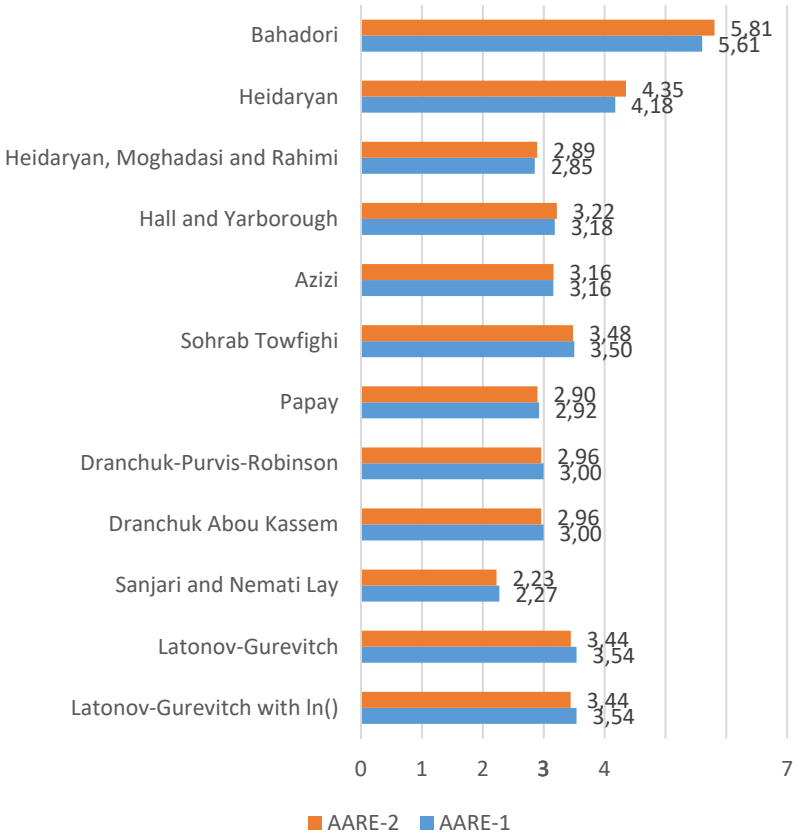

Figure 7. *AARE of the compressibility factor with pseudocritical consitions calculated: AARE-1 using Kay's rule (Equations 120-121), AARE-2 – using Equations 122-123*

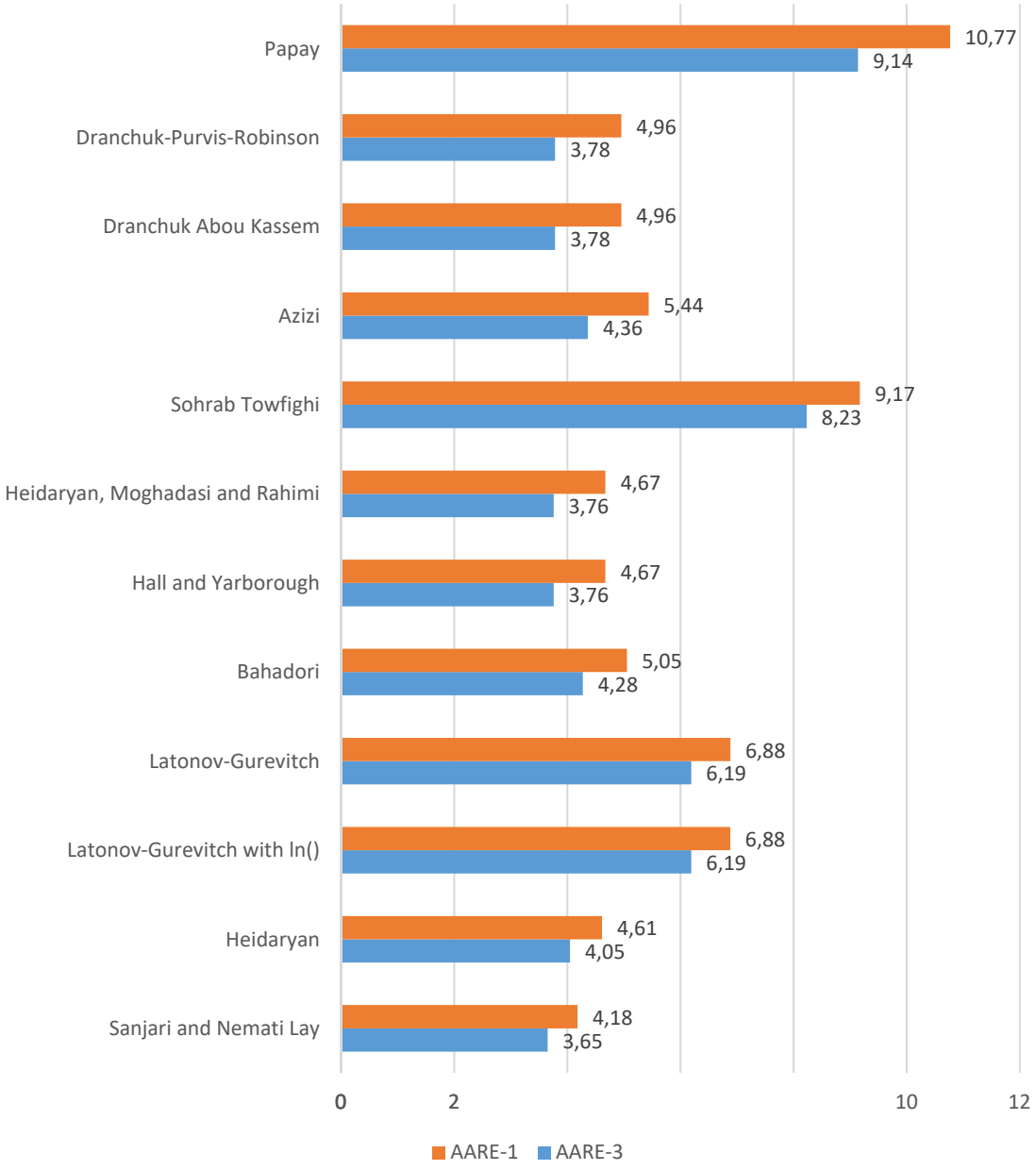

Figure 8. *AARE of the compressibility factor of acid gas with pseudocritical conditions calculated: AARE-1 using Kay's rule (Equations 120-121), AARE-3 – using Equations 129-131*

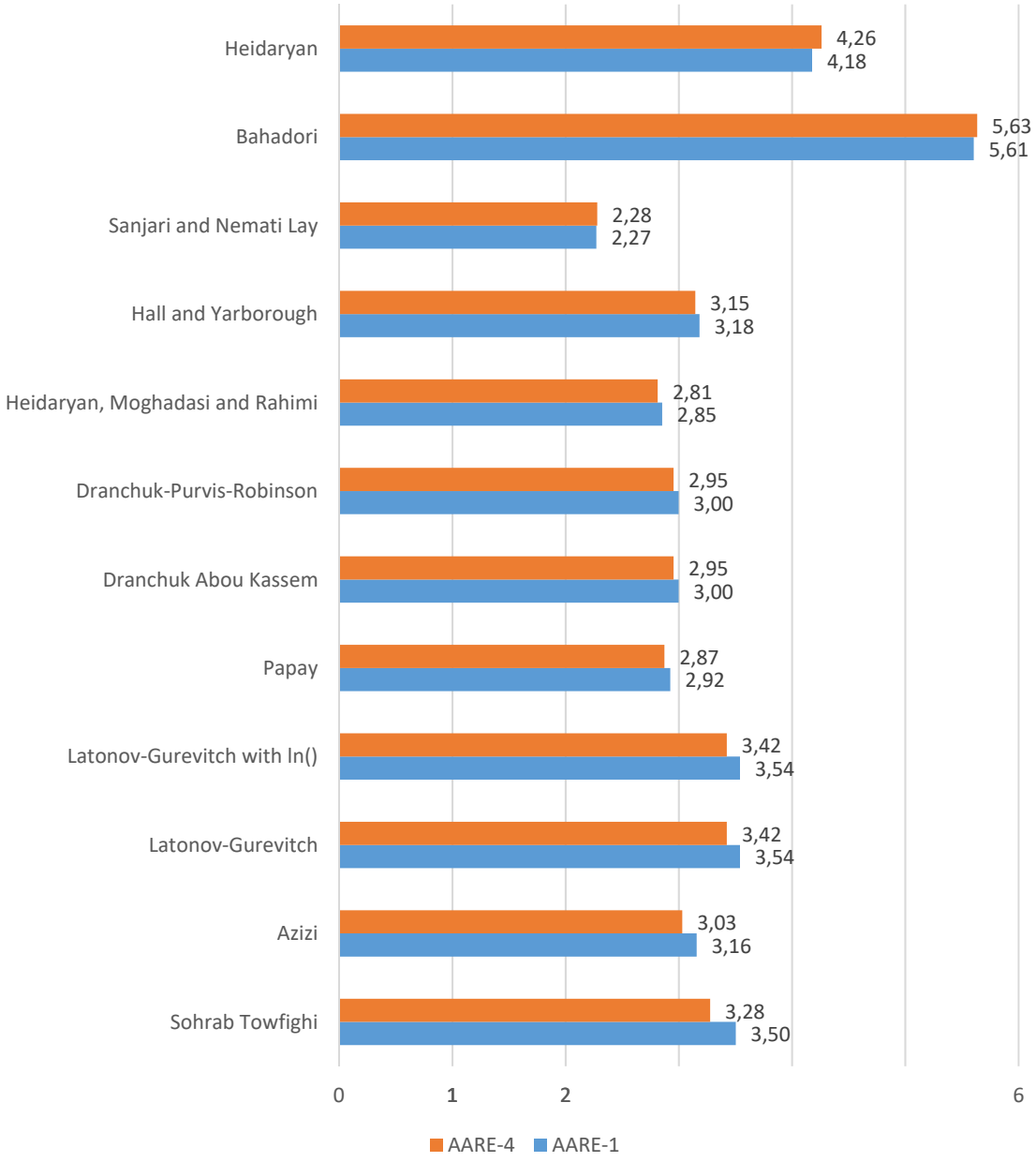

Figure 9. *AARE of the compressibility factor with pseudocritical conditions calculated: AARE-1 using Kay's rule (Equations 120-121), AARE-4 – using Prausnitz and Gunn rule (Equations 122,124)*

PERIÓDICO TCHÊ QUÍMICA
ARTIGO ORIGINAL

ISOLAMENTO, CARACTERIZAÇÕES, ANTICÂNCER, CITOTOXICIDADE, TOXICIDADE *IN SILICO* E AVALIAÇÕES ANTIMICROBIANAS DA PROTEÍNA DE SEMENTES DE *MORINGA OLEIFERA*

ISOLATION, CHARACTERIZATIONS, ANTI-CANCER, CYTOTOXICITY, *IN SILICO* TOXICITY, AND ANTIMICROBIAL EVALUATIONS OF *MORINGA OLEIFERA* SEED PROTEIN

ATOLANI, Olubunmi[1]*; OLORUNDARE, Olufunke Esan[2]; BANERJEE, Priyanka[3]; ADEYEMI, Oluyomi Stephen[4]; PREISSNER, Robert[3]

[1] Department of Chemistry, University of Ilorin, P.M.B. 1515, Ilorin, Nigeria

[2] Department of Pharmacology and Therapeutics, University of Ilorin, P.M.B. 1515, Ilorin, Nigeria

[3] Institute for Physiology, Charité University Medicine, 10115 Berlin, Germany

[4] Department of Biochemistry, Medicinal Biochemistry, Infectious Diseases, Nanomedicine, and Toxicology Laboratory, Landmark University, PMB 1001, Omu-Aran 251101, Kwara State, Nigeria

** Corresponding author*
e-mail:atolani.o@unilorin.edu.ng

Received 07 May 2021; received in revised form 12 July 2021; accepted 21 July 2021

RESUMO

Introdução: A semente de *Moringa oleifera*, que é amplamente utilizada como uma fonte acessível de tratamento doméstico de água, também é conhecida por suas várias aplicações farmacológicas em todo o mundo. **Objetivo:** Este estudo avalia a toxicidade e o potencial farmacológico da proteína da semente de *Moringa oleifera* ao estabelecer o perfil químico. **Método:** Espectrometria de massa de tempo de vôo de dessorção/ionização a laser assistida por matriz (MALDI-TOF-MS) e cromatografia líquida acoplada com espectrometria de massa de ionização por eletrospray (LC-ESI-MS/MS) foram usados para analisar o conteúdo de proteína/peptídeo da proteína purificada. A proteína também foi investigada quanto ao potencial anticâncer *in vitro* nas linhas de células Hela e MDA-MB-231, citotóxica na linha de células 3T3 e toxicidade para camarões de salmoura. Além disso, foi avaliada a ação antimicrobiana da proteína (polipeptídeo). **Resultados e discussão:** O MALDI-MS revelou três frações de proteína com valores de 3,4, 4,6 e 6,9 kDa. Em contraste, a anise por LC-ESI-MS/MS revelou dipéptidos e tripéptidos, que incluem serinilarginina, leucilprolina, leucilmetionilglicina, isoleucilglicilmetinina, ácido glicilarginilaspártico, isoleucylglutamicacidmethionine, di-fenilalanina, asparaginylaspartylhistidine, seril-tirosil tirosina, fenialanilasparaginiltirosina, e proliltrofanilglicina. A proteína da semente exibiu toxicidade extremamente baixa em ambas as linhas de células de câncer de mama 3T3 e MDA-MB-231, enquanto os padrões, doxorrubicina e cicloheximida tiveram IC_{50} = 0,5 ± 0,07 e 0,8 ± 0,10 µg/mL, respectivamente. Além disso, a proteína não mostrou atividade antibacteriana ou antifúngica contra todos os organismos testados. A proteína também não exibiu letalidade contra o camarão de água salgada. Os resultados de toxicidade *in-silico* indicaram que os peptídeos não são imunotóxicos, carcinogênicos ou mutagênicos, pois a maioria pertencia à classe V de toxicidade, exceto serilarginina prevista para classe de toxidade IV (prejudicial se ingerido). Portanto, a ingestão do remanescente de proteína na água pode estar dentro do limite tolerável. **Conclusão:** Os resultados obtidos sugerem que o conteúdo protéico da semente de *Moringa oleifera* é não citotóxico. O resultado valida ainda mais o potencial de segurança do material de sementes desengorduradas e desengorduradas usadas como fontes potenciais de alimento para humanos e animais.

Palavras-chave: *Peptídeo; MALDI; ESI-MS/MS; Doxorrubicina; in sílico*.

DOI: 10.52571/PTQ.v18.n38.2021.15_ATOLANI_pgs_214_223.pdf

ABSTRACT

Background: *Moringa oleifera* seed, which is widely utilized as an affordable source of domestic water treatment, is also reputable for its various pharmacological applications globally. **Aim**: This study evaluates the toxicity and pharmacological potentials of *Moringa oleifera* seed protein while establishing the chemical profile. **Method**: Matrix-assisted laser desorption/ionization time-of-flight mass spectrometry (MALDI-TOF-MS) and liquid chromatography coupled with electrospray ionization mass spectrometry (LC-ESI-MS/MS) were used to analyze the protein/peptide content of the purified protein. The protein was also investigated for *in vitro* anti-cancer potential on Hela and MDA-MB-231 cell lines, cytotoxic on 3T3 cell line, and toxicity to brine shrimps. In addition, the antimicrobial action of the protein (polypeptide) was evaluated. **Results and Discussion**: The MALDI-MS revealed three protein moieties with values of 3.4, 4.6, and 6.9 kDa. On the other hand, LC-ESI-MS/MS analysis revealed dipeptides and tripeptides, which include serinylarginine, leucylproline, leucyl-methionyl-glycine, isoleucyl-glycyl-methinine, glycyl-arginyl-aspartic acid, isoleucyl-glutamyl-methionine, di-phenylalanine, asparaginyl-aspartyl-histidine, seryl-tyrosyl-tyrosine, phenylalanyl-asparaginyl-tyrosine, and propanolyl-trytophanyl-glycine. The seed protein exhibited extremely low toxicity on both 3T3 and MDA-MB-231 breast cancer cell lines, while the standards, doxorubicin, and cycloheximide had IC_{50} = 0.5 ± 0.07 and 0.8 ± 0.10 µg/mL, respectively. Further, the protein showed no antibacterial or antifungal activity against all tested organisms. The protein also exhibited no lethality against brine shrimp. The *in-silico* toxicity results indicated that the peptides are not immunotoxic, carcinogenic, or mutagenic as most belonged to the tox class V except serylarginine predicted for tox class IV (harmful if swallowed). Hence, the intake of the protein remnant in water could be within the tolerable limit. **Conclusion**: The results obtained suggested that the protein content of the *Moringa oleifera* seed is non-cytotoxic. The result further validates the safety potential of the defatted and debittered seed material used as potential food sources for both humans and animals.

Keywords: *Peptide; MALDI; ESI-MS/MS; Doxorubicin; In-silico*

1. INTRODUCTION:

The seed of *Moringa oleifera* Lam. belonging to the family *Moringaceae*, is widely consumed globally, especially in African and Asian rural settings, for its nutritional and medicinal values (Falowo *et al*., 2018). However, some measures of toxicity such as mutagenicity and genotoxicity are reportedly associated with the consumption of the seed (Araújo *et al*., 2013; Villasenor *et al*., 1989). The toxicity associated with seed consumption has been a challenge for the extensive utilization of the seed for various food and ethnomedicinal purposes (Falowo *et al*., 2018; Liu *et al*., 2018). A previous study on the *Moringa oleifera* seed has indicated the various phytochemical constituents, including niazimicin, niazidin, glucomoringin isothiocyanate, niazinin acetate, niazinin triacetate, niazirinin, glucotropaeolin, triolein, and trivaccenin (Atolani *et al*., 2020).

Previous work indicated that the seed extracts with high lipid content possess good antioxidant and low proteinase inhibition potentials, among others (Atolani *et al*., 2018), other studies (Njan *et al*., 2018) further revealed that the alcoholic extract of the *M. oleifera* seed could induce infertility in the male animal by attenuating semen pH, whilst also exhibiting hepatotoxic effects due to persistent increase in ALP and AST even after withdrawal of the extract being administered. We further reported that the seed extractives exhibited high renal toxicity in another (Olorundare *et al*., 2015). Having extensively examined the chemical composition and pharmacological activities and the toxicity associated with the various extracts of the *M. oleifera* seed, we here investigated the composition of the seed protein and the corresponding toxicity potential, which hitherto has not been well explored. The study, among other things, indicates a contribution of the seed protein to the overall inherent toxicity of the *M. oleifera* seed.

2. MATERIALS AND METHODS:

2.1. Plant Material

The seeds of *Moringa oleifera* were obtained as previously indicated (Atolani *et al*., 2020). The seed was authenticated and documented with the voucher number UILH/002/1008 at the herbarium of the Department of Plant Biology, University of Ilorin, Nigeria. The air-dried seeds were de-shielded and pulverized. The powdered material was kept in a cool place for further work.

2.2. Extraction

Powdered seed material (2,000 g) were subjected to exhaustive extraction using ethanol for 9 days to remove all lipid-soluble extractives. This was followed by extraction with water for 5 days. The aqueous extract was thereafter filtered and partitioned with dichloromethane (DCM) to get rid of the non-polar content of the aqueous extract. The resultant aqueous solution was allowed to settle down for the precipitation of the protein. After about five days the precipitate collected via decantation was washed repeatedly with solvents such as hexane, DCM, and ethanol sequentially. The purified protein fraction was dried, and the solid mass obtained was further washed with DCM to remove traces of lipid, followed by methanol to remove other organic impurities, and cold water was finally used to wash it. The purified *M. oleifera* seed protein-tagged (MOSP) was kept in a cool dark place until further analyses (Mann *et al*., 2001).

2.3. Peptide Profiling: HPLC-TOF/Q-TOF-ESI-MS/MS (TANDEM-MS)

The peptide profile of the MOSP was determined by subjecting the digested sample to Agilent Technologies High-Pressure Liquid Chromatography (HPLC) 6200 series-coupled to a Time-of-Flight Mass Spectrometry (TOF/Q-TOF-ESI-MS/MS). The HPLC was equipped with a binary pump, column component, and HiP Sampler Model G4226A, and mass MS Q-TOF component G6550A. Gradient elution mode was applied for the analysis as mobile phase A composed of 100% water and mobile phase B was 100% acetonitrile. The gradient program was set at 95.00. % A: 5.00 % Band increased to A: 0.00 % B:100.00 %. The flow rate was set to 0.3 mL/min as the maximum pressure limit was 1200.00 bars at a stop-time of 30 min. 3.00 µL of the analyte was injected via needle wash injection mode as the right temperature was set at 45°C. The switch time of 0.01 min was used. The MS Q-TOF has a dual AJS ESI ion source and an MS/MS (TANDEM) absorption threshold of 5 with a mass acquisition range of 163 to 1000 at a scan rate of 1.00 spectra per second. The MOSP was dissolved in DMSO and warmed at 50˚C before analysis. The mass determination in selective ion monitoring (SIM) mode was done with both positive and negative ion electrospray ionization methods for effective quantification of the analyte following standard procedure (Grimalt *et al*., 2005).

2.4. Protein Analysis

The MOSP was characterized using Matrix-assisted laser desorption/ionization time-of-flight mass spectrometry (MALDI-TOF MS) Bruker Daltonic, model Ultraflex III, equipped with smart beam laser, Germany. A prepared sinapinic acid matrix was used for a scan range of 5 – 100 KDa. An aliquot (1 uL) of the sample was injected into the machine following standard dried droplet preparation (Gauss et al., 1999).

2.5. Cytotoxicity evaluation – cell viability assay (HeLa, MDA-MB-231, and 3T3 cell lines)

The MOSP was assessed for cytotoxicity via MTT (3-[4,5-dimethylthiazole-2-yl]-2,5-diphenyl-tetrazolium bromide) colorimetric assay (Mosmann, 1983). In this assay, HeLa (Cervical Cancer Cell), MDA-MB-231 (Breast Cancer Cell line ATCC- HTB-26), and 3T3 (Mouse fibroblast, ATCC-1658) were maintained in a standard culture medium consisting of a mixture of streptomycin, penicillin, Dulbecco's Modified Eagle's Medium and 5% fetal bovine serum, in an atmosphere of 5% CO_2 and 37°C. At 80% confluence, cells were sub-cultured and seeded ($1x10^5$ cells/mL) into 96-well plate. After 24 h incubation, test compounds (1-100 µM) prepared in the fresh medium were added, and incubation was carried out for 72 h. Cell viability was assessed by MTT colorimetric measurement at 570 nm on a microplate reader (Molecular Devices, CA, USA). Doxorubucin and cycloheximide were used in this assay as positive drug controls for breast, cervical, and HeLa cancer cell lines. All experimental preparations were made in triplicate. The cytotoxicity was estimated using Equation 1.

$$\%_{\mathbf{Inhibition}} = 100 - [\left(\frac{A_{\text{Sample}} - A_{\text{negative control}}}{A_{\text{positive control}} - A_{\text{negative control}}}\right) * 100] \quad \text{(Eq. 1)}$$

where A is the Absorbance of either sample or control

2.6. Assay for antifungal activity

The antifungal activity evaluation of MOSP, standard agar dilution protocol as described previously elsewhere (Osho *et al*., 2015), was adopted. The test organisms used include *Candida albicans, Aspergillus niger, Microsporum canis, Trichophyton rubrum, Fusarium lini, Candida glabarata.* Briefly, 12 mg/mL MOSP stock solution in

dimethylsulphoxide solution was prepared for further serial dilution. Inoculum of each fungus was introduced to each tube on Sabouraud dextrose agar growth media. Meanwhile, an agar surface streak method was used to evaluate non-mycelial growth. The solvent and miconazole were respectively used as negative and positive controls as the tubes were incubated for 72-168 h at 27-29°C. Linear growth (mm) in media was measured, and growth inhibition was determined with reference to the control. The minimum inhibitory concentration (MIC) for test compounds and reference drugs was estimated dose-response plot obtained by repeating the assay process at different dose levels of test compounds or reference drug (10, 25, 50, 100 $mg.mL^{-1}$).

2.7. Antibacterial assay

The antibacterial potential of MOSP was evaluated against both gram-negative and gram-positive bacterial which include *Salmonella typhi* (ATCC 14028), *Bacillus subtilis* (ATCC 23857), *Staphylococcus aureus* (NCTC 6571), *Escherichia coli* (ATCC 25922), *Pseudomonas aeruginosa* (ATCC 10145), and in Mueller Hinton medium in a 96 well plate following a previously reported protocol (Sarkar *et al*., 2007). The test compounds (300 µg/mL) were added to the wells except for the control well. Imipenem was used as drug control. After 20 h incubation, Alamar Blue Dye was added, and this was followed by a 3h-controlled shaking at 80 rpm. The color change of the dye from blue to pink was taken as the growth of the bacterial strains. Absorbance reading was taken at 570 and 600 nm on a microplate reader. All experiments were carried out in triplicate.

2.8. Toxicity assay using brine shrimp

Brine shrimp toxicity assay, a rapid, inexpensive, general toxicity bioassay was used to examine the toxicity of MOSP following a procedure described previously (Kivack *et al*., 2001). The sample (20 mg) dissolved in DMSO was diluted to concentrations in the range 10 to 1000 µg/mL. Etoposide prepared in a similar solution served as positive control while distilled water served as the negative control. Shrimp survival was estimated periodically for 24 h, and the data was collected appropriately.

2.9. Computational toxicity studies

The *in silico* evaluations of the absorption, distribution, metabolism, excretion, and toxicity, otherwise known as ADMET properties, were performed using the ProTox-II platform and SuperCYPsPred webserver (Banerjee *et al*., 2018; Atolani *et al*., 2020). While ProTox-II is a virtual platform for the evaluation of chemical-based toxicities, the SuperCYPsPred web server is a prediction model for five major CYPs isoenzymes, namely; CYP1A2, CYP2C19, CYP2D6, CYP2C9, and CYP3A4. Precisely, over 80% of clinical drug metabolism are accounted for using the indicated CYPs isoenzymes.

2.10. Data presentation and statistical analysis: Data analysis was achieved using a Finney computer software to estimate IC_{50} values at 95% confidence interval. The results represent the mean ± standard error of the mean values of three different experiments except where indicated otherwise.

3. RESULTS AND DISCUSSION:

3.1. Results

3.1. MALDI-TOF-MS Analysis

The characterization of complex protein mixtures using MALDI and TOF-MS are well established and reported in the literature. The MALDI analysis of MOSP (Figure 1) revealed the presence of three proteins with size values of 5712 (3.4 kDa), 7801 (4.6 kDa), and 11462 (6.9 kDa).

3.2. HPLC-MS/MS Analysis

Electrospray ionization - MS/MS is a viable option for identifying peptides (Ghebremichael *et al*., 2005). Here, an MS/MS with a relative threshold of 0.010% coupled to HPLC operated at both positive and negative modes was used to analyze the MOSP to identify the peptide and amino acid constituents of the digested protein. A total of 8 and 6 peptides/amino acids were obtained in positive and negative modes, respectively (Tables 1 and 2).

3.3. Result of Cytotoxicity Assay

The cytotoxicity of MOSP was examined on HeLa, MDA, and 3T3 cell lines to evaluate its anti-cancer properties or otherwise. A low degree of inhibition (14.3%) was recorded on HeLa cell lines while there was no detectable activity on both MDA-MB-231 and the 3T3 cell lines (Table 3).

3.4 Antibacterial and Antifungal Activities

The result of the antimicrobial activity of the MOSP is as indicated in Table 4. The MOSP did not show significant antibacterial activity against all the organisms (both gram-negative and gram-positive) tested compared to the standard imipenem and miconazole.

3.5. The Brine Shrimp Toxicity Evaluation

The brine shrimp test is a viable means of evaluating the toxicity potential of natural products. The result of the brine shrimp lethality test is as indicated (Table 5).

3.6. In silico Evaluation

Computational toxicity prediction studies using ProTox-II platform (Banerjee *et al*., 2018; Atolani *et al*., 2020) suggest that all the peptides at the positive mode ESI are safe concerning their acute toxicity profiles, mostly belonging to the tox class V (may be harmful if swallowed); except serylarginine predicted for tox class IV (harmful if swallowed). Leucylproline, Glycine, N-(N-L-methionyl-L-leucyl)- shows probable binding to corticotropin-releasing factor Receptor 1(off-targets/toxicity targets) with an average of 71.57 and 74.7. Tanimoto similarity to known ligands of the targets, respectively. N-Formyl-methionyl-leucyl-phenylalanine shows probable binding with the Opioid Receptor Mu with an average similarity of 80.97 (Tanimoto) with its known ligands (Table 6).

3.2. Discussion

The MALDI-TOF-MS analysis (Figure 1) result was corroborated by a previous report where three protein peaks were also obtained (Ghebremichael *et al*., 2005). It was also reported that more than one protein family is present in MOSP (Gassenschmidt *et al*., 1995). Various analyses of plant protein also indicated that closely related proteins are formed during different developmental Stages in plants. Interestingly, a non-protein and non-polysaccharide compound has been isolated from *M. oleifera* seed (Okuda *et al*., 2001).

The DB difference of not more than ± 15 ppm was observed in both modes from the marching (Tables 1 and 2). Peptides are partly hydrolyzed or degraded products of protein which can be further hydrolyzed to the basic amino acid units. Peptides have amino acid units ranging from 2 to 50 linked by peptide bonds (Nelson and Cox, 2005). Naturally occurring peptides have varying complexities, compositions, and functions. Two dipeptides, Serinyl-Arginine (Ser-Arg) and leucyl-proline (Leu-Pro), and four tripeptides obtained include leucyl-methionyl-glycine (Leu-Met-Gly), isoleucyl-glycyl-methinine (Ile-Gly-Met), glycyl-arginyl-aspartic acid (Gly-Arg-Asp), isoleucyl-glutamyl-methionine (Ile-Glu-Met) were obtained in the positive mode. Other peptides detected included N-formyl-methionyl-alanine and N-formyl-methionyl-phenyl alanine; both peptides are amino acids of methionine. Two dipeptides, namely di-phenylalanine (Phe Phe) and tyrosyl-phenylalanine (Tyr-Phe), were obtained in the negative mode. In contrast, four tripeptides obtained are asparaginyl-aspartyl-histidine (Asn-Asp-His), seryl-tyrosyl-tyrosine (Ser-Tyr-Tyr), Phenylalanyl-asparaginyl-tyrosine (Phe-Asn-Tyr), and propanolyl-trytophanyl-glycine (Pro-Trp-Gly). The peptides are well reported in seeds of plants (Gassenschmidt *et al*., 1995; Ghebremichael *et al*., 2005).

From the *In silico* Evaluation result, Table 6. None of the peptides showed inhibitive action against CYP3A4, CYP2D6, CYP2C9, CYP2C19, and CYP2A as predicted using SuperCYPs modeling.

The protein of *M. oleifera* (Table 3) was not active against the cervical, HeLa cancer cell line, MDA-MB-231, and the fibroblast cell line (3T3). The aqueous extract of the seed, which is known to contain glucosinolate and isothiocyanates, has been reported to be cytotoxic to breast adenocarcinoma (MCF-7) cells (Rahaman *et al*., 2017). The chemical compounds include 4(α-L-rhamnosyloxy) phenylacetonitrile, 4-hydroxyphenylacetonitrile, and 4-hydroxyphenylacetamide, isolated from the seed exhibited mutagenic effects in a mouse model (Villasenor *et al*., 1989). The seed extracts are well reported to be cytotoxic to various cancer cell lines while also possessing anti-inflammatory activities (Al-Asmari *et al*., 2015). In light of these previous reports, our results may indicate that the cytotoxic constituent of the seed is not the protein.

The polar and non-polar extracts of *M. oleifera* seed were reported to induce sensitivity in fungi, bacterial and viruses which included: *Scenedesmus obliquus*, *Escherichia coli, Pseudomonas aeruginosa*, *Staphylococcus aureus, Bacillus sterothermophilus,* and *Herpes Simplex* virus type 1 (HSV 1) and *Polio* virus type 1 (Ali *et al*., 2004). The seed extractives have also shown potency against some water-borne bacterial (Ferreira *et al*., 2011; Kumar and Gopal,

1999).

The MOSP showed no lethality (Table 5) compared to the control as the same number of survivors was obtained for all tested concentrations. This implies that the change in concentration does not affect shrimp viability, thereby strengthening the prediction that the protein of the seed of *M. oleifera* is non-toxic at the tested concentrations. This suggests that the toxic characteristic of the seed of *M. oleifera* may not be due to the protein content.

The bioactivities abounding in seeds of plants cannot be over-emphasized. The seeds of plants have been reported to possess significant cytotoxic activity, antimicrobial potential, and antioxidant activities among others (Adeyemi *et al*., 2020). In this study, the protein of the seed of *M. oleifera* has been observed to possess no significant cytotoxic activities on normal (non-transformed) and cancer cell lines. The extremely low activity recorded against the test organisms is an indication that the defatted and debittered seed powder would have no adverse effect in the fortification of flour for edible purposes (Ogunsina *et al*., 2011). Furthermore, it showed no lethality against brine shrimp, and this was also in agreement with existing reports.

4. CONCLUSIONS:

The protein of *M. oleifera* seed from a native source has been purified via a simple technique characterized by ESI-MS and MALDI-MS. The protein showed no lethality on shrimp and no significant toxicity *in silico*. In addition, no cytotoxic action was observed on breast cancer, cervical cancer, and normal cell lines. Thus, the results suggest that MOSP is not responsible for the toxicity reported in the consumption of *M. oleifera* seed. It is presumed that the toxicity of the seed resides in the non-protein extractives of the seed.

.

5. ACKNOWLEDGMENTS:

The authors express their profound gratitude to the Raw Materials Research and Development Council, Abuja, Nigeria, for the grant: RMRDC/AF/20/S.102/1 that supports the research work.

6. REFERENCES:

1. Adeyemi, K.D., Abdulrahman, A., Ibrahim, S. O., Zubair, M. F., Atolani, O., Badmos, A. A. 2020. Dietary Supplementation of *Tetracarpidium conophorum* (African Walnut) Seed Enhances Muscle n-3 Fatty Acids in Broiler Chickens. European Journal of Lipid Science and Technology 122: 1900418.
2. Al-Asmari A.K., Albalawi S. M., Athar M. T., Khan A. Q., Al-Shahrani H., Islam M. 2015. *Moringa oleifera* as an anti-cancer agent against breast and colorectal cancer cell lines, *PLoS ONE* 10, 8
3. Ali, G.H., El-taweel, G. E., Ali, M.A. 2004. The cytotoxicity and antimicrobial efficiency of *Moringa oleifera* seeds extracts. International Journal of Environmental Studies, 61, 699–708.
4. Araújo, LCC, Aguiar, JS, Napoleão, TH, Mota F.V.B., Barros, ALS, Moura, MC, Coriolano, M.C., Coelho, L.C.B.B., Silva, T.G., Paiva, P.M.G. 2013. Evaluation of Cytotoxic and Anti-Inflammatory Activities of Extracts and Lectins from *Moringa oleifera* Seeds. PLoS ONE 8, e81973.
5. Atolani, O., Olorundare, O.E., Anoka, A.N., Osin, A.O., Biliaminu, S.A. 2018. Antioxidant, Proteinase Inhibitory and Membrane Stabilization Potentials of Moringa oleifera Seed Oil. FABAD Journal of Pharmaceutical Sciences. 43, 1-13.
6. Atolani, O., Olorundare, O.E, Banerjee, P., Osin, O.A., Preisner, R., Njan, A.A. 2020. Isolation, Characterisation, and *In Silico* Toxicity Evaluations of Thiocarbamates, Isothiocyanates, Nitrile, Glucosinolate, and Lipids from *Moringa oleifera* Lam. Seed. Journal of the Turkish Chemical Society Section A: Chemistry 7, 233-242.
7. Banerjee, P, Eckert AO, Schrey, AK, Preissner, R. 2018. ProTox-II: a webserver for the prediction of toxicity of chemicals. Nucleic Acids Research, 2018; 46, 257–263.
8. Falowo, A.B., Mukumbo, F.E., Idamokoro, E.M., Lorenzo, J.M., Afolayan, A.J., Muchenje, V. 2018. Multifunctional application of *Moringa oleifera* Lam. In nutrition and animal food products: A review. Food Research International. 106, 317-334.

9. Ferreira, R.S., Napoleão, T.H., Santos, A.F.S., Sá R.A., Carneiro-da-Cunha M.G. Morais M.M., Silva-Lucca R.A., Oliva, M.L., Coelho, L.C., Paiva, P.M. 2011. Coagulant and antibacterial activities of the water-soluble seed lectin from *Moringa oleifera*. Lett Appl Microbiol 53, 186-192.
10. Gassenschmidt, U., Jany, K.K., Tauscher, B., Niebergall, H., 1995. Isolation and characterization of a flocculation protein from *Moringa oleifera* Lam. BBA Biochem. Biophys. Acta 1243, 477–481.
11. Gauss C, Kalkum M, Lowe M, Lehrach H, Klose J. 1999. Analysis of the mouse proteome. (I) Brain proteins: separation by two- dimensional electrophoresis and identification by mass spectrometry and genetic variation. Electrophoresis 20(3):575–600.
12. Ghebremichael, K.A., Gunaratna, K.R., Henriksson, H, Brumer, H, Dalhammar, G. 2005. A simple purification and activity assay of the coagulant protein from *Moringa oleifera* seed. Water Research 39, 2338–2344.
13. Grimalt S, Pozo O.J, Marín J.M., Sancho J.V, and Hernández F (2005). Evaluation of Different Quantitative Approaches for the Determination of Noneasily Ionizable Molecules by Different Atmospheric Pressure Interfaces Used in Liquid Chromatography Tandem. Mass Spectrometry: Abamectin, as Case of Study. American Society for Mass Spectrometry. 16, 1619–1630.
14. Kivack, B., Mert, T., Tansel, H. (2001). Antimicrobial and cytotoxic activities of *Ceratonia siliqua* L. extracts. *Turk. J. Biol*., 26, 197-200.
15. Kumar, S., Gopal, K. 1999. Screening of plant species for inhibition of bacterial population of raw water, J. Environ. Sci. Health 34, 975–987.
16. Liu Y, Wang X, Wei X, Gao Z, Han J. 2018. Values, properties and utility of different parts of *Moringa oleifera*: an overview. Chinese Herbal Medicines. 10, 371-378.
17. Mann M, Hendrickson R.C. and Pandey A. (2001). Analysis of proteins and proteomes by mass spectrometry. Annu. Rev. Biochem. 2001. 70:437–73.
18. Mosmann, T. 1983. Rapid colorimetric assay for cellular growth and survival: application to proliferation and cytotoxicity assays. J Immunol Methods 65: 55-63.
19. Nelson D.L. and Cox M.M. (2005). Principles of Biochemistry. 4th Edition, New York: W.H. Freeman. ISBN 0-7167-4339-6.
20. Njan, AA, Atolani, O, Olorundare, OE, Afolabi, S.O., Ejimkonye, B.C., Crucifix, P.G., Salami, B., Olajide, J.O., Oyewopo, A.O., Oyeleke, S.A. 2018. Chronic toxicological evaluation and reversibility studies of *Moringa oleifera* ethanolic seed extract in Wistar rats. Tropical Journal of Health Sciences 25 (1), 59-71.
21. Ogunsina, B.S., Radha, C., Indrani, D. 2011. Quality characteristics of bread and cookies enriched with debittered *Moringa oleifera* seed flour. International Journal of Food Sciences and Nutrition. 62, 185-194.
22. Okuda, T., Baes, A.U., Nishijima, W., Okada, M., 2001. Isolation and characterization of coagulant extracted from *Moringa oleifera* seed by salt solution. Water Res. 35, 405–410.
23. Olorundare, O.E., Bello, M.K., Billiaminu, S.A., Babatunde, S.A., Ibrahim, O.K., Njan, A.A. 2015. Acute and Subacute Toxicity of Defatted Ethanolic Extract of Moringa oleifera Seed in Albino Rats West. Afr. J. Pharmacol. Drug Res. 30, 46-51.
24. Osho, A., Otuechere, C.A., Adeosun, C.B., Oluwagbemi, T, Atolani, O. 2015. Phytochemical, sub-acute toxicity, and antibacterial evaluation of *Cordia sebestena* leaf extracts. Journal of basic and clinical physiology and pharmacology 27, 163-170.
25. Rahaman, M. H. A., Kadir, N. H. A., Amin, N. M., Omar, W. B. W. 2017. Cytotoxicity effect of water extracts of *Moringa oleifera* leaves and seeds against MCF-7 cells. Acta Horticulturae 1158, 279–286.
26. Sarkar, S.D., Nahar, L. Kumarasamy, Y. 2007. Microtitre plate-based antibacterial assay incorporating resazurin as an indicator of cell growth, and its application in *the in vitro* antibacterial screening of phytochemicals. *Methods* 42, 321–324.
27. Villasenor, I.M., Lim-Sylianco, C.Y., Dayrit, F. 1989. Mutagens from roasted seeds of *Moringa oleifera* seeds. Mutat Res 224, 209-212.

7. OPEN ACCESS

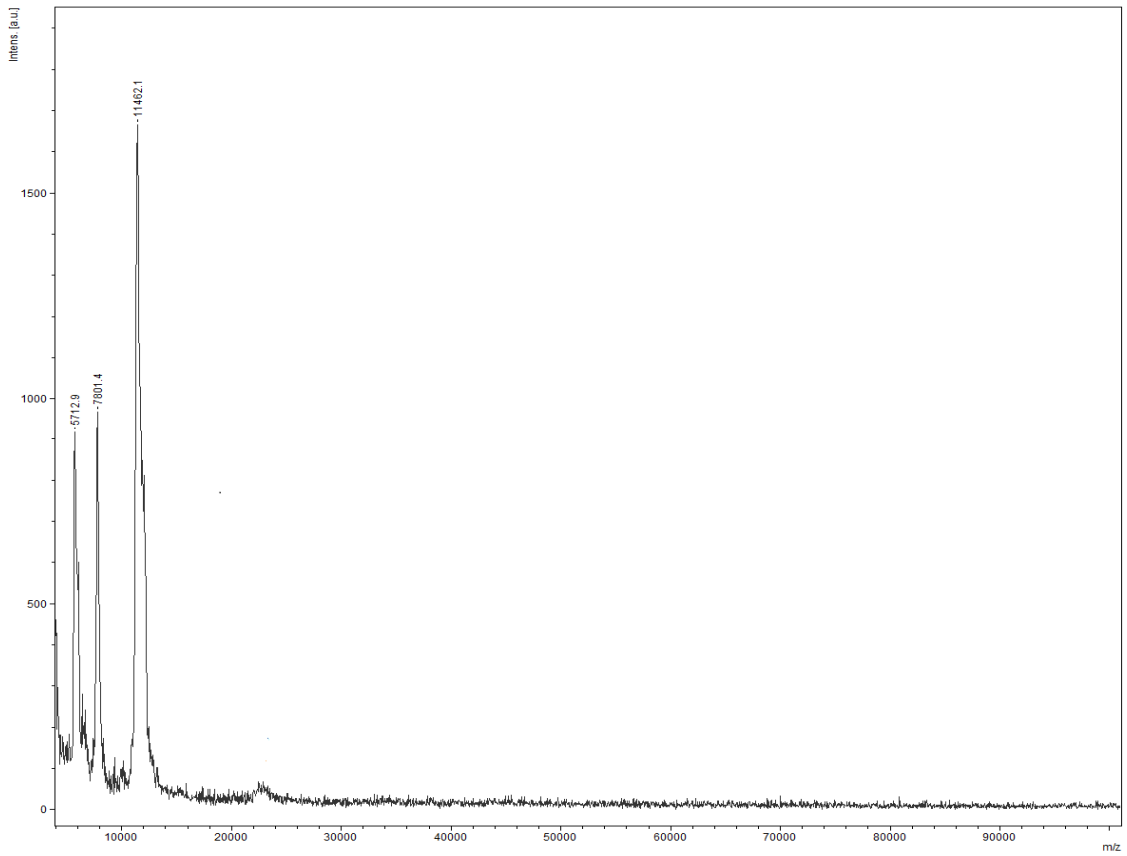

Figure 1: MALDI profile of MOSP

***Table 1**: Qualitative peptide composition at the positive mode ESI*

SN	Name	RT	Mass	Formula	Hits (DB)	DB Diff (ppm)
1	Ser Arg	0.94	261.1415	$C_9H_{19}N_5O_4$	10	8.28
2	Leu Pro	1.00	228.1442	$C_{11}H_{20}N_2O_3$	5	14.19
3	N-formylmethionylalanine	1.26	248.0842	$C_9H_{16}N_2O_4S$	10	-4.46
4	Leu Met Gly	6.19	319.1602	$C_{13}H_{25}N_3O_4S$	10	-11.5
5	Ile Gly Met	8.77	319.1597	$C_{13}H_{25}N_3O_4S$	10	-9.77
6	N-formylmethionylphenyl alanine	8.78	324.1148	$C_{15}H_{20}N_2O_4S$	6	-1.17
7	Gly Arg Asp	8.91	346.1583	$C_{12}H_{22}N_6O_6$	10	5.03
8	Ile Glu Met	9.51	391.1799	$C_{16}H_{29}N_3O_6S$	10	-5.61

***Table 2**: Qualitative peptide composition at the negative mode ESI*

SN	Name	RT	Mass	Formula	Hits (DB)	DB Diff (ppm)
1	Asn Asp His	5.98	384.1451	$C_{14}H_{20}N_6O_7$	6	-15.09
2	Ser Tyr Tyr	8.89	431.1705	$C_{21}H_{25}N_3O_7$	10	-2.83
3	Phe Asn Tyr	15.78	442.1875	$C_{22}H_{26}N_4O_6$	10	-5.18
4	Phe Phe	16.72	312.148	$C_{18}H_{20}N_2O_3$	1	-1.79
5	Tyr Phe	16.94	328.1418	$C_{18}H_{20}N_2O_4$	3	1.55
6	Pro Trp Gly	18.77	358.1652	$C_{18}H_{22}N_4O_4$	10	-3.1

***Table 3:** Cytotoxicity (IC_{50}) of Moringa oleifera seed peptides*

Compounds	HeLa %Inhibition/ [IC_{50} ± SD (µg/mL)]	MDA %Inhibition/ [IC_{50} ± SD (µg/mL)]	3T3 (µg/mL)
MOSP	14.3 [ND]	0.00 [ND]	0.00 [ND]
Cycloheximide	NA [NA]	NA [NA]	89.19 (0.8 ± 0.10)
Doxorubicin	100 (0.90 ± 0.10)	NA [NA]	NA [NA]

ND: Not determined; NA: Not applicable; IC_{50}: 50% inhibition concentration. Results represent mean ± standard error of mean of triplicate determinations

***Table 4:** The antibacterial and antifungal activities of the MOSP*

Organisms	%Inhibition of MOSP	%Inhibition of Imipenem	MIC of Miconazole (µg/mL)
Bacterial (Gram Negative)			
Escherihia coli ATCC 25922	< 30	90	-
Pseudomonas aeruginosa ATCC 10145	< 30	92	-
Salmonella typhi ATCC 14028	< 30	93	-
Bacterial (Gram Positive)			
Bacillus subtilis ATCC 23857	< 30	95	-
Staphylococcus aureus NCTC 6571	< 30	93	-
Fungi			
Trichophyton rubrum	< 10	-	70.00
Candida albicans	< 10	-	110.00
Aspergillus niger	< 10	-	20.00*
Microsporum canis	< 10	-	98.40
Fusarium lini	< 10	-	73.80
Candida glabarata	< 10	-	110.80

* Amphoter cin B was used.

***Table 5**: Effect of MOSP on Brine shrimp viability*

Conc (µg/mL)	Number of Shrimps	Number of Survivors	Mortality via MOSP (%)	Mortality via Etoposide (%)
10	30	27 ± 0.0	10 ± 0.0	-
100	30	27 ± 0.0	10 ± 0.0	-
1000	30	27 ± 0.0	10 ± 0.0	46.6 ± 0.0

Results represent mean ± standard deviation of triplicate determinations

***Table 6**: Computational toxicity prediction using the ProTox-II platform for peptide obtained at the positive mode ESI.*

Compounds	Molecular formula	Predicted Acute Toxicity (LD_{50})	Toxicity Target	Average Similarity (%)
Serylarginine	$C_9H_{19}N_5O_4$	2000 mg/kg Tox Class IV	-	-
leucylproline	$C_{11}H_{20}N_2O_3$	3000 mg/kg Tox Class V	Corticotropin releasing factor Receptor 1	71.57
Glycine, N-(N-L-methionyl-L-	$C_{13}H_{25}N_3O_4S$	3000 mg/kg Tox Class V	Corticotropin releasing factor Receptor 1	74-76
Arginyl-glycyl-aspartic acid	$C_{12}H_{22}N_6O_6$	3000 mg/kg Tox Class V	-	-
N-Formylmethionylalanine	$C_9H_{16}N_2O_4S$	5000 mg/kg Tox Class V	-	-
N-Formyl-methionyl-leucyl-phenylalanine	$C_{15}H_{20}N_2O_4S$	5000 mg/kg Tox Class V	Opioid Receptor Mu	80.97

PERIÓDICO TCHÊ QUÍMICA
ARTIGO ORIGINAL

ESTUDO DA SORÇÃO DE CATIONS DE AMÔNIO EM UM SORVENTE FIBROSO CARBOXÍLICO

STUDY OF THE SORPTION OF AMMONIUM CATIONS ON A FIBROUS CARBOXYLIC SORBENT

ИССЛЕДОВАНИЕ СОРБЦИИ КАТИОНОВ АММОНИЯ НА ВОЛОКНИСТОМ КАРБОКСИЛЬНОМ СОРБЕНТЕ

PEREGUDOV, Yuri Semenovich[1]*; GORBUNOVA, Elena Mikhailovna[1]; OBIDOV, Behzod Aminovich[1]; KIM, Ksenia Borisovna[1], NIFTALIEV,Sabuhi Ilich oglu[1];

[1] Voronezh State University of Engineering Technologies, Faculty of Ecology and Chemical

e-mail: inorganic_033@mail.ru

Received 05 June 2021; received in revised form 19 July 2021; accepted 20 July 2021

RESUMO

Introdução: Águas residuais da produção de fertilizantes minerais, agroindústrias contendo íons amônio, causam prejuízos significativos à piscicultura; portanto, devem ser purificadas antes do descarte. A sorção por troca iônica é um método promissor para o isolamento de cátions amônio. O objeto do estudo foi uma fibra de quimissorção VION KN-1, que desenvolveu superfície e alta taxa de sorção. **Objetivo**: Estudar a cinética de sorção de cátions amônio de soluções aquosas no VION KN-1; treinar uma RNA para prever o grau de recuperação de íons de amônio de águas residuais usando o software *Statistica Neural Networks Versão 13*. **Métodos**: A concentração de íons de amônio na solução foi estabelecida por potenciometria direta. As isotermas de sorção foram construídas usando o método de concentrações variáveis. Para determinar o estágio limite, as dependências cinéticas obtidas foram representadas nas coordenadas das equações de Boyd-Adamson para difusão interna/externa. **Resultados e discussão**: Durante a sorção de soluções com diferentes teores de nitrogênio amoniacal, os valores dos coeficientes de distribuição (Kd) estão no nível de $2{,}3 \cdot 10^3$ cm³/g, o que excede significativamente este parâmetro para ionitas granulares. Os dados experimentais de sorção foram verificados usando as isotermas de Freundlich (R^2 = 0,9224) e Langmuir (R^2 = 0,9996). O grau máximo de recuperação (acima de 96%) foi alcançado passando uma solução com uma concentração de 11,3 mmol/dm³. Usando uma série de dados experimentais, a rede neural MLP-3-5-1 foi treinada. O coeficiente de determinação R^2 = 0,999420 obtido para a amostra de treinamento caracteriza alto desempenho da rede. **Conclusões**: A equação de Langmuir descreve melhor o processo de sorção de NH_4^+ em um sorvente fibroso. É razoável usar VION KN-1 no estágio de tratamento fino. A dessorção do íon amônio da fibra foi realizada por meio de solução ácida. As soluções resultantes de sais de amônio podem ser usadas como fertilizantes líquidos. As redes neurais treinadas podem ser usadas para prever o grau de recuperação de íons de amônio pelo sorvente VION KN-1.

Palavras-chave: *tratamento de águas residuais, quimissorção, íons de amônio, fibra de troca iônica, redes neurais artificiais.*

ABSTRACT

Background: Wastewater from the mineral fertilizer production, agribusiness containing ammonium ions causes significant harm to fish farming; therefore, it must be purified before discharge. Ion-exchange sorption is a promising method for isolating ammonium cations. The object of the study was a chemisorption fiber VION KN-1, which has developed surface and high sorption rate. **Purpose:** To study the sorption kinetics of ammonium cations from aqueous solutions on VION KN-1; to train an ANN to predict the degree of recovery of ammonium ions from wastewater using Statistica Neural Networks Version 13. **Methods:** The ammonium ion concentration in the solution was established by direct potentiometry. Sorption isotherms were constructed using the method of variable concentrations. To determine the limiting stage, the obtained kinetic dependencies were represented in the coordinates of the Boyd-Adamson equations for internal/external diffusion. **Results and Discussion**: During sorption from solutions with different ammonium nitrogen contents, the values of distribution coefficients (K_d) are at the level of $2.3 \cdot 10^3$ cm³/g, which significantly exceeds this parameter for granular ionites. Experimental sorption data were verified using Freundlich (R^2 = 0.9224) and Langmuir (R^2 = 0.9996) isotherms. The maximum degree of recovery (over 96 %) was achieved by passing a solution with a

DOI: 10.52571/PTQ.v18.n38.2021.16_PEREGUDOV_pgs_224_241.pdf

concentration of 11.3 mmol/dm^3. Using an array of experimental data, the MLP-3-5-1 neural network was trained. The coefficient of determination R^2 = 0.999420 obtained for the training sample characterizes high network performance. **Conclusions:** The Langmuir equation better describes the process of NH_4^+ sorption on a fibrous sorbent. It is reasonable to use VION KN-1 at the fine treatment stage. Ammonium ion desorption from the fiber was performed by acid solution. The resulting solutions of ammonium salts can be used as liquid fertilizers. The trained neural networks can be used to predict the degree of recovery of ammonium ions by sorbent VION KN-1.

Keywords: *wastewater treatment, chemisorption, ammonium ions, ion-exchange fiber, artificial neural networks.*

ABSTRACT

Сточные воды производства минеральных удобрений, а также агропромышленного комплекса, содержат ионы аммония. Загрязнённая азотными соединениями вода наносит существенный вред рыборазведению, поэтому перед сбросом ее необходимо очищать. Перспективным способом выделения катионов аммония является ионообменная сорбция. Объектом исследования являлось ионообменное волокно ВИОН КН-1, обладающее развитой поверхностью и высокой скоростью сорбции. Цель работы - изучение кинетики сорбции катионов аммония из водных растворов на ВИОН КН-1. Обучение искусственной нейронной сети для прогнозирования степени извлечения ионов аммония из сточных вод с использованием Statistica Neural Networks версия 13. Концентрацию ионов аммония в растворе определяли на иономере И-130 с ионоселективным электродом. Методом переменных концентраций построены изотермы сорбции. Для определения лимитирующей стадии, полученные кинетические зависимости, представляли в координатах уравнений Бойда-Адамсона для случая внутренней и внешней диффузии. При сорбции из растворов с разным содержанием аммонийного азота значения коэффициентов распределения (K_d) находится на уровне $2.3 \cdot 10^3$ см^3/г, что значительно превышает значения для зернистых ионитов. Экспериментальные данные по сорбции проверены с помощью изотерм Фрейндлиха (R^2 = 0.9224) и Ленгмюра (R^2= 0.9996). Максимальная степень извлечения более 96 % достигалась при пропускании 200 см^3 раствора с концентрацией 11.3 ммоль/дм^3. Используя массив экспериментальных данных, обучили нейронную сеть MLP-3-5-1. Полученный для обучающей выборки R^2 =0,999420 характеризует высокую производительность сети. Уравнение Ленгмюра лучше описывает процесс сорбции NH_4^+ на волокнистом сорбенте. ВИОН КН-1 целесообразно использовать на стадии доочистки. Десорбция ионов аммония из волокна осуществляли раствором кислоты. Образующиеся растворы аммонийных солей можно применить как жидкие удобрения. Обученные нейронные сети могут быть использованы для прогноза степени извлечения ионов аммония сорбентом ВИОН КН-1.

Keywords:очистка сточных вод, хемосорбция, ионы аммония, ионообменное волокно, искусственные нейронные сети

1. INTRODUCTION:

Ammonium ions are present in the gray and agricultural wastewater and in the wastewater from the production of mineral fertilizers. The concentration of ammonium nitrogen varies in the range of 50-200 mg/dm^3. Water purification from ammonium is very important for the ecology and the environment. Such waters cannot be drained into natural water reservoirs, since with increased ammonium content, the ability of hemoglobin in fish to bind oxygen decreases, which leads to a reduction in their numbers and violation of ecological balance (Nageeb, 2013). Groundwater with excessive ammonium content is unsuitable for drinking. According to the standards of the main indicators of water quality, following the requirements of the sanitary standards of the Russian Federation, the World Health Organization (WHO), and the European Community (EU), the concentration of ammonium nitrogen should not exceed 2 mg/dm^3, 1.5 mg/dm^3, and 0.5 mg/dm^3, respectively.

Various methods are used to remove ammonium from wastewater, such as a reagent method, aeration in an alkaline environment, ion exchange, biochemical, and reverse osmosis. Ion exchange sorption is a promising method for the isolation of NH_4^+ (Al-Sheikh *et al.*, 2021; El-Shafey*et al.*, 2014; B. Clark *et al.*, 2020).

The study of the kinetics of ammonium ion sorption makes it possible to establish the rate at

which the equilibrium is reached. An important issue in sorption technology is the determination of the limiting stage of mass transfer. Information about this will help to choose the optimal sorption conditions. It is well known that the exchange process on sorbents consists of five stages:

- diffusion of sorbed ions from an external solution to the surface of the grain ;

- diffusion of sorbed ions through the thickness of the grain to the active ion-exchange groups;

- chemical ion-exchange reaction;

- diffusion of displaced ions towards the surface of the grain;

- diffusion of counterions from the surface of the grain into the volume of the solution.

Stages 1 and 5 are external or film diffusion; stages 2 and 4 are internal or gel diffusion (Kokotov *et al.*, 1970, Riemann *et al.*, 1973).

There is extensive literature on the issue of ammonium sorption on natural and treated with various compounds aluminosilicates (Sakalova *et al.*, 2018, Han *et al.*, 2020) wast. The sorption of NH_4^+ ions on natural mineral sorbents — zeolite, glauconite, and palygorskite — was studied. It was found that in the range of temperatures studied (293–308 K), zeolite exhibits the best sorption properties; the temperature has a slight effect on the sorption process. It is shown that the experimental isotherms for zeolite and glauconite are straight lines. The sorption isotherm of ammonium ions on palygorskite deviates from linearity, which necessitates its analysis using the well-known theoretical models. It is established that the Langmuir equation best describes the process of sorption of ammonium cations on palygorskite (Malyovannyi *et al.*, 2013, Gumnitsky *et al.*, 2013).

The adsorption equilibrium of NH_4^+ions from aqueous solutions on natural clinoptilolite was considered (Ivanova *et al.*, 2010). The possibility of changing the adsorption capacity by chemical modification of natural clinoptilolite was also tested. The zeolite forms enriched with Ca^{2+}, Ba^{2+}, K^+, Cu^{2+}, and Co^{2+} ions were used. The experimental data were verified using the Freundlich and Langmuir isotherms. The kinetics of adsorption were studied and the effect of adsorbent mass, particle size, and contact time of solid and liquid phases on the adsorption capacity. The diffusion coefficients in macropores and in zeolite crystals were calculated using the assumption of a two-porous model.

Sorption of ammonium ions on natural clinoptilolite and artificial zeolite has been studied (Guida *et al.*, 2020; Adam *et al.*, 2020). To effectively remove ammonium from water, a hollow fiber ceramic membrane obtained from clinoptilolite has been proposed. The effect of different sintering temperatures in the manufacture of membranes (900–1150 °C) and the pH of the initial ammonium solution was investigated. The maximum adsorption activity was reached at pH 7.

To increase the efficiency of adsorption of ammonium nitrogen from wastewater, the surface properties of activated carbon were improved by modifying it with iron (III) salt solution (Ren *et al.*, 2021). The total pore volume and specific surface area of the activated carbon increased after modification. The best adsorption effect was achieved under neutral conditions.

It has been shown that it is possible to use the solution to the problem of mixed diffusion dynamics of sorption with a linear isotherm to describe the initial sections of the output curves of ammonium ions on the *Na*-form of clinoptilolite-containing tuff of the Chuguevskoye deposit (Nikashina *et al.*, 2008).

The dynamics and kinetics of the process of adsorption of NH_4^+cations on dispersed silicon earth (Opoka) were studied (Kuzmina *et al.*, 2008). The dependence of the ammonium ion sorption and dynamic capacity on the linear flow rate was considered. It was shown that an increase in the flow rate leads to an increase in the mass transfer coefficient and a significant decrease in the dynamic sorption of NH_4^+. Kinetic studies have shown that the process of ammonium ion sorption on Opoka is a two-stage process.

In Belchinskaya *et al.* (2013), the kinetics and dynamics of sorption of NH_4^+ on natural and activated by sulfuric acid and alkali aluminosilicate sorbent $M_{45}K_{20}$, consisting of montmorillonite and clinoptilolite, were studied. The diffusion coefficients and the adsorption equilibrium constant were calculated. It was shown that an increase in the sorption capacity of the sorbent after acid and alkaline activation is observed.

To recover ammonium ions from wastewater, a zeolite with improved sorption properties was used. Zeolite N was hydrothermally synthesized from kaolin clay with the addition of potassium hydroxide and potassium chloride solutions. The resulting zeolite had increased cation-exchange capacity

and improved ion exchange kinetics (Probst et al., 2021). NaY zeolite obtained from rice husk ash wastes showed a high adsorption capacity of the monolayer (42.37 mg/g) (Alias *et al.*, 2010). Composite adsorbents based on porous hydrogel and zeolite were obtained and recommended for wastewater treatment from ammonium ions (Putra *et al.*, 2020).

The bentonite treated with NaCl solution with a particle size of 0-0.05 mm showed the maximum increase in recovery efficiency (55.7 %) for ammonium ions. The Langmuir adsorption isotherm matched the equilibrium adsorption data well (R^2 from 0.97 to 0.98), while the Freundlich model proved to be mismatched (R^2 = 0.77) (Sakalova *et al.*, 2018).

The ability to remove ammonium ions from an aqueous solution using lightweight expanded clay aggregate (LECA) was investigated. The maximum adsorption capacity of the monolayer, estimated using the Langmuir isotherm, was obtained in the range of 0.229 to 0.254 (mg/g). The contact time required to reach the equilibrium state was 150 min (Sharifnia *et al.*, 2016).

The removal of nitrate and ammonium ions from the water was performed through zeolite (clinoptilolite) filtering material of 400 mm height and particle size 0.315-0.63 mm, at a filtration rate of 5 mg/l. The removal efficiency of NH_4^+ was 95-99.9%. It was noted that zeolite particles of this size are not suitable for the sorption of nitrate ions from aqueous solutions (Mažeikiene *et al.*, 2008).

The study (Kuzmina *et al.*, 2008) devoted to substantiating the theoretical fundamentals of competing for adsorption of multicomponent systems on mineral sorbents is of interest. The sorption capacity of zeolite with respect to ammonium ions in static and dynamic conditions was studied. The authors showed that the presence of foreign ions in the solution significantly reduces the sorption capacity of zeolite with respect to the analyte.

The ion-exchange fiber VION KN-1 is widely used to study the kinetics of the sorption of ammonium ions from solutions. The small diameter of the elementary fiber of 30-50 microns provides a large specific surface area of the fibers (3-10 m^2/g) compared to granular gel ionites (0.1 m^2/g). The fiber has better swelling properties, a high sorption rate, and a high resistance to abrasion by a moving flow. A less regenerating solution is required for the regeneration of fibrous ion exchangers compared to granular ion exchangers (Kuzmina *et al.*, 2008). Besides, the fiber can be used in filters and other equipment of any design used in water treatment processes.

Artificial neural networks (ANNs) are a non-linear and nonparametric data processing method used in various fields of chemical technology for predicting the quality of the resulting product, as well as for automation, optimization, and planning of the technological process (Han *et al.*, 2011; Heddam *et al.*, 2011; Heddam *et al.*, 2018, Alver *et al.*, 2020).

The increasing scarcity of good quality water resources and the growing use of fertilizers imply the use of efficient water and wastewater treatment methods. To predict the performance of biological systems in removing pollutants from water, artificial neural networks were used (Khataee *et al.*, 2011). In (Giwa *et al.*, 2016), a new bioreactor configuration for wastewater treatment was considered. ANNs were also used to simulate the operation of the bioreactor during water treatment from phosphate ions and ammonium cations.

The removal efficiency of ammonia nitrogen was studied from simulated wastewater with spent foundry sand based on 120 serial experiments, which were modeled by a three-layer artificial neural network. The sorption process was well described using the ANN model, and the maximum sorption capacity was 0.9 mg/g (Faisal *et al.*, 2019).

In this study, hybrid prediction models were used to estimate ammonium adsorption from wastewater on zeolite. Feed-forward Neural Network (FF-NN) and Elman-Recurrent Neural Network (ER-NN) containing two different activation functions were used to determine nonlinear dependencies. As a result, the ammonium adsorption rate can be estimated with a 95% probability using the best hybrid model (H-PM4) (Cagcag Yolcu *et al.*, 2021).

This work aims to study the kinetics of sorption of ammonium cations from aqueous solutions on a fibrous carboxyl sorbent VION KN-1, determine the limiting stage of the process, study the effect of the fiber layer height on the degree of recovery of ammonium ions, as well as train an artificial neural network to predict the degree of ammonium ion recovery from wastewater using the software package *Statistica Neural Networks13*

2. MATERIALS AND METHODS:

2.1. Materials (VION KN-1)

The object of the study was VION KN-1. The criteria for choosing VION KN-1 fiber were its characteristics, such as a developed surface, which facilitates the access of reagents to the exchange centers of the fiber; better swelling ability; high sorption rate, and greater resistance to abrasion by a moving flow. For the regeneration of fibrous ion exchangers, a less regenerating solution is required in comparison with granular ion exchangers (Kopylova *et al.*, 2006). In this regard, fibers are widely used both for wastewater treatment from various ions (Xu *et al.*, 2021; Grachek *et al.*, 2020; Wang *et al.*, 2020) and for the recovery of rare earth elements (Li *et al.*, 2020).

Ion exchange fiber VION KN-1 ion exchanger is obtained based on polyacrylonitrile (PAN) fiber (Perepelkin *et al.*, 1985). The radius of the chemisorption fiber PAN = $11 \cdot 10^{-6}$ m. The sorption of water vapor by the nitron fiber at a relative air humidity of 65% is 0.8-1.5 wt. %, and at 95% - 1.5-3.5 wt. %. The swelling of the fiber in water is 3-6 wt.% (Perepelkin *et al.*, 1985).

The fibrous sorbent VION KN-1 is synthesized by the sequential processing of nitron fiber with a 20-25% aqueous hydrazine solution for 1.5-2.0 hours, followed by hydrolysis with caustic soda.

The functional groups of the cation exchange fiber are ~COO^-(H^+carboxyl groups (H^+- or Na^+- forms) (Figure 1).

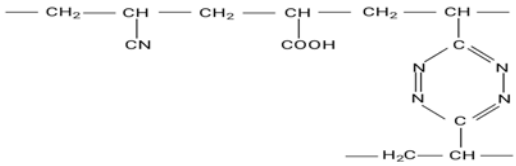

Figure 1. *The structure of the ion-exchange fiber VION KN-1 in the hydrogen form*

This ion exchanger does not dissolve in any known solvent, including when heated. It is capable of multiple regenerations, which are carried out with solutions of acid and alkali. With the help of the fibrous sorbent VION KN-1, wastewater with a concentration of harmful or valuable substances less than 40 mg/l undergoes treatment and additional treatment. At such concentrations, the use of other capture methods is not economically efficient. The sorbent VION KN-1 is produced in the form of chemisorption fiber and nonwoven fabric (Figure 2), the characteristics of which are shown in Table 1.

Table 1*. Characteristics of a chemisorptive fiber and nonwoven fabric VION KN-1*

Characteristics	Value
Static ion exchange capacity (IEC), mg-eq/g	3.5-5.0
Linear density, tex	0.6-0.8
Breaking load, CN / tex	3.5-10.0
Breaking elongation, %	25-40
Fabric width, cm	156-164
Surface density, g/m^2	250, 800

2.2. Experimental procedures or VION KN-1 obtention or synthesis

The ammonium ion concentration in the solution was determined using an I-130 ion meter with an ion-selective electrode according to a calibration graph (voltage dependence on the logarithm of molar concentration).

The study of the equilibrium and kinetics of sorption of ammonium ions was carried out under static conditions from aqueous solutions of ammonium chloride with stirring at a temperature of 298 K.

a

b

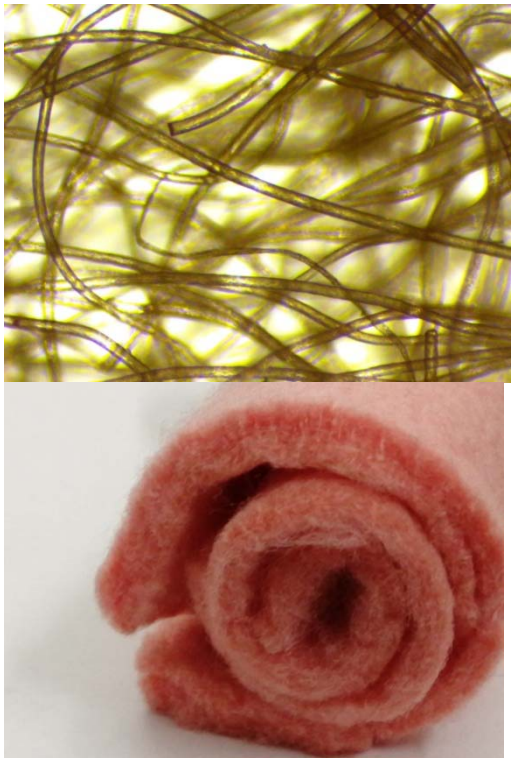

Figure 2.*Image of the sorbent VION KN-1 on Altami BIO microscope in the form of a chemisorption fiber (a) and nonwoven fabric (b)*

In the work, the limited volume method was used (Selemenev *et al.*, 2004), the essence of which was as follows: a sample of an air-dry ion exchanger weighing 0.3 ± 0.0002 g was placed in 100 ml of ammonium chloride solution. The working ammonium chloride solutions were

prepared from a standard solution by dilution. The ammonium ion concentration in the prepared solutions was in the range of 32 to 204 mg/dm^3 (1.78÷11.3 mmol/ dm^3). The experiment was carried out at a temperature of 298±2 K. Constant mixing led to an instantaneous equalization of the concentration of NH_4^+ ions in the solution volume. The change in the ammonium ion concentration was determined by direct potentiometry using an NH_4^+- selective electrode. The amount of the sorbed substance (mol/g) was calculated by the formula (Eq. 1).

$$CE = \left(C_o - C_p\right) \cdot \frac{V}{m} \qquad \text{(Eq. 1)}$$

where *m* is the mass of the fiber sample, g; *V* is the solution volume, dm^3; C_0, C_p is the initial and equilibrium concentration of ammonium ions in the solution, mol/ dm^3.

To calculate the coefficient of internal diffusion (*D*, *m^2/ sec*), the following equation was used(Eq. 2):

$$D = Br^2 / \pi^2 \qquad \text{(Eq. 2)}$$

Where r is the radius of the chemisorption fiber, m (*rPAN = 11·10^{-6}m*); *B* is the slope angle tangent of the direct dependence *Bt = f(t)*, where *Bt=(F/1.08)^2*.

The half-sorption time $T^{1/2}$ (min), indirectly characterizing the sorption rate, was calculated by the equation(Eq. 3):

$$T^{(1/2)} = 0.03r^2(D \cdot 60), \qquad \text{(Eq. 3)}$$

The distribution coefficient of ammonium ions (K_d, sm^3/g) was calculated by the formula(Eq. 4):

$$K_d = \left(R/100 - R\right) \cdot V/m, \qquad \text{(Eq. 4)}$$

where R is the degree of recovery, %.

To calculate the empirical constants *a, b*, and *k*, the Langmuir and Freundlich equations were used. The Langmuir equation (Eq. 5):

$$1/CE = 1/kb \cdot 1/Cp + 1/k, \qquad \text{(Eq. 5)}$$

where *CE* is the sorption value, *mol/g*, *b*, *k* are empirical constants, and *Cp* is the equilibrium concentration of the reagent in the solution, *mol/dm^3*.

The Freundlich's equation(Eq. 6):

$$lgCE = lga + 1/n \cdot lgCp, \qquad \text{(Eq. 6)}$$

Where *CE* is the sorption value, mol/g, a is the empirical constant, and *Cp* is the equilibrium concentration of the reagent in the solution, mol/dm^3.

The procedure for the sorption of ammonium ions under dynamic conditions was as follows. One of the most commonly used and effective options for the sorption process is passing wastewater through a fixed ionite bed (column or filter). The filter was filled with samples of ion-exchange fiber weighing from 0.31 to 0.93 *g*. A solution containing ammonium ions of a known concentration was passed through the filter at a certain rate. The content of ammonium nitrogen in the portions of the filtrate (50 *cm^3*) at the outlet from the filter was determined by the potentiometric method. The passage of the solution was stopped when the concentration of ammonium ions in the filtrate became equal to the initial concentration. The data obtained were used to plot the output curves in the coordinates $C/C_o = f(V)$.

The experimental data were processed using the Statistica Neural Networks software package to predict the degree of recovery of ammonium ions from wastewater. Given the results of the preliminary experiments, the main parameters (input parameters), which have a significant effect on ion sorption, were selected: pollutant concentration, mol/dm^3; the volume of a flowing solution, dm^3; fiber mass, g. The response function (output parameter) was the degree of ammonium recovery, %.

2.3 Neural network models

Based on the data obtained, neural network models were constructed; an automated neural network with the following settings was chosen as the construction strategy: network type - multilayer perceptron, the minimum and maximum number of hidden neurons - 3 and 10, respectively. Five networks with the smallest error with respect to the control sample were saved. The neural network MLP-3-5-1 with high determination coefficients was 0.999420; 0.998767; 0.998572 was selected from them for training testing and sampling control. Such coefficients indicate a high performance of the trained network. The training error was 0.279647; a second-order accuracy training algorithm, BFGS, was chosen. The activation function of

hidden neurons is identical, and of the output neurons are logistic.

3. RESULTS AND DISCUSSION:

The obtained experimental data on the sorption of ammonium ions by the fibrous sorbent VION KN-1 from solutions with different contents of ammonium nitrogen are shown in Table 2. The maximum value of the sorption capacity of the VION KN-1 sorbents at a given concentration of ammonium ions is 2.47 mmol/g. During sorption from dilute solutions, the distribution coefficients (K_d) are at the level of $2.3 \cdot 10^3$ cm^3/g, which is significantly higher than the values for granular ionites.

The degree of recovery *(R)* of ammonium ions increases with decreasing concentration, which indicates the efficiency of the fiber for the additional treatment of diluted effluents to the maximum permissible concentration (MPC). Such indicators of the degree of recovery (less than 90%) can be explained by the fact that the selected ratio of the volume of the solution and the fiber sample (330 cm^3/g) is not the optimal ratio of the parameters: solution volume – ionite sample – pollutant concentration.

Sorption isotherms were constructed using the method of variable concentrations to assess the affinity of the investigated fibrous ionites to ammonium ions. For this, equilibrium concentrations were used, which are the residual content of ammonium ions in the solution after saturation of the fibrous sorbent.

The isotherms of sorption of ammonium ions by ion-exchange fiber in the coordinates CE=f(Cp) have the form of a convex curve (Figure 3). The initial regions for both ionites are close to linear (Henry's region)). The sorption value is practically proportional to the ammonium ion concentration in these regions. At low concentrations (Cp<1 mmol/dm3), almost quantitative sorption occurs in the solution.

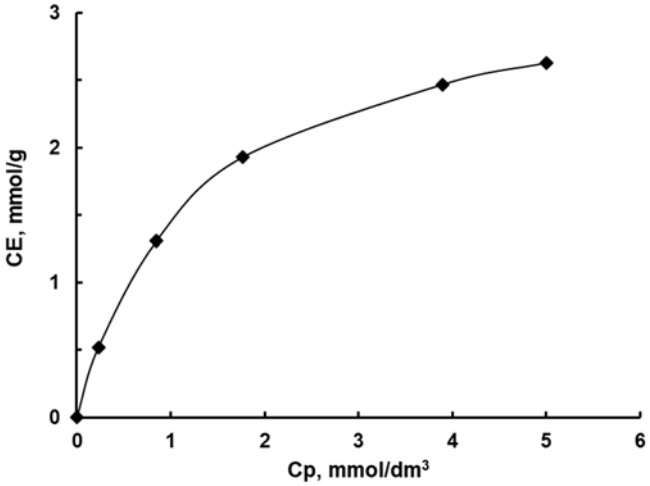

Figure 3. *Isotherms of sorption of ammonium ions by the fibers VION KN-1*

The Langmuir and Freundlich models were applied to quantitatively describe the equilibrium sorption process of ammonium ions. Figure 4 shows that the sorption isotherms by the VION KN-1 sorbent are linearized in the coordinates of the Langmuir equation, as indicated by the values of the reliability R_2. This indicates that sorption has a monolayer character, and its maximum is achieved when the monolayer is completely filled and there is no interaction between the sorbed ions. The values of the parameters in the equations of the Langmuir and Freundlich models and the correlation coefficients are presented in Table 3.

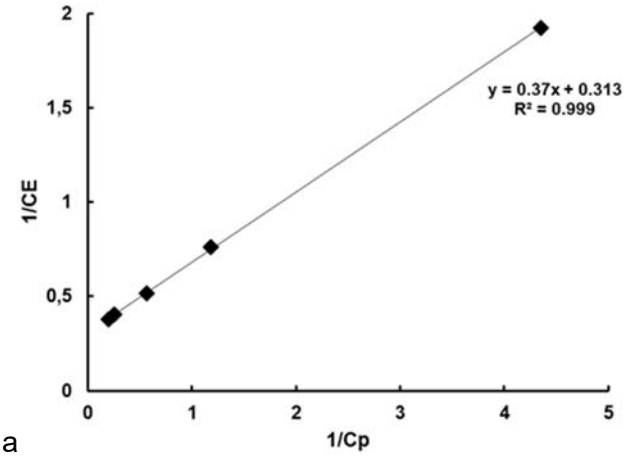

a

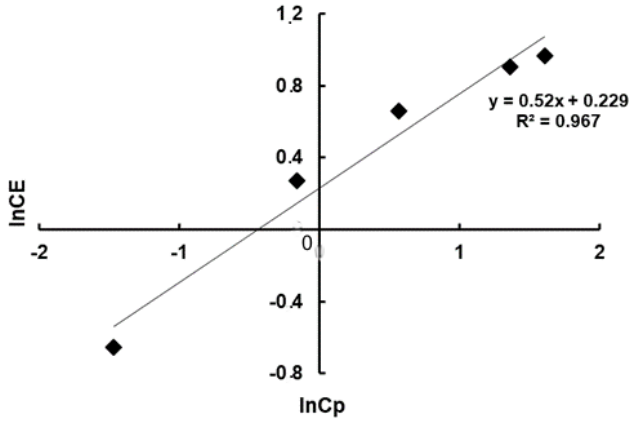

b

Figure 4. Isotherms of ammonium ion sorption by fibrous sorbents in the coordinates of the Langmuir (a) and Freundlich (b) equations

The dependence of the sorption capacity of ionites on the initial ammonium ion concentration in the inverse coordinates *1/CE=f (C$_H$)* (Figure 5) was constructed. This dependence can be used to obtain an analytical equation that makes it possible to predict the sorption capacity of fibrous sorbents.

Based on the obtained straight-line correlations, the values of the *CE$_{00}$* and *K$_L$* constants were reliably calculated. By introducing constants into the Langmuir equation, we obtain analytical equations for predicting the sorption capacity of VION KN-1(Eq. 7):

$$CE = 10.32 \cdot \frac{0.02975C_н}{1 + 0.02975C_н} \qquad \text{(Eq. 7)}$$

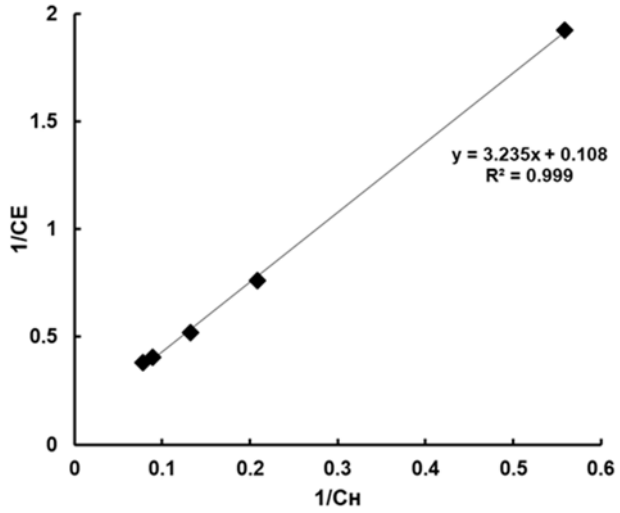

Figure 5. The dependence of the sorption capacity of fibrous sorbents on the content of ammonium nitrogen in the solution in the inverse coordinates

The equation obtained makes it possible to determine the sorption capacity of the test fiber concerning ammonium ions at any initial concentration. The value of the sorption capacity calculated according to the above equation with varying the initial content of ammonium nitrogen agrees well with the experimentally obtained data (Table 4).

Table 4. The calculated and experimental data on the sorption capacities of the fibrous sorbent VION KN-1 for ammonium ions

Ionite brand	$C_н$, mmol/ dm^3	Value CE, mmol/g	
		Calculated	Experimental
VION KN-1	1.79	0.52	0.52
	4.79	1.29	1.31
	7.56	1.90	1.93
	11.3	2.59	2.46

To determine the optimal ratio between the solution volume and the mass of fibrous sorbents, the dependence of the degree of recovery of ammonium ions on the hydromodule was built (Figure 6). The dependences show that with a decrease in the ratio between the volume of solution and the mass of fibers (hydromodule), the degree of recovery increases. In this case, complete recovery of ammonium ions is not achieved (less than 90%). This is due to the fact that the sorption process was carried out at a higher initial concentration of ammonium ions in the solution ($C_н$ = 10 mmol/dm^3).

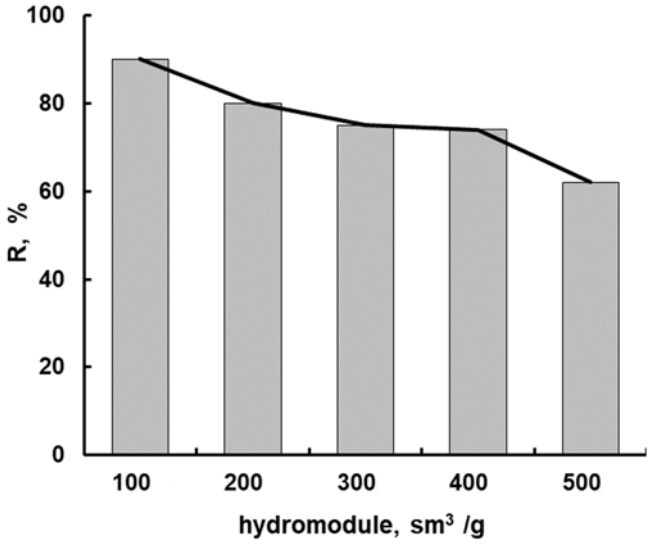

Figure 6. Effect of the hydromodule on the degree of recovery of ammonium ions

Thus, when treating wastewater with a high content of ammonium ions (10 mmol/dm^3), a

two-step process is required. At lower concentrations of ammonium ions, the test fiber can be used to purify water up to the MPC value.

The kinetic dependences of sorption make it possible to determine the time of the establishment of the equilibrium, which characterizes the rate of this process. Figure 7 shows the kinetic curves of ammonium ion sorption by the fiber. It is clear that the type of kinetic sorption curves is similar and is described by the equation $CE = CE_m(1-exp(-\beta\tau))$, where *CE* is the sorption value, τ is the sorption time, $CE_m$and *β* are constant values. The constant CE_mcharacterizes the sorbent capacity at saturation; *β* characterizes the slope of the curve.

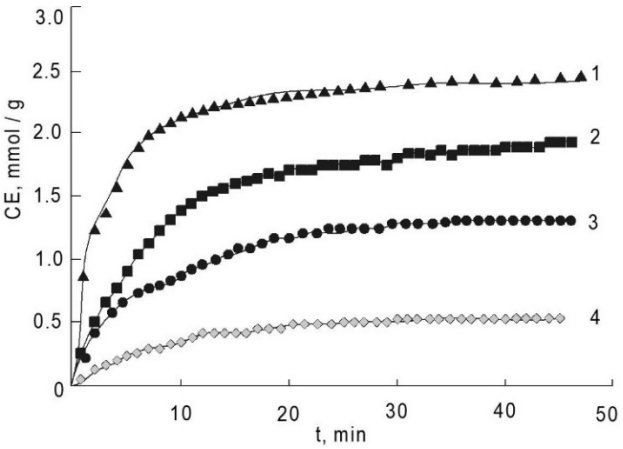

Figure 7. Kinetics of ammonium ion sorption by VION KN-1 fiber. The concentration of the external solution is 1-11.3; 2-7.55; 3-4.72; 4-1.78 mmol/dm^3, respectively.

The sorption rate of ammonium cations on a fibrous sorbent is maximal during the first 10 minutes. The high sorption rate is explained not only by the structural characteristics of the fiber but also by the mixing of the external solution - sorbent system. This probably leads to a decrease in film thickness and an increase in mass transfer. With an increase in the concentration of the external solution, the time of the establishment of the equilibrium state and the sorption capacity increase.

To assess the contribution of the diffusion of ammonium ions through the “film” and inside the VION KN-1 fiber matrix, the kinetic dependences obtained in this work were presented in the coordinates of the Boyd – Adamson equations for the case of internal and external diffusion. To determine the limiting stage, the following dependences of the degree of conversion (*F*) on the sorption time τ were obtained and analyzed: $F - \sqrt{\tau}$ and $-ln(1-F) = f(\tau)$, where $F = CE\tau/CEm$, *CEτ* is the sorption capacity of the fiber for a certain sorption time, CEm is the maximum sorption capacity of the fiber.

Figure 8 shows the kinetic curves. The correlation coefficients are close to unity; the linearity of the dependencies in these coordinates indicates the contribution of internal diffusion. For a cylinder-shaped ion exchanger, linearity must be observed with practical exactness at F~0.5.

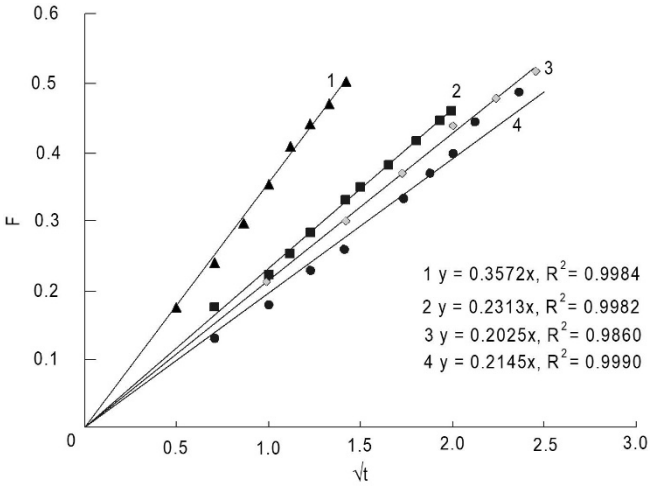

Figure 8. Kinetic curves of ammonium ion sorption by VION KN-1 fiber in the coordinates of the Boyd-Adamson equations for the case of internal diffusion. The concentrations of external solutions: 1 - 11.3; 2-7.55; 3-4.72; 4 - 1.78 mmol/ dm^3, respectively.

To assess the effect of external diffusion, the kinetic sorption curves were considered in the coordinates $-ln(1-F) = f(t)$ at different degrees of sorbent filling (Figure 9).

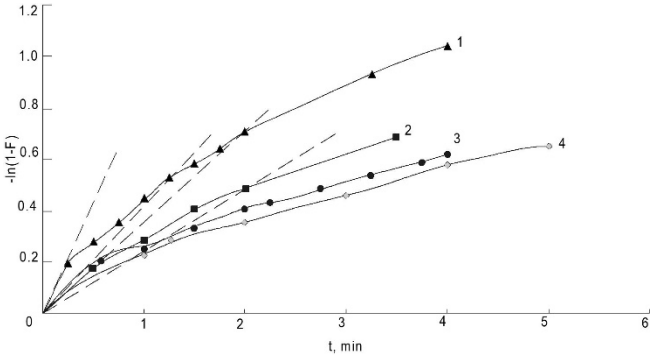

Figure 9. Kinetic curves of ammonium ion sorption by VION KN-1 fiber in the coordinates of the Boyd-Adamson equations for the case of external diffusion. The concentrations of the external solution: 1 - 11.3; 2-7.55; 3-4.72; 4 - 1.78 mmol/dm^3, respectively.

It is clear that linearity is observed in the low concentration region. However, with increasing F, the curves cease to be linear, which emphasizes the effect of internal diffusion on

sorption at a certain degree of fiber filling.

The value of the kinetic coefficients B for the ion exchange fiber was determined from the linear dependences (*Bt - f(t)*) (Figure 10). The obtained correlation coefficients (R_2) confirm the limiting contribution of internal diffusion to ammonium ion sorption.

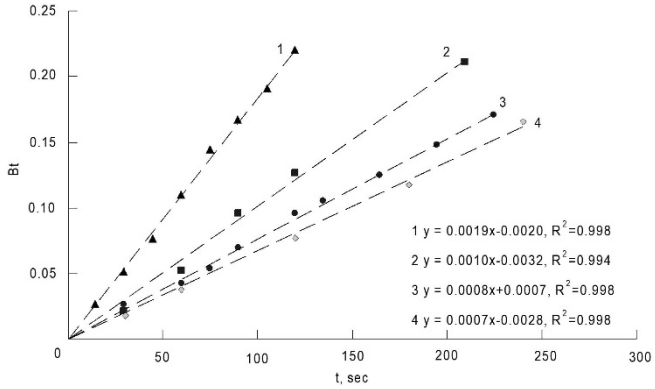

Figure 10. Dependence of the parameter Bт on the duration of ammonium ion sorption by VION KN-1 carboxyl fiber. The concentrations of the external solution: 1 - 11.3; 2-7.55; 3-4.72; 4 - 1.78 mmol/dm^3 , respectively.

In order to make sure that the sorption by VION KN-1 fiber is limited by intradiffusion restrictions, the method with interruption of the ionite-solution contact, described by Kressman and Kitchener (Nesterov *et al.*, 2007), was applied.

Figure 11 shows that after a certain time ("storing" of the ionite, 10 min) and the resumption of contact of the solution with the fiber, the rate of the ion-exchange process at the initial moment increases. This also indicates the gel kinetics of the sorption of ammonium ions by the VION KN-1 fiber.

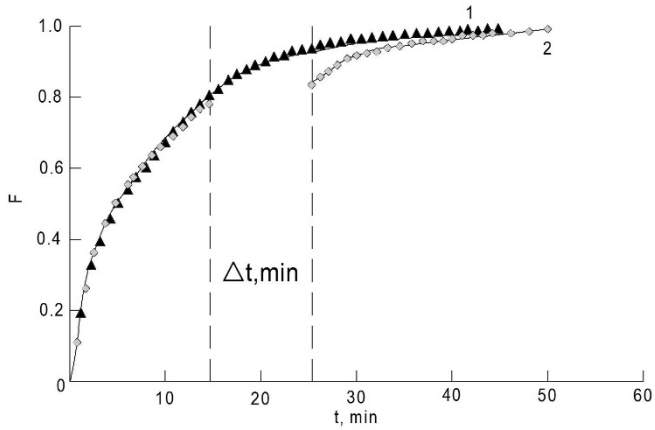

Figure 11. Kinetic dependences of the ammonium ion sorption taking into account the time of interruption of the ionite-solution contact (1); without interruption (2)

The calculated values of the kinetic characteristics are shown in Table 5.

With a decrease in the external solution concentration, the degree of recovery of ammonium ions by VION KN-1 fiber increases.

The Langmuir and Freundlich models were used to quantitatively describe the equilibrium process of ammonium ion sorption by a fibrous sorbent. The calculation results are presented in Table 6.

Table 6. Calculation results for Langmuir and Freundlich models

Model	Parameters	Confidence value
Langmuir	k = 3.233 b = 773.27	R^2= 0.9996
Freundlich	a	R^2 = 0.9224

The obtained confidence values of R^2 show that the isotherms are linearized only in the inverse coordinates of the Langmuir equation and are not described in the coordinates of the Freundlich equation. Empirical constants k and b are found for the studied isotherms. The possibility of using the Langmuir equation to describe the ammonium ion sorption indicates the equivalence of all active centers of the ion exchange fibrous sorbent, which contributes to the formation of a monomolecular sorption layer on the surface of the ion exchanger.

In this work, the study of sorption under dynamic conditions was carried out. To find the optimal fiber height in the dynamic mode, the output curves of the ammonium ion sorption were obtained (Figure 12).

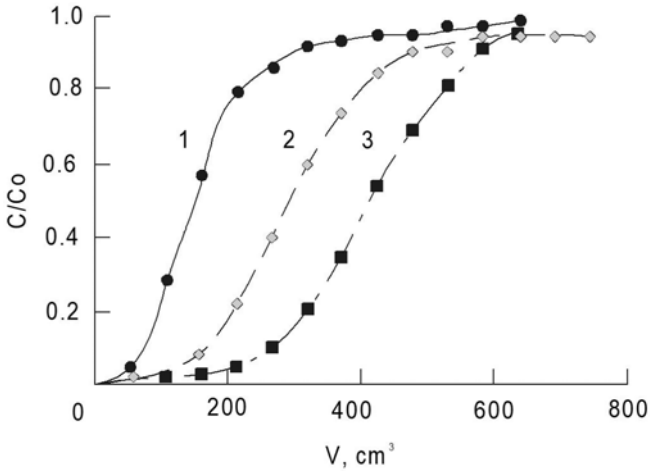

Figure 12. Output curves of the ammonium ion sorption by VION KN-1 fiber. The solution concentration is 11.3 mmol/dm^3; the solution flow

rate is 3 cm^3/min.

The total dynamic exchange capacity (TDEC) with respect to ammonium ions for VION KN-1 fiber is ≈ 4.3 mmol/g.

To determine the efficiency of the degree of recovery, the curves of the dependence of the degree of recovery on the mass of the fiber sample and the volume of the solution were constructed and analyzed (Figure 13). As can be seen from Figure 13, the increase in the weight of the sample results in an increase in the degree of recovery of ammonium ions. Thus, by passing 200 cm^3 of a solution with a concentration of 11.3 mmol/dm^3 through a layer of VION KN-1 fiber weighing 0.93 g, a recovery rate of more than 96% can be achieved.

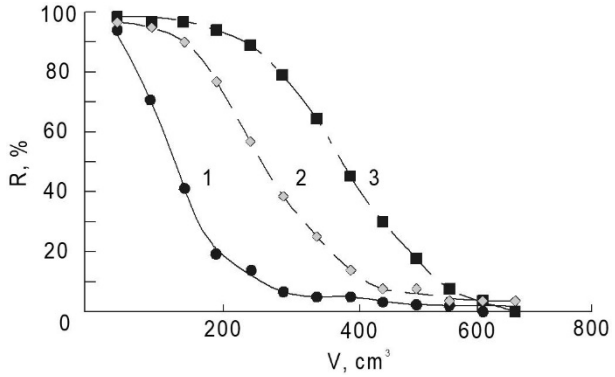

Figure 13. Curves of the dependence of the degree of recovery on the height of the layer (weight of the sample) and the volume of the passed solution (1 –m=0.31 g, h = 0.5 cm; 2 –m=0.62 g, h = 1.0 cm; 3–m=0.93 g, h = 1.5 cm)

To assess the effect of the initial solution concentration on the form of the output curves, the dependences of the relative concentration of C/C_o on the volume of the outflowing solution and on the concentration were obtained and analyzed (Figure 14).

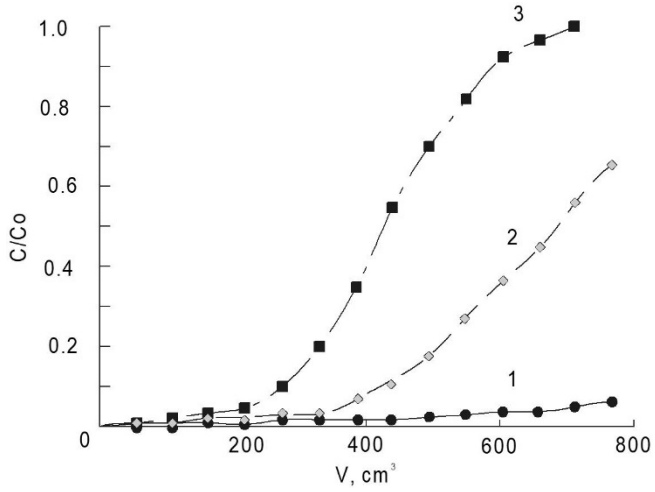

Figure 14. Output curves of ammonium ion sorption by the fiber VION KN-1 with different solution concentrations. The solution flow rate is 3 cm^3/min (1 – 3.34 mmol/dm^3; 2 – 7.10 mmol/dm^3; 3 – 10.00 mmol/dm^3)

Figure 14 shows that at the lowest content of ammonium ions in the initial solution (3.34 mmol/dm^3), the relative concentrations for VION KN-1 are less than 0.065. This means that with a decrease in concentration in a dynamic mode, the sorption characteristics of the fibers do not decrease, which makes their use relevant for the purification of dilute solutions containing ammonium ions.

The proof of these statements can be found in Figure 15.

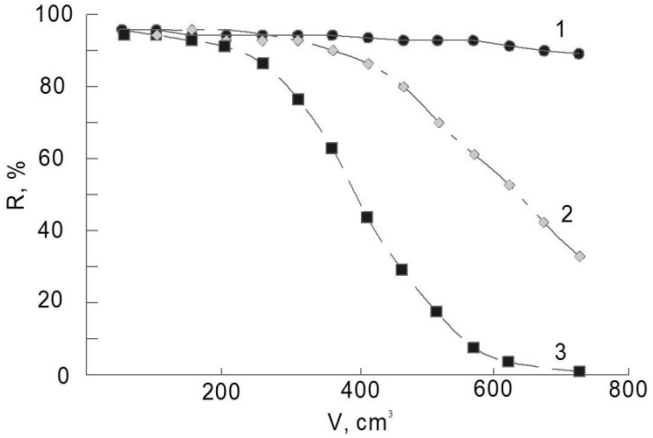

Figure 15. The curves of the dependence of the degree of recovery on concentration and on the volume of the passed solution (1 – 3.34 mmol/dm^3; 2 – 7.10 mmol/dm^3; 3 – 10.00 mmol/dm^3)

As can be seen from Figure 15, when a 700 cm3 solution is passed through a VION KN-1 layer (mfiber= 0.93 g) at low concentrations of ammonium ions in the initial solution, the recovery is greater than 93.

The ammonium ion desorption from the fiber is carried out using acid solutions. As a result, solutions of ammonium salts are formed. The solutions obtained contain ammonium nitrogen, a biogenic element, and can be used to produce liquid mineral fertilizers.

The prediction of the degree of recovery of ammonium ions from wastewater was carried out using the STATISTICA neural network. To establish the dependence of the degree of recovery (R) on the factors listed, the values of the levels and variation intervals of which are shown in Table 7, an experiment has been planned.

A dataset was obtained to train the neural network. This is a set of experiments for which

the values of the input factors and the output parameter (the degree of recovery of ammonium ions) are indicated. An element of the dataset is presented in Table 8.

The adequacy of the trained neural network was checked graphically. For this, a histogram of residues was constructed, i.e., the difference between the input and the output by the network values of the degree of recovery (*R*) of ammonium ions by the fibrous sorbent (Figure 16).

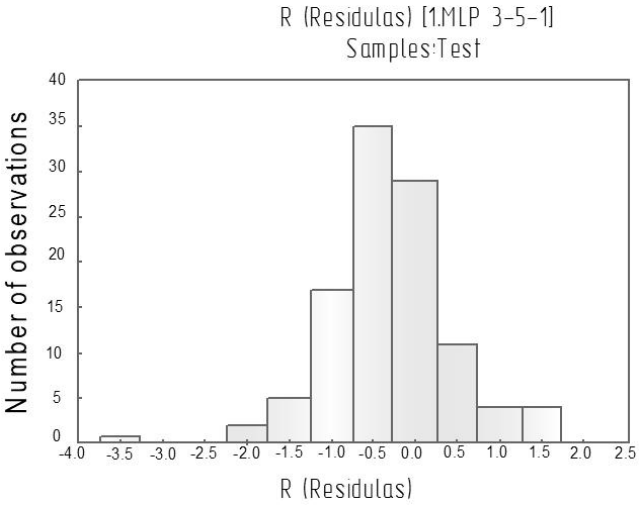

Figure 16. Histogram of the dependence of residues on the number of observations

As can be seen, there are outlying elements, i.e., deviations in some input values of the degree of recovery from the values of the trained network. These are residues equal to -3.5; -2; -1.5; 1; 1.5. The bulk is concentrated in a small range of residues from -1 to 0.5.

The scattering dependence of the target and output values of the neural network is shown in Figure 17. It is clear that most of the input (target) values are on a straight line at an angle of 45°, i.e., they match the output values.

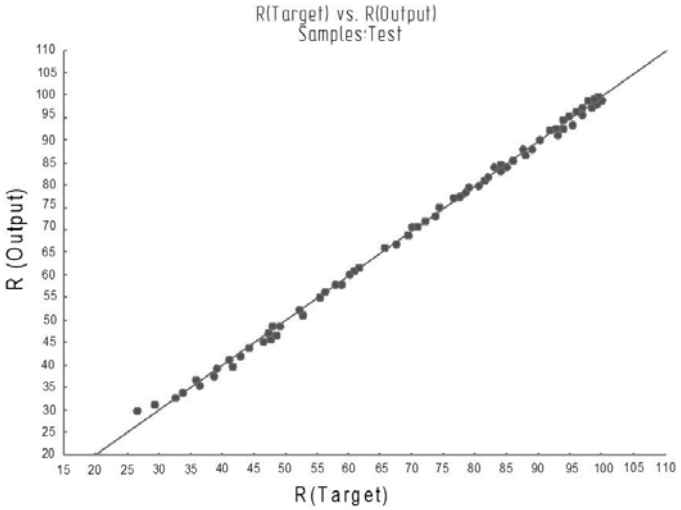

Figure 17. The dependence of the target values of the degree of recovery of ammonium ions on the output values.

When sorption is carried out under industrial conditions, to maximize the recovery of ammonium ions from wastewater, it is advisable to take into account the boundary conditions of the action of the influencing factors. For this, the pairwise influence of the parameters on the course of the sorption process was studied.

Figure 18 shows the response surface of the output parameter (degree of recovery) depending on the pollutant concentration and the volume of the flowing solution.

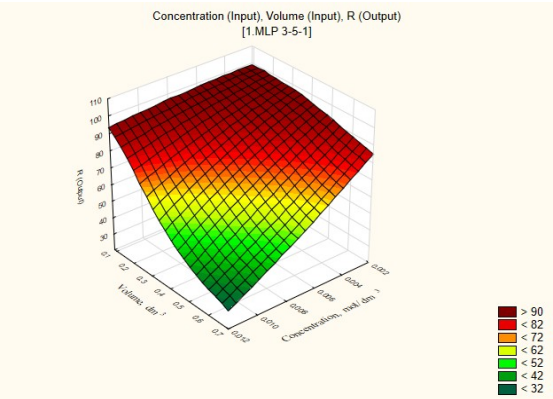

Figure 18. The response surface of the output parameter depending on the pollutant concentration and the volume of the flowing solution.

The analysis of the graphical dependencies shows that an increase in the ammonium ion concentration and the volume of the flowing solution reduces the degree of recovery. A value of R greater than 90% can be achieved by passing a solution of volume up to 0.2 dm^3 and a concentration of 0.002 mol/ dm^3.

Figure 19 shows the response surface of the output parameter (degree of recovery)

depending on the fiber mass and the volume of the flowing solution.

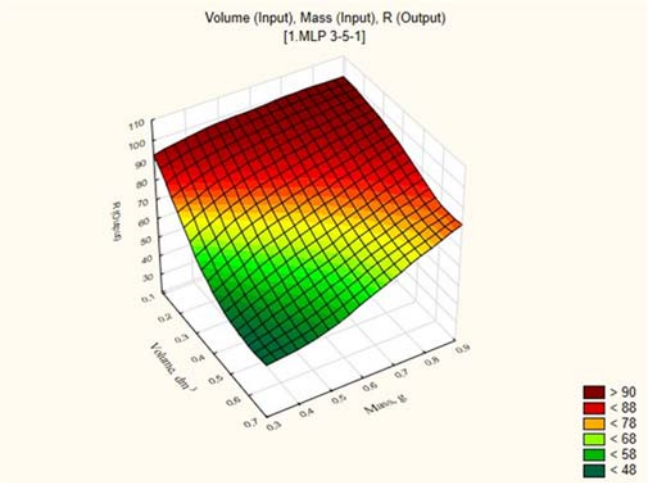

Figure 19. The response surface of the output parameter depending on the fiber mass and the volume of the flowing solution.

With an increase in the volume of the flowing solution and a decrease in the fiber mass, the degree of recovery decreases. When a solution with a volume of 0.3 dm^3 is passed through a fiber layer with a mass of more than 0.6 g, then the ammonium ion concentration decreases by 84%.

Figure 20 shows the response surface of the output parameter (degree of recovery) depending on the fiber mass and the pollutant concentration.

With a decrease in concentration and an increase in fiber mass, the degree of recovery of the pollutant increases. At a concentration of less than 0.009 mol/dm^3 and a fiber mass of more than 0.6 g, the degree of recovery is more than 90 %.

To predict the degree of recovery as a result of ammonium ion sorption under industrial conditions, the test data were analyzed (11 values) (Table 9).

After the analysis, the model was launched using the new input data. Similar sampling was generated, and the saved model with the network identifier, which was previously selected as the best one, was uploaded. A small value of the mean square error indicates a good quality of the constructed model based on the new input data (Table 10).

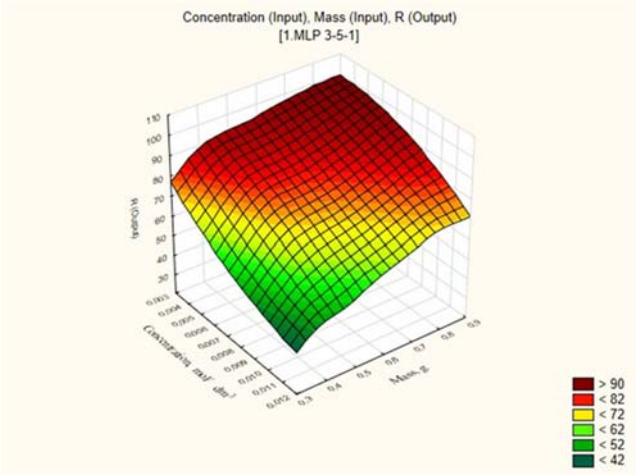

Figure 20. The response surface of the output parameter depending on the fiber mass and the pollutant concentration.

In Table 10, the column Target presents the data obtained during the experiment, in the column Output - the predicted values of the output parameter for predicting the degree of recovery of ammonium ions. These values were produced by a trained neural network MLP 3-5-1. By comparing the first and second columns, the values of the absolute deviation are calculated. The absolute deviation for the entire data selection does not exceed 1.384330 (the column Absolute residues). The parameters of the relative deviation (Squared residues) are also obtained. The residual sum of squares is minimal and ranges from 0 to 1.916369.

The mean square error of the test sampling is 0.596459226. The low value of the mean square error of the introduced new data indicates a sufficient amount of data for training and the existence of a consistent connection between the ammonium ion concentration in the solution, the volume of the passed solution, the ionite mass of the ion exchanger, and the degree of recovery.

4. CONCLUSIONS:

The assessment of the kinetic characteristics of the ammonium ion sorption by VION KN-1 fiber showed that a high rate characterizes the absorption of the analyte by the fibrous sorbent. A decrease in the concentration of the external solution leads to a decrease in the time for the establishment of the equilibrium state and in the value of the sorption capacity. The experimental data obtained as a result of studying the kinetics of ammonium ion sorption by a carboxyl fiber sorbent under static conditions and the calculations performed made it possible to establish the approximation of the kinetic

equations, which are valid for the case of internal diffusion. The experimental data on the sorption were verified using the Freundlich and Langmuir isotherms. The Langmuir equation best describes the process of ammonium cation sorption on VION KN-1 fibrous sorbent. A trained neural network can predict the parameters of the technological process for the treatment of ammonium ions wastewater with high accuracy.

The parameters affecting the ammonium ion sorption from solutions have been established. The maximum recovery of more than 96% was achieved when passing through a 200 cm3 solution with a concentration of 11.3 mmol/dm3. It is shown that it is reasonable to use ion-exchange fibers at the stage of additional treatment. The solutions obtained after desorption VION KN-1 contain ammonium ions, which allows their use as liquid nitrogen-containing fertilizers.

The trained neural networks can be used to predict the degree of recovery of ammonium ions by the fibrous sorbent VION KN-1, which is proved by the data obtained to verify the adequacy of neural network models.

6. REFERENCES:

1. Adam, M. R., Othman, M.H., Puteh, M. H., Ismai,l A.F., Mustafa, A., Rahman, M. A., Jaafar, J. (2020). Impact of sintering temperature and pH of feed solution on adsorptive removal of ammonia from wastewater using clinoptilolite based hollow fibre ceramic membrane. Journal of Water Process Engineering, 33 (101063), https://doi.org/10.1016/j.jwpe.2019.101063
2. Alias, M. Y., Lee, K. K., Zaharah, I., Zaiton, A.M., Nik, A. N. (2010). Kinetic and equilibrium studies of the removal of ammonium ions from aqueous solution by rice husk ash-synthesized zeolite Y and powdered and granulated forms of mordenite. Journal of Hazardous Materials, 174 (1–3), 380-385, https://doi.org/10.1016/j.jhazmat.2009.09.063
3. Alver, A., Kazan, Z. (2020). Prediction of full-scale filtration plant performance using artificial neural networks based on principal component analysis, Separation and Purification Technology, 230, 115868, https://doi.org/10.1016/j.seppur.2019.115868.
4. Al-Sheikh, F., Moralejo, C., Pritzker, M., Anderson,W.A., Elkamel,A. (2021). Batch adsorption study of ammonia removal from synthetic/real wastewater using ion exchange resins and zeolites. Separation Science and Technology, 56(3): 462-473. https://doi.org/10.1080/01496395.2020.1718706
5. Belchinskaya, L.I., Novikova, L.A., Khokhlov, V.Yu., Tkhi, Jen LY (2013). Contribution of Ion-Exchange and Non-Ion-Exchange Reactions to Sorption of Ammonium Ions by Natural and Activated Aluminosilicate Sorbent. Journal of Applied Chemistry, V.2013, 1-10. http://dx.doi.org/10.1155/2013/789410
6. Cagcag Yolcu, O., Temel, F. A., Kuleyin, A. (2021). New hybrid predictive modeling principles for ammonium adsorption: The combination of Response Surface Methodology with feed-forward and Elman-Recurrent Neural Networks, Journal of Cleaner Production, 311, 127688, https://doi.org/10.1016/j.jclepro.2021.127688
7. Clark, B., Tarpeh, W.A. (2020). Selective Recovery of Ammonia Nitrogen from Wastewaters with Transition Metal-Loaded Polymeric Cation Exchange Adsorbents. Young Chemists, 26(44), 10099-10112. https://doi.org/10.1002/chem.202002170
8. El-Shafey Ola, I., Fathy Nady, A., El-Nabarawy Thoria, A. (2014). Sorption of Ammonium Ions onto Natural and Modified Egyptian Kaolinites: Kinetic and Equilibrium Studies. Advances in Physical Chemistry, V.2014, 1-12. http://dx.doi.org/10.1155/2014/935854
9. Faisal, A., Naji, L. (2019). Simulation of Ammonia Nitrogen Removal from Simulated Wastewater by Sorption onto Waste Foundry Sand Using Artificial Neural Network. Association of Arab Universities Journal of Engineering Sciences, 26 (1), 28-34. https://doi.org/10.33261/jaaru.2019.26.1.004
10. Farhi, N., Kohen, E., Mamane, H., Shavitt, Y. (2021). Prediction of wastewater treatment quality using LSTM neural network. Environmental Technology & Innovation, 23,101632 https://doi.org/10.1016/j.eti.2021.101632

11. Giwa, A., Daer, S., Ahmed, I., Marpu, P.R., Hasan, S.W. (2016). Experimental investigation and artificial neural networks ANNs modeling of electrically-enhanced membrane bioreactor for wastewater treatment. Journal of Water Process Engineering, 11, 88-97, https://doi.org/10.1016/j.jwpe.2016.03.011
12. Guida, S., Potte,r Ch., Jefferson, B., Soares A. (2020). Preparation and evaluation of zeolites for ammonium removal from municipal wastewater through ion exchange process. Scientific Reports, 10 (1246), 1-11, https://doi.org/10.1038/s41598-02069348-6
13. Gumnitsky, Ya. M., Sabadash, V.V., Matsus'ka, O. V. (2013). Extraneous diffusion kinetics of ammonium ions adsorption in the presence of other ions. Vostochno-Evropeiskii zhurnal peredovykh tekhnologii, V.4. No. 6 (64), 19-23.
14. Grachek, V .I., Shunkevich, A. A., Polikarpovn, A. P., Isakovich, O. I. (2020). Proceedings of the National Academy of Sciences of Belarus. Chemical Series, 56(2): 206-21 https://doi.org/10.29235/1561-8331-2020-56-2-206-211
15. Han, B., Butterly C., Zhang W., He J., Chen D (2020). Adsorbent materials for ammonium and ammonia removal: A review. Journal of Cleaner Production, 283 (10), 124611, https://doi.org/10.1016/j.jclepro.2020.124611
16. Han, H.-G., Chen, Qi-li, Qiao, Jun-Fei (2011). An efficient self-organizing RBF neural network for water quality prediction. Neural Networks, V.24 (7), 717-725 https://doi.org/10.1016/j.neunet.2011.04.006
17. Heddam,S., Bermad, A. Dechemi, N. (2011). An efficient self-organizing RBF neural network for water quality prediction. Journal of Environmental Engineering, V.137 (12), 717-725. https://doi.org/10.1061/(ASCE)EE.1943-7870.0000435
18. Ivanova, E., Karsheva, M., Koumanova, B. (2010). Adsorption of ammonium ions onto natural zeolite. Journal of the University of Chemical Technology and Metallurgy, 45 (3), 295-302.
19. Jayaweera, C.D., Aziz, N. Proceedings of the Future Technologies Conference (FTC). (2018) https://doi.org/10.1007/978-3-030-02686-862
20. Khataee, A. R., Kasiri, M. B. (2011). Modeling of biological water and wastewater treatment processes using artificial neural networks. Clean Soil Air Water, 39 (8), 742-749, https://doi.org/10.1002/clen.201000234
21. Kokotov, Yu. A., Pasechnik, V. A. (1970). Equilibrium and Kinetics of Ion Exchange. Leningrad: Khimiya: 336.
22. Kopylova, V. D., Zverev ,O. V., Astapov, A. V., Peregudov, Yu. S., Fibre Chemistry. (2006) https://doi.org/10.1007/s10692-006-0061-9
23. Kuzmina,R.I, Kondrashova, A.V. (2008). Dynamics and kinetics of the adsorption of ammonium ions on the opok. Khimiya i Khimicheskaya Tekhnologiya, 5(10), 72-74.
24. Mažeikiene, A., Valentukevičiene, M., Rimeika, M., Matuzevičius, A. B., Dauknys, R. (2008). Removal of nitrates and ammonium ions from water using natural sorbent zeolite (clinoptilolite). Journal of Environmental Engineering and Landscape Management, 16 (1), 38-44. https://doi.org/10.3846/1648-6897.2008.16.38-44
25. Malyovannyi, M., Sakalova, G., Chornomaz, N., Nahursky, O. (2013). Water Sorption Purification from Ammonium Pollution. Chemistry & Chemical Technology, 7 (3), 355-358. https://doi.org/10.23939/chcht07.03.355
26. Nageeb, R.M. (2013). Organic Pollutants—Monitoring, Risk and Treatment. Published by InTech, chapter 7, 229. http://dx.doi.org/10.5772/55953
27. Nesterov, Yu. V. (2007). Ionites ad Ion Exchange. Moscow: 480.
28. Nikashina, V.A., Serova, I.B., Katz, E.M. (2008). Purification of artesian drinking water from ion ammonium on natural clinoptilolite-containing tuff. Mathematical modeling and calculation sorption process. Sorbtsionnyeikhromatograficheskieprotsessy, 8 (1), 23-29.
29. Probst, J., Outram, J. G., Couperthwaite, S. J., Millar, G.J., Kaparaju, P. (2021). Sustainable ammonium recovery from wastewater: Improved synthesis and performance of zeolite N made from kaolin. Microporous and Mesoporous Materials. 316, 110918,

https://doi.org/10.1016/j.micromeso.2021.110918
30. Perepelkin, K. E. (1985). Structure and Properties of Fibers. Moscow: Chemistry, 208.
31. Putra, R. N., Lee, Y. H. (2020). Entrapment of micro-sized zeolites in porous hydrogels: Strategy to overcome drawbacks of zeolite particles and beads for adsorption of ammonium ions. Separation and Purification Technology, 237, 116351 https://doi.org/10.1016/j.seppur.2019.116351
32. Ren, Z., Jia, B., Zhang, G., Fu, X., Wang, Z., Wang, P., Longyi, Lv. (2021). Study on adsorption of ammonia nitrogen by iron-loaded activated carbon from low temperature wastewater. Chemosphere, 262. (127895), 1-5, https://doi.org/10.1016/j.chemosphere.2020.127895
33. Riemann W., Walton G. (1973). Ion-Exchange Chromatography in Analytical Chemistry. Moscow: 375.
34. Sakalova, G., Vasylinych, T., Shevchuk, O., Tkachuk, O. (2018). Perspectives of integration the technology of ion-exchanging ammonium extraction from the system of municipal drain water purification. Ukrainian Journal of Ecology, 8(1), 568-572 , https://doi:10.15421/2018_250
35. Selemenev, V.F., Slavinskaya, V.G., Khokhlov, V.Yu., Ivanov, V.A. (2004). Practical course on ion exchange. Voronezh: Voronezh. University Press: 160.
36. Seruga, P., Krzywonos, M., Pyżanowska. J., Urbanowska, A., Pawlak-Kruczek, H., Niedźwiecki, Ł. (2019). Removal of Ammonia from the Municipal Waste Treatment Effluents using Natural Minerals. Molecules, 24(20), 3633; https://doi.org/10.3390/molecules24203633
37. Sharifnia, S., Mohammad, A. K., Shojaeimehr, T., Shavisi, Ya. (2016) Characterization, isotherm and kinetic studies for ammonium ion adsorption by light expanded clay aggregate (LECA). Journal of Saudi Chemical Society, 20 (1), 342-351. https://doi.org/10.1016/j.jscs.2012.12.003
38. Wang, F., Wang ,X., Jiang, Yu., Ni, Zh., Wu, W., Zhang, H. (2020). Study of adsorption performance and adsorption mechanism for U (VI) ion on modified polyacrylonitrile fibers. Journal of Radioanalytical and Nuclear Chemistry, 323 (7), 365–377. https://doi.org/10.1007/s10967-019-06928-5
39. Xu, Li, Qi, Zh., Yang, H. (2020). Ultrafast and Stable Adsorption–Desorption Performance for Recovery of Valuable Rare-Earth Ions using High-Density Polyacrylic Acid Brush-Grafted Polypropylene Fibers Optimized by RSM Models. Industrial & Engineering Chemistry Research, 59(16), 7746–7754 https://pubs.acs.org/doi/abs/10.1021/acs.iecr.9b05793
40. Xu, W., Zheng, W. Wang, F. Xiong, Q. Shi, X.-L.Kalkhajeh, K Yu., G. Xu, H. Gao (2021). Using iron ion-loaded aminated polyacrylonitrile fiber to efficiently remove wastewater phosphate. Chemical Engineering Journal, 403(1) https://doi.org/10.1016/j.cej.2020.126349

7. OPEN ACCESS

Table 2. *Sorption properties of the fibrous sorbent VION KN-1 during the recovery of ammonium ions*

Ionite	$C_{initial}$, mmol/dm^3	C_p, mmol/dm^3	CE, mmol/dm^3	R, %	K_d, cm^3/g
VION KN-1	1.79	0.23	0.52	87.25	2281.07
	4.79	0.85	1.31	82.30	1549.53
	7.56	1.77	1.93	76.59	1090.40
	11.3	3.9	2.47	65.49	632.48

Table 3. *Models and constants of sorption isotherms*

Ionite	Langmuir model			Freundlich model		
	CE_{00}, mmol/g	K_L, dm^3/mmol	R^2	K_F, mmol/g	1/n	R^2
VION KN-1	3.1898	0.8526	0.9999	1.2596	0.5214	0.9665

Table 5. *Kinetic parameters of the process of ammonium ion sorption by VION KN-1 fiber*

C_{NH4}^+, mol/dm^3	CE, mmol/g	R, %	K_d, sm^3/g	B·10^4	D·10^{15}, m^2/sec	$\tau^{1/2}$, min
0.0113	2.468	65.52	633.41	19	23.31	2.59
0.00755	1.921	76.57	1089.34	10	12.27	4.93
0.00472	1.3135	82.29	1548.84	8	9.81	6.17
0.00178	0.5214	87.25	2281.04	7	8.59	7.3

Table 7. *Values of the levels and variation intervals of the factors*

Factor		Factor variation levels			Variation interval
Name	Notation				
Ammonium ion concentration	C, mol/dm^3	0.002	0.007	0.012	0.005
Solution volume	V, dm^3	0.05	0.35	0.65	0.3
Ionite mass	m, g	0.31	0.62	0.93	0.31

Table 8. *Data element of the sorption process by the fiber VION KN-1*

Test No.	Ammonium ion concentration, mol/dm^3	Solution volume, dm^3	Mass, g	Purification degree , %
1	0.002	0.05	0.31	99.40
2	0.002	0.35	0.31	98.70
3	0.002	0.65	0.31	96.40
4	0.007	0.05	0.93	99.50
5	0.007	0.35	0.93	97.35
6	0.007	0.65	0.93	83.80
7	0.012	0.05	0.62	99.05
8	0.012	0.35	0.62	58.70
9	0.012	0.65	0.62	32.00

Table 9. *Test values*

Concentration, mol/dm^3	Volume, dm^3	Mass, g	R,%
0.0065253940	0.35	0.3128	53.37069
0.0100000000	0.20	0.3136	57.20000
0.0115954000	0.15	0.6272	91.37589
0.0099900000	0.30	0.9378	93.42342
0.0060673890	0.45	0.6272	77.66356
0.0040765630	0.55	0.6282	84.48161
0.0019952620	0.70	0.6290	95.71635
0.0033431070	0.60	0.9347	98.04329
0.0070961730	0.65	0.9411	83.81542
0.0019319010	0.35	0.3113	89.10855
0.0078406740	0.50	0.4545	60.49453

Table 10. *Predicted values. Neural network: MLP 3-5-1 (test sampling)*

Observation No.	R Target	R- Output MLP 3-5-1	R- Absolute residues MLP 3-5-1	R- Squared residues MLP 3-5-1
1	53.37069	54.55938	1.188691	1.412987
2	57.20000	57.20866	0.008663	0.000075
3	91.37589	91.39071	0.014817	0.000220
4	93.42342	92.44196	0.981461	0.963265
5	77.66356	77.34208	0.321479	0.103348
6	84.48161	85.86594	1.384330	1.916369
7	95.71635	95.62773	0.088623	0.007854
8	98.04329	99.27424	1.230950	1.515239
9	83.81542	83.89240	0.076987	0.005927
10	89.10855	89.79660	0.688049	0.473411
11	60.49453	60.89747	0.402934	0.162356

INSTRUCTIONS FOR AUTHORS

We ask authors always to visit the online instructions for the use of the latest instructions available. Manuscripts must be submitted using the template available on the Journal's website.

PREPARATION OF MANUSCRIPTS

---

1. PREPARATION OF MANUSCRIPTS (TEMPLATE):

All manuscripts must be written in English or Portuguese and submitted as a Microsoft Word document only using the template of the Journal. Manuscripts should be written following the guidelines below. Please, observe the following points in preparing manuscripts. Papers not conforming strictly to these instructions may be returned to their authors for appropriate revision or may be delayed in the review process.

READABILITY: Manuscripts should be written in clear, concise, and grammatically correct English (British or American English throughout). The editors can not undertake wholesale revisions of poorly written papers. Every paper must be free of unnecessary jargon and readable by any specialist in the related field. The Abstract should be written in an explanatory style that will be comprehensible to readers who are not experts in the subject matter.

PROOFREADING: Please proofread carefully for both errors and inconsistencies in the following: spelling (especially of scientific terminology, proper names, and foreign words), mathematical notation, numerical values in tables and text, and accuracy of quotations. The Journal will evaluate the file seeking English grammatical issues, correctness, clarity, and engagement errors. There will be a tolerance of up to 100 errors in all manuscripts. In case more errors were found, editors will allow the authors to resubmit again and, in case these errors persist, a proofreading fee will be charged.

GENERAL FORMAT: The completed paper has to be written in English and submitted as a **Word document only** using the template of the Journal. Page size: A4, line spacing: single, font type: Arial. Please leave headers and footers unchanged since the editors should fill it. Please check guidelines for accurate information based on all different categories (review articles and technical notes). A single file of the whole manuscript should then be submitted through TCHE QUIMICA JOURNAL's e-mail (journal.tq@gmail.com) along with the COVER LETTER. ***The Journal no longer accepts submissions in any other form than by E-MAIL*** (journal.tq@gmail.com).

FORMAT FOR INITIAL SUBMISSION: Title, Author(s), Abstract (maximum 300 words),

Keywords (at least 3, maximum 5), Main text (Introduction, Review of Literature, Definitions (if any), Materials and Methods or Methodology, or Development, or Background, Results and Discussion or Findings, Conclusions), Acknowledgements (if any), References, Appendix (if any). This structure of the main text is not obligatory, but the paper must be logically presented. Footnotes should be avoided. The main text must be written with font size 11, justify. Within each main section, three levels of subheadings are available, and the titles must be bold, bold, and italic, italic, respectively. The manuscript should contain the whole text, figures, tables, and explanations. For more details, please check the template of the Journal.

2. THE FIRST PAGE OF THE MANUSCRIPT

TITLE: PORTUGUESE, ENGLISH, and the third language if the author's native language is not English or Portuguese. The editors can provide the title in Portuguese for those whose Portuguese is not the first language. It should be brief and informative. The title should reflect essential aspects of the article, in a preferably concise form of not more than 100 characters and spaces: font size 12, capital letters, center alignment.

BY-LINE: Names (size 12, Arial, small capital) of the authors. No inclusion of scientific titles is necessary. In the case of two or more authors, place their names in the same row, separate them with a semicolon (;) and please indicate the corresponding author with * in superscript. The corresponding author should be the one submitting the article online and an e-mail given (only one e-mail) below the addresses of all authors. Authors from different institutions must be labeled with numbers in superscript after the names. The affiliation of the authors should also be given (size 10).

ABSTRACT: PORTUGUESE, ENGLISH, and a third language if the author's native language is not English or Portuguese. Required for all manuscripts in which the **IMRAD (Introduction, Methods, Results and Discussion)** format should be summarized. It should not contain formulas, references, or abbreviations. The name ABSTRACT should be written in capital letters, Arial, size 12, bold, left alignment. The abstract should be written font Arial, size 10, justify. The editors can provide the translation of the abstract to Portuguese for those who Portuguese is not the first language. The journal adopts the **STRUCTURED ABSTRACT from 200 to 300 words as follows**:

Background: Introduction and statement of problem; identifies the need for the research question. In rigorous research, may include a hypothesis which is supported or refuted accordingly. What is the subject and relevance of the study? What does it intend to demonstrate or describe? This should be written succinctly; it might be eventually necessary to refer briefly to a context. What is the importance of the research? Why would a reader be interested in the larger work? The background (introduction) must clearly state the problem, the reason for doing the work, the hypotheses or theoretical predictions under consideration, and the essential background. **Aim:** the purpose of the work (objective); What is the aim of the study? The exact question(s) addressed by the article; the primary objective of the review. Begin with a clear, concise statement of the precise objective or question addressed in the manuscript. If more than 1 objective is addressed, the main objective should be indicated and only key secondary objectives stated. If an a priori hypothesis was tested, it should be stated. Example: This study aimed to...or...The purpose of this study was to... **Methods:** the basic design of the study; state the duration of follow-up, if any; explains the methods so others can replicate the study. How are the objectives achieved? Include the main method(s) used for the research; data collection - describes the process and points out potential omissions; What is the method of study? Show the methodology used, the form of data and sample collection. If it is a theoretical essay, what is the approach adopted. Provide sufficient details to the reader to understand how the study was performed. **Results and Discussion:** The purpose of a Results and Discussion section is to present the key results of your research. What are the main results? The main outcomes of the study should be provided and quantified, including confidence intervals or P values. For comparative studies,

confidence intervals should relate to the differences between groups. Results should be presented concisely. Point out the significance of the results, and place the results in the context of other work and theoretical background. It is important to plan this section carefully as it may contain a large amount of scientific data that needs to be presented in a clear and concise fashion. **Conclusions:** Provide only conclusions directly supported by the results; avoid speculation and overgeneralization. Indicate whether additional study is required; Give equal emphasis to positive and negative findings of equal scientific merit; points out things that may have been overlooked, and suggests areas for further research. summary of your research. Some researchers also include: knowledge contribution, research limitation and future research recommendation in conclusions section. It should not contain formulas, references, or abbreviations.

KEYWORDS: PORTUGUESE, ENGLISH, and a third language if the author's native language is not English or Portuguese. The editors can provide the title in Portuguese for those whose Portuguese is not the first language. Authors should provide appropriate and short keywords that encapsulate the principal topics of the paper. *The maximum number of keywords is 5* not including items appearing in the title. The keywords should be supplied, indicating the scope of the paper. Size 10, italic, justify, only the word Keywords must be bold, left alignment.

The authors should include Abbreviations and Nomenclature listings when necessary.

3. THE MAIN TEXT PART OF THE MANUSCRIPT

The words Introduction, Review of Literature, Definitions (if any), Materials and Methods or Methodology, or Development, or Background, Results and Discussion of Findings, Conclusions must be written in capital letters, Arial, font size 12, left alignment, bold.

INTRODUCTION: The introduction must clearly state the problem, the reason for doing the work, the hypotheses or theoretical predictions under consideration, and the essential background. It should not contain equations or mathematical notation. A brief survey of the relevant literature so that a non-specialist reader could understand the significance of the presented results. A good introduction should ideally have 3-5 well-explained paragraphs and should finishing pointing out the AIM of the study.

MATERIALS AND METHODS OR METHODOLOGY, OR DEVELOPMENT: Provide sufficient details to the reader to understand how the study was performed. The technical description of methods should be given when such methods are new. It is generally recommended that the materials and methods should be written in the past tense, preferably in the passive voice. In this section, ethical approval, study dates, number of subjects, groups, evaluation criteria, exclusion criteria and statistical methods should be described sequentially. The following questions should be absolutely provided: the beginning, and termination dates of the study period; number of subjects/patients/experimental animals etc. enrolled in the study; has the approval of the ethics committee been obtained? Study design (prospective, retrospective or other); still additional features of the study design (cross-sectional) should be indicated. Apart from this, other types of study designs (randomized, double-blind, placebo-controlled or double-blind, parallel control etc.) should be revealed. Before you finish your manuscript, ask yourself the following questions about your Materials and Methods section to ensure that you have included all important information. Is there sufficient detail so that the experiments can be reproduced? Is there excess information that could be removed without affecting the interpretation of the results? Are all the appropriate controls mentioned? Are all appropriate citations included? Is the source of each reagent listed? The Materials and Methods section is a vital component of any manuscript. This section of the report gives a detailed account of the procedure that was followed in completing the experiment(s) discussed in the paper. Such an account is very important, not only so that the reader has a clear

understanding of the experiment, but a well written Materials and Methods section also serves as a set of instructions for anyone desiring to replicate the study in the future. Considering the importance of "reproducible results" in science, it is very relevant why this second application is so vital. Some general rules for Methods sections are:

- It should be clear from the Methods section how all of the data in the Results section were obtained.
- The study system should be clearly described. In medicine, for example, researchers need to specify the number of study subjects; how, when, and where the subjects were recruited, and that the study obtained appropriate 'informed consent' documents; and what criteria subjects had to meet to be included in the study.
- In most cases, the experiments should include appropriate controls or comparators. The conditions of the controls should be specified.
- The outcomes of the study should be defined, and the outcome measures should be objectively validated.
- The methods used to analyze the data must be statistically sound.
- For qualitative studies, an established qualitative research method (e.g. grounded theory is often used in sociology) must be used as appropriate for the study question.
- If the authors used a technique from a published study, they should include a citation and a summary of the procedure in the text. The method also needs to be appropriate to the present experiment.
- All materials and instruments should be identified, including the supplier's name and location.
- The Methods section should not have information that belongs in another section (such as the Introduction or Results).
- You may suggest if additional experiments would greatly improve the quality of the manuscript. Your suggestions should be in line with the study's aims. Remember that almost any study could be strengthened by further experiments, so only suggest further work if you believe that the manuscript is not publishable without it.

RESULTS AND DISCUSSION OR FINDINGS: Results should be presented concisely. Also, point out the significance of the results, and place the results in the context of other work and theoretical background. The results and discussion sections are one of the challenging sections to write. It is important to plan this section carefully as it may contain a large amount of scientific data that needs to be presented in a clear and concise fashion. The purpose of a Results section is to present the key results of your research. Results and discussions can either be combined into one section or organized as separate sections. Use subsections and subheadings to improve readability and clarity. Number all tables and figures with descriptive titles. Present your results as figures and tables and point the reader to relevant items while discussing the results. This section should highlight significant or interesting findings along with P values for statistical tests. Be sure to include negative results and highlight potential limitations of the paper. The results and discussion section of your research paper should include the following: Findings; Comparison with prior studies; Limitations of your work; Casual arguments; Speculations; Deductive arguments.

CONCLUSION: Summarize the data discussed in the Results and Discussion or Findings section showing the relevance of the work and how different it is from other researches. Also, point out the benefits and improvements that can be observed to develop new science standards that can change something in the related field.

ACKNOWLEDGMENTS: (if any) These should be placed in a separate paragraph at the end of the text, immediately before the list of references. It may include funding information too.

REFERENCES: References should be cited in the text using the **name-and-year system (Author, year) (APA FORMAT).** Alternatively, the author's surname may be integrated into the text, followed by the year of publication in parentheses. **Examples:** Grasslands are regarded as important foraging areas for many insectivores in Europe, such as birds (Vichery, 2001; Barnet *et al*., 2004), bats (Guttinger, 1997) or amphibians and reptiles (Langton and Burton, 1997). However, the knowledge of the overall arthropod availability in such grasslands is scarce, since many studies about insect populations concentrate on extensive grasslands on poor, dry or wet soils include only few species or systematic groups (Ellgsen *et al*., 1997; Gibson *et al*., 1992; Hansel and Plachter, 2004; Manhart *et al*., 2004; Kruess and Tscharntke, 2002a, b; Wingerden *et al*., 1992; Sjodin, 2007a, b; Perner *et al*., 2005). Carbon dioxide produced by the combustion of biodiesel can be recycled by photosynthesis, thereby minimizing the impact of biodiesel combustion on the greenhouse effect (Korbitz, 1999; Agarwal and Das, 2001).

- *Cite only essential resources, avoid citing unpublished material. References to papers "in press" must mean that the article has been accepted for publication. At the end of the paper list references alphabetically by the last name of the first author. Please, list only those references that are cited in the text and prepare this list as an automatically numbered list. The word References with size 12, bold, capital letters, left alignment*

---

4. GUIDELINES FOR REFERENCES:

- **The Journal uses the APA (American Psychological Association) FORMAT CITATION as follows**:

GENERAL RULE FOR ACADEMIC PAPERS:

Author's surname, initial(s). Year of publication after the name of the authors (between parentheses). Title of the paper. Name of the journal in italic, number of the edition also in italic, volume between parentheses and finally initial and final page, and, if the case, retrieved from (what website) or DOI

Examples:

1. Nikolaeva, L.P., Cherdantsev DV., Titiv K.S. (2017). Characteristics of bone marrow stem cells in patients with complicated diabetes mellitus. *The Russian biotherapeutic journal, 16*(1): 47-50.
2. Mitchell, J.A. (2017). Citation: Why is it so important. *Mendeley Journal, 67*(2), 81-95. Retrieved from https://www.mendeley.com/reference-management/reference-manager
3. Karthiga, N., Rajendran, S., Prabhakar, P., Rathish, R.J. (2015). Corrosion inhibition by plant extracts - An overview. *Int. J. Nano. Corr. Sci. Eng, 2*(4):31-49.
4. Akbulut, S., and Bayramoglu, M.M. (2013). The Trade and Use of Some Medical and Aromatic Herbs in Turkey. *Ethno Med, 7*(2): 67-77.

- ✓ **For different types of references than of scientific papers, the Journal recommend to visit the websites below for a more detailed information.**

< https://www.mendeley.com/guides/apa-citation-guide >
< https://libguides.murdoch.edu.au/APA6/all >
< https://aut.ac.nz.libguides.com/APA6th/referencelist >

---

5. FIGURES:

The number of pictures (including graphs and diagrams) should not exceed 15 and should be submitted either in JPEG or PNG formats. All photographs, charts, and diagrams should be numbered consecutively (e.g., Figure 1, Figure 2, Figure 3,…..) in the order in which they are referred in the text. Caption must appear below the figure (size 11, bold, italic) and should be sufficiently detailed to enable us to understand apart from the text. Explanation of lettering and symbols should be also given in the caption and only exceptionally in the figures. Figures should be of good quality. Scanned figures should be at a resolution of 800 dpi/bitmap for line graphs. Diagrams containing chemical structures should be of high graphical quality and always be of the same size so that they can be uniformly reduced. Figures should have a maximum width of one Journal column (8.5 cm) to be inserted on the body of the text so that they can be applied to the standards of the Journal. If the figures exceed 8.5 cm, they will be placed at the end of the article. Also, authors may be requested to submit each figure as an image file in one of the following formats: jpeg or png. For pictures, graphs, diagrams, and tables identical to material already published in the literature, authors should seek permission for publication from the companies or scientific societies holding the copyrights and send it to the editors of Tche Quimica Journal along with the final form of the manuscript.

Important summarized information:

- Upload the images either in JPEG or PNG formats. Poor quality and resolution figures will not be accepted. Pay attention when scanning or making print screen of an image. In these cases, the resolution is usually low and it becomes challenging to the reader to see the information of the figure;

- Figures should be numbered consecutively, in Arabic numerals, according to the order in which they have been first cited in the text;

- All information including numbers and symbols should be clear and of uniform size. The lettering for figures should be large enough to be legible either in the two or one column format;

- Any details to point out a specific view like symbols, arrows, or letters used in photomicrographs should contrast with the background;

- Titles and detailed explanations belong in the legends for illustrations not on the illustrations themselves.

- When graphs, scatter-grams or histograms are submitted the numerical data on which they are based should also be supplied and clear enough.

- The photographs and figures should be trimmed to remove all the unwanted areas. Also, if photographs of individuals are used, their pictures must be accompanied by written permission to use the photograph.

- If a figure has been published elsewhere, acknowledge the original source and submit written permission from the copyright holder to reproduce the material. A credit line should appear in the legend for such figures.

- Legends for illustrations: When symbols, arrows, numbers, or letters are used to identify parts of the illustrations, identify and explain each one in the legend. Explain the internal scale (magnification) and identify the method of staining in photomicrographs when suitable;

- The Journal reserves the right to crop, rotate, reduce, or enlarge the photographs to an acceptable size.

6. TABLES:

Tables should be self-explanatory and should not duplicate textual material. They should be mentioned in the text, numbered consecutively (e.g., Table 1, Table 2, Table 3,....), and accompanied by a title at the top (size 11, bold, italic). Please insert all the tables in the text and do not enclose huge tables that cannot fit within the page margins. Other important considerations.

- Tables with more than 15 columns and 30 rows are not acceptable.
- Number tables, in Arabic numerals, consecutively in the order of their first citation in the text and supply a brief title for each.
- Place explanatory matter in footnotes, not in the heading.
- Explain in footnotes all non-standard abbreviations that are used in each table. If necessary, use symbols (*, †, ‡, §, ||, ¶ , **, ††, ‡‡) to explain and make all abbreviations clear to the reader.
- Obtain permission for all fully borrowed, adapted, and modified tables and provide a credit line in the footnote.
- Tables with their legends should be provided at the end of the text after the references. The tables along with their number should be cited at the relevant place in the text.
- In the text, do not use Tab. For an abbreviation of a Table. Write Table 1, Table 2 instead of Tab.1, Tab.2;

7. MATHEMATICAL EXPRESSIONS:

In general, minimize unusual typographical requirements, use solidus, built-up fractions. Avoid lengthy equations that will take several lines (possibly by defining the terms of the equation in separate displays). For drawing equations, please use the Equation Editor of Word, if possible. Make subscripts and superscripts clear. Display only those mathematical expressions that must be numbered for later reference or that need to be emphasized. The equations displayed should be consecutively numbered throughout the paper. The numbers should be placed in parentheses on the right of the equation, e.g. (Eq. 1).

8. SUPPLEMENTARY MATERIAL:

Any Supplementary material (extra figures, tables, diagrams, appendix, abbreviations list) should be placed at the end of the manuscript and indicated as such. All supplementary material should also be cited in the text.

Editors, at any time of the editing process, may ask authors to split off part of the manuscript, presenting it as supplementary material.

9. ARTICLE PROCESSING CHARGES (APC)

PUBLICATION FEES (1), ADDITIONAL FEES FOR PUBLICATION (2), DISCOUNTS (3), AND FREE PUBLICATION OPPORTUNITIES (4)

Authors are required to pay a publication fee to share in the costs of production. The fee will be asked **if, and only if, the article is accepted for publication**. Once full payment has been made (PayPal, Bank Transfer, or Western Union Services), the paper will be published at the Ahead of Print and scheduled for the next available issue. All waivers (as well as the publication fee requests) are **applied to the accepted papers after successful peer-review only**.

Please observe the flowchart below to understand how the Journal works.

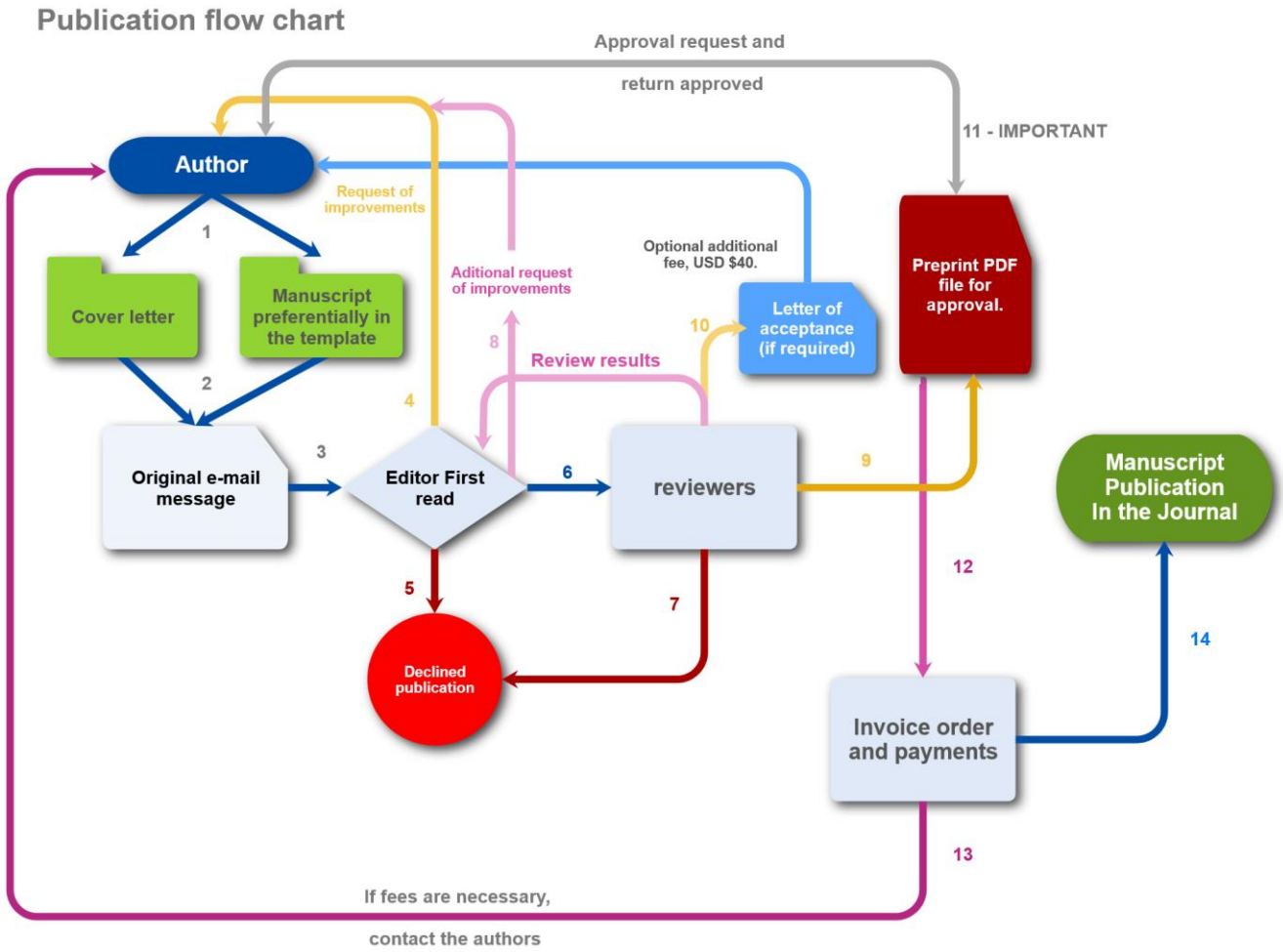

1. PUBLICATION FEES

*Brazilian authors, R$ 600,00

*Other countries income groups:

High income and nuclear-capable countries ***(Israel, India, Pakistan, United Kingdom, China, France,***

United States, Russia, North Korea) - USD 300

Upper middle-income USD 250

Lower middle-income USD 120

Lower middle income (Heavily indebted poor countries (HIPC)) USD 100

Low-income USD 100

Low income (Heavily indebted poor countries (HIPC)) USD 80

- ✓ (*) Classification according to the World Bank list of economies (June 2020). Please check https://datahelpdesk.worldbank.org/knowledgebase/articles/906519-world-bank-country-and-lending-groups

2. ADDITIONAL FEES FOR PUBLICATION

a) Proofreading and / or plagiarism

If the submitted manuscript has more than 100 grammatical errors or plagiarism greater than 5%, **a fee of USD 200** will be charged. This fee does not guarantee publication of the manuscript and is non-refundable.

b) Changing PDF pre-printing files

After the final verification of the manuscript and the generation of the PDF pre-print file, **a fee of USD 100** will be charged to authors who wish to make any changes. For each new change, the fee is charged again.

c) Acceptance Letter for article publication

The acceptance letter is an **optional service** of the Journal. If the authors need a document to prove that their article has been peer-reviewed and accepted for publication, they may request, upon payment of **a fee of USD 40**, an acceptance letter for publication of the article.

NOTE 1: THE LETTER OF ACCEPTANCE may be issued **if, and only if,** the article has undergone a complete peer-review and is considered ACCEPTED for publication. Letters will NOT be issued for newly sent articles that have not yet been appropriately evaluated and peer-reviewed.

NOTE 2: The Journal does not agree with the trade-in documents that can attest to the publication of articles that have not gone through the due process of peer-review and are legitimately considered approved for publication in the subsequent edition.

NOTE 3: THE LETTER OF ACCEPTANCE may be revoked at any time if, concerns about the manuscript emerge.

d) Formatting the manuscript according to the template of the Journal

The use of the template is mandatory. All authors must submit their papers according to the official model of the Journal available at www.journal.tchequimica.com (Downloads >> Templates and Instructions). In case the authors do not have time or proper conditions to execute the formatting of the manuscript, we can provide all the adaptation to the template of the Journal. However, this is an

optional service, and **a fee of USD 80** will be charged on top of the Article Processing Charges.

If there is no need, additional fees are not charged.

3. DISCOUNTS

a) **50% discount** for authors who support other journals from the team (*Southern Brazilian Journal of Chemistry* - this is a 100% free journal), ***with 1 manuscript approved*** for publication;

b) **100% discount** for authors who support other journals from the team (*Southern Brazilian Journal of Chemistry* - this is a 100% free journal), ***with 2 manuscripts approved*** for publication;

c) **Volume discount.** If you are an author/collaborator of the Journal that has ***published with us 4 manuscripts*** (paid your full corresponded price), your fifth manuscript will be free of charge. Later the counting cycle restart.

4. FREE PUBLICATION OPPORTUNITIES

a) Young scientists that are publishing the first manuscript of their career. **Requirements:** Copy of the curriculum without publications; maximum of 2 authors; one manuscript previously accepted in the ***Southern Brazilian Journal of Chemistry*** (the manuscript may be from the author or from colleagues, provided that the extra purpose of the collaboration is notified at the time of submission), or two manuscripts previously accepted in the ***Journal of Law, Public Policies, and Human Sciences*** (manuscripts may be from the author or from colleagues, provided that the extra purpose of the collaboration is notified at the time of submission). (Last revision of the rule: 15th of October 2020);

b) All personal related to the production of the journals, from Brazil and abroad;

c) Longtime collaborators. Authors who have published four (4) articles with us during the past decade will be rewarded with one (1) free publication. After that, this cycle starts again, that is, for every five (5) articles published, one will be free of publication fees. Thank you for choosing and trusting the Journal to publish your research.

d) Paper considered by the Editors of high quality, priority, and relevance for the development of the society shall pay no fees. Note that this condition is a small recognition prize, not something that you may request. Thank you for your comprehension.

Thank you very much for choosing Tche Quimica Journal to publish your paper! We would be happy if you consider the Journal to submit any further paper in the near future.

Kind Regards,

Editorial Team

Dr. Luis Alcides Brandini De Boni

Dr. Eduardo Goldani